AFRL-HE-BR-PC-1999-0002

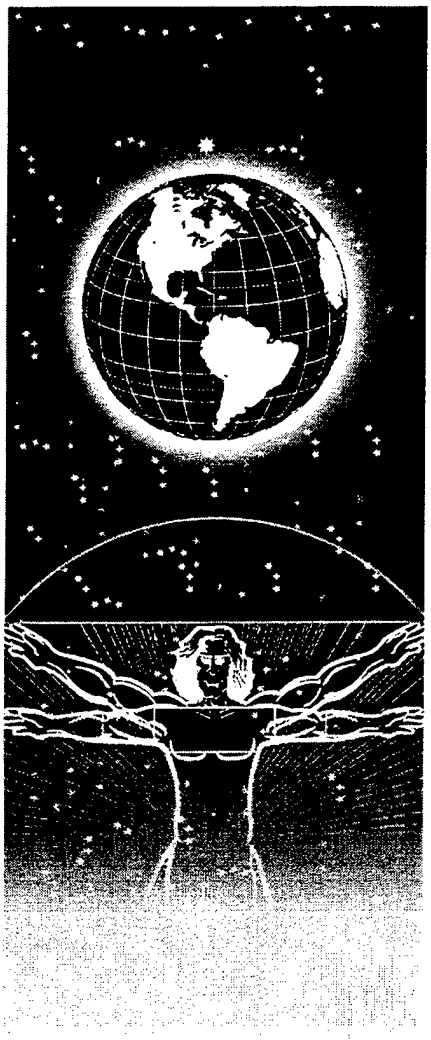

UNITED STATES AIR FORCE RESEARCH LABORATORY

INFRARED LASERS & MILLIMETER WAVES: THE LINKS BETWEEN MICROWAVES AND LASER OPTICS

ELEANOR R. ADAIR
(Editor)

HUMAN EFFECTIVENESS DIRECTORATE
Directed Energy Bioeffects Division
8315 Hawks Road
Brooks AFB TX 78235-5324

February 1999

NOTICES

These proceedings are published in the interest of scientific and technical information exchange and does not constitute approval or disapproval of their ideas or findings.

Using Government drawings, specifications, or other data included in this document for any purpose other than Government-related procurement does not in any way obligate the US Government. The fact that the Government formulated or supplied the drawings, specifications, or other data, does not license the holder or any other person or corporation, or convey any rights or permission to manufacture, use, or sell any patented invention that may relate to them.

The Office of Public Affairs has reviewed this document and it is releasable to the National Technical Information Service, where it will be available to the general public, including foreign nationals.

These proceedings have been reviewed and are approved for publication.

Eleanor R. Adair

ELEANOR R. ADAIR, Ph.D
Editor

RICHARD L. MILLER, Ph.D
Chief, Directed Energy Bioeffects

REPORT DOCUMENTATION PAGE

Form Approved
OMB No. 0704-0188

1. AGENCY USE ONLY (Leave blank)	2. REPORT DATE	3. REPORT TYPE AND DATES COVERED
	February 1999	Interim, 21-22 January 1997

4. TITLE AND SUBTITLE
Infrared Lasers & Millimeter Waves: The Links Between Microwaves and Laser Optics

5. FUNDING NUMBERS
PE – 62202F
PR – 7757
TA – B3
WU – 30

6. AUTHOR(S)
Eleanor R. Adair (Editor)

7. PERFORMING ORGANIZATION NAME(S) AND ADDRESS(ES)
Air Force Research Laboratory (AFMC)
Human Effectiveness Directorate
Directed Energy Bioeffects Division
8315 Hawks Road
Brooks Air Force Base TX 78235-5324

8. PERFORMING ORGANIZATION
AFRL-HE-BR-PC-1999-0002

9. SPONSORING/MONITORING AGENCY NAME(S) AND ADDRESS(ES)

10. SPONSORING/MONITORING AGENCY REPORT NUMBER

11. SUPPLEMENTARY NOTES:
Proceedings of the Infrared Lasers & Millimeter Waves Workshop, The Links Between Microwaves and Laser Optics, Brooks AFB TX, 21 - 22 Jan 97. "USAF Armstrong Laboratory" has been reorganized into the "Air Force Research Laboratory, Human Effectiveness Directorate."

12a. DISTRIBUTION/AVAILABILITY STATEMENT
Approved for public release; distribution unlimited.

12b. DISTRIBUTION CODE

13. ABSTRACT (Maximum 200 words)

The goal of this project is to reconcile the guidelines for human exposure at the frequency interface (300 GHz) between millimeter waves and infrared lasers and to derive means for this reconciliation in terms of existing and proposed scientific data requirements. To this end, a two-day workshop was convened at Brooks Air Force Base on 21-22 January 1997 at which experts in the technology and biological effects of exposure to both millimeter wave frequencies and infrared laser optics presented papers on the state of the art in their respective disciplines. Several informal discussions and a final panel discussion illuminated the key questions requiring answers and proposed research that would help define these answers. A significant step toward future refinement of the exposure guidelines was the establishment of a six-person ad hoc committee, under the Chairmanship of Dr Kenneth R. Foster, to serve as a liaison between radio frequency and infrared laser standards-setting organizations. This committee would determine research and modeling needs that would provide the basis, in terms of both field strength and averaging time, for a reconciled exposure guideline for humans at 300 GHz.

14. SUBJECT TERMS
Millimeter Waves; Infrared Lasers; Radio Waves

15. NUMBER OF PAGES
456

16. PRICE CODE

17. SECURITY CLASSIFICATION OF REPORT	18. SECURITY CLASSIFICATION OF THIS PAGE	19. SECURITY CLASSIFICATION OF ABSTRACT	20. LIMITATION OF ABSTRACT
Unclassified	Unclassified	Unclassified	UL

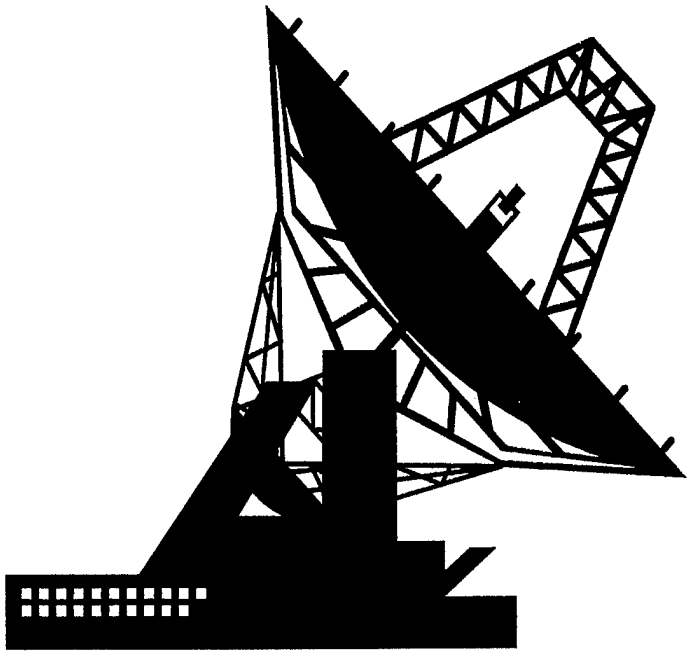

Infrared Lasers & Millimeter Waves Workshop
The Links Between Microwaves & Laser Optics

Brooks AFB, Texas
on
21 Jan 1997 - 22 Jan 1997

TABLE OF CONTENTS

INTRODUCTION

Eleanor R. Adair
AFRL/HEDR
Brooks AFB, TX

The biological consequences of exposure to radio frequency fields at millimeter wavelengths are a subject that has assumed considerable importance for the military in recent years. This is primarily due to the fact that this part of the electromagnetic spectrum is more heavily used by the military than by commercial groups. Furthermore, the subject relates directly to specific issues of health and safety for human beings. There are several recent events that have intensified this importance, of which the following are a sampling:

In 1996 the Federal Communications Commission (FCC) adopted new guidelines for evaluating human exposure to radio frequency electromagnetic fields. The FCC had adopted, in 1985, the American National Standards Institute (ANSI) C95.1-1982 guidelines. When these guidelines became obsolete, the FCC published in 1993 a Notice of Proposed Rulemaking (NPRM) that suggested adoption of the 1992 revision of ANSI 1982. This suggested document, promulgated by the Institute of Electrical and Electronics Engineers (IEEE) in 1991 as IEEE C95.1-1991, became ANSI/IEEE C95.1-1992 upon adoption by ANSI. One feature of ANSI/IEEE C95.1-1992, not shared by any other extant exposure guideline, is the equalization of exposure limits at 300 GHz, where millimeter waves meet the far infrared spectral band. However, under pressure to comply with the U.S. Telecommunications Act of 1996, the FCC adopted guidelines based principally on a recommendation published in 1986 by the National Council on Radiation Protection and Measurements (NCRP). The NCRP document provided guidance for both occupational and general public exposure across a frequency range of 3 kHz to 100 GHz and was endorsed by the U.S. Federal Government health and safety agencies, especially the EPA. By truncating the microwave frequencies at 100 GHz, the FCC failed to resolve the question of the interface between millimeter wave and IR laser standards. In addition, the FCC guidelines at millimeter wave frequencies are a factor of 10 lower than the C95.1 standard, thus suggesting to some that this part of the spectrum is more dangerous than the lower frequencies where the FCC rules and C95.1 standard are similar.

In recent years, there has been a rash of published papers from the former Soviet Union, many of which suggest the existence of resonant athermal effects at millimeter wave frequencies (cf. Pachomov, et al, 1998). Often these papers claim therapeutic effects from the clinical use of millimeter wave fields. On the other hand, many papers are widely quoted by alarmists who believe in the existence of important bioeffects at extraordinarily low field strengths. One alarmist is W. R. Adey who, during a 1992 Senate Hearing on Police Radar, cited published papers from Germany (Grundler, 1983;

Grundler, et al., 1992) claiming resonance effects at ultra-low levels. Careful examination reveals that many of the cited papers are of questionable quality and some are clearly impaired by artifacts related to the characterization of the power source (Osepchuk and Petersen, 1997). In a preliminary proposal for this Workshop on Infrared Lasers and Millimeter Waves, Dr. John Osepchuk noted that the United States military have succeeded in working well with health agencies in developing rational voluntary standards for human exposure to lasers. He believes it is reasonable to require that there be a match between laser and microwave standards at 300 GHz. He further noted that if the alarmists are found to be correct, the permitted exposure levels in the laser standards should be challenged and perhaps tightened by at least a factor of 10. In such a case, the military use of laser technology could be impacted severely.

The foregoing provides a brief background to the subject matter covered by the Workshop held at Brooks Air Force Base on 21-22 January 1997. On that occasion, more than 70 engineers and scientists assembled to discuss a most timely topic: the interface between infrared lasers and millimeter wave microwaves, their similarities and differences, and the import for setting rational exposure guidelines across these frequency bands. The Workshop was sponsored by the Tri-Service Directed Energy Bioeffects Program at Brooks (Project Reliance), with supplementary technical support by Systems Research Laboratories and very generous travel funding from Lucent Technologies through the good auspices of Ronald C. Petersen.

As a basis for the two days of talks and discussions, some pertinent questions were posed to the participants in the Announcement for the Workshop; these questions are listed below. In addition, all speakers were asked to submit abstracts and copies of their visual materials, all of which were bound into two volumes that were distributed at the meeting. These volumes served as the basis for these Proceedings and, in many cases, the abstracts were replaced by formal papers submitted after the Workshop. Originally, we hoped that a publisher could be found to print a volume of technical papers on this topic, based on the lectures given at the Workshop. Unfortunately, the several publishers contacted were in agreement that there was insufficient market for such a volume. Early in 1998, I approached Dr. Michael Murphy, Chief of the Directed Energy Bioeffects Branch, with the request to publish the materials on hand as an Air Force Proceedings. The volume you hold in your hands is the result.

It is important to note that one clear benefit of the Workshop was the formation of a joint IR lasers/millimeter wave subcommittee to investigate the matter of reconciliation of standards at the interface between the two spectral bands, averaging time, dependence on area of irradiation, peak exposure limits, etc. This six-person committee is chaired by Dr. Kenneth Foster and other members are Drs. Russ McCally, Benjamin Rockwell, Bruce Stuck, Marvin Ziskin and Eleanor Adair. Although the committee has never met in person, we exchange ideas frequently via e-mail. In addition, Dr. Foster has prepared a theoretical paper that was recently published in Bioelectromagnetics (Foster, 1998). The paper discusses averaging time for exposures to millimeter wave fields in terms of a

theoretical model of physiological events that occur in the exposed skin. The subcommittee is dedicated to examining the other relevant exposure variables and to designing an appropriate experiment to test a specific biological response to an electromagnetic energy challenge at both IR laser and millimeter wave frequencies, which are normalized to generate equivalent energy absorption by the exposed tissues.

As Chief Organizer of the Workshop and Editor of the volume, I am indebted to several individuals who helped bring this project to a satisfactory conclusion. Drs. John Osepchuk and David Sliney had the initial vision of the Workshop and its importance to standards setting and guided my selection of program and speakers. Ms Debra Jurek ably handled the requests to participate, the submitted visual materials, the local arrangements, and the collation and reproduction of the materials for the Workshop. SSgt. Jesse Hightower assisted Ms Jurek with mailings and collation of materials, manned the registration desk and organized the meeting room and the audio-visual aids. Assisting SSgt. Hightower were many Air Force military personnel, many of whom have since moved on to other careers. Jodie and her staff at the Brooks Club ably managed the facilities for the meeting room and the delicious luncheons we enjoyed. Dr. Michael R. Murphy generously provided the wherewithal to publish these proceedings. Mr. Ron Petersen, valued friend and colleague, convinced Lucent Technologies to part with substantial funds to underwrite the travel expenses of several participants. And Mr. Kevin Mylacraine and Ms. Brenda Cobb have overseen the assembly and reproduction of the materials that constitute this report. To all, I give my sincere thanks.

REFERENCES

1. Foster, K.R., Lozano-Nieto, A. and Riu, P. (1998) Heating of tissues by microwaves: A model analysis. *Bioelectromagnetics* 19:420-428.

2. Grundler, W. (1983) Biological effects of RF and MW energy at molecular and cellular level. In: Rindi, A., Grandolfo, M. and Michaelson, S.M. (Eds.) *Biological Effects and Dosimetry of Nonionizing Radiation. Radiofrequency and Microwave Energies.* New York: Plenum Press, pp. 299-318.

3. Grundler, W., Keilman, F. and Froehlich, H. (1977) Resonant growth rate response of yeast cells irradiated by weak microwaves. *Phys. Rev. Lett.* 62A:463-466.

4. Osepchuk J.O. and Petersen, R.C. (1997) Comments on "Resonance effect of millimeter waves in the power range from 10^{-19} to 3 x 10^{-3} W/cm^2 on *Escherichia coli* cells at diferent concentrations," Belyaev, et al., *Bioeectromagnetics* 17:312-321 (1996). *Bioelectromagnetics* 18:527-528.

5. Pakhomov, A.G., Akyel, Y., Pakhomova, O.N., Stuck, B.E. and Murphy, M.R. (1998) Current state and implications of research on biological effects of millimeter waves: A review of the literature. *Bioelectromagnetics* 19:393-413.

UNDERLYING QUESTIONS FOR THE WORKSHOP

1. Is there any physical (scientific) reason to expect different interaction with material (living or not) of microwaves (6 to 300 GHz) and lasers (300 to 6000 GHz)?

2. If skin depths are similar then shouldn't the effects be the same regardless of frequency in the frequency range of 6 to 6000 GHz?

3. Is there a difference between the effects of coherent and incoherent radiation on materials (living or not) in this frequency range?

4. Is there an auditory effect with only skin absorption -- airborne sound, bone conduction?

5. Is there a database for long-term exposure (chronic)?

MEETING OVERVIEW

David H. Sliney
Laser Microwave Division
U.S. Army Environmental Hygiene Agency
Aberdeen Proving ground, MD

In his opening remarks, David Sliney noted that he had been active in the ACGIH Physical Agents TLV Committee and also in the IRPA Committee, now the International Commission on Non-Ionizing Radiation Protection (ICNIRP). Both of these groups had to recommend human exposure limits for both the optical spectrum and the RF spectrum. As such, it was quite interesting that a much more conservative safety stance had traditionally been taken outside the optical spectrum. Perhaps this was done because of the good press that was received by the major optical radiator, the sun. Certainly, many members had concerns about a step function at 300 GHz (1mm wavelength). He also noted that the laser/optical radiation community had fortunately not had to face the special interest pressures to declare RF at very low exposure rates as hazardous because of concerns about the unsightliness of large antenna structures or power transmission towers. Both committees had resisted the pressures to set very low limits based upon concerns about hypothetical effects, but rather set the limits only on well understood and replicated biological effects. He stressed the importance of understanding the damage mechanism in order to have scaling factors for adjusting limits with wavelength (frequency), area of illumination, duration of exposure, etc. He took excellent notes on all of the lectures delivered in the Workshop. These notes are transcribed and edited in the paragraphs that follow.

1. Dr. Robert Adair (a physicist at Yale University) spoke on interaction mechanisms of electromagnetic fields with matter and started at the level of the effects of fields upon dipoles. He emphasized the relaxation mechanism (cf., Foster and Schwan, CRC Handbook) in studying interactions with dipoles. He then described the known effects of electromagnetic field interactions with the water dipole. He argued that by employing maximum cross sections for resonant absorption, he could show that no interaction could occur with DNA. Furthermore, even if one were to assume coherent effects with DNA, he argued that one could never see such effects. It was noted that membranes were in effect an array of coupled oscillators, but even so, even if one were to assume that these were not damped oscillators, one simply cannot calculate that there is a significant energy transfer to be of concern.

2. Dr. Paul Kennedy, USAF Armstrong Laboratory (USAF/AL), gave an overview of the mechanisms of laser-induced biological interaction with tissue. He stated that virtually all interactions were very superficial and thresholds of damage were generally of the order of 1 J/cm^2 within a range of about one order of magnitude, plus or minus. After briefly describing thermal and photochemical damage of the skin, he described the differing effects upon ocular tissues with change in wavelength. He noted that transient

effects of glare and flash blindness were of interest for vision, but permanent effects on the eye were thermal burns, acoustic effects, photochemical injury, and, in the sub-nanosecond regime, non-linear effects.

3. Dr Steven Chalfin, an ophthalmologist at the University of Texas at San Antonio, gave an overview of the human eye and measures of visual function and damage. He described visual acuity and measures of function. He noted that the cornea and lens were possible targets of infrared and millimeter wave exposures. He stated that the cornea and sclera differed largely in the level of hydration and that affected the clarity. He showed examples of holmium laser burns of the cornea, used clinically in refractive surgery. Slit-lamp biomicroscopy was the standard measure of corneal or lenticular clarity. As an adjunct, he stated that two stains were helpful; fluorescein dye showed areas of corneal epithelial cell loss, whereas rose bengal dye showed dead or dying epithelial cells. Quantitative measures of corneal endothelial cell loss were best measured with a specular microscope. Keratoscopes were used to measure surface optical power and topography, therefore structural changes. With regard to the lens, he described the epithelium, endothelium, cortex and nucleus. He stated there had long been a problem in describing lenticular changes and grades of cataract, but that Scheimpflug photography was particularly effective for visualizing changes in the lens. Also, the IR LED opacity lens meter was quite useful. Finally, he noted that the scanning confocal microscope offered a very powerful tool for studies of thick tissues. He showed a nasal corneal burn from a victim of the Hiroshima A-bomb blast.

4. Dr. Marvin Ziskin, Temple University, Philadelphia, PA, gave a very detailed description of skin anatomy and physiology. He emphasized the great complexity of skin structure, with many specialized cells, such as sebaceous cells, free nerve endings and Langerhans cells. He thought that Langerhans cells might be a special absorber of millimeter waves. He noted that thermally sensitive nerve endings were quite numerous in the skin of the fingertips and the lips, but much less concentrated on the back.

5. Dr. S.I. Alekseev, Temple University (formerly of Puschino, Russia), described the use of millimeter waves in therapy in Russia, since these waves are absorbed very superficially in the skin - - generally within 1 mm skin depth. He showed a plot of changes in the firing rate of RP-4 neurons during and after exposure at a SAR of 3150 mW/g. He showed that for increasing SAR (500 to several thousand W/kg) this rate changed steadily. He presented data and calculations that showed that sensitivity was relatively flat with frequencies below approximately 10 GHz. Above 10 GHz, the sensitivity increased strongly. He stated that his SAR was determined by temperature rise and calculated over a 0.3 mm depth. He stated that the change in firing rate was a thermal effect and directly proportional to temperature increase. He explained that the free-field power density of his 60-70 GHz applicator was about 10 mW/cm^2.

6. William D. Hurt (USAF/AL) spoke on the dielectric properties of tissue and the dosimetry of millimeter waves. He showed photographs of 35 and 94 GHz sources used at USAF/AL. They use dielectric lenses to increase power densities up to 1 W/cm^2. He described instruments used for field measurements (e.g., the Narda field sensor). The

standard gain horns for 35 and 94 GHz sources are quite small. An infrared camera was used to chart temperature distributions in absorbing materials. From the IR camera, they were able to estimate the localized SAR. The skin depth for 35 GHz was about 0.66 – 0.76 mm, at 94 GHz was 0.33 – 0.41 mm, and at 300 GHz was 0.23 – 0.32 mm. Reflection coefficients varied from 0.43 – 0.49 at 35 GHz down to 0.16 – 0.18 at 300 GHz. They had not looked at variations of dielectric properties with field strength, but he stated that in theory this should not take place until very high power densities. They used 5 seconds after exposure to measure the SAR.

7. David Sliney spoke on radiometric parameters used in describing infrared bioeffects. He pointed out that because of the superficial penetration of the skin and thin-layer absorption in skin, cornea or retina, irradiance and radiant exposure were used to provide surface dose rate and dose. He then spoke on the impact of heat flow, eye movements and averaging areas for describing the dose. He thought these concepts were relevant to millimeter wave work. He also noted that power density and energy density in optics referred to power and energy per unit volume and not to surface power density and surface energy density as in the RF spectrum. He also explained that fluence and fluence rate - - although having the same units as radiant exposure and irradiance - - were in fact different concepts. Fluence included backscatter and had no cosine dependence, whereas, radiant exposure referred to the cosine-corrected radiant energy incident upon a surface, that which is normally measured.

8. Dr. Eleanor R. Adair (USAF/AL) spoke on the variables that influence thermal sensation derived from infrared exposure. She described research performed at the John B. Pierce Foundation Laboratory, New Haven, CT back in the 1960's under the leadership of Dr. Joseph Stevens. She explained that thermal sensation is essential for effective body temperature regulation and it registers "how much", regardless of the exact spatial and temporal distribution of skin stimulation. She showed that studies in this area of skin sensation revealed that so-called "cold spots" were far more frequent than the spatial density of "warm spots", e.g., on the forearm. The map of warm spots varied from day to day, which was rather curious. She presented a graph of the temporal summation of warmth for IR stimuli and showed reciprocity between duration and irradiance at the absolute threshold; the reciprocity ended at ~ 1 second at the warmth threshold for a 22 cm^2 stimulus area. She also showed a plot of the irradiance required to stimulate a given sensation as a function of irradiated area. Beyond 30-50 cm^2, spot size no longer seemed to have an effect. The forehead and cheek were the most sensitive, then abdomen and chest, then back, and finally the extremities were least sensitive of all. The pain threshold varies with stimulus duration and spot size, but the functions all converge to one level at about 45 °C for lengthy exposures. [David Sliney noted that in his own experience with a 647-nm krypton laser beam of 2 mm diameter, he could move the beam around and as the beam struck a "hot spot" he could sense a tingling heat sensation at incident powers of 10-50 mW. However, it took 400-500 mW to sense the beam as really uncomfortably hot within a few seconds.]

9. Dr. Dennis Blick, Systems Research Laboratories at USAF/AL, spoke about a recent study on the variation of skin warmth sensations for wavelengths from IR-C to 2.45 GHz.

His group exposed 15 male Caucasian subjects to 10-s exposures of RF energy over a defined area of 327 cm^2 of their back to determine detection thresholds. They employed a number of different RF sources and two T3 quartz heat lamps (operated at low voltage to achieve 2-4 μm infrared radiation on the back). The thresholds dropped by 15-fold when going from 2.45 to 94 GHz. The IR threshold was about the same as the 94 GHz threshold (about 5 mW/cm^2). He noted that the 1064 nm IR laser MPEs were far greater than the millimeter-wave value of 10 mW/cm^2. But, Dr. Sliney explained that the far-infrared laser limit for large areas was really 10 mW/cm^2 (MPE) for skin areas exceeding 1,000 cm^2, and up to 100 mW/cm^2 for areas less than 100 cm^2. The averaging area was an 11 mm diameter circular aperture (about 1 cm^2) for IR wavelengths greater than 0.1 mm.

10. Dr. Cliff Sherry, Systems Research Laboratories at USAF/AL, stated that skin temperature typically varied from about 32 to 37 °C, that the pain threshold was 45-47 °C and thermal damage occurred at 55-60 °C. He described the challenge of tracing neural fibers by various experimental techniques. Type A myelinated fibers could be more readily detected and traced than Type C non-myelinated fibers. His report was largely the result of a literature search of recent publications since about 1985.

11. Dr. Joseph Zuchlich, TASC, Inc. at Brooks AFB, gave a broad overview of retinal injury data from exposure to visible light and infrared lasers in the retinal hazard region of 400-1400 nm. He focused in on his studies in the 1300 nm spectral region, where effects could be seen in the cornea, lens and retina. He showed again the great impact of irradiated spot size. He also noted that the variation of threshold with wavelength had more fine structure than that with exposure limits. He suggested that some of the step functions of exposure limits as a function of wavelength could be eliminated.

12. David Sliney gave an overview of ocular exposure to optical radiation in the industrial environment, with emphasis on infrared exposure in the foundry, metal works, steel mills, welding, and glass industries. He stated that welding arcs produced little significant IR compared to large hot metal surfaces. He stated that workers exposed to irradiances of the order of 80-400 mW/cm^2 over a working lifetime developed cataracts at an earlier age than unexposed workers, but modern labor practice did not really permit such high exposures. Eva Lydahl (1984) of the Karolinska Institute, Stockholm had done the best recent epidemiological study of IR heat cataracts. Her collaborators measured IR irradiance in the workplace.

13. Bruce Stuck, Army Medical Research Detachment (AMRD), Brooks AFB, compared IEEE/ANSI C95.1 radio frequency and LIA/ANSI Z136 laser MPEs as a function of exposure duration, taking into account the area of irradiation and comparative penetration depth. He presented a number of experimental data for laser-induced skin burns and histological studies of skin damage that varied with spot size, time of assessment (1 hour or 24 hours) and wavelength. For pulsed CO_2 (10.6 μm) exposures, only the stratum corneum would be affected at threshold, and some surface white powder appeared at the irradiation spot. He also showed a number of plots of the absorption depth of water and the similar variation of pulsed thresholds. But he also showed the impact of different

penetration depths and spot sizes, when the time-temperature history over the pulse might look similar but the Arrhenius integral could differ. He then cited several mathematical models that had been developed over the past two decades. These would allow the estimation of a "SAR" in order to put the thermal thresholds for small volumes into a data base for those working in the millimeter wave spectrum.

14. Prof. Myron L. Wolbarsht, Duke University, spoke on infrared cataractogenesis. He began by describing the structure of the lens and the nature of lens fiber cells. Epidemiological studies were seen as fraught with problems of confounders; however, experimental data from the laboratory can be very useful, such as the well known studies of Donald Pitts and coworkers using a filtered xenon arc. Wolbarsht, et al., performed some in vitro studies with enucleated rabbit lenses kept in a 37 °C water bath; they showed that without IR-A illumination the lenses remained clear, but with IR-A illumination over 24 hours, an opacity was observed. He therefore was skeptical that IR cataract was purely the result of a temperature elevation. He then reviewed the classical Vogt-Goldmann debate on whether direct lenticular absorption or indirect heating by iris absorption was the primary damage mechanism. Using a laser, Wolbarsht was able to experimentally irradiate only the lens or iris. He showed that both of these two Swiss ophthalmologists were correct, but the irradiance necessary for the iris heating was much more than encountered in industry. In an in vivo experiment, his results of fractionating the exposure in different ways over a period of two days did not result in any different total dose. A threshold of approximately 100 J/cm^2 was found for the production of an acute cataract developing within an hour or less. He reported that even Pitts' data showed approximate dose exposures of 1400, 3500, and 10,000 J/cm^2. The quantum energy near 1000 nm is of the order of 1 eV and there could be a photochemical mechanism operating.

15. Prof. Om P. Gandhi, University of Utah, spoke on millimeter wave dosimetry. He presented some data from his 1986 article with Riazi for penetration depth and reflectance for the skin at 30-300 GHz (reflectance from 0.49 to 0.18; skin depth from 0.78 to 0.23 nm). He suggested that while clothing absorbed IR, the millimeter waves may penetrate to the skin. He noted a report by Webb and Booth that suggested that E. coli were absorbing and affected differently by different frequencies in the millimeter wave band. Therefore, the University of Utah team used frequencies between 25 and 90 GHz to study yeasts, bacteria, viruses, etc., but was unable to find the resonances postulated by Froehlich. He did conclude that it was conceivable that there were dimensionally related longitudinal modes, which could be excited in biological media, that should be detectable by Raman spectra, but they did not conduct those studies. Ken Foster took issue with this conclusion because of the damping existing in biological media, a damping that was not present in a solid state crystal. He suggested that Grundler was finding effects because he was using a less stable microwave source.

16. Dr. Andrei Pakhomov, McKesson BioServices, Brooks AFB, spoke on the widespread use in Russia of millimeter wave therapy with power densities less than 10 mW/cm^2. Out of more than 500 medical scientific papers, he chose 90 papers with English abstracts or written in English. Millimeter wave therapy was used for

gastrointestinal, cardiovascular, respiratory and other diseases. The most commonly used generating devices were the YAV-1, operating at 7.1 mm and 5.6 mm, and the Electronica at 4.9 mm. The most common area of application was the sternum. Other application points were the same as acupuncture points. He described a number of studies where treatment was reported to have been effective and some other control studies. He explained that, like acupuncture, it was not well understood what the underlying mechanisms might be. He felt that the dosimetry was very poor, but large numbers of patients argued for the effectiveness of treatments. He suggested that these effects should be taken into account in setting human exposure limits. In the discussion, he explained that there was no evidence that specific placebo type studies had ever been performed.

17. Dr. Yevgenyi (Eugene) P. Khizhniak, a physicist at the Fox Center for Biomedical Physics, Temple University, described infrared thermography in studies of millimeter wave bioeffects. He showed thermographic patterns in tissue phantoms irradiated by horn applicators. He showed computer profiles from these data and also stated that thermal gradients were quite high. He said that the threshold for hydrodynamic convective changes in water was only 1 nW/cm^2. He noted physiological surface changes in irradiated mouse skin that could be produced by millimeter waves but not by infrared of the same irradiance and same gross temperature change. His hypothesis for the effect was that water in the epidermis and stratum corneum was selectively vaporized. If sweat pores were closed there was little thermal spatial gradient, but when opened (stimulated by millimeter-wave exposure) the strong spatial gradients were noted.

18. Dr. Kathy L. Ryan (working with Melvin Frei), Trinity University, San Antonio, spoke on circulatory failure resulting from sustained millimeter wave irradiation. Irradiating Sprague-Dawley rats at 75 mW/cm^2 at 35 GHz (SAR of 12 W/kg), they were able to produce shock with the colonic temperature not even 40 °C, but of course the subcutaneous temperature was much higher (about 48 °C). As in infrared radiant heat stress, blood pressure falls with the large movement of blood to the peripheral vasculature. But she reported that the fatal effect could result from irradiating only 10% of the total body surface. She looked for physiological (biochemical) mediators but as yet had not pinpointed the critical one.

19. Dr. Yun Wang, a mathematical modeler from USAF/AL, spoke on microwave-induced acoustic effects. Her model considered that the heat pulse was much longer than the RF exposure pulse, whereas earlier models did not.

20. Dr. John Osepchuk, Chair of the IEEE SCC28 Committee on RF Standards, gave an overview of the rationale for human exposure limits for electromagnetic energy. He compared RF limits with optical radiation limits and promulgating bodies such as ACGIH, NCRP, ANSI, etc. He noted that the C95 standard of 1965 was only a few pages and one number: 10 mW/cm^2 averaged over 6 minutes from 10 MHz to 100 GHz. But today, the C95.1 standard is over 70 pages long. He explained that as the result of an eleventh-hour concern in the committee in 1989, a caution was added to the standard regarding SAR averaging over the eyes. He noted that the time constant for thermal dissipation varied from 5 to 10 minutes for the eyes or testes, but nearly an hour for the

whole body. In safety standards, the averaging times varied considerably from seconds to 6 minutes or more. He noted that he had performed studies at 2.45 GHz of optimum auditory detection, which was around 8-13 kHz (pulse modulation frequency). He cited the problems of determining the criteria upon which the limits should be based, e.g., was the auditory effect a potentially adverse health effect? Dave Sliney pointed out for historical note that the original C95-1966 standard had a correction factor for very hot environments, but this was later dropped. Dr. Sliney also noted that if the optical radiation community were to accept the very large safety factors employed in the RF standards community, the optical limits would not permit a person to stand outside in sunlight.

21. Ron Petersen, (Bell Laboratories) Lucent Technologies, Murray Hill, NJ, showed that by applying microwave engineering principles, one could probably explain the strong "frequency dependant or athermal effects" reported in the millimeter wave bioeffects literature by resonant effects in microwave components. For example, the insertion losses associated with waveguides and variable attenuators get more dramatic as one moves to higher frequencies. He concluded that one can not rely on variable attenuators for extrapolating the RF power delivered to a biological sample. This can be misleading in waveguide delivery systems. Harmonics can also be significant at higher frequencies because of the penetration depth.

22. Dr. Kenneth Foster, University of Pennsylvania, Philadelphia, PA, spoke on thermal models in general. He presented the standard bioheat equation and showed how different exposure parameters affected RF heating of tissue. He then described how he and his colleague Pere Riu had solved the bioheat equation for the data presented earlier in this Workshop by Dennis Blick. The thermal analysis suggested that the measured thresholds corresponded to a localized temperature increase of about 0.07 °C at or near the surface of the skin. The modeling effort also showed that, even at 94 GHz, the depth at which the temperature receptors are located in the skin is not a relevant parameter as long as it is within 0.3 mm of the surface. For the 10-sec exposures in Blick's experiment, the results of the thermal model were insensitive to blood flow, but were sensitive to thermal conduction, which increased strongly with frequency.

23. Dr. Russ McCally, Johns Hopkins Applied Physics Laboratory, reported on studies of CO_2 (10.6 μm) corneal thermal injury. He stated that the absorption length in the epithelium was 10.5 μm and 98% would be absorbed in 40 μm. His formulation of single-pulse ED50 data was: $0.592 + 6.064\ \tau^{0.66}$ J/cm^2 over the range of 10 ms to 10 s. This led to a critical temperature of single-pulse ED50 data of 42 ±2 °C, although the data fit an empirical formulation of $72\tau^{-0.02}$ °C. Spot size dependence varied with exposure duration and he showed a spot averaging of about 1 mm for 0.1 s, 2 mm for 1 s, and slightly larger than 3 mm for longer times. He then showed a phase transition model to predict single-pulse damage and temperature modulation with a repetitively pulsed laser. The total energy required increased as $N^{0.75}$ (the same as the $N^{-0.25}$ safety rule). Dr. Sliney noted that in deriving the limiting apertures for safety limits, the committee routinely enlarged the averaging area for the skin and cornea and then reduced the size of the safety factor for very small hot spots.

24. Dr. Mary Potasek, USAF/AL, gave an overview of her efforts to mathematically model the propagation of optical waves through the ocular media. She described non-linear self-focusing, pulse-steepening, Raman scattering, etc. and how they dominated in different time domains. She showed a plot of the second-order dispersion of water, which changes sign near 1000 nm; this anomalous dispersion can occur at the 1064-nm wavelength. She presented calculations and data to show soliton transmission in an optical fiber, but this phenomenon had not been modeled for the optical media.

25. Dr. Arthur W. (Bill) Guy, Wireless technology research, Seattle, WA, spoke on the near-field hot-spot dosimetry problems encountered in estimating the localized SAR in the head of a cellular phone user. He described some experiments in a TEM exposure cell in order to show the uniformity of SAR in vials and petrie dishes. The lack of uniformity in the vial was shown as a potential problem in some in-vitro studies. He noted that the current ANSI/IEEE C95.1 standard allows hot spots of 20 W/kg, except for the eyes and testes; hence, for cellular phones, the problem relates back to the eye's exclusion from the averaging criterion.

26. Dr. David Freund, Johns Hopkins Applied Physics Laboratory, Laurel, MD, spoke on mathematical modeling of gaussian and rectangular-beam induced retinal thermal injury. Assuming the thermal properties of water for most of the retinal layers, he calculated the time-temperature histories for a spot 5 μm in front of the RPE inside the photoreceptor layer. All retinal irradiances were normalized to 1 W/cm^2. He assumed that the RPE had an attenuation factor of 1587 cm^{-1}. The rectangular image cases generally produced higher peak temperatures than the Gaussian beam profiles for a 1-s exposure when the two beams had equal power. But this ratio was reversed for short-pulse exposures. Temperature rise was faster in the rectangular beam than in a square beam, but a lower temperature was reached in the former. He found that the ratios did not vary with depth, with RPE thickness, or with absorption coefficient. Interestingly, the ratio was always greater than 1.0 for rectangular aspect ratios of 1 to 3, but was less for higher aspect ratios. This work was inspired by the frequent use of rectangular sources, such as laser diodes, in laser technology.

27. Ron Petersen, Lucent Technologies, gave a brief history of the ANSI C95.1 standards from 1966 to the present. In 1974 the standard separated out the E and H fields, and in 1982 the SAR was introduced. In 1991 the standard introduced two tiers, but had a number of minor problems/inconsistencies. The standards-setting process was complex, from generation and approval in Subcommittee 4 to the parent committee (SCC28), then to ballots within SCC28 until consensus was achieved and negative ballots resolved. One third of Subcommittee 4 participants were engineers and physical scientists and 43% were life scientists. A number of working groups were involved in evaluating the literature database, a process that required several years. Subcommittee 4 concluded that the most sensitive measures of potentially harmful biological effects were based on the disruption by RF exposure of food-motivated behavior in laboratory animals. The MPEs from 100 MHz to 6 GHz are based upon a fixed SAR for controlled (and 1/5th that SAR for uncontrolled) populations. Only within this frequency range was there considered to

be differences in individual sensitivity due to body size or health status. In their current process of revising the 1991 standard, more than 1100 citations are presently included in the database organized by Dr. Martin Meltz. Dr. Meltz has designed standardized evaluation forms to be used by different specialized experts to evaluate each publication for scientific merit. Mr. Petersen outlined several current questions that he felt needed to be resolved in the next iteration of the standard. He suggested the need to develop frequency dependent mass and time averaging criteria as well as to re-evaluate the need for two tiers.

28. Prof. Myron L. Wolbarsch, Duke University, spoke on the derivation of laser exposure limits. There was general agreement worldwide among ACGIH, ANSI, ICNIRP, IEC, etc. for the same MPEs. He stated that the ACGIH TLVs were the most modern since they could be revised quickly, e.g., on a one-year basis. By contrast, the CDRH/FDA performance standards take a long time to revise. In his opinion, the ACGIH, ANSI, and ICNIRP limits were based strictly on medical scientific criteria, but the IEC standard has a history of influence by political and commercial agendas, where there appeared to be clear efforts to develop emission limits that misrepresented the biological data. He felt that the laser field had the advantage of having a very large biological database. He complimented the military services for funding the extensive amount of biological research upon which these limits are based. He felt that there was a large safety factor in most of the limits, which led many experts to actually work above the limits. This was particularly true for skin exposures. He thought the time may have arrived to abandon the curve-fitting efforts and replace them by simple tabular values at each wavelength.

29. Prof. Om Gandhi discussed some weaknesses that he perceived in the ANSI/IEEE C95.1-1992 standard. He argued that the standard did not protect against startle reactions caused by transient spark discharges and data from the laboratory on transient discharge currents as a function of frequency. Also, he felt that there was a potential problem with shocks and burns that should be dealt with. He expressed his belief that there was a need to re-examine the low-power device exclusion and he argued for more research funding.

30. At the close of the meeting, a panel discussion was held, which led to the conclusion that spatial and temporal averaging rules need to be more sophisticated for the 0.1 to 6 mm spectral region. It was suggested that mathematical thermal models be employed to give a better idea of how the scaling factors (apertures and times) should be set. Dr. Sliney suggested that an experiment be performed with an IR laser and a millimeter wave source, under the same protocol, to determine if the threshold for a minimal reactive dose in the skin was the same for the same penetration depth. A more detailed account of the panel discussion can be found at the end of this report.

Infrared Lasers & Millimeter Waves
Workshop
The Links Between Microwaves
& Laser Optics

21 Jan 1997 - 22 Jan 1997

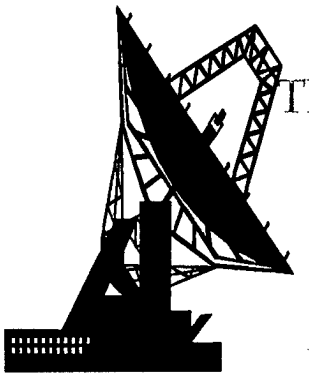

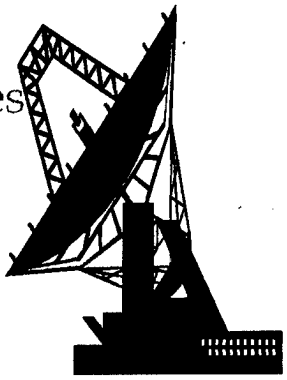

SECTION I:

MECHANISMS

The Physical Bases for the Interaction of Millimeter Waves with Biological Systems

Robert K. Adair
Department of Physics, Yale University
New Haven, CT 06520-8121

April 27, 1997

Abstract

We examine physical properties and constraints concerning the biological effects of the interactions of millimeter wave electromagnetic radiation with special emphasis on the effects of radiation at power densities of $I = 10$ mw/cm^2 (or $E_{rms} = 200$ V/m), a level characteristic of occupational exposure limits. Effects of the interactions of radiation with wavelengths λ, such that $10\,\mathrm{mm} > \lambda > 1\,\mathrm{mm}$, can be divided usefully into two different categories: (a) There are effects that can be described in terms of relaxation times or the time-variation of the response of the system to a disturbing field. And, (b), there are effects that can be described in terms of resonances where energy is stored and released in a time that is long compared to the period of the electromagnetic wave. We examine the characteristics of such processes and show that resonance responses to oscillating fields that generate mm wavelengths cannot be expected to be biologically important.

The Electromagnetic Field

Charges exert forces on one another as described by Coulomb's law. From a reductionist view, Coulomb's law (together with special relativity) contains the whole content of classical electromagnetism. And, in Dirac's rhetoric, Coulomb's law, together with the proper (quantum) mechanics, accounts for most of physics and the whole of chemistry – and by extension, almost the whole of biology. But a description of these forces through the concept of the electromagnetic field is, at the least, a more convenient way of describing the forces, and perhaps the more fundamental way.

Hence, by definition, electromagnetic fields act on matter only through forces applied to electric charges; the force on a charge at rest is proportional to the product of the magnitude of the charge and the magnitude of the electric field, $\mathbf{E}q$. As a consequence of relativity and the limit of signal transmission to the speed of light, that description is modified if the charge moves and that modification, of relativistic origin, is labeled the magnetic field[1], $\mathbf{B}$. The force applied by the magnetic field is proportional to the magnitude of the charge and, in natural units, the ratio of the velocity, $\mathbf{v}$, of the charge to the velocity of light. In SI units (which obscure the relativistic origin of magnetism and, hence, are not used in fundamental physics) the Lorenz force law expressing the vector force, $\mathbf{F}$, on a charge can be written as,

$$\mathbf{F} = q(\mathbf{E} + (\mathbf{v} \times \mathbf{B})) \tag{1}$$

Though it is often useful to describe the effects of fields in terms of scalar and vector potentials, a description of effects in terms of forces on charges must be complete.

In this essay, we consider the physical bases of the effects on biology of electromagnetic radiation, with wavelengths in the mm region, *i.e.* 1 cm $\geq \lambda \geq$ 1 mm, or frequencies such that 30 GHz $\leq \nu \leq$ 300 GHz. We are especially interested in fields that are large enough to effect biology (in general, through mild heating), but are not so large as to be biologically destructive. In this spirit we will often consider a canonical intensity level of 100 W/m^2 (or 10 mW/cm^2) which corresponds to a root-mean-square electric field strength of about 200 V/m and an rms magnetic field of 0.67 μT.

Thermal and Athermal Effects

Thermal effects are defined as those that follow from a modification of the mean energy – that is the temperature – of biologically sensitive elements that are in local thermal equilibrium with nearby matter. Such elements will have an energy distribution such that the probability of a state having an energy E is proportional to $e^{-E/kT}$. Biological processes are almost exquisitely sensitive to that distribution which is shown in Fig. 1 for a temperature T and temperatures $T' = 1.05\,T$ and $T" = 0.95\,T$. If $T \approx 313$ °K, as the characteristic "life-temperature", by and large, T' will not sustain life and T'' will not sustain human life.

[1]In common with much modern usage, I call $\mathbf{B}$, the magnetic field, correcting an ancient error; $\mathbf{H}$ is a subsidiary quantity parallel in meaning to the electrical displacement, $\mathbf{D}$.

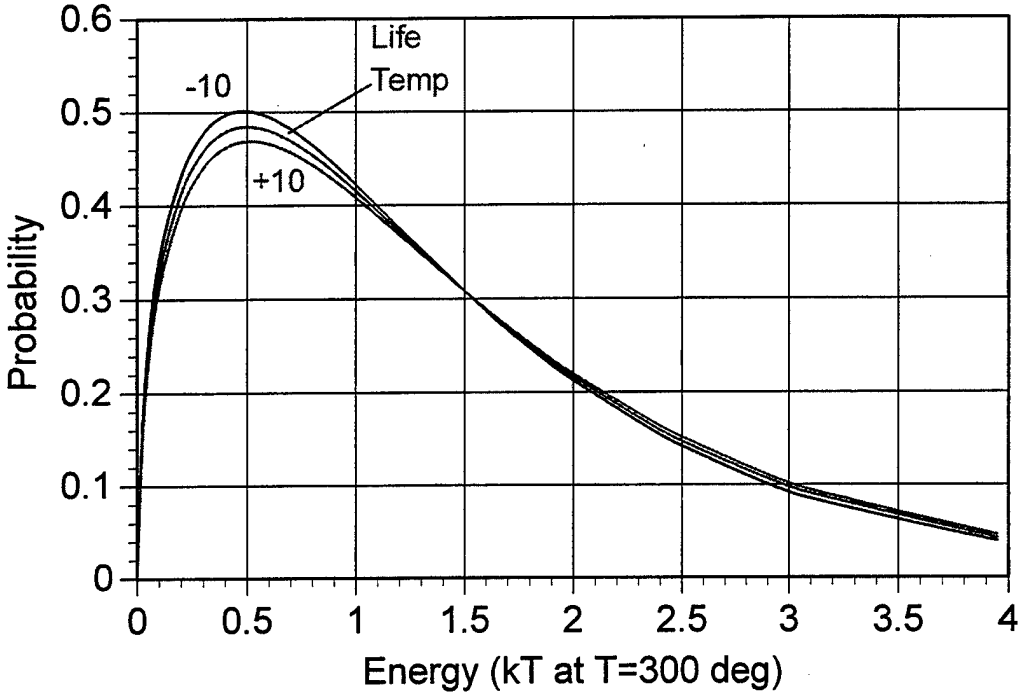

Figure 1: The Boltzmann distribution for a temperature T and for temperatures, $T' = 1.05\,T$ and $T'' = 0.95\,T$.

Conversely, *athermal* effects are those effects that follow from energy excursions in a system – or degree of mechanical freedom in a system – that are not described by the Boltzmann distribution; literally as well as etymologically, *athermal* is defined negatively as simply that which is not *thermal.*

Often, complex systems such as proteins will change conformation and thus biological properties when a specific excitation energy, w, exceeds a threshold value w'. For a system in thermal equilibrium at a temperature T, that probability, $P(T, w')$ can be expressed in terms of the Arrhenious integral,

$$P(T, w') \propto \int_{w'}^{\infty} e^{-w/kT}\, dw \tag{2}$$

Because of the close coupling of elements of a biological system, elements with non-thermal energy distributions are brought back into thermal equilibrium after excitation in a characteristic *relaxation time,* τ_r. While a detailed calculation is required for many purposes, for biological systems excited by electric fields, these time constants will not usually be very different

than that calculated using the relation,

$$\tau_r \approx \left(\frac{1}{10}\right) \frac{C\rho}{\kappa}\, a^2 \approx \cdot 10^6\, a^2 \text{ seconds} \tag{3}$$

where a is a characteristic length measured in meters. Here, $C\rho = 4.18 \cdot 10^6$ J/m^3 is a heat capacity, $\kappa = 0.6$ W$\cdot$m^{-1}deg$^{-1}s^{-1}$, is a thermal conductivity and the numerical values are those of water – which makes up much tissue[2]. While the relaxation times defined in Eq. 4 are derived implicitly for macroscopic systems, the results are found to be a good approximation for systems as small as individual molecules.

While excitations of systems through effects of electric fields generally have small relaxation times as expressed by Eq. 3, systems that are excited to a higher energy through a change in magnetic moment generated by a special orientation of an electron spin or nuclear spin will usually have much longer relaxation times even as the electrical forces between elements in the solid state of matter are much stronger than the magnetic forces. Roughly speaking, states with higher – non-equilibrium – energies as a consequence of a special electron spin orientations have relaxation times of the order of microseconds, while states excited by a variance in nuclear spin orientation will have relaxation times measure in seconds[3].

The time constant enters macroscopically for the interaction of millimeter wave radiation with flesh inasmuch as the energy is absorbed very near the surface. The absorption length – defined as the $1/e$ attenuation length for the electric field vector and, hence, $1/e^2$ for the intensity – for millimeter wave radiation in tissue is approximately one-tenth of a wave length.

[2]For mechanical systems undergoing linear or rotational motion, the relaxation times can be estimated as

$$\tau_r \approx \frac{\rho}{\eta}\, a^2 \approx \cdot 10^6\, a^2 \text{ seconds} \tag{4}$$

where ρ is the density of the element – taken here as that of water – and η is the viscosity of the medium, taken, again, as the viscosity of water. The near equivalence of the time constants calculated in different ways, follows from the close relation between heat capacity and mechanical energy and between thermal conductivity and viscosity.

[3]At room temperature, the spins of the two protons in the H_2 molecule are parallel (thus the nuclear spin is $1\hbar$) in 3/4 of the molecules and anti-parallel (spin 0) in 1/4.of the molecules which is just the statistical weight. But the spin 0, singlet, singlet state has a somewhat lower energy than the spin 1 triplet state, though the energy difference is much less than kT for T=300 °K. But at the temperature of liquid hydrogen, T=27 °K, kT is less than the energy difference and the triplet molecules then make transitions to the singlet state over a period of about one day. Thus, this ortho-para transition in liquid hydrogen at 27 °K, the boiling point at atmospheric pressure, has a relaxation time of about one day and the heat released by the transition contributes significantly to the evaporation of stored liquid hydrogen.

Hence, for modulations with periods $P < \tau$, thermal effects in the zone of large energy deposition will depend only on the average intensity and will not be affected by the modulation. And that time limit, τ, varies roughly as the inverse square of the basic frequency.

Quantum Effects

At these wavelengths quantum effects can be considered to be small – though, perhaps, not so small as to be wholly insignificant. For radiation with a wavelength of 1 mm, and a frequency, $\nu = 300$ MHz, the photon energy, $h\nu \approx 10^{-3}$ eV which can be compared to, $kT \approx 0.025$ eV, to van der Waals bonds with an energies of the order of 0.07 eV, to hydrogen bonds and ionic bonds with strengths in the range of 0.25 eV, and to covalent bonds, e.g. the C-H bond, with a binding energy of about 4 eV. (For chemists, 0.001 eV is about 0.023 kilocalories per mole.) Hence, we do not expect to see mm wave electromagnetic fields generate significant quantum effects, but that need not be the case for frequencies in the infrared with wavelengths twenty-five times smaller.

Of course, quantum effects are, manifestly, athermal. They can be distinguished from thermal effects in principle by their dependence upon the total energy absorbed, independent of the rate. The number of quantum transitions, N, generated by an incident intensity, I, over a time Δt on a system held at a temperature, T, can be expected to proportional to,

$$N = k(T) \int_0^{\Delta t} I(t)\, dt \tag{5}$$

where $k(T)$ is a constant depending on the density of targets and the probability, or cross section, of a quantum interaction with the target. Usually, k will be independent of T.

Conversely, thermal transitions will depend sensitively on temperature often following the Arrhenious prescription,

$$N = k(w', T) \int_0^{\Delta t} P(T, w'), dt \tag{6}$$

where $P(T, w)$ is the Arrhenious integral (Eq. 2).

In either case, the simple exposition may be complicated by relaxation effects for times $\Delta t < \tau$, where τ is a relaxation time.

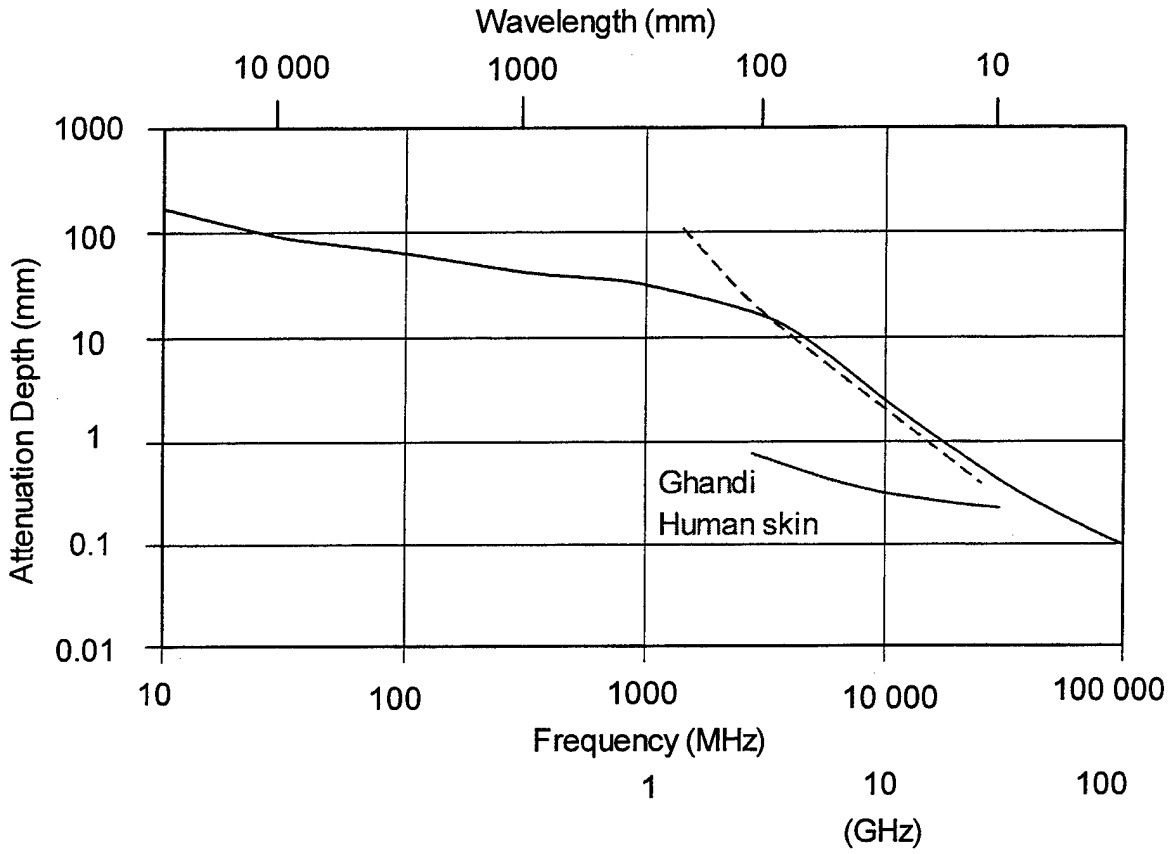

From Polk, Handbook of Biological Effects of Electromagnetic fields, Polk & Postow, CRC, 1996

Figure 2: The energy attenuation length as a function of frequency for microwaves. Here we define the attenuation length L_a as the depth in which $1-1/e^2 = 86.5\%$ of the energy is absorbed. Other definitions are sometimes used.

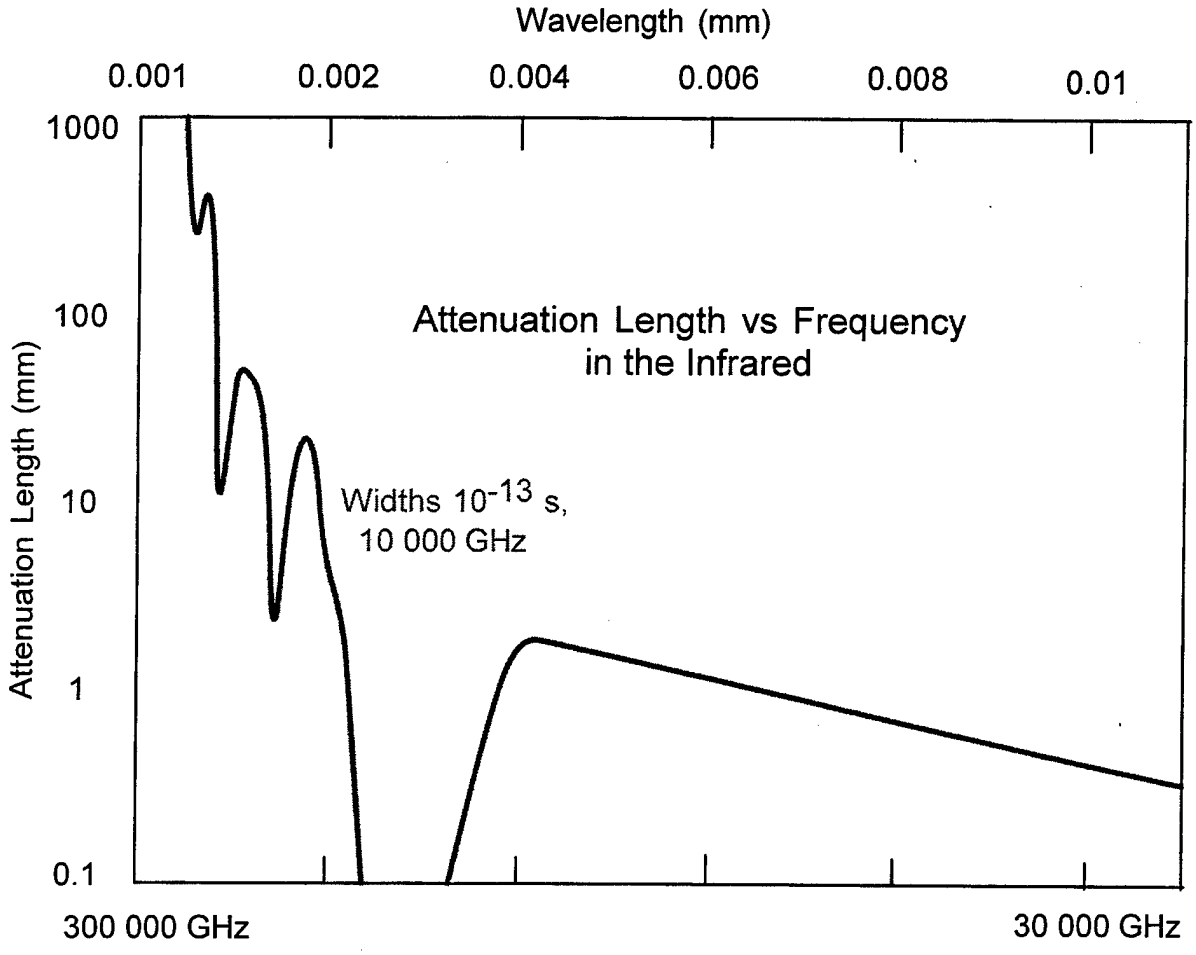

Figure 3: The energy attenuation length as a function of frequency for the near infrared.

Interaction Mechanisms

With quantum effects of little importance, the interactions of the electromagnetic field with biological matter will largely follow from classical forces on charges held in the matter and the following discussions are largely classical.

For illustration, we describe the effect of electric fields on charged systems by a displacement of positive and negative charged systems impeded by the resistance of a spring and a dashpot as shown in Fig. 4. The spring exerts a restraining force, $F_s = -Kx$, where K is a spring constant and x the displacement; the dashpot resistance takes the form, $F_d = -\kappa\, dx/dt$. If the characteristic mass of the system is taken as m, the characteristic time for the spring motion is, $\tau_s = \sqrt{m/K} = 1/\omega$ where ω is the angular frequency of oscillation, while, $\tau_d = m/\kappa$, is the natural dissipation time.

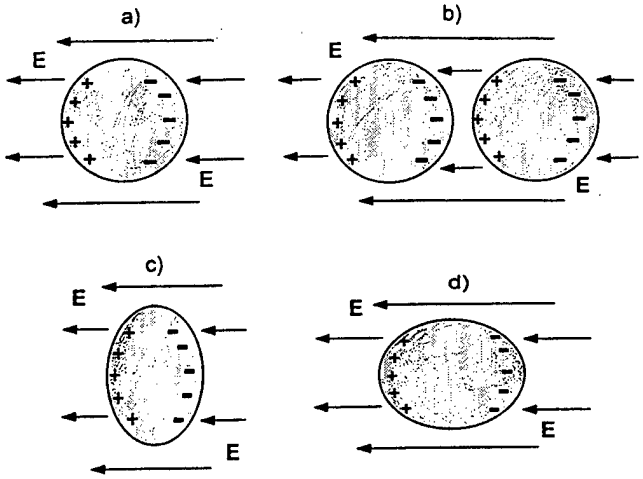

Figure 4: Schematic diagram of the displacement of charge in elements that can be induced by an electric field.

If $\tau_d \ll \tau_s$, the motion of the charged elements will largely be determined by the dissipation of the dashpot. If the field is turned on at time $t = 0$, the displacement x will vary as,

$$x \approx x_0 \left[1 - e^{t/\tau_d}\right] \quad \text{where} \quad x_0 = \frac{Eq}{K} \tag{7}$$

However, if $\tau_s \ll \tau_d$, the motion will be mainly determined by the spring

constant and can be approximated by the relation,

$$x = x_0 \left[1 + \cos(t/t_d)e^{-\omega t}\right] \quad \text{where} \quad \omega = \frac{1}{t_s} \tag{8}$$

Relaxation Mechanisms

Even as the Fourier transformation of a step function, contains all frequencies, the response of a system to a voltage step involves the response of the system to all frequencies. That alone only is only tautology. But the analysis is important inasmuch as the response to a step function over some specific period of time can often be understood physically in a simple manner, hence the modeling of that physically simple response constitutes a modeling of the frequency response of the system over a frequency interval complementary to that time.

The description is especially useful if the electric field imposed on the sample is described, conventionally, as generating an induced dipole moment, or aligning a permanent dipole moment, to create a dipole moment per unit volume or polarization P, which then "relaxes" in a characteristic time τ according to the relation,

$$P = P_\infty + P' \left(1 - e^{-t/\tau}\right) \tag{9}$$

where P_∞ is the very fast change due to the polarization of the electron fields about the atoms. We can describe this in terms of the permittivity,

$$\epsilon = \epsilon_0 + P/E = \epsilon_\infty + \epsilon_s(1 - e^{-t'\tau}) \tag{10}$$

Applying a Laplace transformation,

$$\epsilon = \epsilon_\infty + \frac{\epsilon_s - \epsilon_\infty}{1 + i\omega\tau} \tag{11}$$

where ϵ_∞ is the permittivity at infinite frequency and ϵ_s is the permittivity for a constant field.

Noting that the index of refraction, $n = \sqrt{\epsilon/\epsilon_0}$ we can write the index of refraction of water as a function of frequency as,

$$n_w = \left[N_\infty^2 + \left(\frac{K-1}{1 - i\omega\tau}\right)\right]^{1/2} \quad \text{where} \quad K = \left[\frac{\epsilon}{\epsilon_0}\right]_{\nu=0} \approx 81 \tag{12}$$

and the attenuation length is, $L_{att} = \lambda/(2\pi \text{ Im n})$.

The time constant, τ is a parameter which is adjusted to fit the data – or better, the experimental results, usually expressed in terms of the relaxation length, interpreted through these formulae, results in a measure of the relaxation time. This can be defined usefully in terms of the mean collision time defined simply as $\tau_c \approx \ell/v_{kT} = 6.5 \cdot 10^{-13}$ from the mean-free-path, $\ell \approx (1/N)^{1/3} = 3 \cdot 10^{10}$ m and the thermal velocity of water molecules $v_{kT} = \sqrt{3kt/2m} = 460$ m/s. The fit to the data shown in Fig. 2 follows from a choice of $\tau = 15 \cdot \tau_c = 10^{-12}$ seconds. Also, $\tau = 1/\omega_0$ where $\nu_0 = \omega_0/2\pi = 16$ GHz.

Of course, the description of as complex a system as a water molecule and its interactions with its surroundings in liquid water by one parameter – a relaxation time – must, necessarily be a rough approximation at best, but that this one parameter describes the interaction of water with microwave fields over a considerable frequency interval, is surely interesting.

Forces on Elements Carrying Charge

Translational Motion

We first examine the effects of fields on the translational motion of charged elements in an inertial system where the mean or initial velocity of the charged element is zero and the neglect of effects of the magnetic part of the field introduces no significant error. In particular, we describe the effects of an electric field, taken in a y-direction, of angular frequency ω and amplitude E_0, on an element of mass m holding a (monopole) charge q. The total force on the element can be described as a binding force, $F_b = -Ky$, a driving force $F_d = E_0 q \cos\omega t$, where y is the displacement of the element from an equilibrium position in the direction of the field $\mathbf{E}_0$, and a stochastic noise force, $\xi(t)$. For small elements on the cell level, this noise, derived from interactions with their neighborhood environment, can be approximated by a viscose resistance, $F_r = -\gamma\, dy/dt$. Further dissipation effects will only reduce the energy transfer. For free elements, $K = 0$, though even nominally free elements may have interactions with neighboring molecules that result in some degree of restraint. Equating the sum of these forces,

$$\gamma\dot{y} + Ky = E_0 q \cos\omega t \tag{13}$$

Writing the variation of y with time as $y = y_0 \cos(\omega t + \phi)$,

$$y_0^2 = \frac{(E_0 q)^2}{K^2 + \gamma^2\omega^2} \tag{14}$$

and the mean kinetic energy, W_T of the element is,

$$W_T = \frac{1}{4}\, m\omega^2 y_0^2 = \frac{1}{4}\, \frac{(E_0 q)^2 m\omega^2}{K^2 + \gamma^2\omega^2} \approx \frac{1}{4}\, \frac{E_0 q^2 m}{(K/\omega)^2 + \gamma^2/4} \qquad (15)$$

We estimate the viscous resistance from Stoke's Law, $\gamma = 6\pi\eta r$, where r is a characteristic length of the element; for a sphere, r is the radius. Outside of cells, η will be the viscosity of the tissue electrolyte; inside of cells, η will be the viscosity of the cytoplasm; for elements held in the membranes, η will be the viscosity of the dilipids making up the membrane. For general estimates, we take that viscosity η, conservatively, as that of water, where $\eta = 7{\cdot}10^{-4}\ Ns/m^2$ at life temperatures. The viscosity of cytoplasm has been reported to be much greater than water[2], and the viscosity of the dilipid cell membrane material is not likely to be much less than that of water.

For unrestrained (i.e. with $K \approx 0$) cell-size systems in an aqueous solution, any charge carried by the system tends to be partially neutralized by counter ions and $q/\gamma = \mu$ where $\mu \approx 3 \cdot 10^{-8}\ m^2/Vs$ is a mobility that is nearly independent of the size of the charged sphere, its composition, or the magnitude of the charge, if the charge is large enough. With this substitution in Eq. 15, the maximum kinetic energy for a cell of mass m is $W_t = (E_0\mu)^2 m/4\gamma^2$, and for the canonical cell with a radius, $r = 10\ \mu m$, and $E_0 = 282$ V, $W_t = 0.018\ kT$.

Since $W_T \propto m/\gamma^2 \propto r$, for very large spheres, or large cells, W_T will be somewhat larger but will not likely exceed kT. Conversely, smaller elements will have energies much less than kT.

The maximum value of W_t is largely set by the dissipative factor $\gamma = 6\pi\eta r$, where,

$$\tau_\gamma = m/\gamma \approx 2.2 \cdot 10^{-5}\ \text{seconds} \qquad (16)$$

is the characteristic viscous time constant for the canonical cell with a radius, $r = 10\,\mu m$. Time constants derived in different ways should have similar values. The thermal relaxation time can be expressed as,

$$\tau_t = \frac{C}{4\kappa} a^2 = 1.6 \cdot 10^6 \cdot a^2 \text{ seconds} \qquad (17)$$

where C is the volume thermal capacity and κ the conductivity of water while a is a characteristic length. Taking $a = r = 10\ \mu m$ for the cell, $\tau_t \approx 1.6 \cdot 10^{-4}\ s$. The rough equivalence of τ_γ and τ_t suggests that the estimate is reliable to within an order of magnitude.

Rotational Motion

Effects may follow from torques, $N = (p \times E)$ produced by the interaction of electric fields $\mathbf{E}$ with elements carrying permanent electric dipole moments $\mathbf{p}$. The total torque on an element with a electric dipole moment d will be made up of a binding torque, $T_b = -N_b\theta$, and a driving torque, $T_d = N\cos\omega t$, where θ is the angle of rotation and a stochastic noise torque. Again, we approximate the effects of such noise by a resistive torque, $T_r = -\beta\dot{\theta}$, and write an equation with a form like Eq. 5:

For free elements, $N_b = 0$, though even nominally free elements may have interactions with neighboring molecules that result in some degree of restraint. Equating the sum of these forces to the acceleration,

$$\beta\dot{\theta} + N_b\theta = E_0 d\cos\omega t \tag{18}$$

Writing the variation of θ with time as $\theta = \theta_0\cos(\omega t + \phi)$,

$$\theta_0^2 = \frac{(E_0 d)^2}{N_b^2 + \beta^2\omega^2} \text{ where } \omega_0^2 = \frac{N_b}{I} \tag{19}$$

and the mean kinetic energy, W_T of the element is,

$$W_T = \frac{1}{4}I\omega^2\theta_0^2 = \frac{1}{4}\frac{(E_0 d)^2 I\omega^2}{N_b^2 + \beta^2\omega^2} \approx \frac{1}{4}\frac{(E_0 d)^2 I}{(N_b/\omega)^2 + \beta^2} \tag{20}$$

where I is the moment of inertia of the element. Again it is important to couch conclusions in terms of some particular, but simple, structure in order to provide insights into general behaviors. Hence, we state energies and torques in units of kT, and we use the easily visualized sphere of radius r and the density of water as a surrogate model for both the moment of inertia and the viscous resistance. Using Stokes Law as a guide, we estimate the resistive torque, $\beta\dot{\theta}$, on a rotating system by taking $\beta = 6\eta V$ where V is the volume of the system. This relation is exact for a sphere with a diameter larger than 1 μm and an adequate approximation for this purpose for elements with other shapes and smaller sizes.

It is helpful to make some numerical estimates of possible interactions of electric fields, such that $E_0 = 282$ V/m, with elements holding permanent electric dipole moments. In particular, we consider the hemoglobin macromolecule, which has an effective dipole moment of $d = 1.6 \cdot 10^{-27}\ Cm$ and a moment of inertia $I \approx 8 \cdot 10^{-40}\ kg\,m^2$. The length of the molecule is $L \approx 7 \cdot 10^{-9}\,m$ and we take the volume of the molecule as $v \approx 10^{-25}\ m^3$, $\beta \approx 6 \cdot 10^{-28}\ Nms$. With these values, $W_T \leq 2.8 \cdot 10^{-14}\ kT$. The energy transfer is small and can be significant only if the relaxation time were

about 7 orders of magnitude longer. Dimensionally, $W_T \propto Lq^2$, and smaller systems have even stronger energy constraints.

Properties of water.

If the simple model describing the transmission of energy from microwaves to large molecules is valid, the model should describe the known absorption of microwave energy to water. The diagram of Fig. 4 suggests the character of the water molecule. For a free molecule in a gaseous state at low pressure, the angle between the linkage of the two hydrogen atoms to the oxygen atom is about 104.5° and the bond lengths are about 0.096 nm. The valence bonds are such that the hydrogen atom valence electron occupies the vacancy in the $n = 2$ shell of the oxygen atom about 32% of the time so as to generate a permanent dipole moment of about $6 \cdot 10^{-30}$ mC.

The heat of condensation of water of about 540 calories per gram, at a pressure of one atmosphere, represents about 500 calories of binding energy plus about 50 calories of PV work. The 500 calories of binding energy represents about 15 kT per molecule. The water molecules are attached to each other loosely through weak hydrogen bonds connecting the oxygen atom of one molecule with the hydrogen atom of another molecule. The binding energy of such a bond is, hence, only about 4 kT. The mean bond length is about 0.285 nm. The bonds are continually being made and broken as the molecules change partners. These bindings are sufficiently loose so that the characteristic vibrational frequency, $\nu_r < 4kT/h \approx 2.6 \cdot 10^{13}$ Hz at $T = 310$ °K, and is not then completely "frozen out quantum mechanically at the temperatures characteristic of liquid water.

While the interaction with the other molecules modifies the shape and the mean charge held by the atoms somewhat from the values cited, those values will be adequate for the estimates we make for the interaction of water with high frequency electromagnetic fields. Then, we can assign moments of inertia, $I_x \approx 2.1 \cdot 10^{-47}\ kg\,m^2$, and $I_y \approx 1.2 \cdot 10^{-47}\ kg\,m^2$ and $I_z \approx 3.3 \cdot 10^{-47}\ kg\,m^2$ where the coordinate axis are those shown in Fig. 4.

Power absorbed by water.

The power, P, absorbed by a dipole is,

$$P = (\beta\dot{\theta}) \cdot \dot{\theta} = \beta\dot{\theta}^2 = \beta\omega^2\theta^2 \tag{21}$$

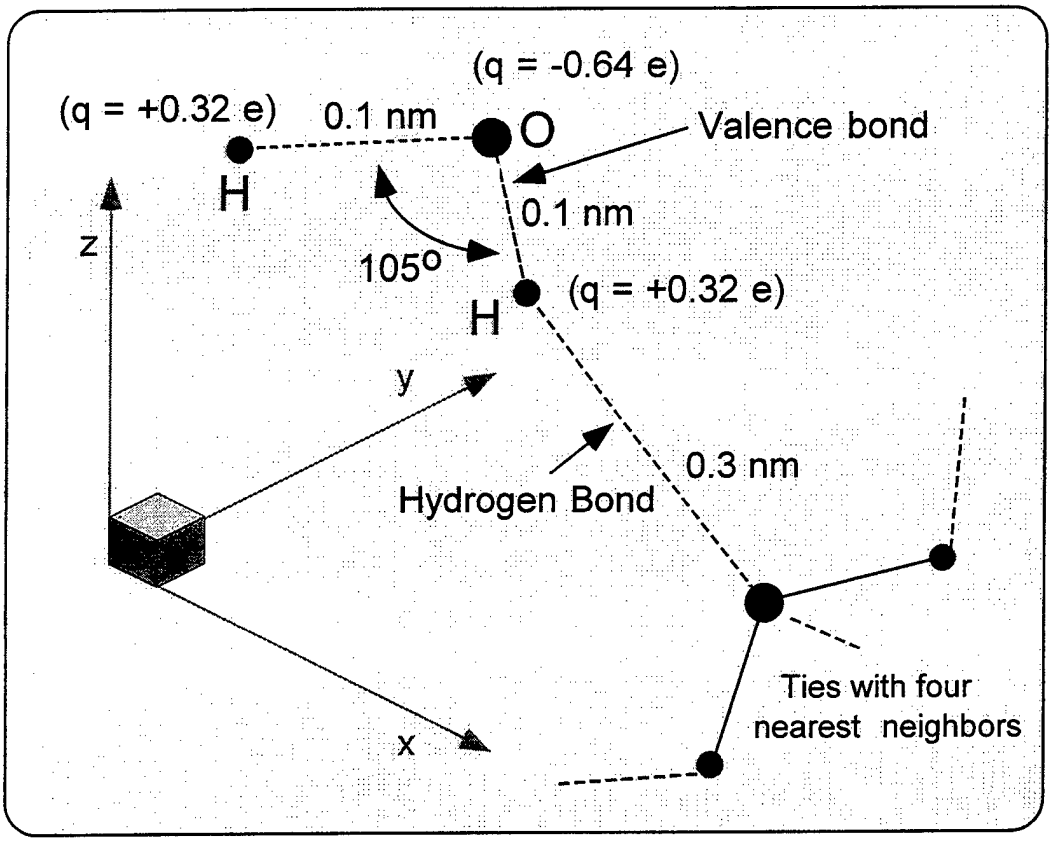

Figure 5: A diagram suggesting the character of an H_2O molecule in liquid water.

Then the time-average power is,

$$\overline{P} = \frac{\beta\omega^2\theta_0^2}{2} \text{ where } \theta_0^2 = \frac{(Ed)^2}{N_b^2 + \beta^2\omega^2} \tag{22}$$

Taking the average over orientations of the dipole moment,

$$\overline{(E \cdot d)^2} = \frac{E^2 d^2}{2} \tag{23}$$

and

$$\overline{P_1} = \frac{\beta\omega^2\theta_0^2}{4} \approx \frac{(Ed)^2}{4\beta} \tag{24}$$

is the power absorbed by one molecule of water. The absorption of a unit volume of water will be $P_N = N \cdot P_1$. where N is the number of molecules of water in a unit volume and $N = A\rho/M = 3.33 \cdot 10^{28}$, where $A = 6 \cdot 10^{26}$ is Avogadro's number, $\rho = 1000$ kg/m^3 is the density of water, and $M = 18$ is the molecular weight of water. The minimum attenuation length λ_0 is then the ratio of the maximum absorbed power in the unit volume to the incident power density,

$$\lambda_0 = \frac{I}{P_N} = \frac{\epsilon_0 E^2 c}{NE^2d^2/(4 \cdot 6\eta V)} = \frac{\epsilon_0 c \cdot 24\eta}{N^2 d^2} = 1.1 \cdot 10^{-3} \text{ m} \tag{25}$$

which is about that measured for a wavelength of 3 mm and in reasonable accord with experiment.

Resonance Absorption

Previous discussions emphasized the non-resonant interactions of electromagnetic waves with systems damped by viscous impedance. Generally the damping was sufficient to preclude strong resonant effects. We consider here the absorption of electromagnetic energy in a formally different manner through a partial wave analysis which emphasizes resonant absorption[5]. Here the damping of the system is described in terms of the removal of energy from the system through thermal conductivity.

The absorption of energy by a resonant system from a plane wave can be expressed in terms of an absorption cross section, σ_a where,

$$\sigma_a = 3\frac{\lambda^2}{4\pi} \frac{\Gamma_s \Gamma_a}{(\omega - \omega_r)^2 + \Gamma^2/4} \tag{26}$$

where Γ_a is the absorption width, Γ_s is the scattering, or emission, width, $\Gamma = \Gamma_a + \Gamma_s$ is the total width; the lifetime $\tau = 1/\Gamma$. The resonant frequency

is ν_r, and λ is the wavelength of the radiation. The cross section $\sigma - a$ is defined as the power absorption per unit incident power flux and, thus, has the dimensions of area.

The energy absorption can be calculated using the relation,

$$\int_{\omega_i}^{\omega_j} \sigma_a \, d\nu \leq 6\lambda^2 \Gamma_s \tag{27}$$

where the equality holds if the frequency spread of the incident radiation, $\Delta\omega = \omega_j - \omega_i$ encompasses the whole resonance, $\Delta\omega > \Gamma$, and $\Gamma_a \gg \Gamma_s$. Here, $\Gamma_s = 1/\tau_s$ where $\tau_s = W/P \approx Q/\omega$ where W is the energy stored in the resonance and P is the power radiated through the oscillating electric dipole moment. If there were no dissipative effects and $\Gamma_a = 0$, τ_s would be the lifetime of the state.

From Eqs. 26 and 27, for $\Gamma_a \gg \Gamma_s$ and for an incident power density P, the power absorbed by the system will be,

$$P_a \leq 6P\lambda^2 \frac{\Gamma_s}{\alpha} \tag{28}$$

Where α can be taken as the larger of the quantities, $2\pi\Gamma_a$ or $\Delta\nu$.

Since, biological systems tend to be much smaller than the microwave wavelengths, which by definition are greater than 1 mm, the coupling of the dipole moment to the radiative field tends to be small and the maximum absorption by the system will be small. we estimate Γ_s, and then the absorption cross section integral, using classical electrodynamics. The power P_s radiated by an oscillating electric dipole is,

$$P_s = \frac{1}{4\pi\epsilon_0} \frac{d_0^2 \omega^4}{3c^3} \text{ where } d_0 = qA_0 \tag{29}$$

where $\omega = 2\pi c/\lambda$ is the radial frequency of the oscillator, p_0 is the maximum dipole moment which I describe in terms of an amplitude A_0 and charge, q. With this model, we consider the energy of the oscillator as,

$$W = \frac{1}{2} m\omega^2 A_0^2 \text{ and } \Gamma_s = \frac{1}{\tau_s} = \frac{P_s}{W} = \frac{q^2\omega^2}{6\pi\epsilon_0 mc^3} \tag{30}$$

where m is a characteristic mass. Combining Eqs. 29, 30, and 31,

$$P_a \leq \frac{I}{\alpha} \cdot \frac{4\pi q^2}{\epsilon_0 mc} \text{ and } W_a = P_a \cdot \tau \approx \frac{P_a}{\Gamma_a} \leq \frac{I}{\alpha\Gamma_a} \cdot \frac{4\pi q^2}{\epsilon_0 mc} \tag{31}$$

where W_a is the maximum absorbed energy and $\Gamma_a = 1/\tau_a \approx 1/\tau$.

We use these relations to consider energy transfers to several specific systems to provide general quantitative insights. (We note the claims of Grundler and Kaiser[6] that there are biological resonances in the frequency range of $45 \cdot 10^9$ Hz, hence, $\lambda = 6.67\ mm$.) We use the canonical power level of $I = 10\ mW/cm^2 = 100\ W/m^2$ for numerical calculations and assume conservatively that the incident electromagnetic waves are nearly monochromatic and that $\Delta\nu$ is very small.

1 Assume the effective oscillator is a $^{40}Ca^{++}$ ion. From Eq. 3, taking $r = 1$ Å, we have assumed the relaxation time as $\tau_r = 1/\Gamma_a \approx 10^{-14}$ s. With this value, the maximum energy transfer to the system will be $5.6 \cdot 10^{-15}\ kT$. Only if the relaxation time is 8 orders of magnitude longer, will the absorbed energy be greater than kT and larger than thermal fluctuations.

2. I consider a macromolecule where the effective charge is $q = 10e = 1.6 \cdot 10^{-18}\ C$ and the mass is $5 \cdot 10^{-22}\ kg$. Taking the characteristic length as $a = 5 \cdot 10^{-9}\ m$ (the radius of a volume of water of mass m.), the thermal relaxation time from Eq. 3 is $\tau_r = 4 \cdot 10^{-11}$ seconds and the maximum energy transfer as $1.5 \cdot 10^{-10}\ kT$. Again the energy transfer is small and can be significant only of the relaxation time were about 5 orders of magnitude longer.

Coherence

If two systems close together resonate at the same frequency, their interaction with electromagnetic fields is proportional to the sum of their vector dipole moment *amplitudes,* and the systems are *coherent.* Otherwise, the interaction is proportional to the sum of the squares of the amplitudes; the *intensities* add and the systems are *incoherent.* Hence, the interaction of N equal coherent systems results in energy absorption and reemission equal to N^2 times that for one system while the absorption and reemission will be equal to N times one system if the systems are incoherent. Therefore, the energy absorbed from an electromagnetic wave by a N resonant systems can be as much as N times greater if the systems act coherently than if they are incoherent. Frölich[7] has emphasized the possibility that coherent effects may be important at frequencies near the infrared level if the incident energy is sufficiently large.

If systems are to be coherent, two conditions must apply. (i) The systems must be sufficiently close together so that the phase of the incident electromagnetic wave, of wavelength λ, acting on them will be nearly the same. This will be the case if the distance a between the systems will be such that $a < \lambda/2\pi$. (ii) The frequency, ν, of the systems must be nearly the same.

For two systems i and j, $|\nu_i - \nu_j| < 1/(2\pi\tau_r)$, where τ_r is the relaxation time. If that frequency equivalence is to hold over large regions of generally heterogeneous structure, the elements must be mechanically coupled. That coupling will extend over a characteristic length that we can estimate as $\lambda \approx v_s/\nu$, where ν is the frequency of the electromagnetic wave and v_s is the velocity of sound in the system. However, if the system is sufficiently homogenous, the dipole-dipole coupling of the individual oscillators maybe sufficient and the limitation on the characteristic length may be relaxed.

We consider typical systems that may act coherently.

3. A sector of the cell membrane, with an electric dipole density taken from the known potential difference of about 70 mV across the membrane, could interact with a high frequency electromagnetic wave. We estimate the relevant area of membrane $A_m \approx \lambda^2$, where $\lambda = v_s/\nu$ over which coherence can be expected to obtain where $v_s \approx 1500$ m/s, the velocity of sound in water, is an estimate of the velocity of sound in the membrane and $A_m \approx 1.1 \cdot 10^{-15}\ m^2$.

Taking the thickness of the membrane as $d = 10^{-8}\ m$ and the potential across the membrane as $dV = 100\ mV$, we estimate the dipole charge density as $\sigma = K\, dV\, \epsilon_0/d$ where we take the dielectric constant of the membrane, $K \approx 5$. For the mass, we assume a membrane density twice that of water. Estimating the thermal relaxation time $\tau_r = 1/\Gamma_a \approx 10^{-9}$ seconds from Eq. 3, the maximum energy transfer is $3.7 \cdot 10^{-12}\ kT$. Following Frölich, the vibrational frequency must be near $\nu = v_s/d \approx 1.5 \cdot 10^{11}\ s^{-1}$ –or a wavelength, $\lambda \approx 2\ mm$.

4. Perhaps the region of coherence is larger. I modify the above model by assuming a coherent region $A = r^2$ where $r = 10\ \mu m$ is the radius of a typical cell. For a sheet, the thermal relaxation time will depend only upon the thickness of the membrane and that time will be the same as for the smaller membrane sector considered in (3) and the maximum energy transfer is, $W_a = 1.2 \cdot 10^{-7}\ kT$, again too small to be significant.

Forces on Induced Charges

Induced moments with interaction energies $W > kT$ can be created by electric fields of the order of 100 V/m (power densities, I=25 W/m2) but only at frequencies such that the angular frequency, $\omega < 1/RC$, the inverse of the natural time constant of the element. But $RC \approx \epsilon_0\rho$, where $\rho \approx 1\ \Omega$·m, which places a high frequency cutoff of $\nu = 10$ GHz on such induction hence we should not expect induced effects at mm wavelengths, where 30 GHz $<\nu <$ 300 GHz to be important.

Appendix A, Resonances in Rotational Motion

We have proceeded under the approximation that inertial effects can be neglected. It is interesting to review that in detail and in that review, consider in more detail the limitations on resonances that might follow from vibrations of whole molecules or large portions of a molecule.

While the argument presented here, and applied specifically to possible rotational states of water as it is loosely bound in the liquid to four other water molecules through hydrogen bonds, is directed to rotational motion generated by the coupling of the electric field to permanent dipole moments, the same arguments, with the same conclusions, can be presented concerning linear displacements of charged elements.

Rotational effects may follow from torques, $N = (p \times E)$ produced by the interaction of electric fields $\mathbf{E}$ with elements carrying permanent electric dipole moments $\mathbf{p}$. The total torque on an element with a electric dipole moment d will be made up of a binding torque, $T_b = -N_b\theta$, and a driving torque, $T_d = N\cos\omega t$, where θ is the angle of rotation and a stochastic noise torque. For free elements, $N_b = 0$, though even nominally free elements may have interactions with neighboring molecules that result in some degree of restraint. And we approximate the effects of such noise by a resistive torque, $T_r = -\beta\dot{\theta}$. Equating the sum of these forces to the acceleration,

$$I\ddot{\theta} = -\beta\dot{\theta} - N_b\theta + E_0 d\cos\omega t \tag{32}$$

Writing the variation of θ with time as $\theta = \theta_0\cos(\omega t + \phi)$,

$$\theta_0^2 = \frac{(E_0 d)^2}{I^2(\omega_0^2 - \omega^2)^2 + \beta^2\omega^2} \text{ where } \omega_0^2 = \frac{N_b}{I} \tag{33}$$

and the mean kinetic energy, W_T of the element is,

$$W_T = \frac{1}{4}I\omega^2\theta_0^2 = \frac{1}{4}\,\frac{(E_0 d)^2 I\omega^2}{I^2(\omega_0^2 - \omega^2)^2 + \beta^2\omega^2} \approx \frac{1}{4}\,\frac{(E_0 d)^2 I}{2I^2(\omega_0 - \omega)^2 + \beta^2} \tag{34}$$

where I is the moment of inertia of the element.

Again it is important to couch conclusions in terms of some particular, but simple, structure in order to provide insights into general behaviors. Hence, we state energies and torques in units of kT, and we use the easily visualized sphere of radius r and the density of water as a surrogate model for both the moment of inertia and the viscous resistance. Using Stokes Law as a guide, we estimate the resistive torque, $\beta\dot{\theta}$, on a rotating system by taking $\beta = 6\eta V$ where V is the volume of the system. This relation

is exact for a sphere with a diameter larger than 1 μm and an adequate approximation for this purpose for elements with other shapes and smaller sizes.

With so definite a model, we review the effects of inertial forces by considering the time constant, $\tau_I = I/\beta$. For a sphere, $I = (2/5)V\rho r^2$ and $\beta = 6\eta V$, where $\rho = 1000$ kg/m^3 is the density of the material, which we take as that of water, $\eta = 7 \cdot 10^{-4}$ Nms^{-1}, is the viscosity of water, and V is the volume of the system. Then $\tau \approx 10^{-14}$ for $r = 3 \cdot 10^{-10}$m, which is a reasonable radius for water. In this approximation, one can then neglect inertial terms up to frequencies of $\omega_{lim} = 1/\tau \approx 10^{14}$ or $\nu_{lim} = 2 \cdot 10^4$ GHz which is well into the infrared.

In general, we should not then expect microwave resonances related to the vibrations of molecules or elements of molecules that contain whole atoms.

Looking at the same problem from a different viewpoint, we make some numerical estimates of possible interactions of electric fields, such that $E_0 =$ 282 V/m, with elements holding permanent electric dipole moments. In particular, we consider the hemoglobin macromolecule, which has an effective dipole moment of $d = 1.6 \cdot 10^{-27}\ Cm$ and a moment of inertia $I \approx 8 \cdot 10^{-40}\ kg\,m^2$. The length of the molecule is $L \approx 7 \cdot 10^{-9}\,m$ and we take the volume of the molecule as $v \approx 10^{-25}\ m^3$, $\beta \approx 6 \cdot 10^{-28}\ Nms$. With these values, $W_T \leq 2.8 \cdot 10^{-14}\ kT$. The energy transfer is small and can be significant only if the relaxation time were about 7 orders of magnitude longer. Dimensionally, $W_T \propto Lq^2$, and smaller systems have even stronger energy constraints.

References

1. R. K. Adair, Constraints on biological effects of weak extremely-low-frequency electromagnetic fields, *Phys. Rev.* **A43** 1039 (1991).

2. A. D. Keith and W. Snipes, Viscosity of cellular protoplasm, *Science* **183**: 666 (1974).

3. R. P. Blakemore, Magnetotactic bacteria, *Science* **190**:

4. M. M. Walker and M. E. Bitterman, Conditioned responding to magnetic fields by honeybees, *J. Comp. Physiol.* **A157**:

5. These standard techniques are described in, J. B. Marion and M. A. Heald. "Classical Electromagnetic Radiation," Harcourt Brace Jovanovich, New york (1980).

6. W. Grundler and F. Kaiser, *Nanobiology* **1**: 7. H. Frölich, Long range coherence and energy storage in biological systems, *International Journal of*

Quantum Chemistry **2**: 641 (1968).
8. H. P. Schwan, EM-field induced force effects, in "Interactions between Electromagnetic fields and cells," Editors, A. Chiabrera, C. Nicolini, and H. P. Schwan, Plenum Publishing Corp. (1985).
9. K. Montaigne and W. F. Pickard, Offset of the vacuolar potential of charocean cells in response to electromagnetic radiation over the range of 250 Hz to 250 kHz, *Bioelectromagnetics* **5**: 31 (1981).
10. J. C. Weaver and R. D. Astumian, The response of living cells to very weak electric fields: limit *Science,* **247**:
11. R. D. Astumian and B. Robertson, Quadratic response of a chemical reaction to external oscillations, *J. Chem. Phys.* **96**:
12. K. Foster and H. Schwan, Dielectric properties of tissues, "CMC Handbook of Biological
Effects of Electromagnetic Systems," Editors, C. Polk and E. Postow, CMC Press, Boca Raton, Florida (1985).
13. H. P. Schwan, Interactions of ELF fields with excitable tissues, and Biophysical principles of the interaction of ELF fields with living matter, II coupling considerations and forces, "Biological Effects and Dosimetry of Static and, EMF Electromagnetic Fields," Editors, M. Grandolfo, S. M. Michaelson and A. Rindl, Plenum Publishing Corp. (1985).
14. H. P. Schwan, Dielectric spectroscopy and electrorotation of biological cells, *Ferroelectrics,* **86**: 205(1988).
15. J. C. Lin, Computer methods for field intensity predictions, "CMC Handbook of Biological Effects of Electromagnetic Fields," Editors, C. Polk and E. Postow, CMC Press, Boca Raton (1986).
16. F. S. Barnes, Extremely low-frequency (ELF) and very low-frequency electric fields; rectification, frequency sensitivity, noise, and related phenomena, "CMC Handbook Biological Effects of Electromagnetic Fields," Editors, C. Polk and E. Postow, CMC Press, Boca Raton (1986).

Presentation to the Infrared Lasers and Millimeter Waves Workshop; 21 Jan. 1997

Laser Bioeffects and Damage Mechanisms

Paul K. Kennedy, Benjamin A. Rockwell, and Mark E. Rogers

Optical Radiation Division, U.S. Air Force Armstrong Laboratory
Brooks Air Force Base, TX 78235

Abstract

Both continuous wave (cw) and pulsed (microsecond to femtosecond) lasers, emitting in the ultraviolet (uv), visible, and infrared (IR) regions of the spectrum, have the potential to inflict severe biological damage on unprotected humans and animals. Mechanisms for laser-tissue damage fall into three catagories: photochemical damage from short wavelength radiation, photothermal damage from bulk tissue heating, and photomechanical damage (ripping and tearing) due to bubble formation or shock wave emission from vaporized or superheated tissue. As most laser energy is absorbed near the surface of the body, the damage is done primarily to the eyes and skin. Skin damage can occur from uv, visible, or IR exposure to cw lasers with high average power or pulsed lasers with high peak power and irradiance. Both surface burns and skin ablation (removal of surface tissue) can be produced, depending on the type and duration of the exposure. Biological effects on the eye may be either transient or permanent. Transient impairment of eyesight (glare, flashblindness) only occurs with visible light and is produced by saturation of the photoreceptors on the retina. Permanent ocular effects include corneal burns (from uv and IR exposure) and retinal burns and hemorrhages (from visible and near-IR radiation). The retina is the organ most at risk because ocular focusing increases the irradiance (power/area) by a factor of 100,000 as light propagates from the cornea to the retina. Ultrashort pulses (sub-microsecond) in the visible and near-IR are the greatest retinal hazard, since very low pulse energies (millijoules) can cause retinal hemorrhages and temporary or permanent loss of vision.

Presentation to the Infrared Lasers and Millimeter Waves Workshop, 21 Jan 97

LASER BIOEFFECTS AND DAMAGE MECHANISMS

by

P. Kennedy, B. Rockwell, and M. Rogers

USAF Armstrong Laboratory

Overview

- Characteristics of Lasers
- Biological effects of lasers
  - Summary: Types of Bioeffects
  - Mechanisms for Permanent Damage
- Biological effects on Skin
- Biological effects on the Eye
- Laser Eye Safety

Characteristics of Lasers

- Highly Directional Beam (low beam divergence)
- High Irradiance (high power in a narrow beam)
  - deliver significant energy at long range to small area
- Highly Monochromatic
  - Damage depends on absorption coefficient
- Pulsed or Continuous Wave (CW) Output
  - very high peak powers (pulsed)
  - very high average powers (CW)

Biological Effects of Lasers: Summary

- Light is usually absorbed near the surface
  - Usually not deep-penetrating damage
  - Fairly inefficient at transferring energy
- Different effects possible:
  - Eye effects (glare, flashblindness, lesion, hemorrhage)
  - Skin effects (surface burns, deep tissue ablation)
  - Pressure effects (ear damage, internal organ damage)
- The eye is the most light-sensitive part of the body
  - Eye focusing increases intensity of visible and near infrared light by ≅ 100,000 from cornea to retina
  - Very low energy pulsed lasers can cause immediate, catastrophic damage to the retina and to sight

Biological Effects of Lasers: Mechanisms for Permanent Damage

- Three types of permanent damage from optical radiation
  - photothermal: damage from heating of tissue
    - » Lasers can burn skin, cornea, and retina
    - » Damage due to denatured proteins
    - » Typical of long-pulse to CW lasers
    - » Damage thresholds ~ 1 J/cm^2 at absorbing tissue
  - photomechanical: structural damage from stress
    - » Rapid tissue heating (or vaporization) causes shock waves or cavitation
    - » Ripping and tearing of tissue
    - » Typical of short-pulse lasers (sub-microsecond)
  - photochemical: biochemical damage from uv radiation

BIOLOGICAL EFFECTS OF LASERS

Anatomy of Skin

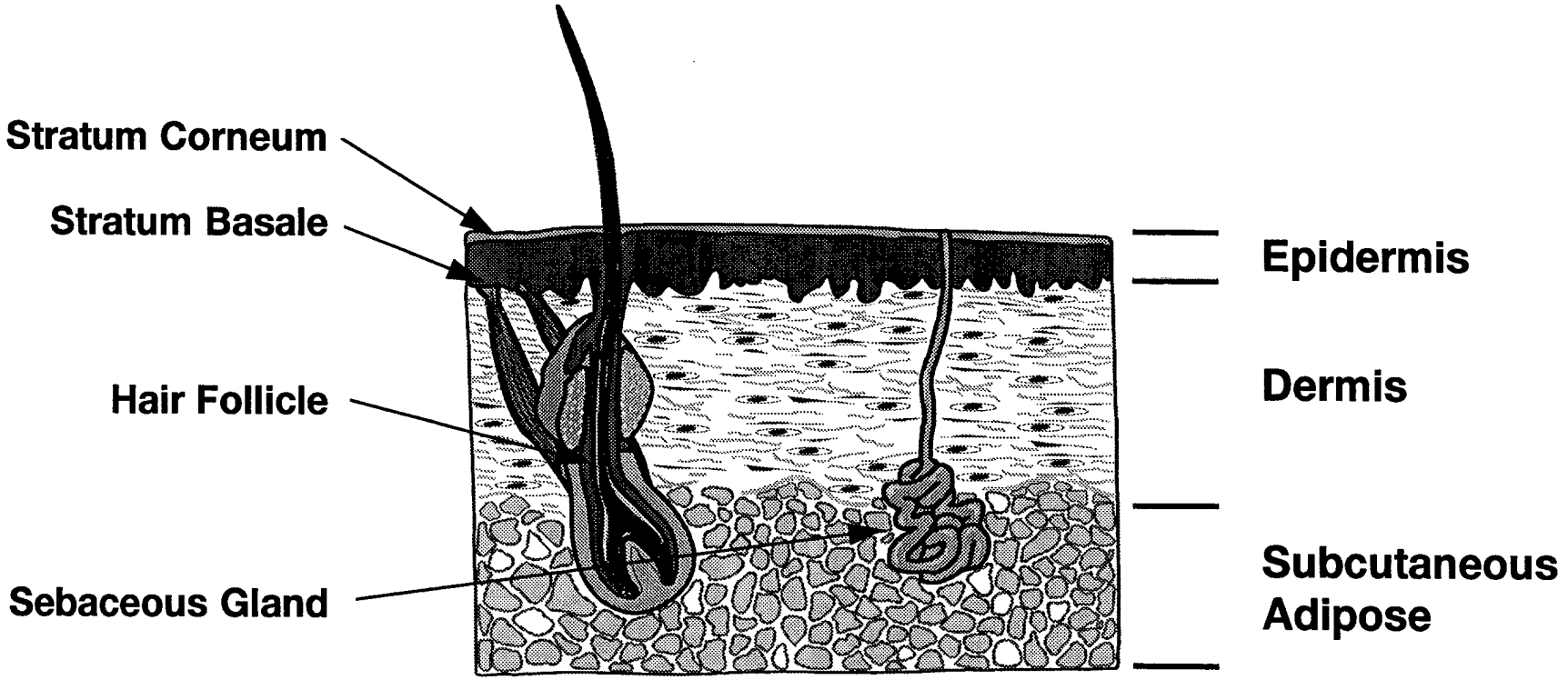

Nerves and blood vessels lie below the epidermis.

Biological Effects On Skin

- Skin damage can occur from uv, visible, or infrared radiation during pulsed or cw exposure
- Skin burns
  - Can be photothermal or photochemical (sunburn)
  - Dominant mechanism for cw or long-pulse exposure
- Skin ablation (removal of surface tissue)
  - Photomechanical damage through tissue vaporization or photodisruption (laser-induced breakdown)
  - Dominant mechanism for short-pulse exposure (less than a microsecond)
  - Couples mechanical impulse into body

BIOLOGICAL EFFECTS OF LASERS

Anatomy of the Eye

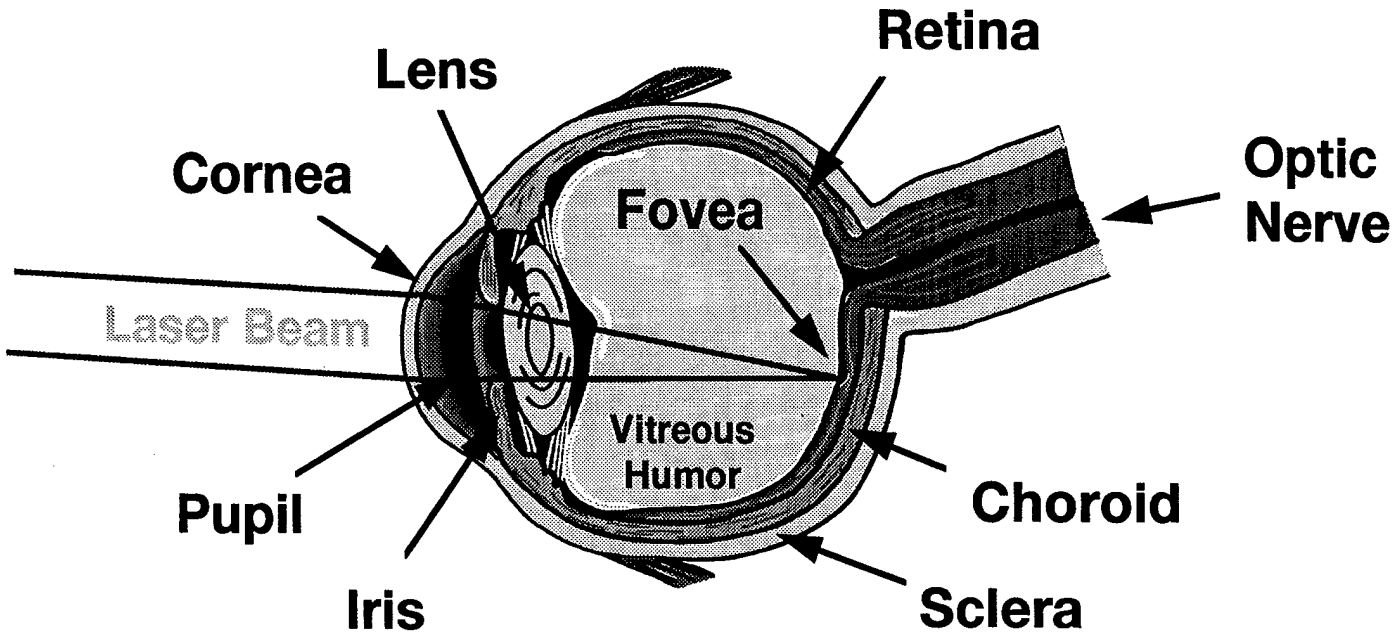

- Light passes through transparent cornea (λ = 0.4 to 1.2 microns)
- Focusing by cornea & lens concentrates beam by about 100,000X
- Central (20/20) vision occurs at fovea
- Pupil adjusts from 7 mm dia (night) to 2 mm dia (bright day)

Biological Effects on the Eye

TRANSIENT OCULAR EFFECTS

GLARE

FLASHBLINDNESS

PERMANENT OCULAR EFFECTS

RETINAL/CORNEAL BURNS

RETINAL HEMORRHAGES

Transient Ocular Effects on Eyesight

- Only produced by visible light (due to saturation of photoreceptors)
- Glare = obscuring vision while the laser is on
- Flashblindness =diminishing blind spot after laser is off
- Both effects give time-dependent blind spot
- Scenario-dependent:
  - how bright the laser is
  - target/background contrast
  - ambient light level (day, night)
  - task acuity (reading text versus seeing a car)

Permanent Ocular Effects

- UV and IR lasers can burn the cornea
  - Damage thresholds about 1 J/cm^2 at eye surface
  - High energy pulses can rupture globe of eye
- Visible and Near-IR lasers can damage the retina
  - Retinal lesions (burns) or retinal hemorrhages may produce temporary or permanent loss of vision
  - For short pulse durations (nanoseconds) only need
    - » microjoules at cornea to obtain retinal lesions
    - » millijoules at cornea to obtain retinal hemorrhage
  - Degree of vision loss depends on type of damage and on where damage site lies on the retina

Ultrashort Pulse Ocular Effects

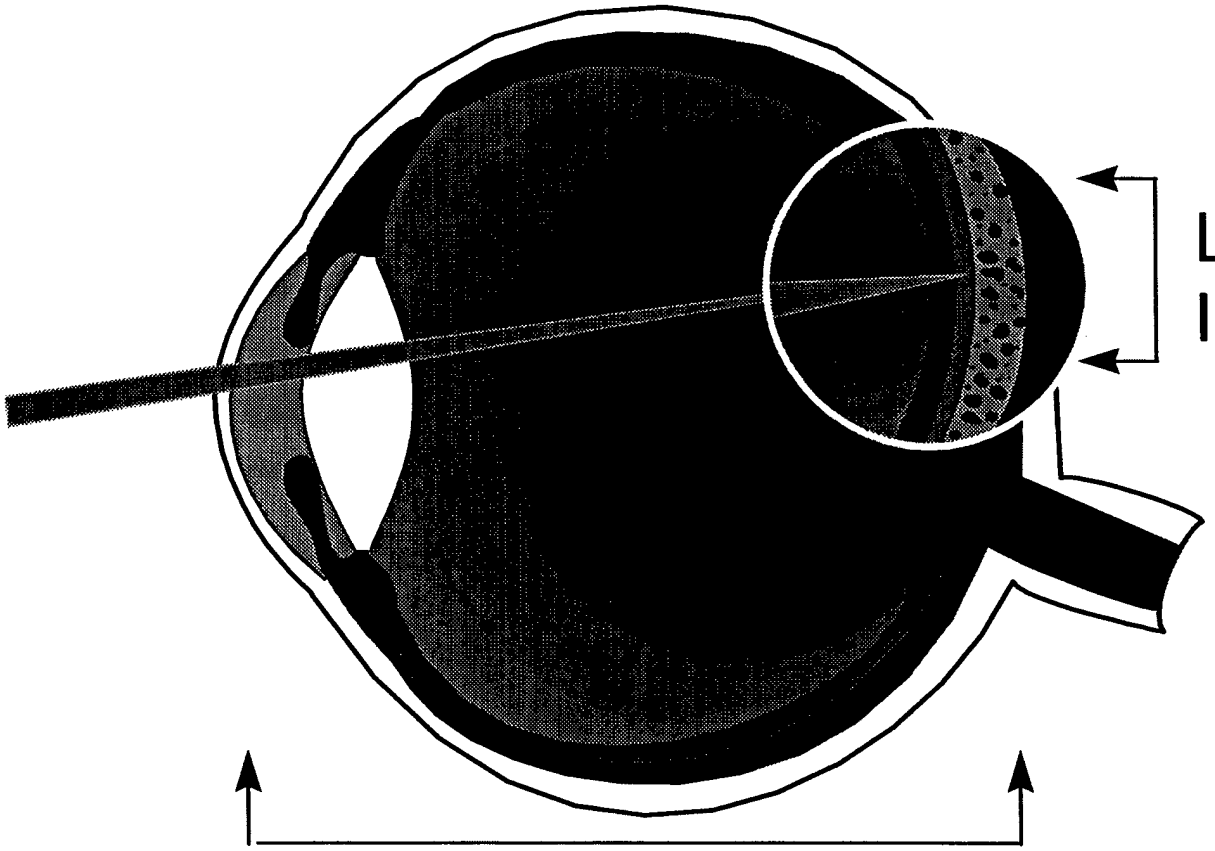

Laser -Tissue Interaction

thermal damage (ns - ks)
photochemical (> ks and UV)
melanin mediated
- photo-mechanical
- bubble
- laser induced breakdown

Propagation

self-focusing
nonlinear absorption
laser Induced breakdown

second harmonic generation
supercontinuum generation
stimulated Brillouin scattering

AL/OEO, BROOKS AFB, TX

Laser Eye Safety

- Minimal Visible Lesion (MVL)
  - Smallest visible lesion (d = 20 - 50 microns)
  - Threshold exposure level is the ED50 (estimated dose for 50% probability of producing an MVL)
- Maximum Permissible Exposure (MPE)
  - Equivalent to roughly 0.1 ED50
  - Exposure at or below MPE is considered safe
- Nominal Ocular Hazard Distance (NOHD)
  - Range where laser energy density decreases to MPE
  - Temporary effects can occur at ranges much greater than NOHD
  - Permanent damage usually occurs at much shorter ranges

Effective Ocular Damage Range

All laser beams diverge with distance, decreasing the energy density in the beam

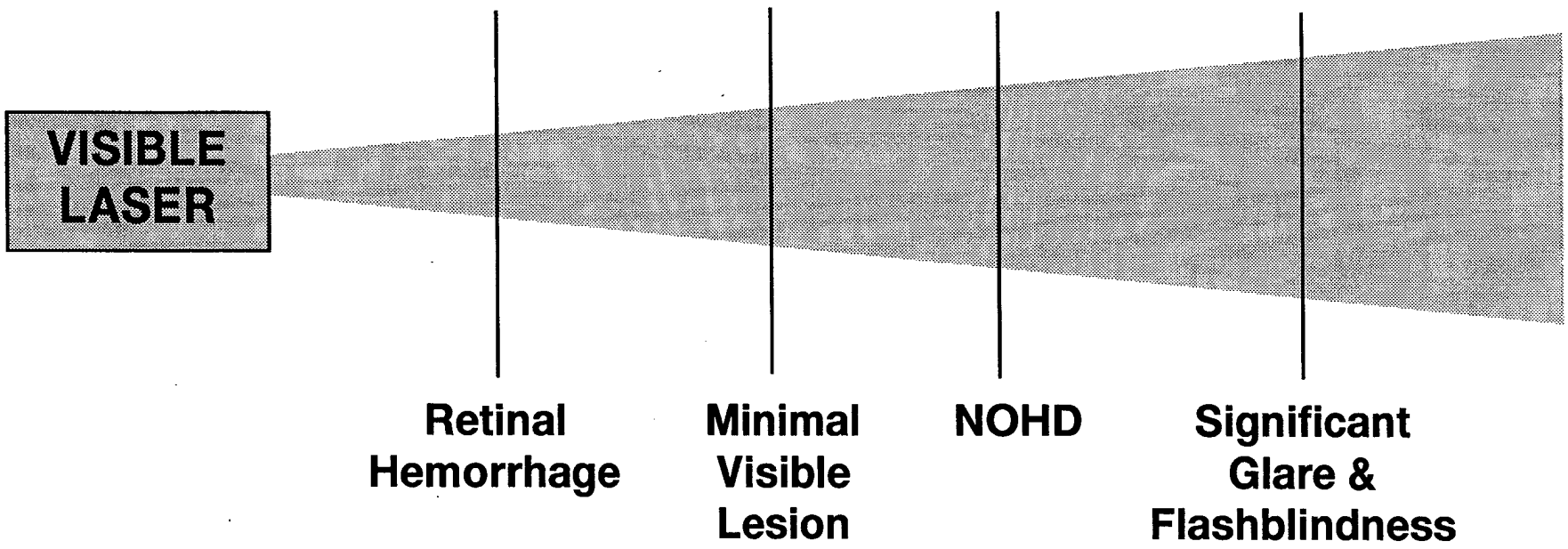

Actual ranges highly dependent on laser and scenario

"Blinding" Laser Damage

- Most retinal lesions produced by lasers do not produce damage severe enough to meet definitions of "blindness"
  - Not "all or nothing"
  - Retinal lesion produces blind spot in visual field
  - Vision loss depends on
    - » Lesion location
    - » Lesion size
- World Health Organization (WHO) definition of "blindness"
  - 20/400 or worse in the better eye
- Legal blindness in the United States
  - 20/200 or worse in the better eye

Assessment of Anterior Segment Ocular Bioeffects

Steven Chalfin, MD
Ophthalmology Department – UTHSCSA
7703 Floyd Curl Drive, San Antonio, TX 78284-6230
(210) 567 8411 chalfin@uthscsa.edu

Abstract: Both millimeter wave (MW) microwaves and infrared (IR) lasers are known to produce significant biological effects in the anterior segment of the eye. This presentation will provide an overview of the principles and methodologies used to detect, characterize, and quantify anterior segment bioeffects in the human (or other primate) eye.

MW or IR exposure may produce changes in ocular structure, which can be detected directly, or indirectly by their effect on visual function. Visual function is typically assessed by testing either visual acuity or contrast sensitivity. The technique of slit lamp bio-microscopy may be used to qualitatively observe structural changes in the conjunctiva, cornea, iris, and lens. Computerized corneal topography is used to detect and quantify minute changes in corneal curvature, which affect the refractive status of the eye. Corneal endothelial cell density, morphology, and (indirectly) function can be measured using the technique of specular microscopy. Cataract formation may be quantified using either Scheimpflug photography or an opacity lensmeter.

Emerging technologies which may have a role in the assessment of anterior segment bioeffects, such as the confocal microscope, will be briefly discussed.

Measurement of Visual Function: The traditional assessment of visual function has been accomplished by measurement of visual acuity. Using black optotypes on a white background, visual acuity provides a measure of the resolution of the eye for high (95-100%) contrast targets. Contrast sensitivity measurements using sinusoidal gratings at varying spatial frequencies, allows testing a wider spectrum of visual function. Both visual acuity and contrast sensitivity measure the function of the eye as a whole, and decrements in these parameters cannot be directly related to a specific anatomical defect.

Electrophysiologic testing such as the electroretinogram (ERG) or visual evoked potential (VEP) allows determination of retinal and visual pathway function and may be used in conjunction with other testing to relate visual impairment to anterior segment pathology. Unlike visual acuity and contrast sensitivity, which are somewhat subjective, electrophysiologic testing is completely objective.

Anterior Segment Anatomy: The anterior segment of the eye consists of the conjunctiva, cornea, anterior chamber, iris, and lens. Because of their short wavelength, millimeter waves only superficially penetrate biological tissue. This localized absorption can produce very high specific absorption rates (SAR) in a relatively small volume of tissue. In addition to high SARs, the heating pattern of millimeter wave energy that is

absorbed in tissue can be non-uniform, with local SAR values exceeding the average SAR by a factor of ten (hot spots). Almost all previous studies of millimeter wave absorption have used skin as the target tissue. The highly vascularized structure of skin may allow significant heat removal by conduction, and an increased threshold to millimeter wave damage. The cornea and lens of the eye, however, are avascular, and may be especially vulnerable to millimeter wave injury.

Corneal Anatomy: The cornea is composed of five histologic layers: epithelium, Bowman's layer, stroma, Descemet's membrane, and endothelium. Of these, epithelium, stroma, and endothelium are most likely to show acute and chronic changes secondary to millimeter wave absorption.

Slit Lamp Biomicroscopy: The technique of slit lamp biomicroscopy allows high quality, high magnification, stereoscopic imagery of the entire anterior segment. In clinical ophthalmology, it is considered the 'Gold Standard'. It is excellent for detection and characterization of damage to the anterior segment structures, but less useful for quantification of damage. Widely available and relatively inexpensive, it is the primary instrument used for anterior segment examination. A number of topical stains may be used in conjunction with the slit lamp to highlight corneal epithelial damage. These include fluorescein, which stains areas of corneal epithelial cell loss, and rose bengal, which stains dead or dying epithelial cells.

Specular Microscopy: This technique uses a high magnification camera with a contact or non-contact objective to image the corneal endothelium by specular reflection. It allows photography of the corneal endothelium *in vivo*. Endothelial cell density may be measured by means of a standardized counting grid, and cell morphology may also be assessed. Specular microscopes also have the ability to measure corneal thickness (pachymetry), which is an indirect indication of endothelial cell function.

Corneal Topography: This technique uses the principle of the Placido disk, a series of dark and light rings, to measure the shape of the corneal surface. A digital camera captures an image of the reflected rings and a computer analyzes the image to calculate the corneal curvature and construct a topographic map. Corneal topography is able to detect very small changes in the surface on the order of 0.1 diopter. Corneal stromal heating secondary to millimeter wave absorption may result in collagen shrinkage and irregularities in corneal topography.

Lens Anatomy: The crystalline lens is a multilaminar structure, which is particularly sensitive to ionizing and non-ionizing radiation. It consists of a central nucleus, which grows throughout life surrounded by a softer cortical layer. The lens epithelium, which overlies the cortex, contains dividing cells, which add layers to the lens. Surrounded by an acellular capsule, the lens is suspended in the eye by the zonule.

Measurement of Lens Opacity Slit lamp examination of the lens through a pharmacologically dilated pupil with grading of opacities using predetermined criteria is

the method used in clinical ophthalmology. For research purposes, it requires the use of a masked examiner and suffers from problems with sensitivity and reproducibility. Scheimpflug photography uses a special slit lamp camera with the illumination source and camera 45 degrees apart to obtain standardized images of the lens. These images may be scanned on a densitometer or computer to yield a quantitative measure of lens opacity. This device is expensive and not widely available. A modern adaptation of this principle is called the Anterior Eye Segment Analysis System (Nidek).

Another device which can be used to measure lens pathology is the Opacity Lensmeter (Interzeag). Operating on the principle of backscatter from an infrared laser diode, this device is especially suited for measurement of anterior lens opacities.

Confocal Microscopy: This technique uses a confocal optical system to examine histology of the cornea and conjunctiva *in vivo*. It is particularly well suited for observation of corneal epithelium, endothelium, and stromal keratocytes. Currently, these systems are not widely available outside ophthalmic research laboratories.

Ophthalmic Pathology: Histopathologic examination of exposed tissue can provide valuable information on cellular and histologic sequelae of millimeter wave exposure. It suffers from the requirement for sacrifice of a large number of expensive subjects to fully assess the course of damage induction and repair.

Summary: With the increasing power output and widespread use of millimeter wave devices, safety concerns have grown. Ocular bioeffects, predominantly in the anterior segment, have not been well characterized. New and existing ophthalmic technologies will be utilized to characterize these effects and develop rational safety standards.

MILLIMETER WAVES AND NEURONAL MEMBRANES: BIOEFFECTS AND MECHANISMS

S.I. Alekseev and M.C. Ziskin

Center for Biomedical Physics
Temple University Medical School, Philadelphia, PA 19140

Millimeter waves are widely used in the former Soviet Union for therapeutic treatment [Vetkin, 1991]. In most cases the optimum modes of irradiation were determined empirically in a hospital environment. However, the primary mechanisms of the biological effects of mm-waves have been insufficiently studied.

Millimeter waves are totally absorbed within 1 mm in the superficial layers of the skin [Gandhi, 1983]. Therefore the primary effect of mm-waves is limited to an interaction with structures located within the skin, such as receptors, nerve endings, and immunocompetent cells. Recent data have demonstrated that exposure potentiates the immune system of mammals [Rojavin et al., 1997]. This effect may involve two mechanisms. Exposure may affect the immune system either directly or indirectly via the nervous system, as the immune and nervous systems are closely related to each other [see, i.e. Rabin et al., 1989; Hosoi et al. 1993]. To study the effects of mm-waves on receptors and nerve endings, we selected nerve cells of the mollusc *Lymnaea stagnalis* to be used as a natural model. Pacemaker neurons of this mollusc

have been widely used in experiments with microwave irradiation [Bolshakov and Alekseev, 1987; 1992; Alekseev et al., 1997].

METHOD

Experiments were conducted using pacemaker neuron BP-4 [Zherelova, 1971] of the large parietal ganglia of the mollusc *Lymnaea stagnalis*. The firing rate of the neurons was recorded using a conventional microelectrode technique [Purves, 1981].

The cells were irradiated with continuous mm-waves at frequencies of 61.22 and 75.00 GHz. The open end of a rectangular waveguide with a 3.6 x 1.8 mm cross-section was covered with a thin waterproof Teflon film and served as an irradiator. It was inserted into the solution close to the neuron studied. The absorbed energy of the mm-wave irradiation was evaluated by measuring the specific absorption rate (SAR) in the 0.1 mm thick layer of solution closest to the waveguide outlet [Alekseev and Ziskin, 1995]. SARs were within the range of 0-4200 W/kg which corresponded to temperature rises of 0 - 2.2°C. Measurements of the firing rate were conducted at 18°C. When studying the thermal reactions of the nerve cells, the desired temperature rise rate was achieved by carefully controlling the temperature and flow rate of the heated solution through the chamber.

RESULTS AND DISCUSSION

Effects of mm-waves

The BP-4 neuron generates a steady spontaneous firing rate under normal physiological conditions. Millimeter wave exposure causes changes in the firing rate of this neuron. Immediately after the switching on of irradiation we observed a transient decrease in the firing rate (Fig. 1). The transient inhibition becomes more pronounced with increasing the output power or SAR [Alekseev et al., 1997]. At higher levels of SAR (4200 W/kg), pacemaker generation in some neurons was stopped completely. For a longer period of irradiation the transient decrease was followed by slower increase in the firing rate to a new stable level (Fig. 2). On the average, exposures with an SAR of 4200 W/kg caused a transient inhibition of the firing rate by 69 ± 22% (n = 23) and steady-state increase in the firing rate by 68 ± 21% (n = 9). These effects did not reveal the frequency dependence for two frequencies that we used (61.22 and 75 GHz). As can be seen in Fig.2, the transient decrease in the firing rate developed within the first 10 s of irradiation. The rising phase was well fitted by an exponential with a time constant of τ = 3.7 ± 1.9 min (n = 7). When the irradiation was turned off, reversible changes in the firing rate were observed.

A possible explanation for the transient decrease in the firing rate is a hyperpolarization of the neuronal membrane due

to an increase in the activity of the sodium pump. In the presence of ouabain, a relatively specific inhibitor for the sodium pump [Willis et al., 1974], the neuronal membrane was depolarized by 6±2 mV. The spontaneous firing rate increased almost two times. The transient response of the neuron to mm-wave irradiation disappeared entirely. These results suggest that an electrogenic sodium pump is responsible for the transient decrease of the firing rate during mm-wave irradiation.

Irradiation produced a temperature rise in the medium. We tried to reproduce the temperature effect of irradiation by simple warming to produce a temperature rise of 2°C at a temperature rise rate of 0.96°/s. This corresponds to an SAR of 4030 W/kg. The transient decrease in the firing rate of neurons in these experiments was 72±15% (n = 8). The steady-state level of the firing rate increase was 60±20% (n = 8). The results are in agreement with the mm-wave exposure data. Thus, the effect of mm-waves is qualitatively and quantitatively equivalent to warming of the neurons. The thermal mechanism seems to be main cause of the effects of millimeter waves on the firing rate of the neurons studied.

The rate of temperature rise was critical for reproducing the transient response of the neuron. In a study of the threshold sensitivities of the neuron to heating, the temperature was increased to 0.3 °C at different rates. The minimal temperature

rise rate for observing the transient response was 0.0025 °C/s. The statistically reliable decrease in the firing rate was recorded at a 3% level. In humans, the threshold stimulus is 0.001 °C/s for warmth and 0.004 °C/s for cold receptors [Iggo A, 1962]. It is obvious that the thermal sensitivity of the mollusc neuron is within the range of the thermal sensitivity of human thermoreceptors.

Modeling the changes in the firing rate

As most experiments are time consuming, we tried to predict some effects using a model. It was shown that the spontaneous firing rate of molluscan pacemaker neurons is a direct function of membrane potential [Willis et al., 1974] which results mainly from a sum of two potentials produced by the passive ion transport system and electrogenic Na-pump [Marmor and Gorman, 1970]. Warming results in an increase of the activity of the Na-pump hyperpolarizing the membrane [Carpenter, 1981; Carpenter and Alving, 1968]. The time constant of this process estimated from our data and the data by Carpenter and Alving [1968] is about 6 s. The component of the membrane potential dependent upon ionic gradients and permeabilities can be determined primarily by the ratio P_{Na}/P_K [Gorman and Marmor, 1970; Moreton, 1968]. On warming, this component produces depolarization of the membrane because of an increase of the ratio P_{Na}/P_K. The time constant for depolarization of the neuron or increase in the firing rate was

calculated as 3.7 min. Difference in the rates of hyperpolarization and depolarization is a main cause of the biphasic changes in the firing rate (Fig. 3). If the time constant of the temperature rise exceeds the time constant for thermal depolarization of the neuron due to the ionic component, we can expect only an increase in the firing rate without the appearance of the transient response. This was confirmed in the experiment with a very slow temperature rise. When the time constant of the temperature rise is smaller than that of the thermal depolarization, then the initial hyperpolarization of the membrane due to increase in the activity of Na-pump dominates over depolarization giving rise to the initial transient inhibition of the firing rate.

The changes in the firing rate during irradiation and warming were calculated using following equation:

$$FR(T + \Delta T, t) = FR_o(T) - FR_A(\Delta T, t) + FR_P(\Delta T, t), \quad (1)$$

where $FR_o(T)$ is the firing rate in control, $\Delta FR_A(\Delta T, t)$ and $\Delta FR_P(\Delta T, t)$ are changes in the firing rate due to sodium pump and ionic component, respectively. The temperature rise during irradiation was simulated using exponential function:

$$\Delta T = \Delta T(\infty) \; [1 - \exp(- t/\tau)], \quad (2)$$

where $\Delta T(\infty)$ is the steady-state temperature. Time constants τ were calculated following equation [Foster et al. 1978]:

$$\tau = \mu L^2 , \quad (3)$$

where $\mu = \rho c/k = 1000$ s/cm^2 for muscle, L is the penetration depth. The penetration depths for different frequencies were taken from Polk [1968].

Our model reproduces the typical changes in the firing rate during irradiation (Fig. 2). Fig. 4 shows the changes in the firing rate at different SARs. In this study we generated the same steady-state temperature rise of 2°C in every simulation. In our model it was done by choosing appropriate SARs at different frequencies. The dependence of the magnitude of the transient response on SAR has an S-shape with midpoint at 170 W/kg (Fig. 5). The transient response reaches maximal value at 2000-3000 W/kg and then does not depend on SAR.

We estimated the threshold SARs at different frequencies when exposure produces a 3% transient decrease in the firing rate (Fig. 6). The threshold SARs increase with frequency. For example, at 75 GHz the threshold SAR is about 110 W/kg which is close to the experimental value of 120 - 140 W/kg. At 1 GHz the threshold SAR is only 9 W/kg.

Fig.7 shows the frequency dependence of the threshold incident power density for producing a 3% transient response of a neuron. The threshold curve has a strong frequency dependence with a minimum (~ 4 mW/cm^2) in the range of 7-70 GHz. At constant level of the incident power density the temperature rise rate decreases with decreasing the frequency (< 7 GHz). At higher

frequencies (>70 GHz), the temperature rise rate decreases due to decrease in the steady-state temperature rise. Both these events result in an increase of the threshold power densities.

Experiments show that a temperature increase by even several tenths of a degree is capable of causing recordable changes in the firing rate of pacemaker neurons if the rate of temperature rise is sufficiently high. Therefore it seems likely that a temperature rise by several degrees as may be brought about by therapeutic devices [Betsky et al., 1989] could produce a notable effect on human thermoreceptors and on other thermosensitive nerve endings in the skin. For example, mechanoreceptors also demonstrate a high thermal sensitivity due to the presence of the Na-pump [Pierau et al., 1974] and, along with thermoreceptors, can play a possibly important role in the therapeutic effects of millimeter waves.

CONCLUSIONS

Millimeter wave irradiation caused biphasic changes in the firing rate of mollusc pacemaker neurons.

The temperature rise rate played an important role in the development of the transient response of the neuron.

Millimeter wave irradiation, at commonly used intensities, is sufficient for activating thermoreceptors and other thermosensitive nerve endings in the upper layers of the skin.

REFERENCES

Alekseev SI, Ziskin MC (1995): Millimeter microwave effect on ion transport across lipid bilayer membranes. Biolectromagnetics 16:124-131.

Alekseev SI, Ziskin MC, Kochetkova NV, Bolshakov MA (1997): Millimeter waves thermally alter the firing rate of the *Lymnaea* pacemaker neuron. Biolectromagnetics 18:89-98.

Betsky OV, Petrov IY, Tyazhelov VV, Khizhnyak EP, Yaremenko YG (1989): Distribution of the electromagnetic fields of mm-waves in models and biological tissues in the near field area of irradiators. Doklady Academy nauk SSSR 309:230-233.

Bolshakov MA, Alekseev SI (1987): Pulse microwave radiation influence on the electrical activity of snail neurons. Izvestia AN SSSR (ser biol) 2:312-314.

Bolshakov MA, Alekseev SI (1992): Bursting responses of *Lymnaea* neurons to microwave radiation. Bioelectromagnetics 13:

Carpenter DO (1981): Ionic and metabolic bases of neuronal thermosensitivity. Federation Proceedings 40: 2808-2813.

Carpenter DO, Alving BO (1968): A contribution of an electrogenic Na^+ pump to membrane potential in *Aplysia* neurons. J gen Physiology 52:1-21.

Foster KP, Kritikos HN, and Schwan HP (1978): Effects of surface cooling and blood flow on the microwave heating of tissue.

IEEE Trans. Biomed. Eng. 25: 313-316.

Gandhi OP (1983): Some basic properties of biological tissues for potential biomedical applications of millimeter waves. J. Microwave Power 18:295-304.

Gorman A.L.F., and Marmor M.F. (1970): Temperature dependence of the sodium-potassium permeability ratio of a molluscan neurone. J.Physiol. 210:919-931.

Hosoi J, Murphy GF, Egan CL, Lerner EA, Grabbe S, Asahina A, Granstein RD (1993): Regulation of Langerhans cell function by nerves containing calcitonin gene-related peptide. Nature 363: 159-163.

Iggo A (1962): An electrophysiological analysis of afferent fibers in primate skin. Acta neuroveg (Wien) 24:225-240.

Marmor M.F., and Gorman A.L.F. (1970): Membrane potential as the sum of ionic and metabolic components. Science. 167: 65-67.

Moreton RB (1968): An application of the constant-field theory to the behaviour of giant neurones of the snail, *Helix Aspersa*.

Pierau F-K., Torrey P., and Carpenter D.O. (1974): Mammalian cold receptor afferents: role of an electrogenic sodium pump in sensory transduction. Brain Research 73:156-160.

Polk C. (1986): Introduction. In "Handbook of Biological Effects of Electromagnetic Fields", CRC Press, Inc., Boca Raton, Florida, pp. 1- 24.

Purves RD (1981): Microelectrode methods for intracellular recording and ionophoresis. Acad. Press, A Subsidiary of Harcourt Brace Jovanovich, London.

Rabin BS, Cohen S, Ganguli R, Lysle DT, Cunnick JE (1989): Bidirectional interaction between the central nervous system and the immune system. Crit Rev Immunology 9: 279-312.

Rojavin MA, Tsygankov AY, Ziskin MC (1997): In vivo effects of millimeter waves on cellular immunity of cyclophosphamide-treated mice. Electro-and Magnetobiol 16: 281-292.

Vetkin AN (1991): Application of millimeter waves in clinics. Digest of papers of Int. Symposium "Millimeter waves of non-thermal intensity in medicine", Moscow, p.7-14.

Willis J.A., Gaubatz G.L., and Carpenter D.O. (1974): The role of the electrogenic sodium pump in modulation of pacemaker discharge of *Aplysia* neurons. J. Cell. Physiol. 84: 463-472.

Zherelova OM (1971): Electrophysiological characteristics of molluscian giant neurons. In:"Biophysics of Living Cells", Puschino, USSR: Scientific Center of Biological Investigations, pp 89-97.

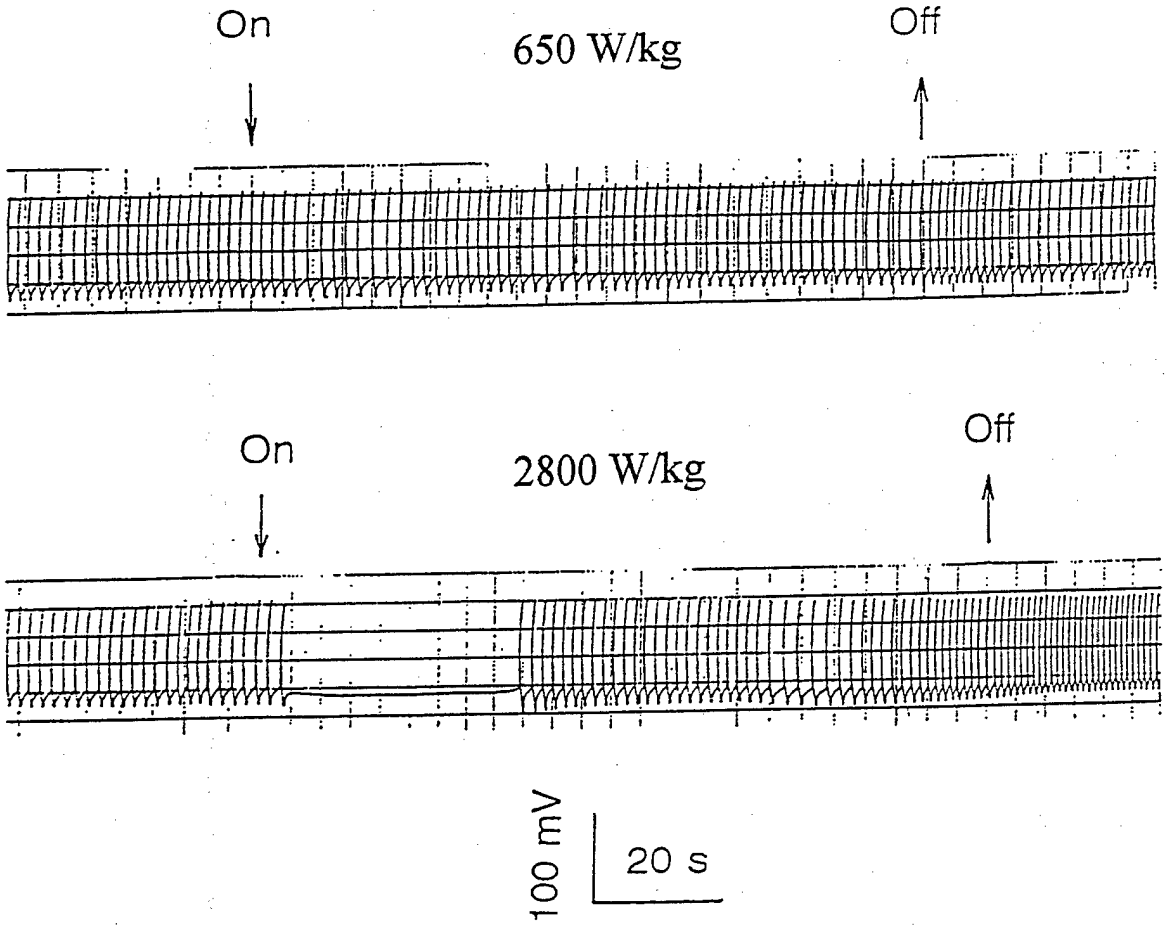

Fig.1. Effect of mm-wave exposure on the firing rate at different SARs obtained by changing the source power.

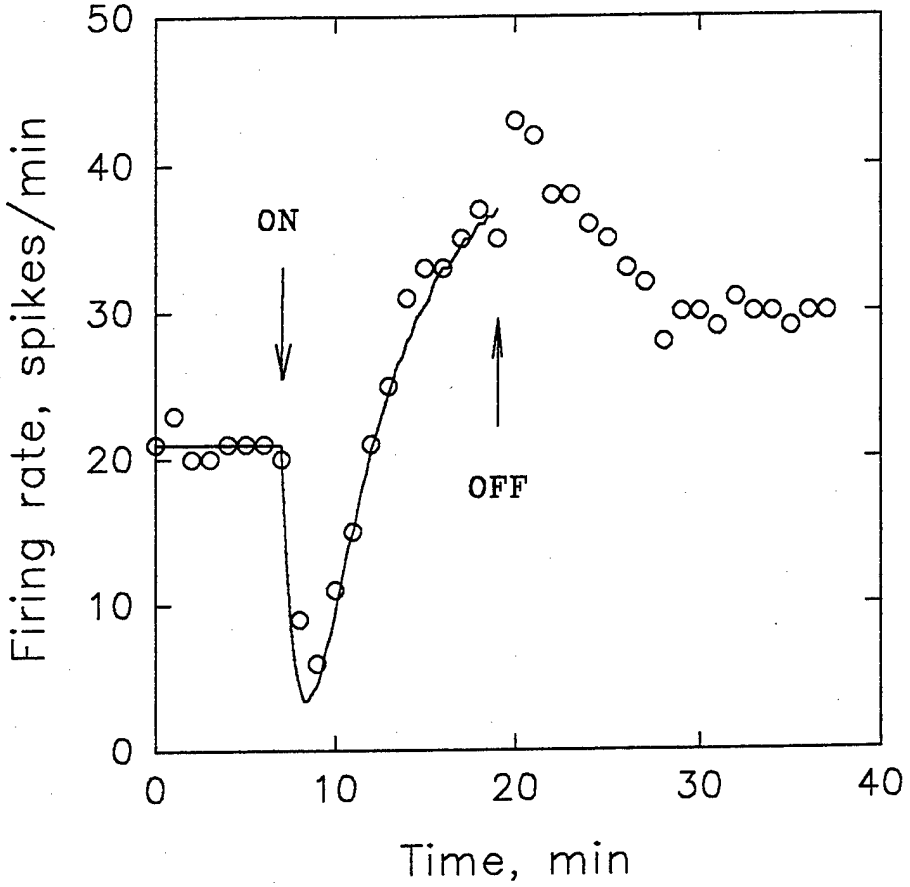

Fig.2. Typical changes in the firing rate of the neuron during and after mm-wave irradiation at an SAR of 3150 W/kg. The solid trace is a fit of the model to the data.

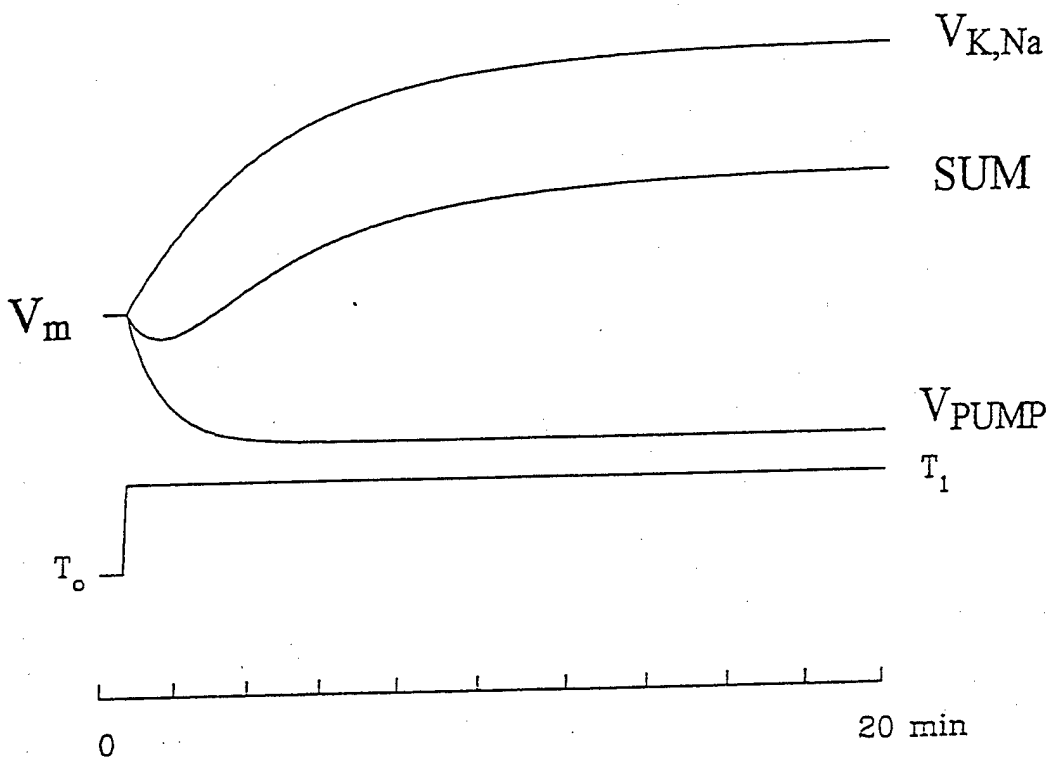

Fig.3. Membrane potential following sudden temperature increase from T_o to T_1. V_m is a resting potential, $V_{K,Na}$ is a potential change due to increase of the permeability ratio for sodium and potassium ions (P_{Na}/P_K), V_{PUMP} is a potential change due to increase of the activity of the Na-pump, and SUM is a resulting membrane potential change.

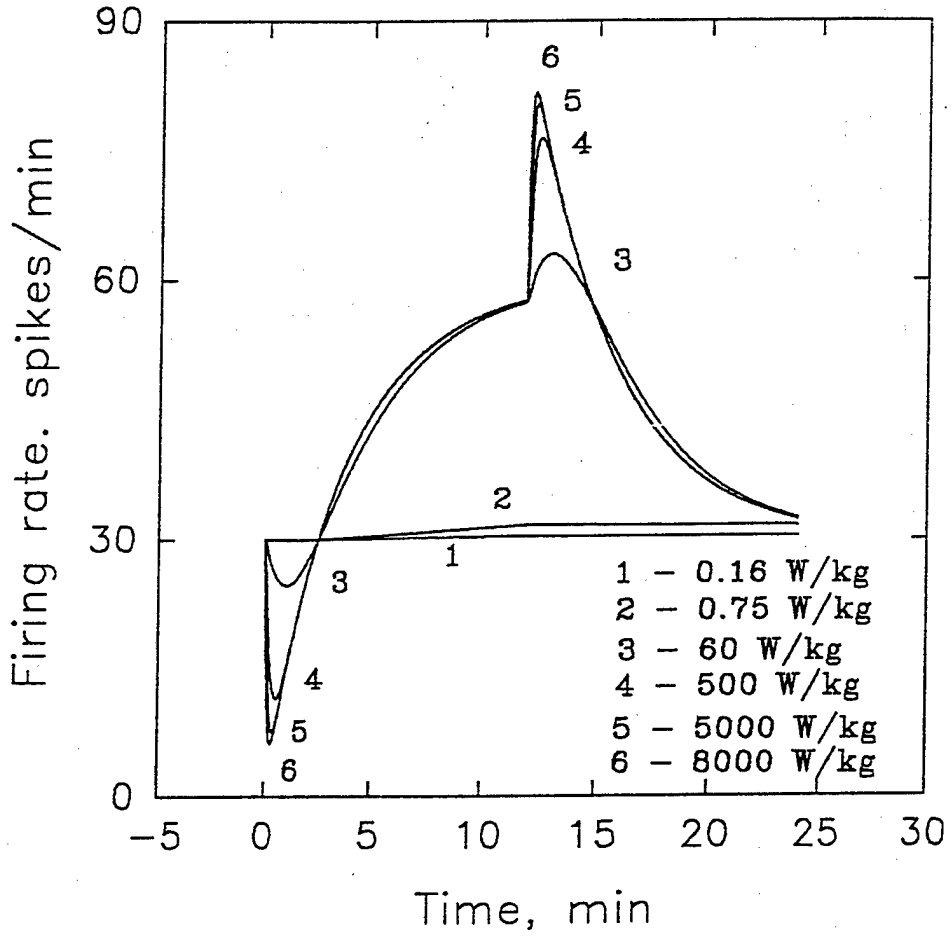

Fig.4. Changes of the firing rate in response to exposure simulation at different SARs to the same steady-state temperature of 2°C.

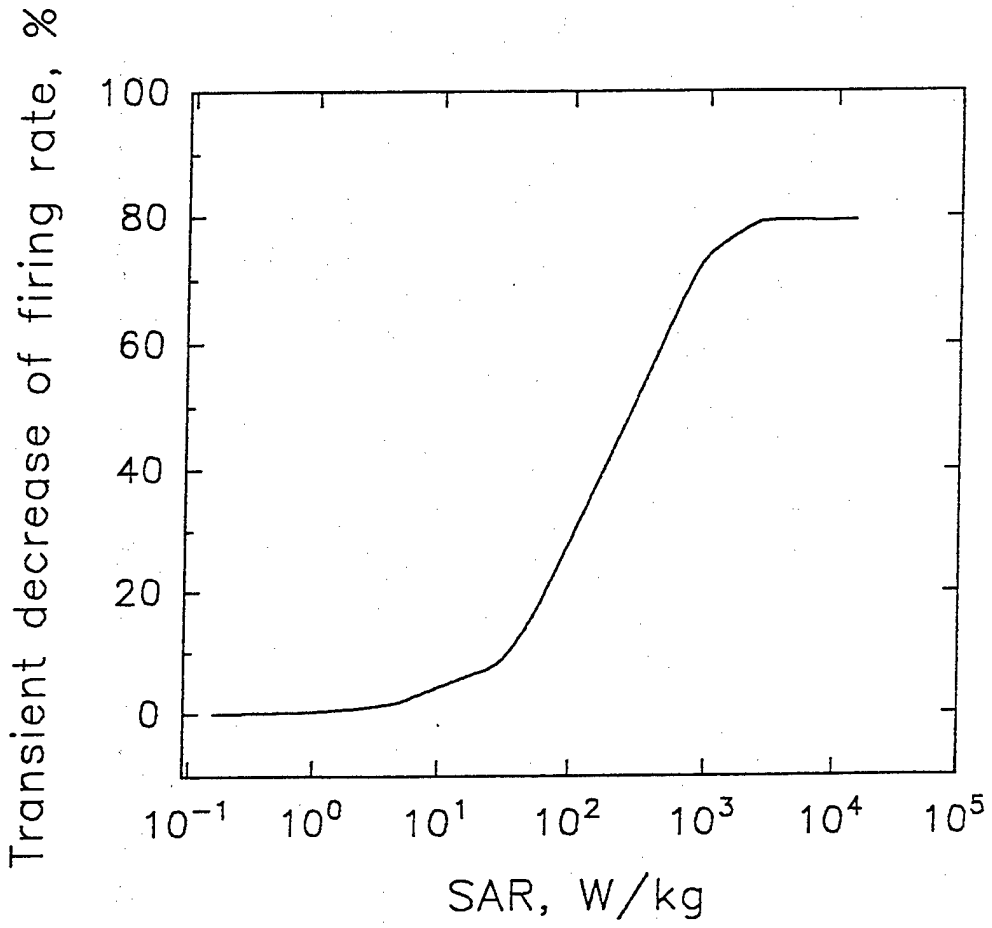

Fig.5. Dependence of the transient response on SAR. Different SARs were obtained using different frequencies which generated the same steady-state temperature of 2°C.

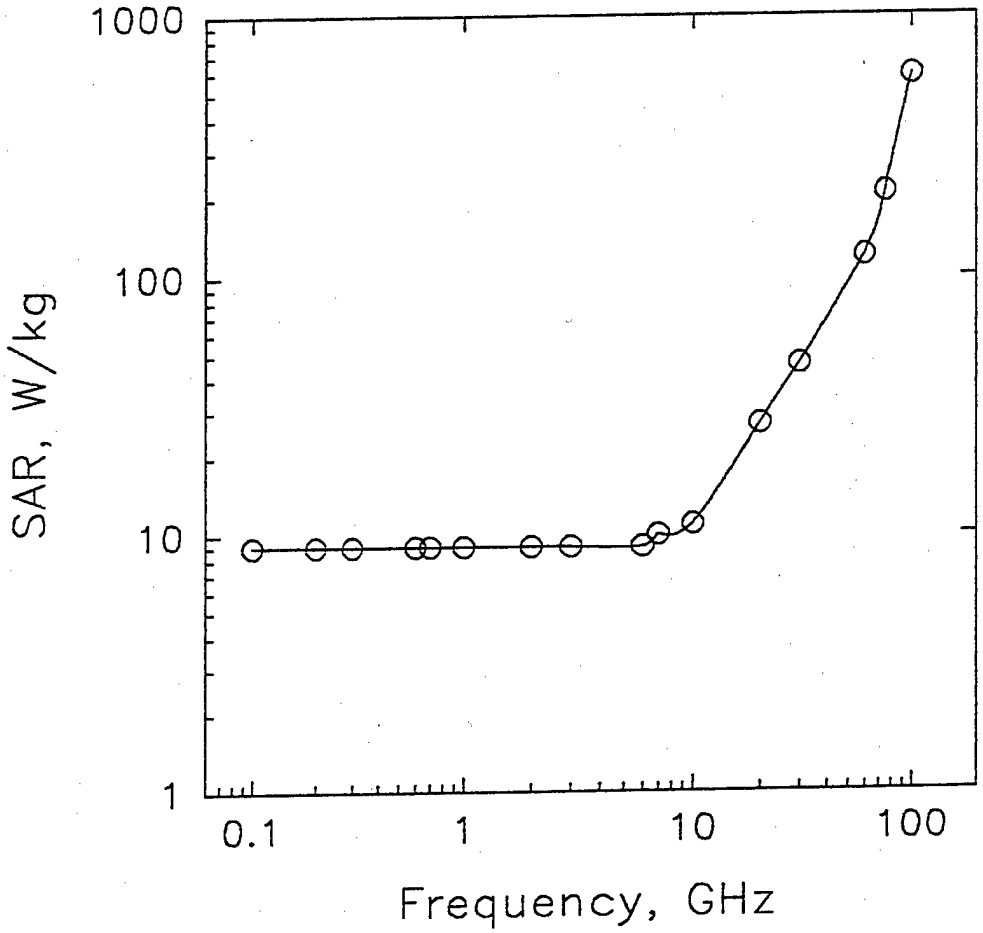

Fig.6. Frequency dependence of SAR producing a 3% transient decrease in the firing rate.

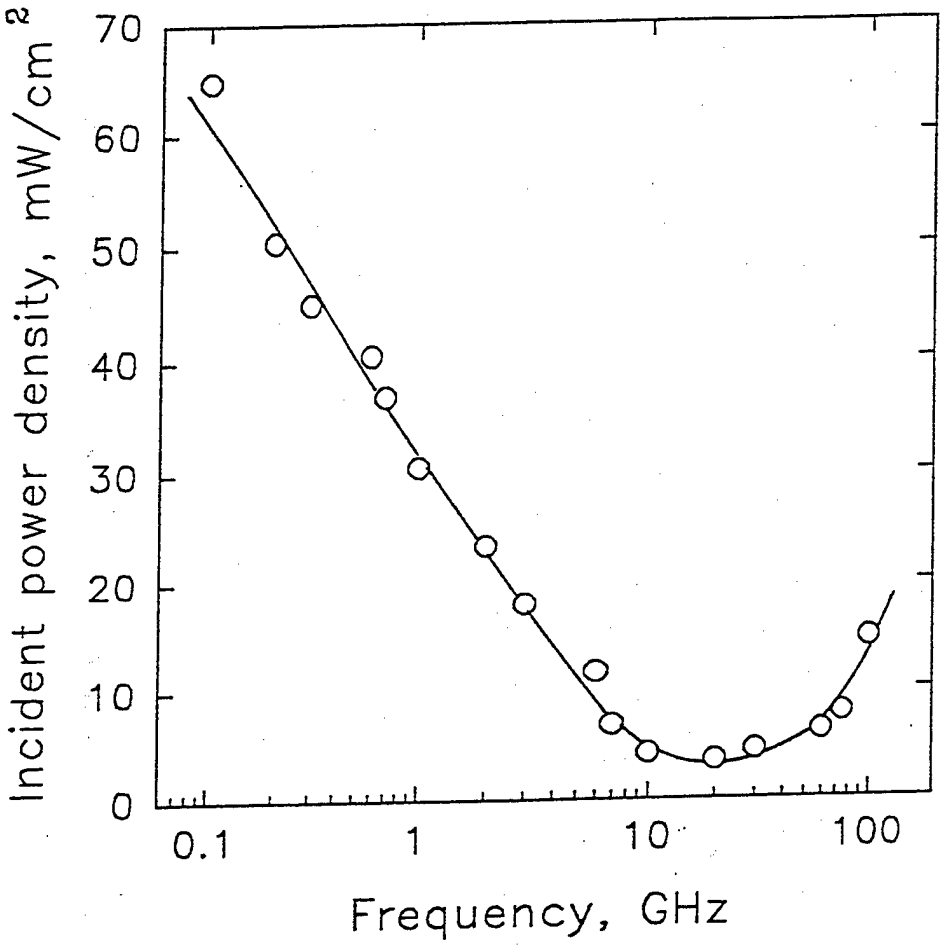

Fig.7. Frequency dependence of the incident power density producing a 3% transient decrease in the firing rate.

FIGURE LEGENDS

Fig.1. Effect of mm-wave exposure on the firing rate at different SARs obtained by changing the source power.

Fig.2. Typical changes in the firing rate of the neuron during and after mm-wave irradiation at an SAR of 3150 W/kg. The solid trace is a fit of the model to the data.

Fig.3. Membrane potential following sudden temperature increase from T_o to T_1. V_m is a resting potential, $V_{K,Na}$ is a potential change due to increase of the permeability ratio for sodium and potassium ions (P_{Na}/P_K), V_{PUMP} is a potential change due to increase of the activity of the Na-pump, and SUM is a resulting membrane potential change.

Fig.4. Changes of the firing rate in response to exposure simulation at different SARs to the same steady-state temperature of 2°C.

Fig.5. Dependence of the transient response on SAR. Different SARs were obtained using different frequencies which generated the same steady-state temperature of 2°C.

Fig.6. Frequency dependence of SAR producing a 3% transient decrease in the firing rate.

Fig.7. Frequency dependence of the incident power density producing a 3% transient decrease in the firing rate.

Infrared Lasers & Millimeter Waves
Workshop
The Links Between Microwaves
& Laser Optics

21 Jan 1997 - 22 Jan 1997

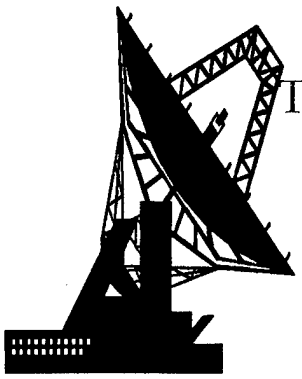

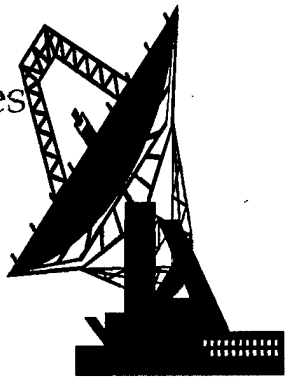

SECTION II:

DIELECTRIC PARAMETERS, SKIN DEPTH & DOSIMETRY

DOSIMETRY AT MILLIMETER WAVELENGTHS

W.D. Hurt[1] and P.A.Mason[2]

[1]Air Force Research Laboratory, Directed Energy Bioeffects Division, Radiofrequency Radiation Branch, Brooks AFB, TX, 78235;
[2]Veridian, Inc., San Antonio, TX, 78216

INTRODUCTION

Interest remains high concerning possible health hazards associated with the ever increasing use of radio frequency (RF) electromagnetic (EM) equipment and the resulting increased exposure of both occupational workers and the general public to RF fields which include millimeter waves. An essential element of the research related to RF biological effects and hazards is dosimetry, the calculation and measurement of the amount of energy absorbed as a result of exposure to RF fields. Energy absorption is expressed in terms of the specific absorption rate (SAR).

SOURCES

The millimeter (mm) wave sources operated by the Radiofrequency Radiation Branch (HEDR), Directed Energy Bioeffects Division, Human Effectiveness Directorate, Air Force Research Laboratory, Brooks Air Force Base, Texas, includes two 35 GHz transmitters and two 94 GHz transmitters. One facility consists of a 75-W, 35 GHz transmitting system; a 50-W, 94 GHz transmitting system; a temperature-controlled, millimeter-wave anechoic exposure chamber; and a set of biconvex dielectric lenses for collimating the mm wave energy. The transmitters are based upon CW Extended Interaction Oscillator tubes. These transmitter-lense combinations can focus mm waves to obtain densities of 1 and 6 W/cm2 for 35 and 94 GHz respectively with 3 dB spot sizes having a diameter of approximately 2.5 cm. [Shelton 1991].

The other 35 GHz source is a GTE Model 01-1374683-1, Pulsed Millimeter Wave Transmitter. This Traveling Wave tube (TWT) amplifier based transmitter also runs into a temperature-controlled anechoic exposure chamber and is capable of an 800 W output. Another 94 GHz transmitter has an output power of 800 W. It is based on a Coupled Cavity TWT amplifier and manufactured by the North Star Research Corp.

FIELD MEASURING

For free field measurements we generally use a Narda model 8700 series radiation survey system. However we also use a variety of mm wave horns (pyramidal, conical, and open ended waveguide by Milltech). The energy captured by the horns is measured with either an Hewlett-Packard (HP) 437B power meter (with HP R8486A power sensor for 35 GHz and HP W8486A power sensor for 94 GHz) or the Milltech series DXP crystal detectors. The crystal detectors are calibrated against the HP power meter by using Millitech series GDM Gunn Oscillators and calibrated attenuators.

During the past several years, we have also been using conductive cloth and infrared (IR) thermography to measure field distribution. These techniques reveal the location and field pattern before an object, such as an animal holder, is placed in front of the waveguide. The time required to map the field using either of these techniques is substantially less than that using power meters or crystal detectors. After the general

field pattern is known, power meters or crystal detectors are then used to measure the field. After an object is placed in the field, the cloth and IR camera have been useful in revealing disturbances to the field and the IR camera has been extremely valuable in revealing localized "hotspots" on the skin, presumably resulting from the animal holder focusing the field.

SKIN HEATING

Although locating "hotspots" on the skin can be accomplished with thermistor type temperature probes that use high resistive leads, the IR camera is much more effective and convenient. A single point measurement is obtained with each temperature probe, whereas a 256 x 256 pixel array denoting temperature is obtained with each IR image. We use a Radiance 1 Infrared Camera System (Amber Engineering, Inc., Goleta, CA), equipped with a 25, 50, 70, or 250 mm lens. The camera contains a focal plane array composed of 256 X 256 indium antimonide sensors. Obtaining this array resolution has considerably increased the usefulness of IR camera in biological research. Knowing the precise location of the temperature increase was difficult when using older cameras having lower resolution. It would be difficult to resolve whether the eye or the tissue surrounding the eye was the warmest. The IR camera system is calibrated using a Mikron M340 black body calibration source. Using supporting hardware and software, images can be sampled at a rate of 5 per second. Real-time and off-line image analysis is performed using ImageDeskTR and Adobe PhotoshopTR software. Real-time image analysis provides instantaneous feedback as to the resulting temperature increases. Exposure parameters may be subsequently modified to produce the desired biological effect. Off-line image analysis is used to determine heating rates as a function of exposure parameters. Since a temperature measurement is available for each pixel, occasionally moderate temperature increases in unexpected locations are revealed. These may have been missed if only temperature probes were used. In addition to the above dosimetric techniques, IR thermography has been recently combined with thermochemiluminescent (TCL) technology to determine mm wave dosimetry [Kiel et al. submitted]. A rat phantom filled with diazoluminomelanin (DALM) has been used as a TCL dosimeter for 35 GHz radiation. The temporal and spatial information provided by the TCL technology was validated by IR thermography.

Observed bioeffects are more closely related to tissue temperature than to the SAR that results from exposure to RF fields. Therefore consideration of heat flow characteristics is essential, especially for mm wave exposures where most of the energy is absorbed so near the surface. Under many circumstances, significant amounts of energy can dissipate from areas of high SAR resulting in temperatures that may be much different from those predicted by schemes that ignore heat flow considerations. For mm wave exposures, Walters et al. [submitted] have found that the a one-dimensional thermal model, based on the solution of the heat conduction equation [Cook 1952 and Foster et al. 1978], compares very well with measurements of skin temperature as a function of time for 3 second exposures to 94 GHz. Dave Nelson [personal communication, Michigan Technological University] has expanded upon this modeling by attempting to extrapolate the skin heating effects observed in rodents to that in monkeys and man. This modeling will incorporate thermal effects due to variations in skin blood flow.

SAR CALCULATIONS

For mm wave exposures, the most practical models for calculating the SAR distribution is the one dimensional model [Hurt 1984] because the curvature of the body can be neglected for these high frequencies. When a planewave is incident on a planar object, the wave transmitted into the object attenuates as it travels and transfers energy to the material. At mm wave frequencies most of the energy from the field is absorbed near the surface. Franzen and Samn [1997] have extended the model of a simple one-dimensional monochromatic planewave normally impinging on a tissue half-space to a multi-layered tissue model irradiated by monochromatic planewaves at oblique incidence. This will allow more realistic predictions of SAR distributions resulting from actual exposure conditions.

The finite-difference time-domain (FD-TD) method for EM calculations has received wide use for a variety of applications in EM radiation, interaction, and scattering problems [Kunz and Luebber 1993]. However due to the small cell size needed to perform FD-TD calculations for mm wave exposure problems, to model a realistic scenario would result in a prohibitively large program.

CONCLUSIONS

In order to support the mm wave bioeffects research performed in HEDR, 35 and 94 GHz field generating equipment is available for use by the researchers. Various types of free field measurement instrumentation is used to determine the incident power density for the different experimental designs. Results of SAR calculations are used in thermal conduction models to predict the temperature distribution history for the various experimental setups so that the researcher will have appropriate information needed to correctly identify the mechanisms causing the observed effects. These thermal models are confirmed through the use of IR thermography.

REFERENCES

Cook, H.F. A Physical Investigation of Heat Production in Human Tissues when Exposed to Microwaves. British Journal of Applied Physics 3:1-6, 1952.

Foster, K.R., Kritikos, H.N., and Schawn, H.P. Effects of Surface Cooling and Blood Flow on the Microwave Heating of Tissue. IEEE Transactions on Biomedical Engineering 25:313-316, 1978.

Franzen, J. and Samn, J. Electromagnetic Fields in a Single Slab for Oblique Incidence. Unpublished internal report. AFRL/HEDB. Brooks AFB, TX. 1997.

Hurt, W.D. Measurements of Specific Absorption Rate in Human Phantoms Exposed to Simulated Air Force Radar Emissions. Report USAFSAM-TR-84-16. Brooks AFB, TX, USAF School of Aerospace Medicine. 1984.

Kiel, J.L., Alls, J.L., Mason, P.A., and Erwin, D.N. Luminescent radio frequency radiation dosimetry. Bioelectromagnetics, Special Durney Symposium edition, submitted.

Kunz, K. and Lubbers, R. The Finite Difference Time Domain Method for

Electromagnetics. CRC Press Catalog Number 8657. 1993.

Shelton, W.W. Millimeter-wave Exposure System Augmentation. Technical Report AL-TR-1991-0056. Brooks AFB, TX, U.S. Air Force Armstrong Laboratory. 1991.

Walters, T.J., Blick, D.W., Johnson, L.R., Adair, E.R., and Foster, K.R. Heating and Pain Sensation Produced in Human Skin by Millimeter Waves: Validation of a Simple Thermal Model. Health Physics, submitted.

Radiometric Parameters Used in Laser Research

David H. Sliney, Ph.D.

US Army Center for Health Promotion and Preventive Medicine

Aberdeen Proving Ground, MD

CIE Infrared Spectral Bands

- The CIE splits the infrared spectrum into three bands: IR-A, IR-B and IR-C
- IR-A: 760-1400 nm. Water is not a strong absorber; penetration is deeper than in any other part of the optical spectrum
- IR-B: 1400-3000 nm. Water is primary absorber; shallow (< 1 mm) penetration
- IR-C: 3000 nm - 1 mm. Water strongly absorbs; only very superficial absorption.

Radiometric Quantities

- CIE/ISO/IEC International Vocabulary
- Power Density is W/m^3 and not W/m^2
- Irradiance has units of W/m^2 and is used to quantify "exposure dose rate" for CW lasers
- Radiant exposure has units of J/m^2 and is used to quantify "exposure dose"
- Fluence and fluence rate are often misused to represent radiant exposure and irradiance

Depth Dose and Backscatter

- *Fluence* and *fluence rate*--when correctly used--refer to the J/m^2 and W/m^2 passing through a plane in tissue and includes all radiant flux coming from all directions, including backscatter.
- No dose concept of energy or power per unit tissue mass or volume is used in laser and optical radiation bio-effects studies, since surface absorption is the general rule.

Units: To use m^2 or cm^2 ?!

- SI Convention encourages m, mm, km, nm, etc. and not the cm, but the cm is just "discouraged"
- Some European standards argue for the use of only m^2 or m^3 in the denominator of units and not the cm or mm
- The medical and biological communities hold to the cm as a more workable unit

Optical Radiation Dosimetry
Special Considerations for the Eye

- The eye transmits and focuses visible and near-infrared radiant energy on the retina within the 400-1400 nm spectral region
- Critical absorption of energy in four structures: cornea, iris, lens, and retina
- **Radiance** of a source determines the retinal **irradiance**
- **Retinal Image Size** is critical in this region

Tissue Optics: Absorbers

- Water dominates tissue absorption in the infrared,
- Proteins dominate absorption in the visible and ultraviolet
- Melanin pigment granules, hemoglobin and rhodopsin are key absorbing molecules in the visible, but others such as xanthraphyl, some lipids, etc. have also been of interest

Tissue Reflectance and Emissivity

- A law of thermal physics: Tissue must be highly absorptive for high radiant emissivity
- The human skin has a spectral reflectance of only a few percent in the IR-C out to at least 20 um and probably much farther out; hence the emissivity is optimum at the black-body peak of emission in the 8-13 μm region
- IR-C is heavily absorbed, but re-emitted

Spot-Size Dependence

- The actual geometrical profile of absorbed energy with depth (e.g., in IR-A) depends on the irradiated area of tissue. Why?
- Radial heat flow and scatter combine to raise the threshold irradiances for injury to small irradiated spot sizes.
- The geometry of redistributed optical energy and heat depends on wavelength.

Measurement Aperture and Averaging of Irradiance

- In laser and optical radiation safety standards, the measurement aperture for averaging MPEs must be provided.
- This necessarily depends on wavelength and exposure duration. During short pulsed exposures, scatter but not heat flow occurs
- In lengthy exposures, heat flow, blood flow & body movements redistribute the energy

IR-C Laser MPEs

- Incident laser beam energy is averaged over a 3.5-mm circular aperture.
- CW MPE is 100 mW/cm^2 averaged over 3.5 mm aperture unless the beam is greater than 100 cm^2
- The MPE decreases, with increasing skin surface area exposed, from 100 to 1000 cm^2 linearly down to an MPE of 10 mW/cm^2

Tissue Absorption and Scattering

- The tissue scattering coefficient has been measured in a number of studies and steadily decreases from the ultraviolet down to at least 900 nm
- Tissue absorption coefficients have been measured for a variety of tissues and depend upon the presence of certain key absorbers, such as melanin and hemoglobin

Photobiological Action Spectra

- *Action Spectrum:* The relative spectral response of a photobiological (photo-chemical) effect as a function of wavelength
- *Chromophore:* The target molecule that undergoes a chemical change when a photon is absorbed. The chromophore(s) in most human tissue responses is (are) generally not known. DNA is one.

Photobiological Effects

- Since photon energy must be sufficient to alter a chomophore molecule, it has traditionally been assumed that these effects are limited to the UV and visible spectrum.
- However, there is evidence in photo-dermatology, enzyme chemistry and ocular research, that there may be a limited amount of photochemistry taking place in the IR-A.

Laser Desorption

- Laser desorption is the selective removal of surface contaminant molecules (adsorbants) by laser resonant absorption
- The technique is used in chemical analysis

Infrared Lasers & Millimeter Waves
Workshop
The Links Between Microwaves
& Laser Optics

21 Jan 1997 - 22 Jan 1997

SECTION III:

THERMAL BIOEFFECTS DATABASE

VARIABLES THAT INFLUENCE THERMAL SENSATION DERIVED FROM INFRARED EXPOSURE

Eleanor R. Adair
Air Force Research Laboratory
Human Effectiveness Directorate
Brooks Air Force Base, Texas, 78218

I. THERMAL SENSATION

The past few years have seen a resurgence of interest in the sensory characteristics that may accompany exposure to microwave and radio frequency energy. This interest has been reinforced by a desire to better quantify the biological effects of human exposure to these fields with the ultimate goal of basing rational exposure guidelines on hard data that relates to human beings. At microwave frequencies above a few GHz, the energy will be deposited principally in the skin of the exposed organism, a situation very similar to that occurring during exposure to infrared energy. Since we know a great deal about the variables that influence the sensory characteristics of infrared exposure, that knowledge can be applied advantageously to the design and interpretation of studies involving microwave exposure.

The temperature sense provides information to an organism about the thermal characteristics of both the external environment and of the body itself. This sense is also referred to as thermal sensation. Several early studies [Eijkman and Vendrijk, 1961; Hendler, et al., 1963; Justesen, et al., 1983] were designed to determine what intensity levels of microwave energy were required to initiate a just-detectable sensation, i.e., to stimulate a sensation of warmth. A recent study of absolute thresholds of warmth across a range of microwave frequencies [Blick, et al., 1997] appears immediately following the present paper in this Technical Report. The information provided through thermal sensation is essential to the effective regulation of the body temperature, called thermoregulation, which can be both behavioral and autonomic. Regardless of the exact spatial and temporal distribution of thermal stimuli that occur on the skin surface, thermal sensation registers "how much" stimulation is present and also "how pleasant or unpleasant" that stimulation may be. As we shall see, the thermal senses function as thermometers because they can also register "what" when warm or cold objects are touched; this information can indicate whether substances are safe to touch or ingest. Thermal sensation is essential to the avoidance of local skin damage, especially from burning, but also from freezing.

Much neurophysiological evidence [cf. Hensel, 1982] indicates that there are specialized receptors residing in the outer layers of the skin that mediate the temperature sense in humans and other mammals. These include "warm" and "cold" receptors that respond respectively to increases or decreases in the temperature of the skin. Other skin receptors include nociceptors, associated with pain, and slowly adapting (SA) fibers associated with mechanical stimulation. Several investigators have reported the existence of sensory spots on the skin surface that may relate to the location of sensory nerve endings in the

epidermal or dermal layers. When the skin is touched with very small warm and cold stimulators, some spots feel warm, others cold, and still others give rise to no thermal sensation whatever. Maps of the skin for warmth and cold, such as the example in Figure 1, show that 1) warmth and cold spots are independently distributed, 2) cold spots are far more numerous than warm spots, 3) spot density varies over the skin surface, and 4) map reproducibility is poor even when charted with great care. Further, there is no clear evidence that spots mark the location of underlying receptors or that warmth and cold are separate sense modalities. Finally, such maps imply that large areas are insensitive (especially to warmth), which is negated by thermal stimulation of larger skin areas.

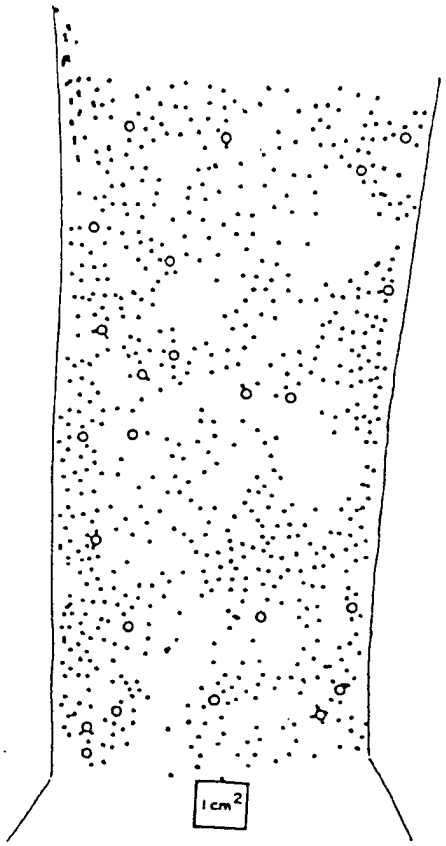

Figure 1. Cold (dots) and warm (circles) spots mapped across 100 cm^2 of the dorsal side of the right human forearm. Map redrawn from Strughold and Porz, 1931.

II. ASOLUTE THRESHOLDS AND TEMPORAL SUMMATION

One important question we can ask about any sensation concerns the minimal intensity, or power density, that is necessary to evoke a just-detectable response such as "Yes, I feel it; it is warm." This intensity is defined as the absolute threshold. For thermal sensation, the physical stimulus may be a change in skin temperature from thermal neutrality or as the radiant energy impinging on the skin. Many classical and modern psychophysical methods have been developed to measure absolute thresholds across the different sense modalities. Often the absolute threshold of a particular stimulus is measured as a function of the duration of that stimulus in order to determine the reciprocity between these two stimulus variables. The resulting function for warmth sensation of a small

stimulus area (21.8 cm^2) is shown as the lower curve in Figure 2 and gives the combinations of duration and infrared power density that produce a constant threshold [Marks and Stevens, 1973].

We can note two important features of this threshold function. First, the power density threshold depends on stimulus duration almost by a complete reciprocity up to a duration of 1 second. This phenomenon is called temporal summation and most of the human senses have been found to exhibit this psychophysical property. The duration at which this reciprocity comes to an end is called the critical duration, after which duration no longer matters. A comparison of these infrared threshold data with similar threshold data for 10-cm microwaves [Eijkman and Vendrik, 1961] shows that the critical duration is probably longer (about 2.5 seconds) for microwaves. Whether this difference in critical duration varies systematically with frequency is unknown and awaits further research. experimentation. But it is clear that the absolute threshold of warmth depends almost as much on how long the stimulus lasts as how intense it is.

It is also of interest to explore how the magnitude of a supra-threshold sensation varies, not only with the intensity but also with other variables. It turns out that for infrared stimuli the rules of temporal summation change as the level of warmth sensation becomes greater. The six upper functions in Figure 2 illustrate this effect. To obtain these functions, arrays of different stimuli were presented to subjects who judged the perceived warmth of each stimulus by the method of magnitude estimation. In this procedure, the subject is asked to assign a number to each stimulus in proportion to its judged magnitude. For example, a stimulus judged twice as warm as a stimulus assigned the number 5 should be assigned the number 10, and so on. Each of the upper functions

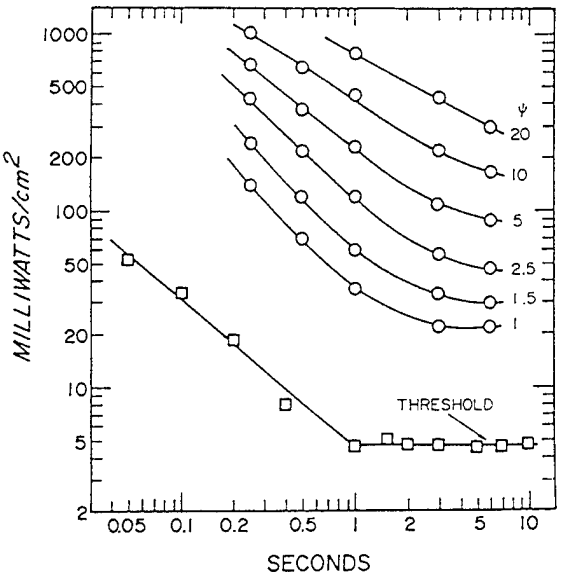

Figure 2. Combinations of infrared power density (mW/cm^2) and duration (seconds) that produce threshold warmth and six constant warmth functions that vary from weak to moderate. (Data of Marks and Stevens, 1973)

in Figure 2 represents the combinations of intensity and duration that cause a particular constant warmth magnitude (Ψ) that ranges from 1 to 20. These functions have a less steep slope as warmth level increases, indicating that duration counts less and less than power density. At the same time, the duration over which temporal summation occurs becomes longer and longer (up to 6 seconds) as magnitude increases. Marks and Stevens [1973] pointed out that this fundamental effect could be explained in terms of the heat transfer properties of the skin.

III. SPATIAL SUMMATION OF WARMTH FOR INFRARED STIMULI

Another variable that influences warmth sensation dramatically is the areal extent of the skin stimulated. In this case, stimulus duration is held constant and the functional relationship between areal extent and intensity are determined for specific threshold or supra-threshold sensations. In general, when an area of irradiated skin is made larger the sensation induced is that of greater warmth, not of increased apparent area. This phenomenon is known as spatial summation. Trading of area for intensity varies from almost complete reciprocity at the absolute threshold to no trading at all near the threshold of thermal pain. Figure 3 shows some examples of how the absolute threshold of warmth for 3-second infrared stimuli varies with the area stimulated. The two lower curves are thresholds for individual subjects, while the upper curve is the geometric mean

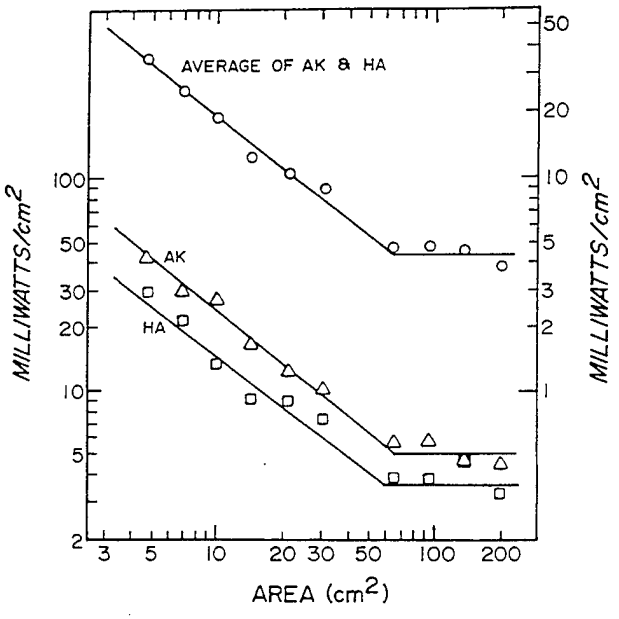

Figure 3. Spatial summation of the warmth threshold for two subjects stimulated with different areas on the skin of the back (lower two curves) and the geometric mean of these data (upper curve, right ordinate). The duration was 3 seconds. (Data reproduced from Stevens, Marks and Simonson, 1974)

function for those two subjects. Clearly there is complete reciprocity between areal extent and power density at threshold up to a critical area of ~60 cm^2, after which area no longer matters. In other words, below the critical area, when the area is doubled the intensity may be approximately halved to preserve the absolute threshold. Above this critical area, spatial summation no longer occurs and the threshold depends on intensity alone. The area stimulated for the functions in Figure 3 was the back; it is not clear that the critical area would be the same for stimulation of other bodily regions.

At levels above the absolute threshold, the area of skin stimulated can influence the magnitude of warmth sensation in interesting ways. If one selects a particular stimulus area and a constant stimulus duration for study, irradiated subjects can use the method of magnitude estimation to judge the magnitude of the warmth sensation produced by different power densities. The psychophysical functions of sensation magnitude versus power density thus produced are power functions, which are rectified when plotted in log-log coordinates. In a landmark study, Stevens, et al. [1974] presented various intensities of infrared radiation to 6 different skin areas (range = 4.7 to 200 cm^2) on the back. Subjects were instructed to assign numbers to represent the apparent magnitude of each warmth sensation experienced during 3-second exposures. In general, the subjects reported that they were unaware that the area of stimulation varied. The resulting data from this study are reproduced in Figure 4, which shows how warmth grows as a function

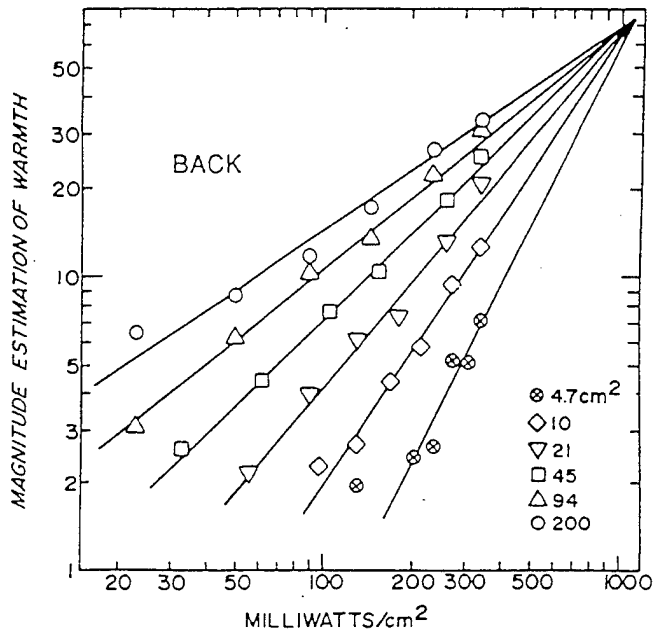

Figure 4. A family of psychophysical functions for subjective warmth as a function of power density (at 6 different areas and a constant duration of 3 seconds). The stimulus was infrared irradiation of the back skin. Extrapolations of the functions intersect at the threshold of pain. (Data of Stevens, Marks and Simonson, 1974)

of power density for each areal extent explored. Several conclusions may be drawn from these data: 1) the functions are approximately linear in log-log coordinates and thus obey the power law of S.S. Stevens [1961]; 2) the slope of the function is greatest for small

stimulus areas and decreases as area becomes larger; 3) for any given power density, the larger the area the greater the warmth sensation; and 4) the functions converge at a high intensity of ~ 1000 mW/cm^2, which approximates the threshold of pain. This latter conclusion is extremely interesting and reinforces the basic fact that thermal pain does not exhibit spatial summation at threshold [Green and Hardy, 1958]. It is fairly certain that the convergence point will depend on the stimulus duration as well as the part of the body stimulated. However, studies such as this have allowed Stevens [1991] to formulate a general principle of thermal sensibility, namely that rich spatial summation always occurs near the warmth threshold but declines gradually to zero summation at the threshold of pain. Thus, the warmth sense functions to allow a compromise between two basic biological needs: 1) the necessary assessment of weak heating over large segments of the body as an aid to thermoregulation, and 2) the sharpening of acuity or localization of strong thermal stimuli to increase the probability of avoiding injury.

IV. REGIONAL SENSITIVITY OF WARMTH TO INFRARED STIMULATION

It has been known for a long time that certain body sites are much more sensitive to thermal stimulation than are others. The early data, consisting of spot mapping, assorted thresholds, etc., were insufficient to allow generalization and quantification of the phenomenon. Recent studies of regional sensitivity to warmth have employed the method of magnitude estimation and other scaling techniques that provide a more comprehensive and functional assessment. Stevens et al. [1974] generated psychophysical functions for graded sets of supra-threshold warmth stimuli applied to

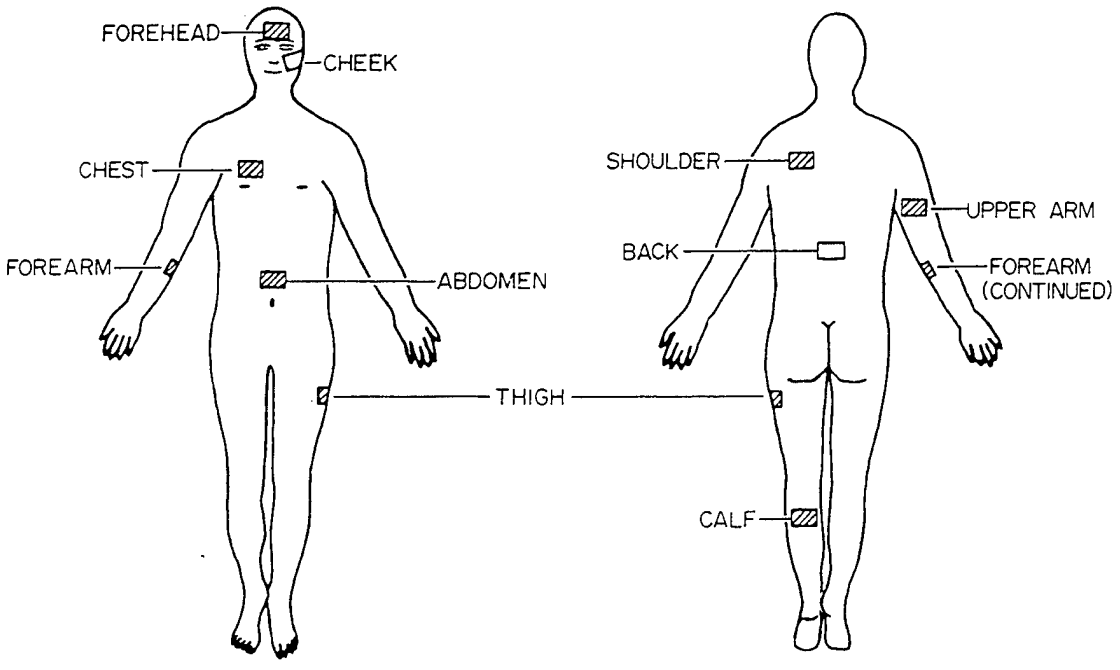

Figure 5. The 10 body sites explored for thermal sensitivity by Stevens, Marks and Simonson (1974)

each of 10 sites on the body, depicted in Figure 5. Although many combinations of areal extent and power density were explored in several experiments, a particular area (22 cm^2) was common to all 10 sites and was used to compare regional sensitivity across the body surface. For each site, a psychophysical function relating estimated warmth to power density for 3-second infrared stimuli was determined for a group of subjects. These functions were then plotted together in log-log coordinates and the array appeared somewhat fan-shaped, like the functions in Figure 4. It was then possible to estimate the power density that produced the same level of warmth sensation across all sites. In practice, this involved making horizontal cuts across the array of functions at specific warmth levels.

Figure 6 shows the resulting set of "equal warmth" contours for the 10 body sites, which are arranged from most sensitive (forehead) to least sensitive (calf). The 6 levels of warmth sensation range from weak (close to absolute threshold) to strong (close to the pain threshold). At the lowest warmth level, the 10 regions differ significantly in sensitivity, with head regions more sensitive than trunk regions, which are in turn more sensitive than the extremities. The figure also shows that the contours become flatter as warmth becomes stronger until, close to the threshold of pain, all regions have a similar thermal sensitivity.

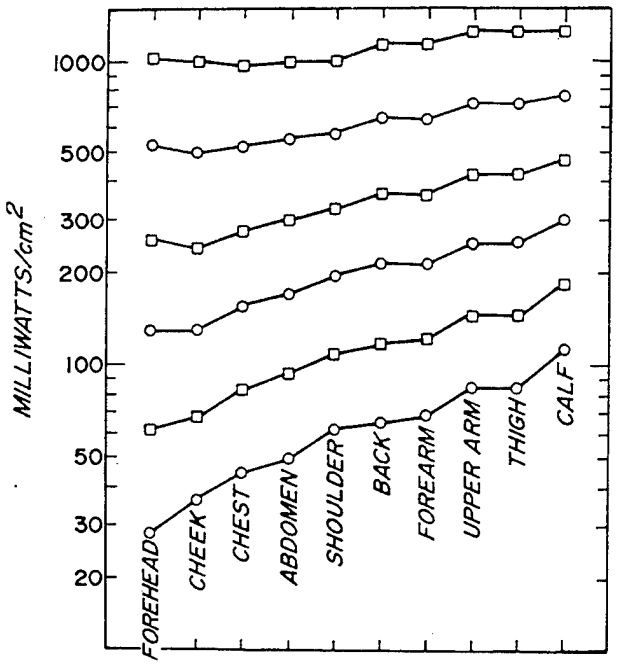

Figure 6. The infrared power density required to produce the same levels of warmth sensation at 10 sites across the human skin. Stimulus area was constant at 22 cm^2 and duration of stimulation was 3 seconds. As the level of warmth increases, the contours flatten out. (Data of Stevens, Marks and Simonson, 1974).

It should be noted that the contours presented in Figure 6 apply only to a stimulus area of 22 cm^2 and a brief stimulus duration of 3 seconds. Other areas and durations would

undoubtedly produce different set of contours but might not alter the relative sensitivity of the different body regions, especially close to threshold.

V. CONCLUSIONS

The above description of some of the parameters that influence the perception of cutaneous warmth aroused by infrared irradiation is meant only as an introduction to the subject. Many other factors such as age, sex, fitness, and body dimensions will also play complex roles in thermal sensitivity, as will adaptation, which occurs over longer periods of stimulation. The paper is intended only as a guide to some of the most relevant parameters that may influence comparable warmth perception in the presence of microwave irradiation of the skin, especially at millimeter wave frequencies. Several general conclusions may well apply to warmth sensations aroused by millimeter waves. These are as follows:

- For warmth sensation derived from near and far infrared stimuli, an absolute threshold of sensation can be determined.
- Both temporal and spatial summation characterize the absolute threshold of warmth.
- Threshold and supra-threshold warmth sensation varies in orderly fashion with power density, areal extent, and duration of stimulation.
- Warmth grows as a power function of intensity, at a rate that depends on stimulus area and/or duration. Warmth functions converge at the threshold of pain at which there is a lack of spatial summation.
- Different body regions vary in their sensitivity to warmth, with the face being the most sensitive and the limbs the least sensitive.

VI. ACKNOWLEDGMENTS AND DISCLAIMER

The author is greatly indebted to her valued colleague, Dr. Joseph C. Stevens for much of the material included in this paper and for his permission to reproduce several figures from his published works. The views expressed in this paper are those of Dr. Stevens and the author and are not to be construed as official policy of the United States Air Force or of the Department of Defense.

VII. REFERENCES

Blick, D.W., Adair, E.R., Hurt, W.D, Sherry, C.J., Walters, T.J. and Merritt, J.H. (1997) Thresholds of microwave-evoked warmth sensations in human skin. *Bioelectromagnetics* 18:403-409.

Eijkman, E.G. and Vendrik, A.J.H. (1961) Dynamic behavior of the warmth sense organ. *J. Exp. Psychol.* 62:403-408.

Green, L.C. and Hardy, J.D. (1958) Spatial summation of pain. *J. Applied Physiol.* 13:457-464.

Hardy, J.D., Wolff, H.G. and Goodell, H. (1952) *Pain Sensations and Reactions.* Baltimore: Williams and Wilkins.

Hendler, E., Hardy, J.D., and Murgatroyd, D. (1963) Skin heating and temperature sensation produced by infrared and microwave irradiation. In: *Temperature: It's Measurement and Control in Science and Industry.* (J.D. Hardy, Ed.) New York: Reinhold, Pp 211-230.

Hensel, H. (1982) *Thermal Sensations and Thermoreceptors in Man.* Springfield, IL: Chas. C. Thomas.

Justesen, D.R., Adair, E.R., Stevens, J.C. and Bruce-Wolfe, V. (1982) A comparative study of human sensory thresholds: 2450-MHz versus far-infrared radiation. *Bioelectromagnetics* 3:117-125.

Marks, L.E. and Stevens, J.C. (1973) Spatial summation of warmth: Influence of duration and configuration of the stimulus. *Am. J. of Psychol.* 86:251-267.

Stevens, J.C. (1991) Thermal sensibility. In: *The Psychology of Touch.* (M.A. Heller and W. Schiff, Eds.) Hillsdale, NJ: Lawrence Erlbaum, Pp.61-90.

Stevens, J.C., Marks, L.E. and Simonson, D.C. (1974) Regional sensitivity and spatial summation in the warmth sense. *Physiology and Behavior* 13:825-836.

Stevens, S.S. (1961) The psychophysics of sensory function. In: *Sensory Communication.* (W.A. Rosenblith, Ed.) New York: Wiley & Sons, Pp. 1-33.

Strughold, H. and Porz, R. (1931) Die Dichte der Kaltpunkte auf der Haut des menschlichen Korpers. *Zeitschrift fur Biologie* 91:563-571.

Bioelectromagnetics 18:403–409 (1997)

Thresholds of Microwave-Evoked Warmth Sensations in Human Skin

Dennis W. Blick,[1]* Eleanor R. Adair,[2] William D. Hurt,[3] Clifford J. Sherry,[1] Thomas J. Walters,[1] and James H. Merritt[3]

[1]Systems Research Laboratories, Inc., Brooks AFB, Texas
[2]John B. Pierce Laboratory, New Haven, Connecticut
[3]USAF Armstrong Laboratory, Brooks AFB, Texas

We measured thresholds for microwave-evoked skin sensations of warmth at frequencies of 2.45, 7.5, 10, 35, and 94 GHz. In the same subjects, thresholds of warmth evoked by infrared radiation (IR) were also measured for comparison. Detection thresholds were measured on the skin in the middle of the back in 15 adult male human subjects at all microwave (MW) frequencies and with IR. Long duration (10-s), large area (327-cm^2) stimuli were used to minimize any differential effects of temporal or spatial summation. Sensitivity increased monotonically with frequency throughout the range of microwave frequencies tested. The threshold at 94 GHz (4.5 ± 0.6 mW/cm^2) was more than an order of magnitude less than at 2.45 GHz (63.1 ± 6.7 mW/cm^2), and it was comparable to the threshold for IR (5.34 ± 1.07 mW/cm^2). *Bioelectromagnetics 18:403–409, 1997.*

Key words: warmth threshold; psychophysics; infrared; microwaves; skin sensation

INTRODUCTION

The sensations evoked by electromagnetic radiation with wavelengths in the millimeter to meter range, i.e., microwaves (MW), are of interest from both practical and scientific standpoints. From the practical standpoint, the recent proliferation of industrial and military devices capable of generating strong MW fields in the vicinity of human operators raises numerous safety issues. It would be useful to know, over the wide range of frequencies used in various devices, at what field intensity the MW field becomes perceptible and how these detection thresholds relate to safety standards that govern permissible exposures.

Many researchers have addressed these questions [Stevens, 1983; Vendrik and Vos, 1958; Osepchuk, 1983; Justesen, 1988; Justesen et al. 1982; Michaelson, 1972; Hendler, 1968]. However, experiments measuring detection thresholds in human subjects are relatively few; they were conducted 10 to 35 years ago and were not standardized with regard to such important independent variables as field characteristics (frequency, polarization, mode, etc.), exposure duration, and areal extent or locus of stimulus application. The existing data, covering a frequency range from 2.45 to 10.0 GHz, indicate that skin sensitivity to MW radiation increases with frequency. The proportion of the MW energy that is deposited superficially, at or near the skin receptors that respond to warmth, also increases with frequency. It is therefore reasonable to expect that higher frequencies would be more efficient at stimulating these receptors. Low frequencies, on the other hand, may be so inefficient in stimulating the skin that dangerous quantities may be absorbed before any basis for an avoidance response is perceptible [Justesen, 1988].

Our study extended the MW frequency range for which human detection threshold data were available by comparing sensitivity to five different MW frequencies in the same group of observers. A standardized exposure protocol was used for all frequencies, including infrared (IR). Based on his review of the literature on warmth sensations evoked in the skin by IR, Stevens [1983] pointed out that the stimulus determinants of the warmth sensation are complex. The detection threshold depends not only on power density, but also on the duration, areal extent, and bodily locus of stimulation. For comparisons of sensitivity across a wide range of frequencies to be valid, it is important that the exposure

*Correspondence to: Dennis W. Blick, Ph.D., Systems Research Laboratories, Inc., P.O. Box 35313, Brooks AFB, TX 78235. E-mail: blick@rfr.brooks.af.mil

Received for review 5 November 1996; revision received 30 December 1996

protocol minimize the risk of interactions between stimulus frequency and other stimulus parameters, such as duration, area, and bodily locus of stimulation.

The temporal resolution of the sensory system for pure sensations of warmth evoked by IR (or presumably by MW) is rather limited, i.e., very brief exposures and rapid or small fluctuations in incident energy tend not to be detected. As a result, duration and intensity can trade off for one another over a substantial range to reach the detection threshold. When stimulus duration is shorter than some "critical duration," which for IR may be as long as a second or more [Stevens, 1983], there is a reciprocal relationship between the power density and the duration of a stimulus that just reaches the threshold for warmth detection. For durations shorter than the critical duration, "temporal summation" is said to occur. At the critical duration, the threshold power density reaches an asymptotically low level that is constant for longer durations. Eijkman and Vendrik [1961] showed that the critical duration for 3.0 GHz MW stimulation on the forearm was about 3 s. Because differences in critical duration as a function of wavelength could contaminate sensitivity comparisons, we chose a stimulus duration (10 s) for these experiments that was longer than any expected critical duration.

The warmth sense is also relatively insensitive to the fine spatial details of stimuli, compared with the senses of vision and touch, for example. Over fairly large areas, the details of input energy distribution (e.g., size, number, or location of stimulated spots) are indiscriminable, as long as the total energy delivered within the area is the same. This lack of spatial acuity implies extensive "spatial summation," so that the area and intensity of stimuli at the detection threshold vary reciprocally, up to some critical area. For IR, Stevens [1983] reported that the critical area may be 60 cm^2 or more, depending on bodily locus. Because the area within which summation occurs could vary with the frequency of the MW stimulus, we chose an area (327 cm^2) that should be larger than any critical area likely to be found for MW-induced warmth detection.

The middle of the back was selected as a stimulus locus where we could stimulate such a large area of relatively homogenous skin. Warmth sensitivity at this site is near the middle of the range for different body sites. Stevens et al. [1974] examined warmth sensitivity to IR at 10 different sites, and found that facial areas were the most sensitive, followed by sites on the trunk, whereas areas on the limbs were among the least sensitive.

METHODS

Subjects

The subjects were 15 male Caucasian volunteers (age, 45.2 ± 6.0 years; height, 182.3 ± 5.6 cm; weight, 83.9 ± 11.1 kg.). All were employed at Brooks AFB, as military or civilian Department of Defense personnel or contractors. Written informed consent was obtained from each subject before testing began. Each subject was tested at all frequencies. The use of human subjects in this research was in accordance with a protocol approved by the institutional committee on human use (Armstrong Laboratory Advisory Committee on Human Experimentation), and by the Office of the Surgeon General of the Air Force.

Stimulus Sources and Calibration

Separate transmitters were used to generate MW at frequencies of 2.45, 7.5, 10.0, 35, and 94 GHz. For each transmitter/antenna combination, subjects were exposed in the E orientation (long axis of subject parallel to E-vector of electromagnetic field) in the far field of the antenna. Field intensities (mW/cm^2) were measured and averaged for 25 locations in the area stimulated (327 cm^2); we used Narda probes calibrated for each transmitter frequency to derive a conversion factor ($mW/cm^2/W_{fwd.pwr.}$) for each testing situation. The characteristics of each transmitter, and the probes and meters used for dosimetry with each, are summarized in Table 1.

The source of IR stimulation consisted of two, T-3 quartz lamps (40.6 cm long) mounted vertically in front of stainless steel parabolic reflectors. The lamps and reflectors were mounted on a hydraulically operated slide, which allowed the lamps to be positioned between 20 and 70 cm from the back of the subject. A hydraulically operated shutter, consisting of two parallel stainless steel plates with a 1-cm air gap between them, was interposed between the subject and the heat lamps, except during exposures. Field intensity was calibrated with a radiometer [Su and Berglund, 1987] located at the center of the exposed area. A cutoff filter (longwave pass with cutoff at 850 nm; stock #32769, Edmund Scientific, Barrington, NJ) was used to avoid contamination of the IR radiometric measurements by energy emitted from the heat lamps in the visible wavelength range.

Because the heat lamps were operated at relatively low color temperatures, it was deemed unnecessary to blacken the skin in the exposure area. Hendler and Hardy [1960] saw "no essential differences" for blackened or unblackened skin in detection thresholds to near IR on the forehead. Their stimulus contained a range of wavelengths (2 to 30 μm, peak at 5 μm, color temperature 245 °C) in which human skin acts essentially as a black body (reflectance well below 5%). In contrast, skin reflectance rises to near 70% for wavelengths in the long end (0.7 μm) of the visible spectrum [Hendler and Hardy, 1960]. The small component of

TABLE 1. Microwave Exposure and Dosimetry Apparatus

Frequency (GHz)	Transmitter model (series)	Magnetron/oscillator	Waveguide/antenna	Maximum power (W)	Narda meter/probe	Horn to subject (cm)
2.45	Cober 1326C (2743)	Litton L-3460A	Type "S" Struther 23.5 × 17.5 cm	500	8716/8725	84
7.5	Cober 1326C (2743)	Litton L-3462A	Type "X" Struther 11.7 × 9 cm	300	8716/8725	57
10	Cober 1326C (2743)	Litton L-3643A	Type "X" Struther 7.5 × 5.9 cm	250	8716/8725	72
35	Applied Electromagnetics, Inc.	Varian VKQ2420L2 GEO[a]	WR-22, Applied Electromagnetics, Inc. 7 × 5 cm	70	8616/8623D	200
94	Applied Electromagnetics, Inc.	Varian VKB2426L2 GEO[a]	WR-8, Applied Electromagnetics, Inc. conical, 3 cm	50	8616/8623D	200

[a]GEO, gridded extended oscillator.

our lamps' output in the visible wavelengths (less than 1% at the lowest lamp voltage to at most 3–5% at the highest voltage) would thus cause the threshold to be underestimated by at most 1–2% in the least sensitive subjects and by far less than 1% in the most sensitive subjects.

Calibration of the IR stimulus was achieved in the following manner: First, a variable transformer was set at the lowest lamp voltage that would produce 30 mW/cm^2 at the radiometer with the lamps in the closest position. Then, lamp position settings were determined that would produce 2 mW/cm^2 steps down from the maximum at this voltage. When the range of movement was exhausted, the lamps were again moved to the nearest position, and a lower voltage was selected to provide an irradiance of 20 mW/cm^2. A set of position settings was then determined for 1 mW/cm^2 downward steps at this voltage. Finally, with the lamps at the most distant position, the voltage was set to produce 1 mW/cm^2 at the radiometer, and positions for 1 mW/cm^2 steps up from this irradiance were determined. With three lamp voltages and the various lamp positionings, we could present IR stimuli to the subjects' backs varying from 0 to 20 mW/cm^2 in 1 mW/cm^2 steps, or from 0 to 30 mW/cm^2 in 2 mW/cm^2 steps. The highest lamp voltage used was less than 50% of the rated voltage for the lamps; only a few subjects required stimuli intense enough for this voltage to be used.

Psychophysical Technique

A modified staircase procedure [Simpson, 1989; Cornsweet, 1962] was used to determine the threshold for the detection of a warmth sensation at each frequency tested. At each frequency, a set of 20 equally spaced stimulus-intensity levels was selected, so that the lowest intensity was below threshold for the most sensitive subject and the highest was above threshold for the least sensitive. The stimulus intensity presented on each trial was selected randomly from one of two concurrently operating step series of stimuli. This procedure made the intensity of the next stimulus unpredictable to the subject.

The step method [Simpson, 1989] is a variant of older, adaptive staircase methods. It is an efficient means to determine sensory threshold values, because it concentrates stimulus presentations in the region of the threshold so that each presentation (after a brief initial period of "homing in") provides maximal information regarding the threshold. Within each step series, the stimulus level in each trial depended on the responses in previous trials. At a given stimulus level, two consecutive "yes" responses (indicating that the subject felt warming from the exposure in that trial)

produced a reduction in intensity for the next presentation from that series. A "no" response (the subject did not detect warming) produced an increase of intensity in the next trial.

Within 30 trials, the two series of steps tended to converge on a stimulus level that evoked "yes" responses two-thirds of the time. When the responses from the two series were combined, the relative frequency of "yes" responses increased monotonically with intensity, and the 66.7% "yes" point was readily determined by linear interpolation between the two intensities that bracketed this point. The interpolated value was recorded as the threshold for that subject at that stimulus frequency. Due to the statistical nature of the process, this threshold value corresponds to the 70.7% probability of a "yes" response on a standard psychometric function [Wetherill and Levitt, 1965]. Whereas this procedure would yield slightly higher threshold estimates than those based on a 50% "yes" criterion, the objective of comparing sensitivity across frequencies is unaffected, because the criterion was uniform across frequencies. Although a more rigorous, forced-choice psychophysical procedure might have reduced subject-to-subject variability in thresholds introduced by individual response biases, there was no reason to expect that subjects' response biases would vary systematically with stimulus frequency. Because the main concern was variation in threshold as a function of frequency, the more time-efficient method was adopted to reduce the demands made on the time of the subjects.

Procedures

Each subject was asked to strip to the waist and remove metallic items (belt buckles, jewelry, and pocket contents). The subject was then seated in a small (approximately 90 × 90 × 180 cm) testing chamber that was constructed from sheets of polystyrene foam 5 cm thick. This chamber was placed within a larger anechoic chamber. The subject's back was exposed to MW or IR through a 20.4-cm diameter circular aperture in one wall of the test chamber; the center of the aperture was located on the antenna boresight. An air-conditioning unit circulated air through the subject's chamber at a temperature of 23 ± 0.5 °C. Ambient temperature outside the test chamber was maintained at 23 ± 1.5 °C. The inside surface of the test chamber, against which each subject's bare back was placed, was in the far field of the transmitter antenna in a plane normal to the boresight.

Exposures of 10-s duration occurred at 1-min intervals. After each exposure, the subject was required to give a yes-or-no decision regarding detection of a stimulus. A 1-s warning tone occurred 4–6 s before each exposure. A light signaled the presence of a microwave or IR exposure (except on "catch" trials, when there was no energy output from the stimulus source). A microwave-absorbent shutter was interposed between the subject and the antenna between exposures. A few seconds before the beginning of each trial, a warning tone was sounded, and the transmitter output was turned on and adjusted to the level required by the staircase procedure. When the selected power level was achieved, the shutter was opened, and the signal light visible to the subject was turned on. On trials in which the subject said "yes" before the end of the trial, exposure was discontinued immediately. Otherwise, transmitter power was turned off and the shutter was closed after 10 s of exposure. No record was kept of the latency or frequency of early "yes" responses.

The subject was visible and audible to the experimenters throughout all experimental sessions via a video monitor and intercom. Frequencies were tested in the same order for all but one subject: 2.45, 10, 35, 94, and 7.5 GHz, followed by IR. One subject was unavailable when the other subjects were tested at 7.5 GHz. On his return, he was tested with IR before being tested at 7.5 GHz. Seven of the subjects were tested at 94 GHz in a preliminary experiment. When they were retested, the results of the two tests were comparable, indicating that little or no carryover or practice effects were present to distort the results.

RESULTS

The thresholds at all MW frequencies and IR are presented in Table 2, along with depth of energy deposition (depth at which incident power density decreases by a factor of 1/e) and the wavelength values corresponding to each frequency. The threshold and skin depth values are illustrated graphically in Fig 1. The threshold data are well fitted by a linear regression between log threshold and log frequency ($r^2 = 0.978$). Depth of energy deposition is similarly well fitted by a line ($r^2 = 0.979$), but its slope in log-log coordinates (-1.22) is different from the slope of the threshold data (-0.69). Sensitivity (the inverse of threshold) increased by more than an order of magnitude as frequency increased from 2450 MHz to 94 GHz. Although the threshold at 94 GHz was slightly lower than the IR threshold, this difference was not significant.

DISCUSSION

Our findings are generally consistent with those reported by earlier investigators. For example, Hendler [1968] reported the following comparison of MW and

TABLE 2. Dermal Warmth Detection Thresholds as a Function of Frequency

Frequency (GHz)	Threshold (mW/cm^2) (mean ± s.e.m.)	Tissue penetration[a] ($1/e^2$ depth, mm)	Wavelength (mm)
2.45	63.1 ± 6.7	32	122
7.5	19.5 ± 2.9	6.3	40
10	19.6 ± 2.9	3.9	30
35	8.8 ± 1.3	0.8	8.6
94	4.5 ± 0.6	0.4	3.2
$1-3 \times 10^5$	5.34 ± 1.1	<0.1	ca. 0.002

[a]Skin depth (δ) is given by: $\delta = (67.52/f)[\sqrt{(\varepsilon')^2 + (\varepsilon'')^2} - \varepsilon']^{-1/2}$, where f is frequency in GHz, ε' and ε'' are the real and imaginary part of the relative permittivity, respectively. (Durney et al., 1986). Relative permittivity (ε^*) of skin is given (Hurt, 1996) by:
$\varepsilon^* = \varepsilon' - i\varepsilon'' = 4.3 - 3.19if + 105/(1 + if/.05) + 32/(1 + if/20)$.

IR thresholds on the forehead: threshold at 3 GHz = 33.5 mW/cm^2; at 10 GHz, 12.6 mW/cm^2; and at IR, 4.2 mW/cm^2. Although these values are somewhat lower than ours, the trend over frequencies is very similar. Others [e.g., Kenshalo et al., 1967] have found that the back is about 2 dB less sensitive than the forearm and that the forehead is among the most sensitive areas. Thus, the differences between our findings and Hendler's may simply reflect the regional differences in sensitivity. Justesen et al. [1982] reported that the threshold at 2.4 GHz is about 15 times the threshold for IR on the forearm. This finding is quite comparable to our finding for the back. Hendler et al. [1963] found that the threshold at 10 GHz was only about twice as great as that of IR, whereas we found it to be nearly four times as great. Hendler and his colleagues tested a 37-cm^2 area on the forehead, so it is unclear whether this discrepancy arises from differences between the back and forehead, from differences in the methods used to measure threshold, or from a possible confounding due to variation in spatial summation as a function of frequency on the forehead.

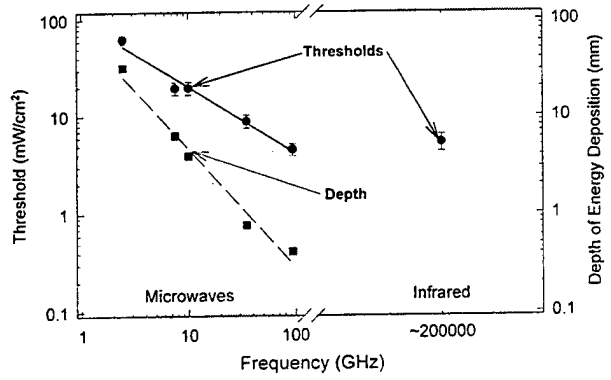

Fig. 1. Detection threshold and penetration depth as a function of MW frequency. Threshold for IR is shown to the right for comparison.

Warmth thresholds in the millimeter-wave range of MW wavelengths (frequencies beyond 30 GHz) have not been reported previously. The finding that warmth sensitivity to millimeter-wave MW is similar to the sensitivity for IR, the natural stimulus for this sensation, has not previously been reported. Although our finding is that thresholds for 94 GHz and IR do not differ significantly, it is possible that future work directed at this specific comparison may find a significant difference in either direction.

There were two minor sources of uncertainty involved in this comparison in the present experiment. First, because the thresholds are expressed in terms of incident energy, the value for the millimeter-waves may be slightly inflated relative to IR, as more of the incident MW energy is probably reflected (about 35% of MW [Gandhi and Riazi, 1986] compared with <5% of IR [Hendler and Hardy, 1960]). Second, the spatial distribution of the incident energy differed between IR and MW in our experiment. The large heat lamps provided an essentially homogenous radiation field over the whole exposure area, whereas the milliter-wave fields were characterized by a peak at the center of the exposed area, with field intensities falling off by about 2 dB near the edges. The effective stimulus area for millimeter-waves (the critical area for complete spatial summation) was undoubtedly smaller than the entire area stimulated, so our use of the average irradiance over the whole area would have somewhat underrepresented the field intensity in the effective stimulus area. That is, the average power density in the critical area in which spatial summation contributed to the threshold was somewhat higher than the average over the whole area stimulated. However, the potential biasing effects of differences in reflectivity and inhomogeneity of the stimulus fields acted in opposite directions, so their net effect should have been small. Less of the incident millmeter-wave power than of the incident IR is absorbed, so it appears that the threshold for 94

GHz may actually be smaller than for IR, in terms of absorbed power.

If future work directed at a precise comparison between IR and millimeter wavelength MW should find a small difference in either direction, the difference is likely to be much smaller than the difference in permissible exposure limits for the two radiation frequencies specified by the applicable safety standards [ANSI Z136.1-1993, 1993; ANSI/IEEE C95.1-1991, 1992]. For lasers with outputs in the IR range, skin exposures as high as 1 W/cm^2 are within permissible limits for exposures exceeding 10 s in duration. The maximal permissible whole-body exposure (MPE) at 94 GHz MW in uncontrolled environments (in which the exposed individual may have no knowledge of or control over the exposure) is 10 mW/cm^2, averaged over 39.8 s [ANSI/IEEE C95.1-1991, 1992]. For partial body exposures like those in our experiments, this standard is relaxed to an MPE of about 40 mW/cm^2. Given our exposure area and duration, the average subject thus received less than 3% of the MPE in a typical trial at the average detection threshold for 94GHz.

If the pain threshold is about 2 orders of magnitude greater than the detection threshold, this implies that exposure of any small area of the body at 94 GHz MW would produce pain at or near the MPE. Gandhi and Riazi [1986] have pointed out that millmeter-waves may more efficiently couple to skin under dry clothing than to bare skin. Thus, under normal exposure conditions, skin pain might be evoked at exposure levels below the MPE. Given that this safety standard includes a 50-fold safety factor, even whole-body exposure to MW in this frequency range is likely to produce sensations that would provoke escape or avoidance responses before damaging levels (as contemplated by the standard) could be reached. Relative to the IR-laser standard, the radio frequency safety standard for millimeter-wavelengths seems very conservative indeed, given that human skin is about equally sensitive to radiation in these two wavelength ranges.

At lower MW frequencies, e.g., 2.45 GHz, where the detection threshold is about 15 times higher than for millimeter-waves or IR, the situation is different. MW energy is deposited relatively deep in the tissues (see Table 2), and unless the subject has knowledge of the presence of a MW source, he or she is likely to attribute sensations of warmth to internal conditions, rather than external sources [Justesen, 1988]. Under these circumstances, appropriate avoidance responses are not likely to be evoked, even at levels of exposure that produce significant (and perhaps damaging) increases in body temperature [Justesen, 1988]. Healthy human adults have thermoregulatory resources more than adequate to counteract the energy deposited at the MPE for low MW frequencies [Adair, ER, personal communication], so the safety standard appears to provide adequate protection, even at frequencies close to resonance for the human body [Adair and Berglund, 1989].

The differences in slope between the functions relating frequency to threshold and penetration depth suggests that penetration depth alone does not explain the variation in sensitivity with frequency. Additional mechanisms related to the thermal properties of the tissue may be involved. Further work is needed to define the properties of these mechanisms.

ACKNOWLEDGMENTS

The authors greatly appreciate the technical support provided by Mr. Kevin Mylacraine, Mr. Robert Plotner, Mr. Clarence Theis, and the staff (especially TSgts. Leland Johnson and Alan Johnston) of the Sources and Measurements Branch, Radiofrequency Radiation Division, Occupational and Environmental Health Directorate, USAF Armstrong Laboratory. Our volunteer subjects displayed great dedication and cooperative spirit in the completion of these experiments. We thank Dr. J. C. Stevens for helpful comments on the manuscript. The extremely timely and helpful comments of the referees and editors are also greatly appreciated.This work was supported by the U. S. Air Force Armstrong Laboratory (Human Systems Center, Air Force Material Command) under Contract Number F33615-90-C-0604. The views expressed are those of the authors and are not to be construed as official policy of the U.S. Air Force or of the U.S. Department of Defense. Portions of this work were presented in preliminary form at the 1995 Annual Meeting of the Bioelectromagnetics Society, and at the Second Annual Michaelson Research Conference, Kalispell, Montana, August 11–15, 1995.

REFERENCES

Adair ER, Berglund LG (1989): Thermoregulatory consequences of cardiovascular impairment during NMR imaging in warm/humid environments. Magn Reson Imaging 7:25–37.

American National Standards Institute (1993): ANSI Z136.1-1993. American National Standard for Safe Use of Lasers. The Laser Institute of America, Orlando, FL, pp 1–121.

Cornsweet TN (1962): The staircase-method in psychophysics. Am J Psychol 75:485–491.

Durney CH, Massoudi H, Iskander MF (1986): Radiofrequency Radiation Dosimetry Handbook (Fourth Edition), USAFSAM-TR-85-73, USAF School of Aerospace Medicine, Brooks Air Force Base, Texas p 3.76.

Eijkman E, Vendrik AJH (1961): Dynamic behavior of the warmth sense organ. J Exp Psychol 62: 403–408.

Gandhi OP, Riazi A (1986): Absorption of millimeter waves by human

beings and its biological implications. IEEE Transactions on Microwave Theory and Techniques. MTT-34: 228–235.

Hendler E (1968): Cutaneous receptor response to microwave irradiation. In Hardy JD (ed): "Thermal Problems in Aerospace Medicine." Surry: Unwin Ltd. pp 149–161.

Hendler E, Hardy JD (1960): Infrared and microwave effects on skin heating and temperature sensation. IRE Trans Med Electron ME-7:143–152.

Hendler E, Hardy JD, Murgatroyd D (1963): Skin heating and temperature sensation produced by infrared and microwave irradiation. In Herzfeld CM (ed): "Temperature: Its Measurement and Control in Science and Industry." New York: Reinhold, p 211.

Hurt WD (1996): Radio Frequency Radiation Dosimetry Workshop: Present Status and Recommendations for Future Research, AL/OE-SR-1996-0003, USAF Armstrong Laboratory, Brooks Air Force Base, Texas, p 51.

IEEE Standards Coordinating Committee 28 on Non-Ionizing Radiation Hazards (1992): IEEE Standard for Safety Levels with Respect to Human Exposure to Radio Frequency Electromagnetic Fields, 3 kHz to 300 GHz. IEEE C95.1-1991. The Institute of Electrical and Electronics Engineers, Inc., New York.

Justesen DR, Adair ER, Stevens JC, Bruce-Wolfe V (1982): A comparative study of human sensory thresholds: 2450-MHz microwaves vs far-infrared radiation. Bioelectromagnetics 3:117–125.

Justesen DR (1988): Microwave and infrared radiations as sensory, motivational, and reinforcing stimuli. In O'Connor ME, Lovely RH (eds): "Electromagnetic Fields and Neurobehavioral Function." New York: Alan R. Liss, Inc. pp 235–264.

Kenshalo DR, Decker T, Hamilton A (1967): Spatial summation on the forehead, forearm, and back produced by radiant and conducted heat. J Comp Physiol Psychol 63:510–515.

Michaelson SM (1972): Cutaneous perception of microwaves. J Microwave Power 7:67–73.

Osepchuk JM (1983): The microwave stimulus. In Adair ER (ed): "Microwaves and Thermoregulation." New York: Academic Press, pp 33–56.

Simpson WA (1989): The step method: A new adaptive psychophysical procedure. Percept Psychophys 45:572–576.

Stevens JC (1983): Thermal sensation: Infrared and microwaves. In Adair ER (ed): "Microwaves and thermoregulation." New York: Academic Press, pp 191–201.

Stevens JC, Marks LE, Simonson DC (1974): Regional sensitivity and spatial summation in the warmth sense. Physiol Behav 13: 825–836.

Su X-H, Berglund L (1987): An uncovered reflecting and absorbing surface thermopile type radiometer. In Foster KR (ed): "Proceedings of the Thirteenth Annual Northeast Bioengineering Conference," Vol 2. New York, The Institute of Electrical and Electronics Engineers, Inc., pp 503–506.

Vendrik AJH, Vos JJ (1958): Comparison of the stimulation of the warmth sense organ by microwave and infrared. J Appl Physiol 13:435–444.

Wetherill GB, Levitt H (1965): Sequential estimation of points on a psychometric function. Br J Math Stat Psychol 18:1–10.

Can Organisms Avoid Injury From Millimeter Wave Electromagnetic Radiation?

Clifford J. Sherry
Systems Research Laboratories, 8305 Hawks Rd, San Antonio, TX 78235

The portion of the electromagnetic spectrum that is commonly called millimeter wave fits in a narrow band between the upper end of the microwave frequencies to the lower end of the infrared portion of the frequency spectrum. Unfortunately, relatively little is known about the effects of millimeter waves on biological systems. Most of the existing work deals with models; in vitro preparations; or lower organisms. Frei and his colleagues, in one of the first studies of the effects of 35 GHz on mammals, found that when skin temperature reached 43-45 °C (Tcore < 39 °C), a dramatic increase in mesenteric flow rate occurred. This was accompanied by a dramatic decrease in mean arterial blood pressure, circulatory shock, and death.

Since civilian and military applications of millimeter wave radar appears to be increasing, it is likely that humans are being and will continue to be exposed to millimeter waves. Therefore, it is important to determine if conscious organisms can "sense" the presence of millimeter waves before damage or a life threatening crisis such as those described by Frei and his colleagues can occur.

Using a now standard technique, Hardy and his colleagues found that the threshold for warmth is 0.00015 gm-cal/sec/cm^2 (millicalories) or a change in skin temperature of 0.003 °C. The amount of a stimulus that will cause a detectable difference in the degree of heat sensation is called a just noticeable difference (JND). There are approximately 90 jnd's between the threshold for warmth and the threshold for pain. It is unlikely that someone engaged in their daily activities would detect and respond to subtle changes in heat sensations. A mild pain sensation, on the other hand, would probably interrupt daily activities and cause the person to orient to the stimulus and respond to it. Hardy found that for a 3 sec exposure, the minimum pain threshold was 0.220 millicalories. Their subjects reported a sharp stab of pain, the culmination of an intense sensation of warmth, just before the termination of the 3 sec exposure. Contrary to popular belief, pain thresholds are fairly similar for humans. For example, the greatest number of people feel pain when a small area of their skin is heated to about 45°C and virtually everyone perceives pain before the temperature reaches 47°C. The upper limit was approximately 480 mcal. Above this value, burns were induced.

The 'sensor' for pain are the free nerve endings found at all of the surfaces of the body (i.e. skin and mucosa) and whose axons are either myelinated (Aδ fibers) or non-myelinated (c fibers). These two types of fibers may be responsible for the 'double pain' phenomena that occurs when intense heat is applied. These two phases are commonly called 'fast' or first and 'slow' and second pain. The 'fast' fibers are potentially located just below the epithelium (i.e. 0.25-0.50 mm), while the 'slow'.

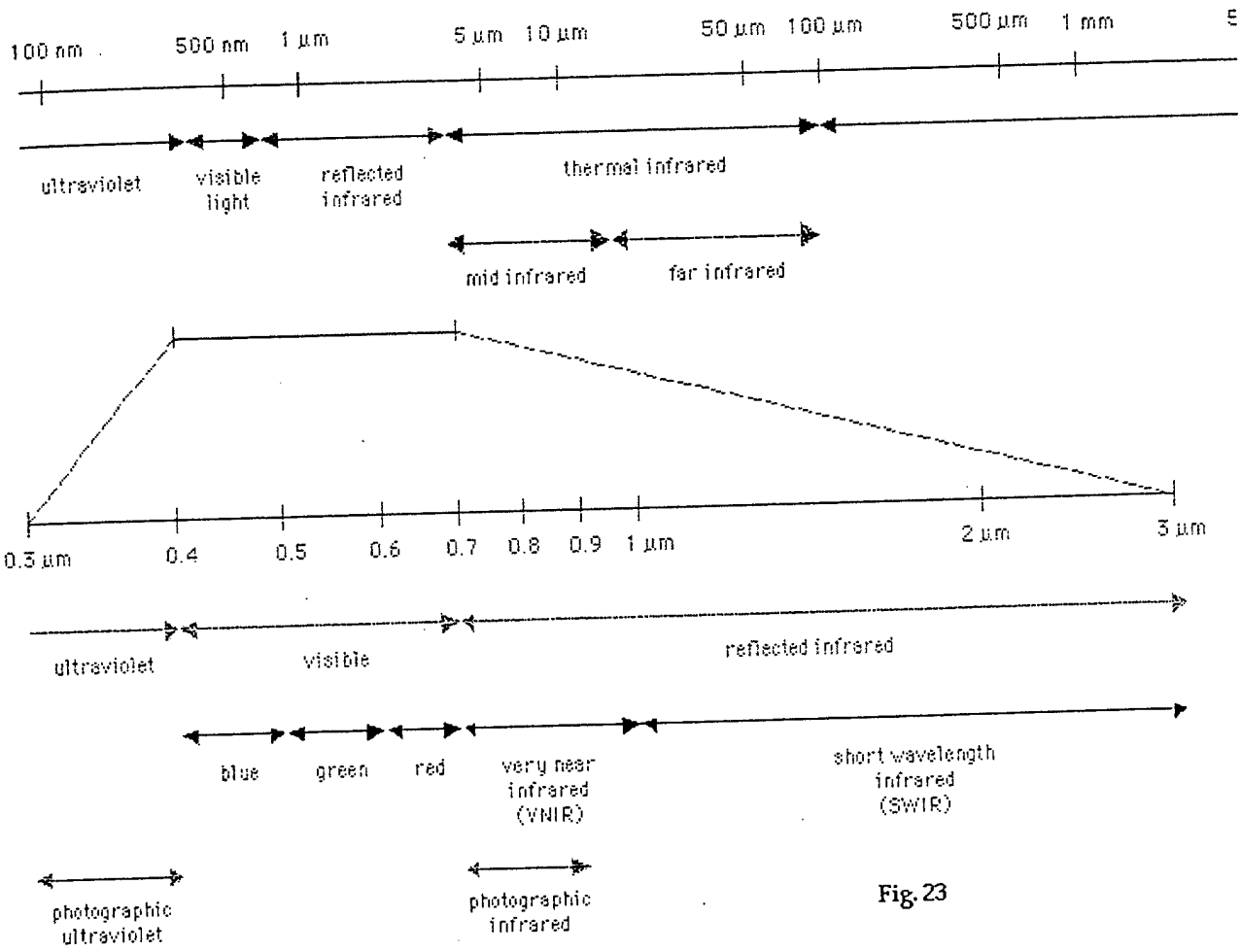

Fig. 23

32-37 °C $\Rightarrow$ 45-47 °C $\Rightarrow$ 55-60 °C

Skin Temperature $\therefore$ Pain Threshold $\therefore$ Damage

TYPE Aδ

-13-35 °C 46-50°C
-3--20 m/SEC
-MYELINATED

TYPE C

-23-46 °C
-0.5--2 m/SEC
-NON-MYELINATED

-LOW THRESHOLD
MECHANORECEPTORS
-HIGH THRESHOLD
MECHANORECEPTORS
-MECHANOTHERMAL NOCICEPTORS
-THERMAL NOCICEPTORS
-POLYMODAL NOCICEPTORS
-THERMORECEPTORS

Psychophysical Detection and Pain Ratings of Incremental Thermal Stimuli: A Comparison with Nociceptor Responses in Humans

CHARLES J. ROBINSON*, H. ERIK TOREBJÖRK** and ROBERT H. LaMOTTE

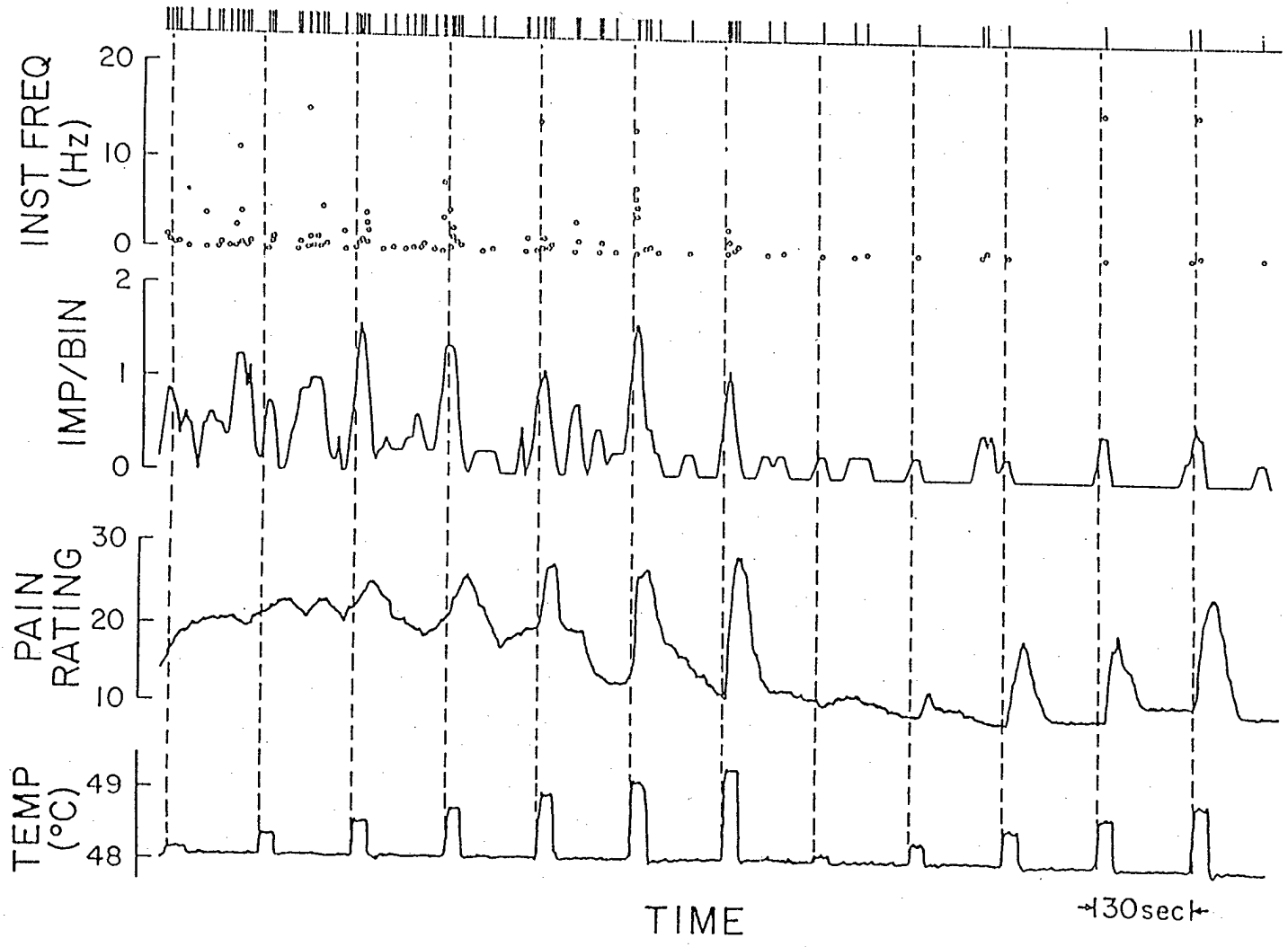

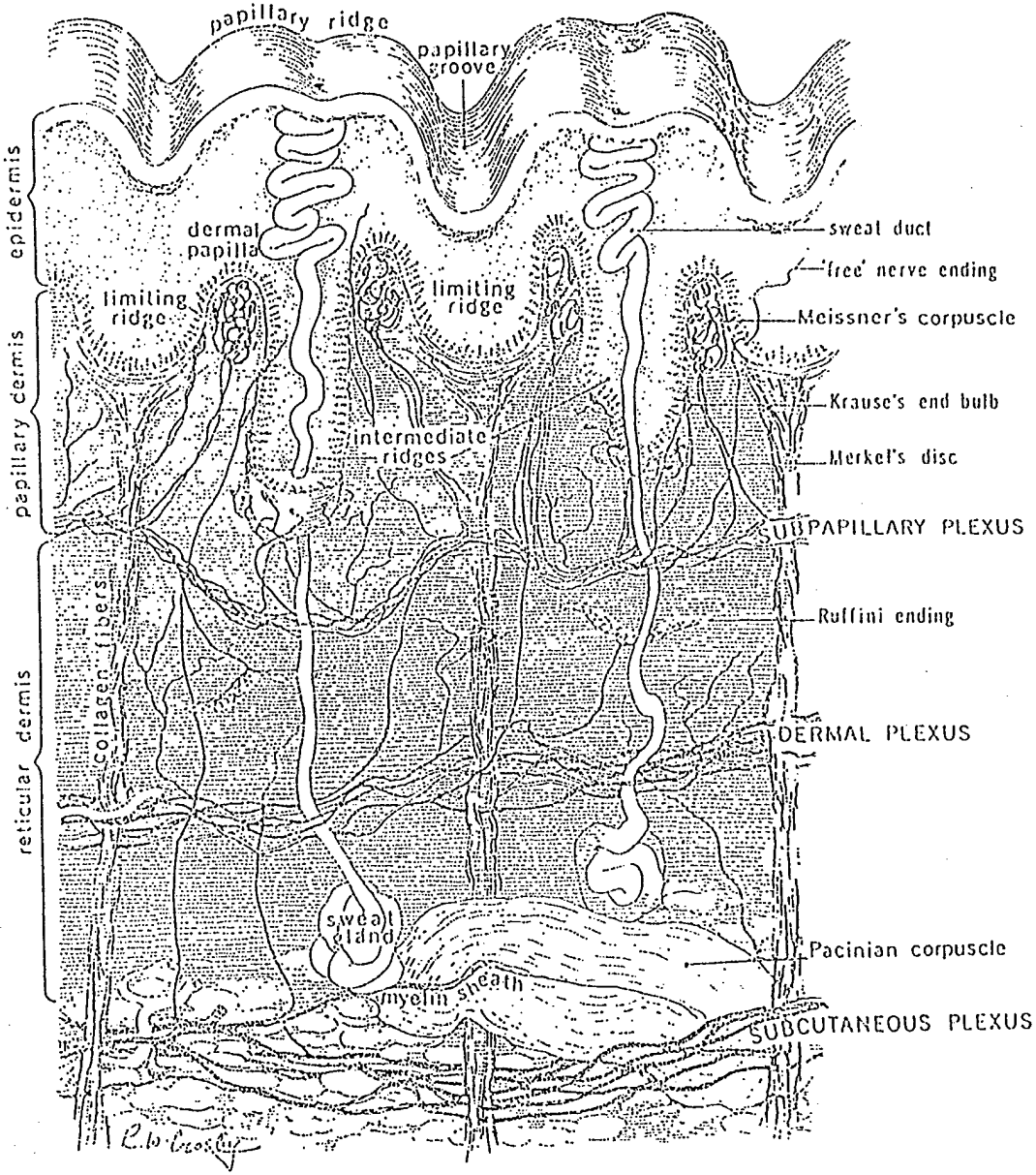
papillary ridge
papillary groove
epidermis
papillary dermis
reticular dermis
dermal papilla
limiting ridge
limiting ridge
intermediate ridges
collagen fibers
sweat duct
'free' nerve ending
Meissner's corpuscle
Krause's end bulb
Merkel's disc
SUBPAPILLARY PLEXUS
Ruffini ending
DERMAL PLEXUS
sweat gland
Pacinian corpuscle
myelin sheath
SUBCUTANEOUS PLEXUS

Influence of the Rate of Temperature Change on Thermal Thresholds in Man

ANTTI PERTOVAARA AND ILPO KOJO[1]

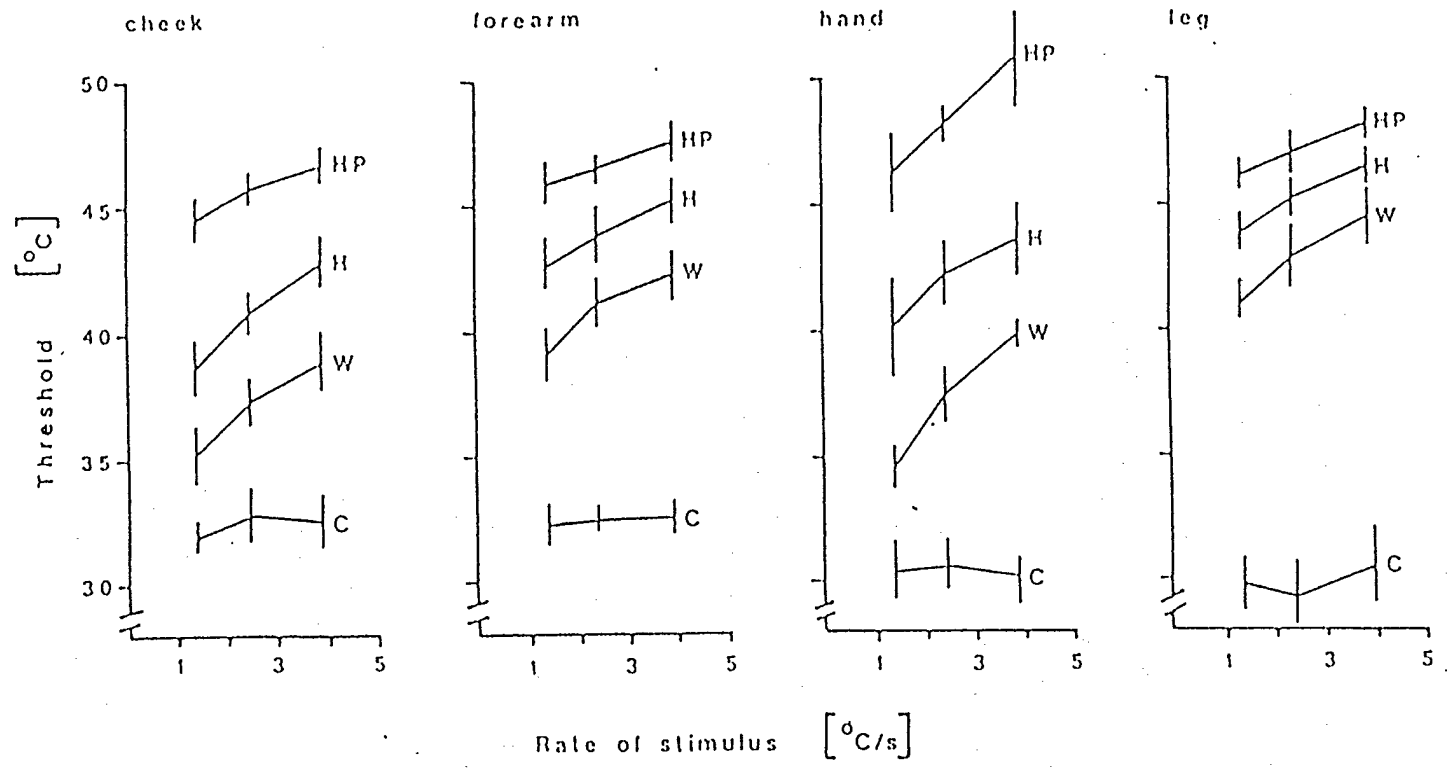

Spatial summation of heat pain: a reassessment

Ruth Defrin and Gid on Urca*

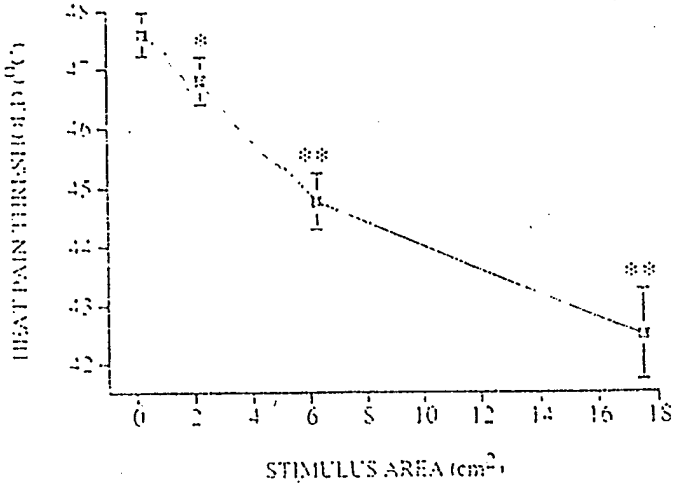

Spatial Summation of Thermal Pain in Human Beings

H. MACHET-PIETROPAOLI AND S. CHERY-CROZE

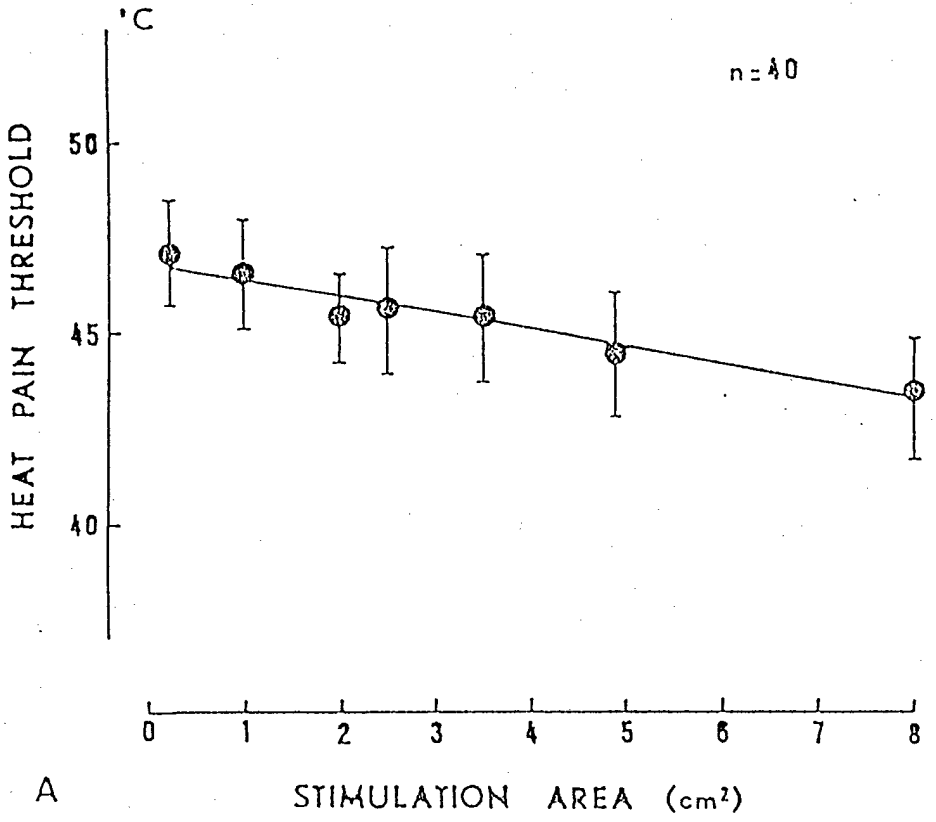

A

Ocular effects of penetrating IR laser wavelengths

J.A. Zuclich[1], D.A. Gagliano[2], F. Cheney[3], B.E. Stuck[2], H. Zwick[2], P. Edsall[1], and D.J. Lund[2]

[1]TASC, Inc., San Antonio, TX 78212-3159
[2]US Army Medical Research Detachment, Brooks AFB, TX 78235
[3]Optical Radiation Division, Armstrong Laboratory, Brooks AFB, TX 78235-5215

ABSTRACT

This study is concerned with ocular effects of laser radiation in the wavelength range from ~1.1 μm to 2.0 μm which includes the so-called "eye-safe" range where retinal and corneal damage thresholds are significantly higher than the corresponding thresholds for more common visible and far-IR lasers. Across this wavelength range, ocular safe exposure limits vary rapidly with wavelength and are up to ~6 orders of magnitude greater than exposure limits for visible wavelengths. However, recent developments in laser technology have yielded a variety of powerful near-IR laser sources. Such lasers are not "eye-safe" but, rather, may emit peak powers orders of magnitude above tissue-damaging levels.

This report focuses on the unique aspects of laser-tissue interactions for "eye-safe" wavelengths. In contrast to past experience where the laser energy is absorbed primarily in a thin layer (either at the corneal or skin surface for longer IR wavelengths or at the retinal pigment epithelium for visible wavelengths), "eye-safe" wavelengths are attenuated gradually through a volume of tissue and may affect any one or several sites within the cornea, lens, and retina. The reaction of the irradiated organism to the volumetric heating associated with such penetrating laser wavelengths does not conform with expectations of an immediate or relatively early observable lesion. Rather, the observable consequences of the laser exposure may take days to become apparent and may involve degeneration across a wider expanse of tissue than that directly irradiated by the laser. For these reasons, IR laser exposures bear close scrutiny to redefine both the usual tissue damage criteria and then the appropriate safe exposure limits.

Keywords: IR laser, eye, ocular damage, safe exposure limits, eye-safe, vision, infrared, safety standard, laser bioeffects

1. INTRODUCTION

Development in the past few years of infrared lasers with high power outputs lends promise of a spate of IR laser applications in the near future. The military communities have long been interested in IR lasers due to their high transmission through the atmosphere coupled with the relatively high exposure levels required to cause ocular damage. The concept of "eye-safe" laser rangefinders is appealing where the application may result in accidental exposure of friendly personnel. The telecommunications industry is gearing up for explosive growth in optical fiber information transmission which will likely involve IR diode lasers emitting at ~1.3 μm and ~1.55 μm, wavelengths which have excellent transmission through optical fibers. Diode lasers with respectable power at these wavelengths are now being produced. With the availability of IR lasers of desirable wavelengths, medical applications are being investigated as physicians find that they can access and treat many body tissues with the relatively high penetration depths of near-IR wavelengths.

0-8194-1738-6/95/$6.00

Against this predicted tide of IR laser applications in the near future, there is a shortfall of detailed studies of IR laser-tissue interactions and precise determination of ocular damage threshold levels. The primary objective of this study is to assess the ocular effects of laser radiation over the transition region as wavelength is varied from visible and near-IR, where the transmission of the ocular medium is high and the retina is at risk from relatively low laser power levels, to the far-IR, where the absorption of the anterior ocular components is so high as to preclude retinal damage. In the latter case, the cornea and lens of the eye are susceptible to thermal damage due to their strong absorption coefficients.

Transmission spectra of the ocular components (cornea, aqueous, lens, and vitreous) of the primate eye are plotted in Figure 1.[1] From this illustration it is seen that transmission through each ocular component (and therefore, transmission to the retina) is high for visible wavelengths and only begins to drop significantly for wavelengths > 1.1 μm where the water content of the tissues begins to absorb. By ~1.4 μm, the absorption of the ocular components is appreciable (save for the relatively thin cornea) and virtually no incident radiation is transmitted to the retina. Between ~1.15 μm and ~1.4 μm, the absorption of an incident laser beam is more evenly distributed across the ocular components and depending upon the precise exposure parameters, damage may be induced in one or more of the cornea, lens, and retina/choroid.

Because of the rapidly varying ocular absorption coefficients and the concomitant uncertainty regarding ocular damage thresholds, safety standards[2,3] for IR lasers are conservatively written and may hinder new applications. Figures 2 and 3 depict the variation in ocular damage threshold with wavelength for two pulsewidth regimes: Q-switched pulsewidths and exposure durations of ~1.0 sec, respectively. In either case, the individual data points represent retinal damage thresholds for wavelengths ≤1064 nm and corneal damage thresholds for longer wavelengths. (Figure 3 includes a corneal threshold reported for 1064 nm.[4] It is seen that this corneal threshold lies 3-4 orders of magnitude above retinal damage thresholds for the same wavelength.)

Also plotted as solid lines in Figures 2 and 3 are the maximum permissible exposure (MPE) levels defined by the ANSI Z136.1 laser safety standard.[2] There are several points to note with respect to Figures 2 and 3. First, MPE levels vary with pulsewidth as well as with wavelength, so the parametric plots of Figures 2 and 3 only depict the wavelength dependence for two pulsewidth ranges of interest. Actually, MPE is invariant to pulsewidth for pulses between 1 nsec and 18 μsec, so all threshold data obtained with Q-switched lasers have been collected in Figure 2 and plotted along with the short pulsewidth (<18 μsec) MPE. Figure 3, on the other hand, shows the MPE applicable for 1-sec exposures plotted with all available threshold data with pulsewidths within a factor of two of the nominal (1 sec) value.

The second point to note with regard to Figures 2 and 3 is that there is almost a total absence of threshold data between 1.1 μm and 1.4 μm where the MPE (and presumably the damage threshold) varies most rapidly with wavelength. (The data plotted at 1.33 μm actually resulted from Nd:YAG laser exposures with simultaneous emissions at several wavelengths clustered about 1.33 μm.[4,5]) MPE levels in this wavelength range are projections based primarily upon variation in absorption coefficients of the ocular components, which to a close approximation, reflects the water content of each tissue. However, the step changes in MPE at several wavelengths (including the step of over 3 orders of magnitude at 1.4 μm, for

short pulsewidths) and the plateaus between the step changes could hardly represent a satisfactory portrayal of variation of damage threshold with wavelength. One of the objectives of the current study is to collect sufficient ocular damage threshold data to more realistically define MPE levels for IR wavelengths.

Third, the genesis of the "eye-safe" laser concept can be seen from Figures 2 and 3. As wavelength is increased from visible into the near-IR, the absorption of the ocular medium becomes stronger and the retinal damage threshold begins to rise - gradually through ~1.1 μm and more rapidly at longer wavelengths. Similarly, as wavelength is decreased from far-IR into the near-IR, the absorption of the cornea (the only ocular tissue affected by far-IR radiation) decreases and the corneal damage threshold rises. The rising retinal and corneal damage threshold curves (as depicted in Figure 4) cross at some intermediate wavelength where the eye is the most resistive to laser-induced damage. The estimate of this crossover wavelength implied by Figure 4 is ~1.3 μm. In contrast, the ANSI standard MPE levels peak and are flat over the wavelength range of 1.4 μm to 1.8 μm. In either case, lasers emitting at or near the crossover wavelength would be the "eye-safest" lasers. Unfortunately, the use of the term "eye-safe laser" in the popular press and to a certain extent in the technical literature has been careless and reports frequently imply, without further discussion of ocular damage thresholds, that there is an "eye-safe" wavelength range where there is no hazard to the eye, regardless of the laser power level. Alternatively, and just as egregiously in error, some papers suggest that if the retina is not at risk from a particular laser, then that laser is "eye-safe," again regardless of the power level and the potential for damage to the anterior ocular tissues.

The fourth and final point to emphasize is that near the crossover wavelength discussed above, incident laser energy is partially absorbed by each ocular component and the safety standard MPE level must be governed by whichever tissue (cornea, lens, or retina/choroid) exhibits the lowest damage threshold. The work reported here presents the results of exposing ocular tissues to two wavelengths, 1.318 μm and 1.356 μm, and discusses the relative susceptibility of the individual ocular components to these wavelengths.

2. METHODS

All laser exposures were accomplished with a CW Nd:YAG laser equipped with pairs of mirrors to optimize the output at either 1.318 μm or 1.356 μm. An intracavity etalon was used to select the wavelength of interest while suppressing other Nd:YAG emission lines. The laser beam was directed through a 0.5-m scanning monochromator to a germanium photodiode to insure that each wavelength selected was free of contaminating laser emissions. CW output was stable at a maximum level of ~2 W for 1.318 μm and 1 W for 1.356 μm. An electronically controlled mechanical shutter was used to select the exposure duration, which was the variable for ocular threshold determinations. Beam profiles were determined using a 2-D laser beam analyzer.

The experimental subjects were rhesus monkeys (*Macaca mulatta*) and Dutch Belted rabbits (*Oryctolagus cuniculus*). All animals used in this study were procured, maintained, and used in accordance with the Animal Welfare Act and the "Guide for the Care and Use of Laboratory Animals" prepared by the Institute of Laboratory Animal Resources, National Research Council; and the ARVO Resolution on the

Use of Animals in Research. All experiments involving animals used appropriate levels of anesthesia so the subjects did not experience pain or distress.

Pre-exposure screening of subjects to insure clear ocular media and normal ocular tissues generally consisted of a slit-lamp examination, a fundus camera examination, fluorescein angiography, baseline photography taken while the subject was still in position at the fundus camera, and refraction to the nearest 0.25 diopter. In the case of rabbit subjects scheduled only for anterior ocular tissue exposures, the pre-exposure screening was limited to the slit-lamp and fundus camera examinations. In cases where laser-induced retinal/choroidal effects were detected or suspected, the subjects were also examined with a scanning laser ophthalmoscope (SLO). The SLO exams included fluorescein and Indo-cyanine green angiographies and were recorded on videotape.

For exposures to anterior ocular tissues, the laser beam was focussed to a 1-mm spot size at the corneal plane, and directed to the selected corneal spot at normal incidence. Beam divergence was always < 1 mrad so the beam is effectively collimated in all instances. In general, nine exposures were delivered to the cornea forming a 3 x 3 grid of exposed sites with ~2 mm between adjacent exposure sites. The grid was centered on the cornea. To insure that the IR beam was delivered to the selected corneal site, two HeNe beams of ~1-mm diameter were made to cross at the corneal plane. The spot where the two HeNe beams crossed was coincident with the passage of the IR beam through the corneal plane. Thus, positioning the cornea with regard to the 1-mm spot defined by the crossing HeNe beams, insured that the selected spot was irradiated by the IR laser.

For retinal exposures, several changes in procedure were instituted. The subjects were placed on an adjustable stage in front of a fundus camera. Laser exposures were delivered to the eye by deflecting the beam off of a sliding gold mirror mounted in front of the fundus camera and adjusted so that when the mirror was in place the deflected laser beam was collinear with the optical axis of the fundus camera. Sliding the mirror to the side allowed normal viewing of the fundus immediately before and after each laser exposure. A gold mirror was chosen because of its high reflectivity to the IR wavelengths being studied. Marker lesions were placed on the subject's retina by means of an air-cooled argon laser using 15-msec exposures to ~60 mW incident at the cornea. For rhesus subjects the marker lesions were placed outside of the pigmented macula in a grid pattern which defined the macular sites for the subsequent IR laser exposures. For rabbit subjects, the marker lesions, when used, were placed below the visual streak again to define retinal sites (also below the streak) for the IR exposures. In order to avoid, or at least minimize corneal and/or lens damage while delivering multiple exposures to the retina, the IR laser beam diameter at the corneal plane was 5 mm instead of 1 mm. The collimated beam was directed so that it passed through the dilated pupil.

Following each exposure session, lesion/no lesion determinations were made for each exposure site in each potentially affected ocular tissue. Although a 1-hr postexposure criterion is standard when reading eyes for laser-induced thermal damage, such a fixed criterion was inadequate in this instance since we discovered that some of the visible consequences of penetrating IR wavelengths were not visualized via slit-lamp, fundus camera, or SLO examination until several days postexposure. Thus, selected subjects were periodically examined at times up to 3-months postexposure to document the temporal development of the various types of observed ocular lesions. When lesion/no lesion data were sufficient, ED_{50} thresholds and confidence limits were calculated by probit analysis.[6]

3. RESULTS

Exposures of rabbit and rhesus subjects to 1.318-μm radiation were conducted with the laser power at 2 W, a corneal spot size of 1.0 mm when irradiating anterior ocular tissues or 5.0 mm when targeting the retina, and exposure times ranging from ~0.2 sec to 1 sec (or longer when searching for retinal effects). Under these conditions and over a fairly narrow range of exposure doses laser-induced damage was observed in the cornea, lens, iris, and retina of the Dutch Belted rabbit. Exposures to rhesus subjects yielded a similar array of lesions save for the fact that retinal damage was not observed.

In the rabbit, the threshold dose required to induce a corneal lesion was 175 J/cm^2. In the rhesus it was 72 J/cm^2. These values may be compared to a rhesus threshold of 212 J/cm^2 reported for 5-sec exposures to the simultaneous 1.318/1.338 μm output from a Nd:YAG laser.[4]

Exposure to doses slightly in excess of the corneal threshold yielded highly reflective corneal spots which were observed immediately following exposure (Figure 5). Through a slit-lamp examination it was determined that the threshold lesion involved the full thickness of the cornea (Figure 6), instead of just the epithelial layer as had been found following threshold exposures to far-IR wavelengths.[7]

By 48-hr postexposure the corneal epithelial damage had repaired (as expected). At that time, slit-lamp examination revealed a stromal lesion which generally had a smaller diameter than the initial epithelial effect, as well as an underlying endothelial lesion whose diameter was equal to or slightly greater than the initial lesion (Figure 7). In both rabbit and rhesus subjects, stromal and endothelial effects were found for almost every case where the epithelium had initially been affected. In the rhesus, several threshold exposures yielded a minimal endothelial effect at ~48-hr postexposure even though no corneal lesion had been observed in the first few hours following exposure. If these data points are changed from "no lesion" readings at 1-hr postexposure to "lesion" readings at 48-hr postexposure, then the rhesus corneal threshold is reduced from 72 J/cm^2 (for 1-hr readings) to ~50 J/cm^2 (for 48-hr readings).

Stromal and endothelial lesions observed in this study had much longer persistence than corneal epithelial effects. Nevertheless, if induced by exposure doses only slightly in excess of threshold, the lesions fully resolved within several weeks postexposure. Lesions induced by doses 2-3 times threshold or more persisted for as long as we monitored the subjects and are thought to represent permanent corneal scarring. At these suprathreshold exposure doses, we also detected cataracts directly behind the corneal lesion site (Figure 8). The threshold for cataract induction was ~260 J/cm^2 incident at the cornea for both the rabbit and the rhesus.

An interesting feature of the IR-laser-induced cataract was that the damage was often visualized as two discrete lesions, hereafter referred to as the anterior surface cataract and the cortical cataract. The anterior surface cataract was observed at the capsule or just sub-capsular with little axial depth perceived by slit-lamp observation. Directly behind the anterior surface cataract the lens appeared to be normal. Directly behind that, the cortical cataract was found and had significant associated depth, appearing to involve as much as one third of the lens thickness. In those cases where the cortical cataract thickness was most pronounced, a tapering of the lesion diameter with increasing depth was observed (Figure 9).

Following exposures slightly in excess of threshold, the anterior surface cataract generally resolved within a few weeks postexposure, whereas the cortical cataract often persisted, although with diminished intensity. Cataracts induced by exposures of at least twice the lens threshold showed undiminished intensity over several months and are assumed to reflect permanent lens damage.

A third category of IR-laser-induced cataract was observed by irradiating the iris rather than the lens directly. This observation may be relevant to daytime field exposures since the eye would not be dilated and assuming an incident laser beam diameter much larger than the pupil size, more energy could easily be absorbed by the iris than that which passes through the pupil to irradiate the lens directly. Therefore, we directed the 1-mm-diameter beam to selected locations on the iris of the undilated eye. Exposure doses sufficient to induce cataracts when the beam was directed through the pupil also induced lesions on the iris. The latter effect may or may not, in itself, have any consequences for visual function. More importantly, when the iris irradiated eye was later dilated, anterior surface cataracts were found beneath the projected irradiated spots (Figures 10 and 11). The threshold for induction of this indirect cataract was ~130 J/cm^2 or ~50% of the threshold for induction of cataract by directly irradiating the lens. With suprathreshold exposure doses, the diameter of the indirect cataract was significantly larger than the diameter of a cataract formed by directly irradiating the lens with the same exposure. Also, with such suprathreshold exposures, two potential ocular complications were noted. First, in some instances the iris-irradiated eye would not dilate for at least several days postexposure because of iris adhesions to the lens surface. Second, in a few cases, a perforation of the iris was found at several weeks postexposure even though the initial iris effect did not involve perforation. The visual consequences of this latter effect (if any) are unknown, but it is obvious that the iris adhesions would interfere with accommodation for as long as they persist.

In order to investigate the possibility of retinal damage resulting from 1.318-μm laser radiation, the laser beam diameter incident at the cornea was enlarged from 1.0 mm to 5.0 mm. Thus, the corneal irradiance was kept below the level required to induce the anterior ocular effects while selected retinal sites were irradiated for exposure durations of up to ~20 sec. In no instance was a retinal effect detected immediately or within the first few hours postexposure. However, in the rabbit, retinal lesions in the form of relatively large reflective spots (~200-500-μm diameter) developed over the 24-hr period following exposures of ~10 sec or longer (Figure 12). In terms of corneal irradiance, the retinal threshold dose is estimated to be ~75 J/cm^2. By 48-hr postexposure the retinal lesions had increased significantly in intensity, but the funduscopically detected lesion diameter was unchanged (Figure 13). Beyond 48-hr postexposure the lesion appearance stabilized for several days to weeks.

In one rabbit eye, an ~500-μm retinal lesion was induced by a suprathreshold corneal exposure even though a 1.0-mm laser spot size was incident at the cornea and an intense corneal lesion and cataract were produced and were visible immediately following exposure. In such a case it is unknown how much energy was transmitted to the retina before the developing corneal and lens lesions shielded the posterior of the eye from further exposure. As in other instances, the retinal effect was not apparent on the day of the exposure but was first found at 24-hr postexposure and observed to have the same size (~500 μm) at 48-hr and 1-week postexposure. When the eye was examined at 2-months postexposure, a much larger (> 1 mm) and irregularly shaped lesion was found overlaying the original lesion site (Figure 14). The lesion seen in Figure 14 is interpreted as a late-developing inflammatory response to the full-thickness retinal damage induced by a suprathreshold 1.318-μm laser exposure. Scanning laser ophthalmoscopy (SLO) was

performed on eyes exhibiting IR-laser-induced retinal damage to aid in the interpretation of the effects illustrated in Figures 12-14. The SLO observations and the associated pathology will be discussed in a subsequent paper.

Exposure of rabbit and rhesus subjects to the 1.356-μm emission of the Nd:YAG laser encompassed a similar series of experiments to that described above for 1.318-μm radiation. At 1.356 μm, the maximum output of the laser was ~1 W and a corneal spot size of 0.7 mm was used so that the corneal irradiance would be comparable to that for the 1.318-μm exposures. Under these conditions, the corneal threshold for 1.356-μm exposures was 58 J/cm^2 in the rabbit and 86.9 J/cm^2 in the rhesus. The cataract threshold for the rabbit was approximately twice the corneal threshold and for the rhesus was about 5 times the corneal threshold (compared to the factor of 4 found at 1.318 μm). The general appearance and temporal development of each type of lesion was similar for the two wavelengths. Corneal and lens thresholds for the two species at the two wavelengths are summarized in Table 1. Since *in situ* lens threshold data are biased by any changes in corneal absorption which occur as corneal damage accrues during the exposure, lens thresholds are only quoted relative to the corneal threshold for identical exposure conditions.

At 1.356 μm, retinal lesions were not observed in either species.

4. DISCUSSION

The IR-laser-induced ocular effects reported in this paper are unique both in terms of the multiple lesion sites which may result from a given exposure and in the differing time frames for development of the ultimate consequences of the laser insult. Virtually all previous studies of laser-induced ocular damage are characterized by strong absorption of laser energy in an axially thin layer - either at the retinal pigment epithelium for visible and near-IR wavelengths up to the more frequently studied 1064-nm Nd:YAG emission, or at the anterior corneal surface for far-IR wavelengths. In the current study the laser energy is gradually absorbed along the entire axial path from cornea through choroid, and numerous sites along that path may be affected. The reaction of the irradiated organism to the volumetric heating associated with such penetrating wavelengths has been shown to sometimes deviate from expectations of a thermal lesion observable immediately or shortly following exposure. Rather, the observable consequences of a penetrating laser insult may take days to become apparent and longer to reach maximum expression, which may include degeneration across a wider expanse of tissue than that irradiated by the laser. For these reasons, IR laser exposures bear close scrutiny to redefine both the standard tissue damage criteria and then the appropriate safe exposure limits.

In considering the implications of this work for extrapolation to the human and for impact on laser safety standards, one must carefully examine the absorption of laser radiation in each ocular component as a function of wavelength. Figure 15 presents the transmission of 1.318-μm radiation through the ocular components (cornea, aqueous, lens, and vitreous) and through the ocular medium as a whole ("eye") for each of the rhesus, rabbit, and human. The plots are based upon the rhesus absorption data of Maher.[1] The rabbit and human transmissions are calculated by correcting transmission based on differences in thickness of the ocular components between species.[8,9]

It is seen from Figure 15 that at 1.318 μm, absorption of the cornea and aqueous is nearly equivalent for the three species. Absorption of the rabbit lens is significantly greater than that for the rhesus or man simply because the rabbit lens is over twice the thickness. This is countered by a thinner vitreous in the rabbit (6.7 mm compared to 11.6 mm in the rhesus and 17 mm in man). The net result is that transmission of 1.318-μm radiation through the ocular medium approximates 6% in the rabbit but only 3.6% in the rhesus and 1% in man. We were able to induce a retinal effect in the rabbit but not in the rhesus with the 1.318-μm laser. Since transmission through the human eye is even lower than that in the rhesus, no retinal hazard is anticipated.

At 1.356 μm absorption of each ocular component is measurably greater than at 1.318 μm, and the percent of incident radiation reaching the retina is lower by about a factor of 10. Thus, it is not surprising that retinal effects were not observed in either the rabbit or rhesus at 1.356 μm.

Lens thresholds in both the rabbit and rhesus showed little change as wavelength was varied from 1.318 μm to 1.356 μm suggesting that the increasing lens absorption coefficient with increasing wavelength was approximately offset by the lower transmission through the cornea and aqueous. The decrease in rabbit corneal threshold from 175 J/cm^2 at 1.318 μm to 58 J/cm^2 at 1.356 μm seems greater than would be anticipated on the basis of increase in corneal absorption but, in general, the relative threshold doses across wavelength and species are consistent with the variation in absorption of the ocular tissues.

Recognizing that tissue absorption coefficients vary rapidly with wavelength in the near-IR/far-IR transition region, as do the factors for extrapolating threshold data across species, we offer the following guidance for assessing potential ocular hazards for this wavelength range.

1. At wavelengths ≤1.15 μm, the transmission of the ocular medium is relatively high, and laser radiation primarily presents a retinal hazard. Safety standard considerations need only be based on the potential retinal hazard.

2. Between ~1.15 μm and ~1.4 μm the cornea, lens, and iris (and, therefore, also the lens due to indirect thermal heating via the iris absorption) may all be affected at comparable threshold levels. From ~1.15 μm to ~1.3 μm the retina is also at risk at comparable exposure doses. For high-power lasers within this wavelength range, safety standard considerations should perhaps be more conservative than for other wavelengths. The strategy for determining safety standard MPE levels is generally to reference the MPE to experimental threshold data for production of a minimum visible lesion (MVL) which, in most instances, if produced, would have no or only a minor transient impact on visual function. For wavelengths under consideration here, the "threshold dose" or doses only slightly in excess of threshold could induce ocular lesions at several sites within the eye and with potentially significant and long-lasting impact on visual function. Thus, a larger margin of safety may be desirable between the threshold dose and the safety standard MPE.

3. For far-IR wavelengths (>1.4 μm), the ocular hazard is probably restricted to the cornea due to the relatively low transmission through the cornea and aqueous humor. However, for the short end of the far-IR range (say ~1.4 μm to 2.5 μm) MPE levels should continue to be expressed with relative caution

since threshold lesions involve corneal layers deeper than the epithelium and, hence, imply a longer lasting, if not permanent, visual deficit.

Figure 16 shows an amended version of Figure 3 with the 1.318-μm and 1.356-μm threshold data from the current study added. The added datapoints provide a basis for extrapolating the retinal and corneal threshold versus wavelength curves to the crossover wavelength at ~1.3 μm. These extrapolations are shown by the heavy dashed lines in Figure 16. The heavy solid lines demonstrate how a revised MPE standard might be drawn. The proposed MPE curve runs roughly parallel to the retinal threshold curve from 1.15 μm to the crossover point at ~1.3 μm and then parallel to the corneal threshold curve from ~1.3 μm to 2.0 μm. Below 1.15 μm and above 2.0 μm, the MPE would remain unchanged. Between 1.15 μm and 2.0 μm several step discontinuities and plateau regions of the MPE are replaced by the two linear segments which present a realistic portrayal of the variation of ocular thresholds with wavelength. Threshold data at several additional wavelengths within the range of 1.15 μm and 2.0 μm are desired to strengthen the basis for the extrapolations drawn in Figure 16 and to lead to a more definitive recommendation for the slopes of the MPE curve within this wavelength range.

5. ACKNOWLEDGMENTS

The research reported here was supported by Contract F33615-92-C-0017 (TASC, Inc.) let by the Optical Radiation Division, Occupational and Environmental Health Directorate, USAF Armstrong Laboratory, Brooks AFB, TX. The work was accomplished at the facilities of the US Army Medical Research Detachment, Brooks AFB, TX.

6. REFERENCES

1. E.F. Maher, "Transmission and absorption coefficients for ocular media of the rhesus monkey," USAF Technical Report, SAM-TR-78-32, Dec 1978.

2. American National Standards Institute, "American national standard for the safe use of lasers," New York, ANSI Standard Z136.1, 1993.

3. Department of the Air Force, "Health hazards control for laser radiation," Washington D.C., AFOSH Standard 161-10, 1980.

4. B.E. Stuck, D.J. Lund, and E.S. Beatrice, "Ocular effects of laser radiation from 1.06 to 2.06 μ," *SPIE Proc.*, Vol. 229, pp. 115-120, 1980.

5. B.E. Stuck, D.J. Lund, and E.S. Beatrice, "Ocular effects of holmium and erbium laser radiation," *Health Phys.*, Vol. 40, pp. 835-846, 1981.

6. D.J. Finney. *Probit Analysis*, Third Ed., Cambridge University Press, 1971.

7. J.A. Zuclich, M.F. Blankenstein, S.J. Thomas, and R.F. Harrison, "Corneal damage induced by pulsed CO_2 laser radiation," *Health Phys.*, Vol. 47, pp. 829-835, 1984.

8. D. Sliney and M. Wolbarsht, *Safety with Lasers and Other Optical Sources*, Plenum Press, New York, 1980.

9. A. Hughes, "A schematic eye for the rabbit," *Vision Res.*, Vol. 12, pp. 123-138, 1972.

Table 1

IR Laser Ocular Threshold Data

Wavelength (μm)	Species	Corneal Threshold (J/cm^2)[1]	Lens Threshold (Relative to Cornea)
1.318 (2 W CW power, 1-mm corneal spot size)	rabbit	175 (154-199)	0.75[2]
	rhesus	72 (68-81)	1.80[2]
1.356 (1 W CW power, 0.7-mm corneal spot size)	rabbit	58 (48-72)	2.0[3]
	rhesus	87 (67-102)	5.0[3]

[1]95% confidence limits in parentheses
[2]Based on iris irradiation
[3]Based on direct irradiation of lens

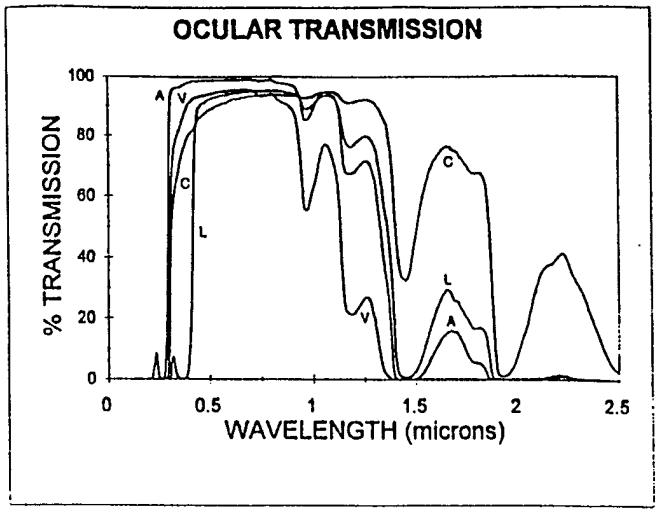

Figure 1. Transmission spectra of the components of the primate eye. C: cornea; A: aqueous humor; L: lens; V: vitreous humor.

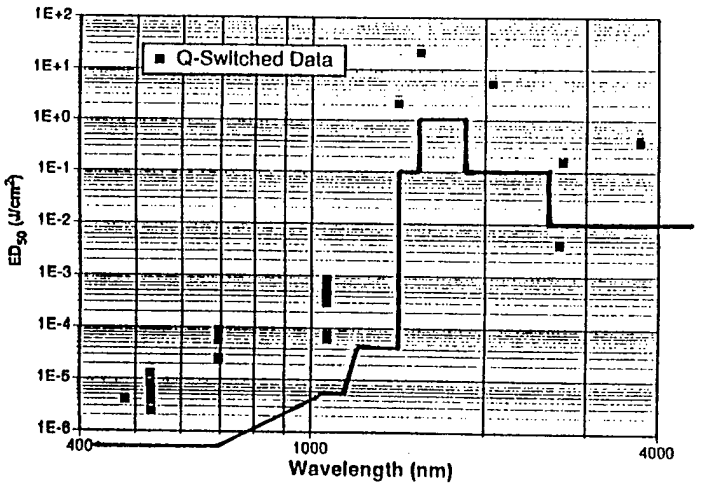

Figure 2. ED_{50} threshold for laser-induced ocular damage plotted as a function of wavelength for Q-switched pulsewidths. The solid curve is the ANSI laser safety standard MPE level applicable to pulsewidths from 1 nsec to 18 μsec.

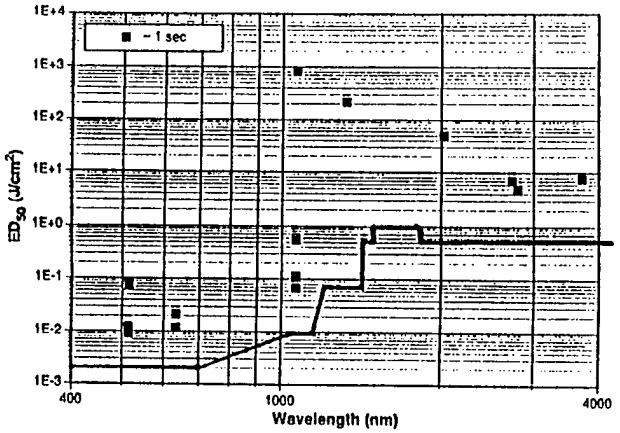

Figure 3. ED_{50} threshold for laser-induced ocular damage plotted as a function of wavelength for 1-sec exposure duration. The solid curve is the ANSI laser safety standard MPE level applicable for 1-sec exposures.

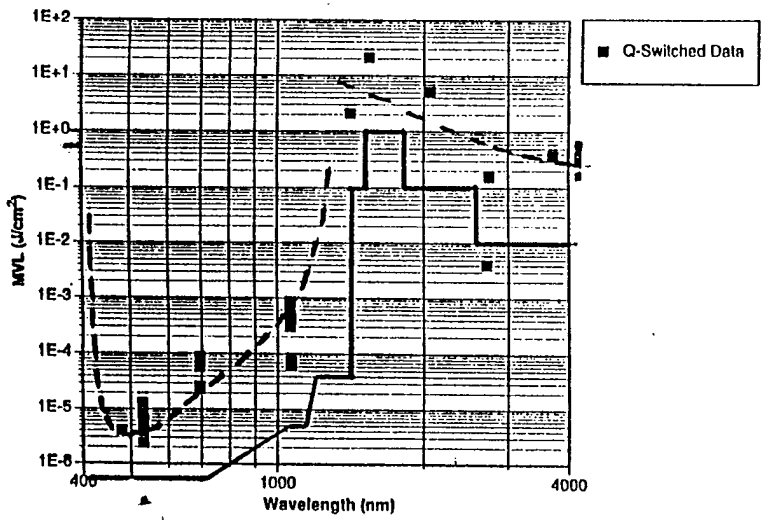

Figure 4. ED_{50} threshold for laser-induced ocular damage plotted as a function of wavelength for Q-switched pulsewidths. This figure is an amended version of Figure 2, with the dashed curves added to illustrate the variation of the retinal (for wavelengths $\leq$1064 nm) and corneal (for wavelengths >1064 nm) damage threshold as a function of wavelength.

Figure 5. Slit-lamp photograph, taken at 1-hr postexposure, of corneal lesions induced by 1.318-μm laser radiation.

Figure 6. Slit-lamp photograph, taken at 1-hr postexposure, demonstrating the full-thickness involvement of corneal lesions seen in Figure 5.

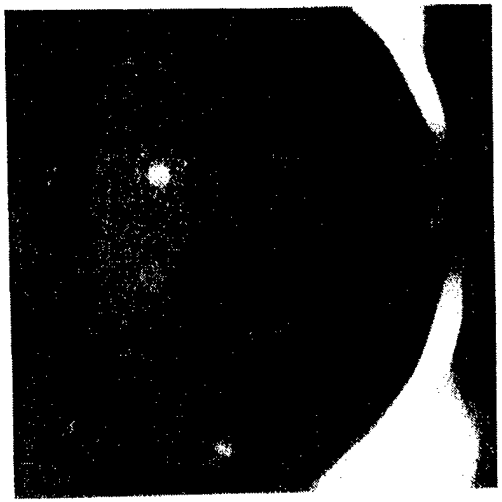

Figure 7. Slit-lamp photograph, taken at 48-hr postexposure, showing stromal and endothelial involvement of corneal lesions induced by 1.318-μm laser radiation.

Figure 8. Slit-lamp photograph, taken at 48-hr postexposure, illustrating an intense cataract lying directly behind a corneal lesion induced by 1.318-μm laser radiation.

Figure 9. Slit-lamp photograph, taken at 6-days postexposure, demonstrating the depth of a cataract induced by 1.318-μm laser radiation. With this side view, the cataract is seen to begin somewhat below the anterior lens surface and to taper off in proceeding deeper into the lens.

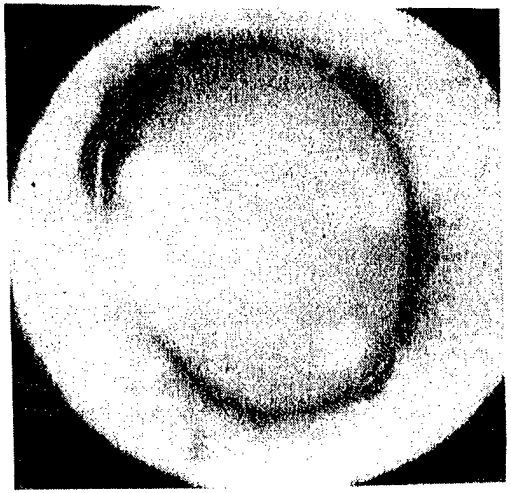

Figure 11. Slit-lamp photograph, taken at 24-hr postexposure, showing the same eye as seen in Figure 10, but with the pupil now dilated to reveal the cataracts induced by 1.318-μm laser irradiation of the iris.

Figure 10. Slit-lamp photograph, taken at 1-hr postexposure, showing iris lesions and associated lens lesions (appearing at pupil border adjacent to iris lesions) induced by 1.318-μm laser radiation directed at the iris.

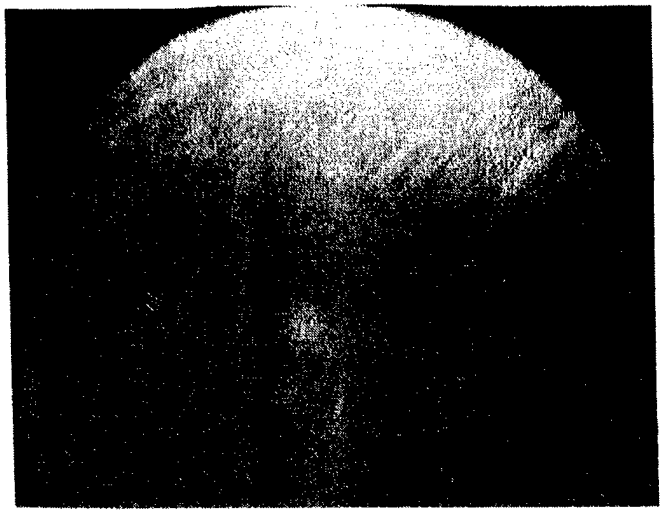

Figure 12. Fundus photograph, taken at 24-hr postexposure, illustrating retinal lesions induced in the rabbit eye by 1.318-μm laser radiation. Two IR-laser-induced lesions are seen directly above two argon-laser induced marker lesions. The IR-laser-induced lesions were not funduscopically visible on the day of exposure.

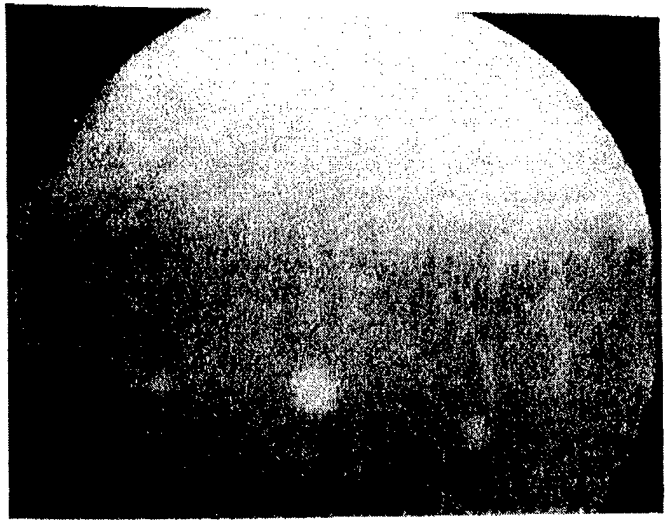

Figure 13. Fundus photograph, taken at 48-hr postexposure, showing the same eye as seen in Figure 12 and demonstrating that the IR-laser-induced lesions were more intense by 48-hr postexposure.

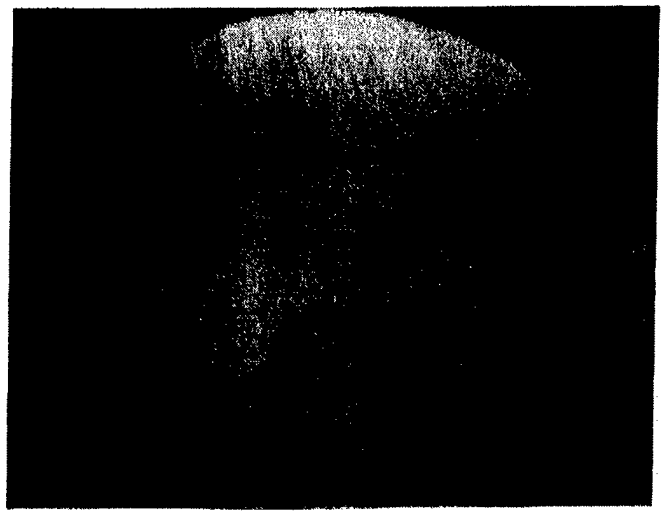

Figure 14. Fundus photograph, taken at 2-months postexposure, illustrating a large (~1 mm) lesion which had developed at the site of a 1.318-μm laser exposure. The appearance of the lesion at 1-day through 1-week postexposure was similar to those seen in Figures 12 and 13.

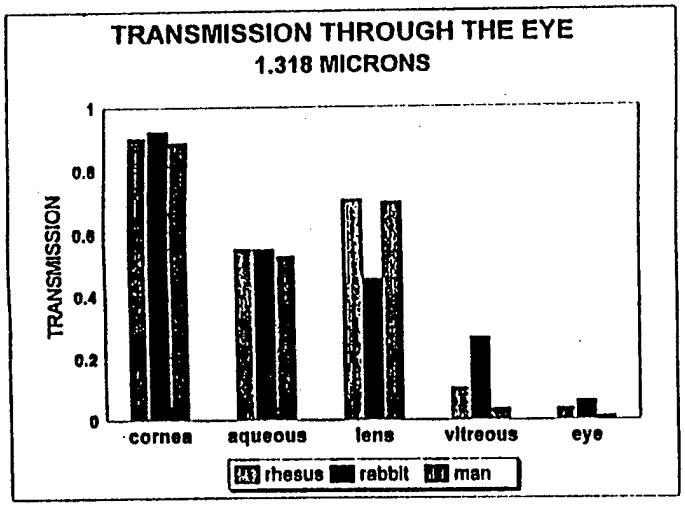

Figure 15. Transmission of 1.318-μm radiation through the ocular components and the ocular medium as a whole (eye) for three species.

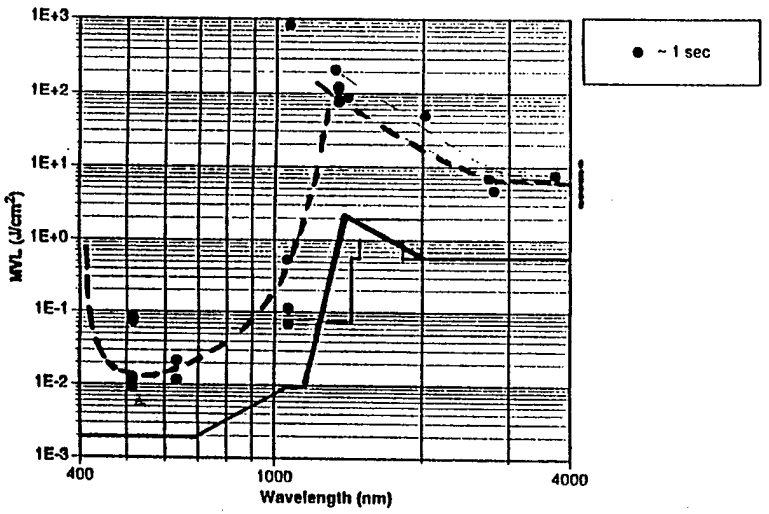

Figure 16. ED_{50} threshold (MVL) and MPE for laser radiation plotted as a function of wavelength for 1-sec exposure duration. This figure is an amended version of Figure 3 with the dashed curves added to depict variation of damage threshold with wavelength and the heavy solid lines drawn over the MPE to suggest a revised safety standard.

Lasers and Light vol. 8 no. 1 pp 15-29 (1997)
Kugler Publications, Amsterdam/New York

A comparison of laser-induced retinal damage from infrared wavelengths to that from visible wavelengths

Joseph A. Zuclich[1], Steven T. Schuschereba[2], Harry Zwick[2], Stephen A. Boppart[3], James G. Fujimoto[3], Frank E. Cheney[4] and Bruce E. Stuck[2]
[1]TASC, San Antonio, TX; [2]US Army Medical Research Detachment, Brooks AFB, TX; [3]Massachusetts Institute of Technology, Cambridge, MA; [4]Optical Radiation Division, Armstrong Laboratory, Brooks AFB, TX; USA

Keywords: infrared laser, retina, ocular damage, SLO, histopathology

Abstract

Corneal, lenticular, and retinal damage have been observed following exposures to a laser emitting in the near-infrared wavelength range (Nd:YAG, 1.318 μm). Ocular damage thresholds are much higher than for visible wavelengths. However, it was found that infrared (IR) exposures may result in multiple damage sites throughout the ocular medium and retina; *that exposure sites which initially appear to be unaffected* may reveal slowly developing (days or longer) degeneration; and that late inflammatory responses may ultimately spread to areas of tissue not directly irradiated by the laser.

The nature of tissue degeneration following IR laser exposure is examined and compared to that following visible wavelength laser exposures *using three approaches: histopathology, scanning laser ophthalmoscopy, and optical coherence tomography. Each approach is shown to reveal unique aspects of the IR laser-tissue interaction when contrasted with effects induced by visible wavelengths.*

Introduction

Recent developments in laser technology have yielded a variety of powerful infrared (IR) laser sources, many of which fall in the wavelength range broadly categorized as 'eye-safe'. Used in this context, the terminology is frequently divorced from its original intent as a relative descriptor meant only to convey the fact that ocular damage thresholds are significantly higher for 'eye-safe' wavelengths than for elsewhere in the visible and IR spectra.

Transmission spectra of the ocular components (cornea, aqueous, lens, and vitreous) of the primate eye are plotted in Figure 1[1]. From this illustration, it can be seen that transmission through each component (and, therefore, transmission to the retina) is high for visible wavelengths and only begins to drop significantly for IR wavelengths above ~1.1 μm, where water absorption becomes appreciable. In the far-IR, the composite absorption of the ocular components is such that virtually no incident radiation is transmitted to the retina. In the near-IR, absorption of incident radiation is distributed across the ocular components and, depending upon the precise exposure parameters, damage may be induced in one or more of the cornea, lens, and retina/choroid.

The simultaneous induction of laser-induced damage in several tissues is perhaps best understood by schematizing the distribution of energy absorption through the ocular medium. This is done in Figure 2 which compares the absorption of 0.514-μm argon laser radiation (Fig. 2a) to that for the 1.318-μm Nd:YAG laser emission used in this study (Fig. 2c). Distance into the eye is meas-

Address for correspondence: Joseph A. Zuclich, PhD, TASC, 4241 Woodcock Drive, Suite B-100, San Antonio, TX 78228, USA

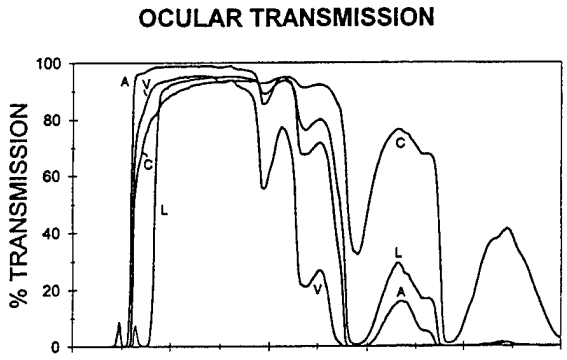

Fig. 1. Transmission spectra of the components of the primate eye. C: cornea; A: aqueous humor; L: lens; V: vitreous humor.

ured along the horizontal axis, as indicated in Figure 2b. Figure 2a remains essentially unchanged if any other visible wavelength is substituted for 0.514 μm.

The solid lines in Figures 2a and 2c show the variation in absorption coefficients as one moves through the ocular medium[1]. Using these absorption coefficients and treating each ocular component as homogeneous, the percent of corneal incident radiation reaching any given depth into the ocular medium is calculated and shown by the dotted curves in Figures 2a and 2c. At 0.514 μm, most of the corneal incident radiation reaches the retina, but at 1.318 μm, the transmission to the retina is ≤5%. Taking the focusing power of the eye into account, the relative laser irradiance at any point along the horizontal axis can be approximated, and is plotted as the dashed curves in Figures 2a and 2c. For visible wavelengths, the retinal hazard is readily appreciated from the high irradiance level at the retina, coupled with a high retinal absorption coefficient[2]. At 1.318 μm, on the other hand, the retinal irradiance exceeds that incident at the cornea by a relatively small margin.

In a preliminary report[3], it was shown that exposures in the 'eye-safe' wavelength range can, indeed, result in multiple damage sites throughout the ocular medium and the retina. It was also noted that initially unaffected IR laser exposure sites, when monitored over time, may reveal slowly developing (days or longer) tissue degeneration, and that the tissue degradation may ultimately progress to involve regions surrounding the discrete areas subjected to laser radiation.

In this report, the laser-tissue interaction at

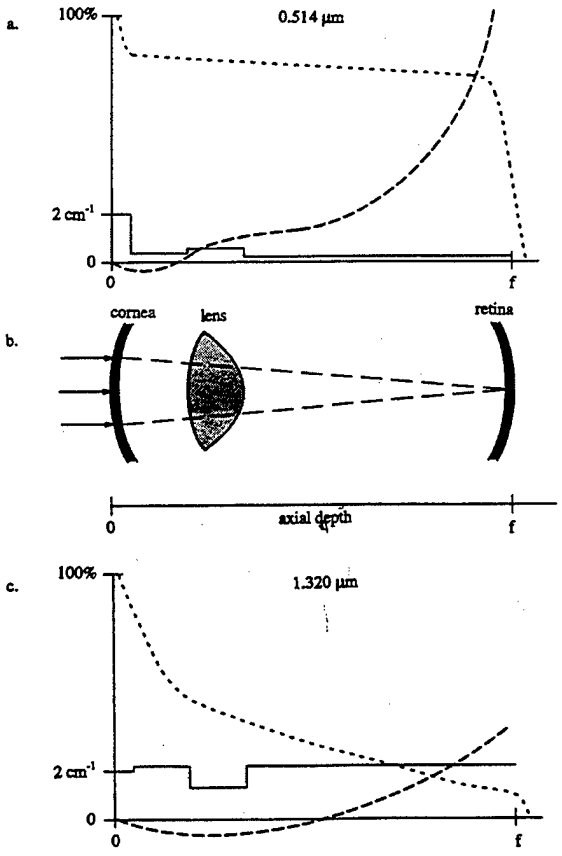

Fig. 2. Schematic depiction of penetration of 0.514-μm and 1.318-μm radiation (*2a* and *2c*, respectively) into an eye of focal length, f (*2b*). The vertical axes of *2a* and *2c* are, in turn, absorption coefficient in cm^{-1} (for the solid lines); percent of corneal incident radiation penetrating to a given depth into the eye (dotted lines); and relative irradiance at a given depth (dashed lines). *The relative irradiance is set equal to 1.0 at the corneal surface.*

1.318 μm is further characterized via *confocal* scanning laser ophthalmoscopy (SLO) and optical coherence tomography (OCT), as well as by examining the associated retinal pathology. For both the imaging approaches and the ocular pathology, the findings in IR laser-exposed retinal tissues are contrasted to those in argon laser-exposed tissues. The SLO and OCT imaging techniques are briefly described below.

Background

Two imaging technologies (SLO and OCT) which employ coherent light sources are applied to yield

non-invasive, *in situ* observations of ocular tissues and, specifically, to detect laser-induced retinal effects. The imaging techniques allow *repeated post-exposure examinations of the progression of damage, potentially yielding a more detailed interpretation* of the laser-tissue interaction and the subsequent tissue reactions than does the static picture(s) captured by pathological evaluation.

While the SLO approach is relatively well established, use of a confocal aperture in the SLO apparatus has not been widely applied[4,5]. The confocal aperture effectively allows adjustment of the depth of the imaged confocal slice within the eye. Coupled with the use of any of several illuminating wavelengths, this technique allows visualization of discrete retinal layers and affords the opportunity to detect differential damage effects within those layers.

OCT is a new imaging modality that permits high-resolution, cross-sectional tomographic imaging of the architectural morphology of biological tissues *in vivo*[6]. Imaging is performed by directing a focused light beam into the tissue *and using low-coherence interferometry to measure the delay time (echo delay) for the backscattered light to return to the instrument. In contrast* to the end-face view provided by slit-lamp and funduscopic observations, OCT permits the imaging of ocular structures from the cross-sectional perspective. The clinical diagnostic potential of OCT has been demonstrated in the transparent tissue of the eye[7-9], as well as in highly scattering tissue[10,11].

Methods

The experimental subjects were *15 Dutch Belted rabbits* (*Oryctolagus cuniculus*). Animals used in this study were procured, maintained, and used in accordance with the Animal Welfare Act and the "Guide for the Care and Use of Laboratory Animals" prepared by the Institute of Laboratory Animal Resources, National Research Council; and the ARVO Resolution on the Use of Animals in Research. All experiments used appropriate levels of anesthesia *(IM injection of ketamine (20 mg/kg) mixed with xylazine (0.5-1.0 mg/kg))*, so the subjects did not experience pain or distress.

Pre-exposure screening of subjects to ensure clear ocular media and normal ocular tissues generally consisted of a slit-lamp examination, a fundus camera examination, fluorescein angiography, baseline photography taken while the subject was still in position at the fundus camera, and refraction to the nearest 0.25 diopter.

Ocular exposures were made with a cw Nd:YAG laser equipped with a pair of mirrors to optimize the output at 1.318 μm. An intracavity etalon was used to select the wavelength of interest while suppressing other Nd:YAG emission lines. The laser beam was directed through a 0.5-m scanning monochromator to a germanium photodiode to ensure that the selected wavelength was free of contaminating laser emissions. CW output was stable at a maximum level of ~2 W. An electronically controlled mechanical shutter was used to select the exposure duration, which was the variable for ocular threshold determinations. Beam profiles were determined using a 2-D laser beam analyzer. Marker lesions were produced on the subjects' retinas with an air-cooled argon-ion laser with a cw power of 60 mW and an exposure duration of 15 msec. Elsewhere, we have reported corneal, lens, and retinal thresholds in both rabbits and primates for 1.318- and 1.356-μm radiation obtained from the Nd:YAG laser[3]. The SLO and OCT observations discussed in this paper, as well as the pathological evaluations, were conducted only in rabbits and only for one IR wavelength (1.318 μm) and one visible wavelength (0.514 μm).

IR laser exposure times ranged from one to ten seconds. The 1.318-μm collimated beam was ~5 mm in diameter when incident at the cornea. This yielded exposure doses of ~10-100 J/cm^2 at the cornea. Procedures for delivering laser exposures and laser beam diagnostics are described elsewhere[3].

Subjects were examined by standard fundus ophthalmoscopy and SLO immediately following laser exposure, and again at 24 and 48 hours postexposure. The Rodenstock SLO was capable of projecting four wavelengths: argon blue (0.488 μm), argon green (0.514 μm), helium neon (0.633 μm), and gallium arsenide (0.780 μm)[5]. A confocal aperture was employed[4]. Images were recorded on super VHS video tape. Individual video frames were digitized with a Delta Tech-

nologies image-processing system, and printed. SLO examinations generally included fluorescein and indocyanine green (ICG) angiographies. The former allowed evaluation of retinal vascular leakage and blockage from lesion sites in the sensory retina, while the ICG angiography was used to detect blockage in the choroidal blood supply.

The OCT instrument utilized a modified ophthalmic slit-lamp to image *in vivo* ocular structures of *two rabbit subjects*. The subjects contained a variety of corneal, lens, and retinal lesions induced by the 1.318-μm Nd:YAG laser[3], as well as retinal lesions induced by the argon laser. The light source for the OCT interferometer was an 830-nm super-luminescent diode laser that enabled imaging with an incident optical power of 200 μW. Images were acquired either vertically or horizontally (as viewed with the slit-lamp) through selected lesions. The instrument achieves a spatial resolution at the retina of ~15 μm in both the longitudinal and transverse directions.

Two rabbits selected for pathological evaluation were euthanized with an overdose of Nembutal. The retinas were processed for routine transmission electron microscopy (TEM)[12]. Briefly, both eyes were enucleated and immersion-fixed within five minutes of death with a cacodylate-buffered solution (4°C) containing 1% glutaraldehyde and 1% paraformaldehyde[13]. Approximately 24 hours later, strips of retina (~2x4 mm) containing the laser-induced lesions were dissected out for further processing. Plastic sections of 1-μm thickness were first examined by light microscopy to determine lesion centers. Then, thin sections for electron microscopy were cut through the lesion centers, using a diamond knife. The thin sections were stained with uranyl acetate and lead citrate, and then examined and photographed with a Zeiss TEM at 60 kV.

Results

Figure 3 is a fundus photograph illustrating retinal lesions induced in the rabbit eye by 0.514- and 1.318-μm laser radiation. The photograph, taken at 24 hours postexposure, *shows three argon-laser-induced marker lesions (arrows) and two IR-laser-induced lesions directly above the central and right-hand marker lesions.* The marker lesions are ~200 μm in diameter and were visible immediately following exposure. The IR lesions were not funduscopically visible on the day of exposure. By 24 hours postexposure, the IR lesions were readily detected with the fundus camera and, as seen in Figure 3, were larger and more reflective than the argon marker lesions. The IR lesions developed somewhat further in size and reflectivity during the ensuing 24-hour period, but beyond 48 hours postexposure, the appearance of the lesions stabilized.

Scanning laser ophthalmoscopy

SLO observations on the eye seen in Figure 3 also failed to visualize the IR lesions on the day of exposure. By 24 hours postexposure, the two IR lesions were apparent with all illuminating wavelengths of the SLO. Figure 4 is an SLO image, at 24 hours postexposure, using 0.488-μm illumination. The smallest confocal aperture (C1) was used, and *the confocal slice (-1.9 D) lies in the inner retina but below the nerve fiber layer (NFL). In this image, both the argon and IR lesions have appearances similar to those seen with normal fundus camera viewing* (Fig. 3). Figure 5 shows a 0.488-μm image of the same eye, but with the confocal plane moved in the anterior direction into the NFL. Intact NFL fibers are imaged over both the argon and IR lesions.

Figure 6 shows an SLO image of the same eye using 0.780-μm illumination, but with all other viewing conditions as in Figure 4. With 0.780-μm illumination, the image is moved deeper into the retina. The argon lesions at this plane are the same size as in Figure 4, but exhibit dark central areas. The IR lesions are considerably larger and more diffuse. Further, several additional IR lesions are now detected. *The additional IR lesions are seen at sites directly* below and in between the argon marker lesions, *and resulted from exposure doses ranging from ~0.25 to 1.0 times the dose required to induce the IR lesions visible in Figures 3 and 4.* These additional lesions were not visualized with the SLO imaging wavelengths other than 0.780 μm, nor with the white light fundus camera illumination.

Fluorescein angiography at 24 hours post-

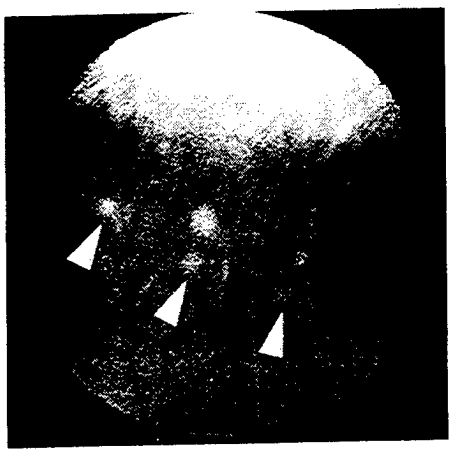

Fig. 3. fundus photograph showing IR (1.318 μm) and argon (0.514 μm) laser-induced lesions in the rabbit eye. *Arrows indicate the three argon marker lesions.* The photograph was taken 24 hours after laser exposures.

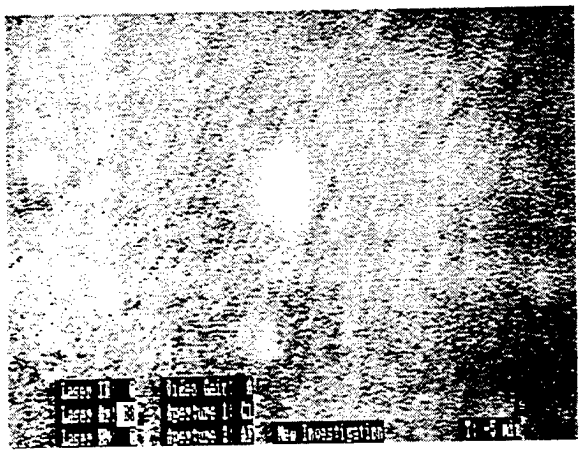

Fig. 4. SLO image (40° field of view) of the same eye as that seen in Figure 3 taken with 0.488-μm illumination and using the smallest confocal aperture. The image was taken at 24 hours following laser exposures.

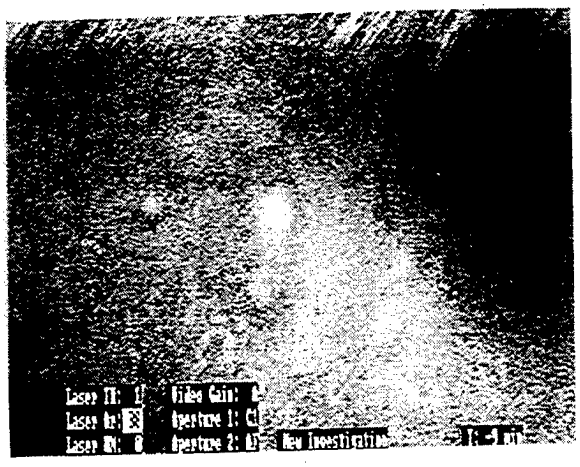

Fig. 5. SLO image (20° field of view) taken with the same viewing conditions as for Figure 4, but with confocal slice moved in the anterior direction to visualize the nerve fiber layer.

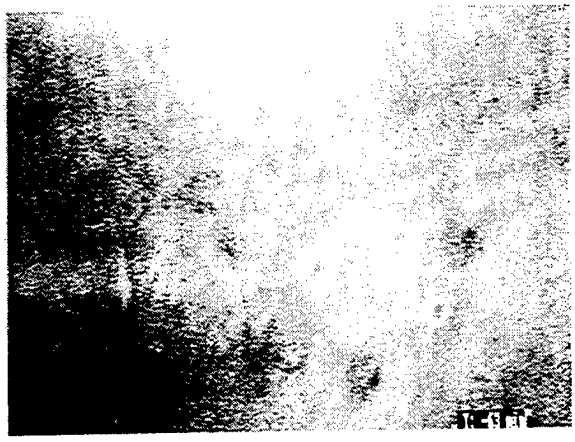

Fig. 6. SLO image (40° field of view) taken with 0.780-μm illumination, but with other viewing conditions the same as for Figure 4.

exposure showed leakage at the argon lesion sites, but not elsewhere. The filling pattern indicated some blockage of retinal vessels across the area between the two argon and two IR lesions in Figure 3. ICG angiography showed choroidal blockage and diffuse staining at the IR exposure sites.

Optical coherence tomography

OCT images through the centers of retinal lesions induced by 0.514- and 1.318-μm laser radiation are shown in Figure 7. The OCT images were also taken at 24 hours postexposure, and laser exposure doses were comparable to those which produced the funduscopically visible lesions seen in Figures 3-6. The top panel of Figure 7 is an image through a 1.318-μm lesion (arrow). The bottom panel is a cut through three adjacent argon lesions (arrows). The color bar under the images scales the intensity of tissue backscatter. The red/white end of the scale represents the highest backscattering, while the blue/black end is associated with the lowest backscattering.

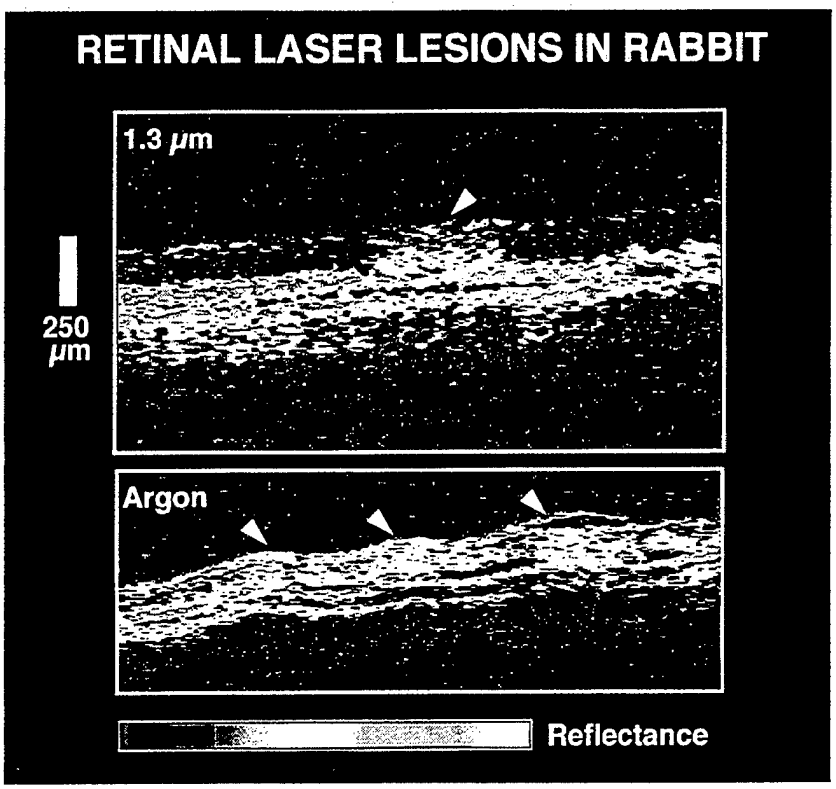

Fig. 7. OCT images comparing a 1.318-μm retinal lesion (upper panel) to three 0.514-μm lesions in the same eye (lower panel). The images were taken at 24 hours following laser exposures.

Several retinal features are explicitly visualized in the OCT images, including *the outer plexiform layer (OPL) and the retinal pigment epithelium (RPE)/choroid interface, which appear as the upper and lower highly scattering red layers, respectively*. Below the RPE, the backscatter signal is gradually attenuated as one moves deeper into the choroid. The inner-limiting membrane (ILM) of the retina is clearly delineated from the vitreous humor. Normal retina is found at the right and left borders of the images.

The 1.318-μm-induced damage seen in Figure 7 (upper panel) is pronounced in the OPL and the adjacent outer nuclear layer (ONL). There is also a noticeable increase in backscatter throughout the inner retinal layers. In contrast, the argon lesions (bottom panel), exhibit more extensive damage in the deeper retinal layers including the RPE and choroid. In all three argon lesions, elevation of the retina is observed, possibly due to the rapid heating and vacuolization within the retina. The right-most lesion also shows a vacuole below the ILM, involving the NFL and ganglion cell layers.

Figure 8 shows OCT images acquired from the anterior chamber (left panel) and retina (right panel) of an eye which, two months earlier, had received a 2 W, ~10-second exposure to the 1.318-μm Nd:YAG laser. Thus, the exposure dose is comparable to those which induced the IR lesions seen in Figures 3-6 but, in this instance, the laser beam diameter incident at the cornea was ~1 mm instead of 5 mm. *As a result of the higher irradiance level incident at the eye, corneal and lenticular lesions were induced in addition to the retinal lesion.* Slit-lamp and fundus camera photographs of these lesions have been published in an earlier report[3].

The corneal and lenticular lesions are visualized in the left panel of Figure 8. Significant opacification is indicated in the nuclear region of the lens, while relatively minor damage is seen in the cornea. The path of the laser beam through the aqueous humor is visualized, although this opacification is also minor.

The retinal image of Figure 8 indicates that, at two months postexposure, the disruption of the inner retinal layers is more pronounced than at 24

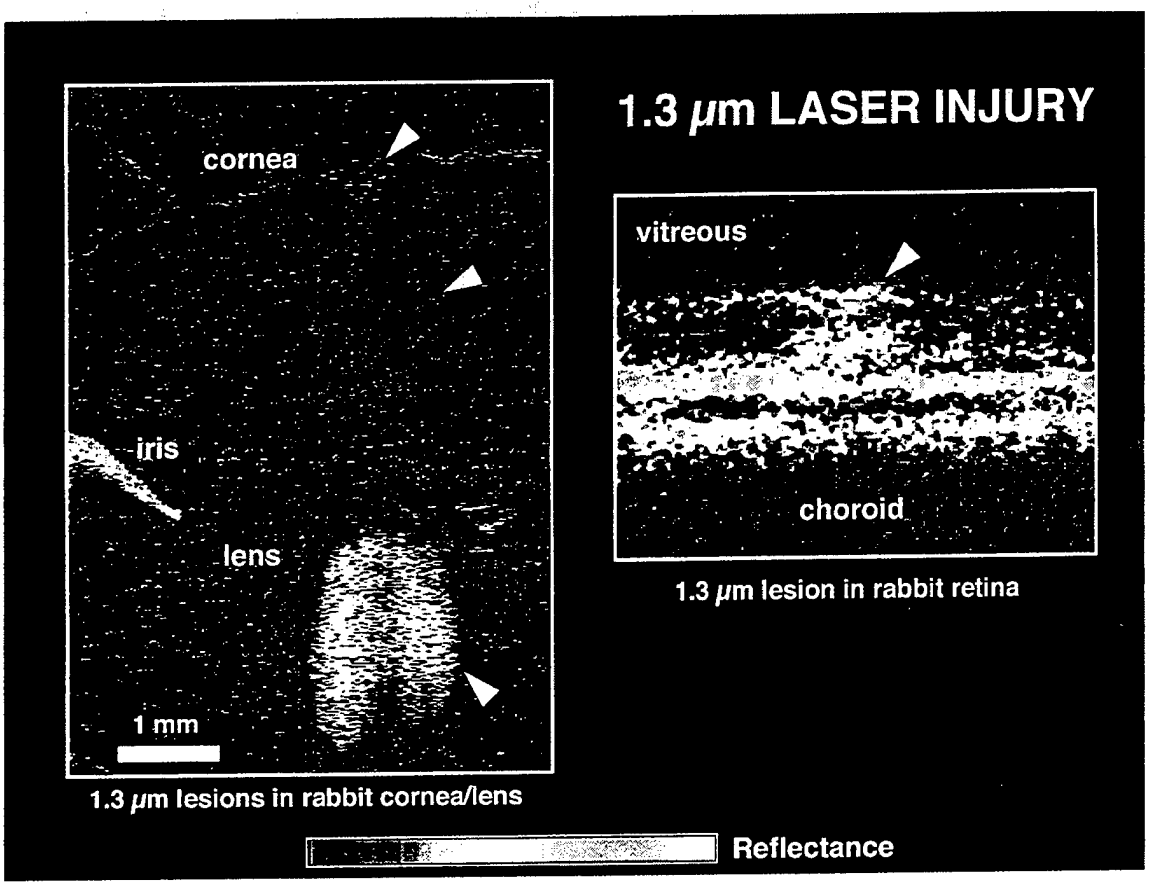

Fig. 8. OCT images, taken at two months postexposure, illustrating 1.318-μm anterior chamber lesions (left panel) and a retinal lesion (right panel) in the same eye, with all the lesions induced by the same exposure.

hours postexposure (Fig. 7). The OPL/ONL damage is similar in appearance to that observed at 24 hours postexposure, while the deeper retinal layers remain relatively unaffected. This OCT image is to be reconciled with the funduscopic appearance of the lesion at two months postexposure, shown in Figure 9. Whereas the 24-hour postexposure fundus camera observation revealed an ~500-μm circular lesion and that appearance was stable with several viewings over the next ten days, by two-months postexposure, the effect had progressed to the large (~1 mm) irregularly shaped lesion seen in Figure 9. This irregularly shaped lesion which, upon funduscopic and SLO observations, appeared to involve the anterior retina, slowly dispersed so that by three months postexposure the underlying circular lesion was again revealed.

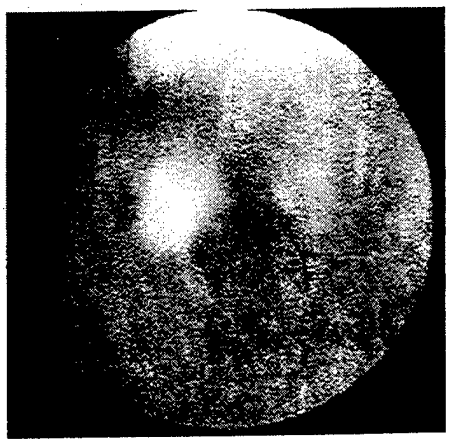

Fig. 9. Fundus photograph, taken at two months postexposure, of the same eye as that seen in Figure 8, illustrating the large (~1 mm), irregularly shaped retinal lesion which had developed at the site of a 1.318-μm laser exposure.

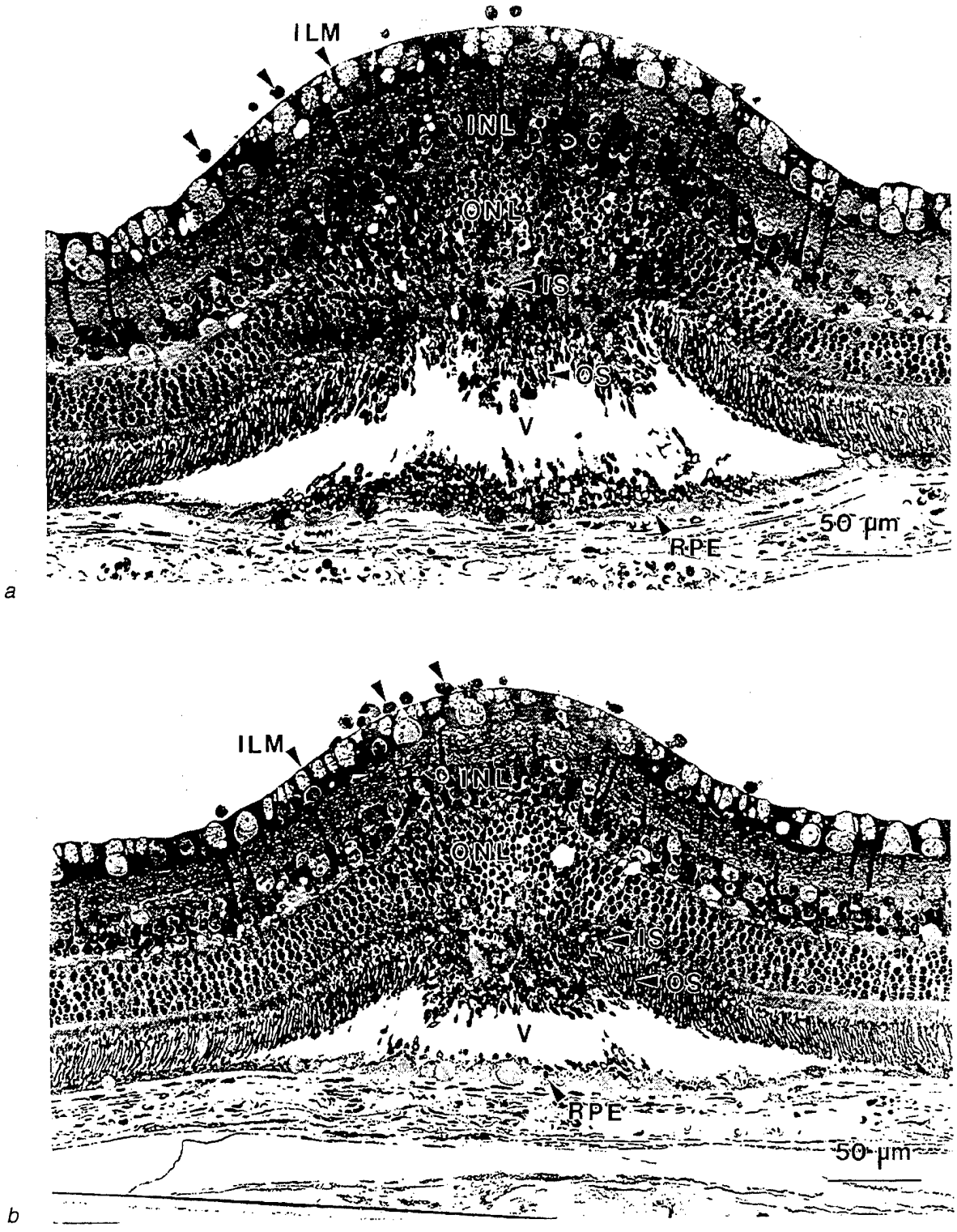

Fig. 10. Light micrographs through the centers of the IR lesions shown in Figure 3. *10a.* Larger of the two IR lesions; *10b.* smaller (right hand) of the two IR lesions. The tissue was fixed at 48 hours following laser exposures.

Retinal pathology

Figures 10a and 10b are light micrographs through the centers of the two IR lesions seen in Figure 3. The ocular tissues were fixed at ~48 hours postexposure. Figure 10a corresponds to the larger ophthalmoscopic lesion but, in fact, the two exposure sites received equal doses of IR radiation. Injury appears to be centered in the ONL. Photoreceptor inner and outer segments (IS and OS, respectively) both show degenerative changes. OSs are separated about halfway along their length, and the OS tips are embedded in the apical portions of the RPE. Inflammatory cells (arrows) are present in the vitreous close to the ILM. Some nuclei in the inner nuclear layer (INL) stain dark, but involvement is much less than in the ONL. The large subretinal vacuoles (V) (typical for suprathreshold laser-induced retinal lesions) are produced by RPE swelling and edema, although they may be exaggerated by additional artifactual separation. (Note that this type of artifact would not be present in the OCT image.) From Figure 10b, it appears that some of the vitreous inflammatory cells are adherent to the ILM and that some OSs are attached to the RPE near the lesion center.

Figures 11a and 11b are light micrographs through the centers of the central and right-hand argon lesions seen in Figure 3. Photoreceptors have darkly stained nuclei (arrows) and show degenerative changes along their full length. The amount of RPE swelling is much greater than in the IR lesions, and vacuoles are apparent in the subretinal space. OS tips are not attached to the RPE apical processes. There are very few inflammatory cells in the vitreous above the lesions. Instead, more macrophages are observed in the subretinal space than were found at IR lesion sites.

Figures 12a and 12b are light micrographs taken near the centers of two lower dose IR exposure sites. Lesions (L) at these sites were visualized only with 0.780-μm SLO observation (Fig. 6). The only evidence of degenerative change at 48 hours postexposure are the few dark nuclei in the ONL (arrows), the slight vacuolization in the RPE, and slight swelling in the inner retina.

Figures 13a, 13b and 13c are TEM micrographs showing control retina, the center of the larger IR lesion seen in Figure 3, and the center of the central argon lesion seen in Figure 3, respectively. The control retina (Fig. 13a) illustrates normal OS, IS, RPE, and choroid. In the center of the IR lesion (Fig. 13b), OSs have rounded up, *i.e.*, outer portions of broken OSs have formed circular profiles with vacuolated membranes found in the centers. The RPE appears to be missing some melanin granules, and the cytoplasm is edematous and lightly stained, but intact. Bruch's membrane shows an increased lamellar density (arrows). Polymorphonuclear leukocytes (PMNs) are present in the choroidal vasculature, which is not congested.

Figure 13c, taken through the center of the argon lesion shows OSs with a finer vesiculation (FV) or none at all. Large macrophages (M) are seen engulfing outer segment debris (double arrows) and melanin granules (arrows). The RPE shows more extensive vacuolization than in the IR lesions and the underlying choroidal vessels show congestion (C).

Discussion

The results demonstrate both the unique nature of the IR-laser-induced ocular damage and the power of the SLO and OCT techniques in detecting such damage and differentiating the effects within the various layers of the ocular medium and retina/choroid. Noteworthy is the fact that the SLO was able to *detect IR-induced lesions in the retina* (Fig. 6) even when the exposure dose was below that which yielded lesions detectable by fundus camera observation. Also of interest is the OCT image revealing the path of the 1.318-μm laser beam through the aqueous humor at two months postexposure (Fig. 8). The 'track' is clearly seen to be in line with the corneal and lens lesions induced by the 1.318-μm exposure, *and is prominent even when the imaging beam is not aligned with normal incidence to the corneal and lens surfaces. This latter observation differentiates the aqueous scattering from OCT artifact usually associated with specular reflection. There may be an analogy between the secondary aqueous reaction (visualized between the corneal and lens lesions) and the delayed inflammatory response (also noted at two months postexposure;*

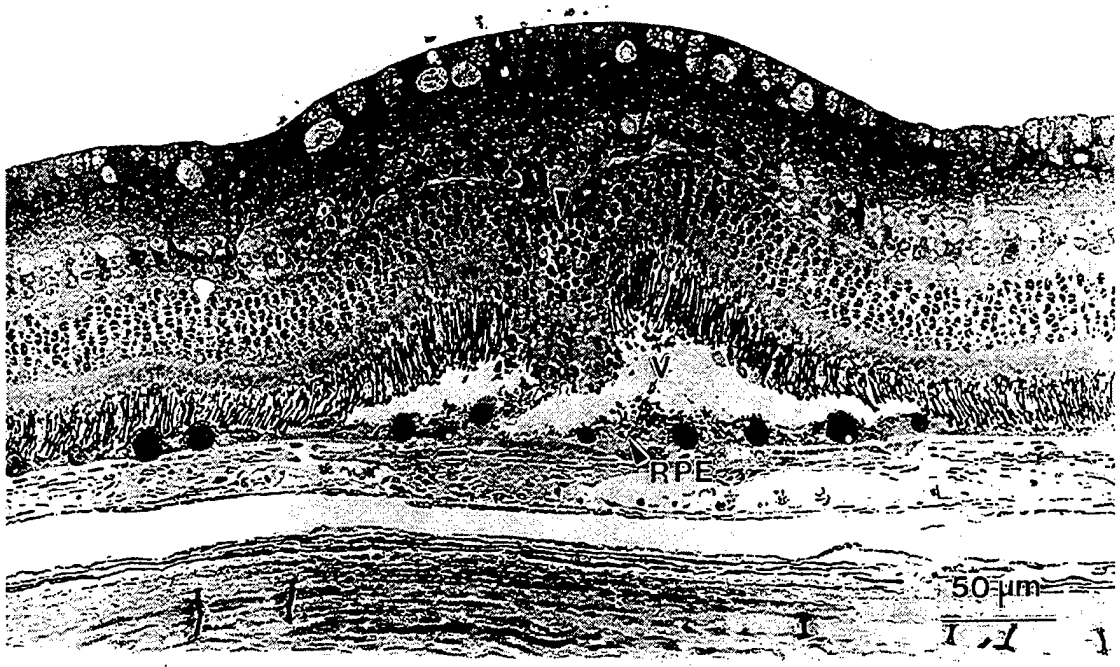

a

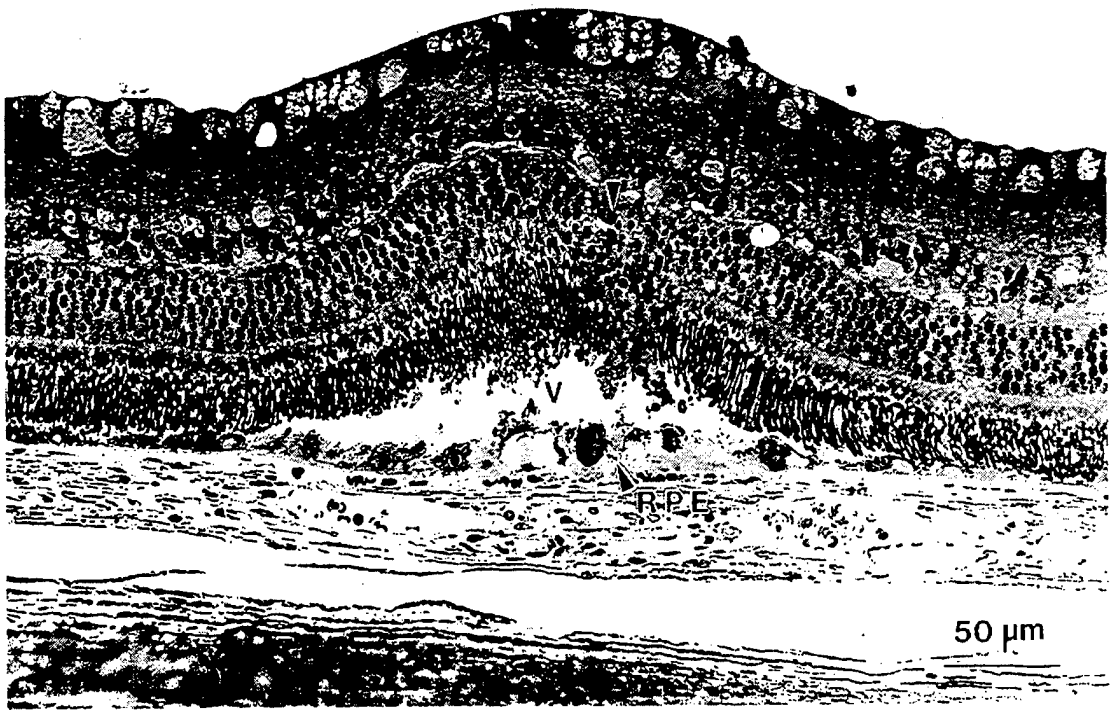

b

Fig. 11. Light micrographs through the centers of the argon marker lesions shown in Figure 3. *11a.* Center marker lesion; *11b.* right-hand marker lesion.

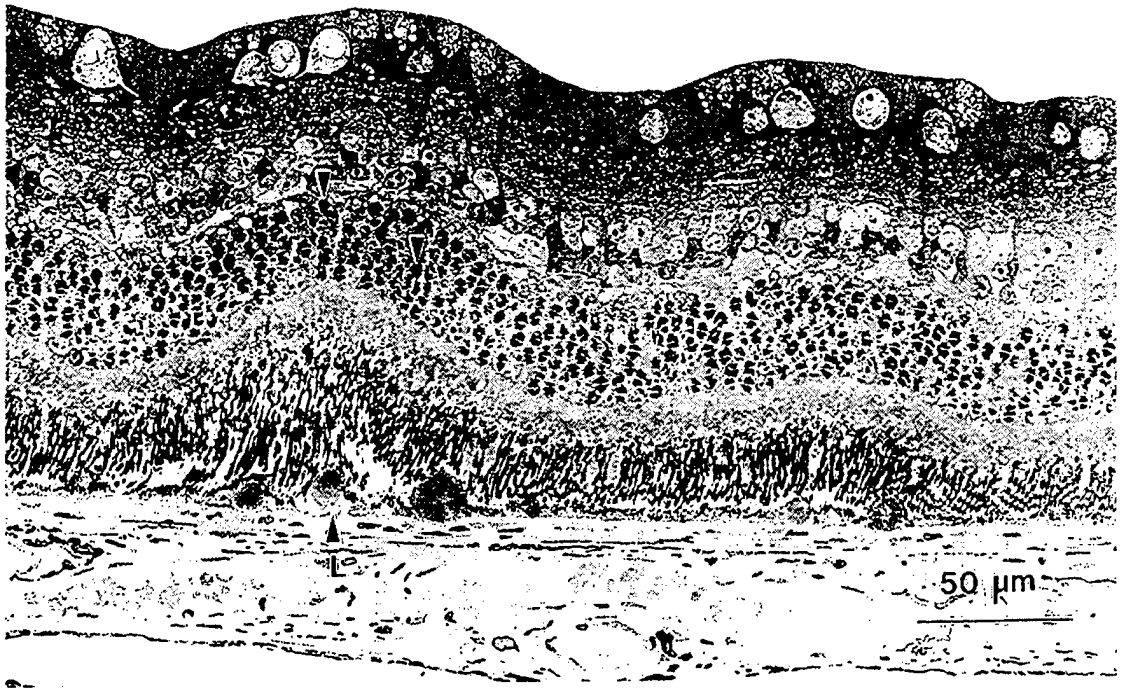

a

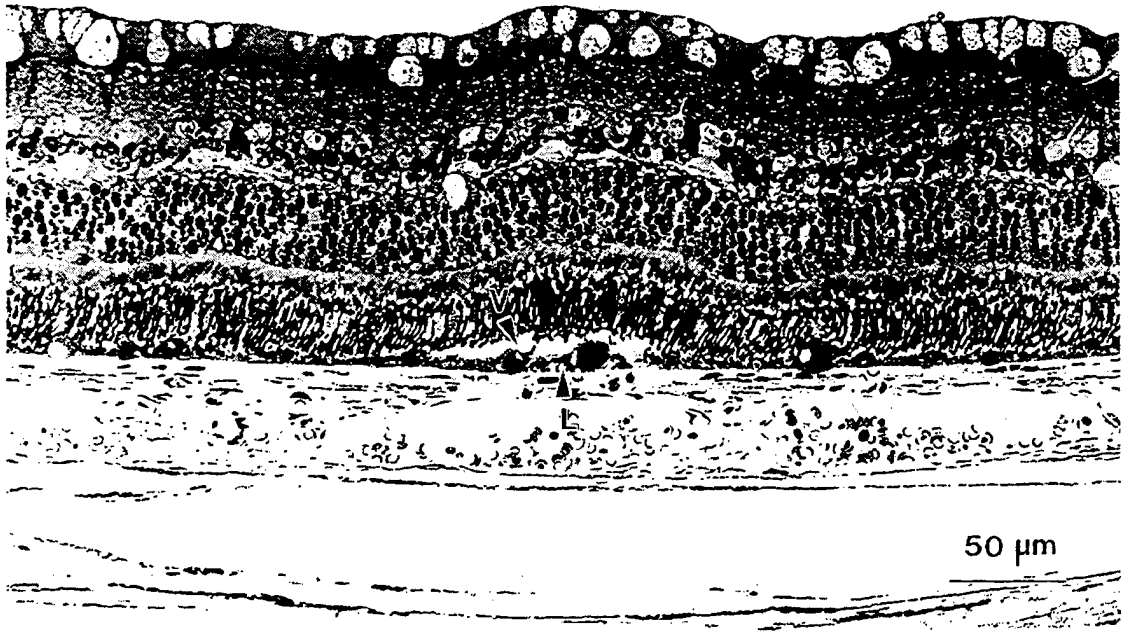

b

Fig. 12. Light micrographs through the centers of the IR lesions in the same eye as that seen in Figure 3, but at exposure sites at which lesions were not ophthalmoscopically visible (see text).

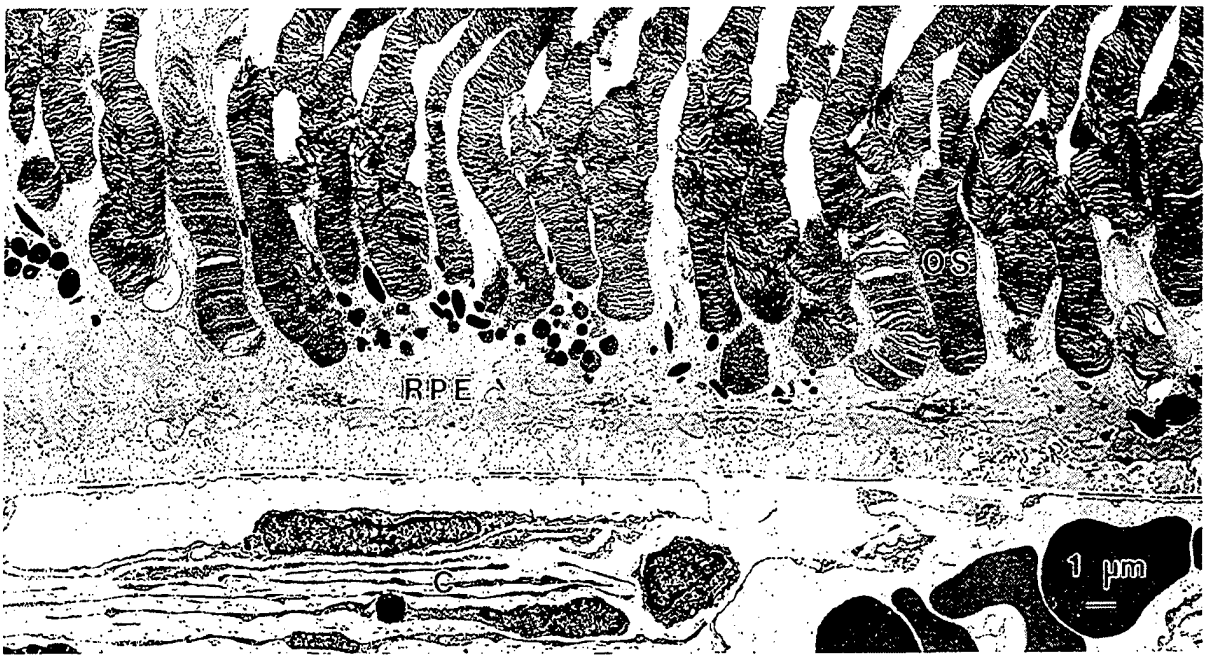

Fig. 13a.

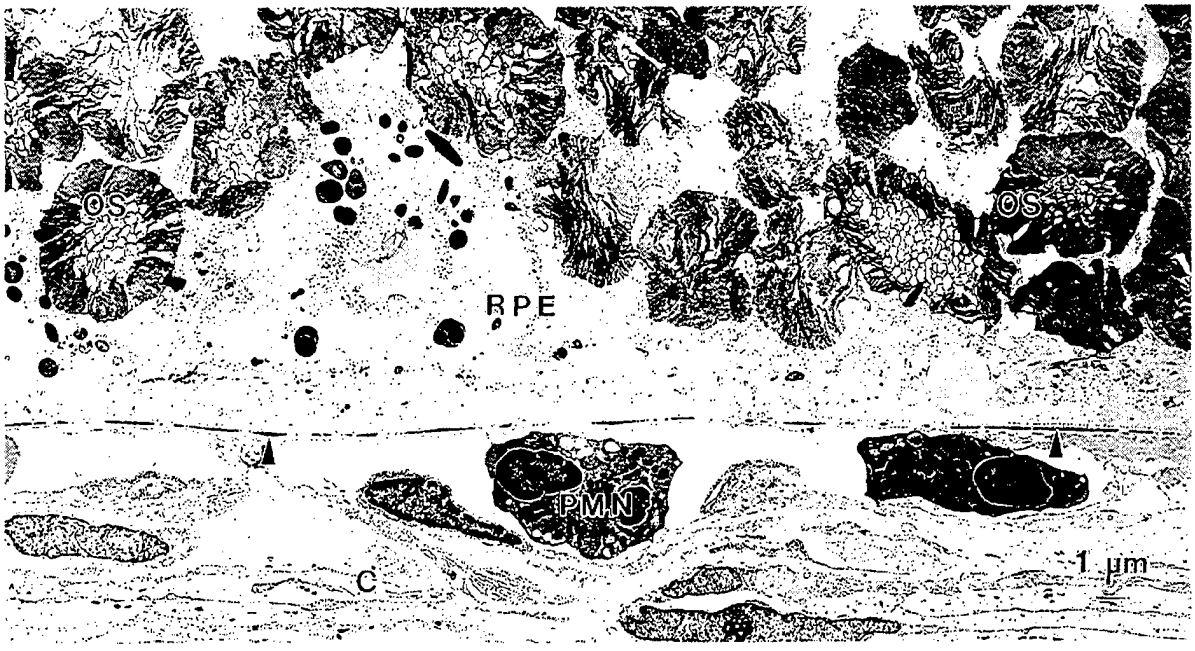

Fig. 13b.

see Fig. 9) involving the retinal lesion and adjacent vitreous.

With 1.318-µm exposure doses sufficient to induce funduscopically visible retinal lesions, both SLO and OCT imaging indicate involvement of the inner retina. But stepping through the retinal layers with the SLO shows that the lesions are largest and most readily detected in the *outer retina* (Fig. 6). Pathological evaluation shows that the 1.318-µm lesions are centered in the ONL.

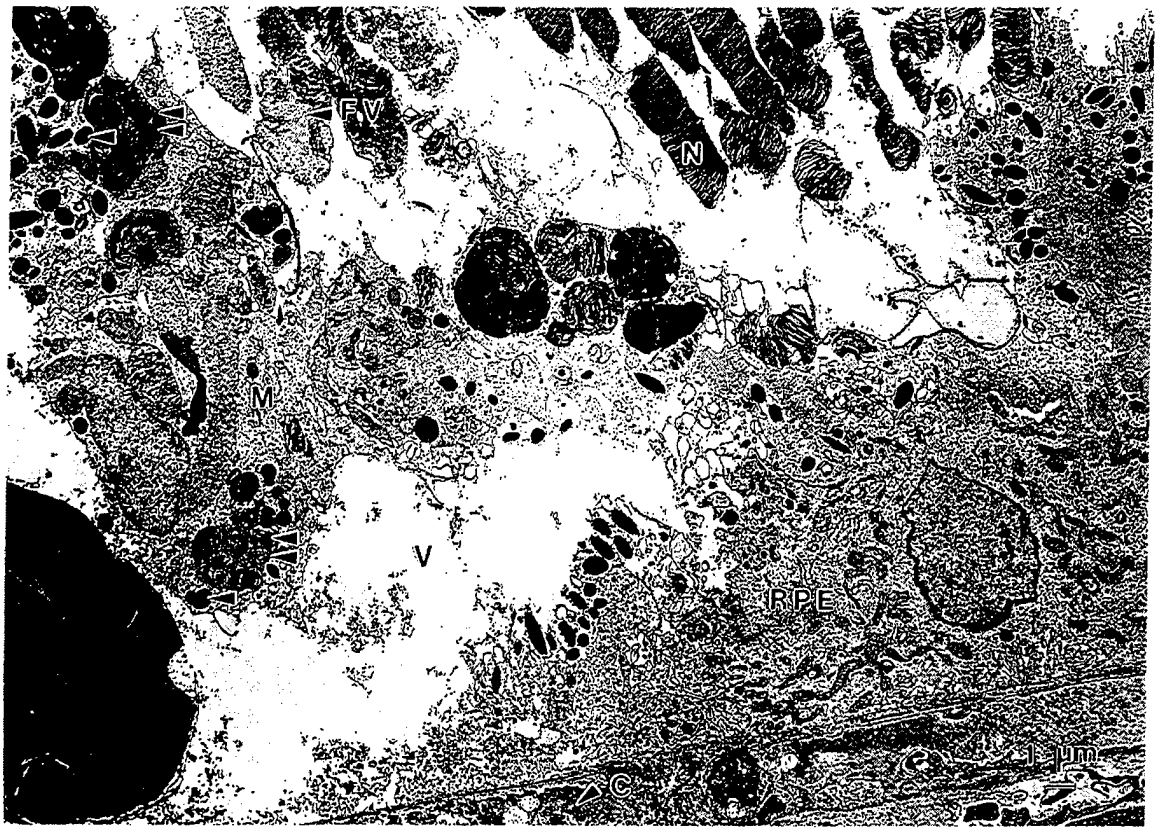

Fig. 13c.

Fig. 13. TEM micrographs through: *13a.* the control tissue; *13b.* the center of the large IR lesion in Figure 3; and *13c.* the center of the central argon lesion in Figure 3.

Comparing the pathology of the argon and IR retinal lesions at 48 hours postexposure (Figs. 10 to 13), reveals that the argon lesions show more RPE involvement than the IR lesions, but that photoreceptor nuclear involvement was greater with the IR exposures. Inner nuclear layer response was also greater in the IR lesions. Further, the pronounced inflammatory reaction observed at the vitreous-ILM interface suggests that the IR exposures induced more inner retinal effects. All these observations emphasize that the gradual tissue absorption of the IR radiation results in involvement of the full retinal thickness.

The argon marker lesions seen in Figures 3 to 6 were induced by exposures much higher than the threshold dose required to produce a minimal visible lesion. At threshold, the argon lesion would be ~20-30 μm in diameter and the damage confined primarily to the RPE layer[14] where the greatest part of the absorption occurs. Only as the exposure does is increased above threshold does the thermal conduction away from the highly absorbing RPE layer result in damage to more distal retinal and choroidal tissues. In contrast, the 1.318-μm lesion at threshold (*i.e.*, at the lowest exposure does which produces an ophthalmoscopically detectable lesion) is already several hundred microns in diameter, in part because chromatic aberrations at this wavelength yield a much larger image diameter at the retina. And, as indicated above, the threshold IR lesions involves the full thickness of the retina. ICG angiography and the pathological evaluation also indicate minor choroidal involvement.

The 1.318-μm retinal effect also differs from thermal damage following visible-wavelength laser exposures, both in the long delay times before ophthalmoscopically visible lesions are first observed and in the late progressive effects which have been detected. Visible-wavelength laser-in-

duced lesions are generally observed shortly following exposure and, within hours, *stabilize so that no further changes in appearance are noted, save for the gradual fading in* reflectivity over a period of months. In contrast, the IR retinal lesions were first detected only upon re-examination of subjects on the day following exposure, and thereafter. This delay time in the formation of observable damage is suggestive of a damage mechanism such as thermally-induced programmed cell death or apoptosis[15]. Funduscopically, the IR lesions reached maximum intensity at ~48 hours postexposure. *Pathological evaluation at that time revealed the presence of* numerous inflammatory cells in the vitreous and at the ILM interface directly above the IR retinal lesion. The suggestion is made that this finding is a prognosticator of the late inflammatory response which expressed itself as the large, irregularly shaped opacity found at a 1.318-μm exposure site at two months postexposure (Fig. 9). SLO observation of the two-month inflammatory response indicated strong involvement of the inner retina. Continued monitoring of the subject showed that the inflammatory response gradually cleared during the following month, so that by three months postexposure the underlying circular lesion was again visualized.

In summary, the IR wavelength studied (1.318 μm) defines the upper limit of wavelength where there is still sufficient transmission through the ocular medium to affect the retina of the eye[1,2]. Because such a large percentage of the incident IR laser radiation is absorbed by the ocular medium, and because that radiation which reaches the retina is not focused to as small an image size nor absorbed there as strongly as visible wavelengths, a very high dose of IR must be incident at the cornea to cause detectable funduscopic damage to the retina. Thus, the term 'eye-safe' has been applied even to higher power lasers in this segment of the IR wavelength region. However, it should be emphasized that applying the term 'eye-safe' to a given wavelength or wavelength band without regard to the laser power level and other beam characteristics, is inconsistent with published laser safety standards. Further, we report several observations which belie the 'eye-safe' terminology. First, a threshold IR lesion involves a volume of retinal tissue many orders of magnitude greater than that affected by a threshold-visible laser exposure and, hence, represents a more serious injury. Second, the usual threshold definition of a minimal visible lesion detected by funduscopic observation is not appropriate for the IR wavelength, since the monochromatic SLO imaging can detect retinal effects induced by significantly lower exposure doses. These observations, together with the delayed inflammatory responses observed histologically (Fig. 10) and funduscopically (Fig. 9), suggest that serious visual consequences may develop following a 'threshold' IR laser exposure.

Acknowledgements

The research reported here was supported by the US Army Medical Research Detachment and the Optical Radiation Division, Occupational and Environmental Health Directorate, USAF Armstrong Laboratory, Brooks AFB, TX, under Contract F33615-92-C-0017 (TASC), let by the USAF. SAB and JGF received support from the Air Force Office of Scientific Research (#2312AA-92AL014). The work was conducted at Brooks AFB, TX.

References

1. Maher EF: Transmission and absorption coefficients for ocular media of the rhesus monkey. SAM-TR-78-32, 1978
2. Boettner EA: Special transmission of the eye. University of Michigan, Final Report, USAF Contact F41(609)-2966, 1967
3. Zuclich JA, Gagliano DA, Cheney F, Stuck BE, Zwick H, Edsall P, Lund DJ: Ocular effects of penetrating IR laser wavelengths. SPIE 2391:112-125, 1995
4. Webb RH, Hughes GW, Delori FC: Confocal scanning laser ophthalmoscope. Appl Opt 26:1492-1499, 1987
5. Zwick H, Gagliano DA, Stuck BE, Lund DJ: Comparison of solar and laser macular retinal injury using SLO spectral imaging. SPIE 2134B:54-63, 1994
6. Huang D, Swanson EA, Lin CP, Schuman JS, Stinson WG, Chang W, Hee MR, Flotte T, Gregory K, Puliafito CA, Fujimoto JG: Optical coherence tomography. Science 254:1178-1181, 1991
7. Hee MR, Izatt JA, Swanson EA, Huang D, Schuman JS, Lin CP, Puliafito CA, Fujimoto JG: Optical coherence tomography of the human retina. Arch Ophthalmol 113:326-332, 1995
8. Puliafito CA, Hee MR, Lin CP, Peichel E, Schuman JS, Duker JS, Izatt JA, Swanson EA, Fujimoto JG: Imaging of macular diseases with optical coherence tomography. Ophthalmology 120:217-229, 1995
9. Drexler W, Hitzenberger CK, Sattmann H, Fercher AF: Measurement of the thickness of fundus layers by partial

coherence tomography. Opt Engineer 34:701, 710, 1995
10. Fujimoto JG, Brezinski ME, Tearney GJ, Boppart SA, Bouma B, Hee MR, Southern JF, Swanson EA: Biomedical imaging and optical biopsy using optical coherence tomography. Nature Med 1:970-972, 1995
11. Pan Y, Birngruber R, Rosperich J, Engelhardt R: Low-coherence optical tomography in turbid tissue: theoretical analysis. Appl Opt 34:6564-6574, 1995
12. Schuschereba ST, Bowman PD, Vargas JA, Johnson TW, Woo FJ, McKinney L: Myopathic alterations in extraocular muscle of rats subchronically fed pyrodostigmine bromide. Toxicol Pathol 18:103-123, 1990
13. Karnovsky MJ: A formaldehyde-glutaraldehyde fixative of high osmolality for use in electron microscopy. J Cell Biol 27:137A-138A, 1965
14. Frisch GD, Beatrice ES, Holsen RC: Comparative study of argon and ruby retinal damage thresholds. Invest Ophthalmol 10:911-919, 1971
15. Majno G, Joris I: Apoptosis, oncosis and necrosis: an overview of cell death. Am J Pathol 146:3-15, 1995

Ocular Exposure in the Industrial Environment

David H. Sliney, Ph.D.
Laser/Optical Radiation Program
US Army Center for Health Promotion and Preventive Medicine
Aberdeen Proving Ground, MD 21010

Lengthy Exposures to Infrared from Radiant Heat Sources

- Workers in the glass and metals industries, foundry workers, blacksmiths and others working near molten glass and metals have been traditionally exposed to average irradiances of 80-400 mW/cm^2 over a working lifetime
- Industrial heat cataracts were not uncommon at the turn of the century

Infrared Radiation & Heat Stress

- Heat is a physical agent which is not *toxic* in the usual sense.
- Heat is a physiological factor. It exists.
- Thermal injury is rare because of skin and ocular protective avoidance mechanisms to thermal pain
- Molecular damage occurs at normal body temperature. Heat stress aggravates this

Workshop on **Infrared Lasers and Millimeter Waves**
The Links Between Microwaves and Laser Optics
Brooks AFB, TX
January 21-22, 1997

CO_2 Laser Effects on the Skin and Cornea

Bruce E. Stuck, US Army Medical Research Detachment, Walter Reed Army Institute of Research, 7914 A Drive, Brooks AFB, TX 78235-5138

ABSTRACT

The ANSI Z136.1 - 1993 permissible exposure limits in the far infrared are primarily based on a robust data base describing corneal and cutaneous threshold effects for carbon dioxide (CO_2) laser radiation at 10.6 μm. The dependence of the minimally visible corneal lesion dose and the minimal erythemic dose on exposure durations from 10^{-7} to 10 seconds are described and compared with the Z136.1 permissible exposure limits. In Z136.1, permissible exposure limits are not dependent on wavelength from 2.6 μm to 1 mm. At the wavelength of 1 mm (300 GHz), the IEEE C95.1 - 1991 and the Z136.1 are in harmony at 10 mw/cm^2 for long exposure durations (10 seconds) and large irradiance diameters (area >1000 cm^2 -Z136.1 Section 8.4.2). Absorption coefficients based predominantly on available water absorption data in the infrared (1 - 10 μm) are compared to those in the 1- 10 mm region. While 10.6 μm is absorbed more strongly than mm wavelengths, infrared wavelengths in the 3.6 to 3.9 μm have comparable absorption depths (based on water absorption). The wavelength dependence of corneal thresholds for pulsed laser exposure is indicative of the relative absorption of the cornea. Thermal models which adequately describe corneal and cutaneous injury threshold data should be applied to the mm wavelength region. More experimental data are needed for repetitive pulse and long exposure durations for infrared wavelengths (or mm wavelengths) where the absorption varys significantly.

Workshop on

Infrared Lasers and Millimeter Waves

The Links Between Microwaves and Laser Optics

Brooks AFB, TX

January 21-22, 1997

CO_2 Laser Effects on the Skin and Cornea

Bruce E. Stuck
USAMRD-WRAIR
7914 A Drive
Brooks AFB, TX 78235

Voice: 210-536-4621; Fax: 210-536-3450; EMAIL: Stuck@LASER.BROOKS.AF.MIL

Infrared Lasers and Millimeter Waves

The Links Between Microwaves and Laser Optics

Initial Comments

- **Exposure Sources and Biological End Points:**

Lasers: Available with sufficient power or energy per pulse to produce acute biological effects for "clinical" and pathological criteria.

Millimeter sources: Low power; requiring long exposure durations and biological end points not readily assessable

- **Exposure Standards:**

Z136.1 - Large empirical data base for wide range of exposure conditions; most (not all!) effects understood from mechanism standpoint; MPE exposure doses are directly measurable

C95.1 - Large data base for some exposure conditions, fields altered by specimen geometry/composition; SAR based requiring calculation assumptions

- **Need more biological data**
- **Beware of athermal effects**

The ANSI Z136.1-1993 and the IEEE C95.1-1991 Standards

Wavelength and Frequency ($\lambda\nu = c$)

Wavelength	Frequency
500 nm (0.5 μm)	600,000 GHz
1.0 μm (Neodymium Laser)	300,000 GHz
10 μm (CO_2 Laser)	30,000 GHz
100 μm	3,000 GHz
1000 μm or 1 mm	300 GHz
10 mm or 1 cm	30 GHz
11.8 cm	2.45 GHz

The ANSI Z136.1-1993 and the IEEE C95.1-1991 Standards

ANSI Z136.1-1993

Maximum Permissible Exposures (MPE) to Ocular Exposure to a Laser Beam (Table 5)

Wavelength (λ)	Exposure Duration (t)	MPE (Corneal Radiant Exposure)	MPE (Corneal Irradiance)	Notes
μm	seconds	J/cm^2	w/cm^2	
2.6 - 10^3	10^{-9} - 10^{-7}	0.01		See Tables 8 and 9
2.6 - 10^3	10^{-7} - 10	$0.56t^{1/4}$		
2.6 - 10^3	10 - 3 x 10^4		0.1	

Maximum Permissible Exposures (MPE) for Skin Exposure to a Laser Beam

1.4 - 10^3	10^{-9} - 10^{-7}	0.01		See Tables 8 and 9 and Sec. 8.4.2
1.4 - 10^3	10^{-7} - 10	$0.56t^{1/4}$		
1.4 - 10^3	10 - 3 x 10^4		0.1	

Note: $10^3 \mu$m = 1 mm $\Rightarrow$ 300 Ghz

Section 8.4.2: Wavelengths Greater than 1.4 μm. For beam cross-sectional areas between 100 cm^2 and 1000 cm^2, the MPE for exposure durations exceeding 10 s is 10,000/A_s , where A_s is the area of the exposed skin in cm^2. For exposed skin areas exceeding 1000 cm^2 , the MPE is 10 mW/cm^2.

The ANSI Z136.1-1993 and the IEEE C95.1-1991 Standards

IEEE C95.1-1991

Excepts from Part A of Tables 1 and 2: Electromagnetic Fields
Maximum Permissible Exposure for Controlled and Uncontrolled Environments

1 Frequency Range	2 Electric Field Strength (E)	3 Magnetic Field Strength (H)	4 Power Density (S) E-Field, H-Field	5 Averaging Time $\|E\|^2$, $\|H\|^2$, or S
Mhz	V/m	A/m	mW/cm^2	minutes
100-300	61.4	0.163	1.0	6
300 - 3000			f/300	6
3,000 - 15,000			10	6
15,000 - 300,000 λ = 2 cm - 1 mm			10	$616{,}000/f^{1.2}$
300,000				0.16 ($\approx$ 10 sec)

f = frequency in Mhz

The ANSI Z136.1-1993 and the IEEE C95.1-1991 Standards

MPE Comparison at 300 GHz

	Radiant Exposure		Irradiance	
Exposure Duration seconds	MPE Z136.1 J/cm^2	MPE C95.1 J/cm^2	MPE Z136.1 w/cm^2	MPE C95.1 w/cm^2
10	1	0.1	0.1	0.01
1	0.56	0.1	0.56	0.1
0.1	0.32	0.1 0.02	3.15	1.0 0.2
0.01	0.18	0.02	17.7	2.0
0.001	0.1	0.02	100	20
0.0001 (100 μs)	0.056	0.02	560	200

Z136.1 MPE = $0.56t^{1/4}$ J/cm^2 for $10^{-7} < t < 10$ sec

C95.1 Peak MPE = [MPE x Avg. Time(sec)]/[5 x Pulsewidth] for t < 100 msec
At 300 GHz, Ave. Time = 10 sec and MPE = 10 mw/cm^2

THRESHOLD EFFECTS OF CO_2 LASER RADIATION
AT 10.6 um ON PORCINE SKIN

Irradiance watts/cm^2	Radiant Exposure joules/cm^2	Exposure Duration msec	Irradiance* Diameter cm	Criterion Response
9.5	2.61	275(220,330)**	1.26	24 hr Erythema
9.5	5.60	590(540,640)	1.26	1 hr Blister
37.4	1.48	39.6(37.9,41.4)	1.33	24 hr Erythema
37.4	3.57	95.4(89.8,101.2)	1.33	1 hr Blister
240	0.97	4.05(3.82,4.29)	0.80	24 hr Erythema
240	1.61	6.71(6.36,7.08)	0.80	1 hr Blister

* The irradiance diameter is defined at the 1/e points of the Gaussian intensity distribution.

** The ED_{50} exposure time for the specified exposure condition. The 95% confidence interval about the ED_{50} exposure time is given in the parentheses.

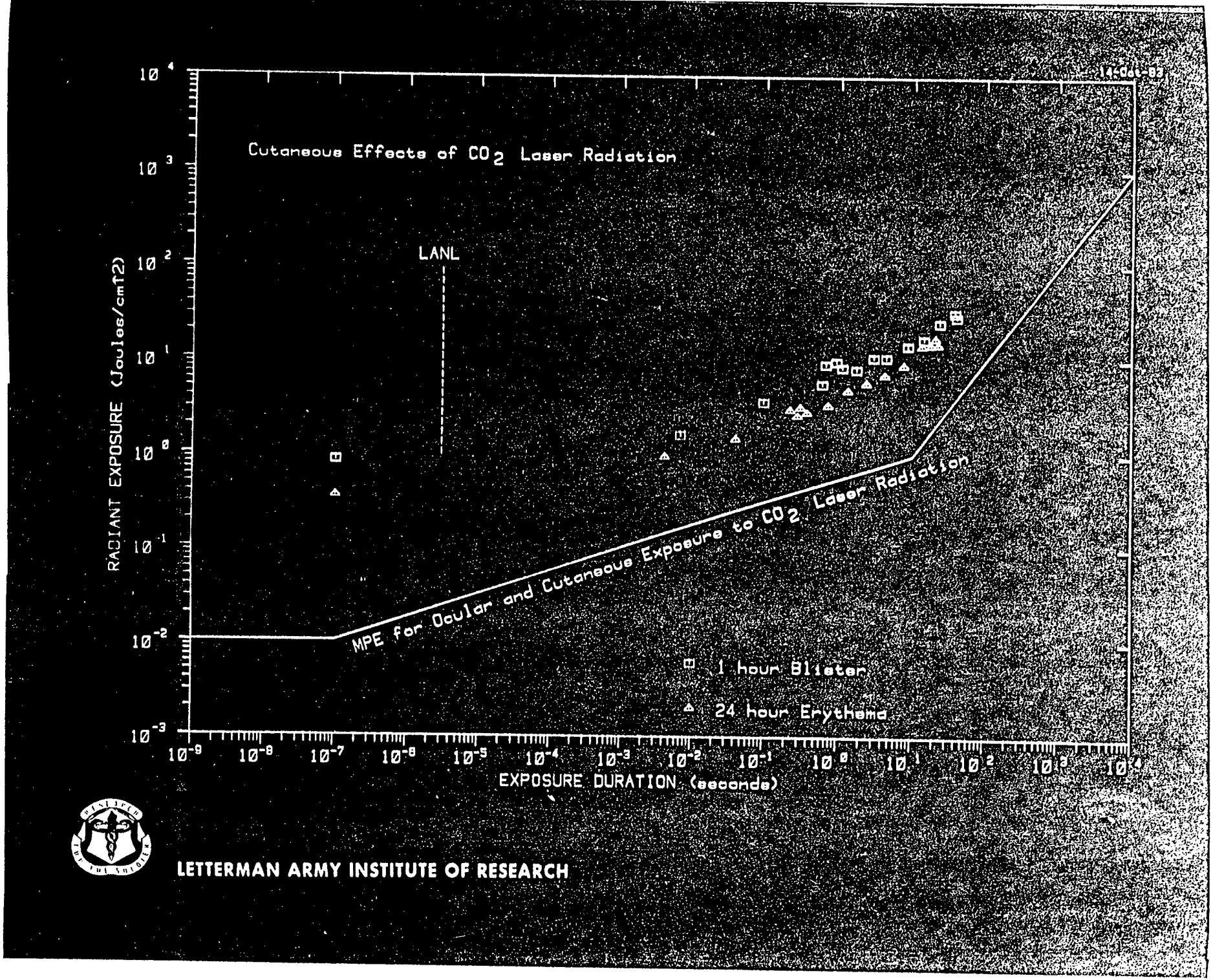
Cutaneous Effects of CO_2 Laser Radiation
LANL
RADIANT EXPOSURE (Joules/cmf2)
10^{4}
10^{3}
10^{2}
10^{1}
10^{0}
10^{-1}
10^{-2}
10^{-3}
MPE for Ocular and Cutaneous Exposure to CO_2 Laser Radiation
1 hour Blister
24 hour Erythema
10^{-9} 10^{-8} 10^{-7} 10^{-6} 10^{-5} 10^{-4} 10^{-3} 10^{-2} 10^{-1} 10^{0} 10^{1} 10^{2} 10^{3} 10^{4}
EXPOSURE DURATION (seconds)
LETTERMAN ARMY INSTITUTE OF RESEARCH

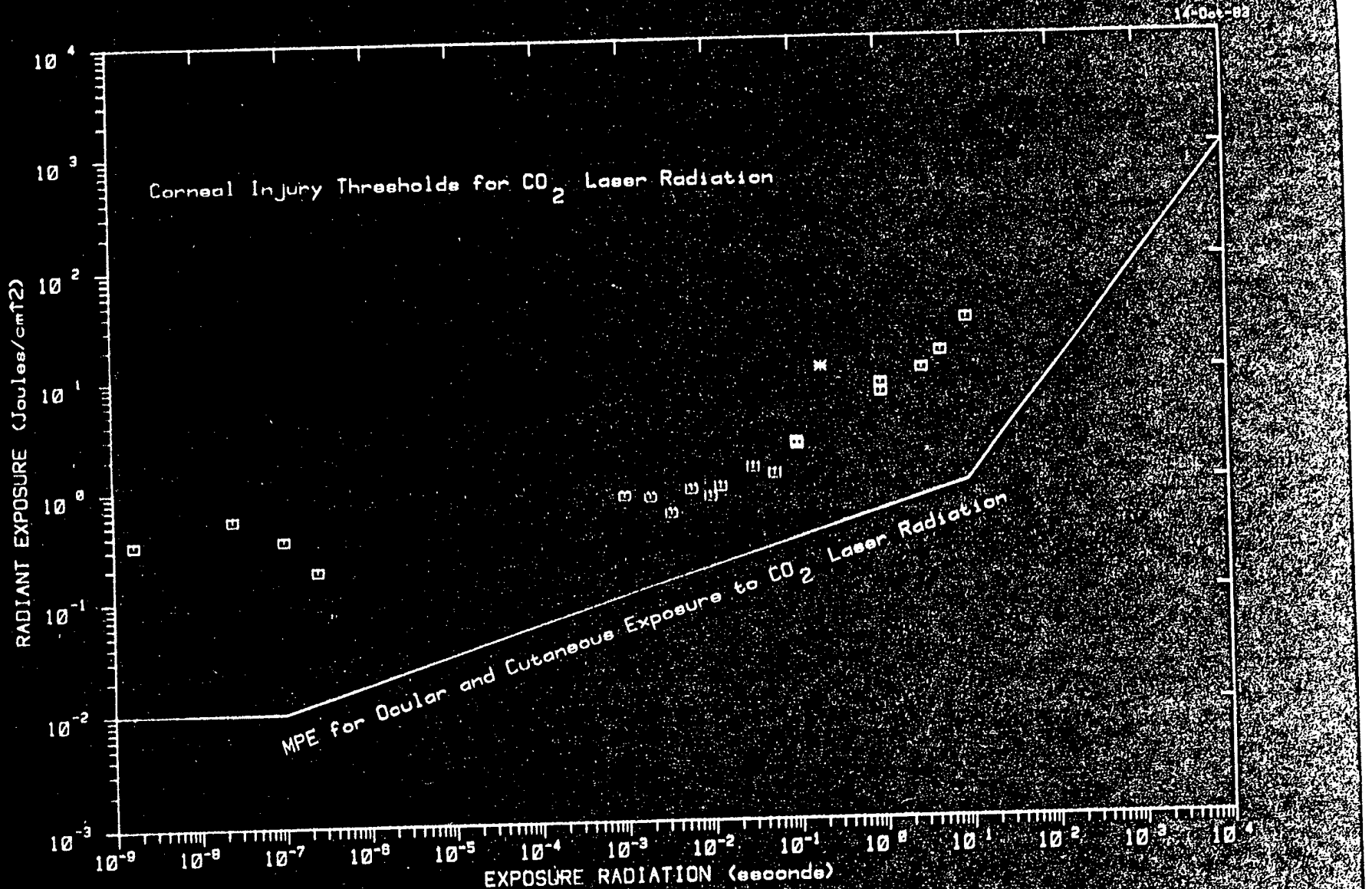

LETTERMAN ARMY INSTITUTE OF RESEARCH

1031-83-1

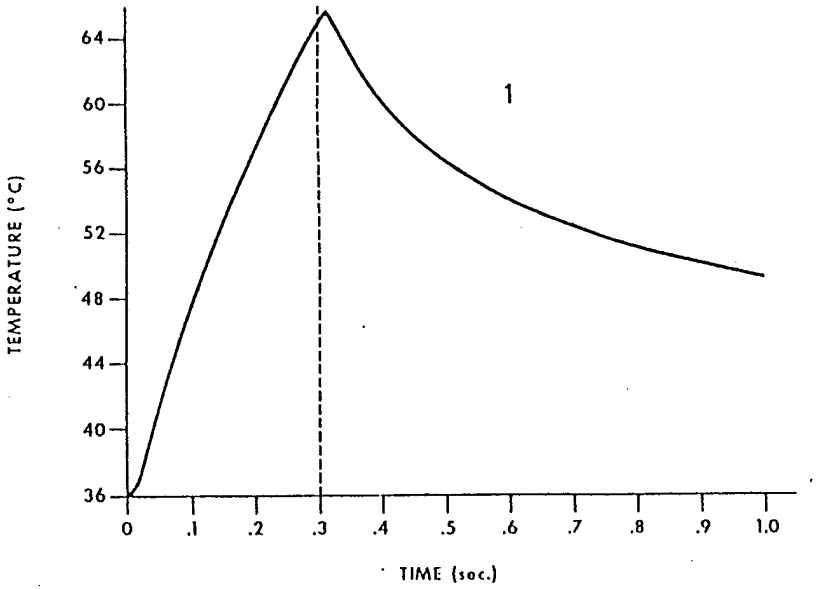
1
TEMPERATURE (°C)
64
60
56
52
48
44
40
36
0
.1
.2
.3
.4
.5
.6
.7
.8
.9
1.0
TIME (sec.)

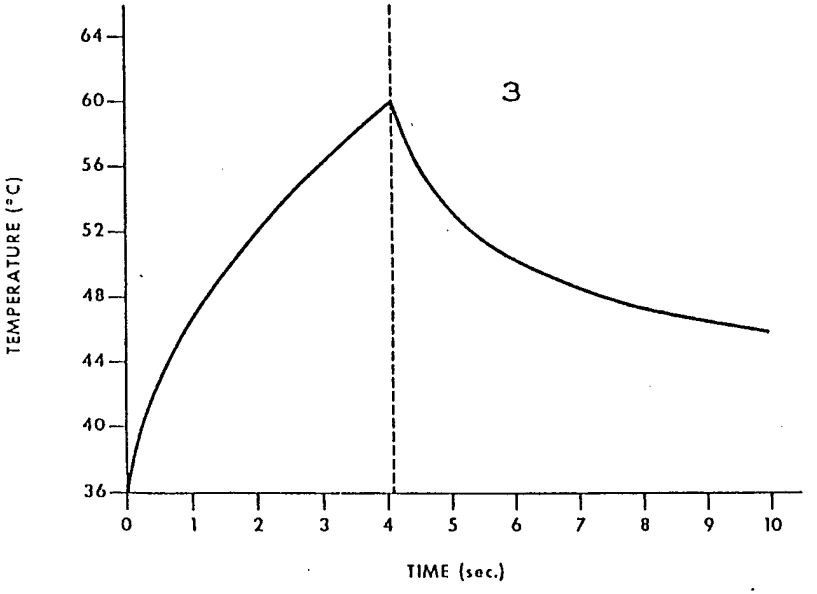
3
TEMPERATURE (°C)
64
60
56
52
48
44
40
36
0
1
2
3
4
5
6
7
8
9
10
TIME (sec.)

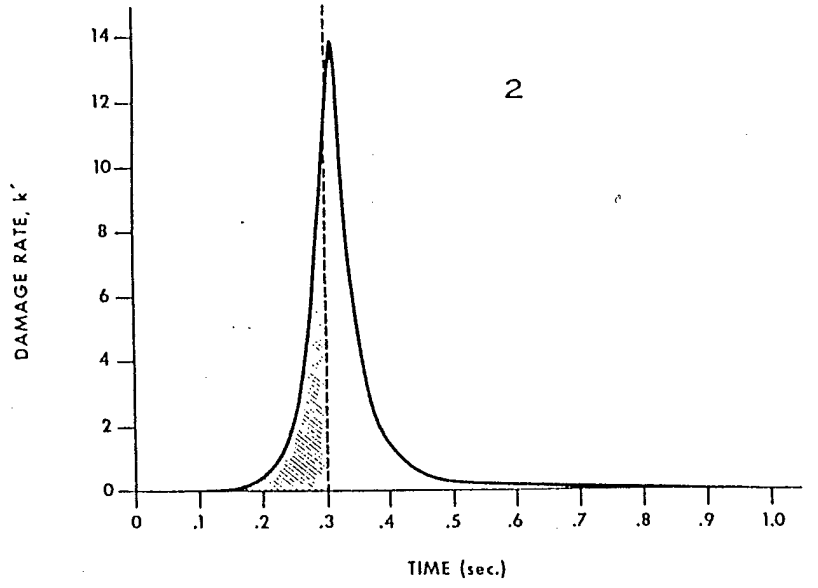
2
DAMAGE RATE, k'
14
12
10
8
6
4
2
0
0
.1
.2
.3
.4
.5
.6
.7
.8
.9
1.0
TIME (sec.)

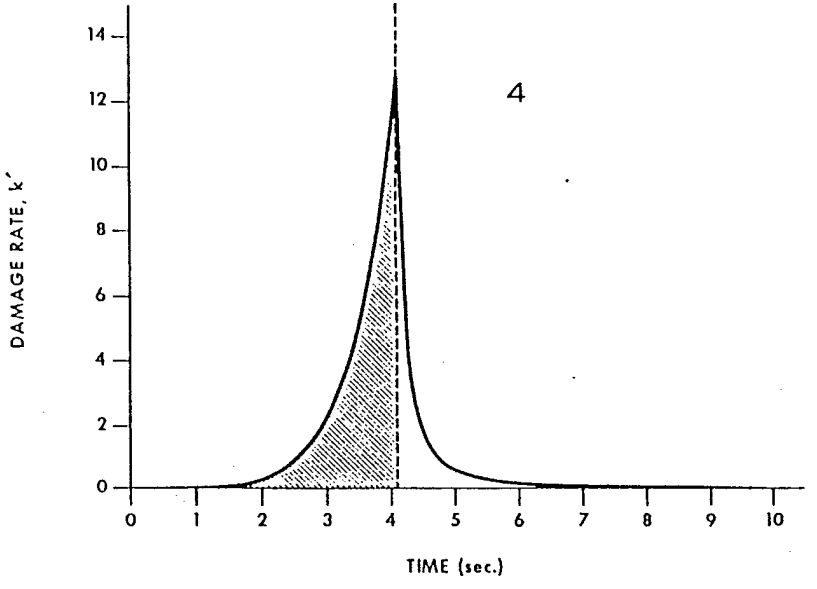
4
DAMAGE RATE, k'
14
12
10
8
6
4
2
0
0
1
2
3
4
5
6
7
8
9
10
TIME (sec.)

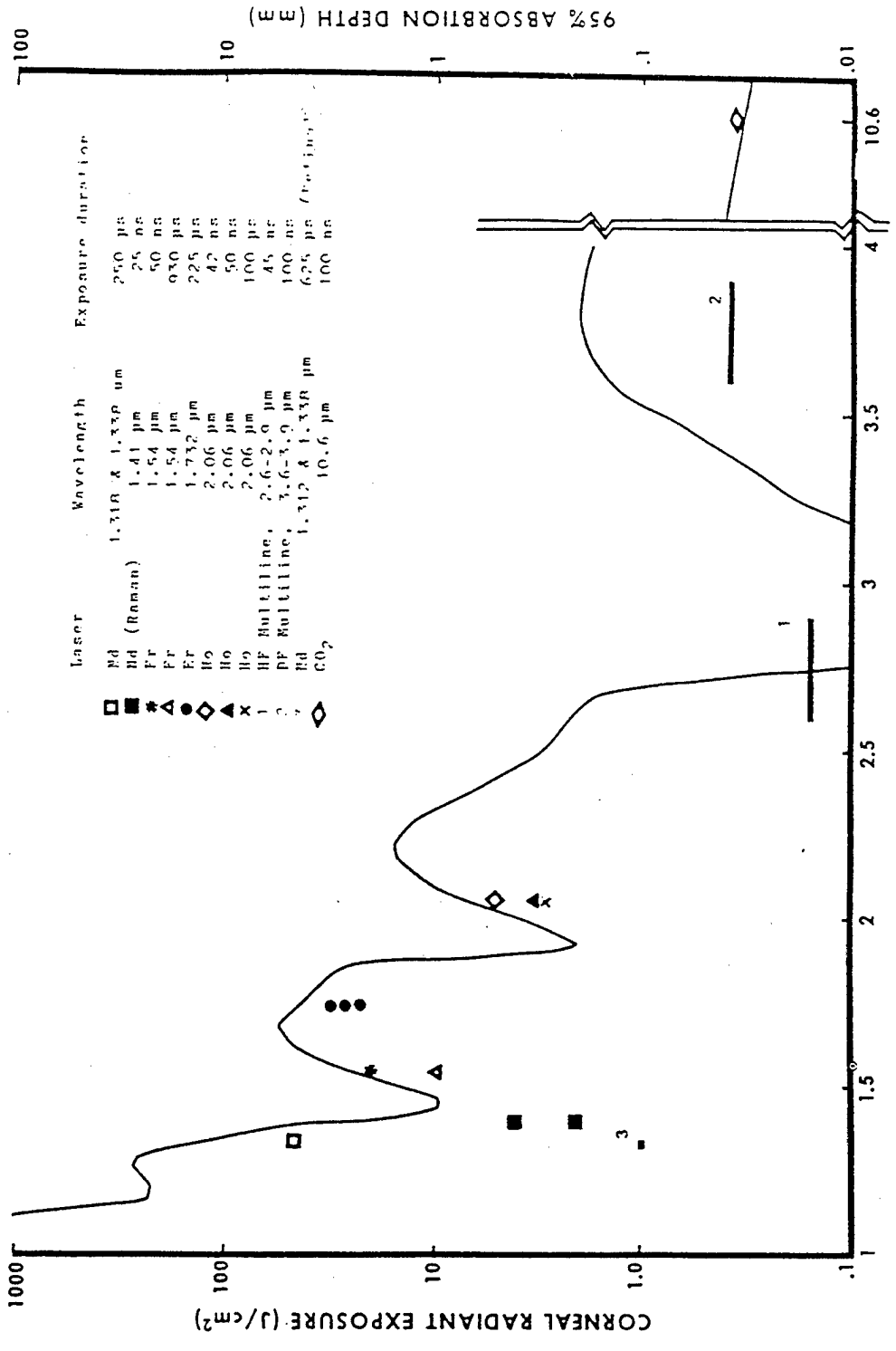

Figure 4. The ED_{50} for the production of a corneal lesion for exposure conditions given in Table 2 as a function of wavelength. The solid curve is the depth (right hand axis) at which 95% of the incident energy is absorbed in physiological saline (the absorption properties of physiological saline approximate those of the outer ocular media). The data point at 3 is the ED_{50} for the production of a retinal lesion obtained at the 1.33 μm.

Infrared Lasers and Millimeter Waves

The Links Between Microwaves and Laser Optics

Water Absorption Coefficients

Wavelength	δ (mm)	α (cm^{-1})	Reference
1.06 μm	21	0.95*	Maher, 1978
1.3 μm	8.69	2.3*	Maher, 1978
1.54 μm	2.22	9.0*	Maher, 1978
2.06 μm	0.71	28*	Maher, 1978
2.9 μm	0.0015	12900	Hale, 1973
3.6-3.9 μm	0.18 - 0.11	112-180	Hale, 1973
10.6 μm	0.024	817	Hale, 1973
1 mm	0.138	144	Ryakovdkaya, 1983
2 mm	0.174	114	Ryakovdkaya, 1983
5 mm	0.302	66	Ryakovdkaya, 1983
8 mm	0.472	42	Ryakovdkaya, 1983
10 mm	0.615	32	Ryakovdkaya, 1983

$\alpha = 2/\delta$: α = absorption coefficient; $\delta = 1/e^2$ depth ($\cong$86% absorbed)

* Corneal absorption coefficients

Infrared Lasers and Millimeter Waves

The Links Between Microwaves and Laser Optics

Conclusions

- **Harmony of Standards**:

Possible at 300 GHz possible with thermal models and careful review of laser biological data base

- **Use the Laser Bioeffects Data Base and Modeling Efforts**
- **Review laser bioeffects dose-response relationships from a SAR perspective** (perhaps already considered or done)
- **Need more data** for repetitive pulse exposure and long duration exposures for the "penetrating" infrared wavelengths (or at mm wavelengths)

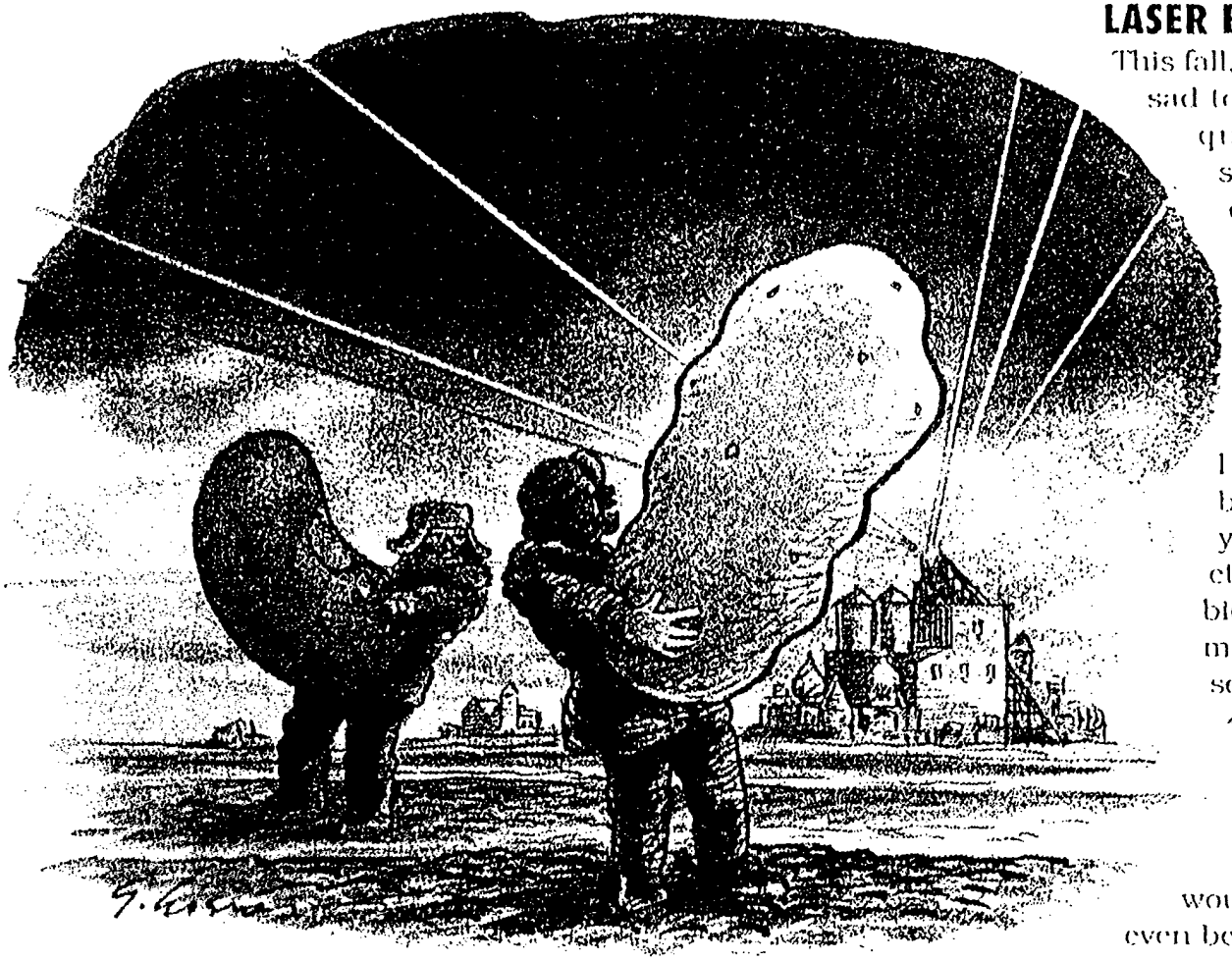

LASER BEANS

This fall, when you're mulling over your sad tomato harvest or the mediocre quality of your homegrown squash, you just might want to contact Tekhnika Co. Ltd., a Moscow firm with some bright ideas on agriculture.

Tekhnika boasts in a recent issue of *Laser Inform*, a newsletter about Russian photonics, that its novel infrared laser/magnetic-field bio-stimulators can optimize your plantings of grains, vegetables and flowers. Placing the biostimulators so that they illuminate a conveyor loaded with seeds can boost harvests by 10 to 40 percent and improve plants' resistance to environmental factors (drought, frost, etc.), the firm says.

If true, such an improvement would be no small beans; it might even be big potatoes. □

ACUTE THERMAL CATARACTS FROM ANIMAL DATA

M.L. Wolbarsht
Duke University

Abstract

Two theories for cataract formation by IR radiation are reviewed: Goldmann's hypothesis that cataracts result from heat transferred to the lens from the IR absorbed by the iris is contrasted with Vogt's hypothesis in which the IR energy is absorbed directly by the lens. Data shows that cataracts can be formed by both mechanisms and that cataracts resulting from long-term exposures are most likely in accord with Vogt's hypothesis. Data from laser and IR heat lamp exposures to in vivo lenses and incubated whole lenses and various extracted lens crystallins, as well as electrophoresis of lens crystallins on polyacrylamide gels and other types of substrates, show conversion of soluble α and β_H crystallins into insoluble protein factions with high molecular weight as a result of exposure to broad band heat or narrow band IR laser radiation. Sub-threshold laser exposure levels produce a markedly decreased mobility of the β crystallins in the lens. Superthreshold exposure levels which produce cataracts show reciprocity between exposure power level and duration over many orders of magnitude even when the dose is fractionated and delivered over several days. This constant energy/dose-related requirement for cataract formation suggests major contributions from photochemical rather than thermal mechanisms, while the partial failure of this relation for longer exposures possibly indicates a some type of repair process.

Introduction

There are two conventional theories for the etiology of infrared cataracts. One theory (Goldmann, 1933) holds that radiant energy in the infrared is absorbed in the iris and converted into heat that is subsequently transferred to the lens leading to a "thermal" cataract. A different theory, also based on a thermally mediated train of events, was proposed by Vogt (1912, 1932) in which direct absorption of radiant energy, particularly in the infrared, by the lens heats it and, thereby, initiates cataract formation. This later theory ignores the relatively low absorption by the lens in the visible spectrum and its only slightly greater absorption in the near infrared. However, present data does, indeed, indicate a possible damage mechanism for IR cataractogenesis depending on direct absorption by the lens, albeit the mechanism is photochemical rather than thermal (Pitts et al., 1981; Wolbarsht, 1980). These data further suggest that such a photochemical mechanism for IR cataractogenesis in humans could act by repeated sub-acute threshold exposures extending over long periods of time, perhaps years, to develop a lenticular opacity. Such an exposure would almost certainly be at a level which exceeds the present environmental exposure limits. However, present data is indirect, as it is based on short-term animal high power level exposures in the laboratory and long-term human epidemiological studies.

There are many kinds of industrial exposures which exceed presently accepted exposure limits: glass blowing, steel puddling, and similar foundry occupations. In general, a higher instance of cataracts in the involved individuals has been reported in these occupations. Reviews of the infrared exposure in the Swedish iron and steel industry (Lydahl et al., 1984; Lydahl, 1980) indicate only that the associated ultraviolet exposures were unlikely to initiate any of the cataracts found, as any ultraviolet irradiance was usually a thousand times or more below that of sunlight. Thus, IR cataractogenesis from industrial exposures seems to be a reality.

The problem of cataractogenesis can be compared to the development of photokeratitis from ultraviolet laser exposures in that there is a delay between the exposure and any obvious symptoms. UV photokeratitis does not appear until hours after the exposure, and this, of course, makes it difficult for the victim to connect the symptoms with the laser exposure. However, any ophthalmologist called upon to examine a patient whose work may allow exposure to a nitrogen laser (337 nm) and who has awakened in the middle of the night with a burning sensation in the cornea will immediately understand that such a laser exposure could be relevant to the patient's symptoms. However, the much longer delay between symptoms and exposure implicit in a chronic situation makes it more difficult to establish a cause and effect relation for this mode of cataractogenesis. The patient who maintains that cataract development has resulted from previous work with Er:YAG lasers (1,300 nm) as long as twenty years ago could well be engaged in a protracted controversy, for experimental evidence is lacking to determine if this type of IR laser either initiated or accelerated the development of a cataract which becomes manifest in later life. However, the data cited from acute experiments in this

report gives a stronger link for the existence of chronic IR cataracts.

Relevant Experimental Data

The main evidence for a photochemical mechanism of cataract formation following IR exposure lies in the reciprocity between the exposure power level and duration, i.e. there is a strong relation between the cataract appearance and total dose. Nevertheless, the same threshold energy is required to give a cataract under the two different power levels of exposure which differed by a factor of 10 with the exposure durations inversely related.

Experiments by Wolbarsht and colleagues (1977), as shown in figure 1, indicate unequivocal cataract development by direct lens irradiation. A CW Nd:YAG laser was used with power levels ranging from 0.1 W to 2 W over exposure periods that varied by a factor of 20 and, in addition, were fractionated over a period of days. The calculated temperature rise in any single exposure was less than 1^0 C. The threshold for cataract formation was around 100 J over an area 3 mm in diameter on the surface of the lens (approximately 1,400 J/cm^2) with a variation of exposure from 50 - 1,050 s. The longest duration spread was two days. This reciprocal relation between power level and exposure duration seems to indicate a true dose related effect. It should be noted that these experiments also confirmed that high levels of the radiation to the iris alone easily produced cataracts in the adjacent lens surface, as suggested by Goldmann (1933). That is, when a sufficiently intense IR laser beam is directed to the iris alone, there is damage to the anterior surface of the lens immediately behind the iris. It is also evident that from this location, the lens opacity spreads through the affected lens fibers to form a larger, perhaps even denser, cataract on the posterior pole due to the enlargement of the individual lens fibers in that region.

Further data is available from Pitts and Cullen (1981) to show a dose related effect as shown in figure 2. Although Pitts and Cullen interpreted their results as supportive of Goldmann's hypothesis in which the cataract results from the transfer of heat from the iris to the lens, nevertheless, an examination of their data shows a strong tendency towards a constant dose relation (approximately 3,500 J/cm^{-2}), and since a large pupil was used during the exposure, some, if not most, of the radiation was delivered directly to the lens. This reciprocity between exposure time and the irradiance level compels serious consideration of a photochemical mechanism located in the lens itself. Although it was true that in some experimental situations, Pitts and Cullen did not confine the radiation to the lens alone and much went through the cornea onto the iris, a major contribution to cataract formation in their experiments must have been a direct radiation effect on the lens. In any exposure in which the cataract is not due to heat transfer from the iris, then any absorption by the iris can be thought of as a shielding effect. When cataracts were obtained by Pitts and Cullen, the threshold was approximately 3,500 J over a power range of 2 to 4 W/cm^{-2}. In the primate (monkey) eye with exposure conditions also involving the iris, the threshold for cataract formation was higher by a factor of almost 3. Part of that may be due to iris shielding, but even with the iris

acting as a shield, a dose related effect is still seen over the range of values given by Pitts and Cullen (1981). However, they made no tests on the monkey with radiation acting directly on the lens without also involving the iris.

The factor of approximately 2.5 difference in dose between the data of Wolbarsht et al. (1977), Wolbarsht (1978a), and that of Pitts and Cullen (1977) may express a real failure in reciprocity. However, there are several other factors contributing whose magnitude is unknown but which would act to bring these two sets of values closer together. The Pitts and Cullen data did not represent any monochromatic exposures, and corrections due to the IR action spectrum could be sizable. Also, the exposures in the earlier experiments were not confined to the lens. Some energy was incident upon the iris which would have lowered the effective lens dose as found in the experiments of Wolbarsht et. al.(1977). Even the monkey data of Pitts and Cullen (1981) is only larger by a factor of 7 which could well be explained by the lens shielding by the iris as discussed above as well as any species differences in lens proteins.

Direct irradiation of in vitro rabbit lenses or calf lens homogenates by IR lasers and IR only heat lamps produced shifts in concentration of various lens crystallins (Wolbarsht, 1980). In these experiments, the whole lenses were also incubated at several different temperatures. As can be seen from this figure, after incubation and irradiation, the α crystallin components were changed markedly. They were less mobile, and the soluble fractions disappeared while large insoluble aggregates appeared. Other changes in electrophoretic gel band structure are probably due to changes in the β crystallins. The control lens band structure remained the same as that in fresh lenses even though the control lenses were incubated for over 24 h at 37° C, thus, indicating the gel changes were due only to the exposure to the heat lamp.

However, in those same studies (Wolbarsht et al., 1977; Wolbarsht, 1978b, 1980), neither electron probe microanalysis of elemental concentrations nor gas chromatography of the relative concentrations of the various amino acids showed any clear cut changes in sub-threshold or markedly cataractous irradiated lenses as compared with controls. This indicated that the IR mediated changes did not result from any specific chemical reactions involving amino acids. Rather, as other data from incubated lenses showed, the cataracts resulted from changes in the concentrations of the various lens crystallins. For example, lenses incubated at various temperatures in the range of 37 to 45° C showed definite changes in their α crystallin components. At the higher temperatures, almost all the soluble α crystallin components disappeared with continued incubation and were replaced by high molecular weight (certainly greater than 5 million) fractions which contained primarily insoluble aggregates of the α crystallin material. Isolated α crystallin proteins went through similar types of changes when incubated. Some mobility changes in isolated β_H and β_2 crystallins are also seen but not to the same degree as in the α crystallins. Low pH accentuated these changes and suggested that, perhaps, some of the development of a cataract may be due to development of an acid pH as a result of the irradiation.

Discussion

Most of the available experimental data shows that cataracts are produced by direct IR irradiation of the lens in a constant energy dose related fashion through an aggregation of the soluble α crystallin fraction into an insoluble high molecular weight form. The Pitts and Cullen (1981) material on cataract formation for long exposures indicated an almost constant energy relationship, although shorter exposures gave a cataract behind the iris at a different and lower energy value. It is not clear from the experimental details given by Pitts and Cullen how much exposure of the iris was involved in their experiments, because they describe merely a "miotic pupil". In the experiments by Wolbarsht (1980), when radiation is confined to the lens, a constant dose is required for cataractogenesis. How this effect changes with much longer duration exposures, however, remains to be seen. One critique of the Pitts and Cullen data is that for experimental reasons, they did not expose the lens long enough to separate the lens damage from corneal and other types of damage. Drip techniques to cool the cornea or the use of sufficiently long and low level exposures might clarify this point. The use of lasers at different wavelengths could also give spectrum related data in a more precise form. Possibly, another technique might be to continue the study of chronic IR types of cataracts and the long-term effects of IR on the isolated lens crystallins to identify the early stages in this process.

All the material presented up to now in part supports the hypothesis by Vogt (1930) that there is cataract development following direct IR exposure to the lens. However, cataractogenesis seems to be photochemical rather than thermal in nature. This is certainly true on an acute or short-term basis and should also apply to chronic exposures where the thermal contributions are even less. However, the experiments by Wolbarsht and colleagues have also shown that under certain conditions, there can be a thermally generated cataract by heat transfer to the lens from the iris, as postulated by Goldmann (1933).

Sliney (1986) has suggested that environmental factors such as ambient temperatures are factors in the development of ultraviolet cataracts. The same may also be involved in infrared cataractogenesis. The temperature of the lens varies with the temperature of the cornea. Calculations indicate that at an ambient temperature of 22° C and a measured corneal temperature of 34.8° C, the lens will be at 35.5° C with the cornea at 43° C, and the lens will be close to 41° C. Obviously, this is an extreme case, but values of elevated lens temperatures such as this may synergize with the IR absorption by the lens to accelerate cataractogenesis by the formation of insoluble lens crystallins.

Stuck (1982) summarized the U.S. Army program at LAIR by indicating that CW IR radiation from a 1.33 μm Nd:YAG laser could produce translucent opacities on the anterior surface of the lens and the cornea, those on the lens having quite a long delay in appearance - up to 4 days. However, once they appeared, the cataracts were permanent, more data suggesting the direct action of the radiation on the lens itself.

Although average and peak irradiances of the exposures necessary for cataractogenesis were measured by Lydahl (1980), what would have been more helpful and in keeping with the experimental data of both Pitts and Cullen (1981) and Wolbarsht (1980) is a calculation of the total dose for cataract formation. For the short-term exposures in rabbits, this value is somewhere between 1,400 to 3,500 J/cm^{-2}. Of course, during protracted or chronic exposures, healing or repair mechanisms could play a significant role. Thus, what is important to specify in any future epidemiological or laboratory study is the average dose per month maintained over a period of years that results in the IR cataract. Possibly, there may be temporary changes in any particular industrial experiment, so the average dose may be exceeded for some weeks or months. Perhaps, this excessive exposure may induce the cataract to reach a point where performance is affected. It is more likely, however, that any cataract will come as a result of cumulative effects. Even as the UV induced brunescent cataracts appear after many years of gradual yellowing of the lenses, so the clouding of the IR cataract may appear in the same gradual way. At present, there seems to be little likelihood of the necessary chronic exposures from available IR lasers in any presently contemplated usage. However, it should be kept in mind that the hazard of cataractogenesis from such an IR laser exposure will add to any environmental IR stress that may be present. Another situation in which such IR hazards may be present is in any Maxwellian projection to the retina in which the source is imaged in the plane of the lens. This is often the optical set-up for ophthalmic instruments, and accordingly, the possible cataractogenesis hazards should be considered.

The shift of the α crystallins and other lens proteins from small soluble molecules to larger aggregated insoluble forms has also been attributed to aging by Zigler (1975). Perhaps, the photochemical process from infrared irradiation is not a new pathway for cataractogenesis but is only an accelerated form of one type of normally occurring age related cataract. There are certainly protective pathways in the lens to mitigate this effect, and that may account for the loss of reciprocity seen in comparisons of the data discussed above, as longer and longer time durations for irradiation are used.

In summary, the material discussed here suggests that there may be two separate but possibly synergistic steps in cataract development from IR laser exposure: thermal stress by heat transfer from the iris maximal for short exposures and high power levels and photochemical effects on lens crystallins from direct absorption of the radiation by the lens for long exposures at lower power levels. To find the cause of any particular cataract, it is necessary to determine the relative contributions from each mechanism. The irradiances required to produce experimental cataracts, either acute thermal or chronic photochemical, were quite high. Certainly, anyone exposed to those levels would be very uncomfortably aware of the exposure. Indeed, if any of the exposures at these power levels cover a significant portion of the body surface, it is doubtful if the person could live through it. Nevertheless, the possibility of chronic IR source exposure as a factor in cataractogenesis is high enough to cause concern about IR laser usage or in any applications where the IR exposure conditions

involve the source being imaged in the plane of the lens such as a Maxwellian projection to the retina.

Acknowledgment

This document is adapted from the publication: "Cataract from Infrared Lasers: Evidence for Photochemical Mechanisms." M.L. Wolbarsht, Lasers and Light in Ophthalmology, volume 4, pages 91-96, 1992.
The original research program that led to the conclusions expressed in this review was carried out with the valuable collaboration of B.S. Yamanashi. Many others who were in this research group at various times also deserve recognition for their help: A.A. Antonucci, R. Kurzel, I.B.C. Matheson, M.A. Orr, and J.S. Zigler, Jr.

References

Goldmann, H. Experimental investigation on the genesis of heat cataract, Arch. Ophth., 130:93-179, 1933.

Lydahl, E. Infrared radiation and cataract, Acta Ophthalmol., Suppl. 166:1-66, 1980.

Lydahl, E.; Glansholm, A.; Levin, M. Ocular exposure to infrared radiation in the Swedish iron and steel industry, Health Physics, 46:529-536, 1984.

Pitts, D.G.; Cullen, A.P. Ocular ultraviolet effects from 295 nm to 335 nm in the rabbit eye, DHEW (NIOSH) Publication No. 77-130, 1-55, 1976.

Pitts, D.G.; Cullen, A.P. Ocular ultraviolet effects from 295 nm to 400 nm in the rabbit eye, DHEW (NIOSH) Publication No. 77-175, 1977.

Pitts, D.G.; Cullen, A.P. Determination of infrared radiation levels for acute ocular cataractogenesis, A.v. Graefes Arch Klin Ophth, 217:285-297, 1981.

Sliney, D.H. Physical factors in cataractogenesis: ambient ultraviolet radiation and temperature, Invest. Ophthalmol. Vis. Sci., 27:781-790, 1986.

Stuck, B. Laser injury to the anterior segment: infrared radiation. In: Symposium Proceedings: Medical Ophthalmic Surveillance of Personnel Potentially Exposed to Laser Radiation, (eds. W.G. Pitts and D.H. Sliney), U.S. Army Environmental Hygiene Agency, Aberdeen Proving Ground, MD 21010-5422, pp. 73-80, 8-9 September 1982.

Vogt, A. Augenschadigungen durch die strahlende energie, Klin. Monatsbl. Augenh: 85:321-344, 1930.

Wolbarsht, M.L. The effects of optical radiation on the anterior structure of the eye. In: Current Concepts in Ergophthalmology (eds. B. Tengroth, P. Epstein, A. Anseth, A. Heading, A. Keenly, M.

Roper-Hall and D. Sliney), Societies Ergophthalmologica Internationalis, Stockholm., pp. 24-46, 1978a.

Wolbarsht, M.L. Safe ocular levels for IR occupational exposure, Final Report, National Institute of Occupational Safety and Health, NIOSH 0053-04, 1978b. Wolbarsht, M.L. Damage to the lens from infrared. In: Ocular Effects of Non-ionizing Radiation (eds., M.L. Wolbarsht and D.H. Sliney,). Proc. Soc. Photo. Inst. Eng. (SPIE), Bellingham, WA, 229:121-141, 1980.

Wolbarsht, M.L. Laser injury to the anterior segment-infrared cataract. In: Symposium Proceedings: Medical Ophthalmic Surveillance of Personnel Potentially Exposed to Laser Radiation (eds. W.G. Pitts and D.H. Sliney), U.S. Army Environmental Hygiene Agency, Aberdeen Proving Ground, MD 21010-5422, pp. 81-86, 8-9 September 1982.

Wolbarsht, M.L.; Orr, Ma.; Yaminashi, B.S.; Zigler, J.S.; Matheson, I.B.C. The origin of cataracts in the lens from infrared laser radiation, Annual Report, U.S. Army Medical Research and Development Command, Contract DAMD-17-74-C-4133, 1977.

Zigler, J.S., Jr. Comparative Studies on a Heterogeneous Family of Vertebrate Lens Proteins--the Beta Crystallins, PhD. Thesis. Duke University, 1975.

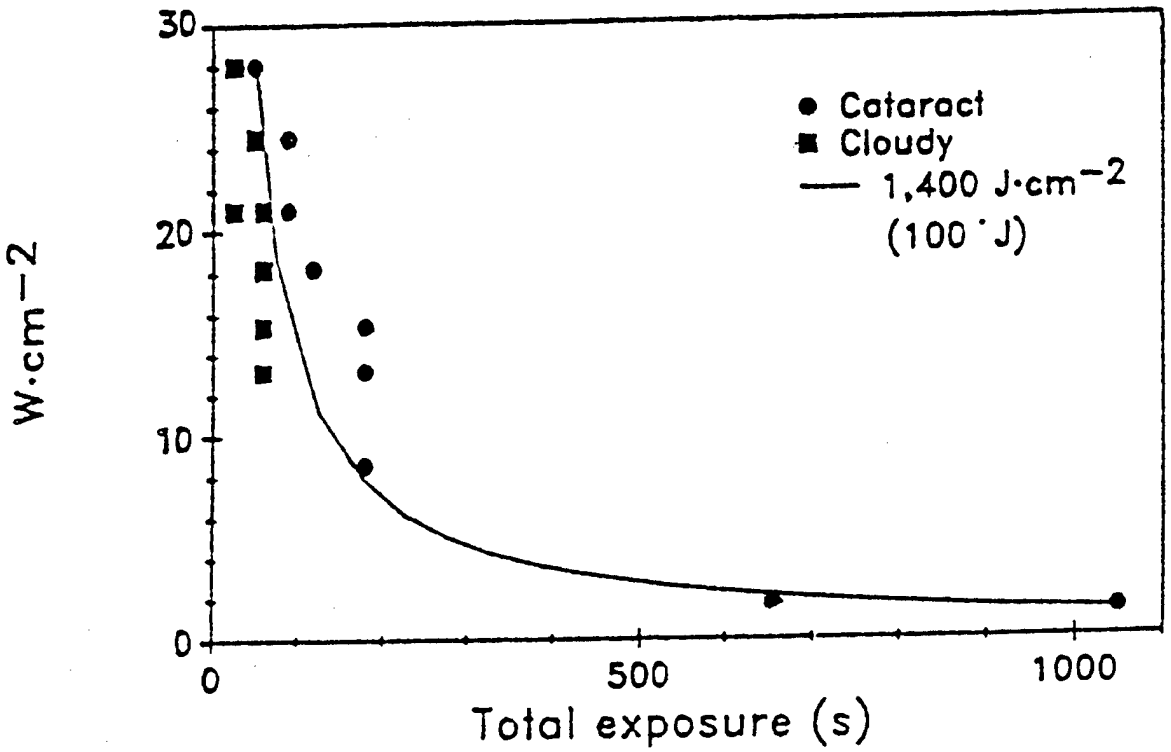

Figure 1. Cataract formation in the rabbit eye by direct exposure to a CW Nd:YAG at 1,064 μm. Markedly cataractous lenses and only slightly affected ones (cloudy) are separated by the 1,400 J/cm^2 constant energy level. The radiation was fractionated over 2 days within a 3 mm diameter area on the lens surface. 1,400 J/cm^2 is slightly less than in the data from Pitts and Cullen (1981) as shown in figure 2. Data from Wolbarsht et al. (1977).

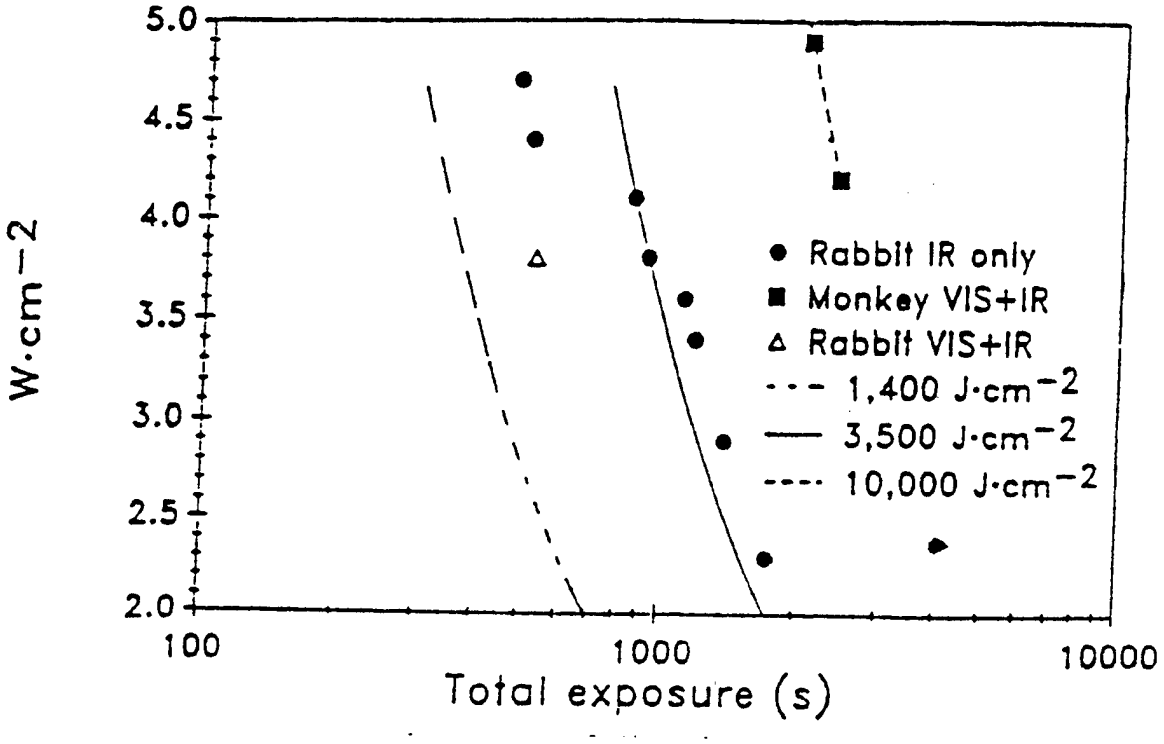

Figure 2. Cataract development following exposure to filtered xenon arc radiation. Cataract in rabbit eyes from "infrared only" at a threshold of 3,500 J/cm^2. A dose related effect holds for all exposures except the shortest which may differ because of iris involvement. All points appear to follow a dose relation. Monkeys have a similar relation at 10,000 J/cm^2. The rabbit IR dose value of 3,500 J/cm^2 is the same order of magnitude as the 1,400 J/cm^{-2} cataractogenesis by a CW Nd:YAG laser shown in figure 1. (Data from table 3 in Pitts and Cullen, 1981).

Measurements of Pulsed IR Laser Induced Acoustic Effects

Jerri Tribble,
NMRI Det Brooks AFB
8308Hawks Rd.
Brooks AFB, TX 78235-5324

Abstract

Absorption of pulsed IR laser energy by tissue results in heating and expansion of the irradiated material. At low energies a traditional thermoelastic response is induced. At higher energies, beyond the linear response of the material, tissue tearing and ejection results in additional pressure due to momentum recoil. Measurements of the acoustic wave generated by short (60 to 200 ns) pulses of IR (3 to 6.45 microns) radiation in gelatin and bovine cornea will be presented. Dependence of these measurements on wavelength, fluence and macropulse duration will be discussed. The laser used for these studies was the Vanderbilt Free-Electron Laser (FEL) which is tunable from 2 to 10 microns and emits pulses of ~ 4 microsecond duration (at 60 Hz) consisting of a train micropulses that are 1 picosecond in duration separated by 350 picoseconds. In this study, the macropulse duration is shortened by a broadband Pockels cell. The shortened macropulses are focused (112-210 microns in diameter) on the surface of a thin (< 1 mm) sample mounted on an acoustic detector which uses 9 micron thick polyvinyldifluoride (PVDF). While a HeNe probe beam monitors ejection of material from the front surface, the acoustic transient travels through the sample and is recorded at the back with nanosecond resolution. In gelatin, at low pulse energies, a bipolar acoustic waveform characteristic of the thermoelastic response at a free surface is measured using FEL wavelengths of 3.36 and 6.45 microns. At higher energies, where the HeNe surface monitor detects material removal, a purely positive (compressive) recoil pressure is superposed with the thermoelastic response.

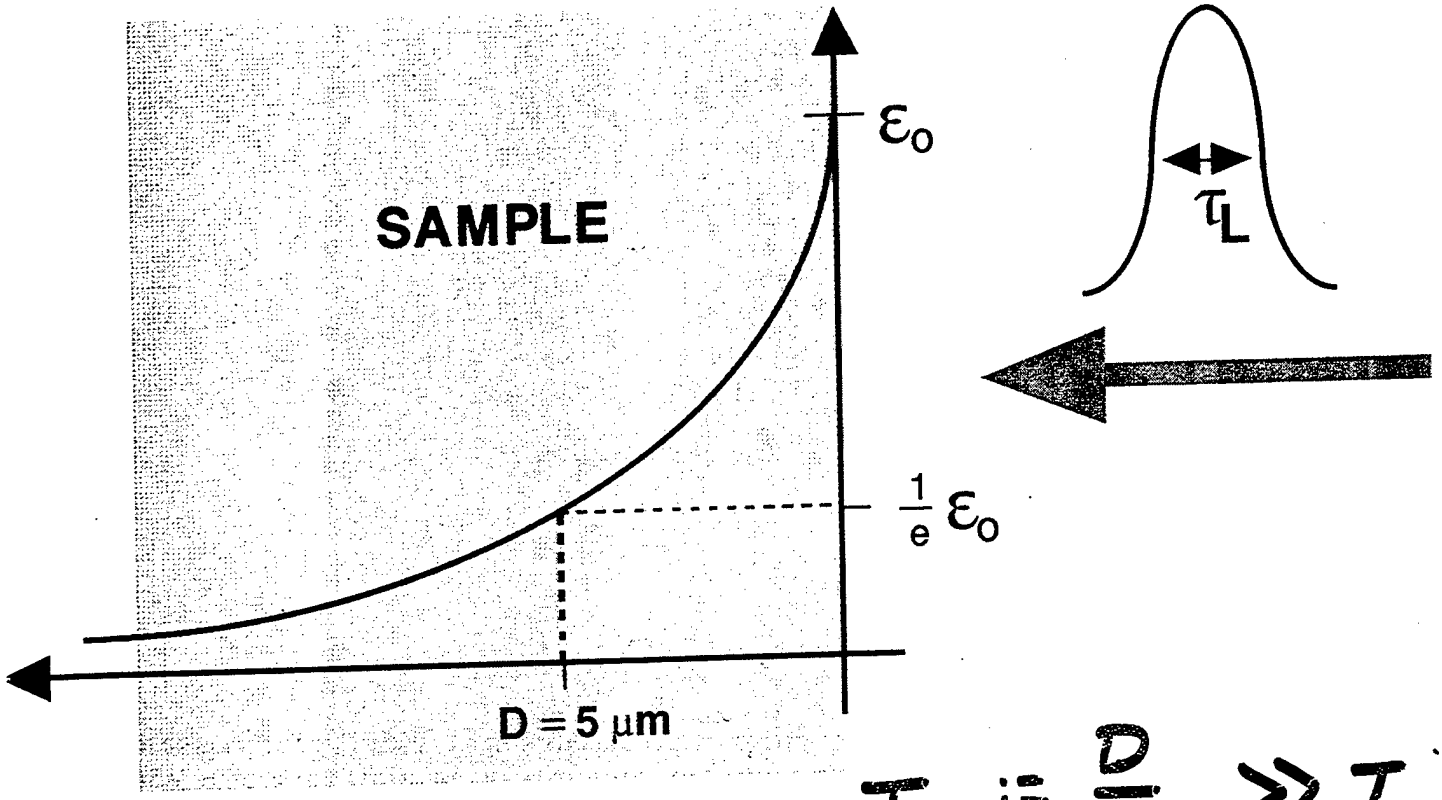

$$\tau_{ac} := \frac{D}{v_s} \gg \tau_L$$

$-(J/m^2)$

$$\varepsilon_o = \frac{\Phi_o}{D}$$ Peak Energy Density

$$\Delta T = \frac{1}{C_V}\left(\frac{\Phi_o}{D}\right)\frac{1}{\rho}$$ Maximum Temperature Rise

$$\frac{\Delta V}{V} = \beta \Delta T$$ Maximum Volume Expansion

$$\sigma_{peak} = \Delta P = v_s^2\left(\frac{\Delta V}{V}\right)\rho$$ Peak Pressure Rise

$$\sigma_{peak} = v_s^2\left(\frac{\beta}{C_V}\right)\frac{\Phi_o}{D} = \Gamma\frac{\Phi_o}{D}$$

Total Stress Amplitude

Developing Stress Waves in the Irradiated Volume

$t = 0$

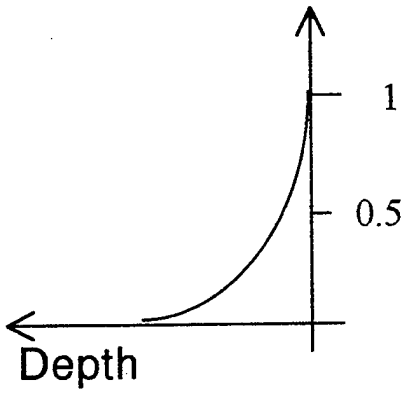

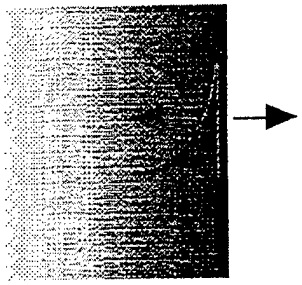

$t = \tau$

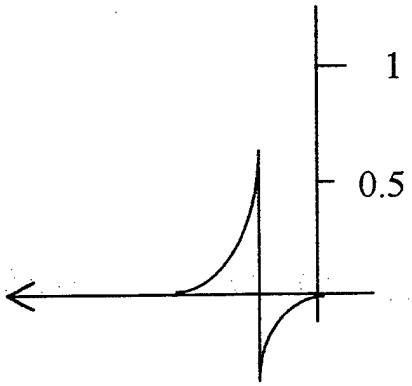

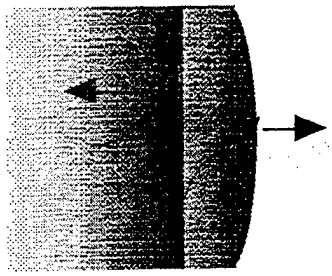

$t = 3\tau$

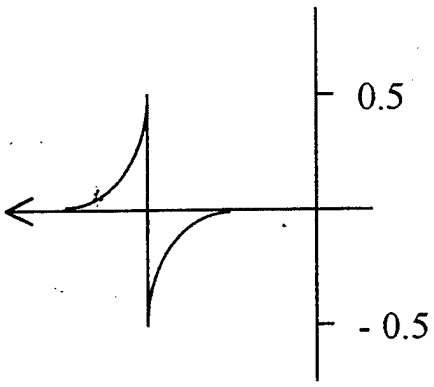

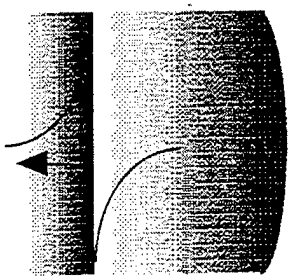

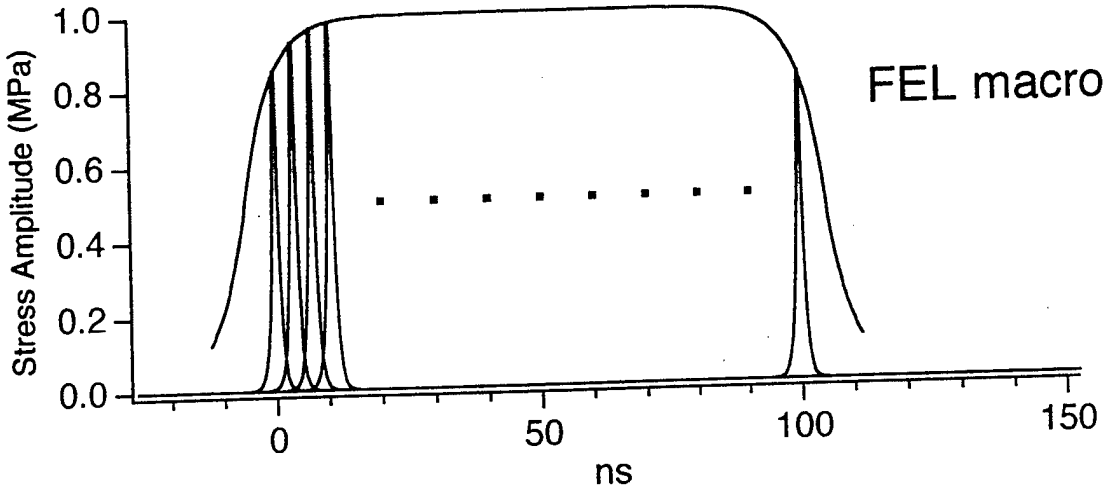

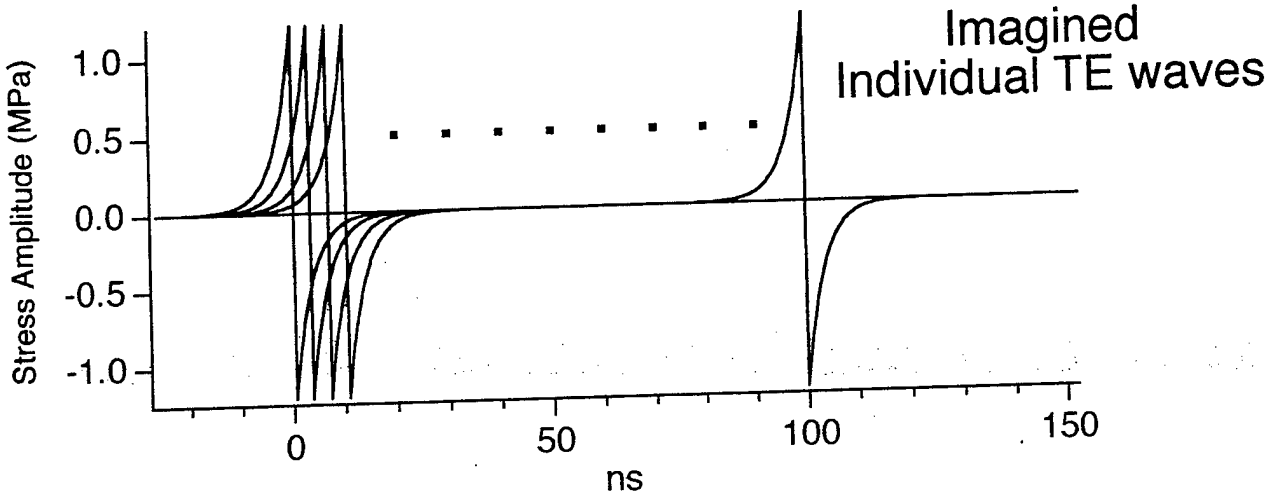

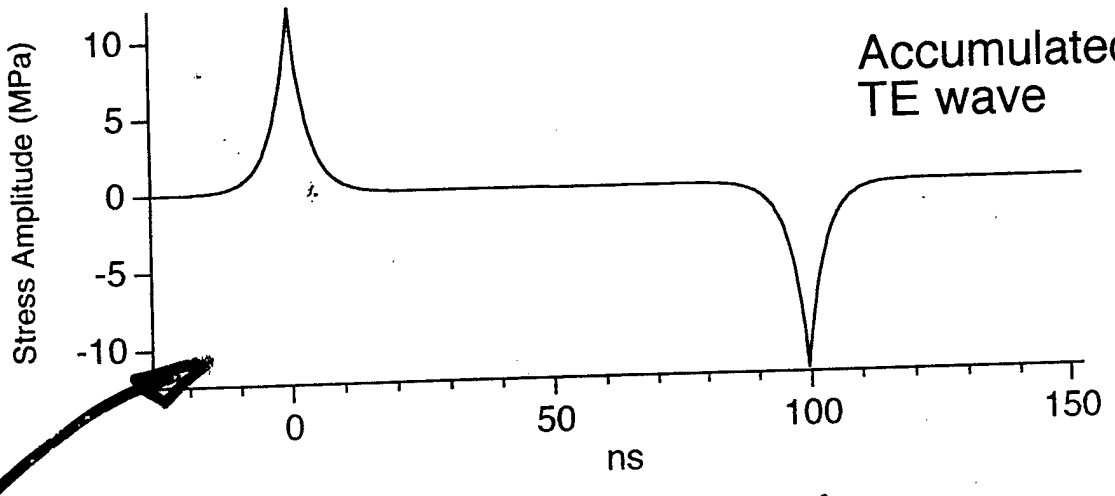

Measured Thermoelastic

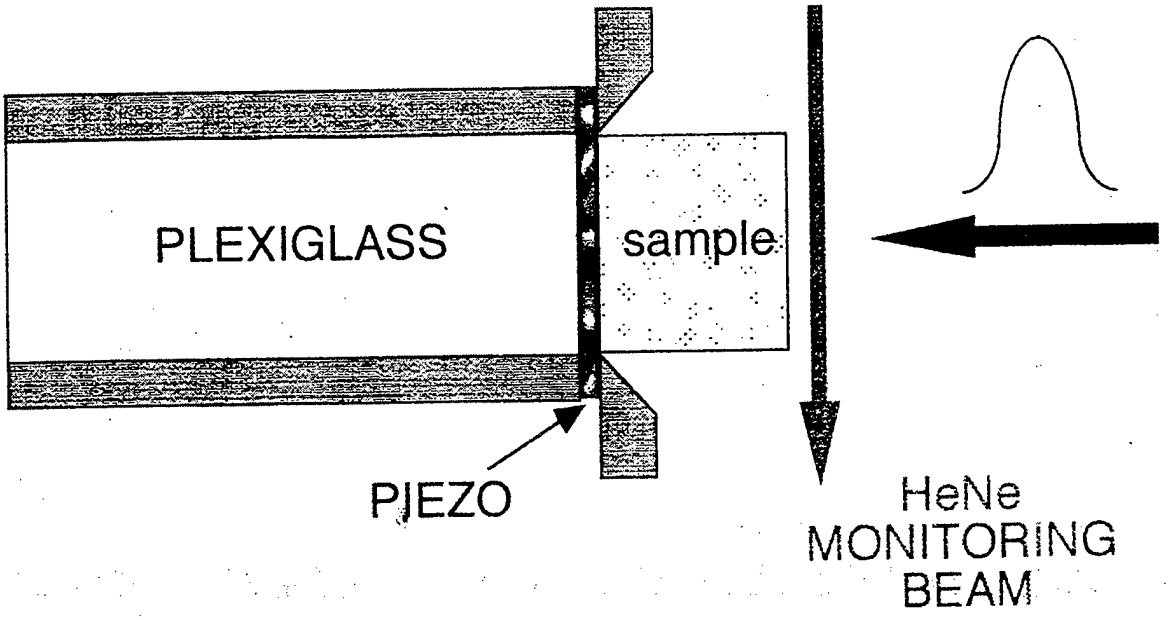
PLEXIGLASS
sample
PIEZO
HeNe
MONITORING
BEAM

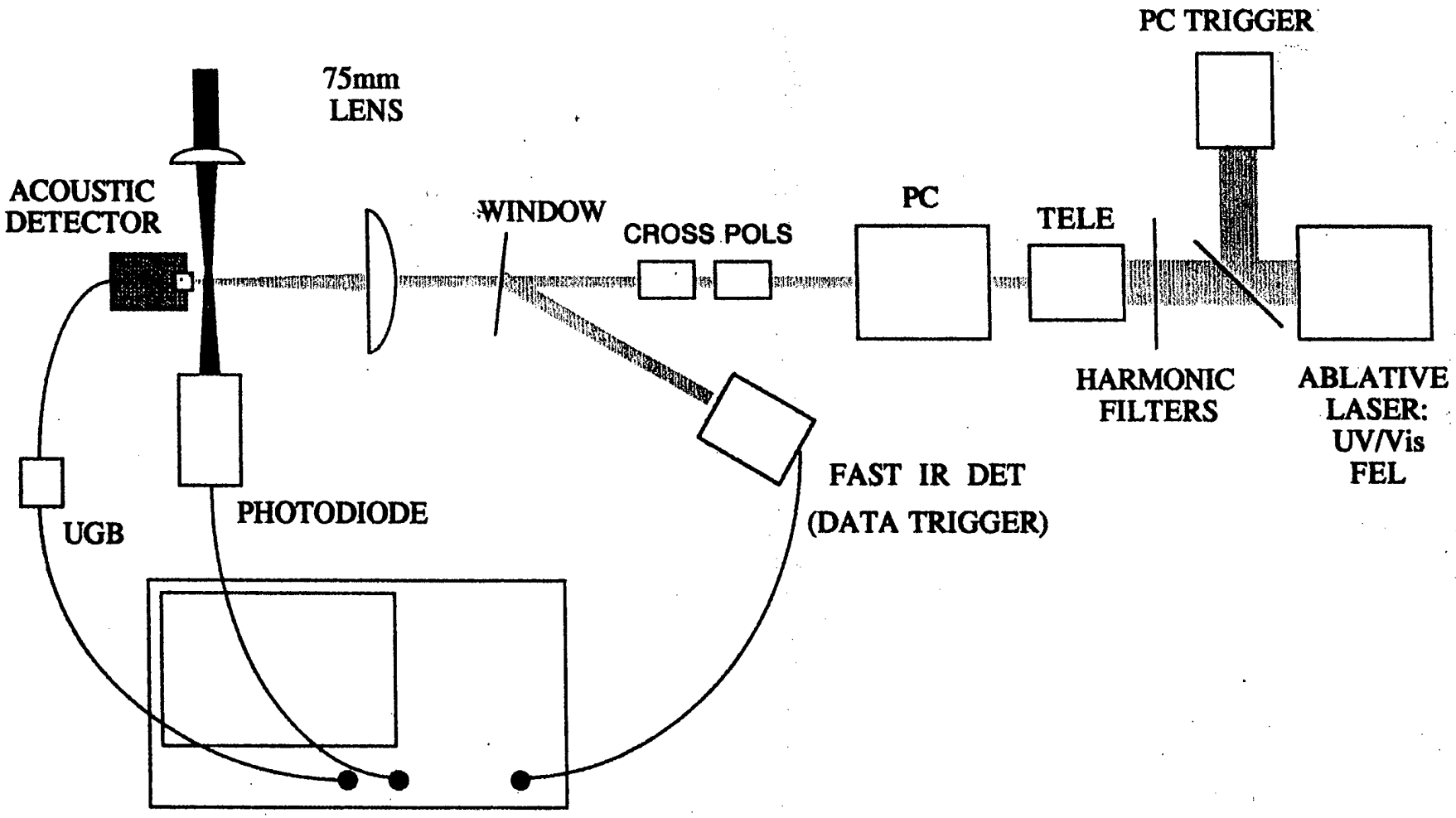
PC TRIGGER
75mm
LENS
ACOUSTIC
DETECTOR
WINDOW
CROSS POLS
PC
TELE
HARMONIC
FILTERS
ABLATIVE
LASER:
UV/Vis
FEL
FAST IR DET
(DATA TRIGGER)
PHOTODIODE
UGB

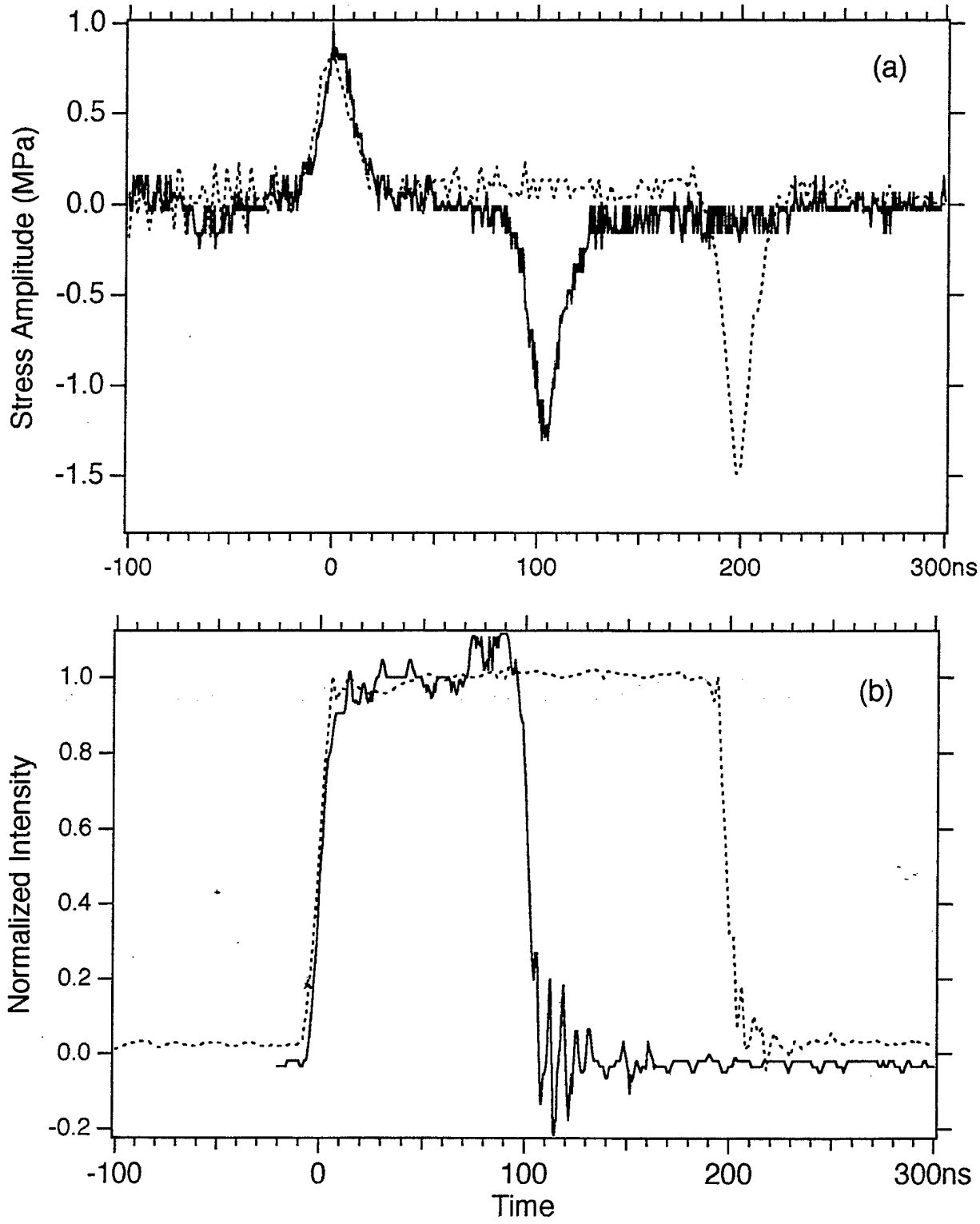
(a)
Stress Amplitude (MPa)
1.0
0.5
0.0
-0.5
-1.0
-1.5
-100
0
100
200
300ns
(b)
Normalized Intensity
1.0
0.8
0.6
0.4
0.2
0.0
-0.2
-100
0
100
200
300ns
Time

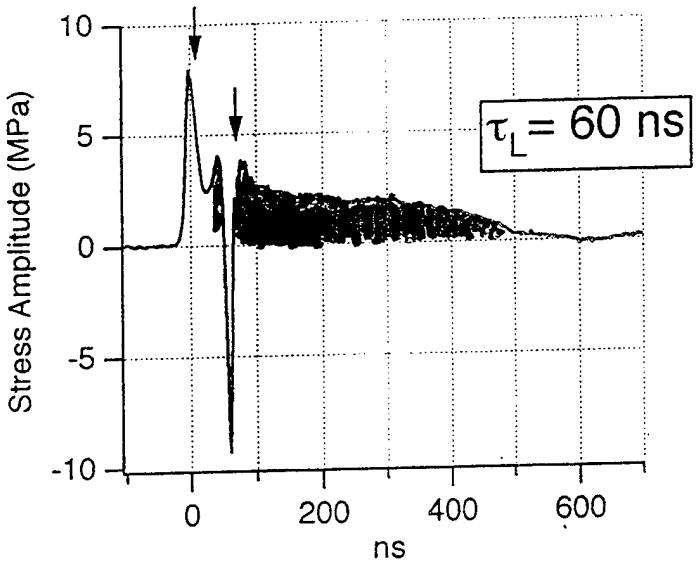
Stress Amplitude (MPa)
10
5
0
-5
-10
0
200
400
600
ns
τ_L= 60 ns

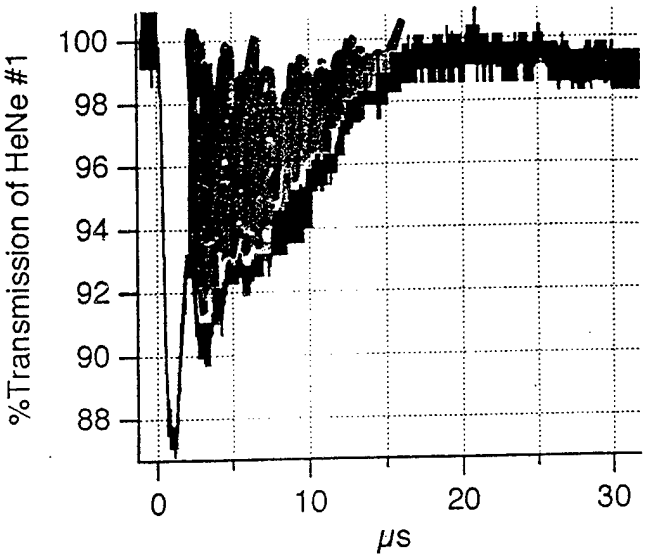
%Transmission of HeNe #1
100
98
96
94
92
90
88
0
10
20
30
μs

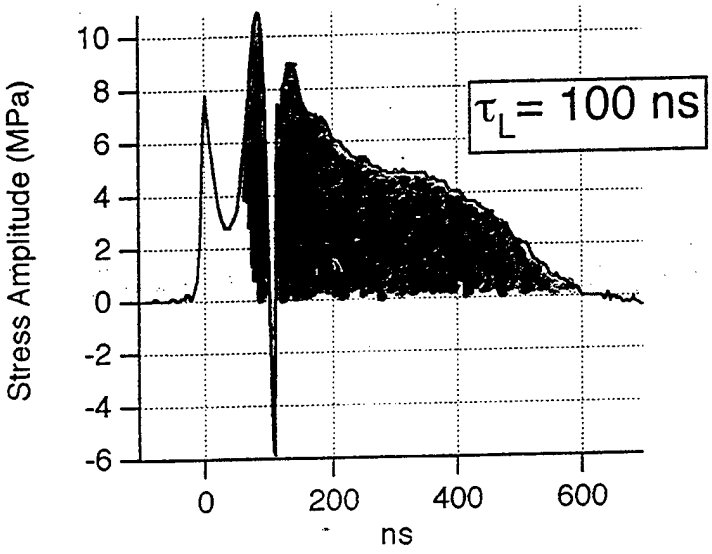
Stress Amplitude (MPa)
10
8
6
4
2
0
-2
-4
-6
0
200
400
600
ns
τ_L= 100 ns

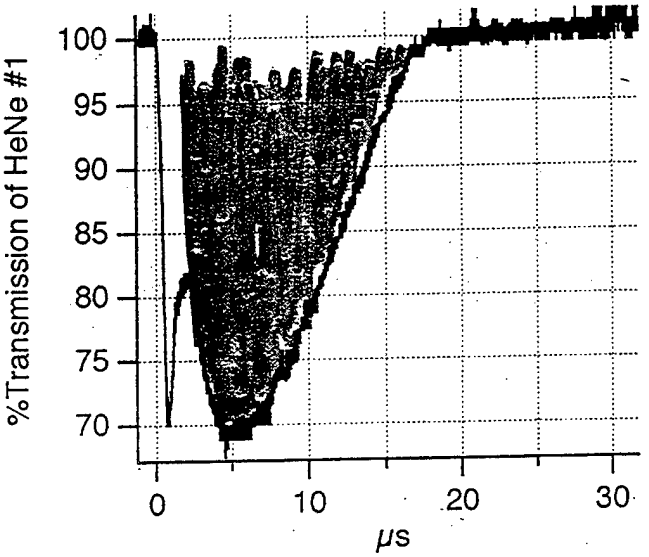
%Transmission of HeNe #1
100
95
90
85
80
75
70
0
10
20
30
μs

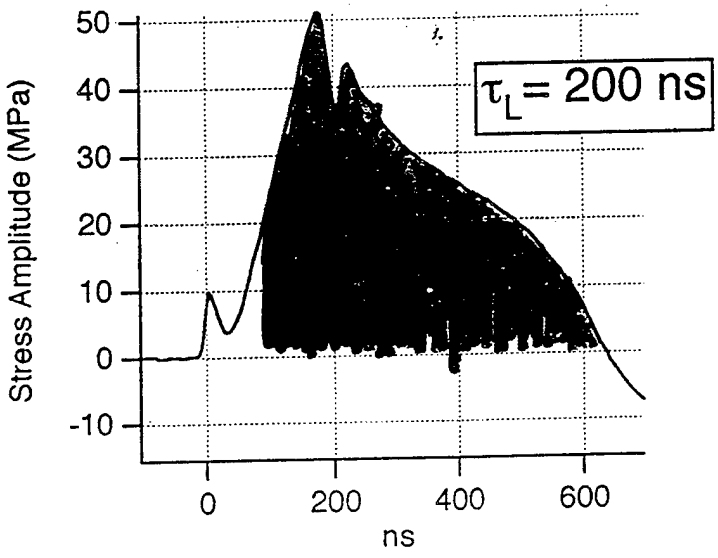
Stress Amplitude (MPa)
50
40
30
20
10
0
-10
0
200
400
600
ns
τ_L= 200 ns

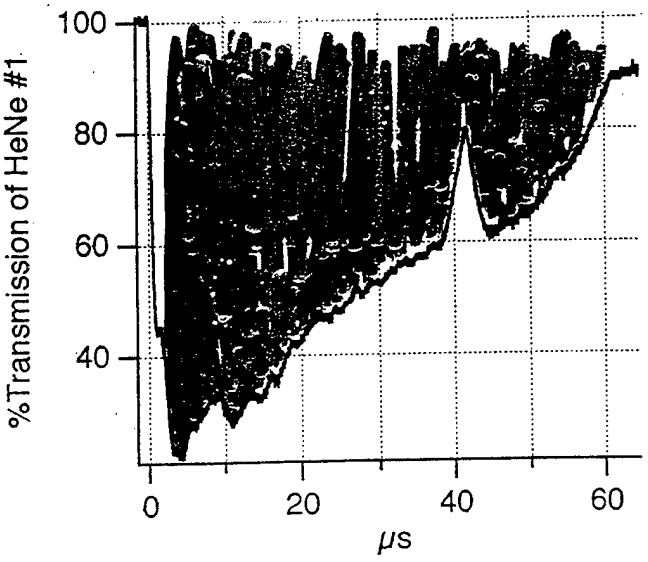
%Transmission of HeNe #1
100
80
60
40
0
20
40
60
μs

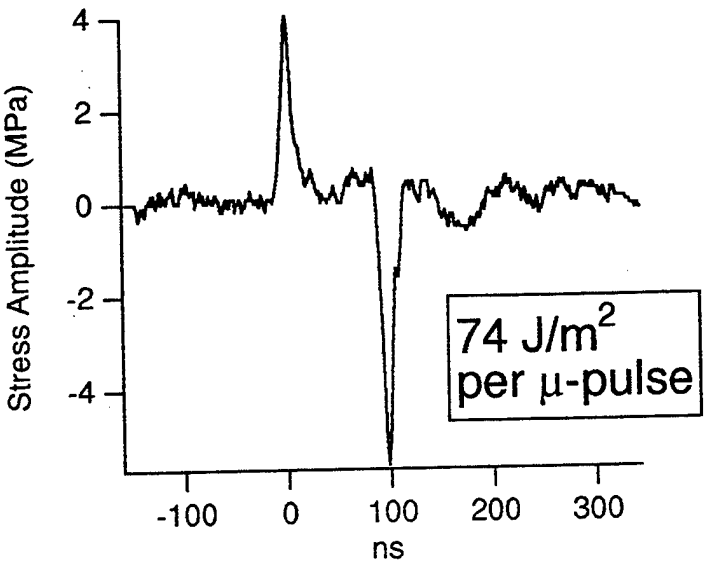
Stress Amplitude (MPa)
4
2
0
-2
-4
-100
0
100
200
300
ns
74 J/m2
per μ-pulse

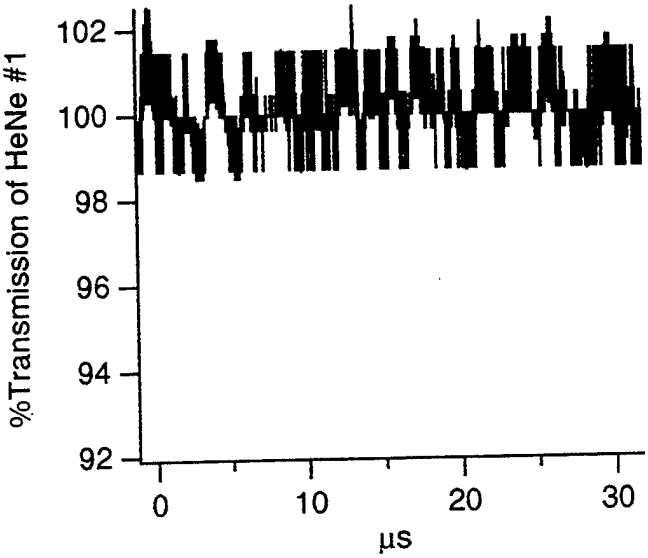
%Transmission of HeNe #1
102
100
98
96
94
92
0
10
20
30
μs

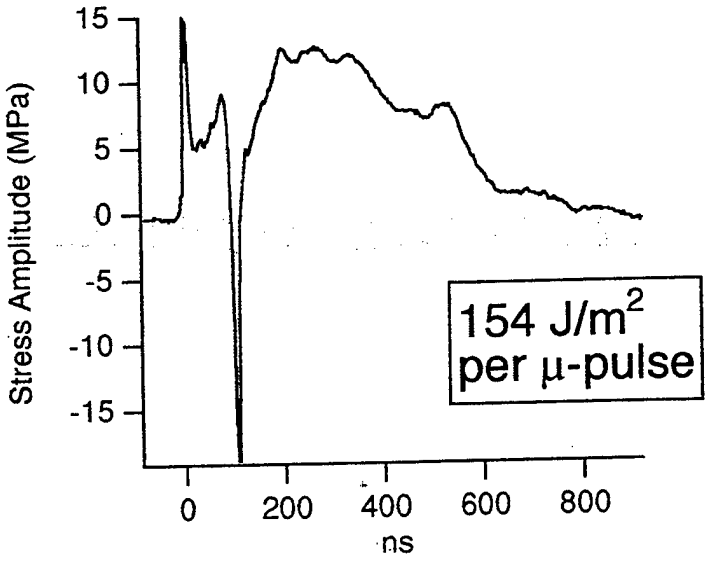
Stress Amplitude (MPa)
15
10
5
0
-5
-10
-15
0
200
400
600
800
ns
154 J/m2
per μ-pulse

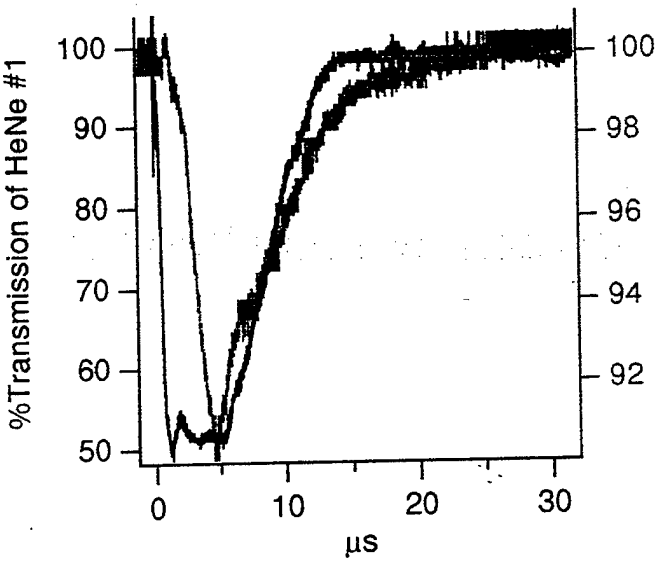
%Transmission of HeNe #1
%Transmission of HeNe #2
100
90
80
70
60
50
100
98
96
94
92
0
10
20
30
μs

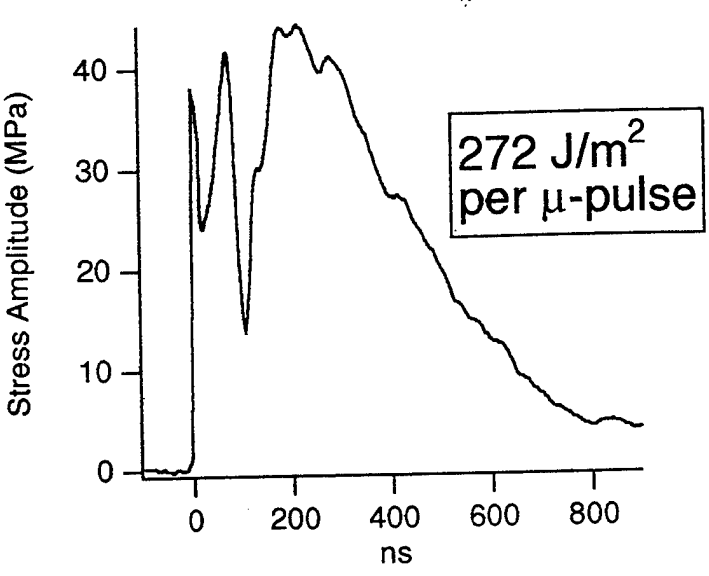
Stress Amplitude (MPa)
40
30
20
10
0
0
200
400
600
800
ns
272 J/m2
per μ-pulse

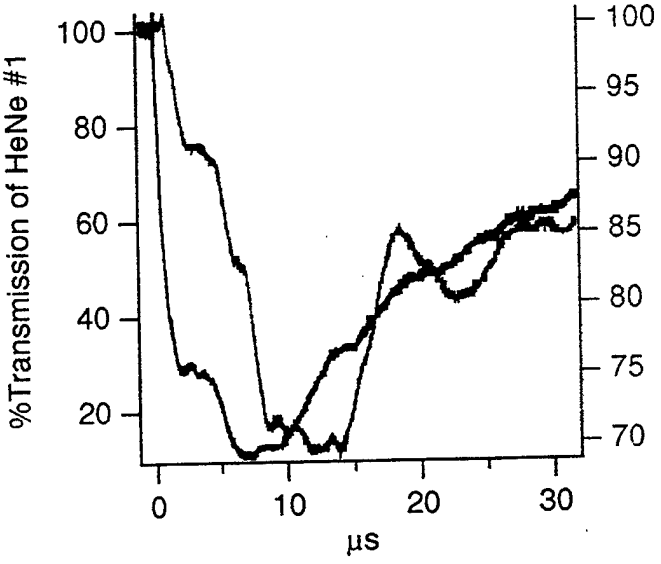
%Transmission of HeNe #1
%Transmission of HeNe #2
100
80
60
40
20
100
95
90
85
80
75
70
0
10
20
30
μs

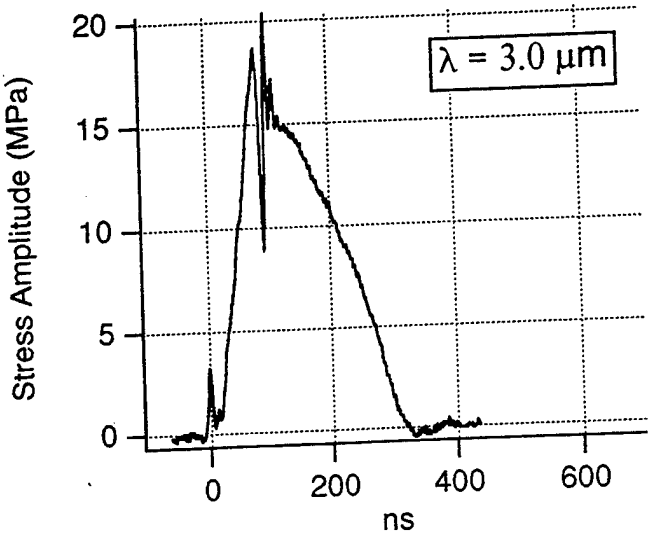
λ = 3.0 μm
Stress Amplitude (MPa)
ns

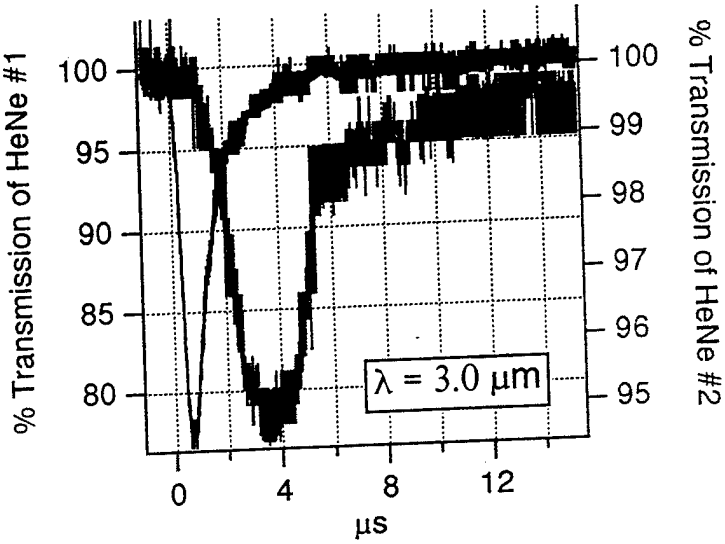
λ = 3.0 μm
% Transmission of HeNe #1
% Transmission of HeNe #2
μs

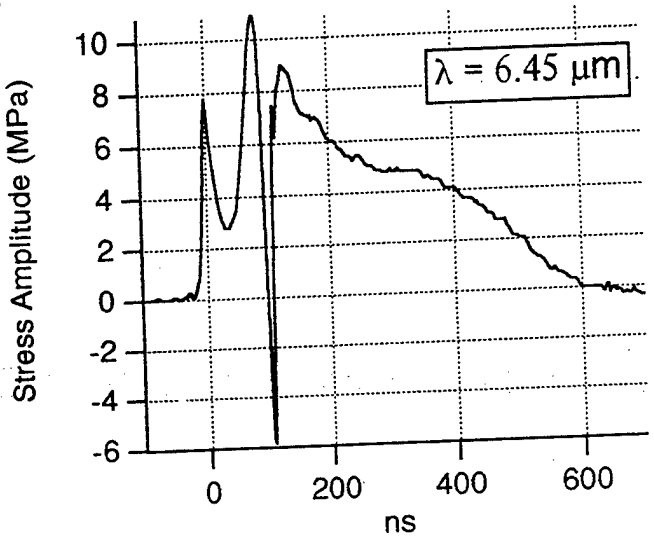
λ = 6.45 μm
Stress Amplitude (MPa)
ns

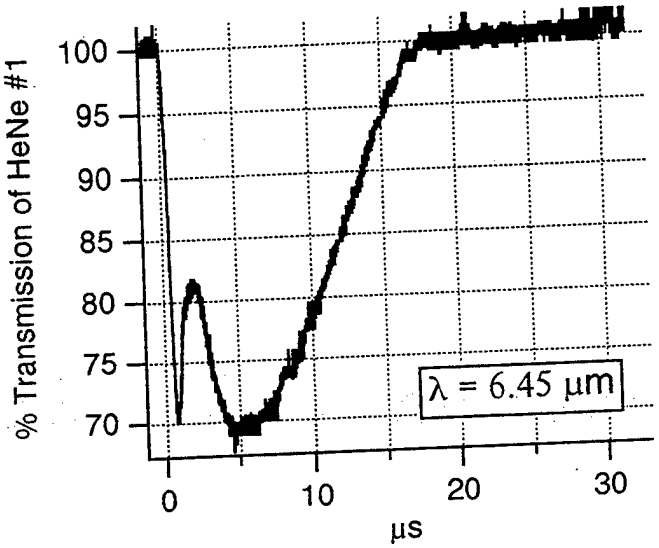
λ = 6.45 μm
% Transmission of HeNe #1
μs

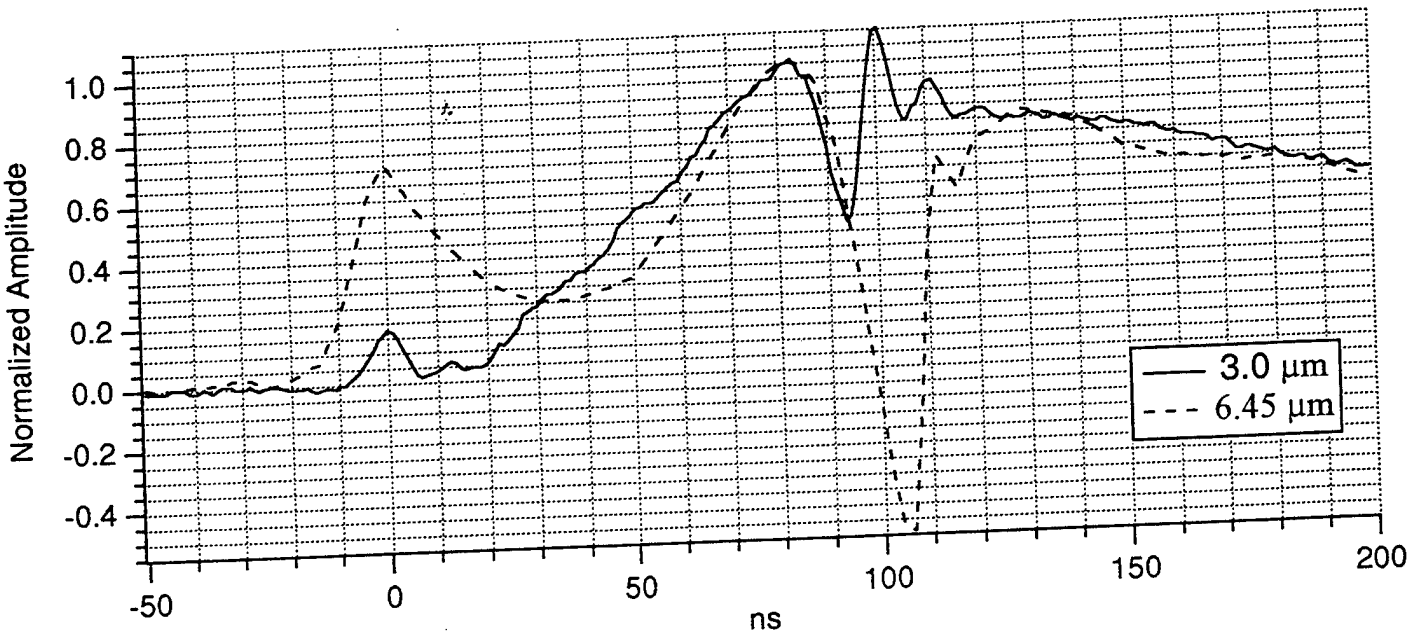
3.0 μm
6.45 μm
Normalized Amplitude
ns

Infrared Lasers & Millimeter Waves
Workshop
The Links Between Microwaves
& Laser Optics

21 Jan 1997 - 22 Jan 1997

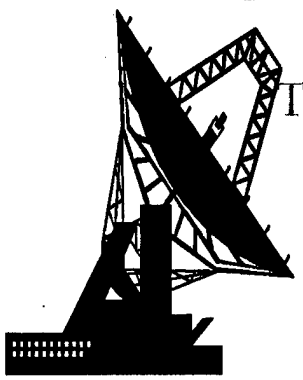

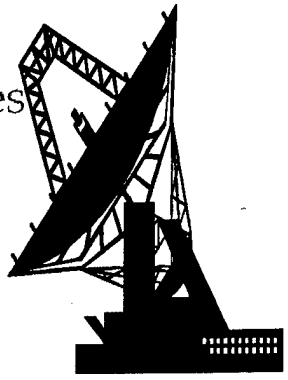

SECTION IV:

LOW LEVEL EFFECTS DATABASE

DOSIMETRY AND BIOLOGICAL EFFECTS OF MILLIMETER WAVES

Om P. Gandhi
Department of Electrical Engineering
University of Utah
Salt Lake City, UT

DEPTH OF PENETRATION AND SURFACE SAR FOR THE HUMAN SKIN*

F GHz	Reflection Coeff.	Skin Depth mm	SAR at Surface for 10 mW/cm^2
30	0.49	0.78	131.0
60	0.41	0.43	276.6
100	0.33	0.32	419.4
200	0.22	0.25	624.0
300	0.18	0.23	714.2

* O. P. Gandhi and A. Riazi, *IEEE MTT-34, pp. 228-235, 1986.*

SOME OTHER ASPECTS OF DOSIMETRY

THICKNESS OF HUMAN CLOTHING ($\varepsilon \sim 4.0 - j0.1$ FOR COTTON) IS ON THE ORDER OF MILLIMETERS.

HUMAN CLOTHING MAY FACILITATE IMPEDANCE MATCHING RESULTING IN NEARLY 60-100 PERCENT COUPLING OF INCIDENT POWER AT MILLIMETER WAVELENGTHS OVER THE WHOLE BODY.

WHOLE BODY EXPOSURES COULD, THEREFORE, RESULT FOR MILLIMETER WAVES RATHER THAN PARTIAL BODY EXPOSURES TYPICAL OF IR RADIATION.

BASED ON THE DATA OF HARDY AND OPPEL, THRESHOLD FOR PERCEPTION OF WARMTH FOR WHOLE BODY EXPOSURE ~ 0.67 mW/cm^2.

SENSATION "VERY WARM OR HOT" MAY RESULT FOR POWER DENSITIES ~ 8.7 mW/cm^2.

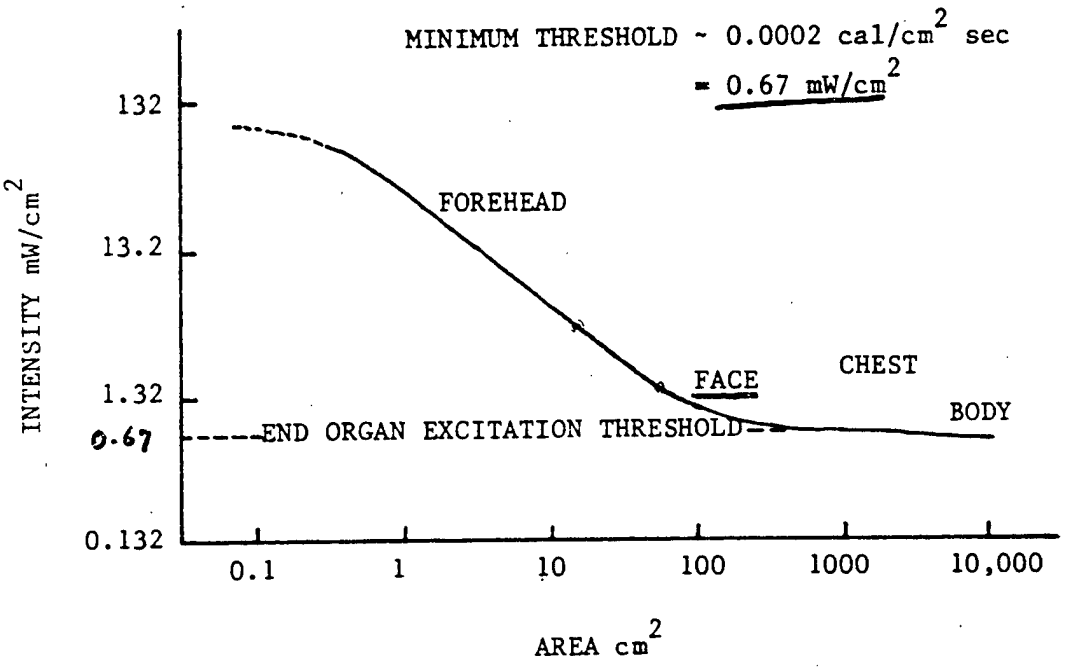

THRESHOLD OF IR PERCEPTION -- INTENSITY VS. EXPOSED AREA
[J. D. HARDY AND T. W. OPPEL, J. CLIN. INVEST. 16, 1937, 533-540]

RELATIONSHIP BETWEEN AVERAGE RATES OF HEAT TRANSFER AND FIRST SENSATIONS REPORTED — DORSUM OF THE RIGHT HAND

ROOM TEMPERATURE 17 ± 1°C
SOURCE OF RADIATION: BLACK BODY AT 130°C ($\lambda > 3\ \mu$)

AREA STIMULATED cm^2	SUBJECT	RATES OF ENERGY ABSORBED mW/cm^2 FAINT WARM	WARM	VERY WARM OR HOT
2.6	1	44.8	56.1	61.1
	2	28.0	41.4	56.1
	3	20.9	22.2	40.6
	4	54.8	62.3	--
	5	42.7	54.0	--
9.6	1	24.3	45.6	61.5
	2	10.9	36.4	54.0
	3	15.5	30.1	52.3
	4	44.7	65.7	--
	5	30.1	59.8	--
		25.1 ± 13.3	47.5 ± 15.1	55.9 ± 4.9*
40.6	1	3.8	12.1	22.6
	2	3.3	10.5	20.9
	3	13.4	10.9	21.3
	4	2.9	10.0	16.3
	5	14.6	16.3	27.6
		7.6 ± 5.9	11.96 ± 2.5	21.7 ± 4.0*

* THE RATIO 21.74/55.39 ≈ 0.4 IS SIMILAR TO THAT FOR THRESHOLDS OF PERCEPTION FOR THE CORRESPONDING INCREASE IN THE EXPOSED AREAS.

REACTION TIME FOR THE SENSATION VERY WARM OR HOT IS TYPICALLY ON THE ORDER OF 1.0 ± 0.6 sec.

P. P. LELE, G. WEDDELL, AND C. M. WILLIAMS, J. PHYSIOL. 126, 1954, 206-234.

MINIMUM PERCEPTIBLE RATES OF ENERGY DEPOSITION FOR DORSUM OF THE HAND[1,2] [EXPOSED AREA = 40.6 cm^2]

$$0.4 \text{ mcal/cm}^2 \text{ sec} \rightarrow 1.67 \text{ mW/cm}^2$$

FOR LARGER AREAS OF EXPOSURE, SUCH AS THE FACE AND THE CHEST, THIS DROPS TO

$$0.67 \text{ mW/cm}^2 \text{ [RATIO } 0.67/1.67 = 0.4\text{]}$$

SENSATION "VERY WARM TO HOT" REPORTED IN REF. 1 FOR 21.74 mW/cm^2 MAY SIMILARLY BE SCALABLE TO $0.4 \times 21.74 = 8.7$ mW/cm^2 FOR AREAS SUCH AS THE FACE AND CHEST AND SOMEWHAT LOWER FOR WHOLE-BODY MILLIMETER-WAVE IRRADIATION.

1. P. P. LELE, ET AL., J. PHYSIOL. 126, 1954, 206-234.

2. J. D. HARDY AND T. W. OPPEL, J. CLIN. INVEST. 16, 1937, 533-540.

BIOLOGICAL EFFECTS OF MILLIMETER WAVE IRRADIATION*

YEARS: 1976-1986

Research Team

D. W. Hill
L. M. Partlow
L. Bush
L. Stensaas
M. J. Hagmann
D. Ghodgaonkar
A. Riazi
L. Furia
R. E. Benner
C. H. Wang

* Work sponsored by
NIH - NCI
USAF (Brooks AFB)
NMRDC

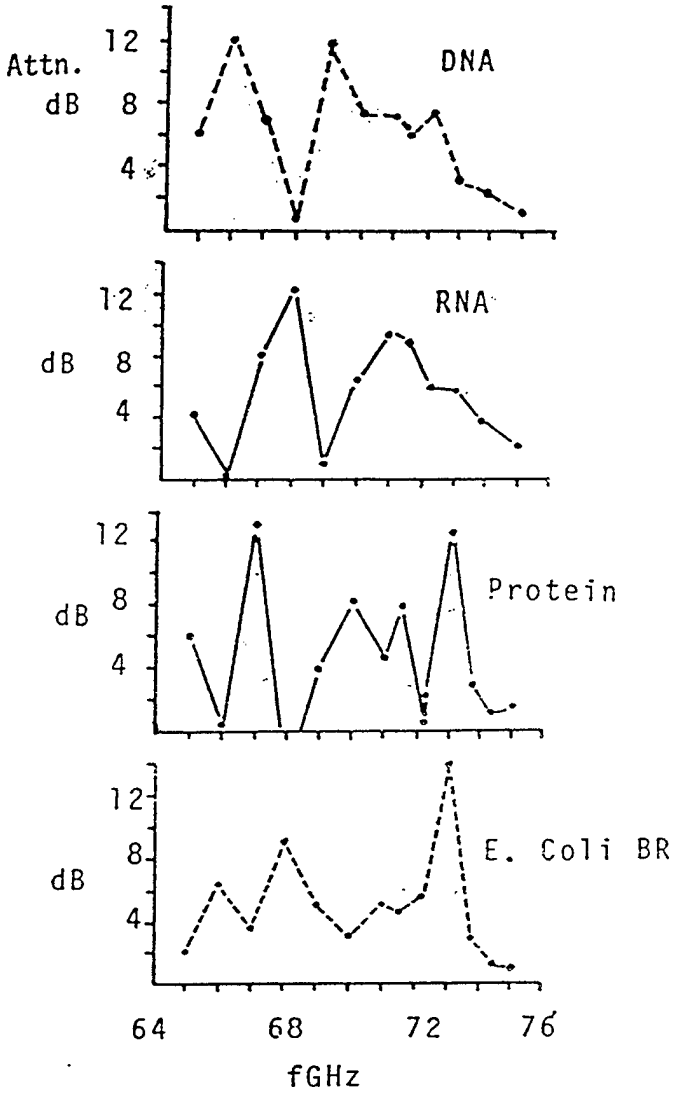

Microwave Absorption Spectra of Biological Entities

From S. J. Webb and A. D. Booth, *Nature*, 222, p. 1199, 1969

SPECTRAL STUDIES

FREQUENCY RANGE: 26.5 - 90 GHz

POWER LEADS: 0.2 - 100 μW

DWELL TIME: 50 ms - 10S

SAMPLE TEMPERATURES: -70°, +20°, + 37°C

BIOCHEMICALS TESTED: RNA (12%)
DNA (4%)

BIOLOGICAL SYSTEMS TESTED: (10^7-10^8/mℓ)

E. Coli
Yeast (2 kinds)
B H K cells
Fibroblasts
RBCs (human, avian)
Viruses

TABLE 1. SUMMARY OF MEASUREMENTS

Test Medium	Comparison Medium	Frequency Range GHz	N	Mean Value	Min. Value	Max. Value
				Relative Insertion Loss, dB		
H_2O	H_2O	26.5-90	5	-.024	-0.20	.16
MEM	H_2O	26.5-90	5	-.13	-0.38	.033
12% RNA	1 M NH_4OH	26.5-90	5	-.71	-1.16	.22
3.6% RNA	1 M NH_4OH	26.5-90	5	-.26	-1.37	.42
0.5% DNA	1 M NH_4OH	26.5-90	5	.020	-0.76	.67
BHK 21/C13 cells	MEM	26.5-90	5	-.14	-0.47	.19
C. albicans	Broth	26.5-60	5	-.21	-0.52	.00
C. albicans	Broth	70-90	5	-.12	-0.24	.032
C. krusei	Broth	70-90	5	-.13	-0.30	-.002
E. coli	Broth	70-90	5	-.12	-0.21	-.023

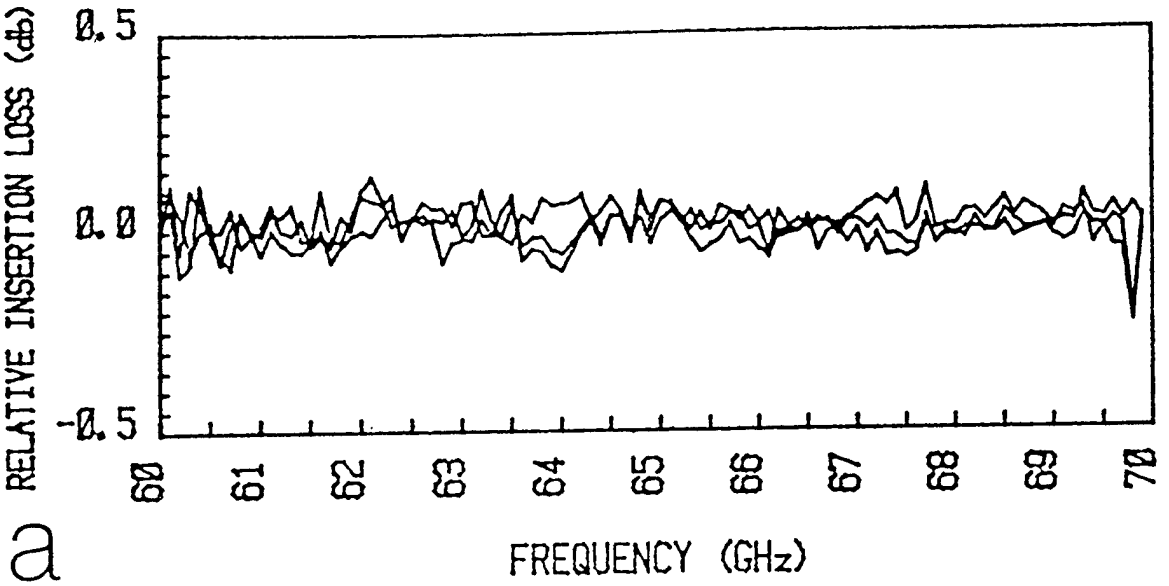

a

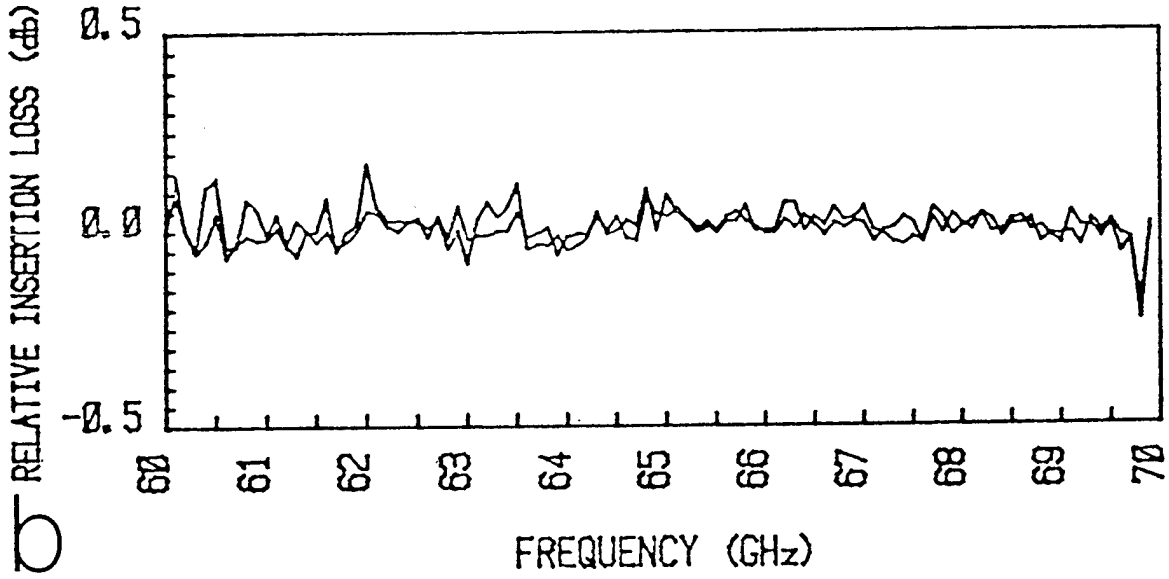

b

Insertion loss of E.coli
(P_{inc} = 8.0 - 24μW with modulation)

a. Broth vs. Broth
b. E.coli vs. Broth

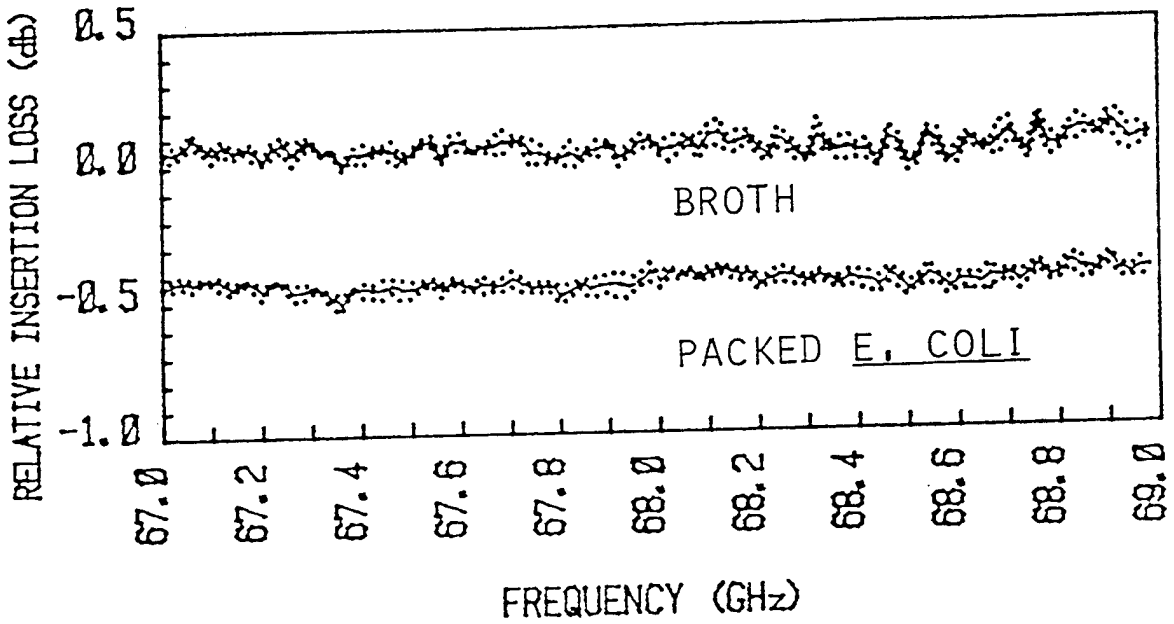

Insertion loss of packed E.coli.

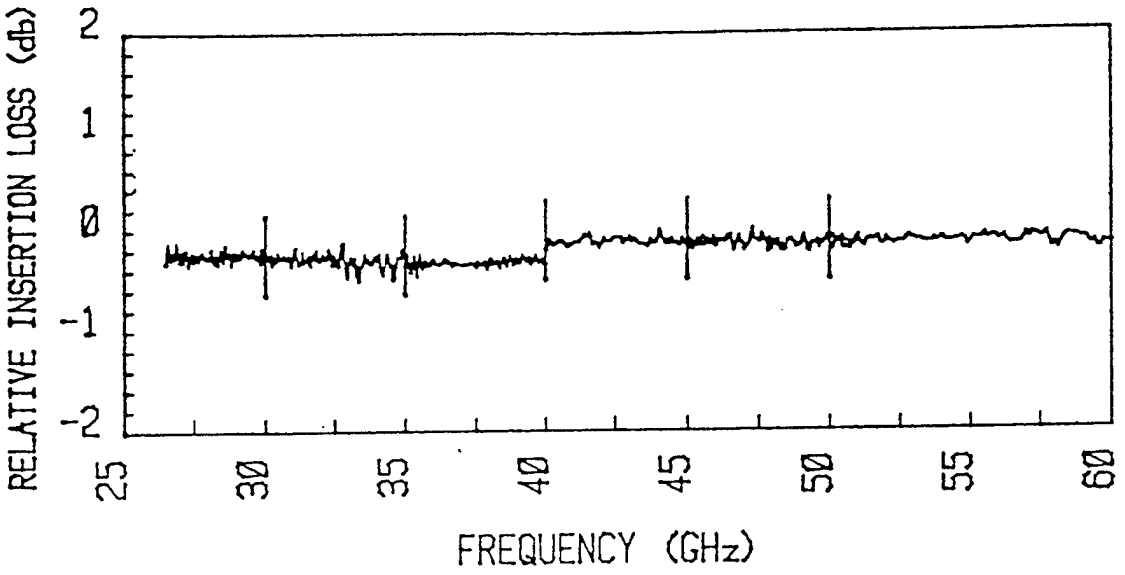

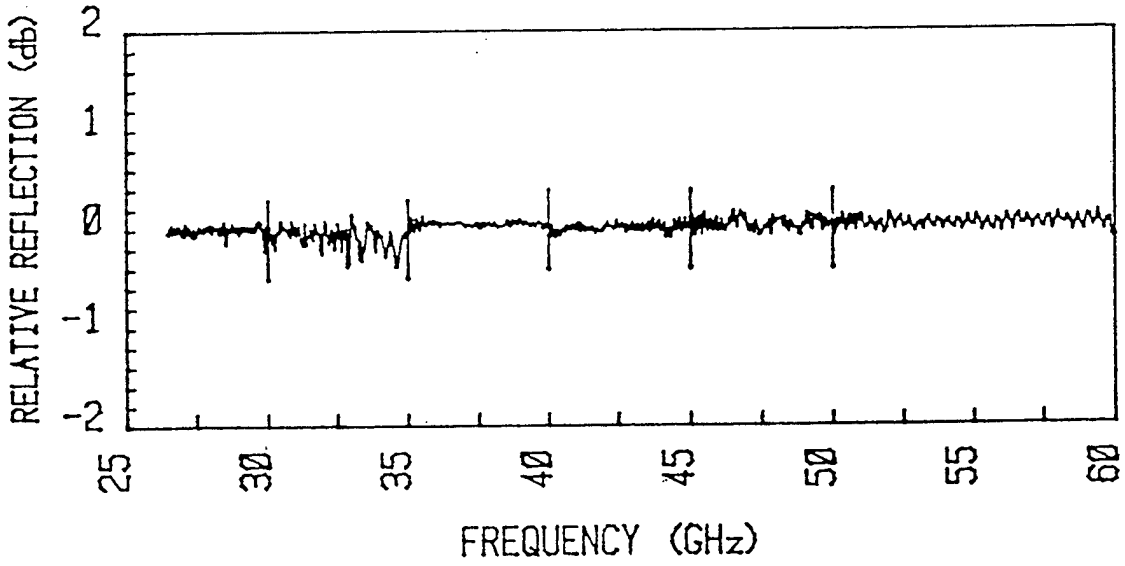

Wideband tests on Candida Albicans.

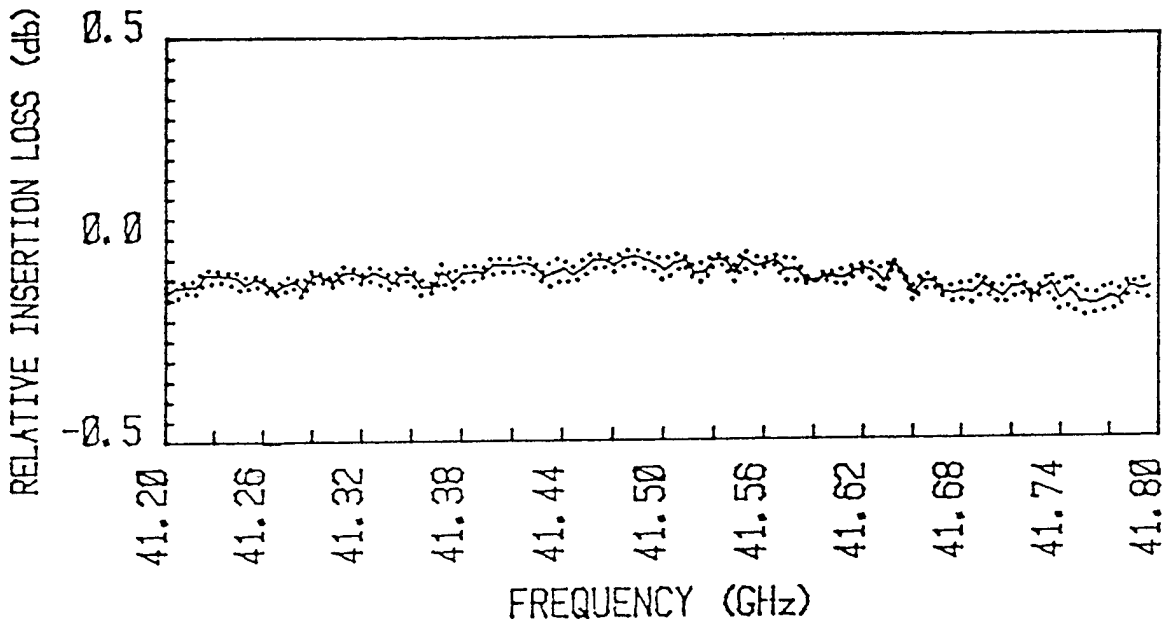

Insertion loss of Candida Krusei (50 ms dwell time; P_{inc} = 10μW; N = 2 x 10^8 cells/mℓ)

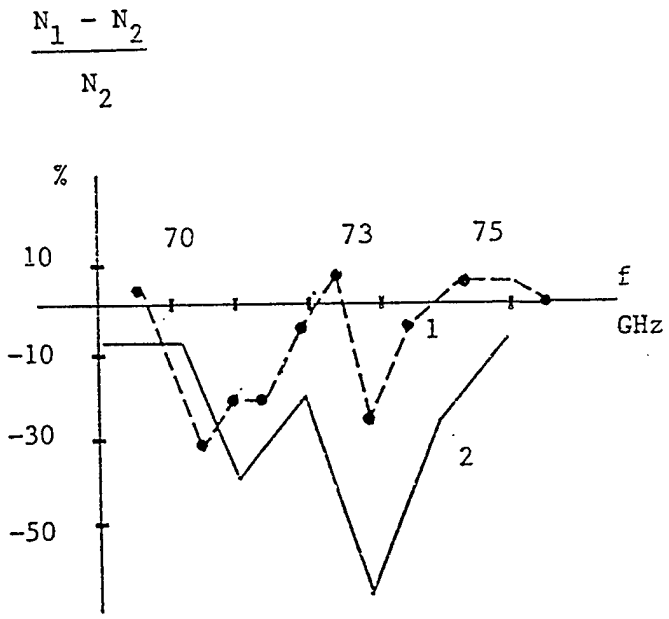

Difference in number of colonies of E. coli between irradiated and control samples.

André

1. A. J. Berteaud et al. *C. R. Acad. Sci.* (D), 281, p. 843, 1975
2. S. J. Webb and A. D. Booth, *Nature*, 222, p. 1199, 1969

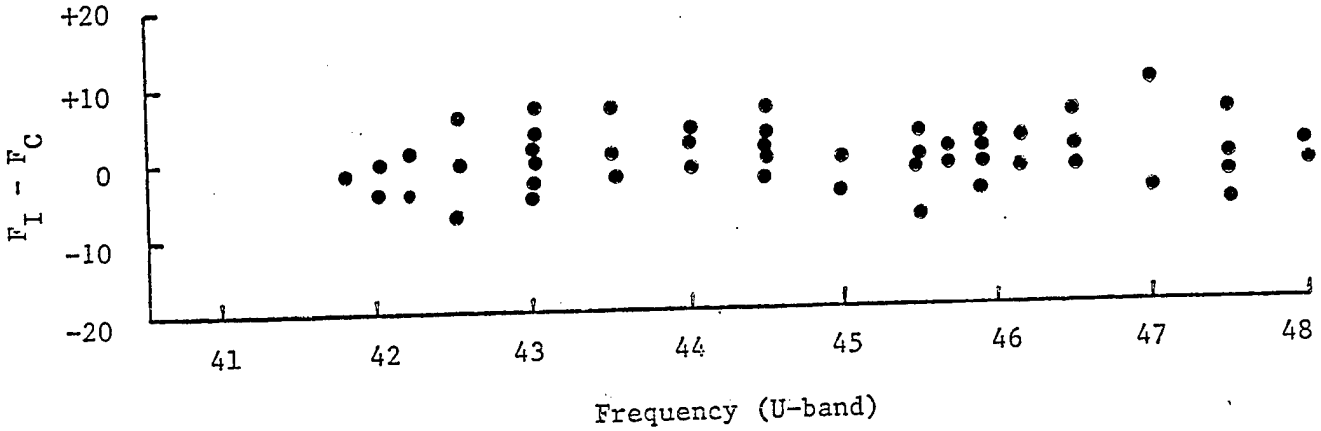

Fig. 4. Effects of microwave irradiation on induction of lambda phage TC600 (λ papa). $F_I - F_C$ denotes the difference in induction rate between irradiated and control samples.

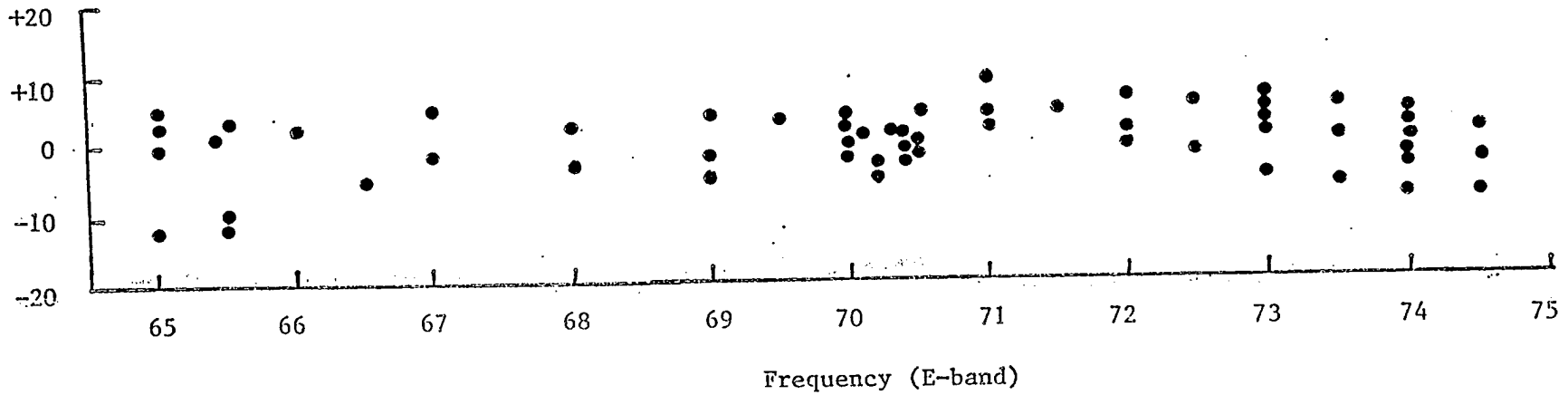

Fig. 5. The difference in induction ($F_I - F_C$) for irradiated and control cells as a function of irradiation frequency (in the E-band) using lambda phage TC600 (λ papa).

PROTEIN SYNTHESIS OF MONOLAYER CULTURES OF BHK-21/C13 MAMMALIAN CELLS STUDIED AT 0.1GHz INTERVALS IN 38.0-48.0 GHz and 65.0-75.0. GHz BANDS (202 FREQUENCIES) FAILED TO REVEAL ANY FREQUENCY OR AMPLITUDE DEPENDENT EFFECTS.

ASSAY INVOLVED INCORPORATION OF ^{3}H-METHIONINE INTO PROTEIN WHICH WAS QUANTIFIED BY MEASUREMENT OF OPTICAL DENSITIES OF AUTORADIOGRAPHS IN CONTIGUOUS RECTANGULAR REGIONS OF WIDTH 0.1 mm.

FOR A LIMITED NUMBER OF EXPERIMENTS WITH INCORPORATION OF ^{3}H-URIDINE INTO RNA FOR IRRADIATION DURATIONS OF 1 HR. ALSO YIELDED NEGATIVE RESULTS.

PARTLOW ET AL.,
BUSH, ET AL.,
STENSAAS, ET AL.

BIOELECTROMAGNETICS, VOL. 2, 1981, PP. 123-159

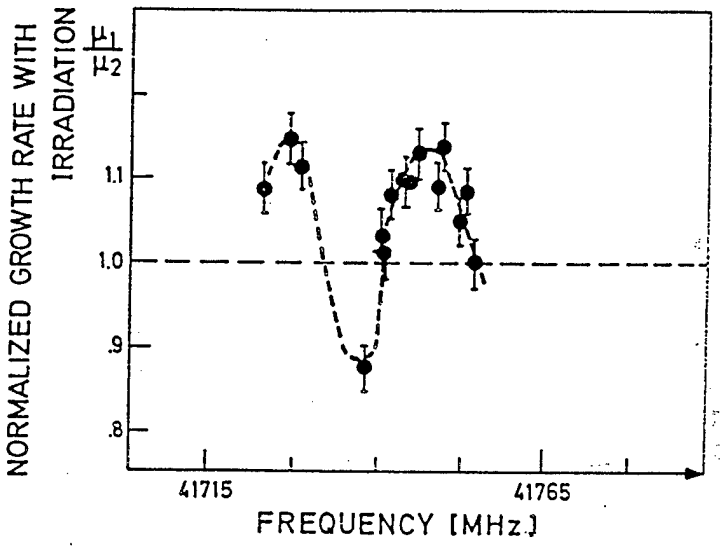

FIGURE 4

Fig. 9. Normalized growth rate of yeast as a function of frequency [from Ref. 11].

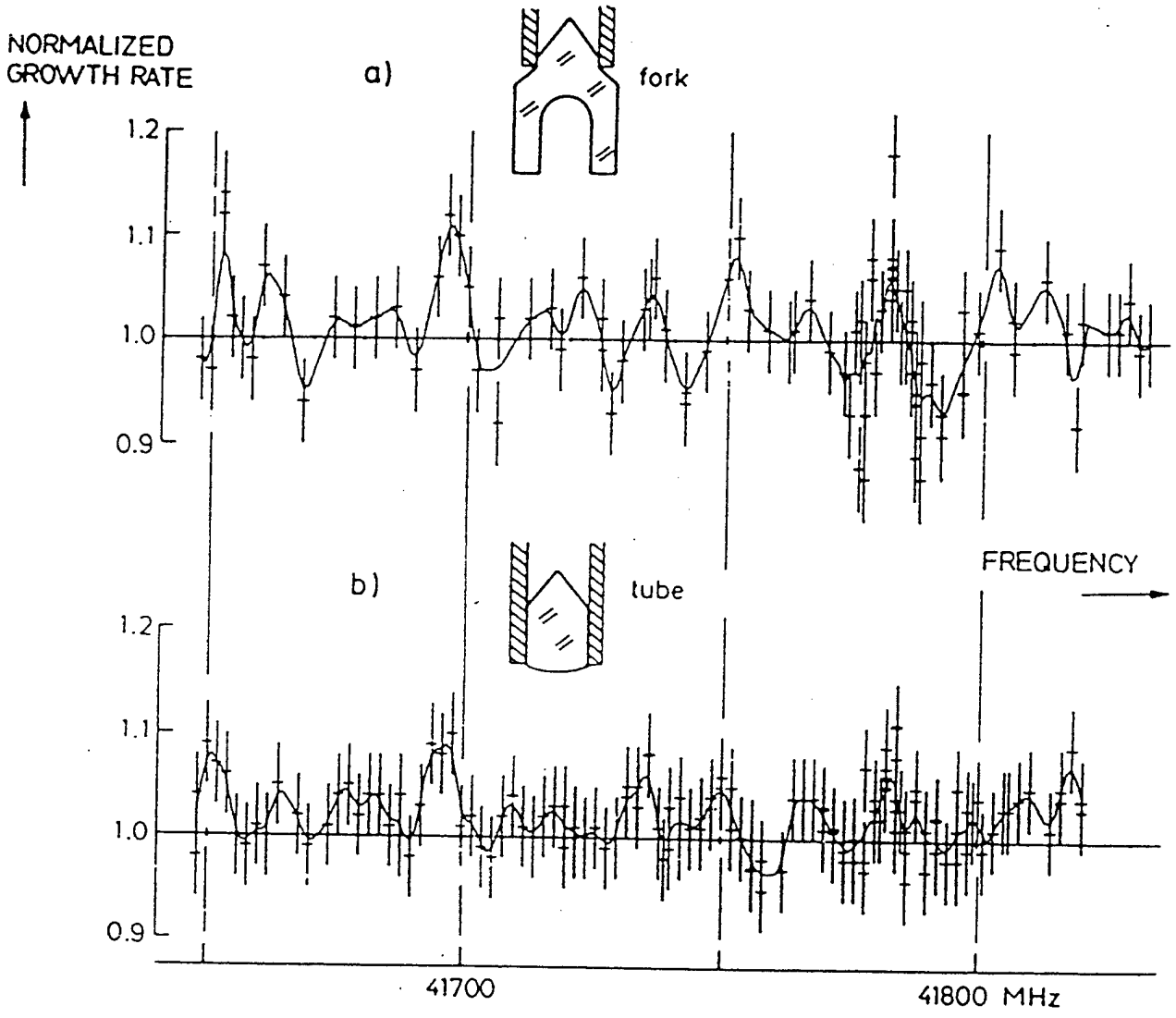

Normalized growth rate of yeast cultures with Mm wave irradiation (W. Grundler and F. Keilmann).

Effects of Millimeter Wave Irradiation on the Growth Rate of Saccaromyces Cerevisiae

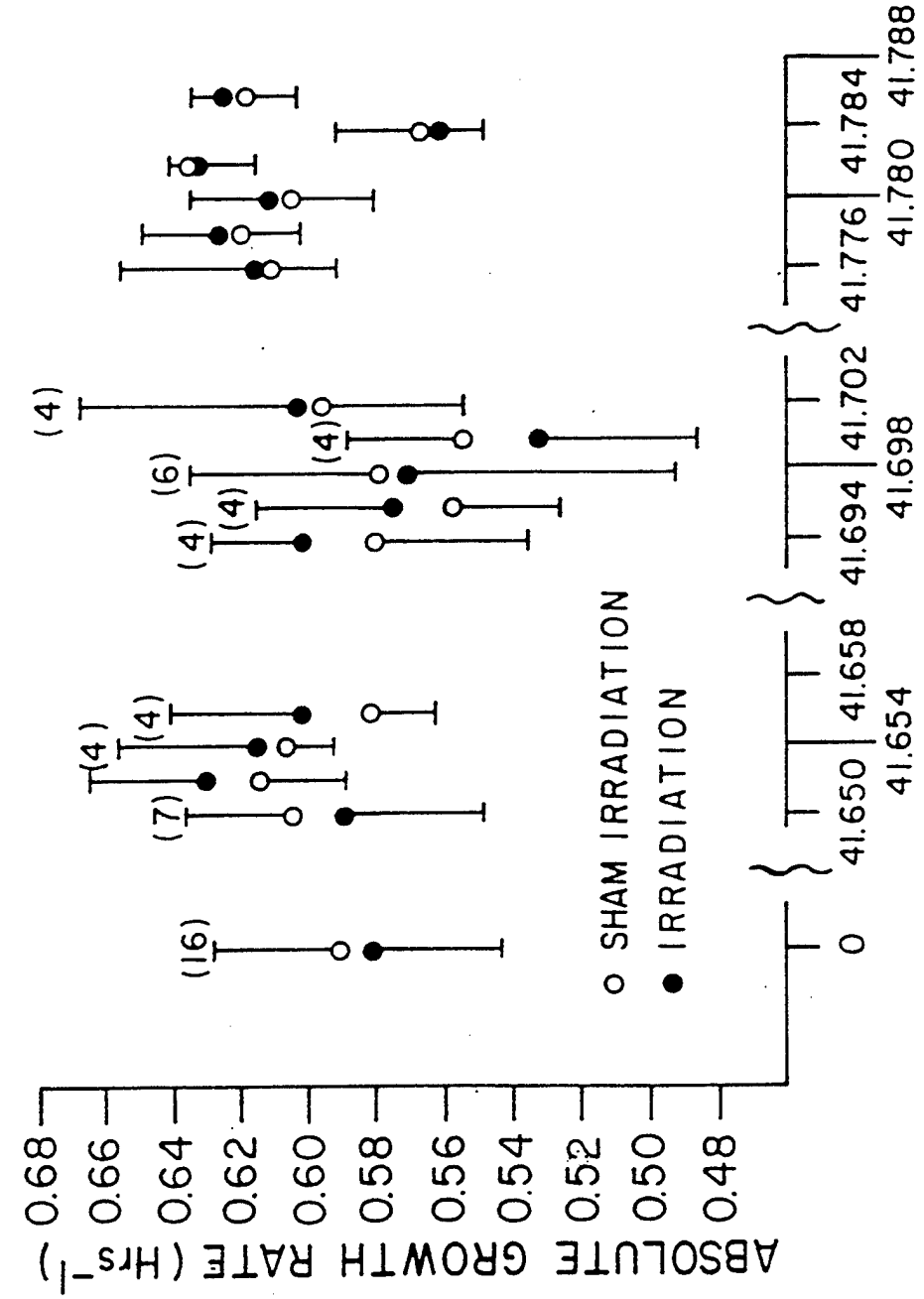

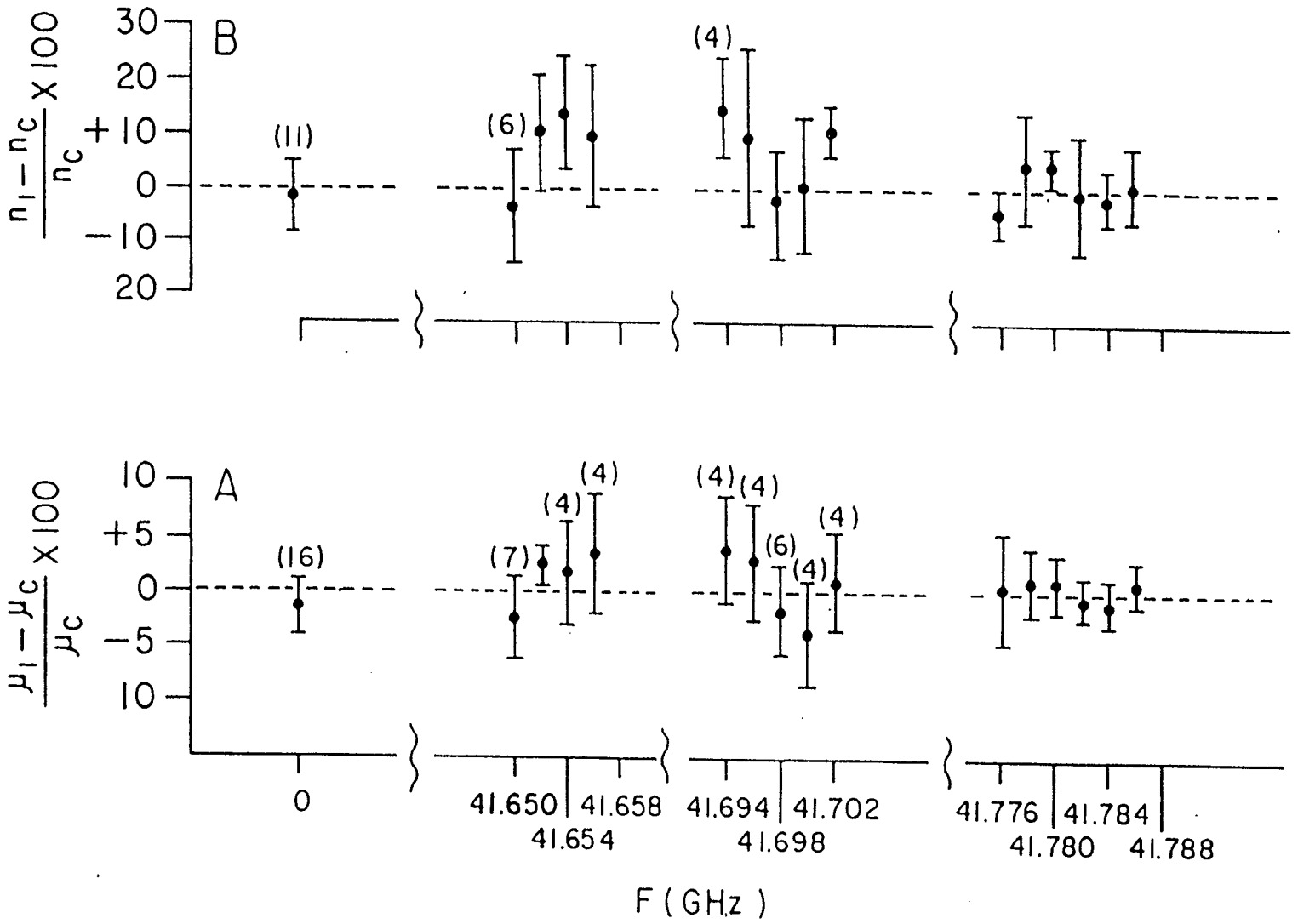

Effects of Mm-wave irradiation on s. cerevisiae

a. Percentage differences in growth rates.

b. Percentage differences in number of viable colonies

Three experiments done at each frequency unless indicated otherwise.

HOPING TO FIND DIMENSIONALLY-RELATED RESONANCES POSTULATED BY FROHLICH FOR CELL MEMBRANES, WE STUDIED RAMAN SPECTROSCOPY OF DPPC VESICLES (~ 70 Å THICK, DIAMETER ~ 300 Å) WITH ARGON-ION LASER AT 514.5 nm.

BELOW AND ABOVE THE PHOSPHOLIPID TRANSITION TEMPERATURE OF 41°C.

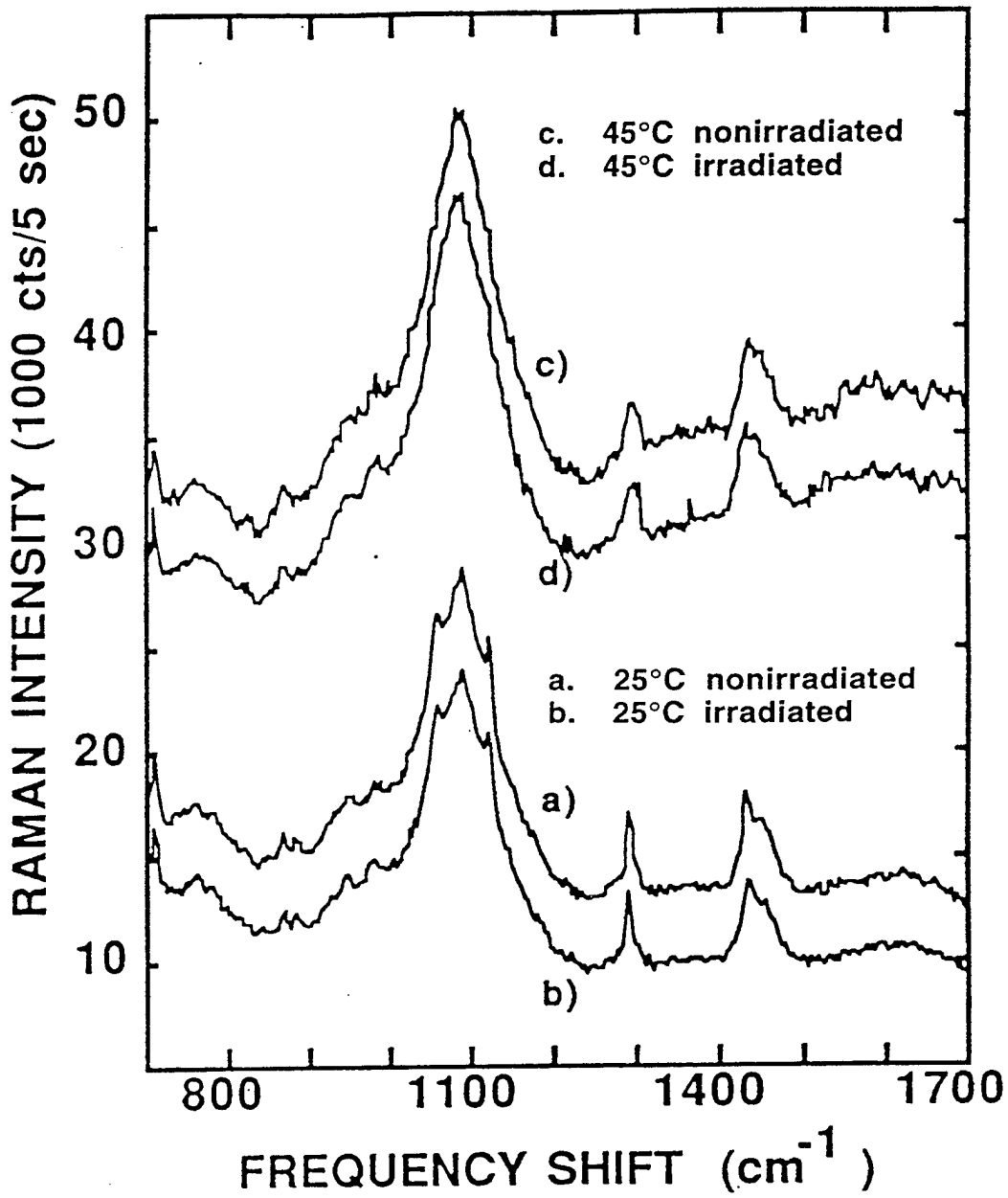

Raman Spectra of Lipid Bilayers with and without Mm wave irradiation.

Dipalmitoyl - Phosphatidylcholine (DPPC) Vesicles
Thickness ~ 70Å; diameter ~ 300 Å

Laser tuned at 514.5 nm

Furia, et al., *Jour. Appl. Phys.* 60, p. 2991, Oct. 15, 1986.

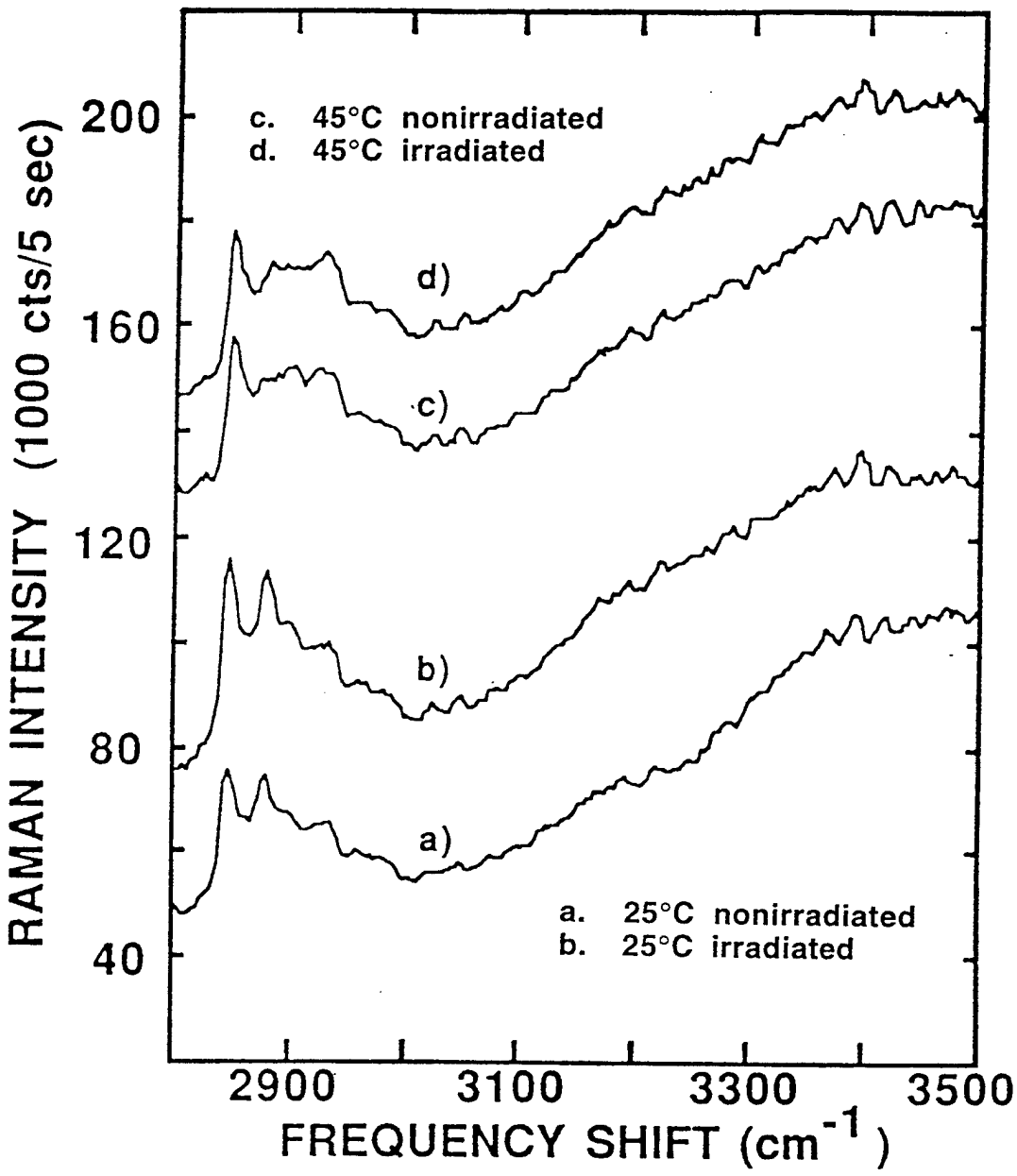

Raman Spectra of Lipid Bilayers with and without Mm wave irradiation.

Dipalmitoyl - Phosphatidylcholine (DPPC) Vesicles
Thickness ~ 70Å; diameter ~ 300 Å

Laser tuned at 514.5 nm

Furia, et al., *Jour. Appl. Phys.* 60, p. 2991, Oct. 15, 1986.

THESE EXPERIMENTS WERE DONE TOWARDS THE END OF THE PROJECT. COUPLING BETWEEN LONGITUDINAL AND OPTICAL PHONONS HAVE CERTAINLY BEEN OBSERVED IN SOLID-STATE PHYSICS.

IT IS CONCEIVABLE THAT AS POSTULATED BY FROHLICH, DIMENSIONALLY-RELATED LONGITUDINAL MODES COULD BE EXCITED IN BIOLOGICAL MEDIA WHICH COULD BE DETECTED BY MEANS OF RAMAN SPECTRA.

Frequencies of maximum coupling to vesicles ~ 70 Å thick, diameter ~ 300 Å assuming $v_s \sim 2\times10^5$ cm/s)

$$f_1 = \frac{v_s}{70\times10^{-8}} \sim 300\ \text{GHz}$$

$$f_2 = \frac{v_s}{300\times10^{-8}} \sim 66\ \text{GHz}$$

Bioelectromagnetics 19:393–413 (1998)

Review Article

Current State and Implications of Research on Biological Effects of Millimeter Waves: A Review of the Literature

Andrei G. Pakhomov,[1]* Yahya Akyel,[1] Olga N. Pakhomova,[1] Bruce E. Stuck,[2] and Michael R. Murphy[3]

[1]McKesson BioServices, Brooks Air Force Base, San Antonio, Texas
[2]U.S. Army Medical Research Detachment of the Walter Reed Army Institute of Research, Brooks Air Force Base, San Antonio, Texas
[3]Directed Energy Bioeffects Division, Human Effectiveness Directorate, Air Force Research Laboratory, Brooks Air Force Base, San Antonio, Texas

In recent years, research into biological and medical effects of millimeter waves (MMW) has expanded greatly. This paper analyzes general trends in the area and briefly reviews the most significant publications, proceeding from cell-free systems, dosimetry, and spectroscopy issues through cultured cells and isolated organs to animals and humans. The studies reviewed demonstrate effects of low-intensity MMW (10 mW/cm^2 and less) on cell growth and proliferation, activity of enzymes, state of cell genetic apparatus, function of excitable membranes, peripheral receptors, and other biological systems. In animals and humans, local MMW exposure stimulated tissue repair and regeneration, alleviated stress reactions, and facilitated recovery in a wide range of diseases (MMW therapy). Many reported MMW effects could not be readily explained by temperature changes during irradiation. The paper outlines some problems and uncertainties in the MMW research area, identifies tasks for future studies, and discusses possible implications for development of exposure safety criteria and guidelines. Bioelectromagnetics 19:393–413, 1998.

Key words: electromagnetic fields; bioeffects; mm wave band; millimeter waves, review

INTRODUCTION

The term "millimeter waves" (MMW) refers to extremely high-frequency (30–300 GHz) electromagnetic oscillations. Coherent oscillations of this range are virtually absent from the natural electromagnetic environment. This absence might have had important consequences. First, living organisms could not have developed adaptation to MMW during the course of evolution on Earth. Second, some specific features of MMW radiation and the absence of external "noise" might have made this band convenient for communications within and between living cells [Golant, 1989; Betzky, 1992]. These arguments, although not adequately proven, are often used to explain the high sensitivity to MMW of biological subjects. Indeed, MMW have been reported to produce a variety of bioeffects, many of which are quite unexpected from a radiation penetrating less than 1 mm into biological tissues. A number of theoretical models have been set forth to explain peculiarities and primary mechanisms of MMW biological action [Fröhlich 1980, 1988; Golant, 1989; Grundler and Kaiser, 1992; Belyaev et al., 1993a; Kaiser, 1995].

One of the most remarkable events in contempo-

Contract grant sponsor: U.S. Army Medical Research and Materiel Command; Contract grant sponsor: U.S. Air Force Armstrong Laboratory; Contract grant number: U.S. Army contract DAMD17-94-C-4069 (to McKesson BioServices).

*Correspondence to: Andrei G. Pakhomov, USA-MCMR, McKesson BioServices, 8308 Hawks Road, Building 1168, Brooks Air Force Base, San Antonio, TX 78235-5324. E-mail: andrei.pakhomov@aloer.brooks.af.mil

Received for review 21 October 1997; final revision received 30 January 1998

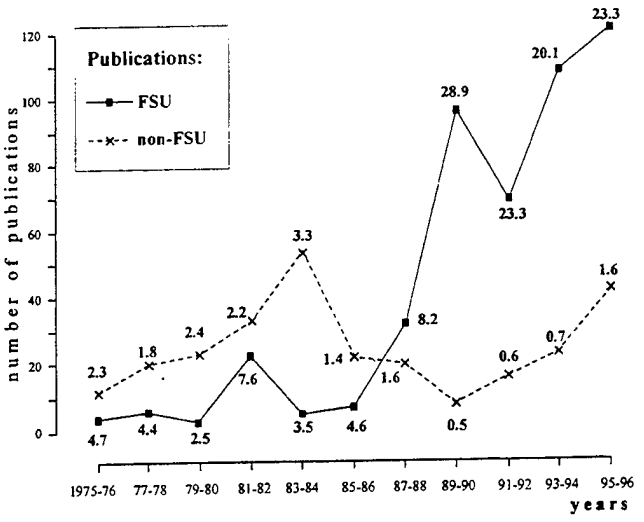

Fig. 1. Absolute numbers and percentages of publications on topics related to biological action of millimeter waves vs. years of publication. The graph is based on counts of citations in the EMF Database version 3.0, 1997. Studies by the former Soviet Union (FSU) scientists and by all other (non-FSU) were counted separately. Vertical scale is the number of published MMW studies per 2-year time intervals (abscissa). Numbers next to the datapoints indicate the weight (%) of MMW studies in the FSU and non-FSU bioelectromagnetic research (i.e., the percentage of MMW studies relative to the total number of studies included in the EMF database for the respective time periods).

rary electromagnetic biology is a surge in interest in MMW biological and medical effects in the countries of the former Soviet Union (FSU). A striking difference in the FSU and "non-FSU" research activity in this area can be seen from counts of related publications. For example, the EMF Database[1] version 3.0 (1997) lists a total of 463 FSU publications on MMW-related topics, and only 261 such publications from the rest of the world. Although these numbers should not be taken as exact (the Database includes most but certainly not all relevant citations), the situation in general is portrayed correctly and is particularly explicit in a historic perspective (Fig. 1). The non-FSU production reached its peak of 52 papers (including meeting abstracts) in 1983–1984, when MMW titles were 3.3% of all non-FSU publications in the bioelectromagnetics area. Then it gradually declined to only seven papers (0.5%) in 1989–1990. Concurrently, MMW research in the FSU expanded greatly: Both the count of publications (up to 120 in 1995–1996) and their portion in the FSU bioelectromagnetic research (20 to 30%) far exceeded these numbers for non-FSU publications.

Aside from the number of studies, there are important qualitative differences. Western (non-FSU) research was largely driven by concerns for public safety. However, safety issues occupy a relatively small portion of the FSU research, whereas far more studies are related to medical applications of MMW. Over 50 diseases and conditions have been claimed to be successfully treated with MMW alone or in combination with other means. Lebedeva and Betskii [1995] have reported more than a thousand MMW therapy centers in the FSU and over 3 million people who received this therapy. Naturally, the extensive medical use of MMW has stimulated basic research as well.

Nowadays, MMW technologies are increasingly being used in practical applications (e.g., wireless communication, traffic and military radar systems), making it imperative that bioeffects data be available for health hazard evaluation and restoring the interest to MMW biological research in the West. The number of non-FSU publications on this topic is again increasing. A specialized MMW session appeared at the 1996 meeting of the Bioelectromagnetics Society and the 1997 Second World Congress on Electricity and Magnetism in Biology and Medicine, and the first Infrared Lasers and MMW Workshop was held at Brooks Air Force Base, Texas in 1997. Unfortunately, the FSU research, a rich source of MMW bioeffects data, is not readily available in the West and is scarcely known by Western scientists.

The present paper is intended to fill in this gap by reviewing recent research in the MMW field, from molecules and cells to MMW therapy. We have analyzed over 300 original FSU publications and about 50 non-FSU papers and selected those which appeared more interesting and credible. This review is primarily focused on experimental and clinical findings reported during the last decade. Therefore, it includes only a few essential citations of earlier publications and does not cover such topics as theoretical modeling of possible interaction mechanisms. Interested readers should see other reviews for additional information [Fröchlich, 1980, 1988 (ed.); Gandhi, 1983; Grundler, 1983; Postow and Swicord, 1986; Belyaev, 1992].

PHYSICOCHEMICAL EFFECTS, MMW ABSORPTION, AND SPECTROSCOPY

A number of independent studies have shown specific MMW effects in the absence of living subjects,

[1]The EMF Database is produced by Information Ventures, Inc. (Philadelphia, PA) and covers topics related to biological effects of electromagnetic fields, from DC to submillimeter wavelengths. The Database contains over 20,000 citations of relevant publications from various sources, including peer-reviewed journals, books, proceedings, and meeting abstracts. Available citations are assimilated in the Database without any preselection based on the language, affiliation of the authors, or relevance to a particular EMF frequency range.

i.e., in solutions of biomolecules and even in pure water. Fesenko and Gluvstein [1995] analyzed MMW effects on periodic voltage oscillations during discharge of a water capacitor. The capacitor, which was a distilled water sample in a 1-mm capillary, was charged by 18 V, 1-ms-wide unipolar rectangular pulses. The capacitor discharged within 500–600 ms after a pulse. The discharge curve contained periodic voltage oscillations reaching 10–15 mV. The Fourier spectrum of these oscillations included two strong peaks, at 5.25 and 46.8 Hz, and these peaks did not change during at least 2 h of experimentation. The water sample was exposed at 36 GHz from an open-ended waveguide (7.2 × 3.4 mm cross-section). Irradiation at 50 μW output power greatly reduced the 46.8 Hz peak in 1 min and virtually eliminated it in 10 min; the 5.25 Hz peak shifted to 6.75 Hz. These changes showed little or no recovery within 2–60 min after cessation of a 10-min exposure. Irradiation at 5 mW output power produced similar changes, but, unexpectedly, was far less effective: the changes developed more slowly, and the original peaks were restored more quickly. Mechanisms of the phenomenon itself, its anomalous power sensitivity, and the long-lasting "memory" of water were not understood. The authors suggested that MMW-induced changes in water properties could underlie biological effects.

Direct MMW effects on pure water properties were also observed by holographic interferometry [Berezhinskii et al., 1993; Litvinov et al., 1994]. Refraction of light in fluid was determined from the width and number of interference bands formed by a He-Ne laser beam (630 nm) passing through the fluid and a referent beam. Irradiation of distilled water at 10 mW output power for 5–7 min caused no effect at 41.5 GHz, but decreased the number of the interference bands from 6 to 5 at 51.5 GHz; the distance between the bands increased 1.2 times. These changes developed faster and were more profound in a 2% human blood plasma solution. The effect reached saturation in 6–7 min and was completely reversible. Both theoretical calculations and direct measurements established that maximal MMW heating was about 1 °C. MMW-induced changes in the light refraction coefficient were almost an order of magnitude greater than produced by conventional heating by 1 °C and, therefore, were attributed to a specific effect of MMW.

Other properties of blood plasma, such as dielectric permittivity and absorption coefficient, could be altered by MMW irradiation as well [Belyakov et al., 1989]. Changes of only 0.05–0.5% in these parameters were measured but were well beyond the limits of the method used (0.01%). The sensitivity of plasma samples to particular radiation wavelengths strongly varied from one blood donor to another.

Khizhnyak and Ziskin [1996] analyzed peculiarities of MMW heating and convection phenomena in water solutions. Besides the most expected reaction (gradual temperature rise), irradiation could induce either temperature oscillations and a decrease in average temperature or a biphasic response in which the temperature initially rises and then decreases. These anomalous effects resulted from convective processes, i.e., the formation of a toroidal vortex. When the vortex became stable, the temperature decreased after the initial rise phase, although the irradiation was constantly maintained. The local temperature could decrease with increasing power density, and, in biological systems, this would appear as an effect opposite to heating. Probably, this phenomena could explain some of reported "nonthermal" MMW effects. If irradiation continued for a long time (30–40 min), the convection phenomena disappeared and could not be reintroduced, even after restoration of the initial temperature. This observation suggested that some irreversible process had occurred in the liquid, which resembles findings of the water "memory" cited above.

The supposed role of water as a primary target for MMW radiation motivated Zavizion et al. [1994] and Kudryashova et al. [1995] to study how MMW absorption at the wavelengths of 2.0, 5.84, and 7.12 mm is affected by the presence of other substances, namely α-amino acids (0.25–2.5 mol/l). Because MMW absorption by amino acid molecules is negligible, the absorption of solutions in most cases decreased proportionally to the amino acid concentration. This difference in absorption by pure water and solutions, called "absorption deficit," increased with increasing length of the hydrophobic radical in a series of homologous amino acids (glycine, alanine, GABA, valine). Paradoxically, the absorption deficit was negative for sarcosine at 5.84 mm and 7.12 mm and for glycine at all the wavelengths, meaning that these two amino acids can increase MMW absorption by water molecules.

A detailed theoretical analysis of MMW absorption in flat structures with high water content was performed by Ryakovskaya and Shtemler [1983]. The authors produced dependencies of the specific absorption rate (SAR) on the radiation frequency, temperature, thickness of the absorptive medium, and presence of dielectric layer(s) above and/or underneath. This work modeled most common biological setups, such as irradiation of cell suspensions in Petri dishes, cuvettes, etc. The wavelength in the medium, reflection coefficients, depth of penetration, and SAR at the surface of a semi-infinite absorptive medium were calculated for wavelengths from 1 to 10 mm, using 1-mm steps. For exam-

ple, the depth of penetration for 1- and 10-mm wavelengths at 20 °C equals 0.195 mm and 0.56 mm, respectively, and the respective surface SARs are 79.4 and 15.5 mW/cm^3 per 1 mW/cm^2. Exposure through a thin dielectric layer (e.g., bottom of a Petri dish) may decrease reflection and further increase SAR by up to 2.5 times. SAR in thin absorptive films (0.1–0.01 mm) increases greatly and may exceed SAR at the surface of a semi-infinite medium more than 10-fold. Furthermore, presence of a dielectric above or below the thin absorptive film may increase SAR in the film by as much as 20-fold. Apparently, the possibility of reaching very high SAR levels and of local heating cannot be underestimated, even for the incident power levels that are often regarded as nonthermal (0.1–1 mW/cm^2).

MMW EFFECTS AT SUBCELLULAR, CELLULAR, AND TISSUE LEVELS

Growth Rate Effects

Debates about resonance growth rate effects of MMW have been going on for over 20 years, and this problem was widely discussed in earlier reviews. In brief, Grundler and coauthors [1977, 1982, 1988] reported that the growth rate of the yeast *Saccharomyces cerevisiae* may be either increased by up to 15% or decreased by up to 29% by certain frequencies of MMW within a 41.8–42.0 GHz band. The effect was established by different methods, both in suspended cells and in monolayer. According to recent observations [Grundler and Kaiser, 1992], an effect of about the same magnitude is produced by field intensities from 5 pW/cm^2 to 10 mW/cm^2 (8 kHz modulation). The width of the resonance peaks increased with the intensity from about 5 MHz to 12–15 MHz over the above intensity range. However, thorough independent attempts to replicate these findings were not successful [Furia et al., 1986; Gos et al., 1997], suggesting that these MMW effects could be dependent on (or even produced by) some as yet unidentified and uncontrolled conditions.

Dardanoni and coauthors [1985] observed frequency- and modulation-dependent effects on the growth of yeast *Candida albicans*. MMW modulated at 1 kHz reduced the growth rate by about 15% at 72 GHz, but not at 71.8 or 72.2 GHz. A 3-h continuous wave (CW) irradiation at 72 GHz had the opposite effect, i.e., the growth rate increased by about 25% over the sham-irradiated control. Remarkable variability of the results was noted, which could be a result of cell subpopulations with different sensitivity.

Golant and coauthors [1994] reported that a marked synchronicity of periodic fluctuations in the growth rate and bud formation in the culture of *S. cerevisiae* can be induced by 0.03 mW/cm^2, 46 GHz irradiation for 50 min. This effect was claimed to persist for over 20 cell generations. Periodicity of bud formation was observed in control samples as well, but it was less pronounced and had a different time duration (60 min vs. 80 min after MMW exposure).

Synchronizing effects of MMW were also observed in higher plant specimens (Shestopalova et al., 1995). Barley seeds were exposed for 20 min at 0.1 mW/cm^2 (61.5 GHz), and then the exposed and control seeds (150 seeds per group) were put into an incubator for sprouting. The incubator was maintained at either 28 °C or 8 °C. Cytologic examination established that the degree of synchronization of cell division in MMW-exposed sprouts increased by 36% (28 °C) and 50% (8 °C) over the respective control plants.

Levina et al. [1989] studied MMW effects on the development of a protozoan *Spirostum sp.* cell population. The population was begun in a saline medium with beer yeast (550 mg/l) as food by adding of 5–6 protozoan cells/ml. The culture was exposed once for 30 min at 1.5 mW/cm^2 (7.1-mm wavelength), between days 2 and 11 of growth. Unexposed cultures grew exponentially up to a density of 100 cells/ml on day 11, then rapidly died without reaching stationary phase, obviously due to poisoning by waste products. Exposures on days 2, 4, or 7 caused the populations to enter the stationary phase on or around day 9. Exposures on day 9 or 11 postponed the population death by 5 days, and the final cell content increased to 115–135 cells/ml on day 14. Irradiation on day 2 also increased the proliferation rate, and by day 7 the cell density was nearly twice as high as in control samples. In another series of experiments, the population began with an initial concentration of 1-2 protozoan cells/ml and stabilized in 8–10 days at 12–13 cells/ml. In these cultures, MMW exposure suppressed proliferation, and the final cell density was only 6–10 cells/ml. This study indicated that irradiation affects the population's own growth control mechanisms and that the effect depends on the stage and other particulars of the population development.

Exposure for 30 min at 2.2 mW/cm^2, 7.1-mm wavelength enhanced the growth of a blue-green algae *Spirulina platensis* by 50% [Tambiev et al., 1989], whereas 8.34-mm wavelength produced no changes compared with sham control. The alga growth rate more than doubled when a 30-min irradiation at 7.1 mm was immediately followed by exposure to high-peak power microwave pulses (15 pulses, 10-ns pulse width, 6-min pause, 3-cm wavelength, 200 kW/cm^2 peak incident power density). Concurrently, photosynthetic oxygen evolution increased about 1.5 times. The

observed stimulatory effects are of considerable promise in biotechnology, in which *S. platensis* is used for production of food protein and biologically active compounds.

Other publications by the same authors [Tambiev and Kirikova, 1992] and independent investigators [Rebrova, 1992; Shub et al., 1995] presented MMW effects on the growth rate of several species of bacteria, Cyanobacteria, algae, yeasts, and higher plants (fennel, lettuce, tomato). For example, in the yeasts *S. cerevisiae* and *S. carlsbergensis* MMW shortened the phases of culture growth 2.3–6.0 times and could increase the biomass production rate by up to 253%. Effects on *Escherichia coli* growth could be either stimulatory or inhibitory, depending on the wavelength (6.0- to 6.7-mm band, $\leq$ 1 mW/cm^2 for 30 min). However, all three papers were summaries of the authors' multiyear experiences with studying these and other MMW effects and did not provide enough detail for full evaluation or possible replication.

Chromosome Alterations and Genetic Effects of MMW

Absence of mutagenic or recombinagenic effects of MMW radiation was clearly demonstrated in the late 1970s [Dardalhon et al., 1979, 1981], and later investigations were consistent with this conclusion. At the same time, a number of studies indicated that MMW could affect the fine chromosome structure and function, cell tolerance to standard mutagens, and lesion repairs.

Best known is the recent work by Belyaev and coauthors [1993a, b, 1994, 1996], who discovered sharp frequency resonances by using an anomalous viscosity time dependence (AVTD) technique. This technique is supposed to reflect fine changes in DNA conformation and DNA-protein bonds. At a resonance frequency, biological changes could be produced by field intensities as low as 10^{-19} W/cm^2. The magnitude of changes gradually increased with the field intensity and reached a plateau between 10^{-17} and 10^{-8} W/cm^2, depending on cell density in exposed samples. Resonance peaks for *E. coli* cells were found at 51.76 and 41.34 GHz; these values decreased in strains with increased haploid genome length. These results pointed to the chromosomal DNA as a target for resonance interaction between living cells and MMW. The width of the resonances increased from units to tens of megahertz by increasing the incident power, and this dependence is in notable agreement with the one reported for cell growth rate effects [Grundler and Kaiser, 1992].

However, the AVTD test is not a conventional technique in cell biology. Interpretation of AVTD data is uncertain and functional consequences of AVTD changes have not yet been convincingly defined. A discussion is continuing as to whether super-low radiation intensities in these studies were measured correctly [Osepchuk and Petersen, 1997a, 1997b; and a reply by Belyaev et al., 1997]. Supposedly, some power at a harmonic frequency might be transmitted to the sample despite large attenuation at the fundamental frequency. Whether this was the case or not, consistent observations of resonance effects represent an important finding, which requires understanding and independent replication.

MMW-induced visible changes in giant chromosomes of salivary glands of the midge *Acricotopus lucidus* [Kremer et al., 1988]. A certain puff, the Balbiani ring BR1 in the chromosome II, reduced in size after irradiation at 67.2 $\pm$ 0.1 GHz or 68.2 $\pm$ 0.1 GHz (5 mW/cm^2), and this effect seemed to be unrelated to heating. Numerous alterations in the giant chromosome morphology were also independently found in *Chironomus plumosus* (Diptera) after a 15-min exposure at 1 mW/cm^2 [Brill' et al., 1993].

Exposure of ultraviolet (UV)-treated *E. coli* culture to MMW at 61 $\pm$ 2.1 GHz, 1 mW/cm^2 increased cell survival [Rojavin and Ziskin, 1995]. The most likely mechanism of this effect was either direct or indirect activation of the dark repair system. No survival effects were found if the sequence of exposures was reversed, i.e., when UV irradiation was performed immediately after a 10- to 30-min MMW exposure.

Genetic effects of 61.02-61.42 GHz radiations were studied in the D7 strain of the yeast *S. cerevisiae* [Pakhomova et al., 1997]. MMW exposures lasted for 30 min at 0.13 mW/cm^2, and were followed in 60 min by a 100 J/m^2 dose of 254 nm UV radiation. Compared with the parallel control, the MMW pretreatment did not affect cell survival or the rate of reverse mutations, but significantly increased the incidence of gene conversions. Sham-exposed samples showed no differences from respective parallel control groups. The data suggested that MMW did not alter the UV-induced mutagenesis, but might facilitate UV-induced recombinagenic processes. A thermal mechanism for this effect was improbable, but could not be ruled out entirely.

Excitable Tissues and Membranes

Along with the genetic apparatus, the cell membrane is another site suspected to be a primary target for MMW radiation. Many of the works discussed below established profound MMW effects; however, only a few attempts have been made to replicate them.

Brovkovich et al. [1991] reported that 61 GHz, 4 mW/cm^2 radiation significantly activates the Ca^{++} pump in the sarcoplasmic reticulum (SR) of skeletal and heart muscles of the rat. The rate of Ca^{++} uptake

by SR membranes was measured by an ion-selective electrode in an ATP-containing medium. An intermittent MMW treatment (5-min exposure, 15-min pause, 3 cycles) of skeletal muscle SR increased the rate of Ca^{++} uptake by 23%, and this increased level was retained for 1 h after the exposure. Uninterrupted MMW irradiation had no effect in 10 min, but increased Ca^{++} uptake by 27% in 20 min; and the effect reached maximum (48%) in 40 min. In heart muscle SR, even a 5-min exposure enhanced Ca^{++} uptake by 18%.

Geletyuk and coauthors [1995] used patch-clamp (inside-out mode) to study 42.25 GHz radiation effects on single Ca^{++}-activated K^+ channels in cultured kidney cells (Vero). Exposure for 20–30 min at 0.1 mW/cm^2, CW, greatly modified the activation characteristics of the channels, particularly the open state probability. The field increased the activity of channels with a low initial activity and inhibited channels with initially high activity. In a subsequent study [Fesenko et al., 1995], these effects were reproduced without direct irradiation of the membrane, just by applying bathing solution pre-exposed for 30 min at 2 mW/cm^2, 42.25 GHz. Irradiation of the solution did not alter its pH or Ca^{++} concentration, and the nature of the MMW-introduced channel-modifying properties of the solution is not understood. The solution retained its biological efficacy for at least 10-20 min after cessation of the exposure.

Kataev and coauthors [1993] used a voltage clamp to study membrane currents in giant alga cells (*Nitellopsis obtusa,* Characea). Irradiation for 30–60 min at 41 GHz, 5 mW/cm^2 suppressed the chloride current to zero with no recovery for 10–14 h. Marked inhibitory effects were also found at 50 and 71 GHz, whereas most of other frequencies tested in the 38–78 GHz range enhanced the chloride current up to 200–400% (49, 70, 76 GHz). This activation was reversible, and recovery to the initial value took 30–40 min. Moreover, "activating" frequencies could restore the chloride current after its complete and normally irreversible suppression by "inhibitory" frequencies. MMW heating did not exceed 1 °C, and neither activating nor inhibitory effects were related to or could be explained by it. Calcium current also changed during irradiation, but this effect was not frequency dependent and could be adequately explained by heating. The authors noted that algae collected in the fall of 1990 and stored over the winter had entirely lost MMW sensitivity by February 1991.

Experiments with artificial bilayer membranes and snail neurons did not reveal any frequency-specific effects of MMW [Alekseev and Ziskin, 1995; Alekseev et al., 1997]. The capacitance of artificial membranes, ionic channel currents, and the transport of tetraphenylboron anions changed proportionally to MMW heating, regardless of the frequency (53–78 GHz range) or modulation used. Irradiation of snail neurons at 75 GHz (600–4200 W/kg) produced biphasic alterations of their firing rate, which were similar to those caused by equivalent conventional heating.

Burachas and Mascoliunas [1989] studied MMW effects on the compound action potential (CAP) in isolated frog sciatic nerve. CAP decreased exponentially and fell 10-fold within 50-110 min of exposure at 77.7 GHz, 10 mW/cm^2. CAP restored entirely soon after the exposure, but the nerve became far more sensitive to MMW: CAP suppression due to the next exposures became increasingly steep and finally took only 10–15 min. This sensitized state persisted for at least 16 h. In addition to this "slow" response, switching the field on increased CAP amplitude instantly by 5–7%, and switching it off caused the opposite reaction. These effects were found in "winter" frogs, but weakened and finally disappeared in spring.

A different effect in the isolated frog nerve was described by Chernyakov and coauthors [1989]. The exposures lasted for 2-3 h, either with a regular frequency change by 1 GHz every 8–9 min or with a random frequency change every 1-4 min (53–78 GHz band, 0.1-0.2 mW/cm^2). The latter regimen induced an abrupt CAP "rearrangement" in 11 of 12 exposed preparations: the position, magnitude, and polarity of CAP peaks (the initial CAP was polyphasic) drastically changed in an unforeseeable manner. The other exposure regimen altered the amplitude and duration of late CAP components in 30-40 min. The authors supposed that MMW increased CAP conduction velocity in fast nerve fibers and decreased it in slow fibers.

Neither of these effects on CAP conduction was observed by Pakhomov et al. [1997a]. Irradiation for 10–60 min, either at various constant frequencies or with a stepwise frequency change did not alter CAP at 0.2–1 mW/cm^2. At 2.0–2.8 mW/cm^2, it produced minor changes, which were independent from the frequency and matched the effect of heating. At the same time, a different MMW effect was revealed using a high-rate nerve stimulation test. MMW attenuated the stimulation-induced CAP decrease in a frequency-dependent manner. The effect reached maximum at 41.34 GHz [Pakhomov, 1997b], and at this frequency the magnitude of changes was the same (20–25%) at 0.02, 0.1, and 2.6 mW/cm^2 [Pakhomov et al., 1997c]. A 100 MHz deviation from 41.34 GHz (to 41.24 or 41.44 GHz) reduced the effect about twofold, and a 200 MHz deviation eliminated it. The field distribution over the preparation at these frequencies was virtually the same, so different MMW absorption or heating patterns could not account for the frequency specificity

of the effect. Interestingly, the most effective frequency in these experiments happened to be the same as the resonance frequency in the cell genome studies of Belyaev et al. [1993a].

Low-intensity MMW radiation effectively changed membrane functions in striated muscle and cardiac pacemaker cells [Chernyakov et al., 1989]. Exposure at 0.1-0.15 mW/cm^2 for 90 s or less (frequencies between 54 and 78 GHz) decelerated the natural loss of transmembrane potential in myocytes, or even increased it by 5–20 mV. Exposure reduced the overshoot voltage, action potential amplitude, and conduction velocity. This effect was observed in 80% of exposures, with no clear dependence on the radiation frequency. MMW influence on pacemaker activity was analyzed in 990 experiments with 80 tissue strip preparations from the frog heart sinoatrial area. In most cases, irradiation immediately decreased the interspike interval, often in less than 2 s. The maximal effect was reached within 30 s. The changes linearly increased with the incident power increase in the range from 20–30 to 500 μW/cm^2. The frequency dependence of the effect was individual, with at least four maximums in the studied range. Maximal preparation heating after a 2 s exposure at 1 mW/cm^2 was calculated as 0.005 °C. With a physiologic response latency of less than 2 s, this response could not be thermal. Exposure to infrared light (4 to 6 μm wavelength) often evoked the same effects as MMW, but the threshold intensity was hundreds of times greater.

In other experiments described in the same paper, low-intensity MMW synchronized firing of urinary bladder mechanoreceptors, suppressed and altered the T-peak on electrocardiography of in situ exposed myocardium, enhanced respiration, altered membrane calcium binding, and reduced the contractility of cardiomyocytes. Summarizing their results, the authors stated that the dependence of bioeffects upon radiation frequency is not monotonic. Peaks of this dependence are individual and are not fixed at particular frequencies, and they become smoother with increased complexity of physiologic control mechanisms involved.

Other In Vitro Effects

Bulgakova et al. [1996] studied how MMW exposure of *Staphylococcus aureus* affects its sensitivity to antibiotics with different mechanisms of action. Irradiations lasted from 1.5 to 60 min (54 or 42.195 GHz, or 66-78 GHz band with 1 GHz steps, 10 mW/cm^2). MMW heating did not exceed 1.5 °C. Over 1000 experiments with 14 antibiotics were completed. A difference in the growth of exposed cells compared with control cells was most often observed with polypeptide antibiotics, which affect the cell membrane (gramicidin group), but not with inhibitors of cell wall synthesis (penicillin group), of DNA-dependent RNA synthesis (actinomycin D), of the RNA polymerase and RNA synthesis (heliomycin), or protein biosynthesis inhibitors (neomycin, tetracycline, etc.). Irradiation either increased or decreased the antibiotic sensitivity, and the probability of these opposite effects depended on the antibiotic concentration. MMW could induce sensitivity to subbactericidal antibiotic concentrations, which normally would not affect the cell growth. Within studied limits, the effect showed no clear dependence on the radiation intensity or frequency. The data suggested that some membrane processes might be a target for the MMW effect. The authors also noted that MMW treatment can reveal (or even induce) the heterogeneity of the sensitivity of a cell population to certain antibiotics.

Rebrova [1992] reviewed various MMW effects on cell metabolism, synthesis of enzymes, and other processes in unicellular organisms, e.g., frequency-dependent enhancement and suppression of colicin synthesis in *E. coli,* stimulation of synthesis of fibrinolytic enzymes in *Bacillus firmus,* increasing of the contents of peptides, DNA, and RNA in *B. mucilaginous,* and suppression of tolerance to antibiotics in *S. aureus.* The maximal magnitude of MMW-induced changes ranged from 20 to 90%, depending on the wavelength and the initial condition of the strain. In contrast to bacteria, reproduction rate and biosynthetic properties of fungi *Aspergillus sp., Endomyces fibuliger,* and *Dacthilyum dendraides* changed only after repeated exposures (10 times). Certain MMW frequencies increased alpha amylase activity in *A. orizae* by 67% and suppressed glucoamylase by 30%; others had the opposite effect. In yeast species, MMW accelerated maltose fermentation by 73%, whereas synthesis of diacetil and aldehydes decreased by 20%. New biosynthetic culture properties introduced by exposure persisted in at least 100 (*S. carlsbergensis*) and 300 (*S. cerevisiae*) cell generations. The selective stimulation of production of some enzymes and suppression of others is promising for biotechnology.

An unusual "double-resonance" effect of MMW was described by Gapeev et al. [1994]. Spontaneous locomotor activity of the protozoan *Paramecium caudatum* was not affected by irradiation unless both the radiation frequency and modulation were tuned to "resonance" values. These values were 42.25 GHz and 0.0956 Hz, respectively (0.5 duty ratio). At these parameters, the threshold field intensity was about 0.02 mW/cm^2. The effect reached maximum (about 20%) at 0.1 mW/cm^2, and remained at this level at intensities up to 50 mW/cm^2, despite increasing heat production (0.1–0.2 °C at 5 mW/cm^2). CW irradiation

or modulation rates of 16, 8, 1, 0.5, 0.25, or 0.05 Hz produced no effect, regardless of the field intensity or heating. At the resonance modulation frequency, a shift of the carrying frequency to 42.0 or 42.5 GHz eliminated the reaction. No effects were observed with heating of samples by other means, e.g., infrared light modulated at 0.0956 Hz. Locomotor activity changes similar to the MMW effect could be evoked by increasing the level of intracellular calcium, pointing to a possible mechanism of the MMW action. However, reasons for the "double-resonance" dependence of this MMW effect remain unclear.

More reported MMW effects in various in vitro systems are summarized in Table 1.

ANIMAL AND HUMAN STUDIES

MMW Effects on Peripheral Receptors

Abundant evidence for MMW effects in specimens directly exposed in vitro neither explains nor predicts possible effects at the organism level. It is clearly understood that MMW penetration into biological tissues is rather shallow, and any primary response must occur in skin or subcutaneous structures, or at the eye surface. This primary response would then mediate all subsequent reactions by means of neural and/or humoral pathways. The nature of the primary response and consequent events has been a subject of intense speculation [Golant, 1989; Mikhno and Novikov, 1992; Rodshtadt, 1993], but there is little experimental proof. As a matter of fact, the link between cellular and organismal effects is missing and remains the least understood area in the MMW field. However, several studies have suggested that peripheral receptors and afferent nerve signaling could be involved in the whole organism's response to a local MMW exposure.

Akoev et al. [1992] studied the response of electroreceptor Lorencini capsules in anesthetized rays. Spontaneous firing in the afferent nerve fiber from the capsule could be either enhanced or inhibited by MMW irradiation (33–55 GHz, CW). The most sensitive receptors increased their firing rate at intensities of 1–4 mW/cm^2, which produced less than 0.1 °C temperature rise. Intensities of 10 mW/cm^2 and higher could evoke a delayed inhibition of firing, so the response became biphasic. The authors emphasized that what they observed was not merely a bioeffect of MMW, but was indeed a specific response of the receptor.

Chernyakov and coauthors [1989] were able to induce heart rate changes in anesthetized frogs by MMW irradiation of remote skin areas. The latency of the changes was about 1 min. Complete denervation of the heart did not prevent the reaction, but decreased its probability. The data suggested a reflex mechanism of the MMW action, maybe involving certain peripheral receptors.

These data are in agreement with later findings by Potekhina et al. [1992]. Certain frequencies from the 53–78 GHz band (CW) effectively changed the natural heart rate variability in anesthetized rats. The radiation was applied to the upper thoracic vertebrae for 20 min at 10 mW/cm^2 or less. The frequencies of 55 and 73 GHz caused pronounced arrhythmia: the variation coefficient of the R-R interval increased four to five times. Exposure at 61 or 75 GHz had no effect, and other tested frequencies caused intermediate changes. Skin and whole-body temperature of the animals remained unchanged. Similar frequency dependence was observed in additional experiments with 3-h exposures; however, about 25% of experiments were interrupted because of sudden animal death that occurred after 2.5 h of exposure at 51, 61, and 73 GHz. A possible role for receptor structures and neural pathways in the development of the MMW-induced arrhythmia was discussed.

Sazonov et al. [1995] compared alterations of spontaneous afferent firing in the bladder nerve in frogs when the bladder was exposed to infrared radiation and to MMW (42.19 ± 0.15 GHz, 10 mW/cm^2). The infrared intensity was adjusted to produce the same heating as MMW. In control experiments, the firing rate was stable for at least 1–1.5 h, but MMW increased it instantly from 30.9 to 32 spikes/s ($P < .05$) and to 48.3 spikes/s ($P < .01$) by the end of a 20-min exposure. Immediately after cessation of irradiation, the rate fell to 35.8 spikes/s, which was still significantly higher ($P < .05$) than before the treatment. Infrared irradiation did not cause statistically significant changes. This difference was interpreted as a proof of a specific (nonthermal) MMW effect, which might in principle take place in skin receptors as well.

In contrast, infrared light and MMW at equivalent intensities produced similar effects on the firing rate of crayfish stretch receptor [Khramov et al., 1991]. Changes were proportional to the average incident power, regardless of modulation or radiation frequency, and were regarded as merely thermal.

The possibility of modifying the peripheral receptor function by low-intensity MMW has been demonstrated directly by Enin and coauthors [1992]. An electrodynamic mechanostimulator was used to apply mechanical stimuli (50-ms duration, 1 to 2 mm amplitude) to individual skin mechanoreceptors on the sole of the hind limb of anesthetized rats. Responses to the stimuli were recorded from afferent fibers in the isolated and cut peripheral end of the tibial nerve. The sole was exposed to 55, 61, or 73 GHz radiation at

TABLE 1. Other In Vitro Effects of Millimeter Wave Radiation

Citation	End points/findings	Exposure conditions	Details
1	2	3	4
Berzhanskaya et al., 1995	Suppression of bioluminescence of *Photobacterium leiognathi*	36.2 to 55.9 GHz 1.3 to 48.0 $\mu W/cm^2$ MMW heating <0.1 °C	The effect reached maximum within 10 min, with a gradual recovery after the cessation of exposure, and could be repeated many times in the same cell culture. The maximal effect (16–18% decrease) was caused by the lower frequencies. At 36.2 GHz, 1.3 and 13 $\mu W/cm^2$ intensities produced virtually the same effect.
Mudrick et al., 1995	Changes in the intensity of $BaSO_4$-induced flash of chemoluminescence in the presence of luminol in human leukocytes	42.19, 46.84, or 53.53 GHz 1 mW/cm^2 30 min	The effect depended on the frequency, and the dependence was individual for blood samples from each particular donor. The maximal observed effect was a twofold flash enhancement ($P < 0.01$) at 42.19 GHz.
Gapeev et al., 1996	Inhibition of the luminol-dependent chemoluminescence of neutrophils activated by opsonized zymosan	41.8 to 42.05 GHz 0.15–0.25 mW/cm^2	In the near zone of the irradiator, the effect depended on the radiation frequency in a quasiresonance manner, whereas in the far field it was independent of the frequency.
Logani and Ziskin, 1996	No MMW effect on lipid peroxidation in phosphatidylcholine liposomes	53.6, 61.2, or 78.2 GHz 10, 1, and 500 mW/cm^2, respectively, 30 or 60 min	MMW did not increase the level of lipid peroxidation under any of the experimental conditions (in liposomes loaded or not loaded with melanin, or in the presence or absence of iron (III) adenosine diphosphate).
Roshchupkin et al., 1994, 1996	MMW changed aggregation of thymocytes with erythrocytes in a dose- and frequency-dependent manner	46.12 or 46.19 GHz either: (1) at 0.35 mW/cm^2, 0 to 120 min, or: (2) 0.05 to 0.5 mW/cm^2, 90 min	(1) The threshold was 60 min for both frequencies, increasing the number of aggregates to 115–140% of the parallel control. The effect of 46.12 GHz did not change when the exposure duration was further increased to 90 or 120 min, whereas the effect of 46.19 GHz fell to 80–90%. (2) The threshold was 0.25–0.35 mW/cm^2. The effect of 46.19 GHz stayed at 110–120% at 0.35 and 0.5 mW/cm^2, whereas the effect of 46.12 GHz grew linearly to 170% at 0.5 mW/cm^2.
Shub et al., 1995	Changes in transmisxsivity of R-plasmids in various strains of *E. coli* and *S. aureus*	6.0- to 6.7-mm band, <1 mW/cm^2 60 min	A number of biologically active frequencies affected the transmissivity of R-plasmids, either decreasing or increasing plasmid- and chromosome-dependent resistivity to antibiotics. Irradiation for 60 min had a bacteriostatic effect, which was not related to the activity of the recA-dependent DNA repair. Cells carrying Iα, I*j*, N, and E plasmids appeared to be protected from the antibacterial effect of MMW.
Kazbekov and Vyacheslavov, 1987	No nonthermal effects in prototrophic, thymidine-deficient, and tryptophan-requiring strains of *E. coli* and *B. subtilis*	6- to 7.8-mm wavelengths 5 mW/cm^2	MMW either had no effect on studied parameters (thymine and thymidine uptake, potassium leakage, hydrogen ion release, uptake of DNA, etc.), or produced the same changes as conventional heating by 1–2 °C.

0.75, 2.90, or 7.81 mW/cm^2, respectively. Exposure lasted for 35 min and caused no changes in the skin temperature (0.01 °C accuracy). MMW did not excite mechanoreceptors, but markedly altered the threshold and latency of their response to mechanic stimuli. In some receptors, the threshold gradually increased, up to 180% of the initial value. In others, the threshold initially decreased by 8–12%, recovered within 10 min, and increased to 160% by the 25th min of irradiation. After that, the receptors became completely inactive and no longer responded to mechanical stimuli. The receptor response latency under exposure could fall to 70% or rise to 120%; the changes could also be biphasic. The MMW-induced changes were maximum at 73 GHz, intermediate at 55 GHz, and minimum at 61 GHz, despite that the incident power at 61 GHz was 4-fold greater than at 55 GHz. The authors supposed that sensations reported by patients under MMW therapy (vibration, warmth, numbness, etc.) may result from functional disturbances and blockage of receptors.

The ability of humans to detect weak MMW has also been repeatedly established under double-blind conditions [Lebedeva, 1993, 1995; Kotrovskaia, 1994]. An examinee was situated in an isolated room and had no contact with the experimenter. The outer surface of the hand was exposed 20 times, for 1 min each. Exposures were separated by 1 min intervals and randomized with sham exposures. The start and end of each irradiation and placebo were accompanied by sound clicks. The examinee had to push a button when he felt the field. Neither examinee nor researcher knew the sequence of exposures and sham exposures; correct and incorrect reactions were recorded automatically. Field perception was characterized by the reaction reliability (the percent of MMW exposures detected) and the false alarms level (the percentage of sham exposures erroneously detected). An examinee was regarded as capable of detecting the field if the reaction reliability consistently and statistically significantly exceeded the false alarm level. With different frequencies (37.7, 42.25, 53.57 GHz), intensities (from 5 to 15 mW/cm^2) and bandwidths, the radiation was detected by 30 to 80% of examinees. Interestingly, 37.7 GHz radiation at 15 mW/cm^2 was detected by far fewer people than 42.25 GHz at 5 mW/cm^2. The reaction latency was usually between 40 and 50 s. It was speculated that MMW perception could involve some types of mechanoreceptors and nociceptors.

Teratogenic effects of MMW

The only study of MMW teratogenic effects was performed in *Drosophila* flies by Belyaev et al. [1990]. Embryos of the blastula and gastrula stages (2.5–3 h after laying) and pupas at the stage of imago tissue formation were exposed in a waveguide at 46.35, 46.42, or 46.50 GHz, for 4–4.5 h at 0.1 mW/cm^2, followed by incubation at 25 °C. Irradiation at 46.35 GHz, but not at 46.42 or 46.50 GHz, caused marked effects. Exposure of pupas increased incidence of morphologic abnormalities 2-4.5 times ($P < .05$), but did not influence imago survival. Exposure of embryos decreased survival by about 30% ($P < .05$) and enhanced morphologic abnormalities, but this effect was rather variable. Supposedly, MMW disturbed DNA-protein interactions that determine the realization of the ontogenetic program.

High-Power MMW Effects

Over the past several years, physiologic effects of high levels of MMW radiation have been intensively studied by Frei et al. [1995], Frei and Ryan [1997], and Ryan et al. [1996, 1997]. In ketamine anesthetized rats, exposure to 35 GHz, 75 mW/cm^2 radiation (12–13 W/kg whole body SAR) increased the subcutaneous temperature by 0.25 °C/min and the colonic temperature by 0.08 °C/min. Concurrently with the hyperthermia, mean arterial blood pressure first increased slightly and then fell until the point of death. Hypotension was accompanied by vasodilation in the mesenteric vascular bed, similar to what occurs in heat stroke induced by environmental heating. However, the onset of vasodilation and hypotension occurred at much lower colonic temperatures (< 37.5 °C vs. > 41.5 °C). The lethal effect became irreversible when the mean arterial pressure fell to 75 mm Hg, even if the exposure was discontinued. Most intriguing, pathologic examination of the skin of lethally exposed animals revealed no significant thermal damage or full-thickness burn, and cardiovascular responses did not mimic those observed in traditional burn models. Searching for physiologic mechanisms mediating the hypotensive response, the authors established that nitric oxide, platelet-activating factor, and histamine did not contribute to it. Exposure of rats at 94 GHz at a similar SAR produced a comparable pattern of heating and cardiovascular responses.

Experimental MMW Therapy: Animal Studies

Except those cited above, virtually all animal studies on MMW effects have been related to various issues of MMW therapy, such as stress relief, wound healing, tissue regeneration, and protection from ionizing radiations. Paradoxically, these animal studies are still less numerous and comprehensive than reports on MMW therapy in humans. Many applications of the MMW therapy seem to have never been adequately tested in animal experiments. For example, we counted 38 publications (including meeting abstracts) on vari-

ous clinical aspects of the MMW therapy for peptic ulcers, but could find just one animal study on this subject. It seems that in some cases animal studies did not precede the clinical use of MMW (as one would expect), but were carried out to create experimental justification for already reported clinical data.

Tissue repair and regeneration. Among possible therapeutic applications of MMW, the more plausible and understandable are treatments of surface lesions (wounds, burns, ulcers), which are directly reachable by the radiation. Indeed, this application has gained sound experimental support from several independent works. Other studies have demonstrated that repair of deep tissues (bone and nerve) could also be stimulated by MMW, suggesting that such effects are mediated by activation of the organism's own recovery mechanisms.

Zemskov et al. [1988] studied MMW effects on healing of skin wounds in rabbits. The animals were randomly assigned to four groups; wounds in groups 1 and 2 were kept aseptic, and those in groups 3 and 4 were infected with a pathogenic *Staphylococcus.* The wound surface in groups 1 and 3 was treated with 37 or 46 GHz CW MMW at 1 mW/cm^2 for 30 min, twice a day for 5 days. A horn irradiator was placed 2–5 mm over the wound surface. Rabbits in groups 2 and 4 served as untreated control animals. MMW decreased swelling of wound edges, hyperemia, and infiltration, and rapidly reduced the wound area in the first 24 h; it also stimulated phagocytosis and reduced bacterial contamination. Complete healing of aseptic wounds in the exposed group took 2.9 days less than in the control group. Infected wounds cleaned up and filled with granulation tissue on days 14–16 in the exposed group and only on days 21–23 in the respective control animals.

A similar protocol was used in a double-blind replicative study by Korpan et al. [1994]. Rabbits with 4 × 6 cm cutaneous wounds were randomly divided into four groups of 18 animals each. The wounds of two groups were rendered septic by inoculating them with 10^9 *Staphylococcus* cells. The wound was exposed for 30 min a day (37 GHz CW, 1 mW/cm^2), for 5 days in one aseptic group and for 7 days in a septic one. The horn aperture was 10 cm from the wound surface. The other two groups were sham-irradiated and served as aseptic and septic control groups. In irradiated animals, wound edge swelling and hyperemia subsided faster, and granulation tissue filled the wound earlier. On day 7, for example, the surface area of septic wounds decreased by 19% in the control group, and by 44% in the irradiated group. The mean daily decrease in wound surface area of the irradiated animals was significantly greater than in the control animals: 7.9% vs. 3.2% in the aseptic groups, and 6.3% vs. 2.7% in the septic groups ($P < .05$). Exposures stimulated phagocytic activity of neutrophils and decreased the blood level of circulating immune complexes. Thus, MMW irradiation enhanced both septic and aseptic wound healing and stimulated immune function.

Detlavs et al. [1993, 1994, 1995, 1996] have extensively studied MMW effects on the composition of granulation fibrous tissue (GFT) during early stages of wound healing. Their experiments were performed in rats with incised full-thickness dermal wounds. The injured area was exposed for 30 min daily for 5 days at 10 mW/cm^2 (53.53 or 42.19 GHz CW, or 42.19 GHz with 200 MHz frequency modulation. Control animals underwent the same manipulations, but were sham exposed. GFT samples from the wound were taken for analysis on the 7th day. CW irradiation significantly decreased the GFT contents of glycoproteins (hexosamines, hexoses, and sialic acids), indicating a suppression of the inflammatory process. In contrast, modulated MMW enhanced the inflammation and increased the production of glycoproteins. CW exposure decreased the GFT content of hydroxyproline, which is a marker for total collagen, to 79–85% of the control ($P < .01$), whereas the modulated regimen increased it to 126-133% ($P < .001$). CW radiation at 53.53 GHz usually was more effective than at 42.19 GHz. Both the anti- and proinflammatory effects of MMW could be useful in clinical practice. CW exposure can be recommended for early stages of the wound healing when control of the inflammatory reaction is desirable. Modulated radiation can be used to promote ultimate recovery in slow-healing wounds or in cases of healing deceleration in the late stages of tissue repair.

Ragimov et al. [1991] used MMW to stimulate the repair of an experimentally produced bone defects in rabbits. A hole 6 mm in diameter was drilled in the lower jaw bone, and the wound was sutured. The first exposure for 30 or 60 min was performed the next day, and six more exposures were done over the next 2 weeks. The shaven nape was exposed from a horn (2-cm^2 aperture) placed 3–4 mm from the skin (5.6-mm wavelength, 25 mW output power). Control animals were handled similarly. Five animals from each group were killed every week for morphologic and roentgenographic analysis of bone repair. One week after the operation, the extent of reparative osteogenesis was the same in all the groups. Later on, the regeneration was faster in exposed animals, particularly in the group with 60-min exposures. By the end of the observation period (28 days), the appearance of the traumatic defect in the control group was nearly the same as it was in exposed animals on day 21.

Hence, irradiation shortened the bone repair time by approximately 1 week.

Kolosova and coauthors [1996a] established that MMW treatment could promote regeneration of a damaged peripheral nerve. The sciatic nerve in 40 rats was transected in the thigh region and sutured. Skin over the injury area was irradiated every third day for 10 min with 4-mW/cm^2, 54-GHz radiation for 7 or 20 days; control rats were sham irradiated. Exposures did not change the skin temperature (0.1 °C accuracy). Upon the completion of the treatment course, the nerve was isolated, and the extent of regeneration was assessed electrophysiologically. After the 7-day course, the regeneration distance was 4.8 mm vs. 3.0 mm in the control animals ($P > .05$). After the 20-day course, the effect became statistically significant: the regeneration distance was 18.4 ± 0.4 mm versus 14.0 ± 1.4 mm ($P < .01$). The nerve conduction velocity also significantly increased, whereas the amplitude and duration of the action potential were not affected.

In a continuation study [Kolosova et al., 1996b], the same irradiations were performed for 2 weeks after the injury, and the nerve was isolated for examination in 5 months. Indices of regeneration were the compound action potential amplitude and conduction velocity at different distances (5 to 19 mm) distal from the suture. Both parameters were higher in the exposed animals. For example, 19 mm from the suture, the velocity was 20.4 ± 0.9 m/s vs. 15.5 ± 0.9 m/s in control animals ($P < .05$), and the amplitude was 313 ± 34 μV versus 156 ± 15 μV ($P < .001$). Hence, exposures not only stimulated the growth of nerve fibers, but facilitated their functional maturation as well.

Tumor growth and development. Experiments by Smirnov et al. [1991] were designed to evaluate the possible use of MMW for the treatment of cancer. VMR tumor cells with a high metastasizing activity were inoculated into the tibial muscle of A/SNL line mice at 5 × 10^5 cells/animal. Exposure for 5 days, 1 h daily (12.5 mW/cm^2, 7.09- to 7.12-mm wavelength, 50 Hz modulation), increased the average life span by 17% compared with sham control cells. The number of visible metastases decreased by more than 50% in lungs, liver, kidney, and adrenal glands, but not in lymph nodes. The authors noted variability of the MMW effect, and in one series exposure even intensified metastasizing.

Chernov et al. [1989] attempted to suppress malignant growth by extremely high peak power nanosecond MMW pulses. Rats were exposed immediately after inoculation with 10, 25, or 50 (× 10^3) Walker tumor cells and received two more exposures during the next 2 days. Each exposure consisted of 43 pulses delivered at 40-s intervals. Two regimens were tested: 8-mm wavelength at 4–5 MW output power, yielding 20 kV/cm E-field level at the skin surface, and 5 mm, 8–10 MW, 30 kV/cm, respectively. The first of these regimens retarded tumor growth 1.5 times and increased the life span by 17–25 days after the inoculations with 10 and 25 (× 10^3) cells the other regimen was less effective. The antitumor effect was presumably mediated by stimulation of immune system, namely the so-called skin-associated lymphoid tissue. Preliminary studies with exposure before tumor inoculation showed that MMW retarded the tumor growth nearly twofold.

Because of concern about possible adverse effects of MMW use in cancer patients, Brill' and Panina [1994] studied the transplantability and growth of a benign tumor (mammary fibroadenoma) in rats. Two tumor pieces were implanted to the right and left sides through a cut in the middle of the abdomen. In 20 of 49 operated animals, tissues in the cut were exposed to MMW (42.0–43.3 GHz band) for 15 min before the implantation, the other animals served as control. In 3 weeks, 39 of 58 tumors (67.3%) resolved in the control group, but only 11 of 40 (27.5%) resolved in the exposed animals ($P < .001$). The percentages of stable and growing unresolved tumors in both the groups were the same. Hence, a single MMW exposure of the implantation area increased tumor transplantability, although did not affect its proliferation.

Stress alleviation and prevention effects. Temur'iants and Chuyan [1992] demonstrated that MMW can alleviate immobilization-induced stress in rats. The authors established that this MMW effect differed in specimens with different characteristic levels of exploratory activity, as evaluated by an open-field testing. In further studies, the open-field testing was always done before stressing and MMW exposures, to divide the population into appropriate groups.

One of these studies [Temur'iants et al., 1993] was performed on 350 animals divided by low (LA), medium (MA), and high (HA) activity. Each activity level was subdivided into five groups; group 1 was cage control, and groups 2–5 were housed for 9 days in individual boxes restricting their motion. Animals in groups 3–5 received daily 30-min MMW exposures of the occipital area, left hip, or right hip, respectively (5.6-mm wavelength, 10 mW/cm^2). Stress severity was quantified by indices of the "nonspecific resistivity" of the organism, which included the lipids and peroxidase contents in neutrophils, and succinate and alpha-2-glycerophosphate dehydrogenases activities in lymphocytes. A typical stress reaction developed in unexposed MA rats: by days 6–9, the contents of lipids and

peroxidase decreased by 21–24%, and the activity of dehydrogenases fell by 36–46%. Occipital or right hip MMW irradiation prevented the stress reaction in MA rats, whereas the left hip exposure was not effective. The immobilization stress was the most pronounced in unexposed HA animals; MMW exposures of the left hip or occipital area prevented stress, whereas exposures of the right hip had little effect. In LA animals, the stress reaction was relatively weak, and all the types of MMW treatment alleviated it.

The next study used 640 albino rats, all with a medium level of locomotor activity [Temur'iants et al., 1994]. The same indices as above were compared in four groups: cage control, hypokinesia without exposures, exposures without hypokinesia, and both. The occipital area was exposed for 30 min/day, 9 days at either 5.6- or 7.1-mm wavelength. Exposures without hypokinesia strongly activated succinate dehydrogenase (up to twofold, $P < .05$). Irradiation at 5.6 mm (but not at 7.1 mm) increased the activities of acid and alkaline phosphatases and glycerophosphate dehydrogenase by 20–30%. Both wavelengths prevented or reversed stress-induced changes, 5.6 mm was more effective. Further experiments with 5.6-mm radiation established that exposures for 15 min/day were less effective than for 30 min/day, and, paradoxically, increasing the exposure duration to 60 min/day eliminated its antistress effect.

A similar exposure technique was independently used by Arzumanov et al. [1994]. The occipital area was exposed at 5.6 mm simultaneously with immobilization of the rat's head for 60 min/day for 10 days. This stressing suppressed feeding and sexual behavior. It also increased the motor activity in a swimming test to the same degree in exposed and unexposed groups. The authors hypothesized that the immobilization stress was too severe and might mask MMW effects, so in the next series rats were immobilized and exposed for only 30 min/day for 9 days. The stress effect was assessed by the electric shock threshold, free-access water consumption, and Vogel's choice test (consumption of water when each attempt to drink is accompanied by an electric shock). Immobilization without exposure decreased threefold the number of attempts to drink in Vogel's test; but, when immobilization was combined with MMW exposures, this index remained the same as in cage control animals. The shock threshold and free-access water consumption were not changed by MMW.

It is interesting to note some parallelism in the above two studies. Using the same exposure procedures, but different protocols and end points, both research groups established that there is an anti-stress effect of a 30-min irradiation, but there is no such effect if the exposure duration is 60 min. The decreased efficacy of a more prolonged MMW irradiation has been observed in some other clinical and experimental studies as well, but this unusual time dependence has not yet been discussed or explained.

Combined MMW and ionizing radiation exposure. Gubkina et al. [1996] researched whether low-intensity MMW can alleviate the effect of X-rays in rats. The abdominal area was shaved and exposed to MMW in a frequency-sweep regimen (38 to 53 GHz) at 7 mW/cm^2 for 23 days, 30 min/day. Control animals not treated by MMW underwent all the same manipulations, including shaving. Exposures to 150 keV X-rays were performed daily during the last 8 days of the MMW course up to a total dose of 24 roentgen. Blood serum and brain tissue samples were collected the next day after the end of exposures. MMW alone did not alter the serum glucose level (6.24 ± 0.79 mM versus 6.53 ± 0.80 mM in control animals); X-ray exposure increased it to 10.37 ± 0.75 mM ($P < .05$), but combining X-rays with MMW prevented this rise (6.81 ± 0.37 mM). MMW decreased the content of the soluble form of the acidic glial fibrillar protein (s-AGFP) 1.5–2 times ($P < .05$) in all analyzed structures of the brain (cerebellum, midbrain, and medulla oblongata) and did not change the content of its fibrillar form (f-AGFP). X-rays decreased the levels of both forms of the protein two to three times. After combined treatment with MMW and X-rays, both s- and f-AGFP levels did not differ from control animals and were significantly ($P < .05$ and $P < .01$) higher than after X-rays only. The authors concluded that MMW alleviated the effect of X-rays at both cellular and organism levels.

Two other studies are of interest, although they are only brief reports that do not contain essential experimental details. Kuzmanova and Ivanov [1995] studied changes in the surface electrical charge of erythrocytes after MMW and γ-ray exposures in rats. The shin of the right hind limb was exposed to 5.6-mm radiation for 10 days, 20 min/day at 1.1 mW/cm^2, followed with a 6 Gy whole-body dose of ^{137}Co γ-rays. The surface charge of erythrocytes was assessed from their electrophoretic mobility (EPM) 3, 7, 14, 21, and 30 days after the exposures. The MMW treatment alone had practically no effect, whereas γ-rays alone decreased EPM for the whole period of observation. When γ-irradiation was preceded by MMW, the EPM remained the same as in control animals. The authors concluded that MMW stabilized the membrane structure and increased its resistivity to γ-radiation.

Tsutsaeva et al. [1995] examined MMW-induced survival changes in mice after a lethal dose of X-rays. Irradiation with pulse-modulated MMW at 1 μW/cm^2 continued for 80 or 24 h before X-ray exposure or was

simultaneous with the X-ray exposure. All tested X-ray doses (7, 7.5, and 8 Gy) were 100% lethal with an average life span of 6–8 days; the first fatalities occurred on days 4–6. MMW treatment for 80 h before 7 Gy of X-rays delayed the first deaths until day 14; 50% of the population died within 30 days, and 100% of the animals died by day 96. The MMW treatment for 24 h appeared even more effective: first deaths occurred on day 8, 50% of the animals died within 30 days, but no more fatalities were observed through day 96. Microwave irradiation simultaneously with the X-rays (7 Gy) increased the survival and life span of mice approximately fivefold. The protective effect of 24-h MMW pretreatment decreased with increasing X-ray dose to 7.5 Gy and became insubstantial at 8 Gy.

MMW Therapy: Clinical Studies

The first clinical trials of MMW therapy began in 1977, and today the method has been officially approved by the Russian Ministry of Health and is used widely. As mentioned in the Introduction section, by 1995 over 3 million people have been treated at more than a thousand specialized centers as well as at regular hospitals [Lebedeva and Betskii, 1995].

General issues of the MMW therapy. MMW therapy involves repetitive local exposures of certain body areas with low-intensity MMW. The area(s) to be exposed, the radiation wavelength, and daily duration of procedures are determined by the physician based on the disease and the condition of the particular patient. The radiation intensity is usually regarded as a less important variable. For most diseases, the daily exposure varies from 15 to 60 min, and the therapy lasts for 8–15 days.

Publications on the clinical use of MMW number in the hundreds. Many of them have claimed that MMW monotherapy is more effective (sometimes, far more effective) than conventional methods, such as drug therapy, for a variety of diseases and disorders. In some cases, MMW has helped the patients who had already tried all other known therapies without success and were considered incurable. At the same time, MMW seldom caused any adverse effects or allergies. MMW in combination with drug therapy facilitated favorable effects and/or reduced adverse side effects of drugs. Some authors reported that MMW might be highly effective or not effective at all, contingent on the patient's condition, individual sensitivity to MMW, and parameters of irradiation. A few authors reported that MMW therapy was always less effective than conventional techniques, and we found only one clinical study saying that MMW therapy was not effective at all [Serebriakova and Dovganiuk, 1989].

Diseases reported to be successfully treated with MMW belong to rather diversified groups. The most common applications of MMW are for gastric and duodenal ulcers (about 25% of studies); cardiovascular diseases, including angina pectoris, hypertension, ischemic heart disease, infarction (about 25%); respiratory sicknesses, including tuberculosis, sarcoidosis, bronchitis, asthma (about 15%); and skin diseases, including wounds, trophic ulcers, burns, atopic dermatitis (about 10%). These percentages are approximate, because we could not cover all clinical studies published and because many authors reported treatment of several diseases in one paper (so the sum would be over 100%). Isolated studies claimed successful MMW treatment for asthenia, neuralgia, diabetes mellitus, osteochondrosis, acute viral hepatitis, glomerulonephritis, alcoholism, etc. MMW were also used for alleviation of toxic effects of chemotherapy in cancer patients and in preventive medicine and health resort therapy.

In most cases, physicians use specialized MMW generators, which are produced commercially by the medical equipment industry. These generators operate at average radiation intensities of 10 mW/cm^2 or less in CW or frequency-modulated regimens at certain fixed frequencies or within a wide frequency band. Three models have been reported used more often than all others together: "Yav'-1-7,1" (7.1-mm wavelength, 42.19 GHz) (36%), "Yav'-1-5,6" (5.6 mm, 53.53 GHz) (31%), and "Electronica-KVCh" (4.9 mm, 59–63 GHz band) (10%). Different generators were often used within a single study to compare their therapeutic efficacy; and more often than not, the efficacy was different, depending on the disease and patients' condition. Some authors used in vitro tests to determine which wavelength is more suitable for a particular patient before the onset of the therapy [Novikova et al., 1995]. However, we have been unable to identify references to the original studies that had shown why the frequencies of 42.19, 53.53, and 59–63 GHz (and not others) should be used for therapy.

In about 30% of clinical studies, the radiation is applied to standard acupuncture points or so-called biologically active points. This procedure is often combined with finding the individual "resonance" frequency based on MMW-evoked "sensations" of the patient (a method called "microwave resonance therapy"). In our opinion, this procedure should be regarded as a variety of acupuncture techniques along with electropuncture, acupressure, etc. Assuming the therapeutic efficacy of these techniques, it is no surprise that MMW can be effective as well: irradiation at about 10 mW/cm^2 can also stimulate acupuncture points by subtle heating or thermal "micromassage." Clinical effects of the "MMW-puncture" are nonspe-

cific, meaning that they are similar to those of traditional puncture-based techniques. These effects are determined by the selection of acupuncture points, intensity and duration of their stimulation, rather than by using MMW or other means for the stimulation. Therefore, studies using the MMW-puncture seem to be of greater interest for the acupuncture practice than for the bioelectromagnetic science; such studies will be left beyond the scope of the present review.

Other areas of MMW exposure include sternum and xiphoid process, skin projection of the diseased organ, large joints, and the surface of wounds and ulcers. Once again, we could not identify the studies that originally provided the rationale and experimental proof for the useful nature of MMW exposure of these particular body areas. Except for the surface lesions, the radiation is unable to penetrate to diseased organs. This fact is understood and discussed by many physicians, but no proven explanation of the MMW therapy has been given yet.

Many clinical studies do not conform to conventional quality criteria (double-blind protocol, placebo treatment, adequate statistics, etc.). However, still others do conform and a lot of matching results have been provided by independent groups of investigators. Some clinical data on the MMW efficacy are quite impressive, and a few examples are given below (see a specialized review by Rojavin and Ziskin [1998] for additional detail).

Examples of MMW therapy. Korpan and Saradeth [1995] performed a double-blind controlled trial of MMW therapy for postoperative septic wounds. The study group consisted of 141 patients, 31–83 yr old, with purulent wounds after an abdominal surgery. The wounds were infected mostly with *S. aureus* and *Bacteroides fragilis*. MMW therapy with 1 mW/cm^2, 37 GHz CW radiation was used in 71 patients. Wound surface and adjacent soft tissue were exposed for 30 min/day for 7 days. The remaining 70 patients received placebo therapy from a similar but defective MMW generator (neither patients nor physicians knew it was defective). Radical surgical cleaning of the wounds was performed regularly in both groups. The MMW-treated patients showed 1.8 times more rapid wound clearance (5.6 ± 0.6 vs. 10.2 ± 0.5 days in control subjects), 1.7 times earlier onset of wound granulation (4.9 ± 0.2 vs. 8.7 ± 0.4 days), and 1.8 times earlier onset of epithelization (7.0 ± 0.4 vs. 12.8 ± 0.6 days). The average daily decrease of wound surface area in the treated patients was twice that of the control subjects (7.1% vs. 3.2%). The authors concluded that low intensity MMW seems to be an effective postoperative wound treatment.

Poslavsky et al. [1989] used MMW as a monotherapy in 317 patients with duodenal and gastric ulcers. The ulcer diameter ranged from 0.3 to 3.5 cm, and the disease duration was from several months to more than 10 years. The epigastric area was exposed at 10 mW/cm^2, 5.6-mm wavelength for 30 min daily, excluding weekends, until complete ulcer cicatrization. A comparable control group of 50 patients received conventional drug therapy. The ulcers cicatrized in 95.3% of MMW-treated patients, with mean healing duration of 19.8 ± 0.45 days. The respective control group values were substantially worse, namely 78% and 33.6 ± 1.12 days. The ulcer relapse rate was significantly lower after the MMW therapy.

Megdiatov et al. [1995] evaluated the efficacy of MMW therapy (42.2 GHz, 10 mW/cm^2) in 52 patients with neuralgia. The radiation was applied to areas where branches of the affected trigeminal nerve approach the skin (10 exposures or sham exposures, 15 min each, concurrently with medicinal therapy). Evident clinical improvement (decrease of the incidence and severity of pain attacks) was achieved in 19 of 27 patients treated with MMW, and only in 4 of 25 patients receiving placebo exposures.

Liusov et al. [1995] studied MMW therapy effects in 100 patients with unstable angina pectoris (this is an intermediate condition between stable angina pectoris and infarction, and is characterized by a high risk of myocardial necrosis). The patients were divided into four groups. Group 1 was treated by MMW only (10 exposures of the right shoulder joint for 30 min/day, 7.1 mm); these patients ceased taking any vasodilators and antianginal medicines. In group 2, the same MMW therapy was combined with drugs (beta-adrenergic antagonists, calcium blockers, organic nitrates, etc.). Group 3 received the same drug therapy and placebo exposures, and group 4 received the drug therapy only. The therapy in groups 1 and 2 substantially decreased the rate and severity of angina attacks, making it possible to reduce the amount of nitroglycerin taken. It also decreased blood levels of malonic dialdehyde and dienic conjugates, normalized T-helper and T-suppresser ratios, reduced the diameter of venules, and increased the diameter of arterioles. No significant improvement of the lipid peroxidation system, immune status, or microcirculation was achieved in groups 3 and 4.

Karlov and coauthors [1991] used MMW in a combined therapy for cerebral circulatory disorders. The 79 patients in the study were mostly 50-80 yr old and suffered from hypertensive disease and/or atherosclerosis; 61 patients were hospitalized for acute ischemic cerebral infarction, 13 for a transient disorder of the cerebral circulation, and 5 for circulatory encephalopathy. Patients were divided into two comparable groups. Both groups received the same drug therapy

(hypotensive, anticoagulant, cardiotonic, and other remedies), whereas the first one was also treated with MMW (10 days, 30 min/day, 4.9-mm wavelength). Patients of the second group were sham-exposed under a double-blind protocol. A favorable therapeutic effect was reported in 70% of the patients in group 1 and in 40% in group 2. MMW procedures helped decrease blood pressure, normalize the blood glucose level, and eliminate serum fibrinogen B.

The efficacy of the MMW therapy is often illustrated by individual clinical cases. Naumcheva [1994] described the history of a 54-yr-old male patient, who had two myocardial infarctions within a 2-yr interval. He experienced severe attacks of angina both on exertion and at rest and took up to 80 nitroglycerin tablets a day (0.4 mg). Repeated courses of in- and outpatient treatment with beta-adrenoblockers, nitrates, plasmapheresis, etc. had little effect. Finally, he was hospitalized in a grave condition with a third infarction. Conventional methods were ineffective, so MMW therapy was ordered on day 10 after admission (7.1-mm wavelength, for 30 min/day to the left border of sternum). Cardialgia decreased after two exposures and nighttime pain attacks ceased after seven procedures. The nitroglycerin intake was decreased to 1–2 tablets/day after 12 exposures. After the MMW course, the patient did not have angina attacks for 3–4 days, was able to walk up to 5 km a day, and was discharged in a satisfactory condition. Another man, age 62, was admitted to hospital with a severe macrofocal infarction, collapse, extrasystolia, and acute insufficiency and aneurysm of the left ventricle. Three days of intensive treatment still left the patient in this critical condition. Even the first MMW irradiation of sternum (5.6-mm wavelength, three 10-min exposures with 5-min intervals) had a striking effect: it arrested angina attacks and normalized sleep, and indices of hemodynamics stabilized within 5 days of the MMW therapy. The patient was discharged in a satisfactory condition and later underwent two additional MMW courses as a preventive measure.

Side effects of MMW therapy. As a rule, MMW therapy is well tolerated by patients, and this is regarded as one of its advantages over a drug therapy. Although most investigators reported no negative reactions to MMW, others observed them in up to 26% of patients [Golovacheva, 1995]. The possibility of induction of adverse health effects by a local, low-intensity MMW irradiation is of potential significance for setting health and safety standards and requires special attention.

Kuz'menko [1989] summarized experience with MMW use in 200 patients with cerebrovascular diseases, such as cerebral circulation insufficiency, discirculatory encephalopathy, and cerebral insult consequences. Irradiation of the sinocarotid zone at various frequencies between 58 and 62 GHz, 0.3–1 mW/cm^2, was performed for 20 min/day or less, for 4 to 10 days. MMW therapy facilitated recovery in 56–77% of patients with different pathologies. However, it also caused adverse side effects, including elevation of the blood pressure (nine cases), induction of a diencephalic crisis or paroxysm during irradiation (seven cases), angina attacks (three cases), fever (five cases), and enhancement of menstrual bleeding (six cases). In hypertension patients, MMW usually decreased blood pressure by 10–15 mm Hg, but occasionally increased it by 20-30 mm Hg. The author concluded that MMW can be successfully used in cerebrovascular therapy, but possible complications must be taken into account.

Afanas'eva and Golovacheva [1997] used MMW therapy in 124 patients with stage II essential hypertension (5.6- or 7.1-mm wavelength, CW, 10 mW/cm^2, 10 procedures for 30 min each). Unfavorable autonomous nervous system reactions (whole-body shivering, sweating, heart pains along with skin paling or reddening) were observed in 18 patients (15.5%). In two cases, these reactions developed into hypertensive crises, which had to be arrested by drug injections. In 33 patients (26.6%), MMW-induced fluctuations of the arterial blood pressure and enhanced headaches. A temporary improvement after four to five exposures was followed by an increase in both systolic (by 25 ± 7.0 mm Hg) and diastolic (by 10.0 ± 2.0 mm Hg) blood pressure, which required medicinal correction. General adverse reactions after the entire MMW course (six patients; 4.8%) included sleeplessness or sleep with distressful dreams, weakness, emotional instability, and irritability. These manifestations were not profound and disappeared without further treatment. The authors emphasized that these adverse reactions were not encountered in patients who received placebo exposures.

Gun'ko and Kozshina [1993] tried MMW therapy in 528 patients with various diseases (ulcerative disease, ischemic heart disease, essential hypertension, bronchitis, pneumonia, and others). Exposures at 5.6- or 7.1-mm wavelength lasted from 15 to 60 min/day, from 5 to 18 days. Three patients being treated for rheumatic polyarthritis, psoriasis, and duodenal ulcer (without any concurrent drug therapy) developed urticaria (hives) on the fifth to seventh day of exposures. An itchy rash appeared first in the abdominal and thoracic areas, and soon spread everywhere. Nevertheless, the treatment of the main disease in all these cases was successful. The rash disappeared 2-10 days after the completion of the MMW therapy but reappeared during

the repeated MMW courses. The authors called for more studies of MMW effects on the immune system.

DISCUSSION

In this review, we have found that recent research in the MMW area covers a variety of subjects. Profound MMW effects were established at all biological levels, from cell-free systems through cells, organs, and tissues, to animal and human organisms. Although trying to avoid a general discussion of thermal versus nonthermal mechanisms in this review, we nonetheless must note that many of the reported effects were principally different from those caused by heating, and their dose and frequency dependencies often suggested nonthermal mechanisms. Regardless of the primary mechanism, the possibility of significant bioeffects of a short-term MMW irradiation at intensities at or below current safety standards deserves consideration and further study.

The major question about FSU publications in the MMW area is their reliability. A number of studies cited here were performed at the highest scientific level. Other studies, perhaps the majority of those cited, were flawed, but may still bear valuable information and should not be discarded without proper analysis. For example, free-field dosimetry in the MMW band is a serious technical problem. To our knowledge, no commercially available probes are rated for near-field measurements in the MMW band even in the U.S. Therefore, it is not surprising that many investigators, particularly clinicians, have had to rely on manufacturer-specified field intensities, such as 10 mW/cm^2 for "Yav'-1" therapeutic generator. One may doubt that the field actually was 5, 10, or 15 mW/cm^2, but under no circumstances could it exceed a spatial average of, say, 50 mW/cm^2, which is beyond the generator's capabilities. Thus, whereas the precise exposure parameters may not be known, a range of possible exposure intensities may be estimated. With an understanding of this fact, the experimental data may still be important and usable.

Another widespread shortcoming of clinical studies occurs when MMW therapy is compared with drug therapy, without using a sham-exposed control group. MMW therapy was often reported to be more effective than drugs. This result could be a placebo effect; but if so, one would have to conclude that placebo was more effective than modern drug therapy. This possibility could certainly be true for certain patients and certain disorders, but does not seem feasible for large populations and a wide scale of diseases.

A further source of skepticism about findings made by FSU scientists is that they have not been replicated in the West. Replication is much needed indeed, but it can hardly be anticipated without adequate attempts. To our knowledge, only three laboratories throughout the U.S. (less than 10 scientists total) are currently doing any research on MMW bioeffects, which is by no means sufficient to match the amount and variety of the FSU research. Besides, many cited studies are very recent (1995–1997), so replication has yet to be expected.

With all the diversity of the MMW research and differences in studied subjects and end points, some particulars seem to be common for various situations and MMW effects. Considering these particulars may be critical for replication studies:

(1) Individuals or groups in a population, which would usually be regarded as uniform, may react to MMW in rather different or even opposite ways. For example, Temur'iants et al. [1993, 1994] divided the vivarium population of rats by their open-field activity before performing exposures. Not only the animal's reactions to MMW, but also their reactions to immobilization stress, were very different in animals with low, medium, and high activity levels. Pooling all the data together, as well as neglecting the intrinsic differences in the population, would have inevitably masked MMW effects.

(2) There seem to exist unknown and uncontrolled factors that determine the MMW sensitivity of a specimen or a population. Irradiation could increase antibiotic resistivity in one experiment and decrease it in the next one [Bulgakova et al., 1996]. It increased the beating rate in one isolated heart and decreased it in the other [Chernyakov et al., 1989]. MMW therapy usually decreased blood pressure, but eventually increased it greatly [Kuz'menko, 1989]. As long as these changes exceeded the "noise" level and were not produced by a sham exposure, they can be regarded as MMW effects. Again, pooling all data together, regardless of the direction of changes, could easily mask an MMW effect.

(3) Even robust MMW effects may be well reproducible for a limited time and then disappear. The effects of complete suppression or 200–400% enhancement of chloride transmembrane current in alga cells were far beyond any spontaneous variations and could hardly be confused with any artifact [Kataev et al., 1993]. However, both effects weakened and disappeared by the end of winter without any apparent reason. MMW effects on isolated frog nerve also disappeared in spring [Burachas and Mascoliunas, 1989], suggesting that MMW sensitivity may be somehow related to the base level of metabolism.

4. MMW effects could often be revealed only in subjects that are experiencing some deviation from the

"normal" state. MMW caused little or no reactions in intact animals, but significantly alleviated effects of immobilization, ionizing radiation, etc. Many clinical studies claim that MMW therapy is effective only when one or another kind of pathology is present, whereas in a healthy organism MMW will not produce any reactions. However, this thesis has not been adequately proven.

5. Increased sensitivity and even hypersensitivity of individual specimens to MMW may be real. Depending on the exposure characteristics, especially wavelength, a low-intensity MMW radiation was perceived by 30 to 80% of healthy examinees [Lebedeva, 1993, 1995]. Some clinical studies reported MMW hypersensitivity, which was or was not limited to a certain wavelength [Golovacheva, 1995]. In a study by Afanas'eva and Golovacheva [1997], adverse health reactions to MMW appeared only in women (100%) who had a labile course of angina pectoris (100%), most of whom were in the menopausal period (66.7%). The authors suggested that this category of people is particularly sensitive to MMW.

It is important to note that, even with the variety of bioeffects reported, no studies have provided evidence that a low-intensity MMW radiation represents a health hazard for human beings. Actually, none of the reviewed studies with low-intensity MMW even pursued the evaluation of health risks, although in view of numerous bioeffects and growing usage of MMW technologies this research objective seems very reasonable. Such MMW effects as alterations of cell growth rate and UV light sensitivity, biochemical and antibiotic resistivity changes in pathogenic bacteria, as well as many others, are of potential significance for safety standards. MMW therapy in many cases uses field intensities comparable to or lower than those allowed by current safety standards, but even local and short-term exposures were reported to produce marked effects. It should also be realized that biological effects of a prolonged or chronic MMW exposure of the whole body or a large body area have never been investigated. Safety limits for these types of exposure are based solely on predictions of energy deposition and MMW heating, but in view of recent studies this approach is not necessarily adequate.

The significance of MMW bioeffects for human health, considering both safety limitations and possible clinical applications, should be neither over- nor underestimated. It is, however, an intriguing and potentially important area that needs to be further explored. If this present review draws attention to the MMW research and stimulates new studies, we will consider its goal accomplished.

ACKNOWLEDGMENTS

The work was supported in part by the U.S. Army Medical Research and Materiel Command and the U.S. Air Force Armstrong Laboratory under U.S. Army contract DAMD17-94-C-4069 awarded to McKesson BioServices. The views expressed in this article are those of the authors and should not be construed as reflecting the official policy or position of the Department of the Army, Department of the Air Force, Department of Defense, or the United States Government.

REFERENCES

Afanas'eva TN, Golovacheva TV (1997): Side effects of the EHF-therapy for essential hypertension. Zvenigorod, Russia: 11th Russian Symposium "Millimeter Waves in Medicine and Biology," April, 1997 (Digest of papers). Moscow: IRE RAN, pp 26–28 (in Russian).

Akoev GN, Avelev VD, Semen'kov PG (1992): Perception of the low-level millimeter-range electromagnetic radiation by electroreceptors of the ray. Dokl Akad Nauk 322:791–794 (in Russian).

Alekseev SI, Ziskin MC (1995): Millimeter microwave effect on ion transport across lipid bilayer membranes. Bioelectromagnetics 16:124–131.

Alekseev SI, Ziskin MC, Kochetkova NV, Bolshakov MA (1997): Millimeter waves thermally alter the firing rate of the Lymnaea pacemaker neuron. Bioelectromagnetics 18:89–98.

Arzumanov YuL, Kolotygina RF, Khonichava NM, Tverytskaya IN, Abakumova AA (1994): Animal study of the stress-protective effect of electromagnetic radiation of the extremely-high-frequency range. Millimetrovie Volni v Biologii i Meditcine 3:5–10 (in Russian).

Belyaev IYa (1992): Some biophysical aspects of the genetic effect of low-intensity millimeter waves. Bioelectrochem Bioenerg 27:11–18.

Belyakov EV, Kichaev VA, Poslavskii MV, Starshinina VA, Soboleva ES (1989): Use of blood radiophysical parameters in the extremely high-frequency range for diagnostic purposes. In Devyatkov ND (ed): "Millimeter Waves in Medicine and Biology." Moscow: Radioelectronica, pp 83–88 (in Russian).

Belyaev IYa, Okladnova OV, Izmailov DM, Sheglov VS, Obukhova LK (1990): Differential sensitivity of developmental stages to low-level electromagnetic radiation of extremely ultrahigh frequency. Dokl Akad Nauk SSSR [Ser B Geol Chim Biol] 12:68–70 (in Russian).

Belyaev IYa, Alipov YD, Polunin VA, Shcheglov VS (1993a): Evidence for dependence of resonant frequency of millimeter wave interaction with *Escherichia coli* K12 cells on haploid genome length. Electromagnetobiology 12:39–49.

Belyaev IYa, Shcheglov VS, Alipov YeD, Radko SP (1993b): Regularities of separate and combined effects of circularly polarized millimeter waves on *E. coli* cells at different phases of culture growth. Bioelectrochem Bioenerg 31:49–63.

Belyaev IYa, Alipov YD, Shcheglov VS, Polunin VA, Aizenberg OA (1994): Cooperative response of *Escherichia coli* to the resonance effect of millimeter waves at super low intensity. Electromagnetobiology 13:53–66.

Belyaev IY, Shcheglov VS, Alipov YD, Polunin VA (1996): Resonance effect of millimeter waves in the power range from 10^{-19} to 3×10^{-3} W/cm^2 on *Escherichia coli* cells at different concentrations. Bioelectromagnetics 17:312–321.

Belyaev IYa, Shcheglov VS, Alipov YD, Ushakov VL (1997): Reply to comments of Osepchuk and Petersen. Bioelectromagnetics 18:529–530.

Berezhinskii LI, Gridina NIa, Dovbeshko GI, Lisitsa MP, Litvinov GS (1993): Visualization of the effects of millimeter radiation on blood plasma. Biofizika 38:378–384 (in Russian).

Berzhanskaya LYu, Berzhanskii VN, Beloplotova OYu (1995): Effect of electromagnetic fields on the activity of bioluminescence in bacteria. Biofizika 40:974–977 (in Russian).

Betzky OV (1992): Use of low-intensity electromagnetic millimeter waves in medicine. Millimetrovie Volni v Biologii i Meditcine 1:5–12 (in Russian).

Brill' GE, Panina NP (1994): Effect of millimeter waves on transplantability and growth of tumors. Fizicheskaia Meditzina 4:25 (in Russian).

Brill' GE, Apina OR, Belyanina CI, Panina NP (1993): Effect of low-level extremely high-frequency radiation on the genetic activity of polytene chromosomes of Chironomus plumosus. Fizicheskaia Meditzina 3:69–71 (in Russian).

Brovkovich VM, Kurilo NB, Barishpol'ts VL (1991): Action of millimeter-range electromagnetic radiation on the Ca pump of sarcoplasmic reticulum. Radiobiologiia 31:268–271 (in Russian).

Bulgakova VG, Grushina VA, Orlova TI, Petrykina ZM, Polin AN, Noks PP, Kononenko AA, Rubin AB (1996): Effect of millimeter-band radiation of nonthermal intensity on the sensitivity of *Staphylococcus* to various antibiotics. Biofizika 41:1289–1293 (in Russian).

Burachas G, Mascoliunas R (1989): Suppression of nerve action potential under the effect of millimeter waves. In Devyatkov ND (ed): "Millimeter Waves in Medicine and Biology." Moscow: Radioelectronica, pp 168–175 (in Russian).

Chernov ZS, Faikin VV, Bernashevskii GA (1989): Experimental study of the effect of nanosecond EHF pulses on malignancies. In: Devyatkov ND (ed): "Millimeter Waves in Medicine and Biology." Moscow: Radioelectronica, pp 121–127 (in Russian).

Chernyakov GM, Korochkin VL, Babenko AP, Bigdai EV (1989): Reactions of biological systems of various complexity to the action of low-level EHF radiation. In Devyatkov ND (ed): "Millimeter Waves in Medicine and Biology." Moscow: Radioelectronica, pp 141–167 (in Russian).

Dardalhon M, Averbeck D, Berteaud AJ (1979): Determination of a thermal equivalent of millimeter microwaves in living cells. J Microw Power 14:307–312.

Dardalhon M, Averbeck D, Berteaud AJ (1981): Studies on possible genetic effects of microwaves in prokaryotic and eukaryotic cells. Radiat Environ Biophys 20:37–51.

Dardanoni L, Torregrossa MV, Zanforlin L (1985): Millimeter wave effects on Candida albicans cells. J Bioelectr 4:171–176.

Detlav IE, Shkirmante BK, Dombrovska LE, Pahegle IV, Slutskii LI (1993): Biochemical parameters of developing granulo-fibrous tissue after the effect of an extremely high-frequency electromagnetic field. Millimetrovic Volni v Biologii i Meditcine 2:43–50 (in Russian).

Detlavs I, Dombrovska L, Klavinsh I, Turauska A, Shkirmante BB, Slutskii L (1994): Experimental study of the effect of electromagnetic fields in the early stage of wound healing. Bioelectrochem Bioenerg 35:13–17.

Detlavs I, Dombrovska L, Shkirmante B, Turauska A, Slutskii L (1995): Some biological effects of mm-wave electromagnetic fields on the granulation-fibrous tissue in a healing wound. Moscow, Russia: 10th Russian Symposium "Millimeter Waves in Medicine and Biology," April, 1995 (Digest of papers). Moscow: IRE RAN, pp 117–119 (in Russian).

Detlavs I, Dombrovska L, Turauska A, Shkirmante B, Slutskii L (1996): Experimental study of the effects of radiofrequency electromagnetic fields on animals with soft tissue wounds. Sci Total Environ 180:35–42.

Enin LD, Akoev GN, Potekhina IL, Oleiner VD (1992): Effect of extremely high-frequency electromagnetic radiation on the function of skin sensory endings. Patol Fiziol Eksp Ter 5-6:23–25 (in Russian).

Fesenko EE, Gluvstein AYa (1995): Changes in the state of water induced by radiofrequency electromagnetic fields. FEBS Lett 367:53–55.

Fesenko EE, Geletyuk VI, Kazachenko VN, Chemeris NK (1995): Preliminary microwave irradiation of water solutions changes their channel modifying activity. FEBS Lett 366:49–52.

Frei MR, Ryan KL (1997): Circulatory failure resulting from sustained millimeter wave irradiation. Brooks AFB, TX: Infrared Lasers and Millimeter Waves Workshop "The Links Between Microwaves and Laser Optics," January, 1997.

Frei MR, Ryan KL, Berger RE, Jauchem JR (1995): Sustained 35-GHz radiofrequency irradiation induces circulatory failure. Shock 4:289–293.

Fröhlich H (1980): The biological effects of microwaves and related questions. Adv Electronics Electron Phys 53:85–152.

Fröhlich H (ed) (1988): Biological coherence and response to external stimuli. Berlin: Springer-Verlag, p 265.

Furia L, Hill DW, Gandhi OP (1986): Effect of millimeter-wave irradiation on growth of Saccharomyces cerevisiae. IEEE Trans Biomed Eng 33:993–999.

Gandhi OP (1983): Some basic properties of biological tissues for potential biomedical applications of millimeter-waves. J Microw Power 18:295–304.

Gapeev AB, Chemeris NK, Fesenko EE, Khramov RN (1994): Resonance effects of a low-intensity modulated EHF field. Alteration of the locomotor activity of the protozoa Paramecium caudatum. Biofizika 39:74–82 (in Russian).

Gapeev AB, Safronova VG, Chemeris NK, Fesenko EE (1996): Modification of the activity of murine peritoneal neutrophils by exposure to millimeter waves at close and far distances from the emitter. Biofizika 41:205–219 (in Russian).

Geletyuk VI, Kazachenko VN, Chemeris NK, Fesenko EE (1995): Dual effects of microwaves on single Ca^{2+}-activated K^+ channels in cultured kidney cells Vero. FEBS Lett 359:85–88.

Golant MB (1989): Resonance effect of coherent millimeter-band electromagnetic waves on living organisms. Biofizika 34:1004–1014 (in Russian).

Golant MB, Kuznetsov AP, Boszhanova TP (1994): Mechanisms of synchronization of the yeast cell culture by the action of EHF radiation. Biofizika 39:490–495 (in Russian).

Golovacheva TV (1995): EHF therapy in complex treatment of cardiovascular diseases. Moscow, Russia: 10th Russian Symposium "Millimeter Waves in Medicine and Biology," April, 1995 (Digest of papers). Moscow: IRE RAN, pp 29–31 (in Russian).

Gos P, Eicher B, Kohli J, Heyer W-D (1997): Extremely high frequency electromagnetic fields at low power density do not affect the division of exponential phase Saccharomyces cerevisiae cells. Bioelectromagnetics 18:142–155.

Grundler W (1983): Biological effects of RF and MW energy at molecular and cellular level. In Rindi A, Grandolfo M, Michaelson SM (eds): "Biological Effects and Dosimetry of Nonionizing Radiation. Radiofrequency and Microwave Energies." New York: Plenum Press, pp 299–318.

Grundler W, Kaiser F (1992): Experimental evidence for coherent excitations correlated with growth. Nanobiology 1:163–176.

Grundler W, Keilman F, Froehlich H (1977): Resonant growth rate response of yeast cells irradiated by weak microwaves. Phys Lett 62A:463–466.

Grundler W, Keilman F, Putterlik V, Strube D (1982): Resonant-like

dependence of yeast growth rate on microwave frequencies. Br J Cancer 45:206–208.

Grundler W, Jentzsch U, Keilmann F, Putterlik V (1988): Resonant cellular effects of low intensity microwave. In Fröhlich H (ed): "Biological Coherence and Response to External Stimuli." Berlin: Springer-Verlag, pp 65–85.

Gubkina EA, Kushnir AE, Bereziuk SK, Potapov VA, Lepekhin EA (1996): Effects of low-intensity electromagnetic radiation of extremely high-frequency on the animal organism in combination with whole-body low-dose X-ray irradiation. Radiats Biol Radioecol 36:722–726 (in Russian).

Gun'ko VT, Kozshina NM (1993): Some complications of extremely high-frequency therapy. Millimetrovie Volni v Biologii i Meditcine 2:102–104 (in Russian).

Kaiser F (1995): Coherent oscillations - their role in the interaction of weak ELM-fields with cellular systems. Neural Network World 5:751–762.

Karlov VA, Rodshtat IV, Kalashnikov IuD, Kitaeva LV, Khokhlov IuK (1991): Experience with using extremely high frequency radiotherapy of the millimeter wave range in cerebrovascular disorders. Sov Med 3:20–21 (in Russian).

Kataev AA, Alexandrov AA, Tikhonova LL, Berestovsky GN (1993): Frequency-dependent effects of the electromagnetic millimeter waves on the ion currents in the cell membrane of Nitellopsis: Nonthermal action. Biofizika 38:446–462 (in Russian).

Kazbekov EN, Vyacheslavov LG (1987): Effects of microwave irradiation on some membrane-related processes in bacteria. Gen Physiol Biophys 6:57–64.

Khizhnyak EP, Ziskin MC (1996): Temperature oscillations in liquid media caused by continuous (nonmodulated) millimeter wavelength electromagnetic irradiation. Bioelectromagnetics 17:223–229.

Khramov RN, Sosunov EA, Koltun SV, Ilyasova EN, Lednev VV (1991): Millimeter-wave effects on electric activity of crayfish stretch receptors. Bioelectromagnetics 12:203–214.

Kolosova LI, Akoev GN, Avelev VD, Riabchikova OV, Babu KS (1996a): Effect of low-intensity millimeter wave electromagnetic radiation on regeneration of the sciatic nerve in rats. Bioelectromagnetics 17:44–47.

Kolosova LI, Akoev GN, Riabchikova OV, Avelev VD (1996b): The effect of low-intensity millimeter-range electromagnetic radiation on the functional recovery of the damaged sciatic nerve in rat. Fiziol Zh Im I M Sechenova 82:85–90 (in Russian).

Korpan NN, Saradeth T (1995): Clinical effects of continuous microwave for postoperative septic wound treatment: A double-blind controlled trial. Am J Surg 170:271–276.

Korpan NN, Resch K-L, Kokoschinegg P (1994): Continuous microwave enhances the healing process of septic and aseptic wounds in rabbits. J Surg Res 57:667–671.

Kotrovskaia TI (1994): Sensory reactions evoked by weak electromagnetic stimuli in humans. Millimetrovie Volni v Biologii i Meditcine 3:32–38 (in Russian).

Kremer F, Santo L, Poglitsh A, Koschnitzke C, Behrens H, Genzel L (1988): The influence of low intensity millimetre waves on biological systems. In Fröhlich H (ed): "Biological Coherence and Response to External Stimuli." Berlin: Springer-Verlag, pp 86–101.

Kudryashova VA, Zavizion VA, Khurgin YuV (1995): Effects of stabilization and destruction of water structure by amino acids. Moscow, Russia: 10th Russian Symposium "Millimeter Waves in Medicine and Biology," April, 1995 (Digest of papers). Moscow: IRE RAN, pp 213-215 (in Russian).

Kuzmanova M, Ivanov St (1995): Effect of millimeter waves and gamma-radiation on the surface electrical charge of erythrocyte membranes. In: "Millimeter Waves in Medicine and Biology," Digest of papers of the 10th Russian Symposium with International Participation, 24–26 April, Moscow, Russia, pp 111–112 (in Russian).

Kuz'menko VM (1989): Indications and contraindications to the use of microwave resonance therapy (MRT) in patients with cerebrovascular diseases. Kiev, Ukraine: First All-Union Symposium with International Participation "Fundamental and Applied Aspects of the Use of Millimeter Electromagnetic Radiation in Medicine," May, 1989, pp 272–273 (in Russian).

Lebedeva NN (1993): Sensor and subsensor reactions of a healthy man to peripheral effects of low-intensity millimeter waves. Millimetrovie Volni v Biologii i Meditcine 2:5–23 (in Russian).

Lebedeva NN (1995): Neurophysiological mechanisms of biological effects of peripheral action of low-intensity nonionizing electromagnetic fields in humans. Moscow, Russia: 10th Russian Symposium "Millimeter Waves in Medicine and Biology," April, 1995 (Digest of papers). Moscow: IRE RAN, pp 138–140 (in Russian).

Lebedeva NN, Betskii OV (1995): Application of low intensity millimeter waves in medicine. Boston, MA: 17th Annual Meeting of the Bioelectromagnetics Society, June, 1995, p 14.

Levina MZ, Veselago IA, Belaya TI, Gapochka LD, Mantrova GM, Yakovleva MN (1989): Influence of low-intensity VHF irradiation on growth and development of protozoa cultures. In Deyatkov ND (ed): "Millimeter Waves in Medicine and Biology." Moscow: Radioelectronica, pp 189–195 (in Russian).

Litvinov GS, Gridina NYa, Dovbeshko GI, Berezhinsky LI, Lisitsa MP (1994): Millimeter wave effect on blood plasma solution. Electromagnetobiology 13:167–174.

Liusov VA, Volov NA, Lebedeva AYu, Kudinova MA, Schelkunova IG, Fedulayev YuN (1995): Some mechanisms of the effect of millimeter-range radiation on pathogenesis of unstable angina pectoris. Moscow, Russia: 10th Russian Symposium "Millimeter Waves in Medicine and Biology," April, 1995 (Digest of papers). Moscow: IRE RAN, pp 26–27 (in Russian).

Logani MK, Ziskin MC (1996): Continuous millimeter-wave radiation has no effect on lipid peroxidation in liposomes. Radiat Res 145:231–235.

Megdiatov RS, Vasilenko AM, Arkhipov VV, Kislov VYa, Kolesov VV, Smirnov VF (1995): Use of a "Sharm" therapeutic-diagnostic system in complex therapy of trigeminal nerve neuralgia. Moscow, Russia: 10th Russian Symposium "Millimeter Waves in Medicine and Biology," April, 1995 (Digest of papers). Moscow: IRE RAN, pp 83–84 (in Russian).

Mikhno LE, Novikov SA (1992): The mechanism of the therapeutic action of millimeter electromagnetic waves and their importance in treating cardiovascular diseases (a review of the literature). Vrach Delo 10:14–18 (in Russian).

Mudrick DG, Golant MB, Izvol'skaia VE, Slutzkii EM, Oganezova RA (1995): Chemoluminescence of human blood leukocytes after exposure to a low-intensity extremely-high frequency electromagnetic field. Moscow, Russia: 10th Russian Symposium "Millimeter Waves in Medicine and Biology," April, 1995 (Digest of papers). Moscow: IRE RAN, pp 109–111 (in Russian).

Naumcheva NN (1994): Effect of millimeter waves on ischemic heart disease patients. Millimetrovie Volni v Biologii i Meditcine 3:62–67 (in Russian).

Novikova LN, Kaminskaia GO, Efimova LN (1995): Significance of the functional state of blood phagocytes in the choice of optimal regime of EHF therapy of patients with pulmonary tuberculosis. Probl Tuberk 6:17–20 (in Russian).

Osepchuk JM, Petersen, RC (1997a): Critical reviews of millimeter-wave athermal effect studies relative to microwave engineering principles. Brooks AFB, TX: Infrared Lasers and Millimeter

Waves Workshop "The Links Between Microwaves and Laser Optics," January, 1997.

Osepchuk JM, Petersen, RC (1997b): Comments on "Resonance Effect of Millimeter Waves in the Power Range from 10^{-19} to 3×10^{-3} W/cm2 on *Escherichia coli* Cells at Different Concentrations," Belyaev et al., Bioelectromagnetics, 17:312–321 (1996). Bioelectromagnetics 18:527–528.

Pakhomov AG, Prol HK, Mathur SP, Akyel Y, Campbell CBG (1997a): Search for frequency-specific effects of millimeter-wave radiation on isolated nerve function. Bioelectromagnetics 18:324–334.

Pakhomov AG, Prol HK, Mathur SP, Akyel Y, Campbell CBG (1997b): Frequency-specific effects of millimeter wavelength electromagnetic radiation in isolated nerve. Electromagnetobiology 16:43–57.

Pakhomov AG, Prol HK, Mathur SP, Akyel Y, Campbell CBG (1997c): Role of field intensity in the biological effectiveness of millimeter waves at a resonance frequency. Bioelectrochem Bioenerg 43:27–33.

Pakhomova ON, Pakhomov AG, Akyel Y (1997): Effect of millimeter waves on UV-induced recombination and mutagenesis in yeast. Bioelectrochem Bioenerg 43:227–232.

Poslavsky MV, Korochkin IM, Zdanovich OF (1989): Experience with application of millimeter-range radiation for treatment and prophylactics of stomach and duodenal ulcer. Vopr Kurortol Fizioter Lech Fiz Kult 4:31–36 (in Russian).

Postow E, Swicord ML (1986): Modulated fields and "window" effects. In Polk C, Postow E (eds): "Handbook of Biological Effects of Electromagnetic Fields." Boca Raton, FL: CRC Press, Inc. pp 425–460.

Potekhina IL, Akoyev GN, Yenin LD, Oleyner VD (1992): Effects of low-intensity electromagnetic radiation in the millimeter range on the cardio-vascular system of the white rat. Fiziol Zh 78:35–41 (in Russian).

Ragimov ChR, Ter-Asaturov GP, Golant MB, Rogov KA, Balakireva LZ (1991): Stimulation of reparative osteogenesis by electromagnetic oscillations in the millimeter range in traumatic defects of the lower jaw in experimental animals. Biull Eksp Biol Med 111:436–439 (in Russian).

Rebrova TB (1992): Effect of millimeter-range electromagnetic radiation on the vital activity of microorganisms. Millimetrovie Volni v Biologii i Meditcine 1:37–47 (in Russian).

Rodshtadt IV (1993): Physiological basis for some immune effects of millimeter-range radiation action on skin. Millimetrovie Volni v Biologii i Meditcine 2:24–35 (in Russian).

Rojavin MA, Ziskin MC (1995): Effect of millimeter waves on survival of UVC-exposed *Escherichia coli*. Bioelectromagnetics 16:188–196.

Rojavin MA, Ziskin MC (1998): Medical application of millimetre waves. Q J Med 91:57–66.

Roshchupkin DI, Kramarenko GG, Anosov AK, Golant MB (1994): Changes in the aggregation ability of rabbit thymocytes under the combined effect of UV-radiation and extremely high frequency radiation. Biofizika 39:1046–1050 (in Russian).

Roshchupkin DI, Kramarenko GG, Anosov AK (1996): Effect of extremely high frequency electromagnetic radiation and ultraviolet radiation on aggregation of thymocytes and erythrocytes. Biofizika 41:866–869 (in Russian).

Ryakovskaya ML, Shtemler VM (1983): Absorption of electromagnetic waves of millimeter range in biological preparations with a plane-layer structure. In: Devyatkov ND (ed): "Effect of Nonthermal Action of Millimeter Radiation on Biological Subjects." Moscow: USSR Academy of Sciences, pp 172–181 (in Russian).

Ryan KL, Frei MR, Berger RE, Jauchem JR (1996): Does nitric oxide mediate circulatory failure induced by 35-GHz microwave heating? Shock 6:71–76.

Ryan KL, Frei MR, Jauchem JR (1997): Circulatory failure induced by 35 GHz microwave heating: Effects of chronic nitric oxide synthesis inhibition. Shock 7:70–76.

Sazonov AYu, Zamuraev IN, Lukashin VG (1995): Effect of the extremely high frequency electromagnetic radiation on bush-like receptors of frog bladder. Fiziol Zh Im I M Sechenova 81:46–49 (in Russian).

Serebriakova SN, Dovganiuk AP (1989): The treatment of patient with peptic ulcer using millimeter-range waves. Vopr Kurortol Fizioter Lech Fiz Kult 4:37–38 (in Russian).

Shestopalova NG, Makarenko BI, Golovina LN, Timoshenko YuP, Baeva TI, Vinokurova LV, Miroshnichenko VS (1995): Modification of synchronizing effect of millimeter waves on first mitoses by different temperature regimens of germination. Moscow, Russia: 10th Russian Symposium "Millimeter Waves in Medicine and Biology," April, 1995 (Digest of papers) Moscow: IRE RAN, pp 236–237 (in Russian).

Shub GM, Luniova IO, Denisova SG, Ostrovskii NV (1995): Effects of millimeter waves on bacteria in in vitro and in vivo experiments. Moscow, Russia: 10th Russian Symposium "Millimeter Waves in Medicine and Biology," April, 1995 (Digest of papers). Moscow: IRE RAN, pp 96–97 (in Russian).

Smirnov AIu, Zinovev SV, Bogoliubov VM (1991): An experimental study of the action of weak-intensity superhigh-frequency electromagnetic radiation in the millimeter range on metastasis of malignant neoplasms. Vopr Kurortol Fizioter Lech Fiz Kult 4:23–27 (in Russian).

Tambiev AH, Kirikova NN (1992): Perspectives of the application of millimeter-range electromagnetic radiation in photobiotechnology. Millimetrovie Volni v Biologii i Meditcine 1:48–54 (in Russian).

Tambiev AKh, Kirikova NN, Lapshin OM, Betzkii OV, Novskova TA, Nechaev VM, Petrov IYu (1989): The combined effect of exposure to EMF of millimeter and centimeter wavelength ranges on productivity of microalgae. In Devyatkov ND (ed): "Millimeter Waves in Medicine and Biology." Moscow: Radioelectronica, pp 183–188 (in Russian).

Temur'iants NA, Chuyan EN (1992): Effect of nonthermal microwaves on hypokinetic stress development in rats with different individual features. Millimetrovie Volni v Biologii i Meditcine 1:22–32 (in Russian).

Temur'iants NA, Chuyan EN, Tumaniants EN, Tishna OO, Victorov NV (1993): Dependence of anti-stress effects of millimeter-range electromagnetic fields on localization of the exposed area in rats with different typological features. Millimetrovie Volni v Biologii i Meditcine 2:51–59 (in Russian).

Temur'iants NA, Chuyan EN, Khomiakova OV, Tishkina OO (1994): Dependence of the stress-protective effect of extremely-high-frequency electromagnetic radiation on parameters of irradiation. Millimetrovie Volni v Biologii i Meditcine 3:11–15 (in Russian).

Tsutsaeva AA, Makarenko BI, Beznosenko BI, Gomosov VI, Simonova NYa, Kovalenko LA, Shatilova LE, Tupchienko GS, Nikitash AV, Kudokotseva OV, Rozniak AI, Lisenko NA, Shurda GG (1995): Radioprotective effect of microwave action. Millimeter Waves in Medicine and Biology, Digest of papers of the 10th Russian Symposium with International Participation, 24-26 April, Moscow, Russia, pp 123–124 (in Russian).

Zavizion VA, Kudriashova VA, Khurgin YuI (1994): Effect of alpha-amino acids on the interaction of millimeter-wave radiation with water. Millimetrovie Volni v Biologii i Meditcine 3:46–52 (in Russian).

Zemskov VS, Korpan NN, Khokhlich IaI, Pavlenko VA, Nazarenko LS, Koval'chuk AI, Stefanishin IaI (1988): Effect of millimeter-band low intensity electromagnetic radiation on the course of wound healing. Klin Khir 1:31–33 (in Russian).

Abstract

IR-THERMOGRAPHY IN STUDIES OF MM-WAVE BIOEFFECTS

Eugene P. Khizhnyak and Marvin C. Ziskin
Richard J. Fox Center for Biomedical Physics
Temple University Medical School
Philadelphia, PA 19140

One of the main effects resulting from mm-waves and infrared (IR) radiation is heating due to absorption of radiant energy in biological structures. IR-thermography is ideal for measuring the rate of heating caused by 6-6000 GHz irradiation in biological tissue and phantoms, because the penetration depth of the 3-5 μm IR-radiation used in thermography is close to the penetration depths of mm-waves and 300-6000 GHz IR. At the same time, the difference in frequency is too great to produce interference between these two types of radiation. Remote temperature sensing, based on measurement of the IR emitted by an object eliminates artifacts that occur when thermo or field sensors are used.

Distribution of mm-wave energy absorption in biological tissue models and in mice and human skin was studied using IR-thermography. 0.1-0.2 mm thin-layer phantoms were used for characterizing the irradiation patterns produced by different types of horn antennas in the near field area in the 37-78 GHz frequency range. It was found that a nonuniform heating pattern can be caused due to geometric resonance and electrodynamic and thermodynamic skin heterogeneity. Depending on the frequency and coupling conditions, local SAR values in hot-spots can exceed the spatially averaged values by over 10 times. These results provide an explanation for a number of frequency-dependent effects of mm-waves. Due to high temperature gradients resulting from nonuniform field distributions and very localized absorption, mm-waves can produce thermal effects at an average incident power density which is much lower than centimeter and decimeter waves. Sweat pore activity which plays an important role in temperature and metabolic regulation was visualized using the IR-thermography method. Concentration of mm-wave absorption in sweat pores was observed together with changes in their opening and closing dynamics.

Many of our methods could also be used for studying biological effects of IR-radiation in the 300-6000 GHz frequency range. The available data shows that in the 300-6000 GHz frequency range the problem related to near field irradiation will diminish with increase of frequency. However, the problem of field concentration due to heterogeneity of biological structures remains very important and may become even more so when compared with mm-wavelengths.

Circulatory Failure Resulting from Sustained Millimeter Wave Irradiation

KATHY L. RYAN*, MELVIN R. FREI* AND JAMES R. JAUCHEM†

**Department of Biology, Trinity University, San Antonio, TX 78212; and,*

† Radiofrequency Radiation Division, U.S. Air Force Laboratory, Brooks AFB, TX 78235

Corresponding Author: Kathy L. Ryan, Ph.D.

Department of Biology

Trinity University

715 Stadium Drive

San Antonio, TX 78212

(210) 536-4825

FAX: (210) 736-7229

E-mail: ryan@rfr.brooks.af.mil

INTRODUCTION

The development of hardware systems capable of generating radiofrequency radiation (RFR) of millimeter wave (MMW) length, as well as the increased use of MMWs for military and civilian purposes, has recently spawned considerable interest in the possible bioeffects of animal exposure to these waves. Theoretical calculations suggest that MMW energy absorption in animals will occur in the skin; for example, the depth of penetration of 30-GHz RFR has been calculated to be 0.78 mm (Erwin and Hurt, 1981; Gandhi and Riazi, 1986), which is certainly within the limits of the cutaneous region. Over the past several years, we have characterized an animal model of circulatory failure induced by sustained, whole-body exposure to 35-GHz radiofrequency radiation. This paper summarizes results from this series of ongoing studies.

CARDIOVASCULAR RESPONSES TO 35-GHz RFR

In our model, ketamine-anesthetized rats are exposed in E orientation (left lateral exposure, long axis of body parallel to electric field and perpendicular to magnetic field) to 35-GHz RFR at an incident power density of 75 mW/cm^2. This power density results in a whole-body specific absorption rate (SAR) of 13.0 W/kg (Frei *et al.*, 1995). During irradiation, mean arterial blood pressure (MAP), mesenteric blood flow, heart rate (HR) and respiratory rate are continuously monitored, along with temperatures at five anatomical sites.

At the onset of irradiation, the subcutaneous temperature of the left abdomen (i.e., the irradiated site; T_{sl}) begins to increase and continues to increase steadily throughout the period of MMW exposure (Figure 1; from Frei *et al.*, 1995). When irradiation is continued until death, the

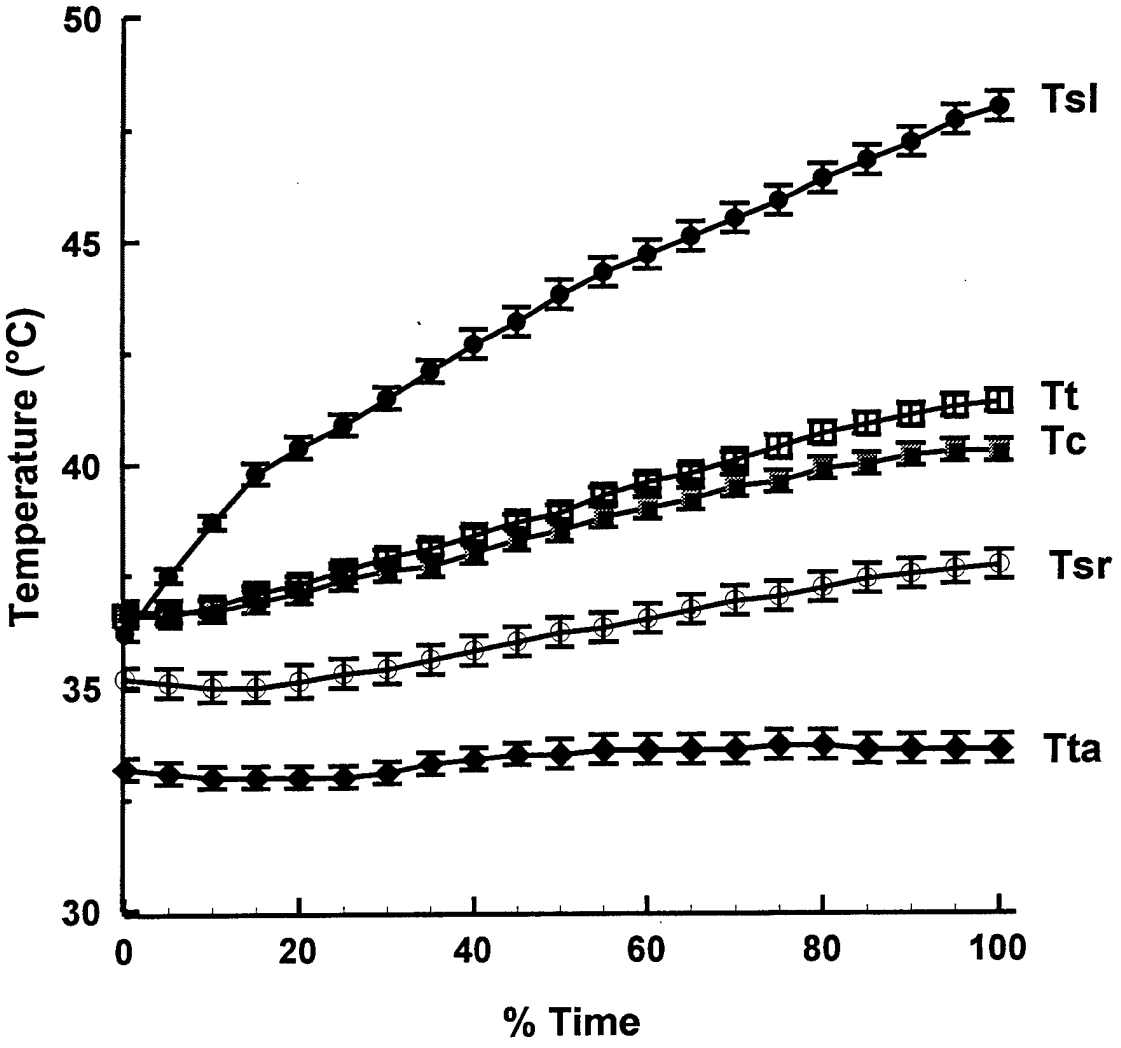

Figure 1. Thermal responses to exposure to 35-GHz RFR in ketamine-anesthetized rats (n=13). Exposure time is represented as a percentage of total time to account for differences in duration of individual experiments. T_{sl}, left subcutaneous; T_{sr}, right subcutaneous, T_t, right tympanic; T_c, colonic; T_{ta}, tail. From Frei *et al.*, 1995, used with permission.

lethal T_{sl} attained is 48.0±0.4°C. Increases in colonic (T_c), right subcutaneous (i.e., non-irradiated side), and right tympanic temperatures temporally lag behind the increase in T_{sl}, suggesting that energy absorption occurs very superficially and that heating of the body core is achieved through circulatory heat transfer from the peripheral site of irradiation. It should be noted that, when irradiation is continued until death, the maximum T_c attained is 40.3°C. The period of MMW irradiation required to elicit death in this study ranged from 32-69 min, with an average of 50 ± 1 min.

Figure 2 depicts the cardiovascular response to MMW exposure (Frei *et al.*, 1995). Because of the extremely rapid and linear rate of rise of T_{sl} during MMW exposure, cardiovascular data are graphed against this variable in Figure 2. During the early phase of irradiation, MAP initially increased slightly. MAP subsequently began to decline, however, when T_{sl} and T_c increased to ≥42.0°C and >37.5°C, respectively. From this point, MAP continued to decline until death. In contrast, HR increased continuously throughout the period of MMW exposure.

During the initial period of irradiation, mesenteric blood flow did not change while mesenteric vascular resistance (MAP/mesenteric blood flow) tended to increase. Mesenteric vascular resistance peaked at T_{sl} = 40.5°C and subsequently began to decline thereafter, reaching statistical significance at T_{sl}≥45.0°C. Concomitantly, mesenteric blood flow tended to increase, although not significantly ($p<0.06$).

Thus, sustained exposure to 35-GHz RFR results in large and rapid increases in skin temperature but only moderate increases in core temperature. This thermal distribution is sufficient, though, to produce a progressive decrease in blood pressure (i.e., hypotension) and circulatory shock

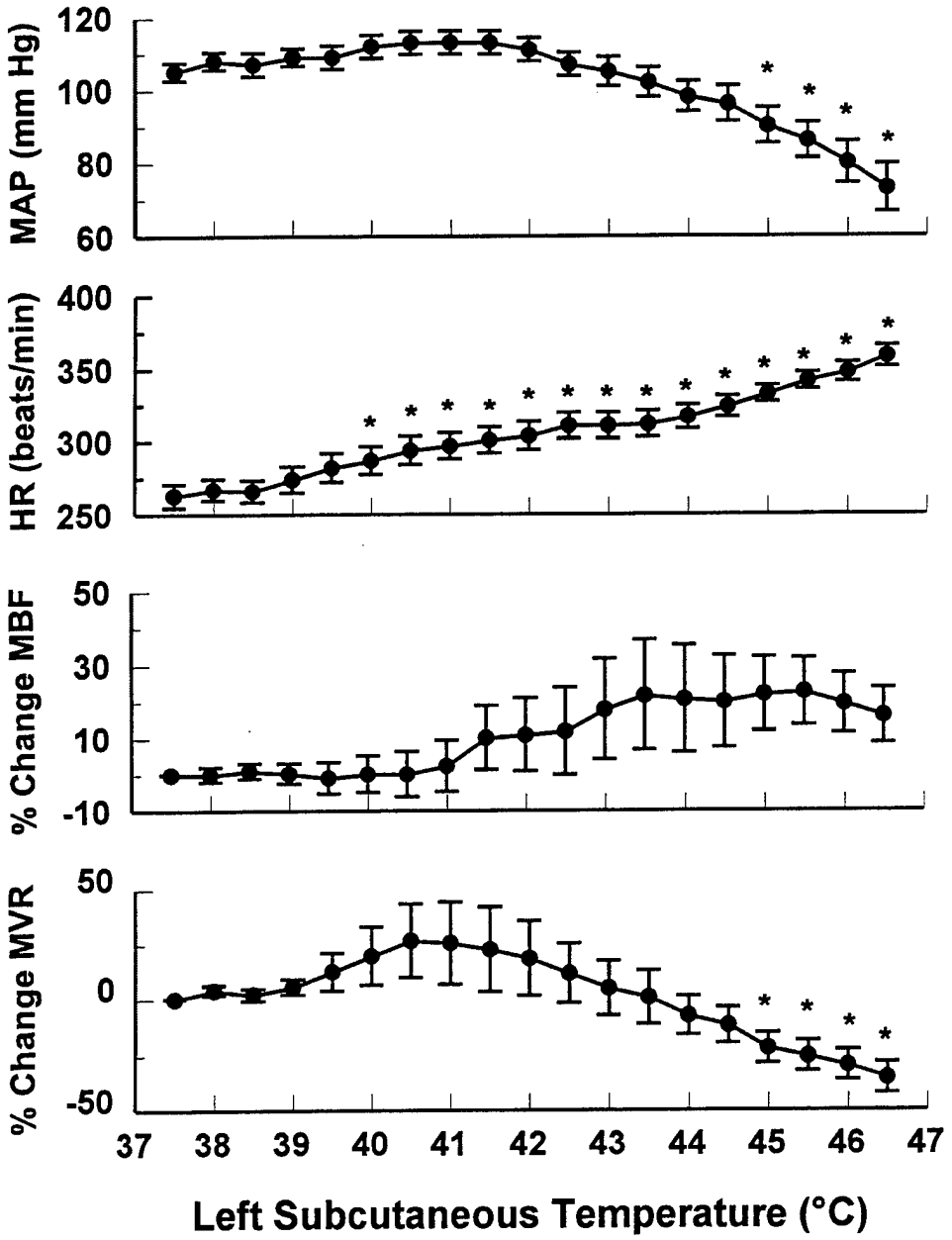

Figure 2. Cardiovascular responses to exposure to 35-GHz RFR in ketamine-anesthetized rats (n=13). Mean arterial pressure (MAP), heart rate (HR), and left subcutaneous temperature (Tsl) are absolute values, while mesenteric blood flow (MBF) and mesenteric vascular resistance (MVR) are presented as percent change from initial values. *Significantly ($p<0.05$) different from initial value. From Frei *et al.*, 1995, used with permission.

in ketamine-anesthetized rats. Parenthetically, MMW exposure also produces identical cardiovascular reactions in rats anesthetized with sodium pentobarbital (Ryan *et al.*, 1997a) or urethane (unpublished observations), indicating that the hypotensive response occurs irrespective of anesthetic choice. This hypotension is accompanied by vasodilation in the mesenteric vascular bed, suggesting that visceral pooling of blood and subsequent loss of functional blood volume may contribute to the hypotension. It should also be noted that exposure to 94-GHz RFR at identical power densities and SARs produces similar thermal and cardiovascular responses to those elicited by 35-GHz (Ryan *et al.*, 1995).

MMW-INDUCED HYPERTHERMIA VS. ENVIRONMENTAL HEAT STRESS

The cardiovascular responses to MMW exposure as outlined above bear certain resemblances to cardiovascular responses produced by exposure to environmental heat stress. If prolonged, environmental heating may produce heat stroke, a condition characterized by hypotension which, in extreme cases, may be fatal (Malamud *et al.*, 1946). Kregel *et al.* (1988) demonstrated that sustained environmental heating of either conscious or anesthetized rats produces hypotension, which is preceded by a large and significant vasodilation of the mesenteric vascular bed. As we have seen, sustained exposure to high levels of MMW also results in a hypotensive state that is accompanied by mesenteric vasodilation. Additionally, both MMW exposure and environmental heating produce large and progressive increases in heart rate (Frei *et al.*, 1995; Kregel *et al.*, 1988).

There are, however, some important differences between this model of MMW-induced heating and environmental heating. First, MMW-induced hypotension occurs at a high cutaneous

temperature but at a relatively low T_c. Indeed, the onset of hypotension in animals heated by MMW exposure occurs at a $T_c < 40°C$ (Frei *et al.*, 1995), while MAP begins to decrease in animals exposed to environmental heating only when T_c rises above 41.5°C (Kregel *et al.*, 1988). Second, the time course of MMW exposure (at the power level used) required for the onset of hypotension is shorter than that for hypotension induced by environmental heating. Despite these differences, the occurrence of mesenteric vasodilation and hypotension in both of these models of heating suggests that the physiological mechanism(s) underlying the development of hypotension in both models may be similar. Potential physiological mediators in both models of severe hyperthermia will be discussed in a subsequent section of this paper.

IS CIRCULATORY COLLAPSE IN MMW-EXPOSED ANIMALS A CONSEQUENCE OF BURN?

Because of the large increases in temperature at the irradiated site, a natural question is whether this level of MMW exposure produces burning of the skin and whether cardiovascular events are a result of this burn. Three lines of evidence argue against this supposition. First, cardiovascular responses to MMW exposure differ significantly from those associated with established experimental models of burn (Lund and Reed, 1986; Speakman and Chapman, 1989). For example, full-thickness (third degree) thermal injury of up to 60% of the body surface area in rats (scalding using the Walker/Mason model) produces decreases in heart rate (Lund and Reed, 1986; Speakman and Chapman, 1989). This is in direct contrast with MMW exposure, in which HR progressively increases throughout irradiation. Furthermore, the MAP of rats with even the most extreme thermal

injury falls only moderately (to 70-80 mmHg) following burn injury and demonstrates some recovery to control levels (Lund and Reed, 1986; Speakman and Chapman, 1989). These animals survive >180 minutes post-burn. MMW exposure, however, produces a progressive decrease in MAP which eventuates in death well before this time.

The second piece of evidence that argues against the production of burn concerns temperature at the surface of the skin. Using infrared thermography, we have determined that T_{sl} (i.e., the temperature in the subcutaneous level under the irradiated skin) corresponds to the actual temperature on the surface of the skin (Ryan et al., 1996b). T_{sl} is thus a valid measure of the maximal surface temperatures attained during MMW exposure. As indicated before, the maximal T_{sl} at death reaches 48.0°C. In order to cause a third-degree burn, this temperature would have to be applied to the skin for at least 14 minutes; production of a first-degree burn (hyperemia without loss of epidermis) would require at least 10 minutes (Moritz and Henriques, 1947). Obviously, this scenario does not occur during our paradigm of MMW exposure.

Finally, we have characterized histopathological alterations in the skin during MMW exposure (Ryan *et al.*, 1996c). Exposure to MMWs at the power density used previously (75 mW/cm^2) produces hemorrhage and congestion in the dermal layer of the skin indicative of hyperemia. Additionally, some vacuolation of the epidermis was noted. Importantly, however, this level of MMW exposure failed to produce full-thickness necrosis; the pathological damage that was noted is characterized as minor thermal injury, akin to that seen in sunburn. Furthermore, there were no pathological alterations produced in any other organ.

In short, MMW exposure sufficient to produce circulatory failure and death does so with only

minor pathology and without evidence of traditional burn injury. It is interesting to note that estimation (from infrared thermography) of the total body surface area irradiated during MMW exposure yields a value of 10-15%, which is much less than that of survivable full-thickness burns in traditional animal models of burn.

IRREVERSIBILITY OF CIRCULATORY SHOCK INDUCTION

We have also performed experiments to determine whether MMW exposure induces an irreversible cascade of events leading to circulatory shock induction. In other words, is there a "point of no return" beyond which cessation of MMW exposure still leads to circulatory collapse and death? In this series of experiments, ketamine-anesthetized rats (n=6/group) were exposed to MMW as before until one of a series of MAP endpoints was reached. Different groups of rats were exposed to MMW until MAP had decreased to: 1) the control (pre-MMW) level; 2) 90 mmHg; 3) 80 mmHg; or, 4) 70 mmHg. MMW exposure times to reach these MAP endpoints in these different groups were 30 ± 2, 30 ± 4, 38 ± 4 and 36 ± 3 minutes, respectively. Animals were then monitored for either 2 hours post-exposure or until death, whichever occurred first. In groups in which MMW exposure was halted when MAP had decreased to the control and 90 mmHg levels, almost all animals survived for a period of 2 hours (6/6 and 5/6, respectively). However, in the group that was irradiated until MAP had declined to 80 mmHg, only 1 animal of 6 survived for a period of 2 hours. Furthermore, no animal survived following exposure to the highest dose of MMW (i.e., until MAP = 70 mmHg); the post-MMW survival time in this group was 15 ± 6 minutes. These data clearly demonstrate that MMW exposure triggers a cascade of events which, at some point, irreversibly leads to death. It is of interest that this point lies at what is, by comparison with other forms of circulatory shock

induction, a fairly high arterial blood pressure level. For example, animals hemorrhaged to a much lower MAP are able to return blood pressure toward normal and to survive this maneuver (Schadt and Ludbrook, 1991).

POTENTIAL PHYSIOLOGICAL MEDIATORS

Determination of the physiological mechanism mediating the hypotensive response to MMW heating is clearly of paramount importance. As indicated above, the hypotension and consequent circulatory failure does not appear to be a consequence of traditional burn injury. Furthermore, if the assumption is made that, because of the similarities in the cardiovascular responses between severe environmental heating and MMW exposure, a similar physiological mechanism may be mediating the two hypotensive states, we can also eliminate a number of other potential mechanisms. That is, it has been demonstrated that the mesenteric vasodilation and subsequent hypotension occurring in response to environmental heat stress is not due to decreases in either sympathetic nerve activity or circulating catecholamines or to a direct effect on the vascular contractile machinery (Gisolfi *et al.*, 1991; Kregel and Gisolfi, 1990).

Recently, nitric oxide (NO) levels in the portal venous blood of severely hyperthermic rats have been shown to be profoundly increased, suggesting that an enhanced release of NO might occur within the splanchnic circulation during environmental heat stress (Hall *et al.*, 1994). NO is a potent endogenous vasodilator molecule. Pathological increases in NO release have been shown to mediate hypotensive states and circulatory shock resulting from a variety of etiologies, including endotoxemia,

sepsis, hemorrhage, trauma and anaphylaxis (Thiemermann, 1994; Szabó and Thiemermann, 1994). It therefore seemed plausible that NO might also contribute to the hypotension induced by severe hyperthermia, whether produced by environmental heating or MMW exposure.

We therefore exposed ketamine-anesthetized rats to MMW irradiation until the point of circulatory shock induction (arbitrarily chosen as MAP = 75 mmHg), discontinued irradiation, and immediately administered a NO synthesis inhibitor (L-NAME; Ryan *et al.*, 1996a). Pharmacological blockade of NO synthesis neither reversed the MMW-induced hypotension nor increased the post-MMW survival time. Furthermore, chronic (14 days) administration of the NO synthesis inhibitor prior to MMW exposure did not in any way protect animals from subsequent MMW exposure (Ryan *et al.*, 1997a). That is, chronic pretreatment with L-NAME did not postpone the onset of hypotension. Furthermore, L-NAME pretreatment actually increased the rate of heating during MMW exposure and therefore decreased the time of MMW exposure required to induce severe hypotension. Taken together, the results from both acute and chronic blockade of NO synthesis indicate that increased levels of NO do not mediate the hypotensive state produced by MMW exposure. It should be noted that NO has also recently been eliminated as a mediator in circulatory failure induced by environmental heat stress (Sils *et al.*, 1996; Tehrany *et al.*, 1997).

Paradoxically, it has been suggested that circulatory shock of varying pathogenetic origins may be the result of endothelial dysfunction and decreased generation of NO, which subsequently results in profound tissue injury (Kovách and Lefer, 1993; Lefer and Lefer, 1993). Some of our results from the aforementioned acute and chronic blockades of NO synthesis (Ryan *et al.*, 1996a; Ryan *et al.*, 1997a) suggested that NO levels might actually be decreased by MMW exposure.

Because administration of NO donors had provided significant protective effects during other forms of shock (see Ryan *et al.*, 1997b, for references), we therefore tested the hypothesis that administration of a NO donor might prove beneficial in animals exposed to MMW irradiation (Ryan *et al.*, 1997b). Administration of a NO donor, however, failed to alter either the thermal or cardiovascular response to MMW exposure. This finding is of interest for two reasons. First, NO depletion does not act to produce the circulatory failure induced by MMW exposure. Second, administration of supraphysiological doses of NO did not produce any evident deleterious effects, which further confirms that increased levels of NO do not contribute to the MMW-induced hypotension.

Recent results from our laboratory have also eliminated platelet-activating factor and histamine as mediators of this response (Skitek *et al.*, 1996; Ryan *et al.*, 1997c). At this point, therefore, it is clear that lethality produced by this model of MMW heating is not the consequence of burn damage to the irradiated skin or the aforementioned endogenous vasodilators. We currently hypothesize that the circulatory failure may result from the release of a vasoactive mediator from the irradiated skin; the minor pathological changes noted are consistent with this event. The identity of this putative mediator, however, is currently unknown but is under active investigation. Alternatively, it is possible that cutaneous thermoreceptors might play a prominent role in triggering an integrated response to MMW exposure, as suggested previously (Frei *et al.*, 1995).

SUMMARY

MMW exposure under these experimental conditions produces a reproducible model of

circulatory failure. Importantly, circulatory failure induced by this form of hyperthermia occurs at only moderate core temperature levels that are much lower than those observed during heat stroke. Furthermore, such profound cardiovascular events occur in the absence of major pathological changes, including those associated with full-thickness burn. This model of hyperthermia-induced circulatory failure is therefore unique and is of intense interest in terms of thermoregulatory physiology, as well as circulatory shock induction.

ACKNOWLEDGMENTS

This work was supported by the United States Air Force Office of Scientific Research and Air Force Contract No. F33615-90-D-0606.

The authors gratefully acknowledge the expert technical assistance of Veronica Guel, Julie D. Lovelace, and Maria R. Tehrany. We are also grateful for the radiofrequency radiation exposure support of the Sources and Measurements Branch, Radiofrequency Radiation Division, USAF Armstrong Laboratory, Brooks AFB, TX.

The animals involved in this study were procured, maintained, and used in accordance with the Animal Welfare Act and the "Guide for the Care and Use of Laboratory Animals" prepared by the National Research Council.

The views and opinions expressed herein are those of the authors and do not necessarily state or reflect those of the U.S. Government.

REFERENCES

Erwin, D. N., and W. D. Hurt. Assessment of possible hazards associated with applications of millimeter-wave systems. *Aeromedical Review USAFSAM Review* 2-81. Brooks Air Force Base, TX: US Air Force Schoole of Aerospace Medicine, 1981.

Frei, M. R., K. L. Ryan, R. E. Berger, and J. R. Jauchem. Sustained 35-GHz radiofrequency irradiation induces circulatory failure. *Shock* 4: 289-293, 1995.

Gandhi, O. P., and A. Riazi. Absorption of millimeter waves by human beings and its biological implications. *IEEE Trans Microwave Theory Tech* 34: 228-235, 1986.

Gisolfi, C. V., R. D. Matthes, K. C. Kregel, R. Oppliger. Splanchnic sympathetic nerve activity and circulating catecholamines in the hyperthermic rat. *J. Appl. Physiol.* 70: 1821-1826, 1991.

Hall, D. M., G. R. Buettner, R. D. Matthes, C. V. Gisolfi. Hyperthermia stimulates nitric oxide formation: Electron paramagnetic resonance detection of ·NO-heme in blood. *J. Appl. Physiol.* 77: 548-553, 1994.

Kovách, A. G. B., and A. M. Lefer. Endothelial dysfunction in shock states. *News Physiol. Sci.* 8: 145-148, 1993.

Kregel, K. C., and C. V. Gisolfi. Circulatory responses to vasoconstrictor agents during passive heating in the rat. *J. Appl. Physiol.* 68: 1220-1227, 1990.

Kregel, K. C., P. T. Wall, and C. V. Gisolfi. Peripheral vascular responses to hyperthermia in the rat. *J. Appl. Physiol.* 64: 2582-2588, 1988.

Lefer, A. M., and D. J. Lefer. Pharmacology of the endothelium in ischemia-reperfusion and circulatory shock. *Annu. Rev. Pharmacol. Toxicol.* 33: 71-90, 1993.

Lund, T., and R. K. Reed. Acute hemodynamic effects of thermal skin injury in the rat. *Circ. Shock* 20: 105-114, 1986.

Malamud, N., W. Haymaker, and R. P. Custer. A clinicopathologic study of 125 fatal cases. *Military Surg.* 99: 397-449, 1946.

Moritz, A. R., and F. C. Henriques, Jr. Studies of thermal injury. II. The relative importance of time and surface temperature in the causation of cutaneous burns. *Am. J. Pathol.* 23: 695-720, 1947.

Ryan, K. L., M. R. Frei, and J. R. Jauchem. Does nitric oxide mediate circulatory failure

induced by 35-GHz microwave heating? *Shock* 6: 71-76, 1996a.

Ryan, K. L., M. R. Frei, and J. R. Jauchem. Circulatory failure induced by 35-GHz microwave heating: Effects of chronic nitric oxide synthesis inhibition. *Shock* 7: 70-76, 1997a.

Ryan, K. L., L. R. Johnson, M. R. Tehrany, and T. J. Walters. Infrared visualization of body surface temperature during 35-GHz radiofrequency radiation (RFR) exposure. Proceedings of the Eighteenth Annual Meeting of the Bioelectromagnetics Society, p. 234, 1996b.

Ryan, K. L., J. D. Lovelace, M. R. Frei, R. E. Berger, and J. R. Jauchem. Cardiovascular and thermal effects of 94-GHz irradiation in rats. Proceedings of the Seventeenth Annual Meeting of the Bioelectromagnetics Society, p. 193, 1995.

Ryan, K. L., J. D. Lovelace, M. R. Frei, and J. R. Jauchem. Exogenous nitric oxide does not affect hypotension induced by 35-GHz microwave heating. Submitted, Life Sci.

Ryan, K. L., M. R. Tehrany, M. R. Frei, and J. R. Jauchem. Histamine receptor blockade does not alter hypotension induced by 35-GHz microwave heating. *FASEB J.* 11:A88, 1997b.

Ryan, K. L., M. R. Tehrany, R. W. Trotter, R. Escarciga, M. R. Frei, and J. R. Jauchem. Lethal heat stress induced by sustained 35-GHz radiofrequency radiation (RFR) exposure:

Pathophysiological alterations. Proceedings of the Eighteenth Annual Meeting of the Bioelectromagnetics Society, p. 232-233, 1996c.

Schadt, J. C., and J. Ludbrook. Hemodynamic and neurohumoral responses to acute hypovolemia in conscious mammals. *Am. J. Physiol.* 260 (*Heart Circ. Physiol.* ???): H305-H318, 1991.

Sils, I. V., P. C. Szlyk-Modrow, K. A. Tartarini, and R. P. Francesconi. Effects of nitric oxide synthesis inhibition on regional blood flow of the rat during hyperthermia. *FASEB J.* 10: A331, 1996.

Skitek, E. B., S. Reddy, K. L. Ryan, M. R. Tehrany, M. R. Frei, and J. R. Jauchem. Inhibition of platelet activating factor (PAF) during hypotension induced by 35-GHz microwave heating. *FASEB J.* 10: A119, 1996.

Speakman, E. A., and B. J. Chapman. Blood volume changes of the anaesthetized rat to a large burn or mock burn injury measured using a continuous measuring circuit. *Burns* 15:322-326, 1989.

Szábo, C., and C. Thiemermann. Invited opinion: Role of nitric oxide in hemorrhagic, traumatic, and anaphylactic shock and thermal injury. *Shock* 2: 145-155, 1994.

Tehrany, M. R., K. L. Ryan, M. R. Frei, and J. R. Jauchem. Effects of nitric oxide (NO) synthesis inhibition on hypotension induced by environmental heating (EH). *FASEB J.* 11:A88, 1997.

Thiemermann, C. The role of the L-arginine:nitric oxide pathway in circulatory shock. *Adv. Pharmacol.* 28: 45-79, 1994.

Microwave / Acoustic Conversion

Yun Wang

Mathematical Products Division
Occupational & Environmental Health Directorate
Armstrong Lab, Brooks AFB, TX

Special thanks to Dr. Richard Albanese

Motivation

- Biological Effects
  - Auditory responses (pulsed microwave radiation) - Frey 1961,62
  - Change of permeability in the brain tissue - Merritt, Frey 1975
  - Thermal stress in animal - Michaelson 1971
  - Observed occupational disorder
    - Decalcification of the bones (small areas seen in X-rays of the bones of the carpus)
    - Injury to soft tissues (of the hands)
    - Osteoarthritis of the joints (of the arms)
    - Varcular disturbance

Motivation

- Questions
  - What is the structure of the acoustic fields associated with electromagnetic exposures?
  - In pulse train exposures, how does the acoustic field serve to scatter later pulses?
  - Can associated acoustic fields harm the organism (intercellular bridges)?
  - Can acoustic field be used diagnostically?
  - What are the mechanisms?

Interactive Mechanisms

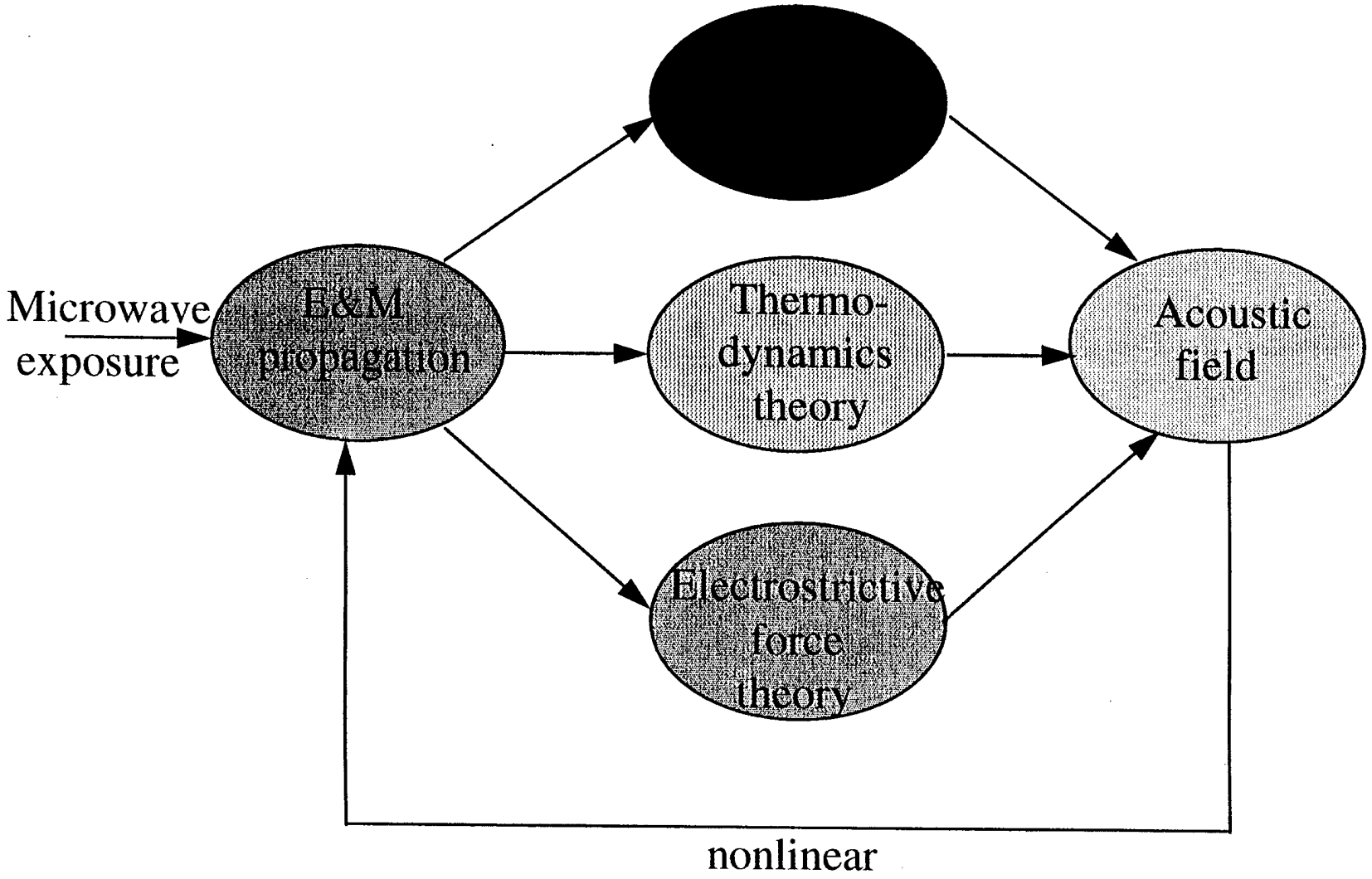

Mathematical Modeling

- Medium: tissue
  - Solid
  - Fluid
    - Newtonian
    - Non-Newtonia
  - Colloid

- Domain $\Omega_t \subset \mathbb{R}^3$ at time t

$z = (z_1, z_2, z_3) \in \Omega_t$

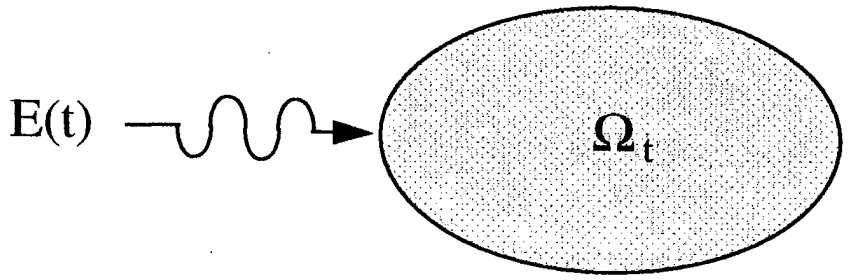

- Electromagnetic wave propagation
  - Maxwell's equations & constitutive relations with dispersion

$$\nabla \times E(z,t) = -B_t(z,t)$$
$$\nabla \times H(z,t) = D_t(z,t) + \sigma(z)E(z,t)$$
$$\nabla \bullet D(z,t) = 0$$
$$\nabla \bullet B(z,t) = 0$$

$$z \in \Omega \subset \mathbb{R}^3$$
$$t > 0$$

$$D(z,t) = \varepsilon_0 E(z,t) + P(z,t)$$
$$H(z,t) = \frac{1}{\mu_0} B(z,t) - M(z,t)$$

$$P(z,t) = \int_0^t g(t-s)E(z,s)ds$$

- Coupled equation of motion & equation of energy

1. Assumptions

  - Sources: Heat

    Electrostrictive force

  - Medium property:

    Newtonia fluid

    Visco-elastic

  - Small deviation around unperturbed states (ρ_0, T_0, p_0, s_0)

  - Relation between entropy (s) and enthalpy (h) governed by *perfect gas* assumption, i.e.

$$\nu \cdot (\rho \nabla h - \nabla p) = \rho \theta \nu \cdot \nabla s$$

2. System of equations

$u(z,t)$ - displacement deviation

$T(z,t)$ - temperature deviation

$p(z,t)$ - acoustic pressure

$$\frac{\partial^2 u}{\partial t^2} - a_1 \nabla^2 u - a_2 \nabla^2 \frac{\partial u}{\partial t} = \mathrm{f}(z,t) - a_3 \nabla T$$

$$\frac{\partial T}{\partial t} - a_4 \nabla^2 T + a_6 T = -a_7 r(z,t) - a_5 a_3 \nabla \bullet \frac{\partial u}{\partial t}$$

$z \in \Omega \subset \mathbb{R}^3$

$t > 0$

$$\nabla T \cdot \boldsymbol{n} + a_8 (T + T_{b0}) = 0 \qquad z \in \partial\Omega$$

$$p = a_9 T - a_{10} \nabla \bullet u$$

3. Coefficients

$$\frac{\partial^2 u}{\partial t^2} - a_1 \nabla^2 u - a_2 \nabla^2 \frac{\partial u}{\partial t} = \mathrm{f}(z,t) - a_3 \nabla T \qquad z \in \Omega \subset \mathbb{R}^3$$

$$\frac{\partial T}{\partial t} - a_4 \nabla^2 T + a_6 T = -a_7 r(z,t) - a_5 a_3 \nabla \bullet \frac{\partial u}{\partial t} \qquad t > 0$$

$$\nabla T \cdot \boldsymbol{n} + a_8 (T + T_{b0}) = 0 \qquad z \in \partial\Omega$$

$$a_1 = \frac{1}{\rho_0 \kappa_T} \qquad a_4 = \frac{\kappa}{\rho_0 c_v}$$

$$a_2 = \frac{\lambda + 2\mu}{\rho_0} \qquad a_5 = \frac{T_0}{c_v}$$

$$a_3 = \frac{\beta}{\rho_0 \kappa_T} \qquad a_6 = \frac{w_b c_b}{\rho_0 c_v}$$

$$a_7 = h$$

ρ_0 = mess density
κ_T = isothermal compressibility
λ,μ= coefficients of viscosity
β = coefficient of thermal expansion
κ = thermal conductivity
c_v = specific heat
T_0 = air temperature
h = heat transfer coefficient
w_b = mass flow rate of blood/volume of tissue
c_b = blood specific heat

- Microwave induced force

Electrostrictive force

$$f(z,t) = -\frac{\varepsilon_0}{2} E^2(z,t)\ \nabla\varepsilon_r(z) + \frac{\varepsilon_0}{6}\nabla\left((\varepsilon_r(z)-1)(\varepsilon_r(z)+2)E^2(z,t)\right)$$

Dissipated (thermal) energy

$$r(z,t) = \sigma(z)\ E^2(z,t) + E(z,t)\frac{\partial P}{\partial t}(z,t)$$

- Literature

$u(z,t)$ - displacement $T(z,t)$ - temperature deviation

$$\frac{\partial^2 u}{\partial t^2} - a_1 \nabla^2 u - a_2 \nabla^2 \frac{\partial u}{\partial t} = \mathrm{f}(z,t) - a_3 \nabla T$$

$$\frac{\partial T}{\partial t} - a_5 \nabla^2 T + a_6 T = -a_7 r(z,t) - a_5 a_3 \nabla \bullet \frac{\partial u}{\partial t}$$

$$\nabla T \cdot \boldsymbol{n} + a_8 (T + T_{b0}) = 0$$

$z \in \Omega \subset \mathbb{R}^3$

$t > 0$

Dafermos 1968

$$\frac{\partial^2 u}{\partial t^2} - a_1 \nabla^2 u = \mathrm{f}(z,t) - a_3 \nabla T$$

$$\frac{\partial T}{\partial t} - a_5 \nabla^2 T = -a_7 r(z,t) - a_5 a_3 \nabla \bullet \frac{\partial u}{\partial t}$$

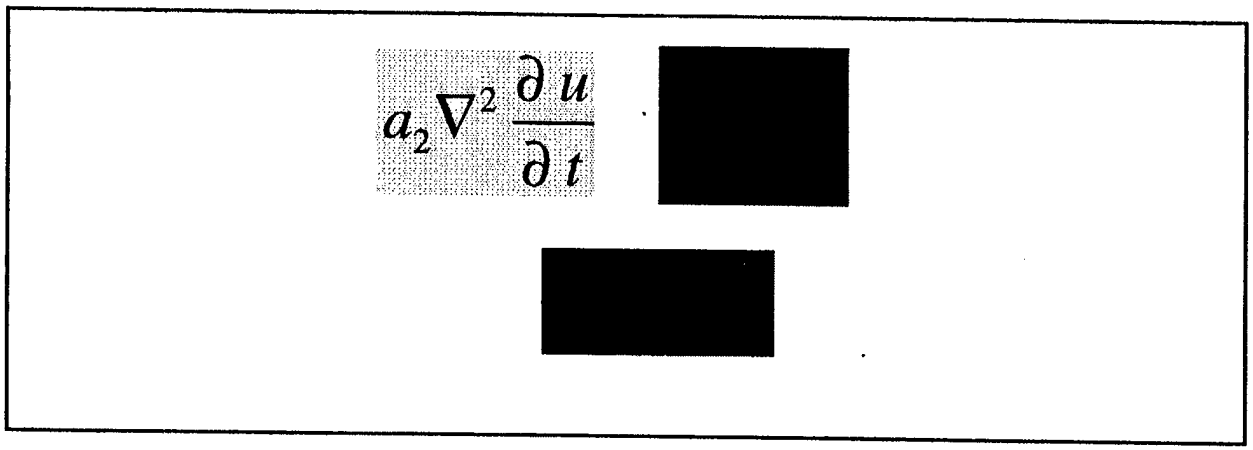

Gibson
Rosen
Tao 1992

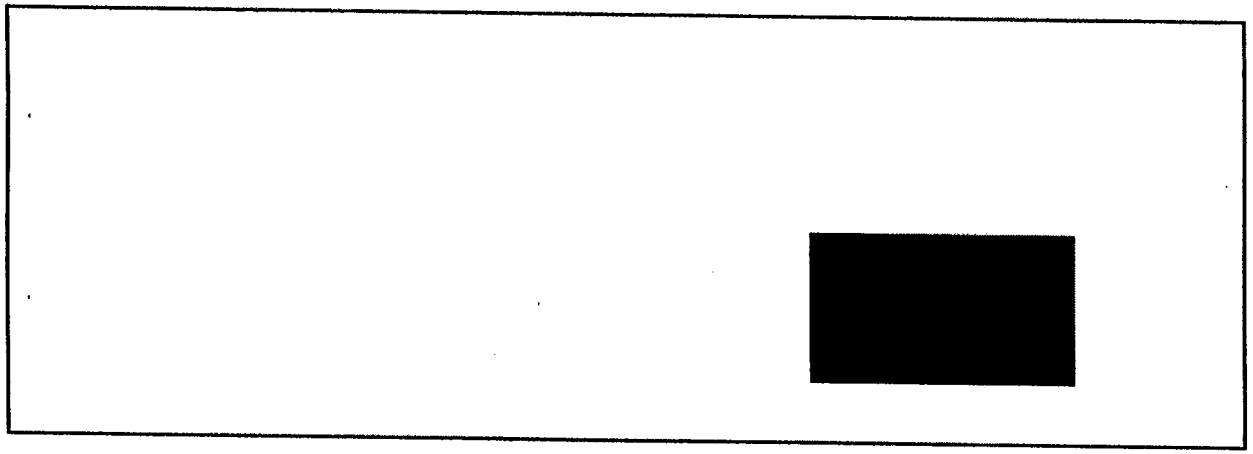

Gibson
Rosen
Tao 1992

Lin 1978

Example

- Geometry: a slab

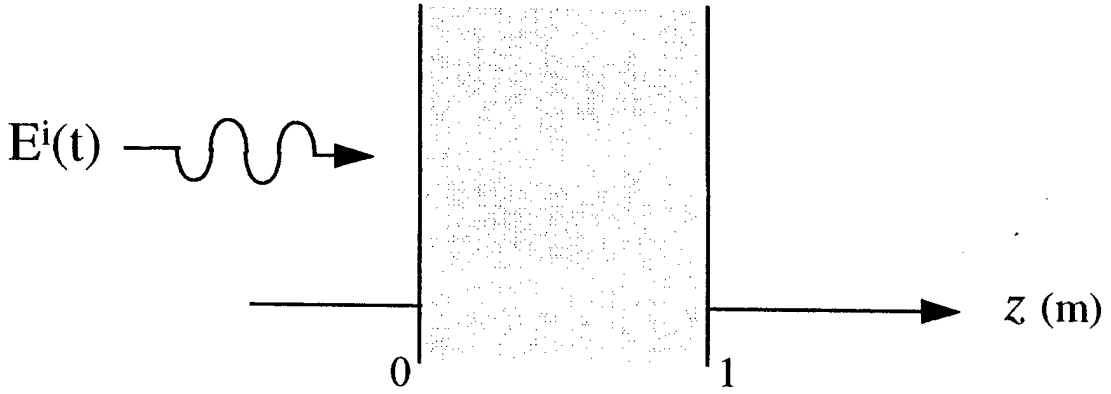

- Incident filed $E^i(t)$: uniform plane wave, single pulse

Pulse with:	4.08 ns
Carry frequency:	2.45 GHz
Peak value:	10^5 V/m

- Medium: Debye

$$\dot{P} + \frac{1}{\tau} P = \frac{\varepsilon_0 (\varepsilon_s - \varepsilon_\infty)}{\tau} E$$

$t = 8.1 \times 10^{-12}$
$\varepsilon_s = 80.1$
$\varepsilon_\infty = 5.5$
$\sigma = 0.05$

- Transmitted E-field

$$E(z,t) \approx E^M(z,t) = \sum_{k=1}^{M} d_k e^{-\alpha_k z} \sin(\omega_k t - \beta_k z + \varphi_k)$$

Peak field: 2.61×10^4 V/m

- System of equations:

$$\frac{\partial^2 u}{\partial t^2} - a_1 \frac{\partial^2 u}{\partial z^2} - a_2 \frac{\partial^3 u}{\partial t \partial z^2} + a_3 \frac{\partial T}{\partial z} = 0 \qquad 0 < z < 1$$

$$\frac{\partial T}{\partial t} - a_4 \frac{\partial^2 T}{\partial z^2} + a_5 a_3 \frac{\partial^2 u}{\partial t \partial z} = -a_7 r(z,t) \qquad t > 0$$

$$\frac{\partial T}{\partial z}(z,t) = a_8 (T - T_0) \qquad z = 0$$

$$\frac{\partial T}{\partial z}(z,t) = -a_8 (T - T_0) \qquad z = 1$$

$$u(0,t) = u(1,t) = 0$$

$a_1 = 1460^2$	$a_4 = 1.5 \times 10^{-7}$
$a_2 = 2.1$	$a_7 = 0.001$
$a_3 = 147.08$	$a_8 = 25$

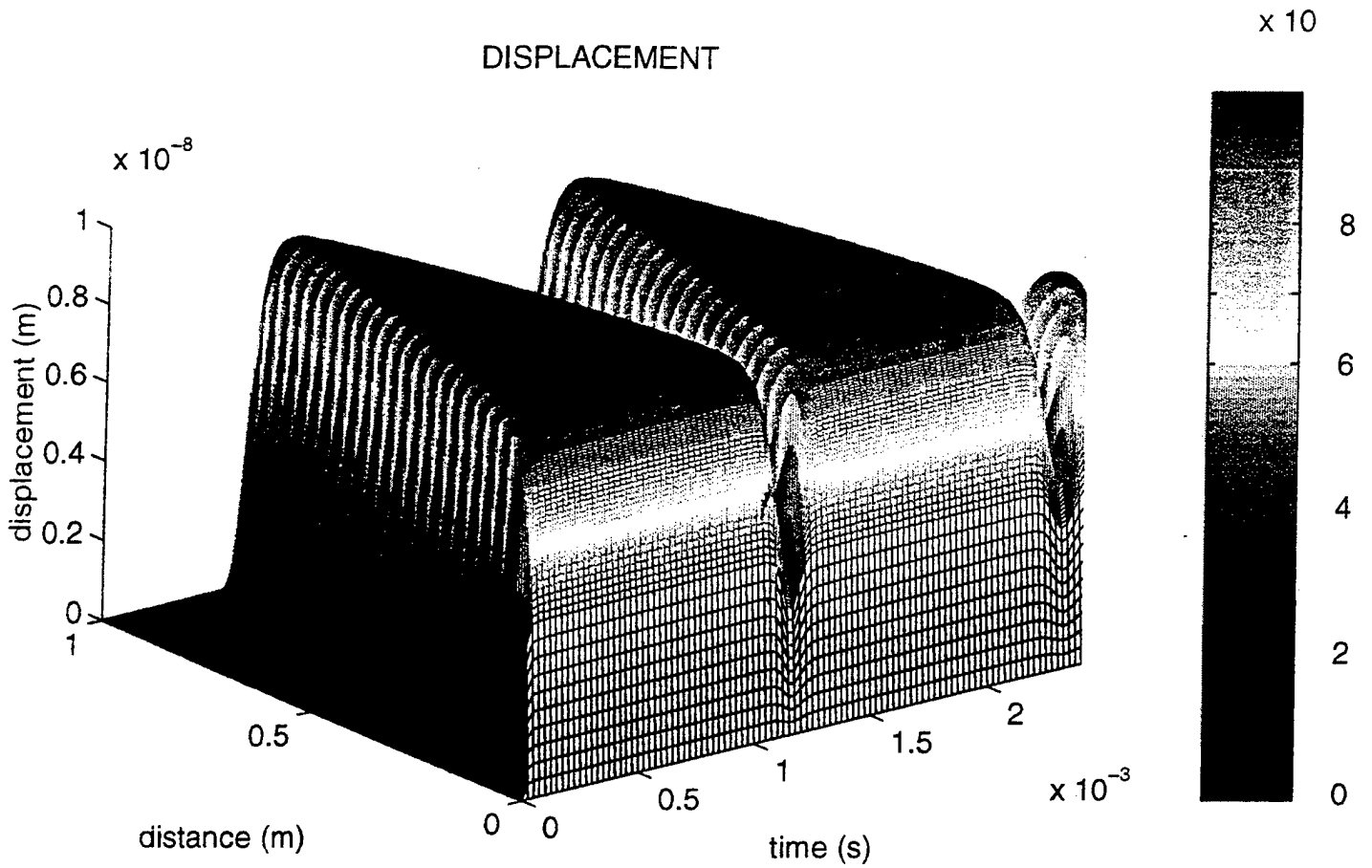
DISPLACEMENT
x 10
x 10^-8
displacement (m)
distance (m)
time (s)
x 10^-3

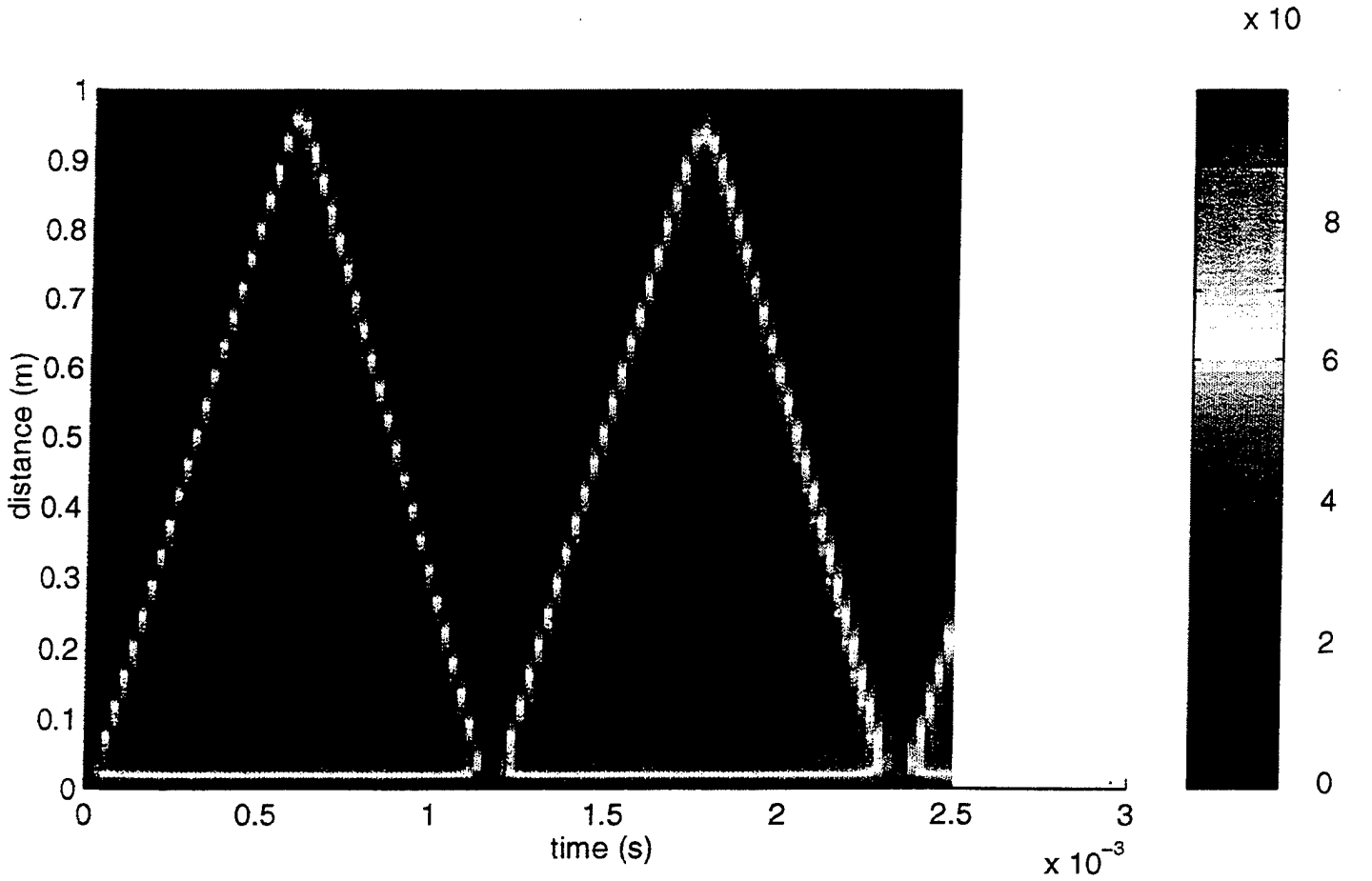
x 10
distance (m)
time (s)
x 10^-3

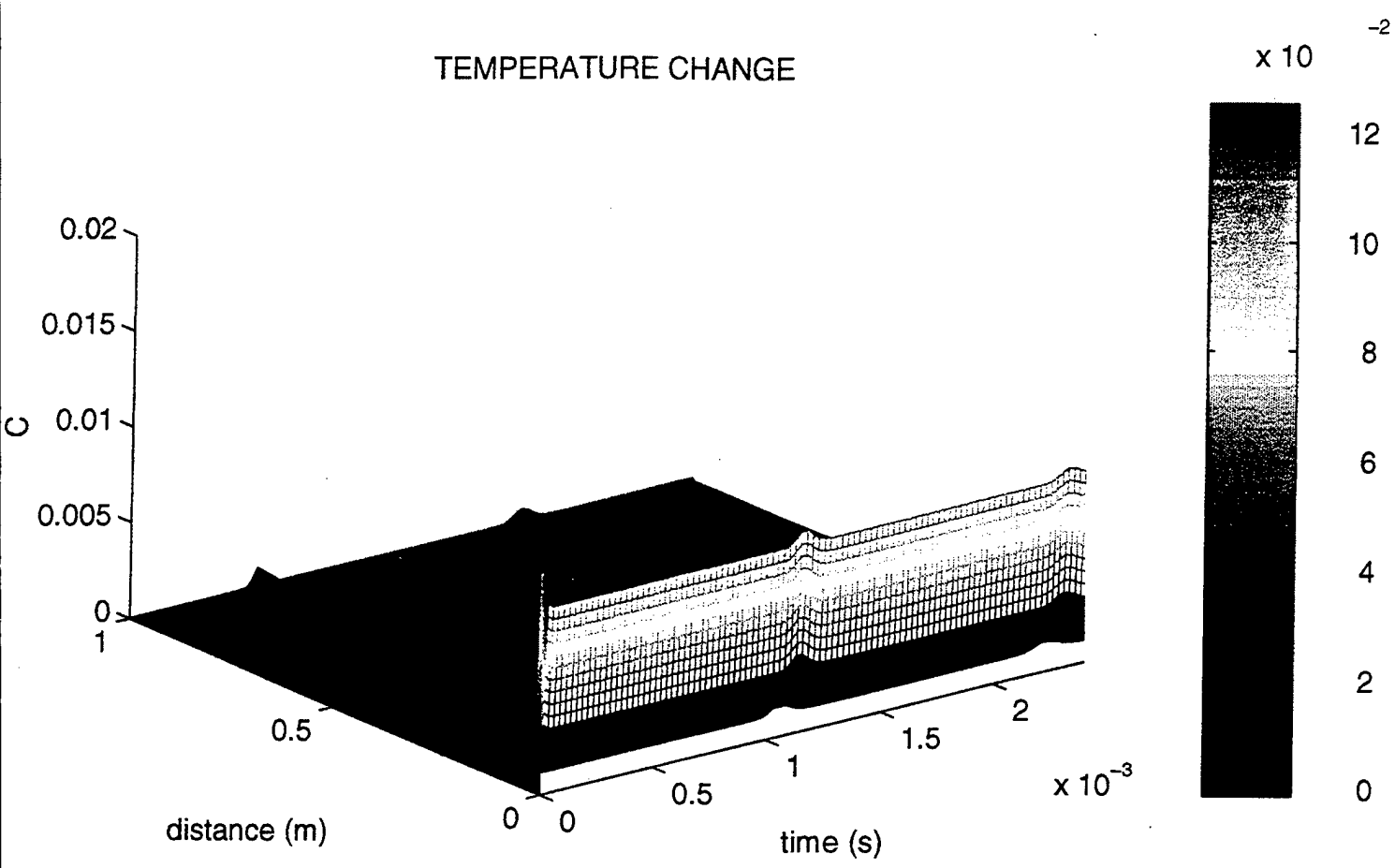
TEMPERATURE CHANGE
x 10^-2
12
10
8
6
4
2
0
C
0.02
0.015
0.01
0.005
0
1
0.5
0
distance (m)
0
0.5
1
1.5
2
x 10^-3
time (s)

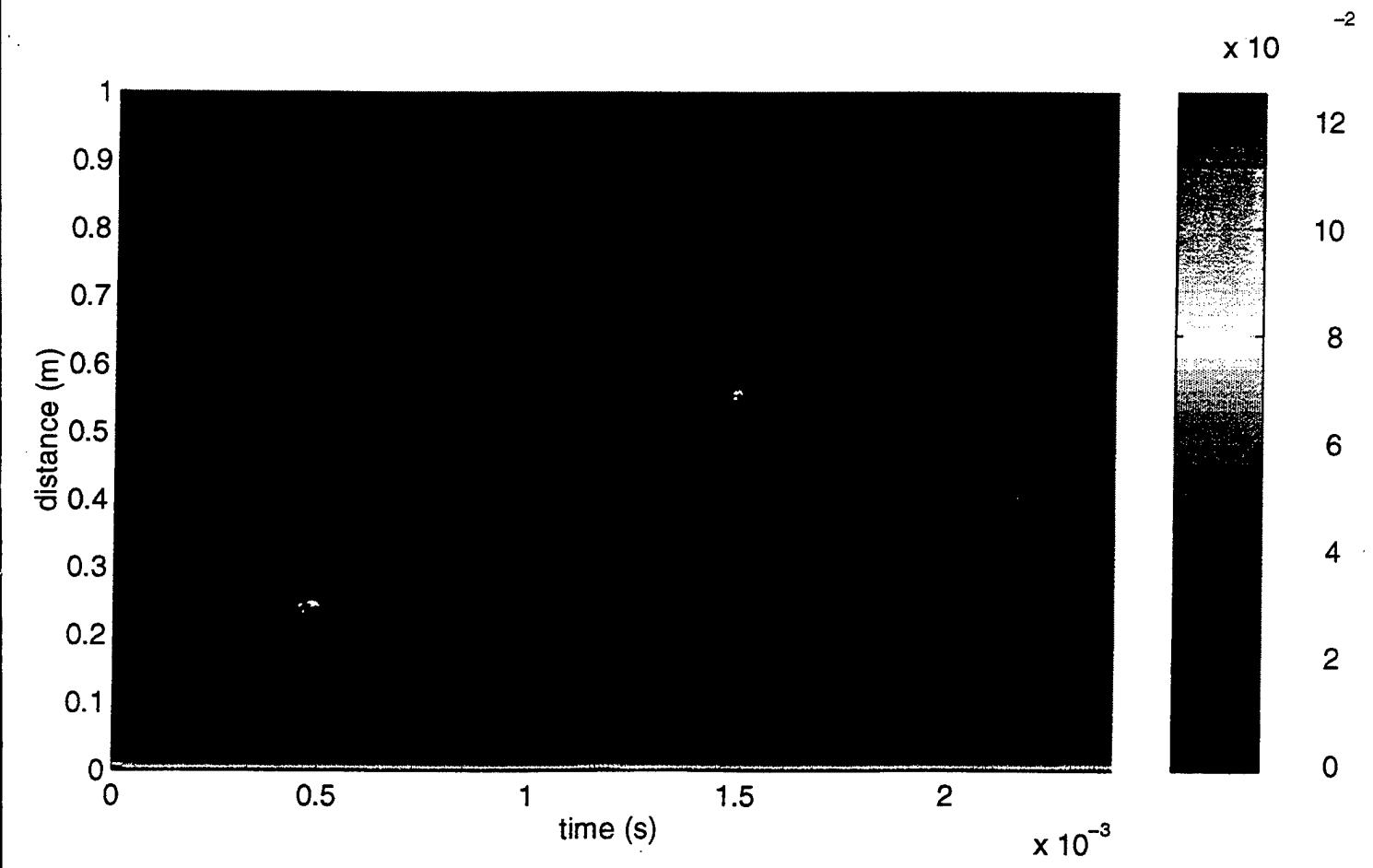
x 10^-2
12
10
8
6
4
2
0
distance (m)
1
0.9
0.8
0.7
0.6
0.5
0.4
0.3
0.2
0.1
0
0
0.5
1
1.5
2
time (s)
x 10^-3

Future Work

- Dynamics of colloid material
- Include Navier-Stokes equation to investigate acoustic field influence to Gel-Sol transformations important to life process (e.g. macrophage movement).
- Inverse problem in cell damage detection. Laser probes can measure vibration of the cells noninvasively which provides data for reconstruction of tissue images.

Spectral and modulation effects: the thermal time constant.

John M. Osepchuk, Ph. D.
Full Spectrum Consulting
Concord, MA 01742

It is a basic premise that standards for safe use of electromagnetic energy should be continuous across the interface between millimeter-waves and infrared. The existing consensus standard, IEEE C95.1-1991, has been criticized by some as being too lax at high frequencies ;i.e. above 6 GHz. The standard also contains a caveat on relaxation of limits for partial-body exposure which is justified today only on the basis that the averaging time in C95.1-1991 may not be conservative enough especially around the range of 10 to 30 GHz.

To meet these objections it is necessary to critically review the possibility of "athermal" effects in the millimeter-wave range and to establish a better scientific basis for averaging time from more accurate information on thermal time constants.

A variety of "athermal" effects are reviewed. It is noted that there is no evidence for such effects in the millimeter-wave spectrum except for frequency-specific effects. The weakness of the experimental data-base for such effects is described by Petersen in the following paper. The rest of speculative "athermal" effects (including pulse effects) have no support in the experimental laser literature (above 300 GHz). The only effect not related to thermalizing levels of exposure is the microwave auditory effect. The evidence for this effect exists up to 5.8 GHz and there are anecdotal reports of such effects by laser experimenters. Research is required to fully establish this effect across the spectrum. It remains questionable whether this is a basis for limits on peak exposure.

The meaning of the classical averaging time of six minutes can be shown to relate to the thermal time constant of small portions of the body e.g. like the eyeball or the testes. Whole-body exposures have been shown to relate to a thermal time constant of about one hour. A review of theoretical solutions for heating of tissue shows an undue emphasis on two-dimensional models which do not yield information on a definitive time constant. A review of work in

the laser field and in heating of non-living materials shows that thermal time constant is determined strongly by heating (or irradiation) area and secondarily by penetration depth. More work is necessary before one can derive meaningful functions of frequency to describe averaging time in the next revision of C95.1. It must relate to the accurate models of thermal time constant as well to averaging times in laser standards.

There is a striking contrast in the nature of literature in the laser field and the microwave (millimeter-wave) field. Speculative papers on "athermal" effect and associated "Cheshire Cat" syndrome are apparent below 300 GHz but not above. It remains to be seen what association this difference has with similar contrast in the prevalence of "risk communication", "prudent avoidance" and Electrophobia below and above 300 GHz.

BASIC PREMISE
for
Rational Standards on
Electromagnetic Energy

Electromagnetic energy is a key tool to improve the quality of life of mankind and can be safely used. It is not a "pollutant" but more aptly a man-made extension of the naturally-generated electromagnetic spectrum that provides heat and light for our sustenance!

Sufficiently high levels of exposure to electromagnetic energy can be hazardous, just as with heat and light. Therefore exposure standards, based on current scientific knowledge, exist to provide guidance on the safe use of electromagnetic energy. Continuing research enables these standards to be refined and improved as the use of electromagnetic energy expands worldwide for the benefit of mankind .

Spectral Regions Associated with Specific Issues and Terms

EMF: Up to 300 GHz

Electrophobia: Up to 300 GHz

Prudent Avoidance: ELF to RF

Risk Communication: ELF to Microwaves

Epidemiology: ELF to Microwaves

Cheshire Cat: ELF to Microwaves

Window Effects: ELF to Microwaves

Auditory Effect: Narrow Microwave Spectrum

Sensation Thresholds: Microwaves to Light

Science-Based Standards: RF to Light

Radiation Thresholds and Safe Limits

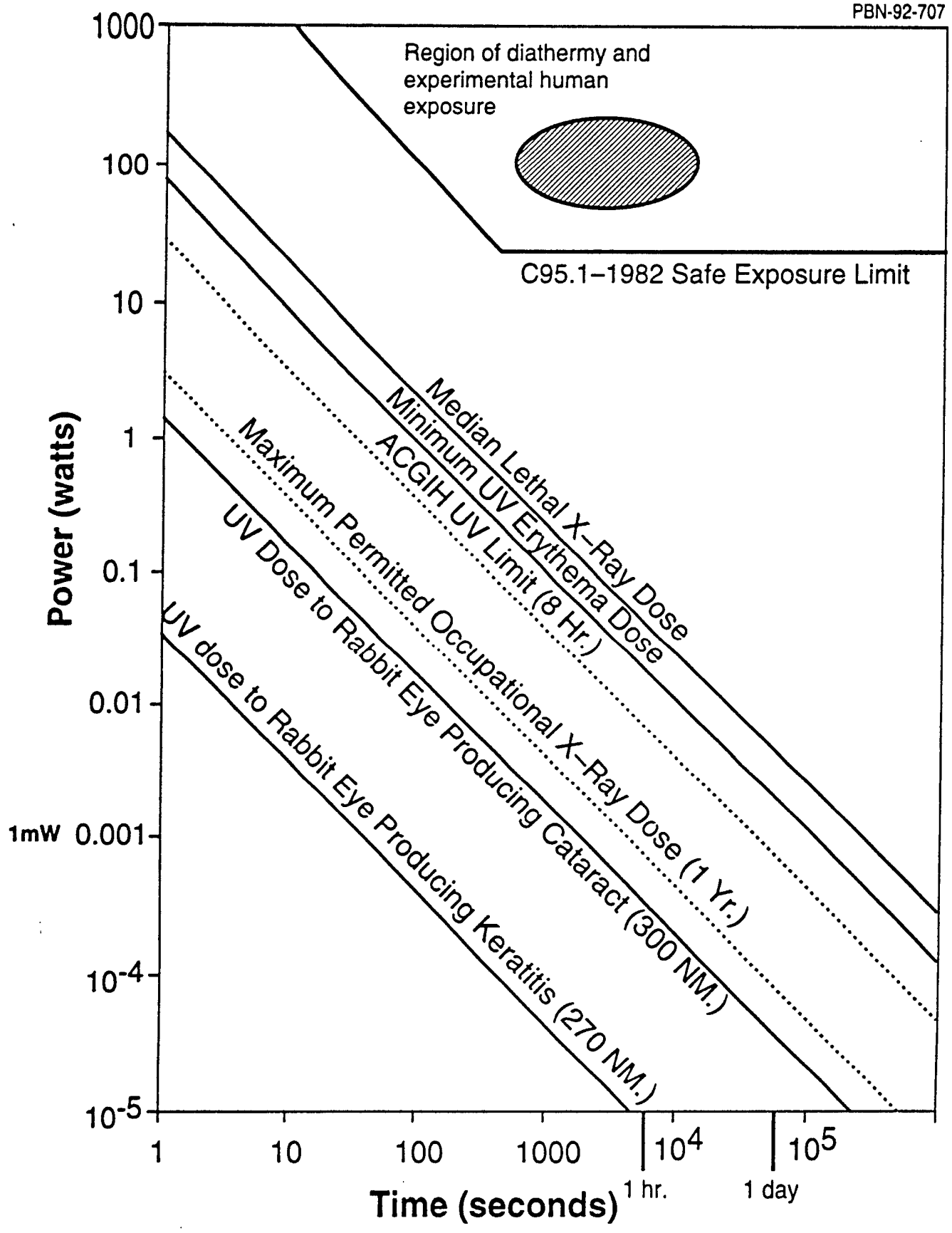

Safe Exposure Limits Across the EM Spectrum

DC - ELF - Microwave/RF - Infrared - Visible - Ultraviolet - Ionizing Radiation

NCRP

? ? C95.1 → | ← 300 GHz ANSI Z136 → ACGIH ACGIH

← Threshold Agent → ← Cumulative Effect → Non-Threshold Agent. Prudent Assumption of Linear Dose Response.

Safe Levels (Dose Rates) and MPEs (SAR, SA, P.D.) → ← Dose → No Safe Level.

Electrostimulation Heating Stochastic Health Effects Risk vs. Benefits

Averaging Time

Seconds	Minutes	Seconds	→	Very long time
	Chronic vs. Acute			
?	No	No	Yes	Yes

PBN-92-713

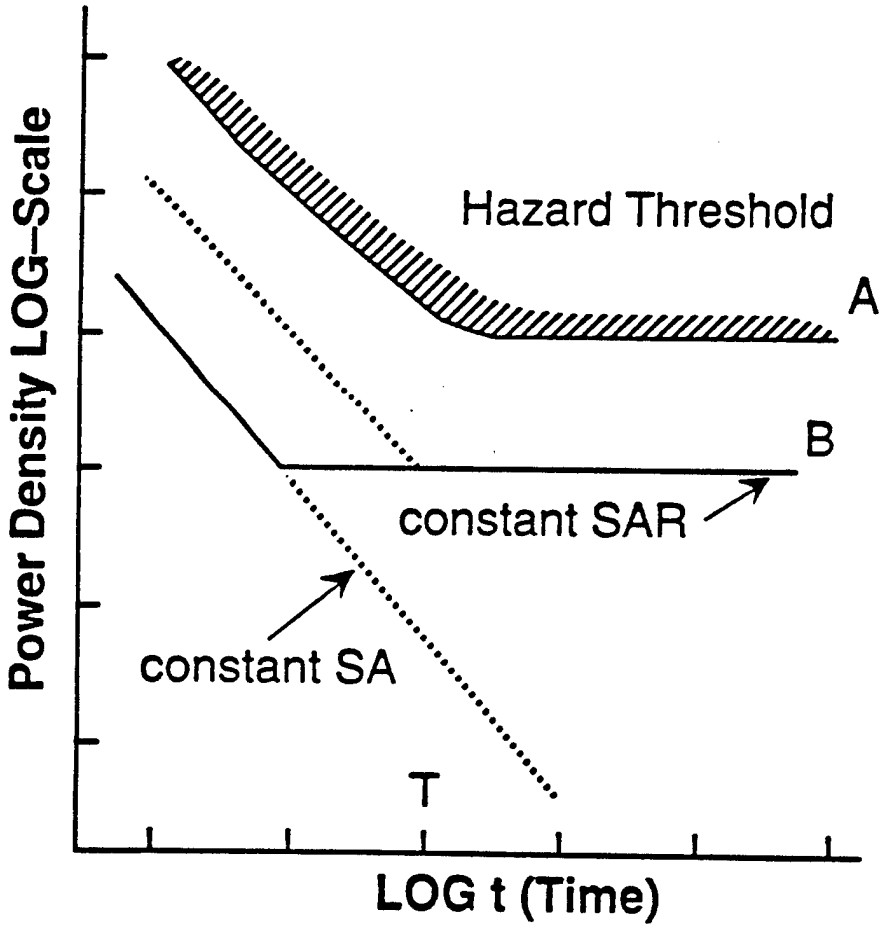
Power Density LOG–Scale
Hazard Threshold
A
B
constant SAR
constant SA
T
LOG t (Time)

A Capsule Guide to IEEE C95.1-1966

PBN-89-1328B

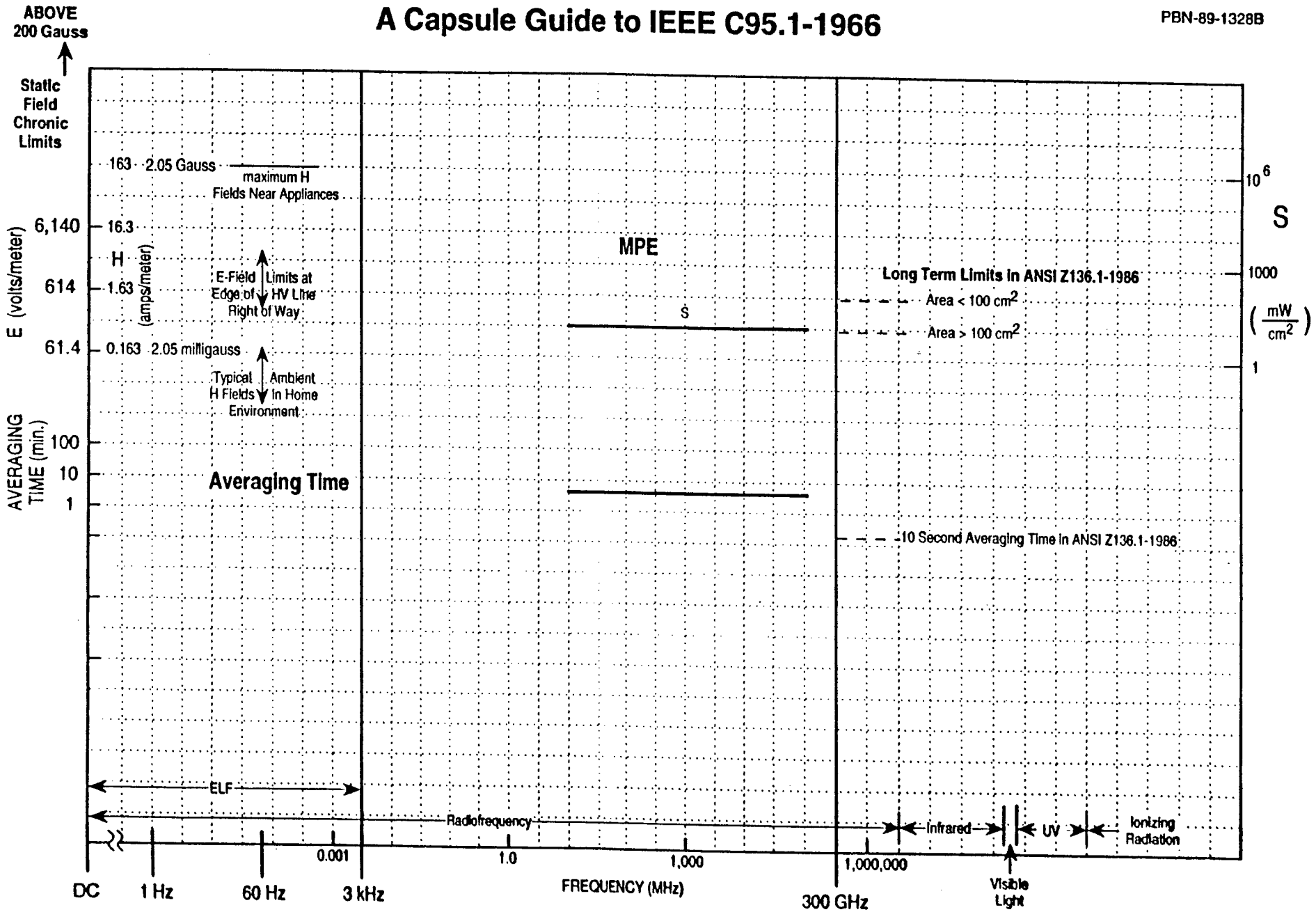

A Capsule Guide to the Final Draft Revision; IEEE C95.1-1991

PBN-89-1328

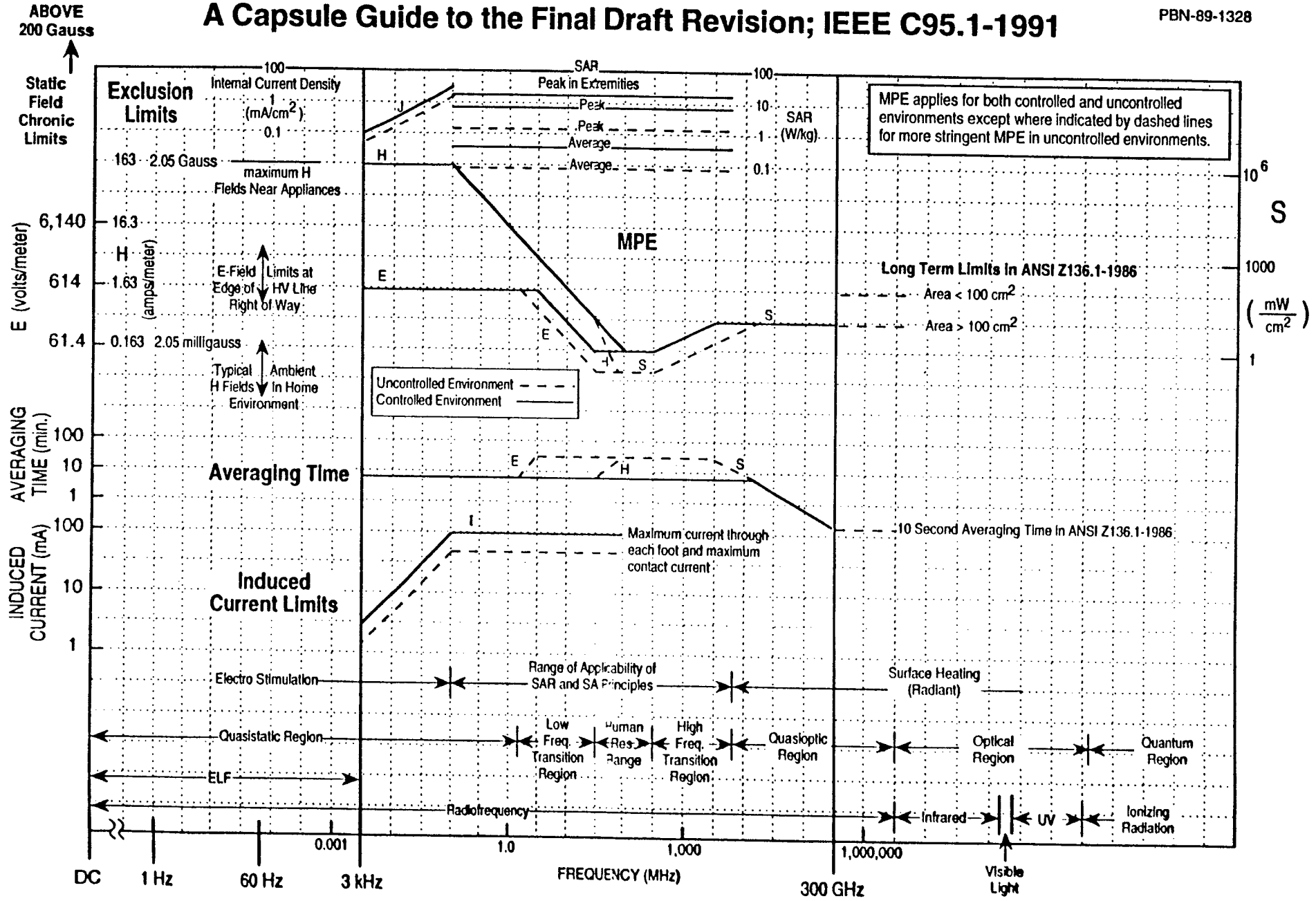

Thermal Time Constants in Bioeffect Literature

Microwave Diathermy: 10 to 15 minutes

Eyes and Testes (Ely): 5 to 10 minutes

Human Whole Body: 30 to 60 minutes
(Hoeft, Tell&Harlen)

Infrared(Hardy): ~ 5 to 20 seconds

Analytical Solutions for Thermal Time Constant in Literature

Two-dimensional: Non-existent
(Buettner, Stoll...)

Curve-Fitting: Non-existent
(Miller et al)

Laser Lierature: Seconds for small spots but lack of application to large areas.

Inanimate Objects: Time constant is proportional to D^2, where D is a diameter of an area heated at the surface

TABLE 1

A List of Some Averaging Times in Standards

Country	τ (hour)	Microwave p_o $\left(\frac{mW}{cm^2}\right)$	$p_o \cdot \tau$ $\left(\frac{mW \cdot hr}{cm^2}\right)$	Comment
Australia (1985)	1/60	1.0 Occ	1/60	Occupational exposures up to 5 p_o ceiling allowed for t < 30 minutes but with 40-minute recovery required.
		0.2 GP	1/300	
Canada	0.1	1.0 Occ	0.1	—
		0.2 GP	0.02	
IRPA	0.1	5.0 Occ	0.5	—
		1.0 GP	0.1	
USSR	8.0	.025 Occ	0.2	These are true averaging times. The new USSR limits are on dose or energy.
	24.0	.010 GP	0.24	
Poland	8.0	0.2	1.6	No true averaging time. Instead a formula $p^2 \cdot t = 32$ is used for t < 8 .0 hr. up to 10 mW/cm^2.
	24.0	.01 GP	0.24	

Averaging Times in Standards at High Frequencies

		T (min)
C95.1	15 - 300 GHz	$616{,}000/f^{1.2}$
NCRP	0.3 - 300	6.0
IRPA	0.3 - 300	6.0
NRPB	10 - 300	$68/f^{1.05}$
Z136	300	~0.15

PBN-95-994

Depiction of Optimum Detection Frequencies and Threshold Power for Eight Subjects ■ and Typical Detection Threshold Curve ×

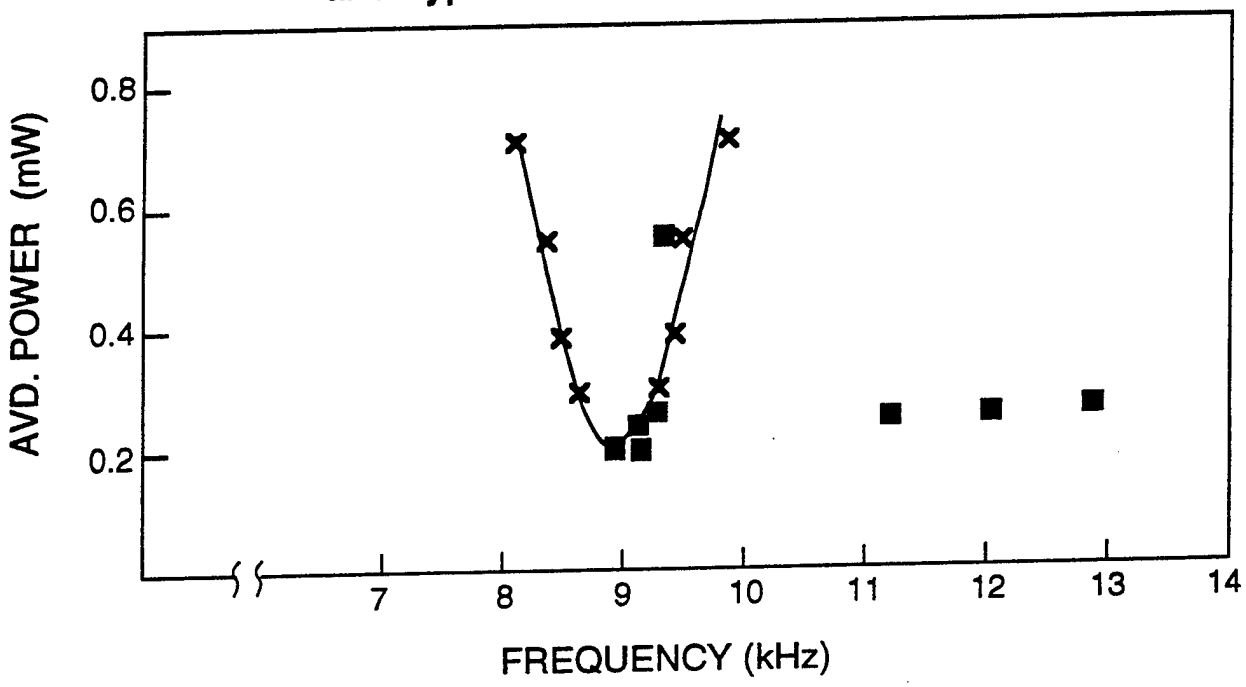

Auditory Thresholds in Human Subjects: 2.45 GHz Monopole

Subject	Age	Sex	Frequency	Power	
				Peak	Average
				Watts	
JO	69	M	8.9 kHz	17	0.2
AV	50	M	9.1	17	0.2
JS	55	M	9.1	21	0.25
RE	58	M	9.3	23	0.27
PG	72	M	9.3	83	0.55
TM	25	M	12.0	20	0.24
PZ	~45	M	11.2	21	0.25
NN	~40	F	12.8	23	0,27
MJH	~50	F	12.1	22	0.26
DP	~35	M	11.8	23	0.28
JA	~45	M	12.3	19	0.23
CS	55	M	8.8	21	0.25
JZ	51	M	9.8	22	0.26
MG	40	M	12.1	20	0.24
MBI	~45	M	9.6	34	0.40
DER	~50	M	9.6	71	1.15
JMO	32	F	9.8	20	0.40
CR	~35	M	12.5	7	0.15
JGO	38	M	11.0	7	0.15

RF	~60	M
WCB	~80	M
RCP	~59	M
EA	~65	F
EB	~65	M
PB	~64	F
SO	62	F

These subjects could not detect the microwave signal within the range of power available--i.e roughly 100 Watts peak.

Many of them could hear airborne sounds from the monopole with lossy sheet load up to 8 kHz. Several with known ear damage could hear the airborne sounds only below 5 kHz.

Normalized Acoustic Signal vs. Normalized Peak Microwave Power

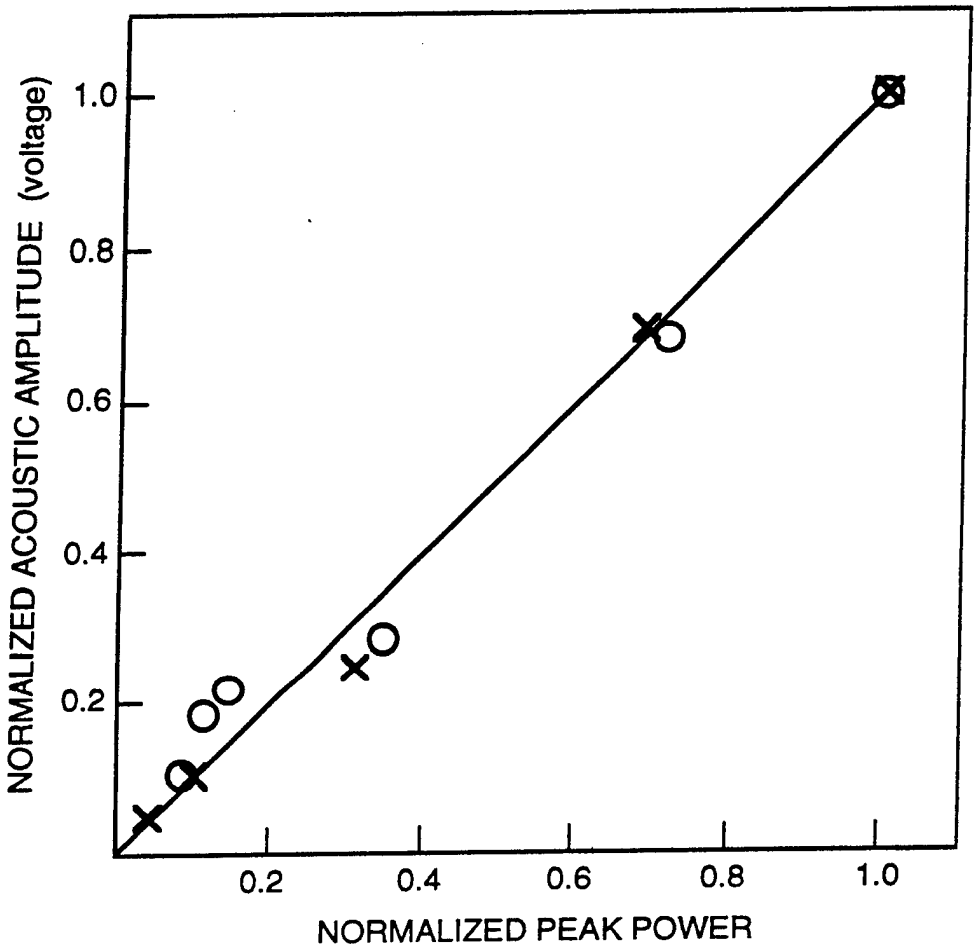

O Microphone Output in Empty Exposure Chamber Driven by Microwave Pulse with Amplitude Modulation

X Transducer Response from Water Load with Nylon Tube in S-Band Waveguide Driven by 28 µsec Pulsed Microwaves

Additional Questions about mm-Waves and Quasi-Optical Radiation

1.Is sensation from exposure considered beneficial or hazardous?

2. Besides sensible heat and vision are there any other sensations ?

3. Are there auditory effects?

4. What are the optimum waveforms and modulation for an auditory effect?

5. Is there a dependence on spatial distribution of radiation in sensations?

6. Is there a minimum irradiation area below which thermal sensation is not assured?

Critical Reviews of Millimeter-Wave Athermal Effect Studies Relative to Microwave Engineering Principles

J. M. Osepchuk, Full Spectrum Consulting, Concord, MA
R. C. Petersen, Lucent Technologies Inc., Murray Hill, NJ

Abstract

This is a preliminary report on a collaborative project on the subject of artifacts in microwave systems and their implications for bioeffect studies. In this paper we report only on one of these artifacts: the presence of and the effect of harmonics that are present in all microwave power sources. This is a fundamental fact well known to older engineers versed in the knowledge that all sources are non-linear devices. A literature survey shows, however, that this subject has been neglected for many years, such that its discovery recently in Russia was described with surprise.

Classically it is well known from studies of radar transmitters that harmonic energies from most sources range from -10 to -30 dB below the fundamental for the 2nd and 3rd harmonic. Solid state devices and traveling wave tubes (TWTs) exhibit high harmonic content — some as high as -8 dB. Resonant devices like the klystron exhibit much less harmonic energy because of inherent filtering. Backward wave oscillators (BWOs) and magnetrons can exhibit significant harmonics as well as spurious signals.

This paper describes one set of experiments concerning the performance of a variable attenuator. The literature contains reports of studies where vane-type attenuators are used with BWO sources as part of an exposure system and resonance effects are reported at levels far below thermal noise. In some of these studies power delivered to the sample is extrapolated from the forward and reflected power and the combined attenuation of one or more variable attenuators. Although the commercial type variable attenuator used in this study is more complex, it serves the purpose of demonstrating that at harmonic frequencies the attenuation will be suppressed in "windows."

In experiments at low frequencies, coaxial cable and circulators will tend to suppress harmonics, e.g., a waveguide-to-coax transducer suppresses certain mode excitations. At high frequencies, where tubes and solid state devices are mounted directly to the waveguide, a variety of waveguide modes at harmonic frequencies will be excited. These harmonics will be significant. Relying on a variable attenuators to vary fundamental power will be misleading because considerable harmonic power will be transmitted despite large attenuation, e.g., 50 or more dB at the fundamental frequency.

The importance of the harmonic energy increases at millimeter-wave frequencies because radiating horns will exhibit uncontrolled radiation patterns at harmonic frequencies under multi-mode conditions. The likely result is hot spots in the radiation pattern at a given distance. Furthermore, because of the shallow penetration depth, significant effects may be expected despite the low power. This harmonic power density will be many orders of magnitude above the assumed levels associated with the fundamental signal.

These effects likely have occurred in many millimeter-wave experiments if there has been no control of harmonics. In some cases they may have been interpreted as due to very low power densities at the fundamental frequency. In some cases they simply clutter the data. In general they would be expected to add a great deal of frequency sensitivity and randomness to the appearance of the data.

Consideration of harmonics should be on the check list for all experiments, even at lower frequencies. Furthermore, it should be one of the check items on literature review forms.

Figure Captions

A. Test of a Western Microwave CTS-24 circulator. The upper two traces show the signal without the circulator (top trace) and the signal between circulator ports 1 and 2 with the circulator in the system. The bottom trace shows the reverse signal (from ports 2 to 1). The results show at least 20 dB of isolation in the reverse direction.

B. Spectrum analyzer display of the harmonics in the 4-6 GHz band from a 2-4 GHz swept signal. (The spectrum analyzer has a YIG preselector.) The top trace is without a circulator in the circuit and the sweeper output unleveled; the green trace (middle) is without a circulator; and the bottom trace is with the sweeper leveled and a circulator present. Note that leveling the solid-state sweeper affects the harmonics and the circulator attenuates the harmonics (which are out of band for the circulator.)

C. Spectrum analyzer display of the harmonics in the 6-8 GHz band from a 2-4 GHz swept signal. The top trace is without a circulator; the bottom trace is with a circulator. A section of "C"-band waveguide, which acts as a high-pass filter ($f_c \approx 4.3$ GHz), is included in the system to show that the harmonics are real and not a spurious response of the spectrum analyzer. Note: Again the harmonics are reduced by the circulator.

D. Spectrum analyzer display of the harmonics in the 8-10 GHz band from a swept 2-4 GHz signal. The top trace is without a circulator; the bottom trace is with a circulator. A section of C-band waveguide is included in the system. There may be overlap of the harmonics, e.g., 3rd and 4th.

E. Spectrum analyzer display of the transmission through back-to-back S-band (2.6 - 3.95 GHz; $f_c = 2.08$ GHz) waveguide-to-coax transducers. The sweep frequency is 4-6 GHz. The top trace is straight through (without the adapters in the system); the bottom trace is the signal through the transducers. Note the presence of cutoff resonances for the various modes — sometimes with significant loss.

F. Spectrum analyzer display of the transmission through back-to-back S-band waveguide-to-coax transducers. The sweep frequency is 6-8 GHz. The top trace is straight through (without the adapters in the system); the middle trace is the signal through the transducers (unleveled); and the bottom trace is the leveled signal through the transducers. Note the significant loss of the cutoff resonances for the various modes.

G. The 2-4 GHz performance of an S-band waveguide attenuator. The sweeper was not leveled and so the traces are not flat. The top trace is with 0 dB attenuation; each successive trace corresponds to a 10 dB increase in the attenuator setting. A circulator is included in the system.

H. The 4-6 GHz performance of an S-band waveguide attenuator. The sweeper was not leveled. The top trace is with 0 dB attenuation; each successive trace corresponds to a 10 dB increase in the attenuator setting. A circulator is included in the system. Note that the attenuator still works even though higher order modes can propagate roughly above 4.4 GHz.

I. The 6-8 GHz performance of an S-band waveguide attenuator. The sweeper was not leveled. The top trace is with 0 dB attenuation; each successive trace corresponds to a 10 dB increase in the attenuator setting. A circulator is included in the system. Note that the attenuator still works but with decreased dynamic range.

J. The same as in the previous figure but with the waveguide-to-coax transducers displaced approximately 0.5 cm along the long axis of the 7.2 X 3.4 cm waveguide. The attenuator still works at many frequencies but collapses at others, e.g., around 6.8 GHz. The explanation is that the misalignment of the transducers helps to excite the TE_{20} mode which may not be affected by the attenuator.

K. Attenuator performance with the axes of each waveguide-to-coax transducer aligned 45° to the corresponding axes of the attenuator waveguide. Even though substantial TE_{01} mode is being excited above 4.4 GHz, the attenuator appears to function well at 2 - 4 GHz.

L. Attenuator performance from 4-6 GHz with the axes of each waveguide-to-coax transducer aligned 45° to the corresponding axes of the attenuator waveguide. A broad "window" is observed above 5 GHz where the variable action of the attenuator disappears. The transmission is reasonably high considering the losses in the feeds and the waveguide-to-coax filtering action. It shows that variable attenuators can be defeated at higher frequencies due to higher modes. The effectiveness of a simple vane (or "flap") attenuator would be decreased if TE_{20} or TE_{01} modes are excited.

M. Attenuator performance from 6-8 GHz with the axes of each waveguide-to-coax transducer aligned 45° to the corresponding axes of the attenuator waveguide. Here the dramatic collapse of the variable attenuation can be seen, e.g., little loss at 7.15 GHz but much more at 7.13 of 7.17 GHz and similar behavior at 7.76 GHz..

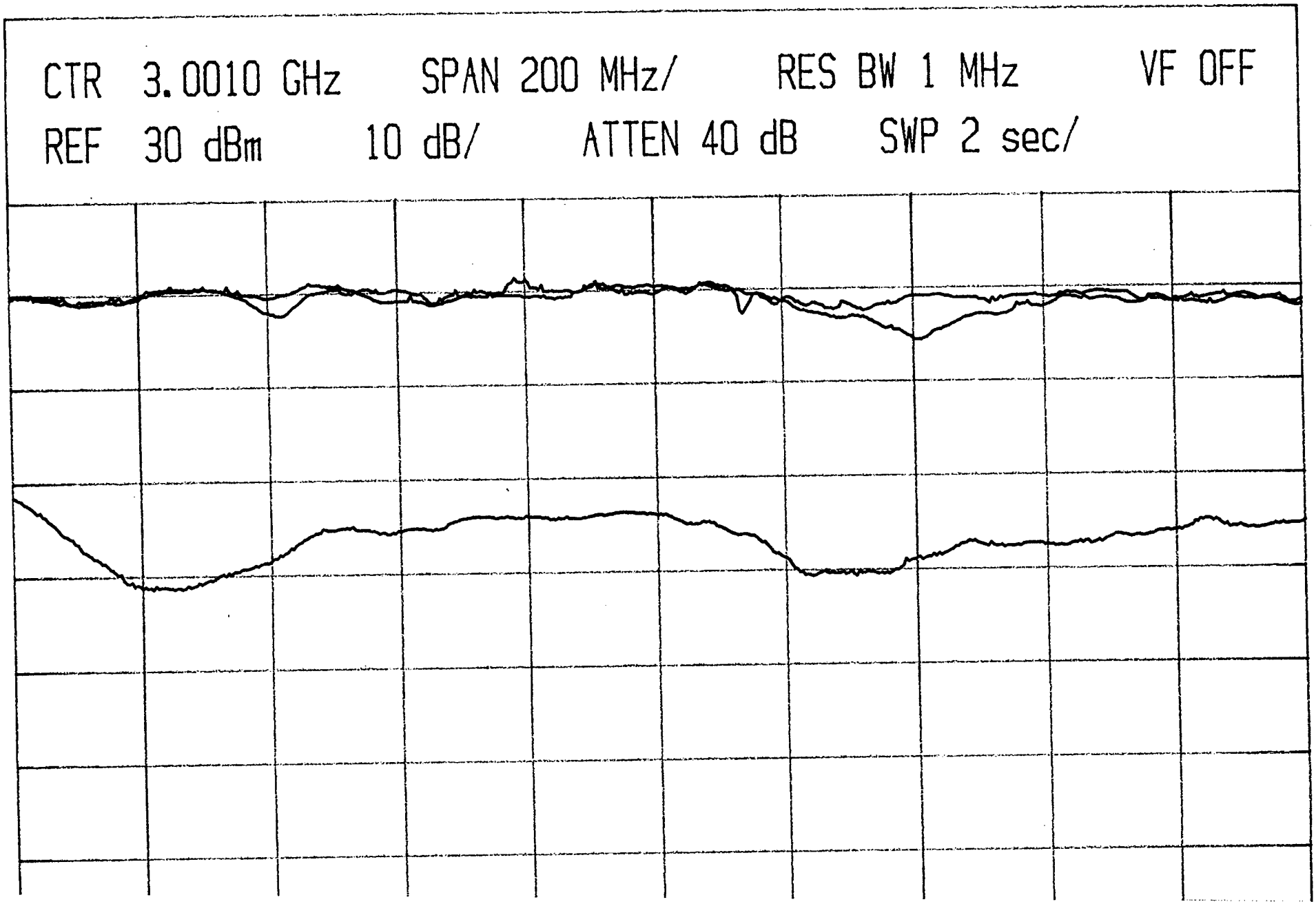

A. Test of a Western Microwave CTS-24 circulator.

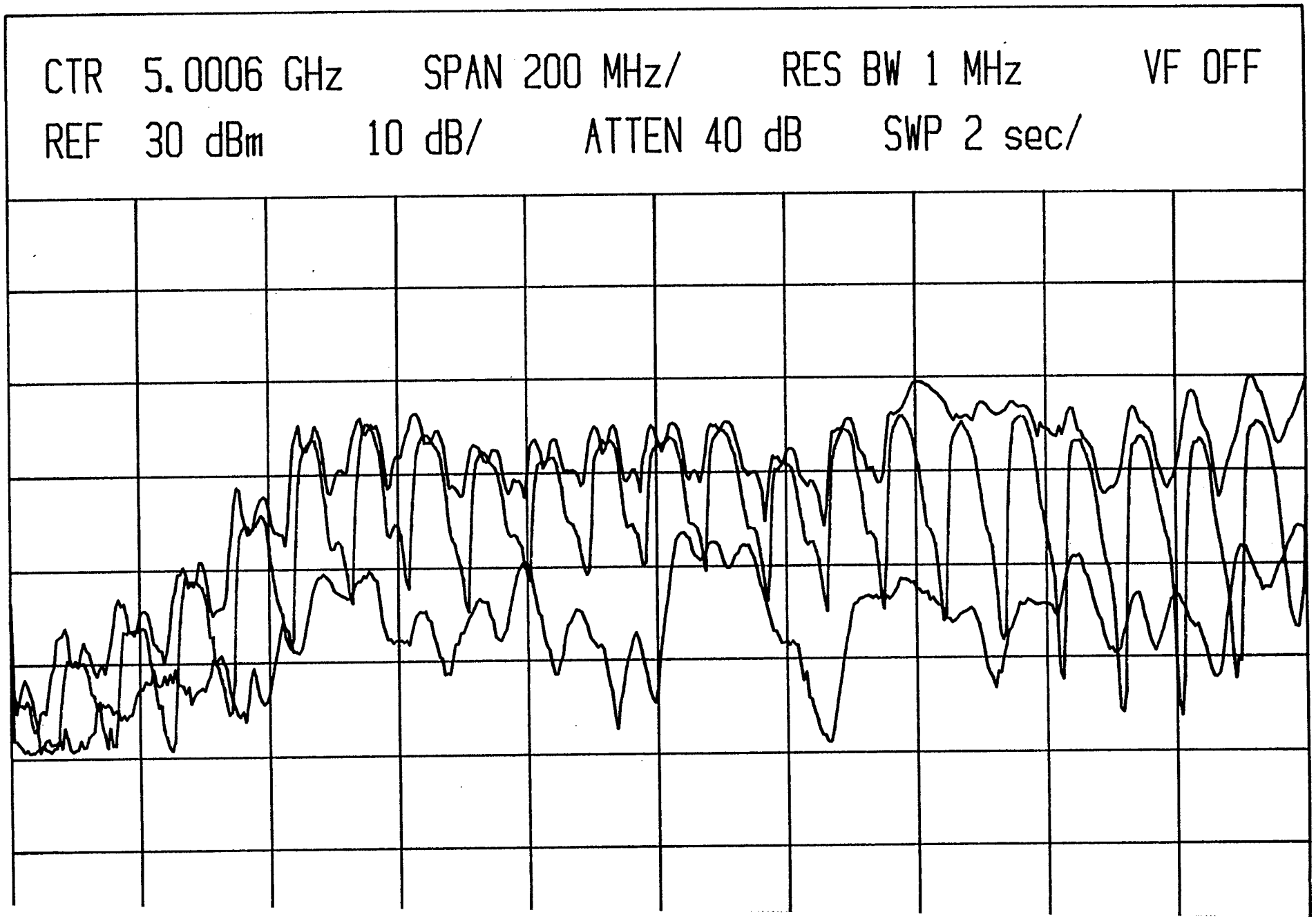

B. Spectrum analyzer (which has a YIG preselector) display of the harmonics in the 4-6 GHz band from a 2-4 GHz swept signal.

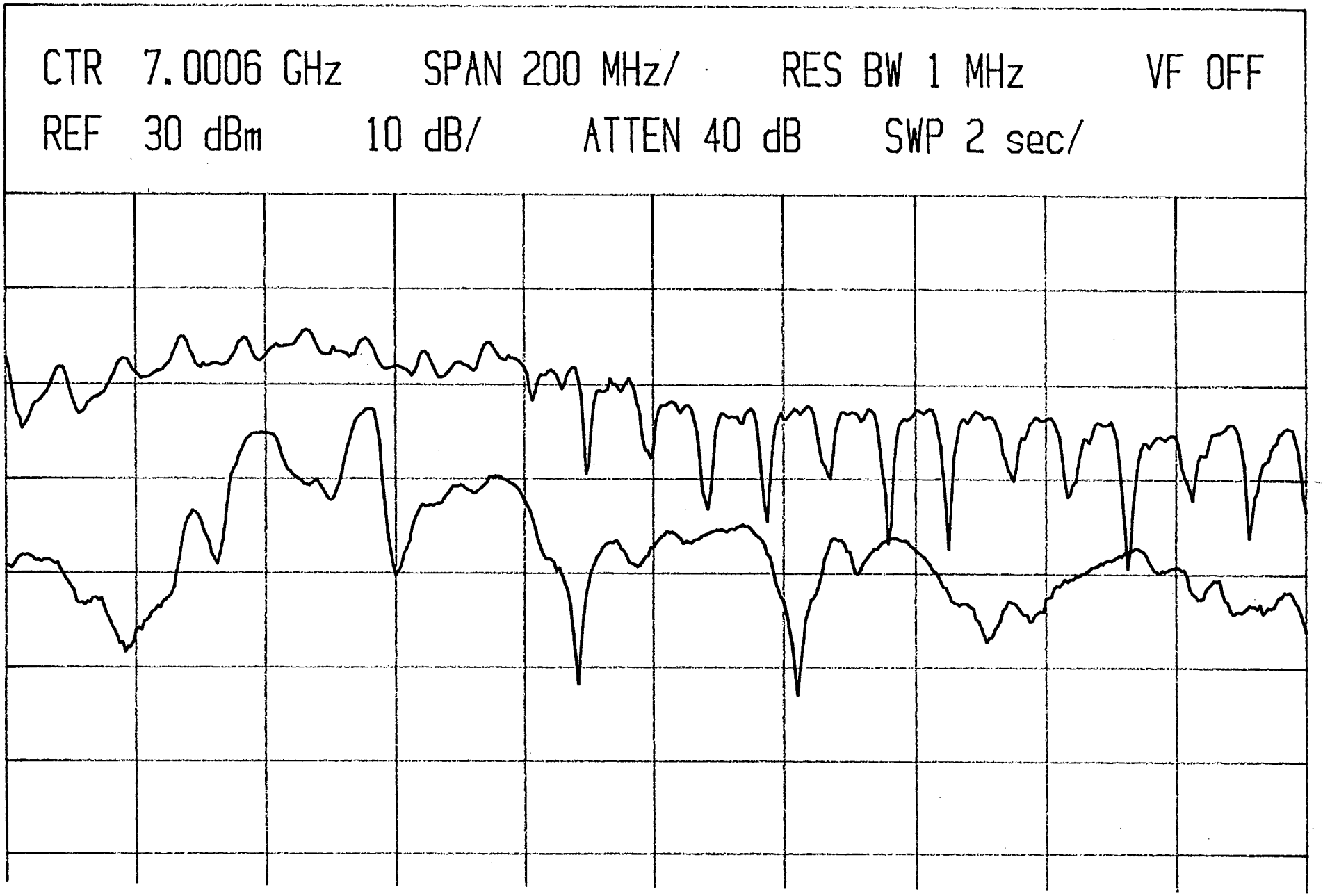

C. Spectrum analyzer display of the harmonics in the 6-8 GHz band from a 2-4 GHz swept signal.

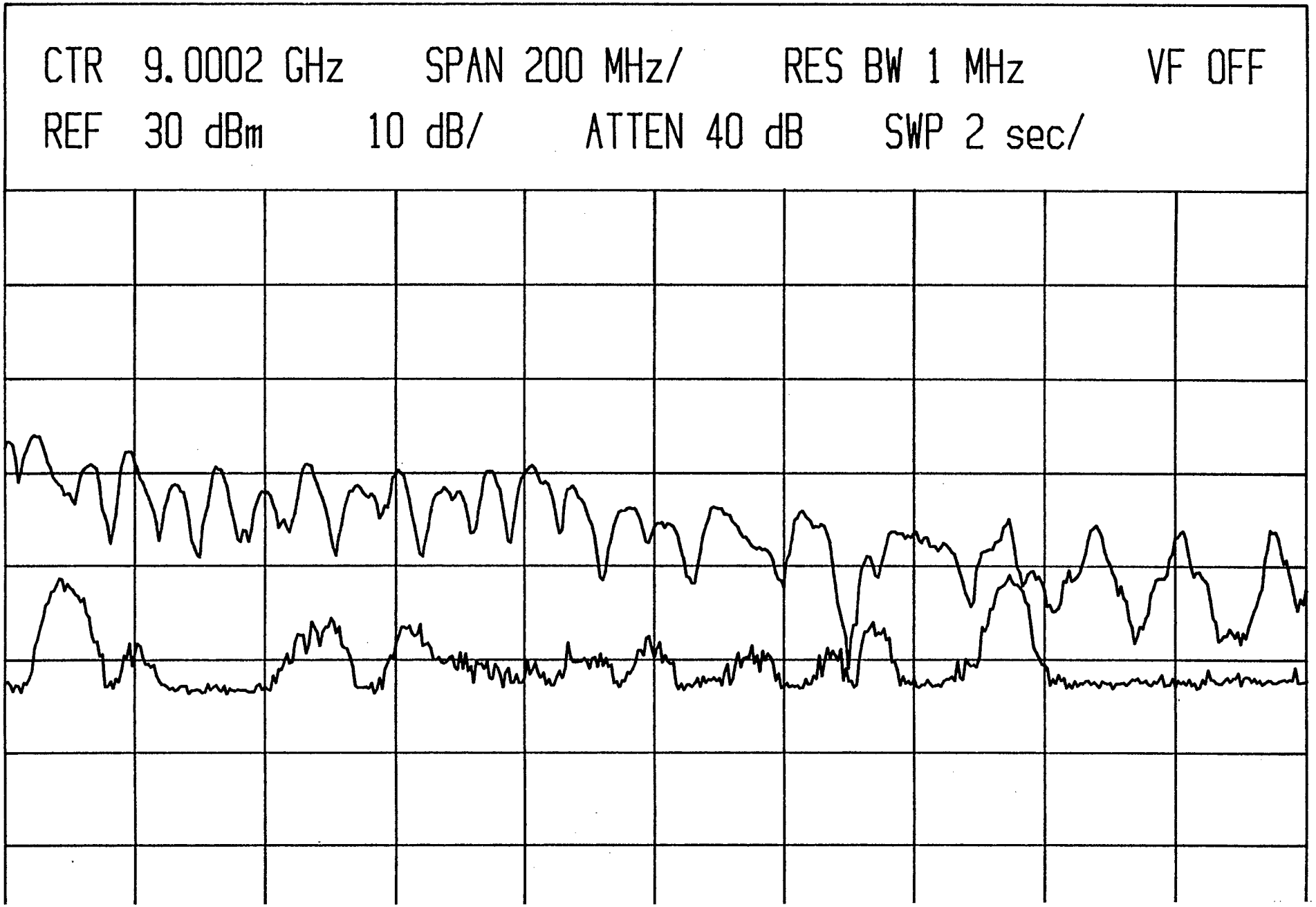

D. Spectrum analyzer display of the harmonics in the 8-10 GHz band from a swept 2-4 GHz signal.

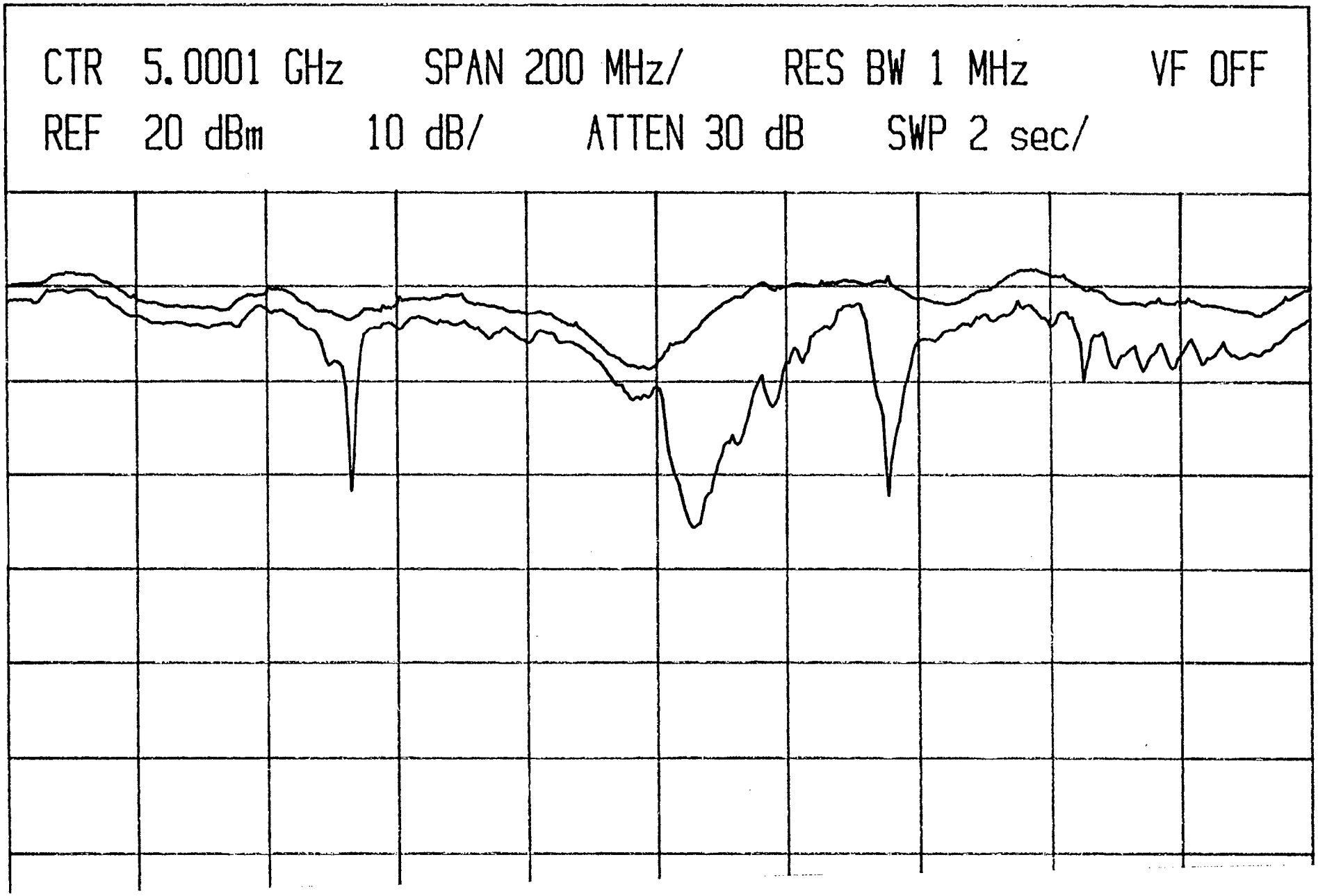

E. Spectrum analyzer display of the transmission through back-to-back S-band waveguide-to-coaxial transducers.

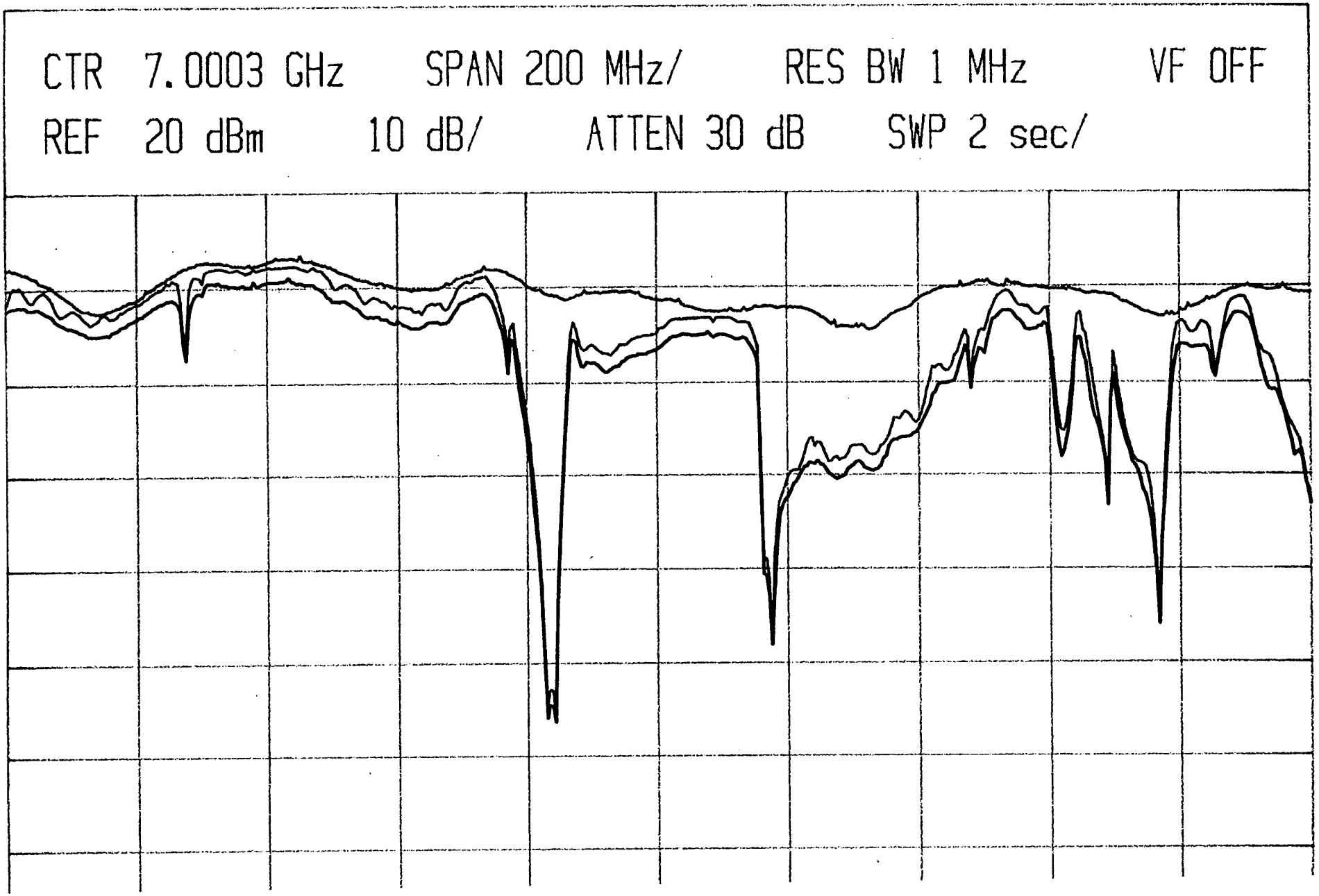

F. Spectrum analyzer display of the transmission through back-to-back S-band waveguide-to-coax transducers.

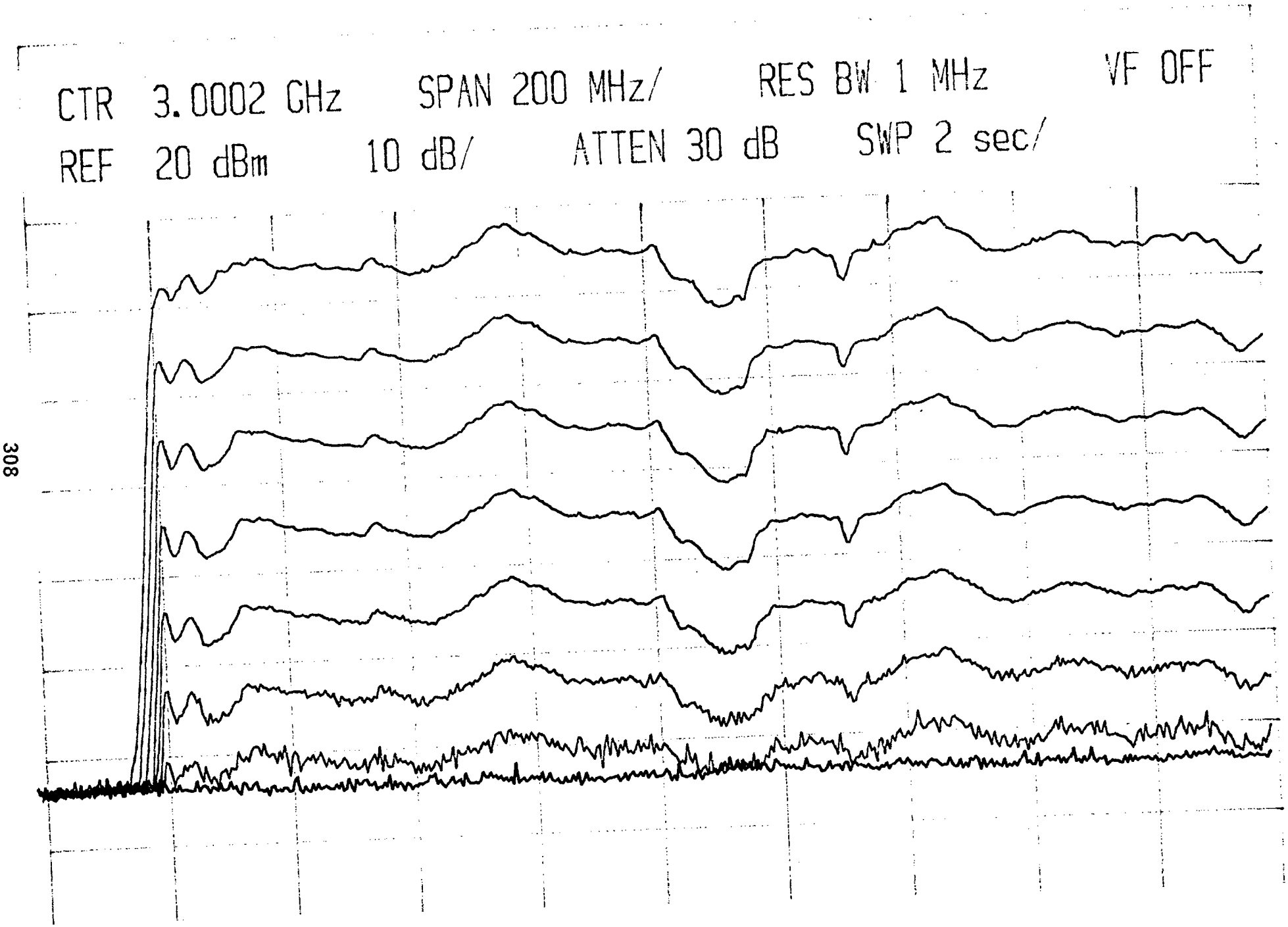

G. The 2-4 GHz performance of an S-band waveguide attenuator.

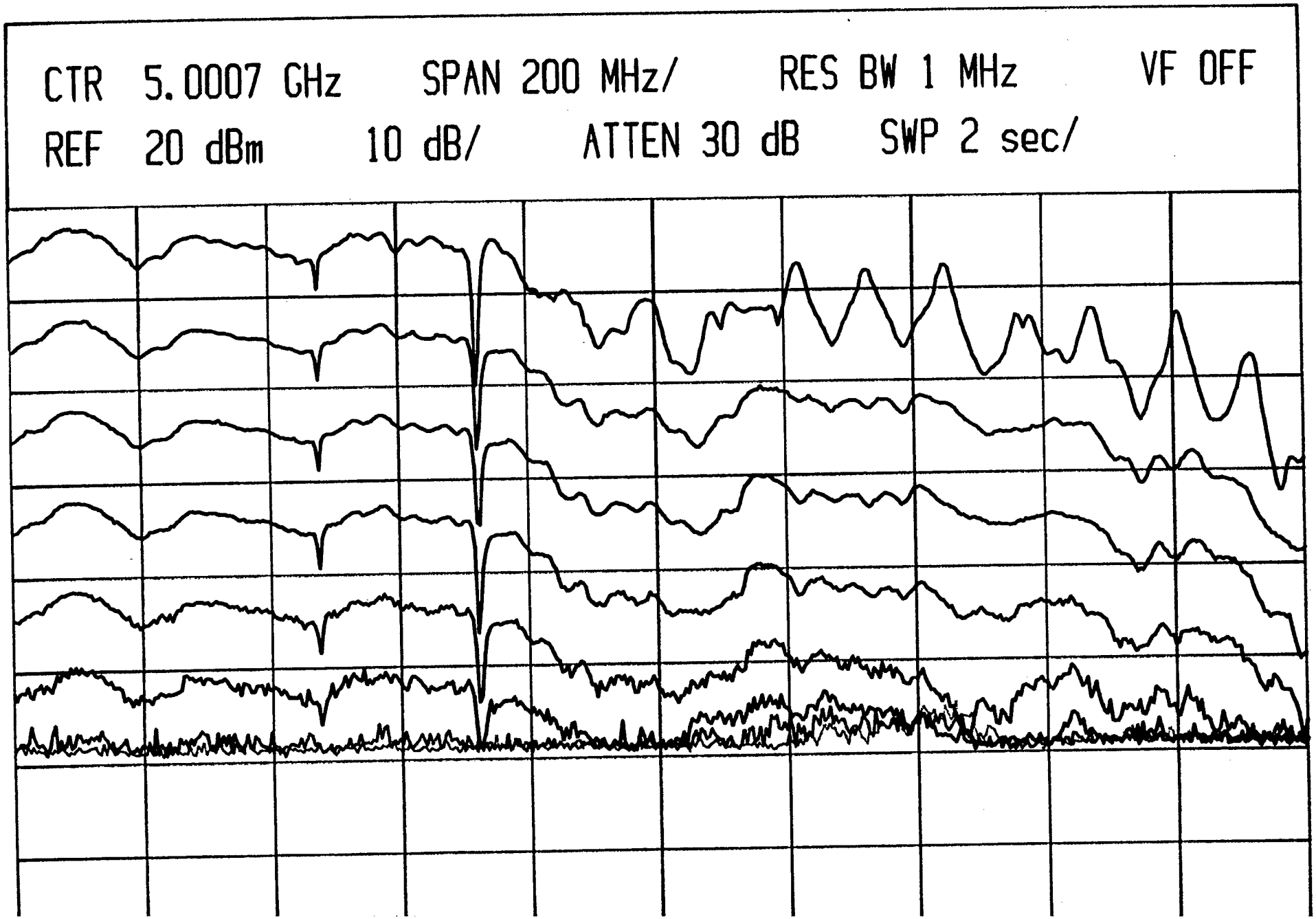

H. The 4-6 GHz performance of an S-band waveguide attenuator.

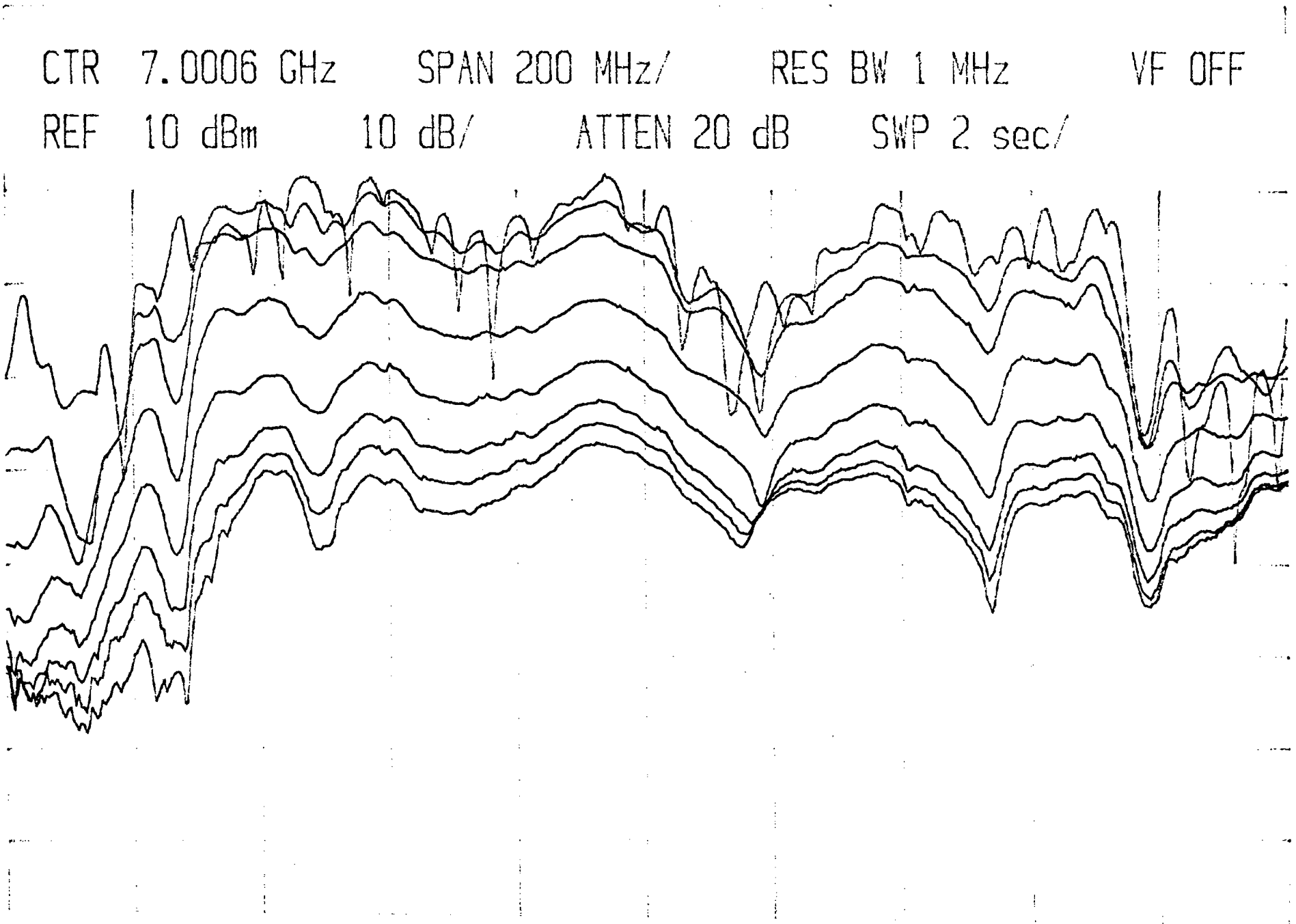

I. **The 6-8 GHz performance of an S-band waveguide attenuator.**

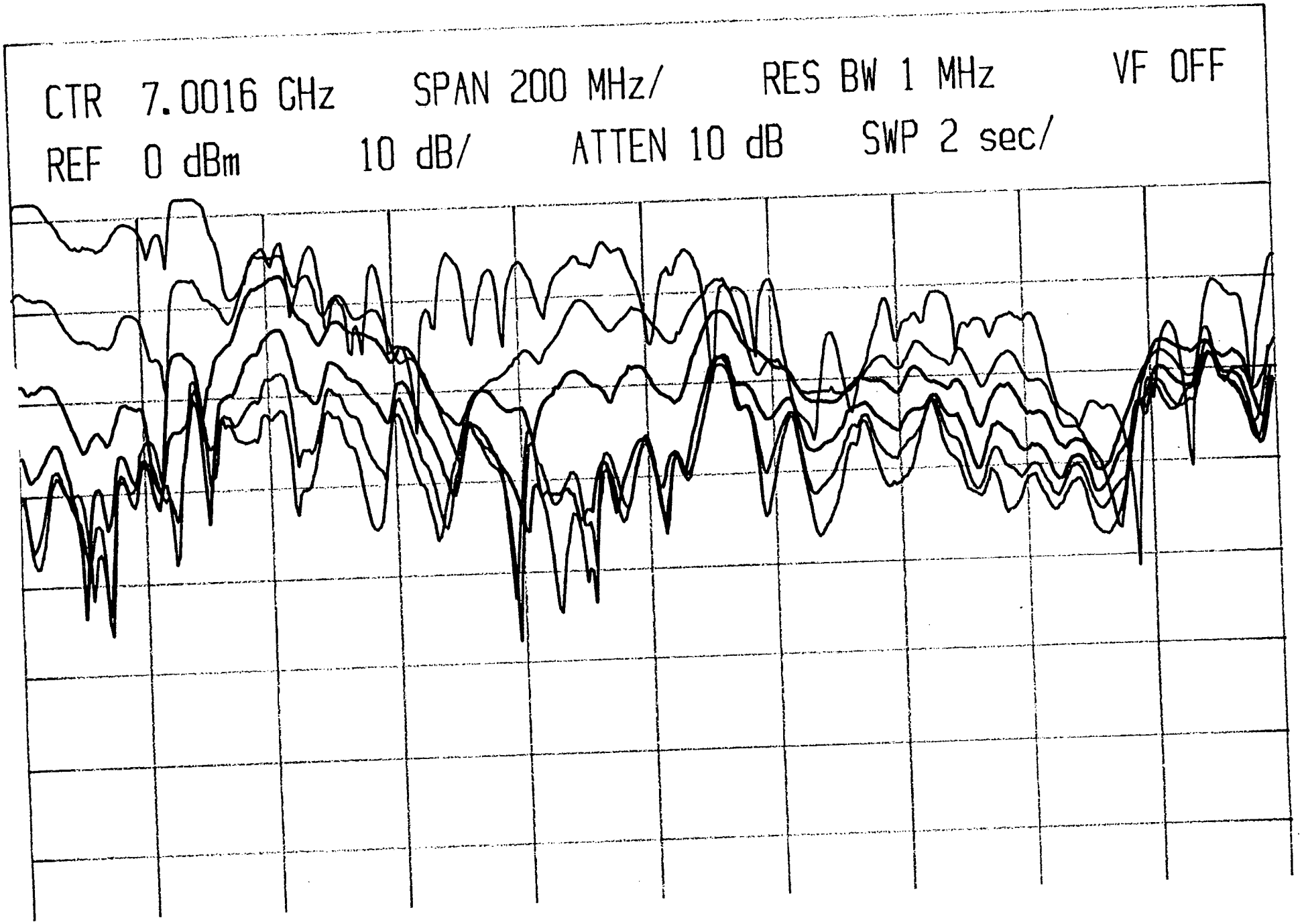

J. The same as in the previous figure but with the waveguide-to-coax transducers displaced approximately 0.5 cm along the long axis of the 7.2 X 3.4 cm waveguide.

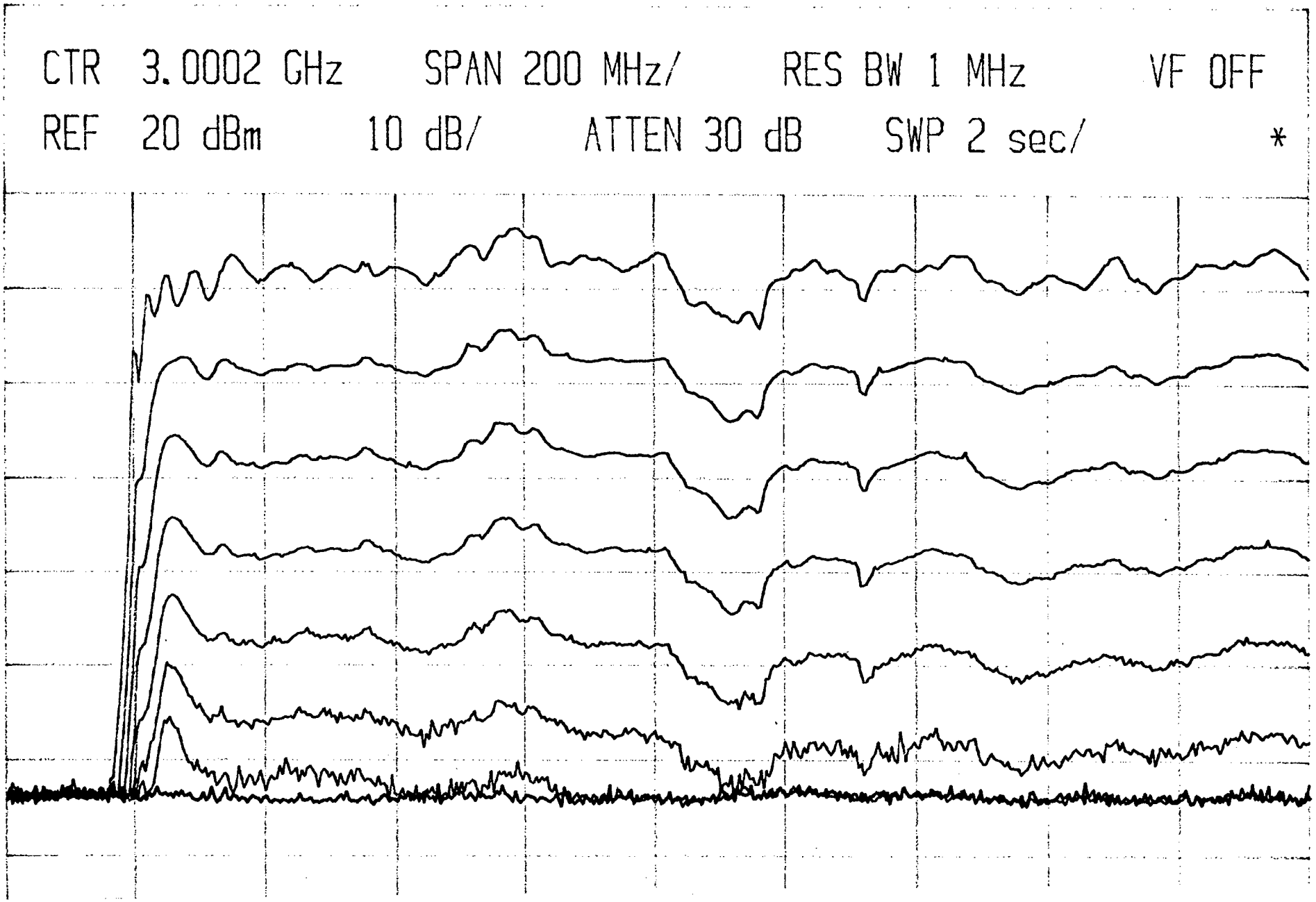

K. Attenuator performance with the axis of each waveguide-to-coax transducer aligned 45° to the corresponding axis of the attenuator waveguide.

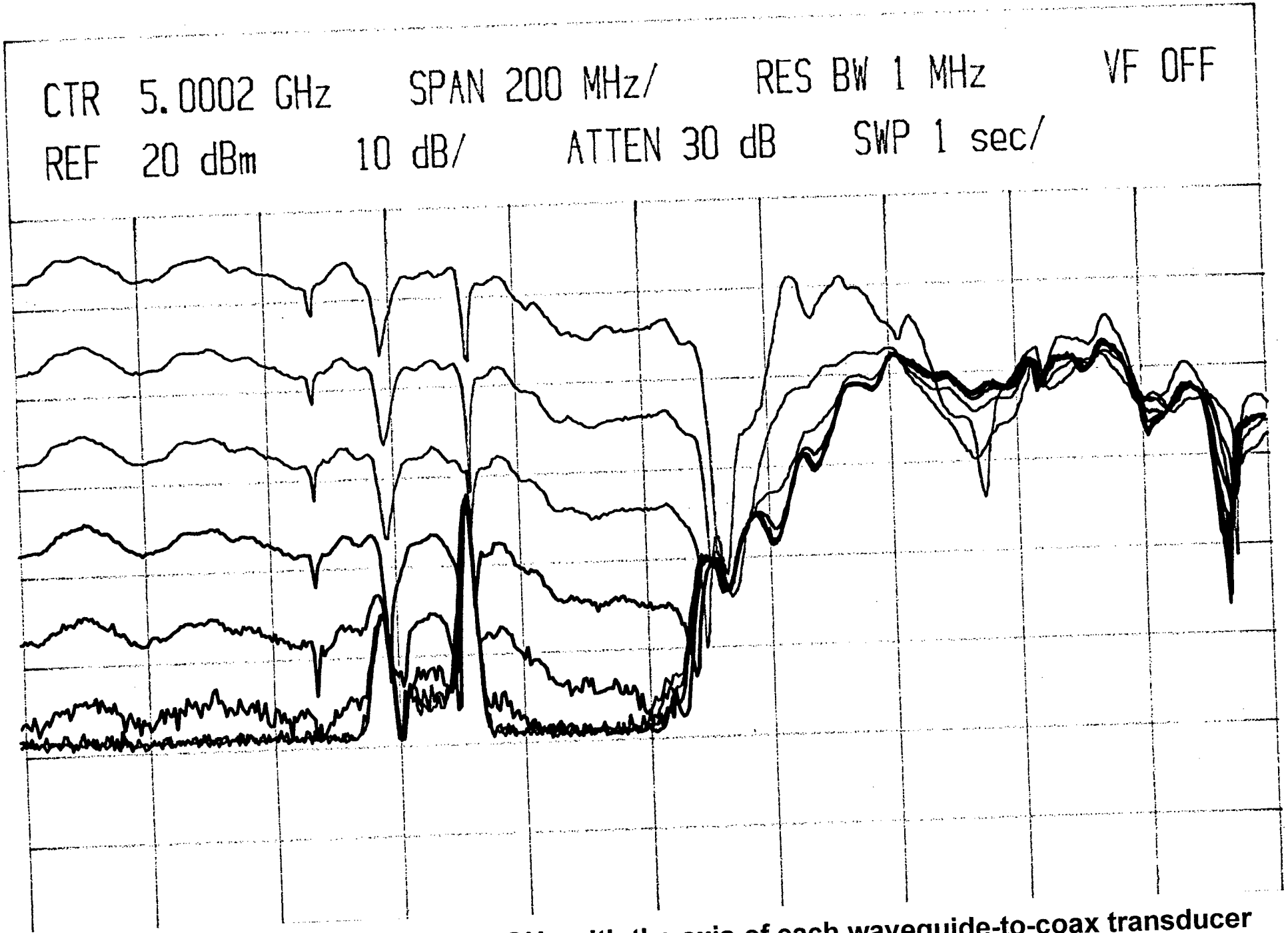

L. Attenuator performance from 4-6 GHz with the axis of each waveguide-to-coax transducer aligned 45° to the corresponding axis of the attenuator waveguide.

(M)

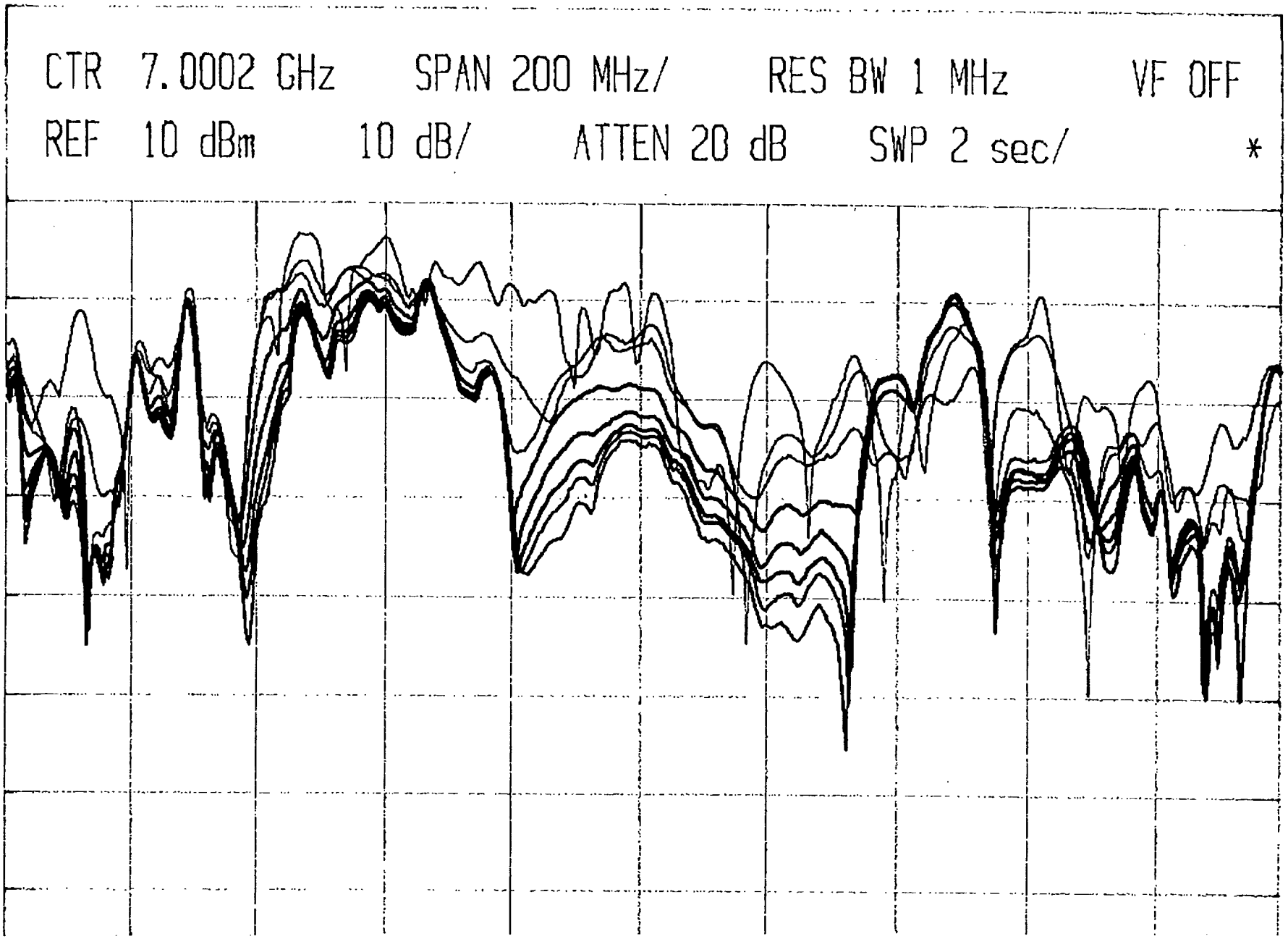

M. Attenuator performance from 6-8 GHz with the axis of each waveguide-to-coax transducer aligned 45° to the corresponding axis of the attenuator waveguide.

Infrared Lasers & Millimeter Waves
Workshop
The Links Between Microwaves
& Laser Optics

21 Jan 1997 - 22 Jan 1997

SECTION V:

THERMAL MODELS OF HEATING AND DAMAGE

Bioelectromagnetics 18:578–583 (1996)

A Thermal Model for Human Thresholds of Microwave-Evoked Warmth Sensations

Pere J. Riu,[1] Kenneth R. Foster,[2]* Dennis W. Blick,[3] and Eleanor R. Adair[4]

[1]*Departament d'Enginyeria Electrònica, Universitat Politècnica de Catalunya, Barcelona, Spain*

[2]*Department of Bioengineering. University of Pennsylvania, Philadelphia Pennsylvania*

[3]*Systems Research Laboratories, Brooks Air Force Base, Texas*

[4]*Radiofrequency Radiation Division, Occupational and Environmental Health Directorate, USAF Armstrong Laboratory, Brooks Air Force Base, Texas*

Human thresholds for skin sensations of warmth were measured at frequencies from 2.45 to 94 GHz. By solving the one-dimensional bioheat equation, we calculated the temperature increase at the skin surface or at a depth of 175 μm at incident power levels corresponding to the observed thresholds. The thermal analysis suggests that the thresholds correspond to a localized temperature increase of about 0.07 °C at and near the surface of the skin. We also found that, even at the highest frequency of irradiation, the depth at which the temperature receptors are located is not a relevant parameter, as long as it is within 0.3 mm of the surface. Over the time range of the simulation, the results of the thermal model are insensitive to blood flow, but sensitive to thermal conduction; and this sensitivity increases strongly with frequency. We conclude with an analysis of the effect of thermal conduction on surface temperature rise, which becomes a dominant factor at microwave frequencies over 10 GHz. *Bioelectromagnetics 18:578-583, 1997.*

Key words: warmth threshold; microwaves; bioheat equation; skin sensation

INTRODUCTION

Numerous attempts have been made to infer the location and functional properties of warmth receptors in the skin from psychophysical data for the threshold of warmth [e.g., Hendler and Hardy, 1960; Eijkman and Vendrik, 1961; Hendler et al., 1963; Hendler, 1968; Stevens et al., 1973]. Most of these attempts have been limited by their restriction of the radiation studied to the infrared and/or one or two microwave frequencies. Modeling efforts, based on physical and physiological principles, have generated three general hypotheses of the adequate proximal stimulus for cutaneous warmth sensation: (1) to reach threshold, the stimulus must produce a fixed increase in temperature (ΔT) in the vicinity of receptors located 150–200 μm below the skin surface [Hendler and Hardy, 1960], (2) a stimulus reaches threshold when it produces a fixed difference in temperature between two subcutaneous layers located about 200 and 1000 μm deep [Hendler et al., 1963], and (3) a stimulus produces a threshold sensation when ΔT at the receptor layer reaches a level that varies with the concurrent level of adaptation [Eijkman and Vendrik, 1961]. To date, the most appropriate among these three hypotheses, or perhaps others, has not been determined.

Recent measurements [Blick et al., 1997] let us reexamine and perhaps resolve this question. In this study, the threshold of human cutaneous warmth sensation was determined by applying 10-s duration pulses

Contract grant sponsor: Dirección General de Investigación Científica y Técnica of the Spanish Government; Contract grant sponsor: U.S. Air Force Armstrong Laboratory (Human Systems Center, Air Force Material Command); Contract grant number: F33615-90-C-0604.

This work was supported in part by the Radiofrequency Radiation Division, Occupational and Environmental Health Directorate, USAF Armstrong Laboratory (Human Systems Center, Air Force Material Command) under Contract Number F33615-90-C-0604. The views expressed are those of the authors and are not to be construed as official policy of the U.S. Air Force or of the U.S. Department of Defense.

*Correspondence to: Dr. K. R. Foster, Department of Bioengineering, University of Pennsylvania, 220 S. 33rd St., Philadelphia, PA 19104-6392. E-mail: kfoster@eniac.seas.upenn.edu

Received for review 27 December 1996; final revision received 19 March 1997

of microwave energy at the frequencies of 2.45, 7.5, 10, 35, and 94 GHz over a region of 237 cm^2 on the back of 16 male adults. The thresholds for detection of the energy decrease as the frequency increases; in other words, less incident power is needed to produce a perceptible sensation at higher frequencies. The experimental data fit a linear regression in log-log coordinates, which can be described by the following expression:

$$P_{th}\ (mW/cm^2) \approx \frac{100}{f^{0.68}} \qquad (1)$$

where P_{th} is the threshold incident power and f is the frequency (in GHz).

It is well known that the energy penetration depth in tissues decreases with frequency. Because of this effect it is expected that the temperature at the surface increases with frequency if the incident power is constant; in other words, the power required to produce the same increment in surface-temperature will decrease with frequency. Data on the field penetration depth (δ) summarized by Blick et al. [1997], however, can be fitted approximately by a power law behavior that is different from that describing sensory thresholds:

$$\delta\ (cm) \approx \frac{10}{f^{1.25}}. \qquad (2)$$

This suggests that another mechanism, probably related to heat transport in tissue, is also significant. To investigate the properties of this mechanism, we modeled the thermal response of the irradiated tissue using the bioheat equation, to predict the temperature increase caused by an incident electromagnetic wave at the skin surface.

METHODS

The bioheat equation, assuming a constant thermal conductivity, can be written [Gao et al., 1995]:

$$\rho c_p \frac{\partial T}{\partial t} - k\nabla^2 T + V(x, t)T = Q(x, t) \qquad (3)$$

where T is the difference between the tissue temperature and the blood temperature (in kelvins), ρ is the density of the tissue (in g/cm^3), c_p is the specific heat of the tissue (in J/gK), k is the thermal conductivity (in W/cmK), V(x, t) is the blood perfusion parameter (in W/cm^3K), and Q is the power deposited in the body (in W/cm^3).

For the purposes of these calculations, the blood perfusion parameter was assumed to be constant over time and space. The power deposited in a semi-infinite body by an incident electromagnetic wave is given by:

$$Q(x, t) = \frac{2I_o\Lambda}{\delta} e^{-2x/\delta} U(t) \qquad (4)$$

where I_o is the intensity of the incident wave (W/cm^2), Λ is the power transmission coefficient between air and the tissue, δ is the field penetration depth (depth where the electric field falls by a factor of e), and U(t) is the unit step function.

Because the area of the heated skin in the experiment was large enough (237 cm^2), the bioheat equation was considered in one dimension only. The analytical solution provided by Foster et al. [1978] was used. Numerical calculations were done using Matlab (MathWorks, Natick, MA). These calculations were supplemented by direct solution of Eq. (4) using a commercial two-dimensional finite element method package (PDEase, Macsyma Inc., Arlington, MA), in part to avoid numerical difficulties in evaluating the complementary error function over certain parameter ranges in the analytical solution and in part to verify the analytical solution; the finite element solution agreed well with the analytical solution. The results shown below are for an insulated boundary condition. The temperature increases are not greatly affected if physiologically relevant heat transfer coefficients from skin to air are assumed, in part because the increase in surface temperature is small and the irradiation times are quite short.

The irradiation frequencies used in the simulation were 2.45, 7, 10, 35, and 100 GHz. They were chosen because they approximate the experimental frequencies, and also because data exist in the literature to calculate the thermal relaxation time, which is defined in the following section. The values used for these parameters, obtained from Foster and Schwan [1989], Polk, [1996], and Lin and Gandhi [1996] are summarized in Table 1.

TABLE 1. Electrical Properties of Tissue Assumed in the Model

Frequency (GHz)	Λ	δ (cm)	τ_2 (s)
2.45	0.4	2	700
7	0.4	0.6	15
10	0.45	0.4	60
35	0.5	0.07	0.9
100	0.56	0.02	0.07

*The values for the thermal parameters were taken from Gao et al. (1995) and are $k = 6 \times 10^{-3}$ W/cmK, $V = 6.7 \times 10^{-3}$ W/cm^3K, $\rho = 1$ g/cm^3, $c_p = 4$ J/gK.

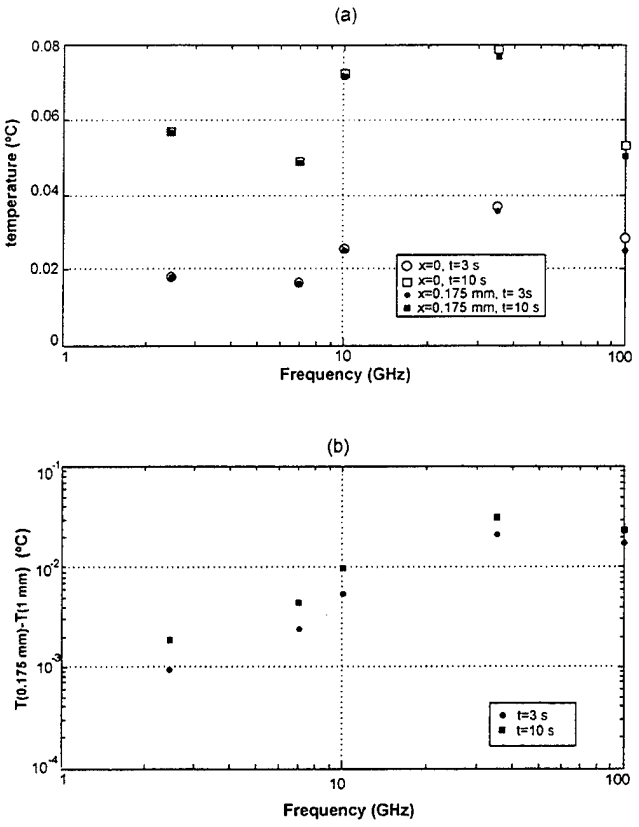

Fig. 1. (a) Calculated temperature increases at skin surface and at a depth of 0.175 mm after 3 and 10 s of irradiation at different frequencies, using the threshold values of incident power density given by Blick et al. [1997]. (b) Temperature difference between depths of 0.175 and 1 mm at different frequencies. The thresholds reported by Blick et al. were 63.1 mW/cm^2 (2.45 GHz), 7.5 mW/cm^2 (7.5 GHz), 19.6 mW/cm^2 (10 GHz), 8.8 mW/cm^2 (35 GHz) and 4.5 mW/cm^2 (94 GHz).

RESULTS

Figure 1 (a) shows the increases in temperature at the surface of the skin and at a depth of 0.175 mm, corresponding to the incident power densities at the sensory thresholds measured by Blick et al. [1997]. There is no significant difference between these two temperatures over the range of frequencies explored, either after 3 s or after 10 s of exposure. The mean temperature increases after 3 and 10 s are 0.025 and 0.062 °K, respectively.

We also calculated the difference in temperature at depths of 0.175 and 1 mm (Figure 1 (b)). In contrast to the temperature increases, these differences vary by more than an order of magnitude over the frequency range of the measurements, because of the corresponding decrease in penetration depth.

To illustrate the spatial and frequency dependence of the tissue temperature, we calculated the temperature profiles at several frequencies as a function of depth (Figure 2). At a depth of 0.25 mm, after 10 s of exposure the temperature is close (within 10%) to its value at the surface, because of the effects of heat conduction. This is true even at 100 GHz, where the penetration depth is of the order of 0.2 mm. The lack of significant temperature gradients over such short distances is consistent with the hypothesis that the threshold is correlated with a given increase in temperature, regardless of whether the thermoreceptors are located at the skin surface or at a depth of a few tenths of a millimeter.

To evaluate the sensitivity of our calculations to parameters chosen in the model, we changed the values of the thermal conductivity (k) and the blood perfusion parameter (V) in steps of one order of magnitude. The results of these calculations for the frequencies of 2.45 and 100 GHz are shown in Figure 3. It is clear that at 2.45 GHz (Figure 3 (a)), effects of heat conduction are not significant over the time scale of the measurements (10 s); at higher frequencies such effects are more pronounced.

At all frequencies, the calculated results are independent of the value of the blood perfusion parameter during the 10 s exposure (Figure 3 (b)), as expected from an analysis of the thermal time constants involved (see below). Indeed, a simple heat conduction model would have yielded essentially the same results for the present situation as the bioheat equation. We note that other thermal models for tissue describe convective heat transport by blood in terms of an "effective" thermal conductivity [Baish et al., 1986]. Such models would yield quite different thermal time constants for convective heat transport by blood than the bioheat equation.

DISCUSSION

Previous psychophysical data for warmth thresholds have been limited to stimulus wavelengths in the

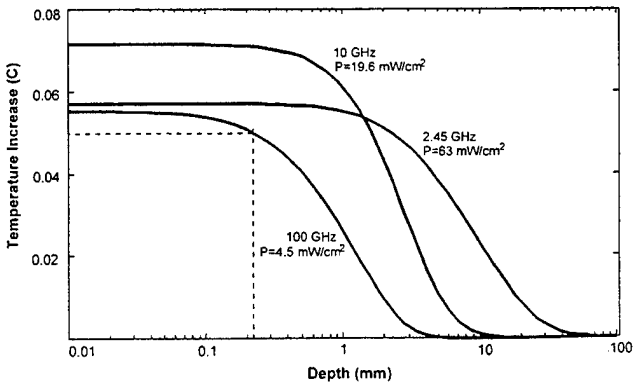

Fig. 2. Temperature profiles after 10 s of excitation at three different frequencies. The −10% decay in the 100 GHz profile is shown.

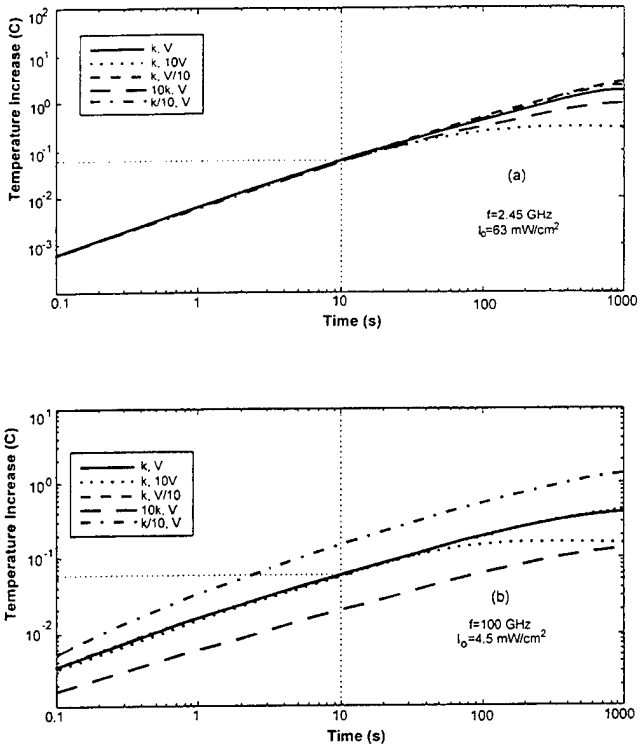

Fig. 3. Change in surface temperature with time, for different values of k and V (**a**) at 2.45 GHz (**b**) at 100 GHz. The incident power coincided with the experimental threshold [Blick et al., 1997].

infrared (IR) or, at most to one or two microwave (MW) frequencies. This has led to some controversy in the interpretation of such data.

For example, Hardy and his colleagues [Hardy and Oppel, 1937; Hendler et al., 1958; Hendler and Hardy, 1960; Hendler et al., 1963; Hendler, 1968], based on extensive experiments with infrared as well as studies at 10 GHz, concluded that ". . . a threshold sensation of warmth is elicited when the temperature of a more superficial layer of subcutaneous tissue, approximately 200 μm below the skin surface, is increased about 0.01 to 0.02 °C over the temperature of a deeper layer in the skin lying about 1000 μm below the surface" [Hendler et al., 1963, p.224].

On the other hand, Vendrik and Vos [1958], on the basis of threshold data for infrared energy and microwaves at 3 GHz, rejected the idea of a temperature gradient as the adequate stimulus and argued ". . . that a threshold sensation is obtained when the temperature of the warmth receptors is increased by a certain amount T" [op.cit, p. 443]. For the forearm skin (13 cm^2) tested by Vendrik and Vos [1958], T varied from 0.2 to 1.0 °C among several subjects. Because they used an unusual method based on response latency to determine thresholds and because the forearm skin is somewhat less sensitive than the back especially for small stimulus areas, it is not surprising that they calculated larger temperature increments at threshold than we did. Like us, when they tested the temperature difference (i.e., gradient) hypothesis, they found that no reasonable values of thermal parameters for skin would produce a large enough thermal gradient to account for the thresholds for perception of microwaves at lower frequencies (<3 GHz).

The 10-s duration of the stimulus pulses may have a significant bearing on the calculations described in this paper. There is a near-complete reciprocity between stimulus intensity and duration (called temporal summation) for the threshold at very short durations. This ceases at a "critical duration" beyond which duration no longer matters [Stevens, 1983]. Eijkman and Vendrik [1961], based on studies of temporal summation for 3 GHz microwaves, concluded that the critical duration was 3 s and that stimulus durations between 1 and 3 s gave rise to temperature increases that varied with stimulus duration. In other words, a relatively fast (time constant of 0.1-0.3 s) adaptation process influences the temperature increases of the receptors required to reach threshold. Because all of the stimuli used by Blick et al. [1997] exceeded the 3 s critical duration, this rapid adaptation phenomenon would not affect the threshold data in a way that depends on irradiation frequency. Thus, our finding of a constant temperature increase at the receptor level at the critical duration is consistent with results of Eijkman and Vendrik.

We conclude that a change in skin temperature on or very near the surface is the actual stimulus for the perception of warmth. Hardy and Bard [1974] remark on the "exquisite sensitivity" of human skin to its own temperature and add that humans are ". . . able to sense changes as small as 0.01 °C in mean skin temperature" [op. cit., p.1309]. This is not to imply that changes in ambient (air) temperature of this magnitude would be discriminated. Because of the inefficiency of convective heat exchange between air and skin, a sudden change in air temperature of this magnitude might not result in a comparable sudden change in the skin temperature [Hardy and Oppel, 1938].

The results of our model are in reasonable agreement with the hypothesis that the threshold for perception depends on skin temperature increases, using the data of Blick et al. [1997]. However, there is significant scatter (10%) in the calculated temperature increase at threshold. This may arise for several reasons. The first is the uncertainty in choosing the electrical properties of skin and superficial tissue. The values in the literature for electrical conductivity and electrical permiti-

vity often vary by 10% or more, even when provided by the same author. These parameters directly affect the calculation of the penetration depth (δ) and the transmission coefficient (Λ):

$$\Lambda = 1 - \Gamma^2; \quad \Gamma = \frac{\eta_2 - \eta_1}{\eta_2 + \eta_1}; \eta_i = \left(\frac{j\omega\mu}{\sigma_i + j\omega\varepsilon_i}\right)^{1/2} \quad (5)$$

$$\delta = \frac{1}{\omega\sqrt{\frac{\mu\varepsilon}{2}\left(1 + \left(\frac{\sigma}{\omega\varepsilon}\right)^2\right)^{1/2} - 1}} \quad (6)$$

thus directly affecting the calculations of the temperature increase. Because the dielectric data used in the present study came, in many cases, from different studies, this could be a source of variability that depends on frequency.

A second reason for scatter is the electrical nonuniformity of the tissues, which include layers of skin and subcutaneous fat. The approximation of a dielectric half space will fail, particularly at lower frequencies for which penetration depth is larger and energy is absorbed by layers of skin, subcutaneous fat, and muscle. A more careful calculation would be needed to take such frequency-dependent effects into account.

A third potential reason for the scatter may be a frequency-dependent variation in the uniformity of irradiation of the subjects' backs. The beam from the microwave antennas is somewhat nonuniform, and the beam pattern may change with frequency. This might have a small frequency-dependent effect on the thresholds for perception.

Probably the most important reason for the scatter in the results are uncertainties in measuring the sensory thresholds. The dispersion in the threshold data reported by Blick et al. [1997] is in the range of $\pm 10\%$ (standard error of the mean), which is comparable to the scatter in the present results.

The present model could be improved in several ways, including by extending it to a multi-layered slab of tissue or optimizing the choice of parameters to best fit the experimental data. Such refinements would not significantly change our conclusion about the agreement of the data with the three hypotheses discussed above. Moreover, it is not clear that the psychophysical data are sufficiently precise to warrant such efforts.

We conclude with a brief comment about the effects of thermal conduction in determining the local rise in temperature. The solution of the bioheat equation for this situation [Foster et al. 1978] yields two time constants τ_1 and τ_2 that characterize the thermal response:

$$\tau_1 = \frac{\rho C_p}{V}$$

$$\tau_2 = \frac{\rho C_p \delta^2}{4k}. \quad (7)$$

The first time constant, τ_1, is associated with heat convection due to blood perfusion and has a value of about 700 s for the parameter values given above. The second parameter, τ_2, is associated with heat conduction and ranges from 0.07 to 700 s for the microwave frequencies considered here (Table 1). Over most of this frequency range, $\tau_1 \gg \tau_2$, which means that heat conduction effects will be more pronounced than those from blood perfusion over the time periods considered in Blick's study.

Short heating times ($\ll \tau_1, \tau_2$) correspond to the transient regime in which the local temperature rise $T_{transient}$ is proportional to the local SAR:

$$T_{transient}(t) = \frac{2I_o\Lambda}{\rho C_p \delta} t \quad (8)$$

At longer times, heat transport by conduction and, still later, by blood flow becomes important. For heating times greater than τ_2, corresponding in the present study to 10 s of irradiation at frequencies above about

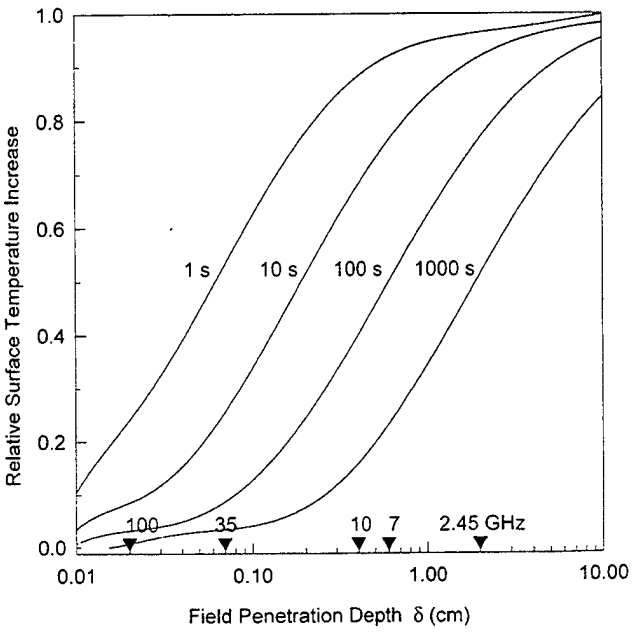

Fig. 4. Surface temperature rise (assuming zero blood flow or heat loss to the surrounding air) divided by the surface temperature rise in the absence of heat conduction (T), as a function of the field penetration depth δ. The symbols indicate the field penetration depths at the frequencies used in the study by Blick et al. [1997].

30 GHz, the surface temperature rise depends weakly on the energy penetration depth, but is limited by diffusion of heat into the tissue. Under such circumstances, the irradiation is equivalent to purely surface heating.

These results are summarized in Figure 4, which shows the surface temperature rise divided by the surface temperature rise in the absence of heat conduction as a function of the field penetration depth. The figure was calculated using the parameters given above, assuming no blood flow or heat loss to the surrounding air. The figure clearly shows the dominant effect of heat conduction in determining the surface temperature rise, even after a few seconds of irradiation, at the frequencies used by Blick et al. [1997].

CONCLUSION

A very simple model based on the one-dimensional bioheat equation with a semi-infinite uniform tissue plane was used to estimate the temperature rise at the skin surface after 10 s of microwave heating. The measured sensory thresholds corresponded to rises in skin temperature of 0.06 to 0.08 °C. If the stimulus duration had been limited to 3 s (the critical duration at which temporal summation is complete) the rise in skin temperature in the vicinity of the receptors would be 0.02 to 0.03 °C. Thermal conduction effects are clearly important in determining the rise in surface temperature over this range of irradiation frequency.

REFERENCES

Baish JW, Foster KR, Ayyaswamy PS (1986): Perfused phantom models of microwave irradiated tissue. ASME Trans Biomech Eng 108:239–245.

Blick DW, Adair ER, Hurt WD, Sherry CJ, Walters TJ, Merritt JH (1997): Thresholds of microwave-evoked warmth sensations in human skin. Bioelectromagnetics 18:403–409.

Eijkman E, Vendrik AJH (1961): Dynamic behavior of the warmth sense organ. J Exp Psychol 62:403–408.

Foster KR, Kritikos HN, Schwan HP (1978): Effect of surface cooling and blood flow on the microwave heating of tissue. IEEE Trans Biomed Eng 25:313–316.

Foster KR, Schwan HP (1989): Dielectric properties of tissues and biological materials: A critical review. CRC Crit Rev Biomed Eng 17:25–104.

Gao B, Langer S, Corry M (1995): Application of the time-dependent Green's function and Fourier transforms to the solution of the bioheat equation. Int J Hyperthermia 11:267–285.

Hardy JD, Oppel TW (1937): Studies in temperature sensation. III. The sensitivity of the body to heat and the spatial summation of the end organ responses. J Clin Invest 16:533–540.

Hardy JD, Oppel TW (1938): Studies in temperature sensation. IV. The stimulation of cold sensation by radiation. J Clin Invest 17:771–778.

Hardy JD, Bard P (1974): Body temperature regulation. In Mountcastle VB (ed): "Medical Physiology, 131st ed." V. St. Louis, MO: CV Mosby Co., pp 1305–1342.

Hendler E (1968): Cutaneous receptor response to microwave irradiation. In Hardy JD (ed): "Thermal Problems in Aerospace Medicine." Surrey: Unwin Ltd., pp 149–161.

Hendler E, Hardy JD (1960): Infrared and microwave effects on skin heating and temperature sensation. IRE Trans Med Electron ME-7:143–152.

Hendler E, Crosbie R, Hardy JD (1958): Measurement of heating of the skin during exposure to infrared radiation. J Appl Physiol 12:177–185.

Hendler E, Hardy JD, Murgatroyd D (1963): Skin heating and temperature sensation produced by infrared and microwave irradiation. In Herzfeld CM (ed): "Temperature: Its Measurement and Control in Science and Industry." New York: Reinhold, pp 211.

Lin JC, Gandhi OP (1996): Computational methods for predicting field intensity. In Polk C, Postow E (eds): "Handbook of Biological Effects of Electromagnetic Fields." Boca Raton, Florida: CRC Press Inc., pp 337–402.

Polk C (1996): Introduction to the Handbook of Biological Effects of Electromagnetic Fields. Boca Raton, Florida: CRC Press Inc.

Stevens JC (1983): Thermal sensation: Infrared and microwaves. In Adair ER (ed): "Microwaves and Thermoregulation." New York: Academic Press, pp 191–201.

Stevens JC, Okulicz WC, Marks LE (1973): Temporal summation at the warmth threshold. Percept Psychophys 14:307–312.

Vendrik AJH, Vos JJ (1958): Comparison of the stimulation of the warmth sense organ by microwave and infrared. J Appl Physiol 13:435-444.

Thermal Models of IR Laser Effects, R. L. McCally[1,2], R. A. Farrell[1,2], C. B. Bargeron[1] and W. R. Green[2], The Johns Hopkins Univertity University Applied Physics Laboratory[1] and The Wilmer Eye Institute[2]

Infrared radiation is absorbed in various depths of the cornea depending on the radiation wavelength. The concomitant temperature increase, which can cause cellular injury, depends on the absorption coefficient, the laser energy density or irradiance and the exposure duration. Damage thresholds for single- and multiple-pulse exposures are discussed in terms of a modified critical temperature model, the damage integral model, and other empirical correlations. We also discuss a simple physical model (i.e., non-empirical) which is appropriate for radiation having very small absorption depths. The model assumes damage is the result of an endothermic phase transition which occurs at temperature T_c and that energy density Q_c is absorbed in the phase transition. We demonstrate that this model accurately correlates single-pulse thresholds for CO_2 laser exposures having durations from 0.001 to 10 seconds with physically reasonable choices for the parameters T_c and Q_c.

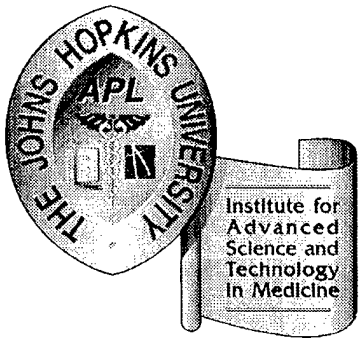

Thermal Models of IR Laser Effects

R. L. McCally [1,2]

Collaborators

R.A. Farrell [1,2], C. B. Bargeron [1] and W. R. Green [2]

[1] The Johns Hopkins University Applied Physics Laboratory

[2] The Wilmer Eye Institute

Support: USAMRMC Contract DSAMD17-96-C-6005

Cornea Cross Section

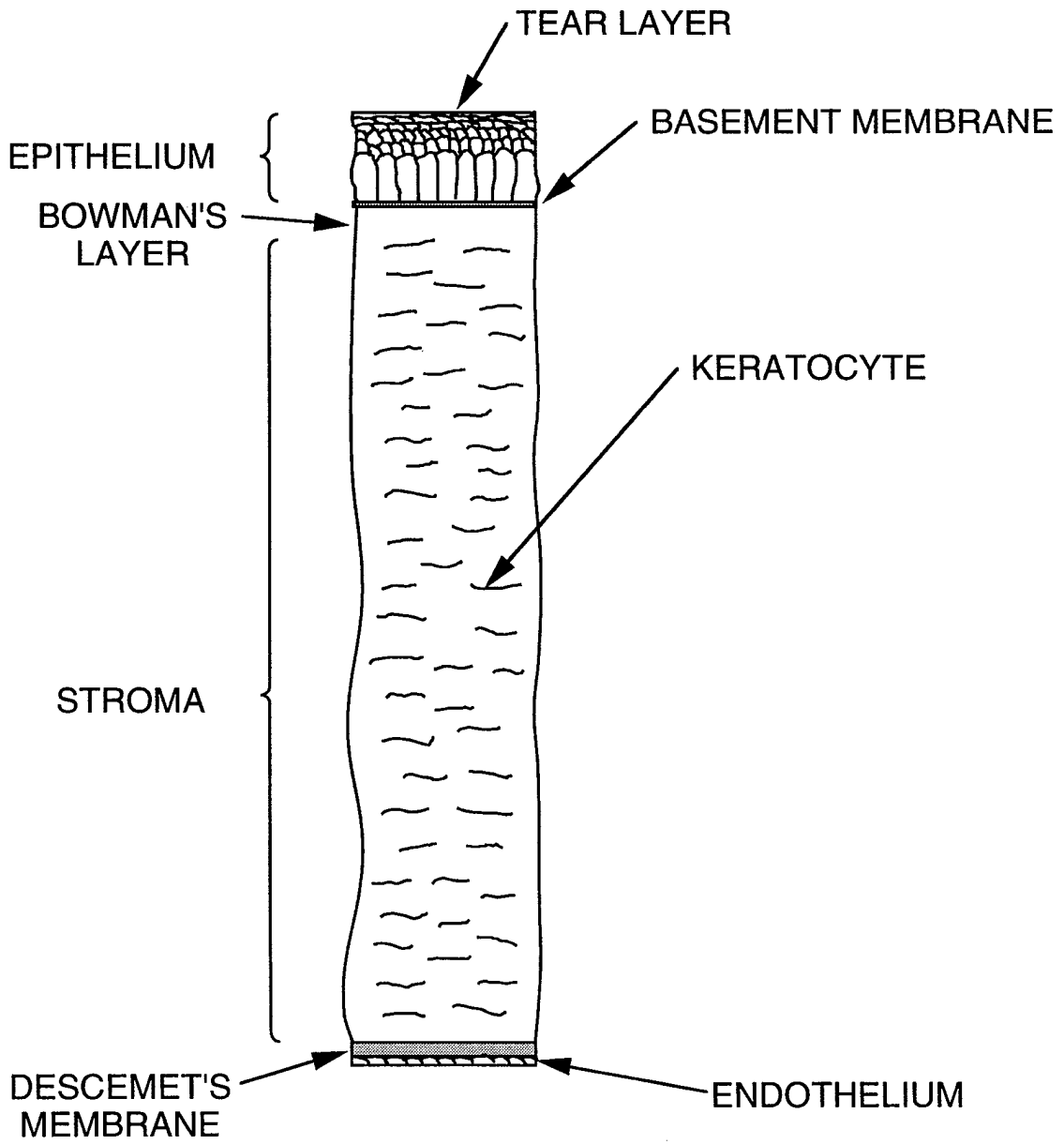

INFRARED LASER ABSORPTION

- Radiation is absorbed by cornea's water.
- Absorption follows Beer's law: $I(z) = I_0 \, exp\,[-\alpha(\lambda)z]$.
- At $\lambda = 10.6$ μm (CO_2 radiation) the absorption length $1/\alpha = 10.5$ μm. (Thus 98% of radiation would be absorbed in a 40 μm thick epithelium.)

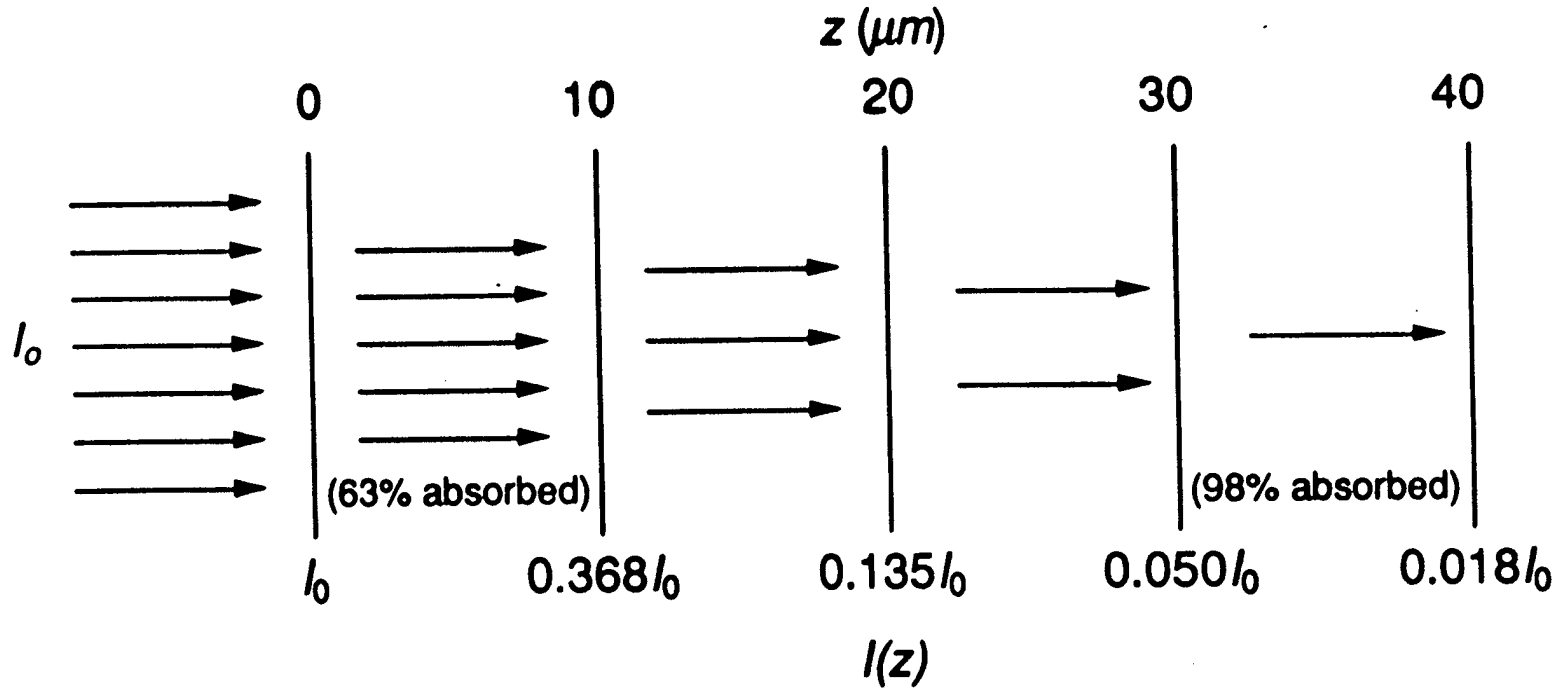

Beam Characteristics

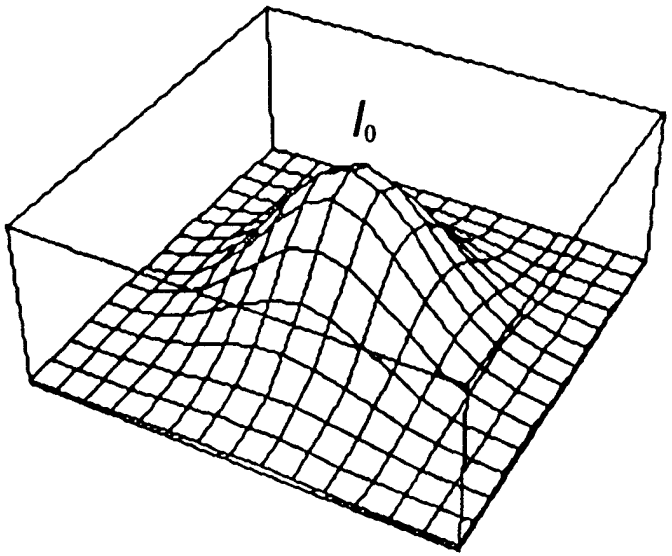

Gaussian Beam Profile (TEM_{00})

$$I = I_0 \exp(-r/r_{1/e})$$

For a Gaussian Beam $I_0 = P / A_{1/e}$, in which $A_{1/e}$ is the area inside the $1/e$ radius, $r_{1/e}$

In an experiment P and $r_{1/e}$ are measured to compute I_0, or $ED = I_0 \tau$.

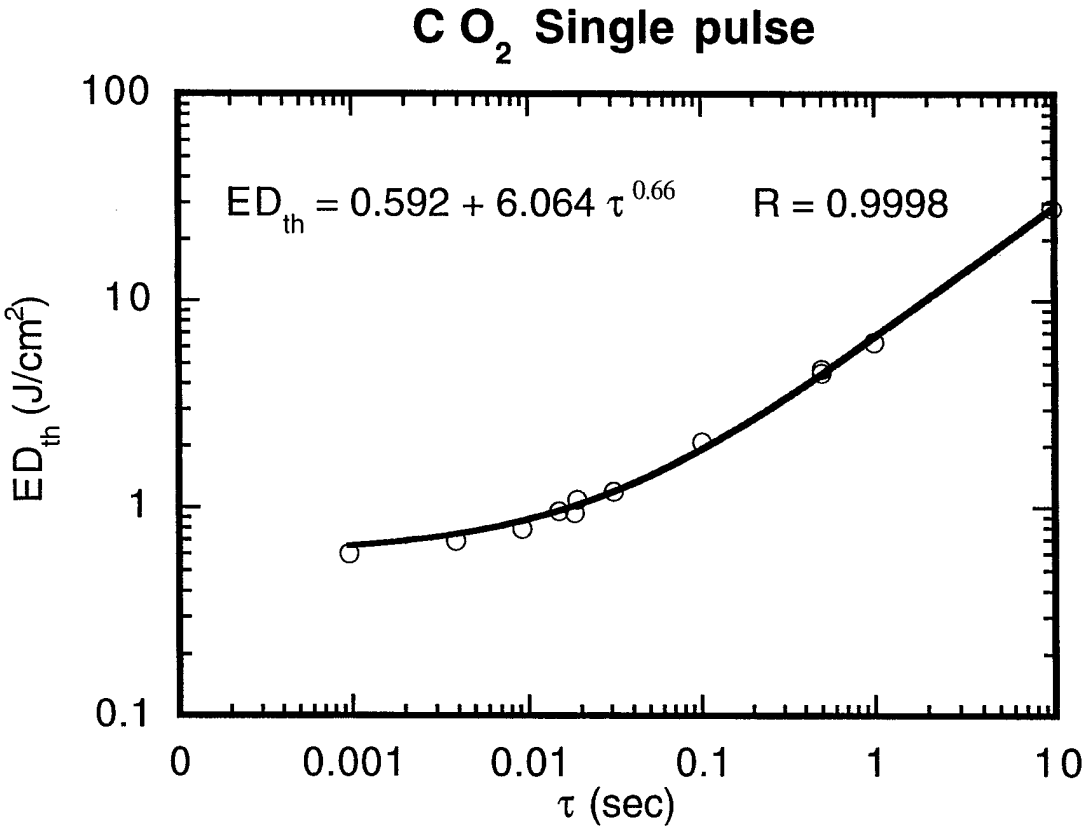
C O2 Single pulse
ED_th = 0.592 + 6.064 τ 0.66
R = 0.9998
ED_th (J/cm2)
100
10
1
0.1
0
0.001
0.01
0.1
1
10
τ (sec)

Single Pulse Damage Thresholds

CO_2 Laser

I_0 (W/cm^2)	τ (sec)	ΔT_{max} (°C)*
624	0.00096	53.9
177	0.0039	47.0
86.2	**0.0092**	**41.4**
64.3	**0.0150**	**42.2**
51.1	**0.0185**	**38.1**
57.2	**0.0191**	**43.6**
38.8	**0.0309**	**39.5**
20.4	**0.101**	**39.5**
8.99	**0.498**	**37.9**
9.29	**0.500**	**41.0**
6.46	**0.977**	**38.3**
2.89	9.730	34.7

Tm:YAG Laser

64.1	0.082	42.4
36.0	0.235	48.4
11.5	4.28	42.0

* Temperature rises calculated on beam axis 10 μm beneath the tear surface.

CO_2 Laser Exposures

For exposures between ~10 ms and ~1 sec (shaded) the temperature rise is essentially constant (empirical **critical temperature damage model)** with

$$\Delta T_{max} = 42 \pm 2 \text{ C}.$$

Variation over entire range leads to an empirical **modified critical temperature model**:

$$CPT = 72\tau^{-0.02} \text{ C}.$$

Data can also be correlated by a physical model based on an endothermic phase transition.

Tm:YAG Laser Exposures

Data also are correlated by a **critical temperature** model with

$$\Delta T_{max} = 44 \pm 4 \text{ C}.$$

Modified Critical Temperature Model
CO_2 Single pulse

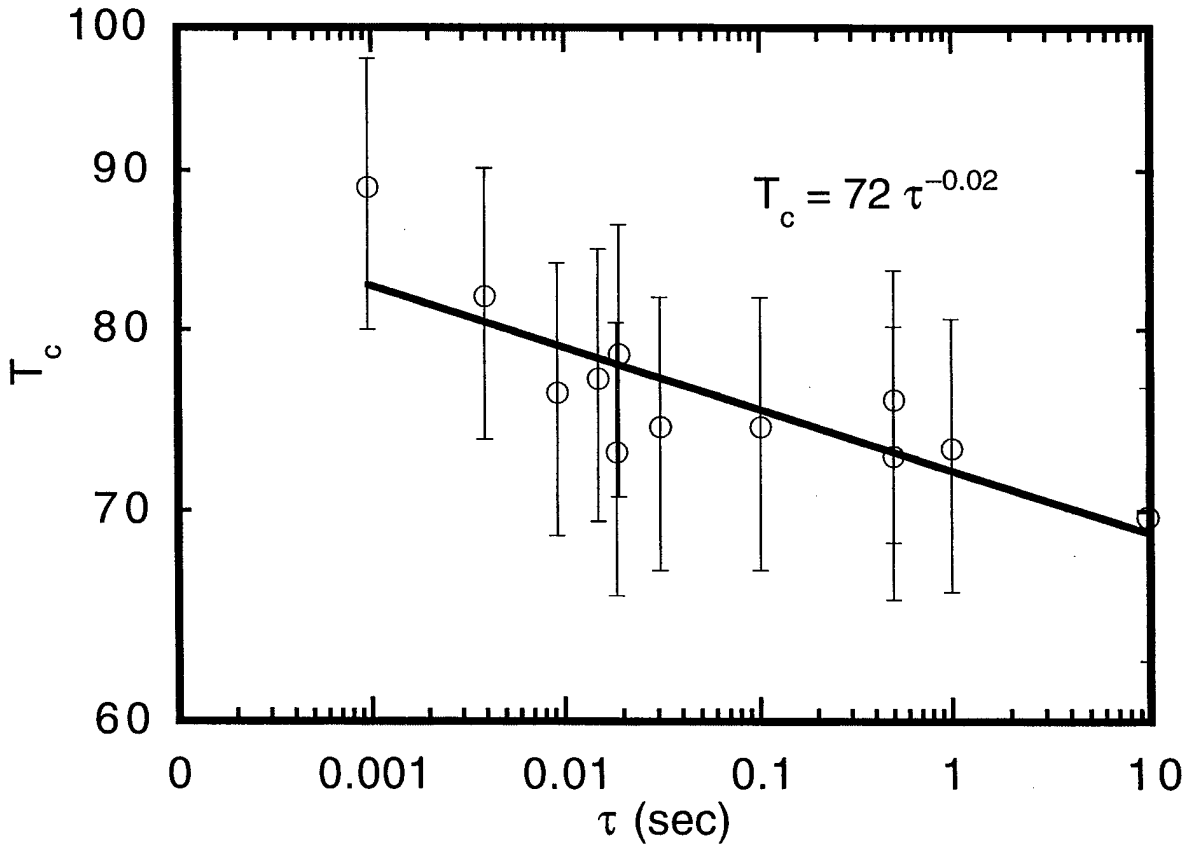

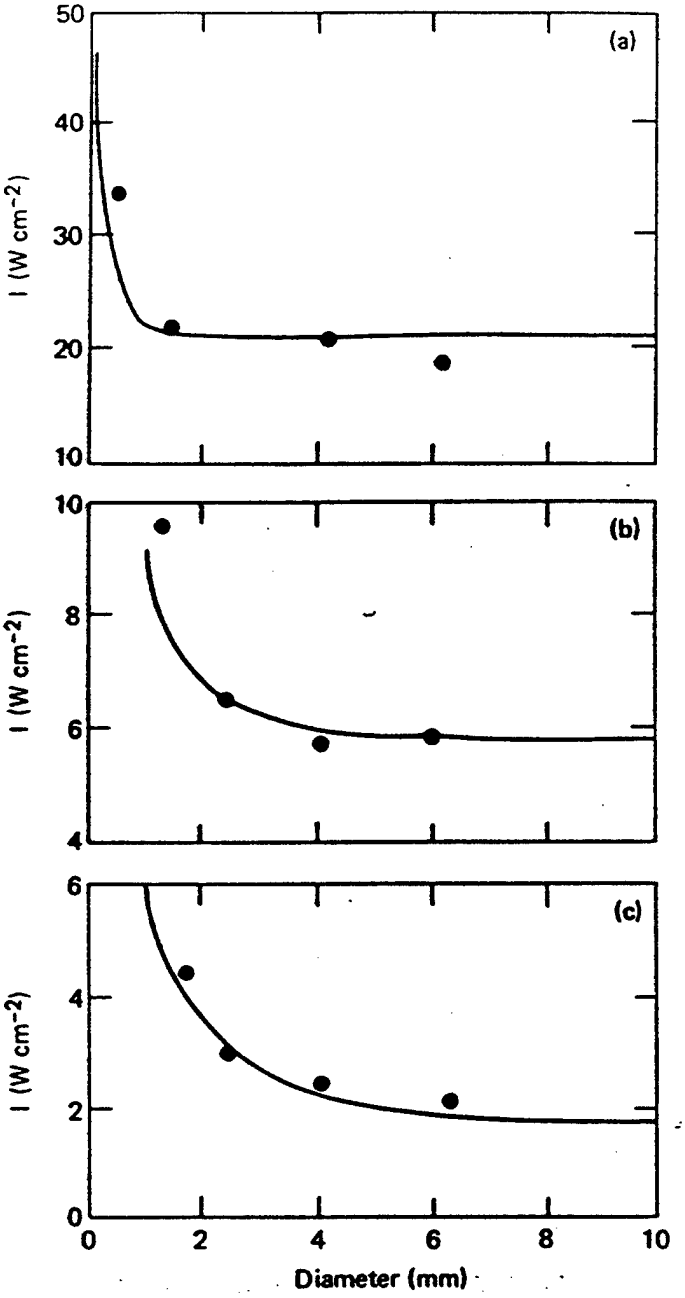

Fig. 5. The data points are the experimental peak irradiances required to produce threshold damage, as a function of beam diameter. The exposure durations were 0.1 s in (a), 1.0 s in (b) and 10.0 s in (c). The solid lines are the calculated peak irradiances needed to produce a fixed temperature rise ΔT_c at a point on the beam axis 10 μm deep into the epithelium. ΔT_c = 41°C in (a), 39°C in (b) and 36°C in (c).

PROBLEM: TO UNDERSTAND THE MECHANISMS RESPONSIBLE FOR THRESHOLD INFRARED DAMAGE TO THE CORNEA. TO OBTAIN A PHYSICAL EXPLANATION FOR THE EMPIRICAL "MODIFIED CRITICAL TEMPERATURE LAW."

OBJECTIVE: TO EXAMINE ENDOTHERMIC PHASE TRANSITIONS (E.G., PROTEIN DENATURATION, ALTERNATIONS IN LIPID STRUCTURES, ETC.) AS A POSSIBLE MECHANISM. TO ANALYZE A SIMPLE THERMAL MODEL INITIALLY.

APPROACH: THEORETICAL ANALYSES CORRELATED WITH EXPERIMENTS.

RESULTS: EVEN THE SIMPLIFIED MODEL CAN EXPLAIN THE THRESHOLD MEASUREMENTS—WITH PHYSICALLY REASONABLE PARAMETERS. APPLIED TO AMRDC FOR SUPPORT FOR MORE REALISTIC ANALYSES.

ASSUMPTION - DAMAGE IS ASSOCIATED WITH THE TRANSFORMATION OF A SPECIFIC AMOUNT OF MATERIAL PER UNIT SURFACE AREA (i.e., WITH A FIXED QUANTITY OF HEAT PER UNIT SURFACE AREA, Q_c, GOING INTO THE TRANSITION)

$$Q_c = \int_{t_c}^{\tau} \left[F_o - K\frac{\partial T}{\partial x}\Big|_{x=o}\right] dt$$

$$= \frac{\{[1 + \theta^2]\tan^{-1}\theta - \theta\}[K(T_c - T_o)]^2}{2\,F_o\kappa}$$

WHERE $\theta = [(\tau - t_c)/t_c]^{1/2}$

κ = THERMAL DIFFUSIVITY K = THERMAL CONDUCTIVITY

SIMPLE MODEL INCORPORATING A PHASE TRANSITION

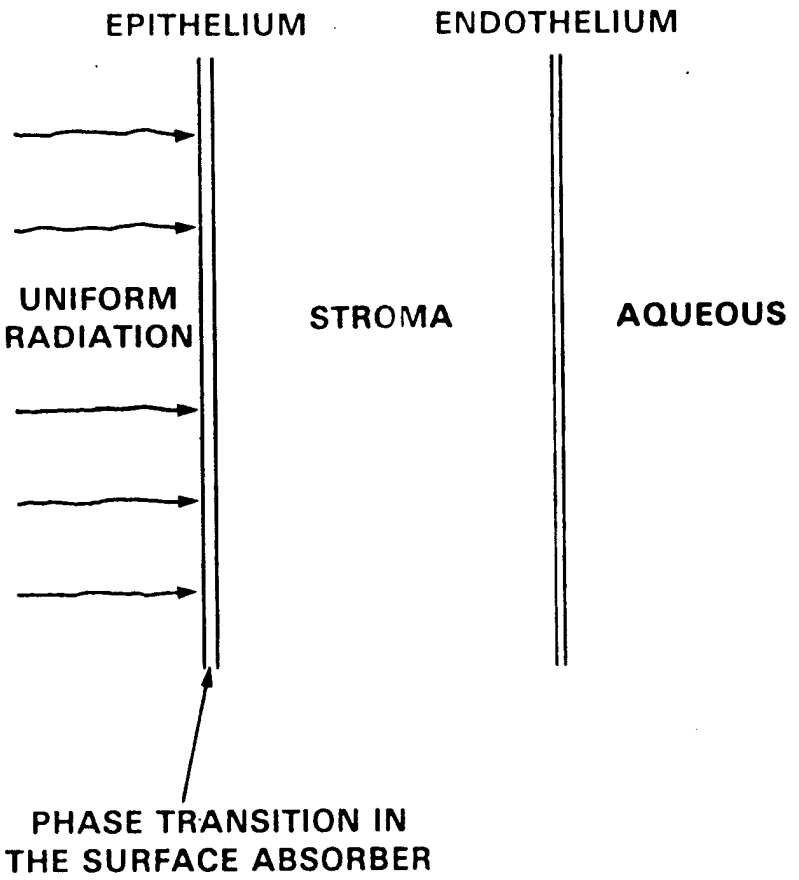

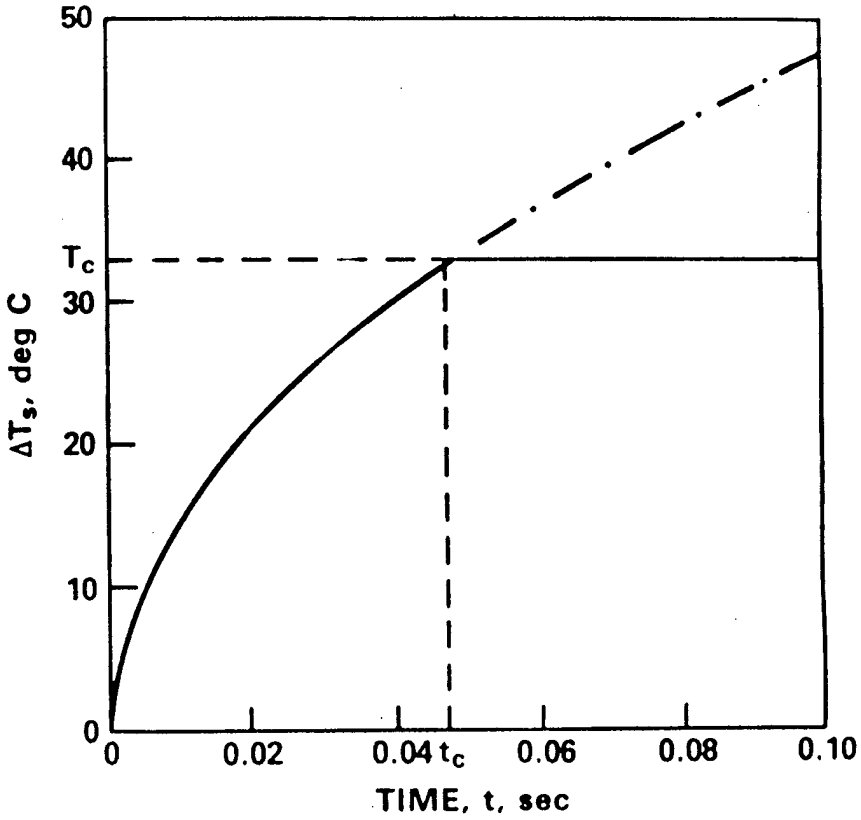

CAN REASONABLE VALUES OF Q_c AND T_c LEAD TO PREDICTED VALUES OF F_o AND τ THAT AGREE WITH EXPERIMENT?

AN APPROXIMATION IS REQUIRED TO TEST MODEL BECAUSE THE EXPERIMENTS HAVE A GAUSSIAN IRRADIANCE PROFILE. THE EXPERIMENTAL IRRADIANCE IS ADJUSTED TO AN EFFECTIVE F_o SUCH THAT, IN THE ABSENCE OF A PHASE TRANSITION, THE CALCULATED TEMPERATURE AT τ WOULD BE THE SAME AS FOR THE ACTUAL GAUSSIAN BEAM.

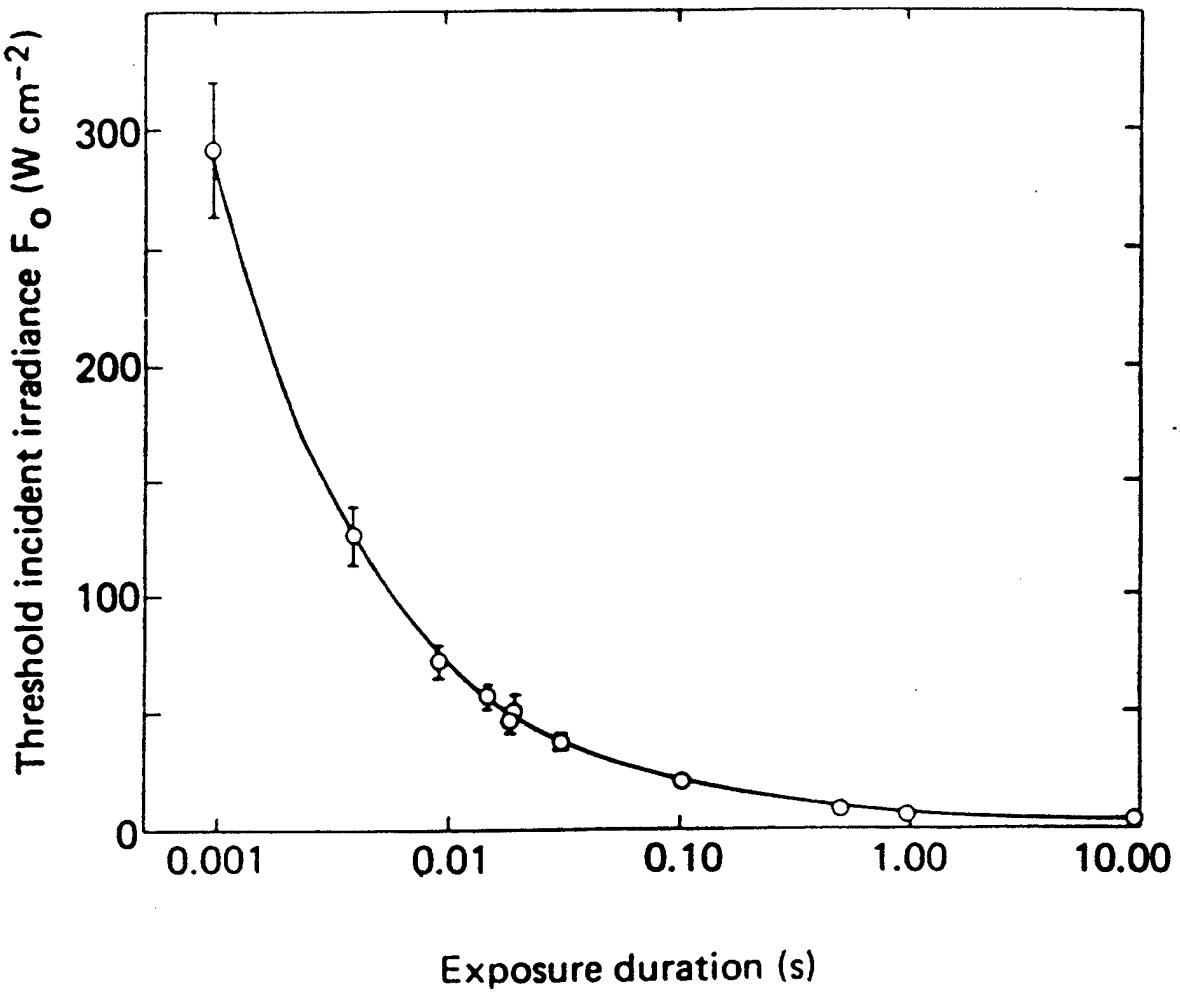
Threshold incident irradiance F_o (W cm^{-2})
300
200
100
0
0.001
0.01
0.10
1.00
10.00
Exposure duration (s)

Table 3. Multiple-pulse exposure damage thresholds.

PRF(Hz)	N	τ(s) x 10^{-3}	I_o(W cm^{-2})	ED_{th} (J cm^{-2})	d(cm)	ΔT_{max} + (C)	$\ell n T_{max}$ xx	Plot Symbol in Figs. 9-11
1*	1	9.2	86.2	0.79	0.252	41.4	4.34	○
1	4	10.1	79.6	3.21	0.172	43.4	4.36	○
1	32	9.3	66.8	19.9	0.250	38.4	4.30	○
10	4	9.7	60.0	2.32	0.256	43.3	4.36	□
10	32	10.9	32.7	11.4	0.244	44.6	4.38	□
10	128	9.2	25.3	29.8	0.270	39.8	4.31	□
20	4	10.0	55.3	2.21	0.252	46.4	4.40	◇
20	32	9.9	27.8	8.82	0.240	47.7	4.415	◇
20	128	8.9	16.4	18.7	0.276	38.8	4.30	◇
1*	1	0.96	624.	0.599	0.102	53.9	4.49	△
20	10	0.94	239.	2.24	0.186	34.7	4.24	△
20	100	0.95	171.	16.3	0.174	39.0	4.30	△
20	500	0.92	122.	56.0	0.190	33.0	4.22	△
100	10	0.96	153.	1.47	0.202	36.0	4.26	▲
100	100	0.95	59.6	5.67	0.196	35.2	4.25	▲
100	999	0.96	42.0	40.3	0.174	40.1	4.32	▲

* From Table I

\+ Maximum temperature rise calculated on the beam axis 10 μm beneath the cornea's anterior surface.

xx $T_{max} = 35C + \Delta T_{max}$

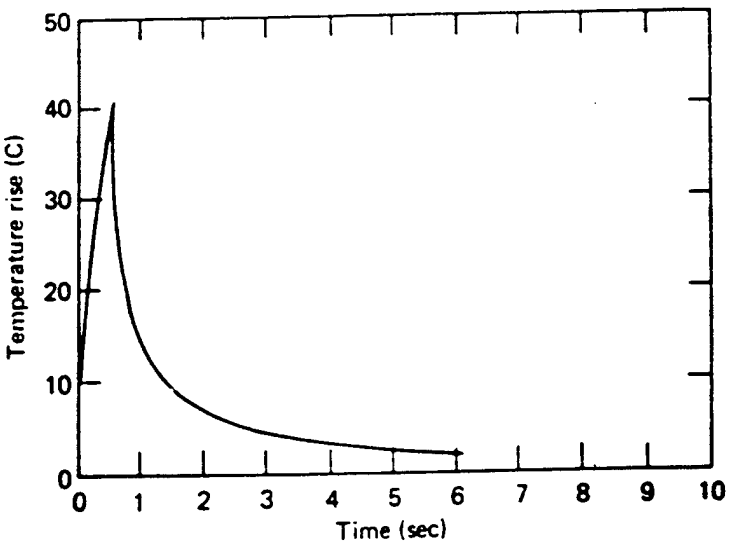
Temperature rise (C)
Time (sec)

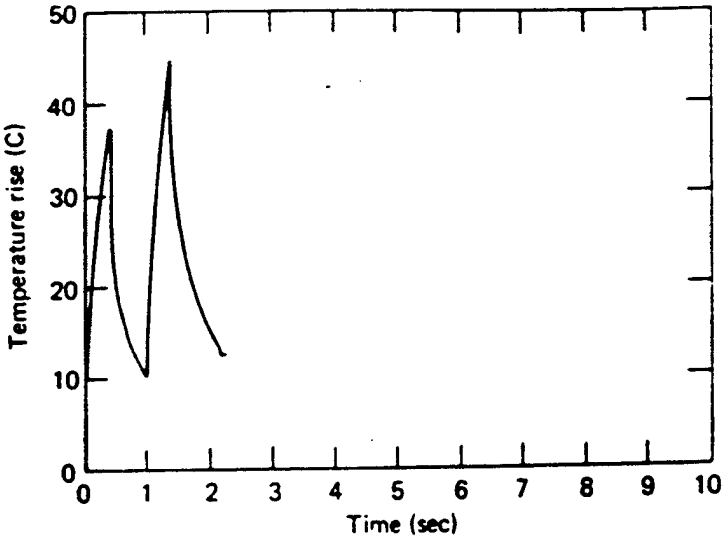
Temperature rise (C)
Time (sec)

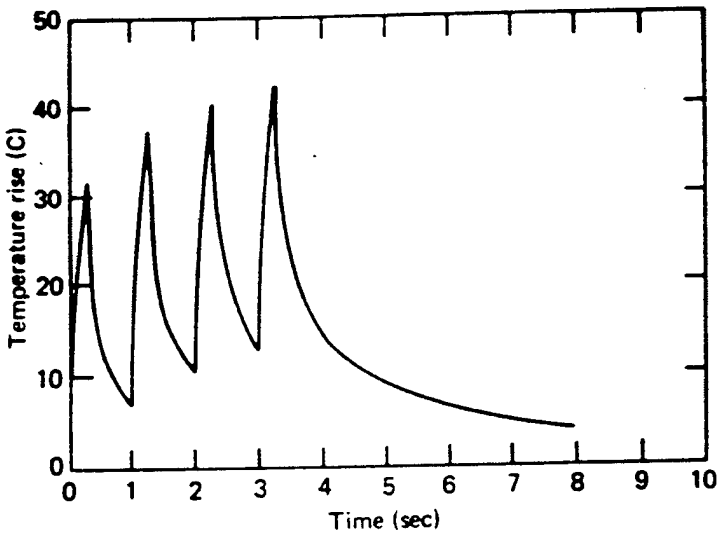
Temperature rise (C)
Time (sec)

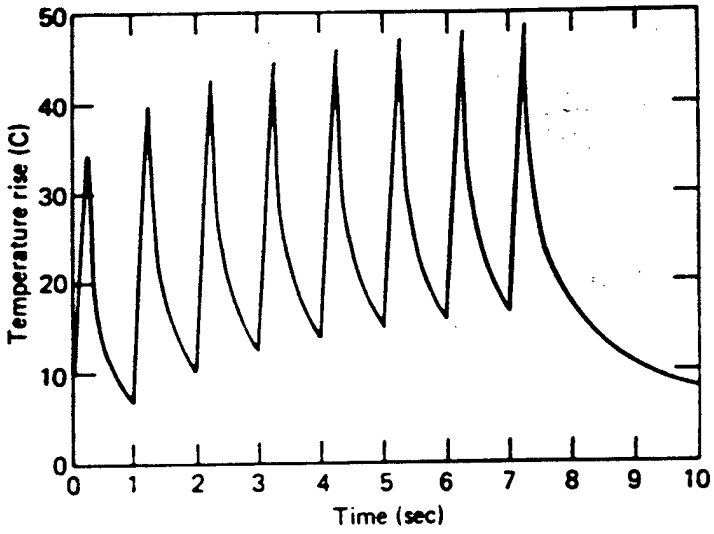
Temperature rise (C)
Time (sec)

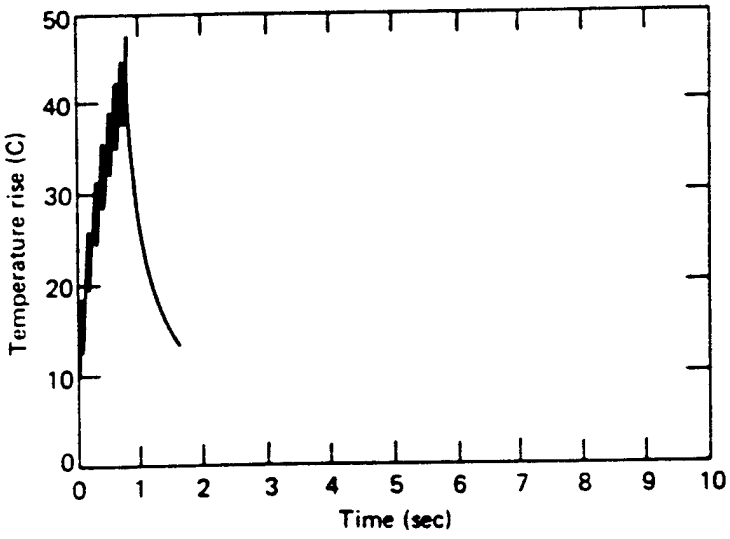
Temperature rise (C)
Time (sec)

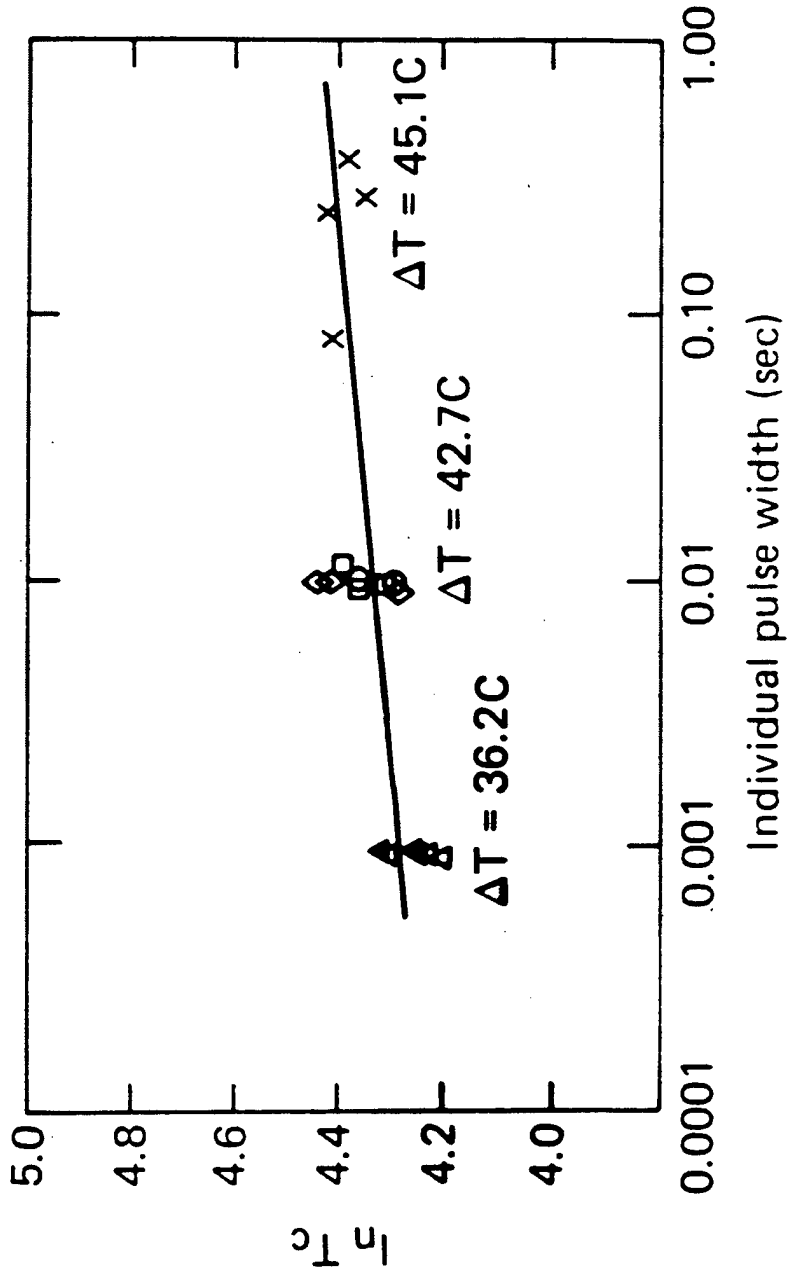
5.0
4.8
4.6
4.4
4.2
4.0
$\bar{n}\ T_c$
0.0001
0.001
0.01
0.10
1.00
Individual pulse width (sec)
ΔT = 36.2C
ΔT = 42.7C
ΔT = 45.1C

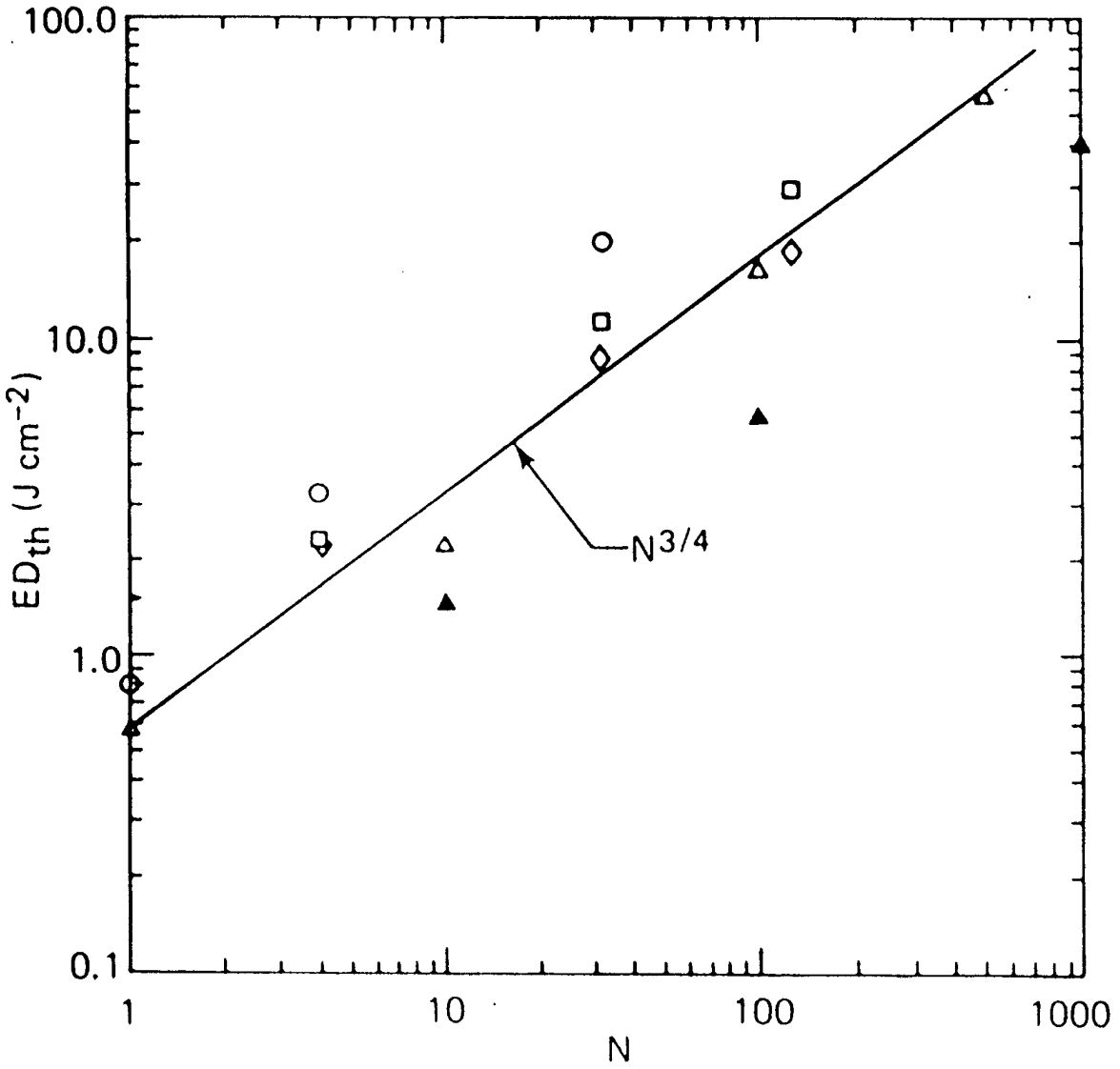

Fig. 10. The measured energy density with various threshold exposures plotted against the number of pulses in the train. The symbols correspond to those in Tables 2 and 3. The data are consistent with a relationship $ED_{th} = CN^{3/4}$, where C depends on the *PRF*.

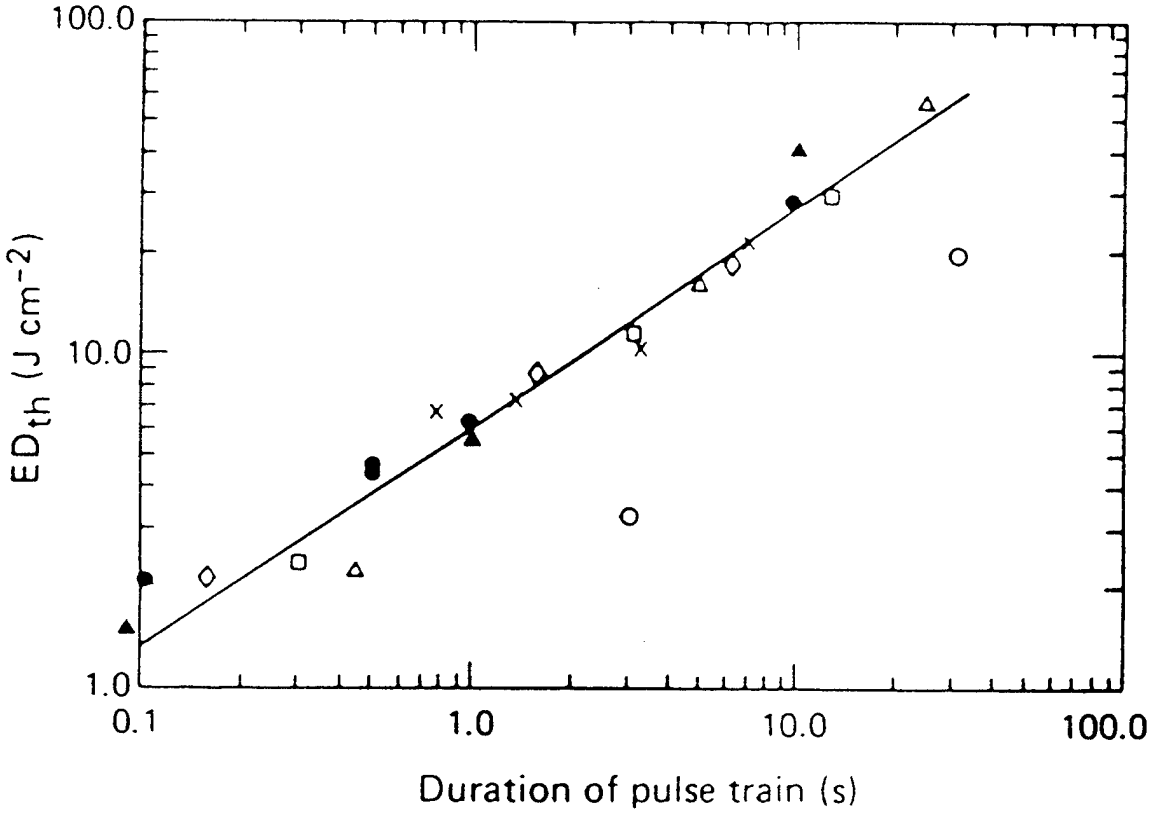

Fig. 11. ED_{th} for the multiple-pulse exposures in Tables 2 and 3 as a function of the total duration of the pulse train. For durations longer than 0.1 s, the data are correlated by an empirical power law of the form $ED_{th} \sim D^{0.66}$. The plot symbols correspond to the respective conditions defined in Tables 2 and 3. The solid circles are for the *single-pulse* exposures that have durations ≥ 0.1 s (cf. Table 1).

Ultrashort Laser Eye Damage: Nonlinear Propagation

M. J. Potasek
Air Force Research Laboratory
HEDB
2503 Gillingham Dr., BLDG 175E,
Brooks AFB, TX 78235

ABSTRACT

The recent development of ultrafast laser systems in the visible and near infrared spectral regions requires detailed knowledge of the material properties of ocular media. Different physical mechanisms play competing roles and give rise to new phenomena as the femtosecond laser pulse propagates in ocular media.

We investigate the relative importance of radial diffraction and material dispersion for a wide range of wavelengths for femtosecond laser pulse propagation. Furthermore, we investigate the significance of the various physical parameters, including the laser's temporal and radial pulse width, intensity and wavelength and the relevant nonlinear and dispersive material properties.

Because no analytical solution exists which can fully explain the laser-material interaction, we use numerical techniques. We give certain numerical results for various incident laser and material parameters associated with the laser-ocular media interaction.

I. INTRODUCTION

The study of spatiotemporal effects of laser propagation is of considerable current interest.[1-24] For the case of intense continuous wave (cw) light beams, the interaction of the nonlinearity and diffraction can lead to self-focusing and, in certain cases, to critical collapse. In the case of temporally pulsed optical beams, the nonlinearity couples the spatial and temporal behavior, resulting in richly complex dynamical results.

The dynamics of nonlinear, dispersive optical pulses combining the effects of diffraction, Kerr nonlinearity and group velocity dispersion (GVD) have been studied[4,5,8,9,11]. Very different behavior occurs depending upon the relative sign of the Kerr nonlinearity and the GVD. In most studies, a positive Kerr nonlinearity is assumed and combined with either a negative (anomalous dispersion) or a positive GVD (normal dispersion). For the anomalous dispersion region, it is suggested that a stable light bullet forms[3]. The situation in the normal dispersion region is more complex.

In the normal GVD region, the pulse is broadened along the time axis but compressed (positive Kerr effect) in the transverse direction. This complex interplay leads to the splitting of the pulse in both space and time. For weak GVD, the pulse can be observed numerically to achieve a high degree of spatial compression before splitting into subpulses (a result of the dispersion).

Nonlinear effects, such as self-focusing, may be responsible for some of the experimental observations for laser eye damage[14-19]. To determine the possible effect of self-focusing on laser propagation in the eye, the ABCD matrix method was used in a calculation of the spot size as the beam propagated in ocular media[15]. The nonlinearity is included using the experimental values for the nonlinear refractive indices for ocular components. It was observed that self-focusing can substantially decrease the spot size and increase laser irradiance at the retina.

It was recently proposed[2] that normal group velocity dispersion (GVD) increases the peak input power required for two-dimensional self-focusing of ultrashort pulses. Several researchers have examined the effects of weak GVD on self-focusing for picosecond (ps) pulses [4,5,7,8,9]. Normal GVD affects self-focusing by spreading the pulse along the propagation direction. Because cross sections of the light pulse differ in power, those possessing powers that exceed the critical power self-focus at different rates. In the absence of GVD and for critical power, the self-focusing leads to a singularity and critical collapse [10].

The situation becomes more complex if the incident pulse is chirped [22-24] (i.e. a phase is added to the initial condition). This chirp can be spatial, as in the case of a lens in the beam path and/or it can be temporal, as in the case of the light beam produced by a semiconductor laser. Several groups have studied the effects of the interaction of nonlinearity, GVD and diffraction for an incident chirped Gaussian pulse[22-24]. It was found that the critical power for self-focusing changes quadratically with the chirp parameter. Numerical studies showed that for chirped pulses propagating in the anomalous GVD region, the self-focusing can be enhanced or suppressed depending upon the value and sign of the chirp parameter. In the normal dispersion region, studies showed that an initially chirped pulse can increase the peak intensity by competing with the temporal pulse splitting. However, if the chirping induces a temporal compression, analytical estimates show that a transverse collapse does not occur. Yet when the chirp causes the pulse to expand in the time domain and compress in the transverse domain, the chirping generates highly peaked field components.

The recent advent of new lasers in the visible and near infrared spectral regions, with pulse durations down to several femtoseconds (fs), requires the extension of the study of spatiotemporal dynamics to new realms. As pulse durations become shorter, the dispersive effects of the light-matter interaction will grow in

importance[12,13,25]. Most studies assumed an instanteous (electronic) Kerr nonlinearity. In many materials, the Kerr nonlinearity consists of both instantaneous as well as time-delayed component (i.e. Raman term). The time-delayed component becomes significant for ultrashort temporal pulses and has been experimentally observed in optical fibers where it manifests itself as a frequency downshifting of the pulse spectrum[26-28].

As the temporal pulse width shortens, higher-order dispersive effects , beyond the GVD, can also contribute to the interplay of spatiotemporal dynamics. These effects include self-steepening in addition to the time-delayed response. In this paper we include these effects, in addition to GVD and diffraction in a nonlinear Kerr medium, and investigate the relative influence and depedence on physical parameters, such as the laser temporal and spatial width, material dispersion . These effects can play a role in ultrashort laser propagation in biological media, such as the eye, two-dimensional waveguides, and in bulk media, including solids, liquids and gases.

II. THEORY

A. Derivation of the propagating field

The propagating electromagnetic field is given by

$$\nabla\times\nabla\times E+\frac{1}{c^2}\frac{\partial^2 E}{\partial t^2}+\frac{1}{\varepsilon_0 c^2}\frac{\partial^2 P}{\partial t^2}=0 \tag{1}$$

where E is the electromagnetic field and P is the polarization vector. In this case we are concerned with the effects of the third-order nonlinear susceptibility, $\chi^{(3)}$. Accordingly, the polarization can be written in terms of its linear (P_L) and nonlinear (P_{NL}) parts,

$$P=P_L+P_{NL} \tag{2}$$

$$P(x,y,z,t)=\varepsilon_0\int_{-\infty}^{\infty}\chi^{(1)}(t-t')E(x,y,z,t-t') \tag{3}$$

$$+\varepsilon_0\int_{-\infty}^{\infty}\int_{-\infty}^{\infty}\int_{-\infty}^{\infty}\chi^{(3)}(t-t_1,t-t_2,t-t_3)E(x,y,z,t_1)E(x,y,z,t_2)E(x,y,z,t_3)dt_1dt_2dt_3$$

The first (second) term corresponds to P_L (P_{NL}). The nonlinear part of the polarization can be written in terms of the dielectric constant,

$$P_{NL}(r,t)=\varepsilon_0\varepsilon_{NL}E(r,t) \tag{4}$$

where ε_{NL} is the nonlinear contribution to the dielectric constant and is defined by[13]

$$\varepsilon_{NL}=\frac{3}{4}\chi^{(3)}{}_{xxxx}|E|^2 \tag{5}$$

The frequency dependent dielectric constant is defined by

$$\varepsilon(\omega) = 1 + \tilde{\chi}^{(1)}(\omega) \tag{6}$$

where $\tilde{\chi}^{(1)}(\omega)$ is the Fourier transform of $\chi^{(1)}(t)$ The real and imaginary parts of ε(ω) are related to the refractive index n(ω) and the absorption coefficient $\hat{\alpha}(\omega)$,

$$\varepsilon(\omega) = \left(n(\omega) + i\hat{\alpha}(\omega)c / 2\omega\right)^2 \tag{7}$$

We write the electric field as a superposition of monochromatic waves

$$E(x,y,z,t) = \int_{-\infty}^{\infty} d\omega\, \tilde{E}(x,y,z,\omega) e^{i(k(\omega)z - \omega t)} \tag{8}$$

where $\tilde{E}$(x,y,z,ω) is the Fourier transform of E(x,y,z,t) and k(ω)=n(ω) ω/c.
Assuming $P_{NL} = 0$, the linear part of Eq. (1) reduces to

$$\nabla^2 \tilde{E} + \varepsilon(\omega)\frac{\omega^2}{c}\tilde{E} = 0 \tag{9}$$

where

$$\nabla x \nabla x \tilde{E} = \nabla(\nabla \bullet \tilde{E}) - \nabla^2 \tilde{E} = -\nabla^2 \tilde{E} \tag{10}$$

in agreement with previous results.[13]

We define the operator

$$\nabla^2 = \frac{\partial^2}{\partial z^2} + \nabla_\perp^2 \tag{11}$$

where $\nabla_\perp^2$ is the radial Laplacian

$$\nabla_\perp^2 = \frac{\partial^2}{\partial r^2} + \frac{1}{r}\frac{\partial}{\partial r}, \tag{12}$$

and $r = (x^2 + y^2)^{1/2}$.
The third order susceptibility is written as

$$\chi^{(3)}(t - t_1, t - t_2, t - t_3) = \chi^{(3)} R(t - t_1)\delta(t - t_2)\delta(t - t_3) \tag{13}$$

In the frequency domain, the propagation of the field,including the nonlinear part becomes

$$\nabla^2 \tilde{E} + \varepsilon(\omega)\frac{\omega^2}{c}\tilde{E} + \frac{3\chi^{(3)}_{xxxx}}{4c^2}\omega^2 \iint \tilde{E}(\omega_1)\tilde{E}(\omega_2)\tilde{E}^*(\omega_1 + \omega_2 - \omega)\tilde{R}(\omega - \omega_1)e^{i\Delta kz} d\omega_1 d\omega_2 = 0 \tag{14}$$

where $\Delta k = k(\omega_1)+k(\omega_2)-k(\omega_1+\omega_2-\omega)-k(\omega)$ and $\tilde{R}(\omega\text{-}\omega_1)$ is the Fourier transform of $R(t\text{-}t_1)$. Expanding $k(\omega)$ in a Taylor series about ω_0,

$$k(\omega) = k_0 + k_1(\omega-\omega_0)+\frac{\mathrm{sgn}(k_2)}{2}(\omega-\omega_0)^2+\frac{\mathrm{sgn}(k_3)}{6}(\omega-\omega_0)^3+\ldots\ldots, \tag{15}$$

$$k_n = \frac{\partial^n k}{\partial \omega^n}\Big|_{\omega_0}$$

where $\mathrm{sgn}(k_2)$, $\mathrm{sgn}(k_3)$ refers to the sign of k_2, k_3, respectively. The normal dispersion region corresponds to $k_2 > 0$ and the anomalous dispersion region corresponds to $k_2 < 0$. For notational simplicity, we will omit the sgn in the following equations. However it should be kept in mind that the physical results will depend upon the signs of the dispersion coefficients. Defining the field envelope $\tilde{A}(r,z,\omega-\omega_0)$,

$$\tilde{A}(r,z,\omega-\omega_0) = \frac{1}{2}\tilde{E}(r,z,\omega)e^{i(k(\omega)-k_0)z}+c.c. \tag{16}$$

where $\tilde{A}(\omega)$ is the Fourier transform of $A(t)$. In many cases the absorption is small compared to the index of refraction. In this case, $\hat{\alpha}(\omega) << 1$, $\varepsilon(\omega) \equiv n(\omega)^2$ and we obtain,

$$\left[i\frac{\partial}{\partial z}+\frac{1}{2k_0}\left(1-\frac{k_1}{k_0}\Delta\omega\right)\Delta_\perp + k_1\Delta\omega+\frac{k_2}{2}\Delta\omega^2+\frac{k_3}{6}\Delta\omega^3\right]\tilde{A}(r,z,\Delta\omega)$$

$$+\frac{3\chi^{(3)}_{xxxx}}{8cn_0}\omega_0(1+q_0\Delta\omega) \tag{17}$$

$$\times\iint \tilde{A}(r,z,\Delta\omega_1)\tilde{A}(r,z,\Delta\omega_2)\tilde{A}^*(r,z,\Delta\omega_1+\Delta\omega_2-\Delta\omega)\tilde{R}(\Delta\omega-\Delta\omega_1)d\omega_1 d\omega_2$$

$$=0$$

where $\Delta\omega = \omega-\omega_0$, $q_0 = 1-\frac{n_1\omega_0}{n_0}$, *and* $n_1 = \frac{\partial n}{\partial\omega}\Big|_{\omega_0}$ and we use the approximations

$$\frac{\partial^2}{\partial z^2} << k_0\frac{\partial}{\partial z},\quad \left(1+\frac{k_1}{k_0}\Delta\omega\right)^{-1}\sim 1-\frac{k_1}{k_0}\Delta\omega,\quad \left(1+\frac{n_1}{n_0}\Delta\omega\right)^{-1}\sim 1-\frac{n_1}{n_0}\Delta\omega \tag{18}$$

The time domain expression is obtained using the inverse Fourier transform; recalling that $\Im\left(\frac{\partial^n}{\partial t^n}\right) \Rightarrow (-i\Delta\omega)^n$, and using the convolution theorem, $f*g = \int g(y)f(x-y)dy$. In actuality the third order susceptibility $\chi^{(3)}$ is complex and can be written in terms of its real and imaginary parts

$$n_2 = \frac{3}{8n_0}\mathrm{Re}\left(\chi^{(3)}_{xxxx}\right), \quad \alpha_2 = \frac{3\omega_0}{4n_0 c}\mathrm{Im}\left(\chi^{(3)}_{xxxx}\right) \tag{19}$$

where n_2 is the coefficient of the nonlinear index of refraction[13] and α_2 is the coefficient for two photon absorption. In many cases the two photon absorption is small compared to the nonlinear index of refraction and we will neglect it. (It can be easily incorporated.[13]) Using these parameters Eq (17) becomes

$$\left[i\left(\frac{\partial}{\partial z}+k_1\frac{\partial}{\partial t}\right)+\frac{1}{2k_0}\nabla_\perp^2-\frac{k_2}{2}\frac{\partial^2}{\partial t^2}-i\frac{k_3}{6}\frac{\partial^3}{\partial t^3}-i\frac{k_1}{2k_0^2}\frac{\partial}{\partial t}\nabla_\perp^2\right]A(r,z,t)$$

(20)

$$+\gamma_0\left[1+i\left(\frac{1}{\omega_0}-\frac{n_1}{n_0}\right)\frac{\partial}{\partial t}\right]A(r,z,t)\int\left|A(r,z,t-t')\right|^2 R(t')dt' = 0$$

where $\gamma_0 = \frac{\mathrm{sgn}(n_2)\omega_0}{c}$. The sgn($n_2$) refers to the sign of n_2. For $n_2 > 0$ self-focusing can occur; for $n_2 < 0$ self-defocusing can occur. Again, for notational simplicity, we will omit the sgn in the following equations. However, its sign can determine the physical situation.

The response function, R(t) includes both the electronic (instantaneous) and vibrational (time-delayed) terms,

$$R(t) = f\,\delta(t) + (1-f)h(t) \tag{21}$$

where f is the fraction of the response that is instantaneous and h(t) is the time delayed response function.. The nonlinear term, NLT (i.e. the last term in Eq (20) is given by

$$NLT = \gamma_0 f\left(1+i\frac{q_0}{\omega_0}\frac{\partial}{\partial t}\right)A(r,z,t)\left|A(r,z,t)\right|^2$$

(22)

$$+\gamma_0(1-f)\left(1+i\frac{q_0}{\omega_0}\frac{\partial}{\partial t}\right)A(r,z,t)\int h(t')\left|A(r,z,t-t')\right|^2 dt'$$

In many physical cases of interest, the incident temporal pulse width is such that A(t-t′) does not differ much from A(t) on the time scale of the response function, so we can expand $|A(t-t')|^2$ in a Taylor series about t

$$|A(s)|^2 = |A(s)|^2_{s=t} + (s-t)\frac{\partial}{\partial s}|A(s)|^2_{s=t} + \ldots\ldots$$

$$= |A(t)|^2 - t'\frac{\partial}{\partial t}|A(t)|^2 + \ldots\ldots \tag{23}$$

where s=t-t′. Then the nonlinear term becomes

$$NLT = \gamma_0\left(1 + i\frac{q_0}{\omega_0}\frac{\partial}{\partial t}\right)A(r,z,t)\int_0^\infty R(t')\left[|A(r,z,t)|^2 - t'\frac{\partial}{\partial t}|A(r,z,t)|^2\right]dt' \tag{24}$$

defining $T_R = \int_0^\infty t'R(t')dt'$, Eq (24) becomes

$$NLT = \gamma_0\left(1 + i\frac{q_0}{\omega_0}\frac{\partial}{\partial t}\right)A(r,z,t)\left[1 - T_R\frac{\partial}{\partial t}\right]|A(r,z,t)|^2 \tag{25}$$

Neglecting second-order derivatives in t, Eq (25) becomes

$$NLT = \gamma_0 A|A|^2 + i\frac{\gamma_0 q_0}{\omega_0}\frac{\partial}{\partial t}\left(A|A|^2\right) - \gamma_0 T_R A\frac{\partial}{\partial t}|A|^2 \tag{26}$$

where A=A(r,z,t). Combining Eqs. (20) and (26) we obtain

$$\left[i\left(\frac{\partial}{\partial z} + k_1\frac{\partial}{\partial t}\right) + \frac{1}{2k_0}\nabla_\perp^2 - \frac{k_2}{2}\frac{\partial^2}{\partial t^2} - i\frac{k_3}{6}\frac{\partial^3}{\partial t^3} - i\frac{k_1}{2k_0^2}\frac{\partial}{\partial t}\nabla_\perp^2\right]A$$

$$+\gamma_0\left[A|A|^2 + i\frac{q_0}{\omega_0}\frac{\partial}{\partial t}\left(A|A|^2\right) - T_R A\frac{\partial}{\partial t}|A|^2\right] = 0 \tag{27}$$

It is convenient to write Eq (27) in the form

$$i\left(\frac{\partial}{\partial z}+k_1\frac{\partial}{\partial t}\right)A+\frac{1}{2k_0}\nabla_\perp^2 A-\frac{k_2}{2}\frac{\partial^2 A}{\partial t^2}+\gamma_0|A|^2A-i\frac{k_3}{6}\frac{\partial^3 A}{\partial t^3}$$

(28)

$$-i\frac{k_1}{2k_0^2}\frac{\partial}{\partial t}\nabla_\perp^2 A+2i\frac{\gamma_0 q_0}{\omega_0}|A|^2\frac{\partial A}{\partial t}+i\frac{\gamma_0 q_0}{\omega_0}A^2\frac{\partial A^*}{\partial t}-\gamma_0 T_R A\frac{\partial|A|^2}{\partial t}=0$$

B. Scaling and Transformation

We assume an incident pulse of the form,

$$A(r,0,t)=A_0\exp(\frac{-r^2}{2a_0^2})\exp(\frac{-t^2}{2T_0^2}) \tag{29}$$

where a_0 is the spatial beam waist, T_0 is the temporal half-width of the pulse intensity and A_0^2 is the peak incident pulse intensity.

In order to examine the physics in more detail, we define the length scales

$L_{DF}=\pi n_0 a_0^2/\lambda_0$	Diffraction Length
$L_{NL}=\lambda_0/2\pi n_2 A_0^2$	Nonlinear Length
$L_{DS2}=T_0^2/k_2$	Second-Order Dispersion Length
$L_{DS3}=T_0^3/k_3$	Third-Order Dispersion Length

As the length scale decreases for a particular effect, the more dominant it becomes relative to the other effects. Therefore, if L_{DF} « L_{DS}, the dominant effect is diffractive; whereas, if L_{DS} « L_{DF} the dominant effect is dispersive. Similarly, if L_{NL} « L_{DF}, the effect is nonlinear.

Assuming the nonlinear diffractive effect is dominant, we define the transformations

$$Q=\frac{A}{A_0},\quad \rho=\frac{r}{a_0},\quad \xi=\frac{z}{L_{DF}},\quad \tau=\frac{(t-k_1 z)}{T_0} \tag{30}$$

and obtain the nondimensioned equation

$$i\frac{\partial Q}{\partial\xi}+\frac{1}{4}\nabla_\rho^2 Q-\frac{1}{2}\bar{\alpha}\frac{\partial^2 Q}{\partial\tau^2}+\bar{\beta}|Q|^2Q-\frac{i}{6}\bar{\gamma}\frac{\partial^3 Q}{\partial\tau^3}$$

(31)

$$-i\bar{\delta}\nabla_\rho^2\frac{\partial Q}{\partial\tau}+i\bar{\varepsilon}|Q|^2\frac{\partial Q}{\partial\tau}+i\bar{\mu}Q^2\frac{\partial Q^*}{\partial\tau}-\bar{\sigma}Q\frac{\partial|Q|^2}{\partial\tau}=0$$

where

$$\overline{\alpha} = \frac{L_{DF}}{L_{DS2}},\ \overline{\beta} = \frac{L_{DF}}{L_{NL}},\ \overline{\gamma} = \frac{L_{DF}}{L_{DS3}},\quad \tau_R = \frac{T_R}{T_0},$$

$$\overline{\varepsilon} = \frac{\overline{\beta} q_0}{\omega_0 T_0},\quad \overline{\mu} = \frac{\overline{\beta} q_0}{2\omega_0 T_0},\quad \overline{\sigma} = \overline{\beta}\tau_R,$$

$$and\ \nabla_\rho^2 = \frac{\partial^2}{\partial \rho^2} + \frac{1}{\rho}\frac{\partial}{\partial \rho}$$

Each coefficient is dimensionless and its magnitude determines the relative importance of its effect.

III. COMPARION OF COEFFICIENTS

When pulses become sufficiently short that higher order dispersive terms cannot be neglected, then Eq. (31) must be investigated. In order to examine the interaction of the various physical properties, it is advantageous to express the coefficients of Eq. (31) in physical terms (i.e. pulse width, pulse intensity, wavelength, spatial beam waist and dispersion coefficients). In many physical cases, we can neglect the frequency dependence of n and obtain $q_0 = 1$. Then, in terms of the input parameters, we have

$$\overline{\alpha} = \frac{\pi n_0 a_0^2 k_2}{\lambda_0 T_0^2}$$

$$\overline{\beta} = \frac{2\pi^2 a_0^2 n_0 n_2 A_0^2}{\lambda_0^2}$$

$$\overline{\gamma} = \frac{\pi n_0 a_0^2 k_3}{\lambda_0 T_0^3}$$

$$\overline{\delta} = \frac{k_1 \lambda_0}{8\pi n_0 T_0}$$

$$\overline{\varepsilon} = \frac{4\pi n_0 n_2 a_0^2 A_0^2}{c\lambda_0 T_0} \qquad (32)$$

$$\overline{\mu} = \frac{2\pi n_0 n_2 a_0^2 A_0^2}{c\lambda_0 T_0}$$

$$\overline{\sigma} = \frac{2\pi^2 n_0 n_2 a_0^2 A_0^2 T_R}{\lambda_0{}^2 T_0}$$

As can be seen from Eq. (32), the coefficients $\overline{\alpha}, \overline{\gamma}, \overline{\delta}$ correspond to linear terms and are coupled to various dispersion coefficients (i.e. k_2, k_3, k_1, respectively). The coefficients $\overline{\beta}, \overline{\varepsilon}, \overline{\mu}, \overline{\sigma}$ correspond to nonlinear terms and depend upon the initial pulse intensity, A_0^2. The functional dependences of some of the coefficients is given in the following figures. Figure 1 shows the dependence of $\overline{\beta}$ on λ_0, a_0, A_0^2. For $\overline{\beta} > 1$, we have nonlinearity and as shown in Fig. 1 the nonlinearity depends on the pulse intensity. Additionally, it can be seen from Fig. 1, that for a given intensity and wavelength, the problem can become linear if the spatial beam waist, a_0, gets so small that $\overline{\beta} < 1$. Figure 2 shows the dependence of the higher order dispersion term, $\overline{\gamma}$ on k_3, a_0, T_0, λ_0. In this case, Fig. 2 shows the strong dependence of this term with decreasing temporal pulse width, T_0. It also shows that this dispersion term is dependent on the spatial beam waist. The dependence of the other coefficients can be observed from Eq. (32) or similar plots to Figs. 1 and 2. However numerical methods must be used to investigate the nonlinear propagation. This is described in the next section.

VI. NUMERICAL PROCEDURE

We use the non-dimensioned equation given by

$$\left[i\frac{\partial}{\partial\xi}+\frac{1}{4}\left(1-i\sigma\frac{\partial}{\partial\tau}\right)\nabla_{\perp}^{2}-\frac{\gamma}{2}\frac{\partial^{2}}{\partial\tau^{2}}-i\frac{\delta}{6}\frac{\partial^{3}}{\partial\tau^{3}}\right]Q$$

$$+ap\{|Q|^{2}+i\sigma\left(2Q^{*}\frac{\partial Q}{\partial\tau}+Q\frac{\partial Q^{*}}{\partial\tau}\right)-\tau_{R}\left(\frac{\partial|Q|^{2}}{\partial t}\right)\}Q=0 \tag{33}$$

where

$$a=\left(\frac{1.22\pi}{4}\right)^{2},p=\frac{1}{a}\frac{L_{DF}}{L_{NL}},\gamma=\frac{a_{0}^{2}k_{0}k_{2}}{2T_{0}^{2}},\delta=\frac{a_{0}^{2}k_{0}k_{3}}{2T_{0}^{3}},$$

$$\sigma=\frac{1}{\omega_{0}T_{0}},\tau_{R}=\frac{T_{R}}{T_{0}} \tag{34}$$

The numerical solution is solved in the form[29]

$$\frac{\partial Q}{\partial\xi}=(D_{DS}+D_{DF}+N)Q \tag{35}$$

where D_{DS}, D_{DF}, and N are operators given by

$$D_{DS}=-\frac{i\gamma}{2}\frac{\partial^{2}}{\partial\tau^{2}}+\frac{\delta}{6}\frac{\partial^{3}}{\partial\tau^{3}}$$

$$D_{DF}=\frac{i}{4}\left(1-i\sigma\frac{\partial}{\partial\tau}\right)\nabla_{\perp}^{2} \tag{36}$$

$$N=ap\left\{i|Q|^{2}-\sigma\left[2Q^{*}\frac{\partial Q}{\partial\tau}+Q\frac{\partial Q^{*}}{\partial\tau}\right]-i\tau_{R}\frac{\partial|Q|^{2}}{\partial\tau}\right\}$$

Equation (35) can be solved using the symmetric split-step method

$$Q(\xi+\Delta\xi)=e^{\frac{\Delta\xi}{2}D_{DF}}\;e^{\frac{\Delta\xi}{2}D_{DS}}\;e^{\int_{\xi}^{\xi+\Delta\xi}d\xi'\,N(\xi')}\;e^{\frac{\Delta\xi}{2}D_{DS}}\;e^{\frac{\Delta\xi}{2}D_{DF}}\;Q(\xi) \tag{37}$$

where the exponential operators are defined by their Taylor series expansion. The problem is solved in three separate parts. The linear dispersion operator, D_{DS} is solved in the Fourier domain using the fast Fourier transform (FFT) method. The nonlinear operator, N, is solved in the time domain using the trapezoid rule and iterated until the algorithm converges,

$$\int_{\xi}^{\xi+\Delta\xi} d\xi' \; N[Q(\xi')] = \frac{\Delta\xi}{2}\{N[Q(\xi)] + N[Q(\xi+\Delta\xi)]\} \tag{38}$$

where the first iteration $N[Q(\xi+\Delta\xi)]$ is set equal to $N[Q(\xi)]$ to obtain a guess for $Q(\xi+\Delta\xi)$ which is used for $N[Q(\xi+\Delta\xi)]$ and the process is repeated until convergence is reached. The terms are evaluated using a discrete space and time grid given by

$$\tau \to \tau_i, \xi \to \xi_n, \rho \to \rho_j$$

Therefore $$Q(\xi,\rho,\tau) \to Q(\xi_n,\rho_j,\tau_i) = Q_{ij}^n$$

Then the nonlinear operator can be written as

$$N(\xi_n) = ap\left\{\left|Q_{ij}^n\right|^2 - \sigma\left[2Q_{ij}^{n*}\left(\frac{Q_{i+1,j}^n - Q_{i-1,j}^n}{2\Delta\tau}\right) + Q_{ij}^n\left(\frac{Q_{i+1,j}^n - Q_{i-1,j}^n}{2\Delta\tau}\right)^*\right]\right\}$$
$$- iap\tau_R\left\{Q_{ij}^{n*}\left(\frac{Q_{i+1,j}^n - Q_{i-1,j}^n}{2\Delta\tau}\right) + Q_{ij}^n\left(\frac{Q_{i+1,j}^n - Q_{i-1,j}^n}{2\Delta\tau}\right)^*\right\} \tag{39}$$

where the "leap frog" method is used to evaluate the derivatives.

The third part involves solving the linear diffraction operator D_{DF}, which is equivalent to

$$\frac{\partial Q}{\partial \xi} = \kappa(\omega)\nabla_{\perp}^2 Q(\xi,\rho,\omega) \tag{40}$$

where $$\nabla_{\perp}^{2} = \frac{1}{\rho}\frac{\partial}{\partial\rho} + \frac{\partial^{2}}{\partial\rho^{2}},$$

and $$\kappa(\omega) = \frac{i}{4}(1-\sigma\omega). \tag{41}$$

Equation (40) is solved using the finite difference scheme,

$$\frac{\partial Q}{\partial\xi} = \frac{Q_{ij}^{n+1} - Q_{ij}^{n}}{\Delta\xi} \tag{42}$$

and

$$\frac{\partial Q}{\partial\rho} = \frac{1}{2}\left\{\frac{Q_{i,j+1}^{n+1} - Q_{i.j-1}^{n+1}}{\rho_{j+1} - \rho_{j-1}} + \frac{Q_{i,j+1}^{n} - Q_{i,j-1}^{n}}{\rho_{j+1} - \rho_{j-1}}\right\} \tag{43}$$

and using the Crank-Nicholson scheme, and assuming equal spacing in ρ,

$$\frac{\partial^{2} Q}{\partial\rho^{2}} = \frac{1}{2}\left\{\frac{Q_{i,j+1}^{n+1} - 2Q_{i,j}^{n+1} + Q_{i,j-1}^{n+1}}{(\Delta\rho)^{2}} + \frac{Q_{i,j+1}^{n} - 2Q_{i,j}^{n} + Q_{i,j-1}^{n}}{(\Delta\rho)^{2}}\right\} \tag{44}$$

Equqtions (42)-(44) are used in Eq. (40) for $0 < \rho_j < \rho_{max}$. Assuming a cylindrically symmetric system,

$$\frac{\partial Q}{\partial\rho} = 0 \quad at \quad \rho = 0$$

Eq (40) becomes (i.e. j=0)

$$\begin{gathered}\left(1+\phi(\omega_i)\right)Q_{i,0}^{n+1} - \phi(\omega_i)Q_{i,1}^{n+1} - \left(1-\phi(\omega_i)\right)Q_{i,0}^{n} - \phi(\omega_i)Q_{i,1}^{n} = 0, \\ \phi(\omega_i) = \frac{2\Delta\xi\,\kappa(\omega_i)}{\rho_1^{2}}\end{gathered} \tag{45}$$

For the maximum radial value, ie $\rho = \rho_{max} = \rho_N$, Eq. (40) becomes

$$\theta(\omega_i)Q_{i,N-1}^{n+1} + [1-\theta(\omega_i)]Q_{i,N}^{n+1} + \theta(\omega_i)Q_{i,N-1}^{n} - [1+\theta(\omega_i)]Q_{i,N}^{n} = 0,$$

$$\theta(\omega_i) = \frac{\Delta\xi\,\kappa(\omega_i)}{2\rho_N(\rho_N - \rho_{N-1})} \tag{46}$$

Using Eqs. (42)-(46), Eq. (40) can be written in the form

$$\Xi_1(\omega_i)\bullet\bar{q}_i^{n+1} = \Xi_2(\omega_i)\bullet\bar{q}_i^{n},$$

$$\bar{q}_i^{n} = \left(Q_{i,0}^{n},\ldots,Q_{i,j}^{n},\ldots,Q_{i,N}^{n}\right) \tag{47}$$

and Ξ_1 and Ξ_2 are tridiagonal matrices. The matrix Ξ_1 is composed of the subdiagonal, diagonal and superdiagonal elements,

$$\bar{a}(\omega_i) = \left[0,\ldots,\frac{\Delta\xi\kappa(\omega_i)}{\rho_{j+1}-\rho_{j-1}}\left\{\frac{1}{2\rho_j} - \frac{1}{\rho_j - \rho_{j-1}}\right\},\ldots,\theta(\omega_i)\right],$$

$$\bar{b}(\omega_i) = \left[1+\phi(\omega_i),\ldots,1+\frac{\Delta\xi\kappa(\omega_i)}{(\rho_{j+1}-\rho_{j-1})}\left(\frac{1}{\rho_{j+1}-\rho_j} + \frac{1}{\rho_j - \rho_{j-1}}\right),\ldots 1-\theta(\omega_i)\right], \tag{48}$$

$$\bar{c}(\omega_i) = \left[-\phi(\omega_i),\ldots,-\frac{\Delta\xi\kappa(\omega_i)}{\rho_{j+1}-\rho_{j-1}}\left(\frac{1}{2\rho_j} + \frac{1}{\rho_{j+1}-\rho_j}\right),\ldots,0\right]$$

and matrix Ξ_2 is composed of the subdiagonal, diagonal and superdiagonal terms,

$$\bar{d}(\omega_i)=\left[0,\ldots,-\frac{\Delta\xi\kappa(\omega_i)}{\rho_{j+1}-\rho_{j-1}}\left\{\frac{1}{2\rho_j}-\frac{1}{\rho_j-\rho_{j-1}}\right\},\ldots,-\theta(\omega_i)\right],$$

$$\bar{e}(\omega_i)=\left[1-\phi(\omega_i),\ldots,1-\frac{\Delta\xi\kappa(\omega_i)}{(\rho_{j+1}-\rho_{j-1})}\left(\frac{1}{\rho_{j+1}-\rho_j}+\frac{1}{\rho_j-\rho_{j-1}}\right),\ldots 1+\theta(\omega_i)\right], \tag{49}$$

$$\bar{f}(\omega_i)=\left[\phi(\omega_i),\ldots,\frac{\Delta\xi\kappa(\omega_i)}{\rho_{j+1}-\rho_{j-1}}\left(\frac{1}{2\rho_j}+\frac{1}{\rho_{j+1}-\rho_j}\right),\ldots,0\right]$$

We can solve a tridiagonal system for each angular frequency, ω_i or construct a super-matrix to solve for all frequencies simultaneously. Using these three methods, Eq.(37) is used to numerically propagate the electromagnetic field in the nonlinear dispersive medium. In the limiting case of the nonlinear Schroedinger equation, the numerical results agree well with analytic solutions.

The effects of both space and time are shown in the following figures. Figure 3 shows the propagation of the nonlinear pulse for self-focusing without dispersion when the input power is less than that required for collapse. The figure shows the pulse propagation at four normalized distances. At $\xi = 0$ the incident pulse is displayed in space and time. As the pulse propagates it narrows in the radial direction but never completely collapses because the peak power is insufficient to produce collapse. However, as shown in Fig. 4, if the incident power is increased above the critical power the pulse initially narrows, and in the limit of zero dispersion, eventually collapses. When dispersion is introduced, as shown in Fig. 5, the pulse initially narrows and then splits in both space and time due to the dispersion. The splitting is also apparent in the spectrum in Fig. 6. These figures illustrate the complex behavior of 3-D spatiotemporal behavior. As the pulse narrows its intensity increases which can lead to damage in biological systems, such as ocular media. Further studies will investigate the effects of spatiotemporal phenomena on biological systems.

ACKNOWLEDGMENTS

This research was supported in part by the Air Force Office of Scientific Research and the Air Force Research Laboratory. Dr Andrew Paul contributed the numerical calculation for the radial part of the propagation code.

REFERENCES

1. J. H. Marburger, "Self-focusing: Theory", Prog. Quant. Electr. 4, 35 (1975).
2. D. Strickland and P.B. Corkum, "Short pulse self-focusing" Proc. Soc. Photo-Opt. Instrum. Eng. 1413, 54 (1991).
3. Y. Silberberg, "Collapse of optical pulses", Opt. Lett. 15, 1282 (1990)
4. P. Chernov and V. Petrov, "Self-focusing of light pulses in the presence of normal group velocity dispersion", Opt. Lett. 17, 172 (1992).
5. J. Rothenburg, "Pulse splitting during self-focusing in normally dispersive media", Opt. Lett. 17, 583 (1992).
6. A.B. Aceves and C. DeAngelis, "Spatiotemporal pulse dynamics in a periodic nonlinear waveguide", Opt. Lett. 18, 110 (1993).
7. G. Luther, J.V. Moloney, A. Newell and E. Wright, "Self-focusing threshold in normally dispersive media", Opt. Lett. 19, 862 (1994).
8. G. Luther, A. Newell and J. Moloney, "The effects of normal dispersion on collapse events", Physica D 74, 59 (1994).
9. G. Fibich, V. Malkin, G. Papanicolaou, "Beam self-focusing in the presence of small normal time dispersion", Phys. Rev. A 52, 4218 (1995).
10. M. Landman, G. Papanicolaou, C. Sulem and P. Sulem, "Rate of blowup for solutions of the nonlinear Schroedinger equation at critical dimension", Phys. Rev. A 38, 3837 (1988); and references therein.
11. Q. Feng, J.V. Moloney, A.C. Newell, E.M. Wright, K. Cook, P.K. Kennedy, D.X. Hammer and C.R. Thompson, "Theory and simulation of laser-induced breakdown and self-focusing of ultrashort focused laser pulses in water", preprint.
12. M.J. Potasek, "Femtosecond solitons in optical fibers", J. Appl. Phys. 65, 941 (1989); and references therein.
13. G.P. Agrawal, Nonlinear Fiber Optics (Academic Press, NY, 1989); and references therein.
14. P. K. Kennedy, S.A. Boppart, D.X. Hammer, B.A. Rockwell, G.D. Noojin and W.P. Roach, "A First-Order model for computation of laser induced breakdown thresholds in ocular and aqueous media: Part II-code description and comparison to experiment", IEEE J. Quant. Electron., 31, 2250 (1995).
15. B.A. Rockwell, W.P. Roach and M.E. Rogers, "Determination of self-focusing effects for light propagating in the eye", Laser-Tissue Interaction V 2134, 2 (1994).
16. P.W. Lappin, "Ocular damage thresholds for the helium-neon laser", Arch. Environ. Health 20, 17 (1970).
17. G.H. Bresnick, et.al., "Ocular effects of argon laser radiation I. Retinal damage threshold studies", Invest. Ophthalmol. 9, 901 (1970)
18. R.G. Allen, S. J. Thomas, R.F. Harrison, J.A. Zuclich,and M.F. Blankenstein,"Ocular effects of pulsed Nd laser radiation: variation of threshold with pulsewidth", Health Phys. 49, 685 (1985).
19. W. P. Roach, C.A. Toth, C.D. Stein, G. D. Noojin, D. J. Stolarski and C. P. Cain, "Minimum visible lesions from pico- and femtosecond laser pulses", Proc. SPIE, Laser-Tissue Interaction V, 2134, 10 (1994).
20. J. Taboada and W. D. Gibbons, "Retinal tissue damage induced by single ultrashort 1064 nm laser light pulses", Appl. Opt. 17, 2871 (1978).
21. A. J. Goldman, W.T. Ham, and H.A. Mueller, "Ocular damage thresholds and mechanisms for ultrashort pulses of both visible and infrared laser radiation in the Rhesus monkey", Exp. Eye Res., 24, 45 (1977).

22.X.D. Cao, G.P. Agrawal and C.J. McKinstrie, "Self-focusing of chirped optical pulses in nonlinear dispersive media", Phys. Rev. A 49, 4085 (1994).
23. A.T. Ryan and G.P. Agrawal, "Pulse compression and spatial phase modulation in normally dispersive nonlinear Kerr media", Opt. Lett. 20, 306 (1995).
24. Berge, J. J. Rasmussen, E. A. Kuznetsov, E. G. Shapiro and S. K. Turitsyn, "Self-focusing of chirped optical pulses in media with normal dispersion", J. Opt. Soc. Am. B, 13, 1879 (1996)
25. P.V. Mamyshev and S.V. Chernikov, "Ultrashort-pulse propagation in optical fibers", Opt. Lett. 15,1077 (1990).
26. F.M. Mitchke and L.F. Mollenauer, "Discovery of the soliton self-frequency shift", Opt. Lett. 11, 659 (1986).
27. J.P. Gordon, "Theory of the soliton self-frequency shift", Opt. Lett. 11, 662 (1986).
28. K.J. Blow and D. Wood, "Theoretical description of transient stimulated Raman scattering in optical fibers", IEEE J. Quantum Electron. 25, 2665 (1989).
29. M. J. Potasek and A. E. Paul, "Investigation of nonlinear ocular media using femtosecond laser pulses", Proc. Laser and Noncoherent Ocular Effects: Epidemiology, Prevention, and Treatment, SPIE, vol 2974, 66 (1997).

FIGURE CAPTIONS

Fig. 1 The dependence of the nonlinear coefficient ($\bar{\beta}$) on wavelength (λ_0), spatial beam waist (a_0), and pulse intensity (A^2_0).

Fig. 2 The dependence of higher order dispersion ($\bar{\gamma}$) on temporal pulse width (T_0), spatial beam waist (a_0), dispersion (k_3) and wavelength (λ_0).

Fig. 3 Pulse propagation as a function of distance in the non-dispersion case.

Fig. 4 Pulse propagation as a function of distance in the non-dispersion case for peak intensity above the critical value.

Fig. 5 Pulse propagation including both self-focusing and dispersion effects.

Fig. 6 The spectra corresponding to the case shown in Fig. 5.

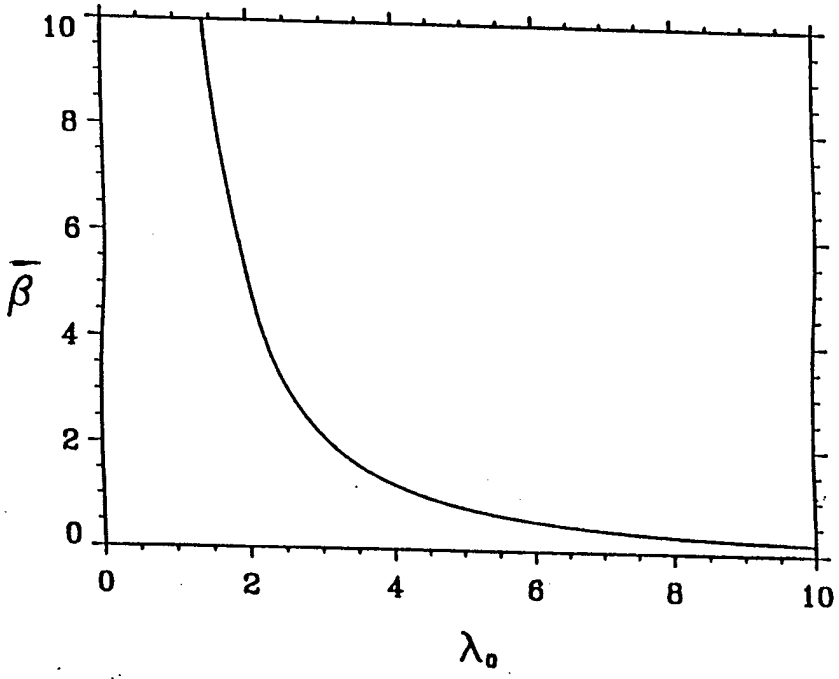
10
8
6
4
2
0
$\bar{\beta}$
0
2
4
6
8
10
λ_0

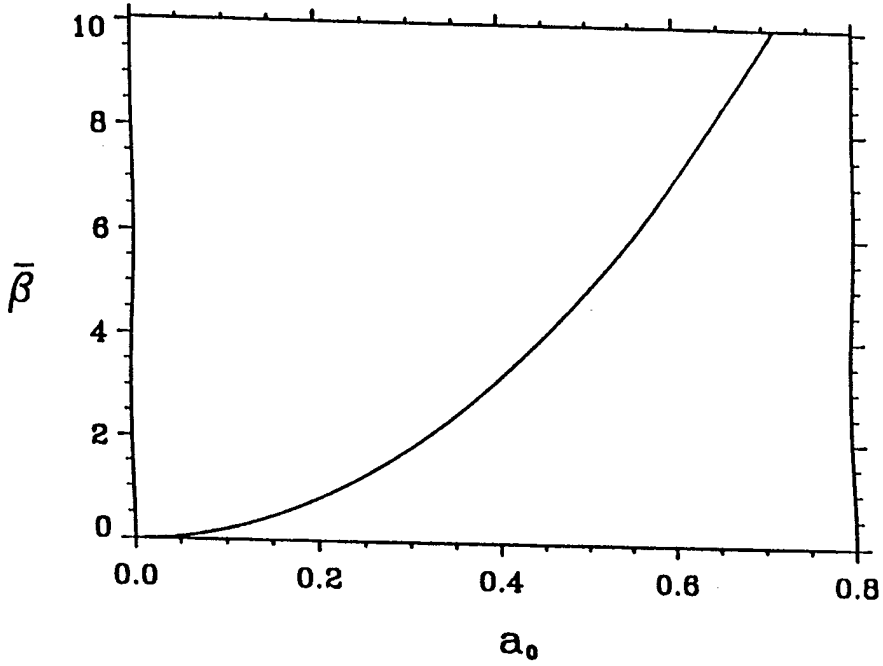
10
8
6
4
2
0
$\bar{\beta}$
0.0
0.2
0.4
0.6
0.8
a_0

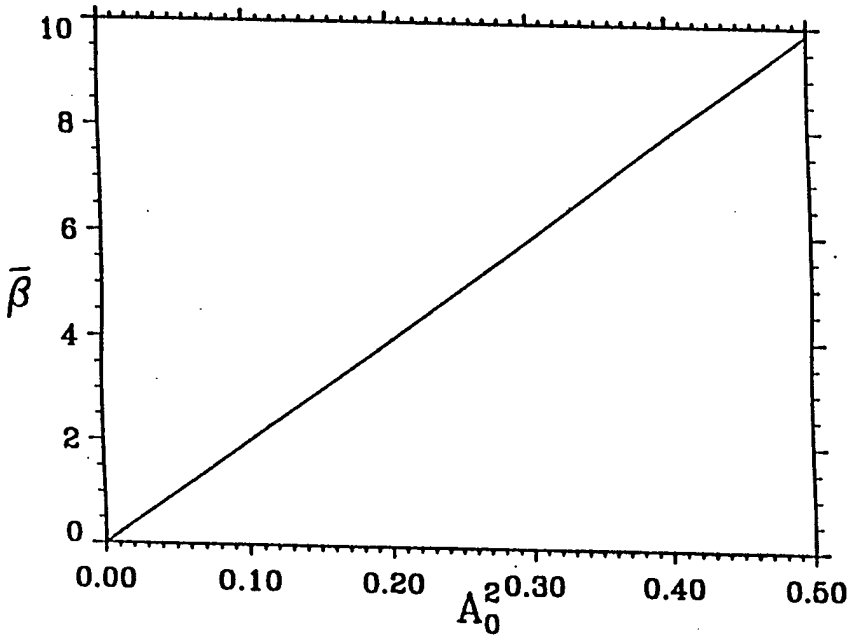
10
8
6
4
2
0
$\bar{\beta}$
0.00
0.10
0.20
0.30
0.40
0.50
A_0^2

Fig. 1

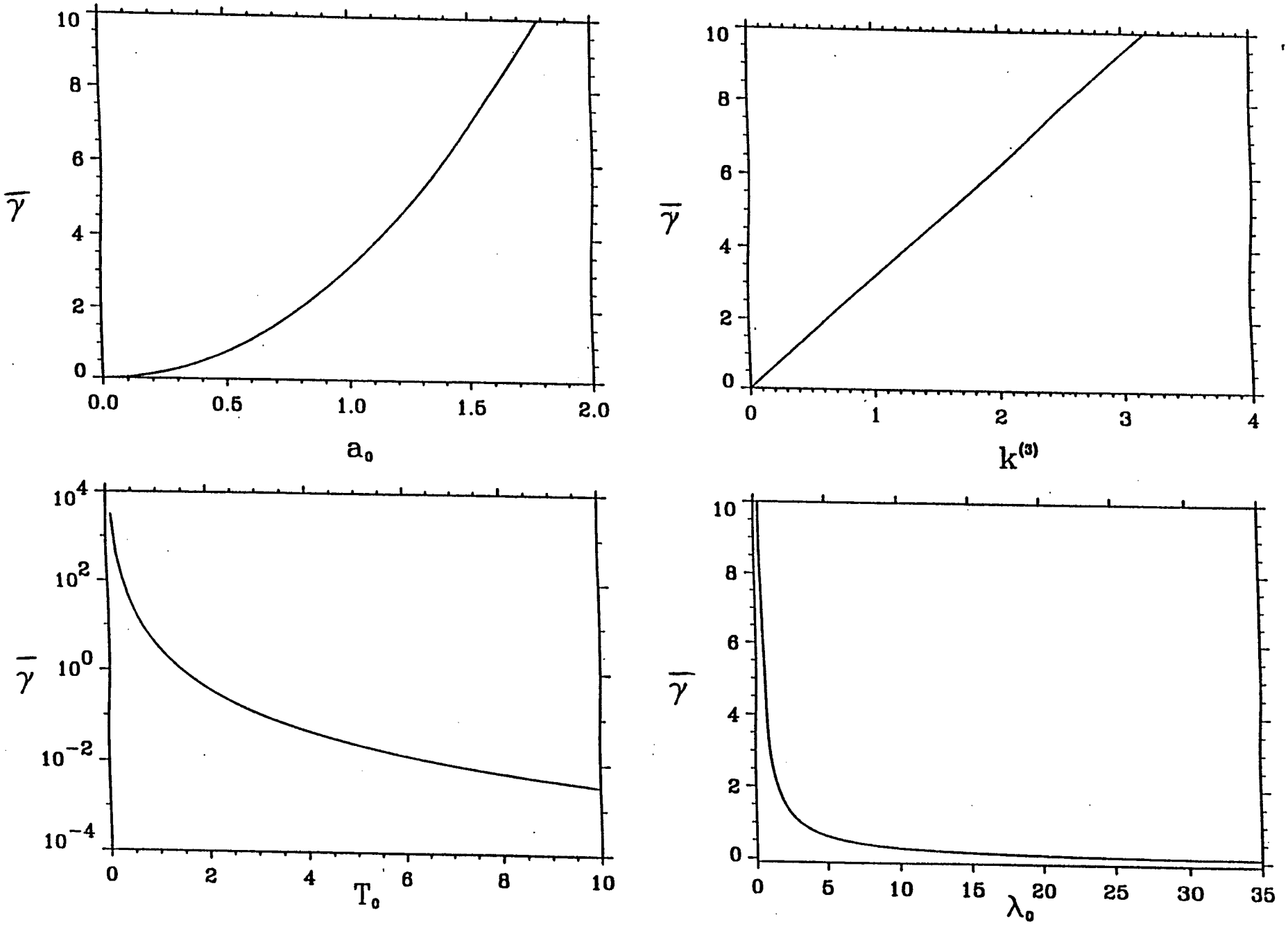

Fig. 2

Self-Focusing with out Collapse

($p = 1$ and $\gamma = \delta = \sigma = \tau_R = 0$)

$\xi = 0$
Peak = 1

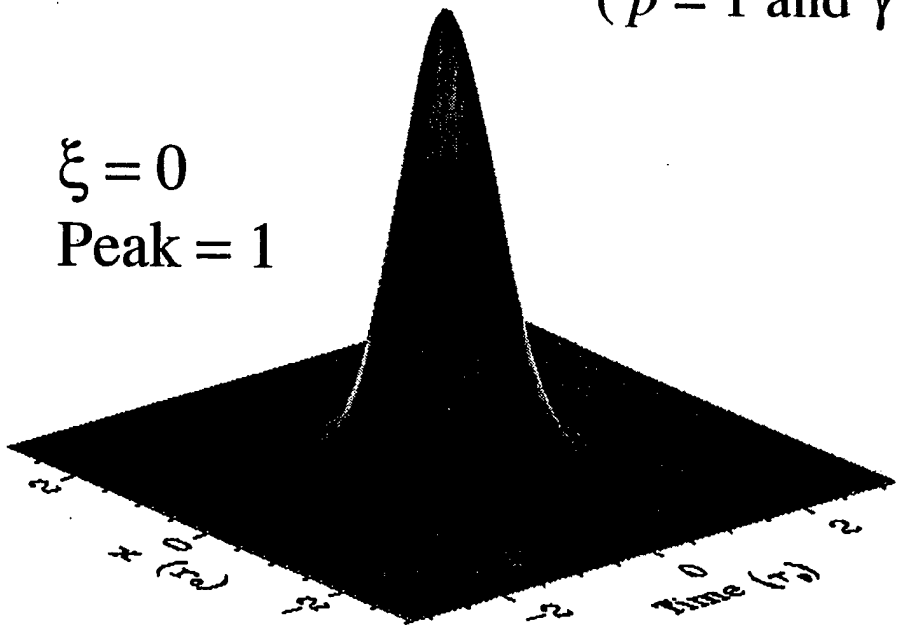

$\xi = 1.2$
Peak = 1.7

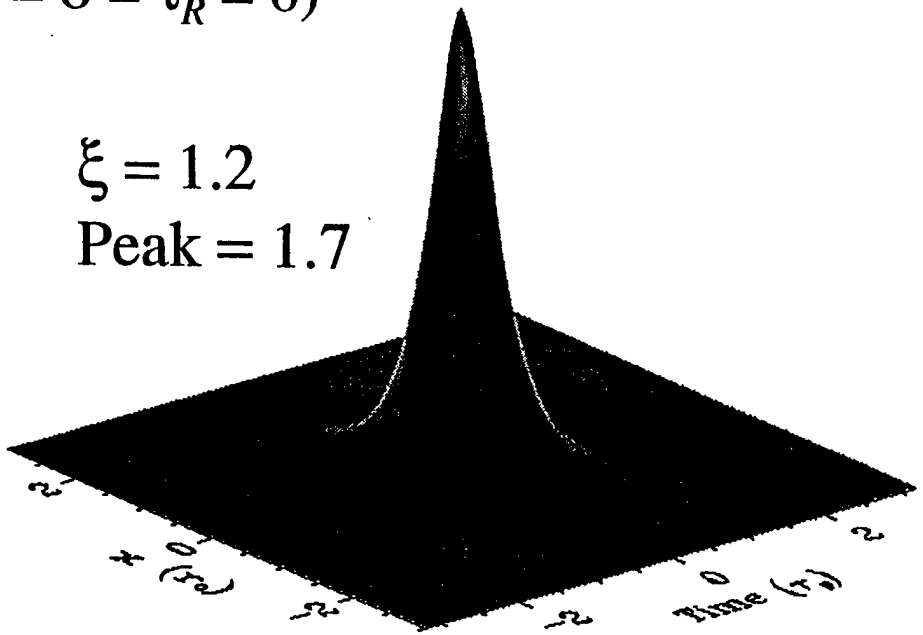

$\xi = 2.6$
Peak = 1.5

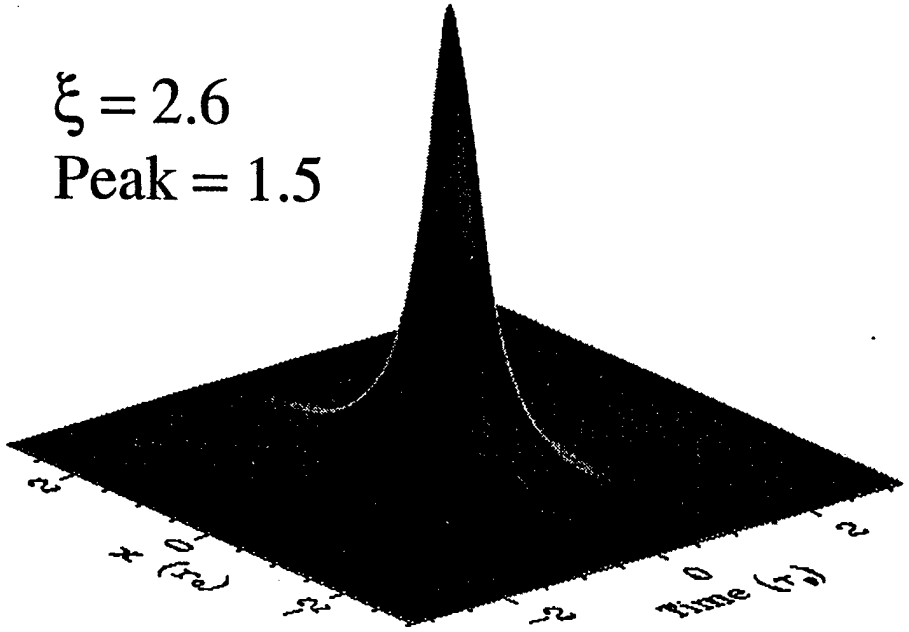

$\xi = 4$
Peak = 0.9

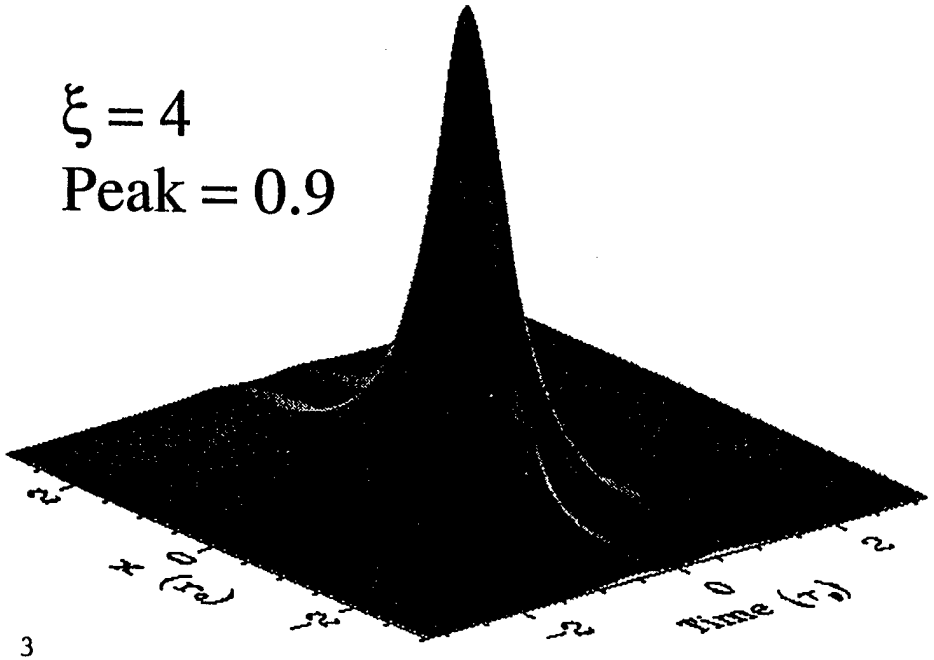

Fig. 3

Critical Collapse from Self-Focusing

($p = 1.2$ and $\gamma = \delta = \sigma = \tau_R = 0$)

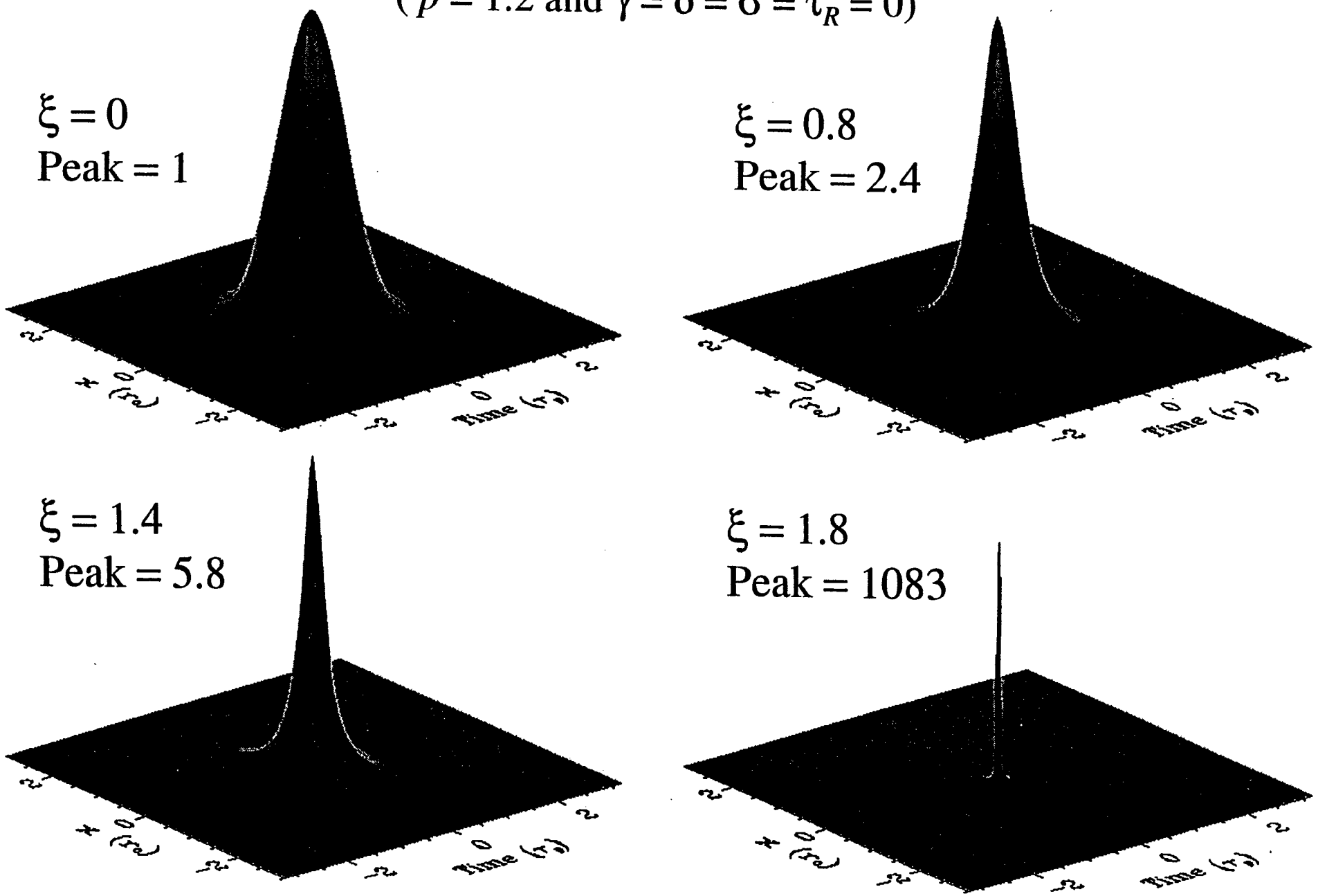

Fig. 4

The Effect of 2nd Order Dispersion on Collapse

($p = 1.475$, $\gamma = 0.0755$, and $\delta = \sigma = \tau_R = 0$)

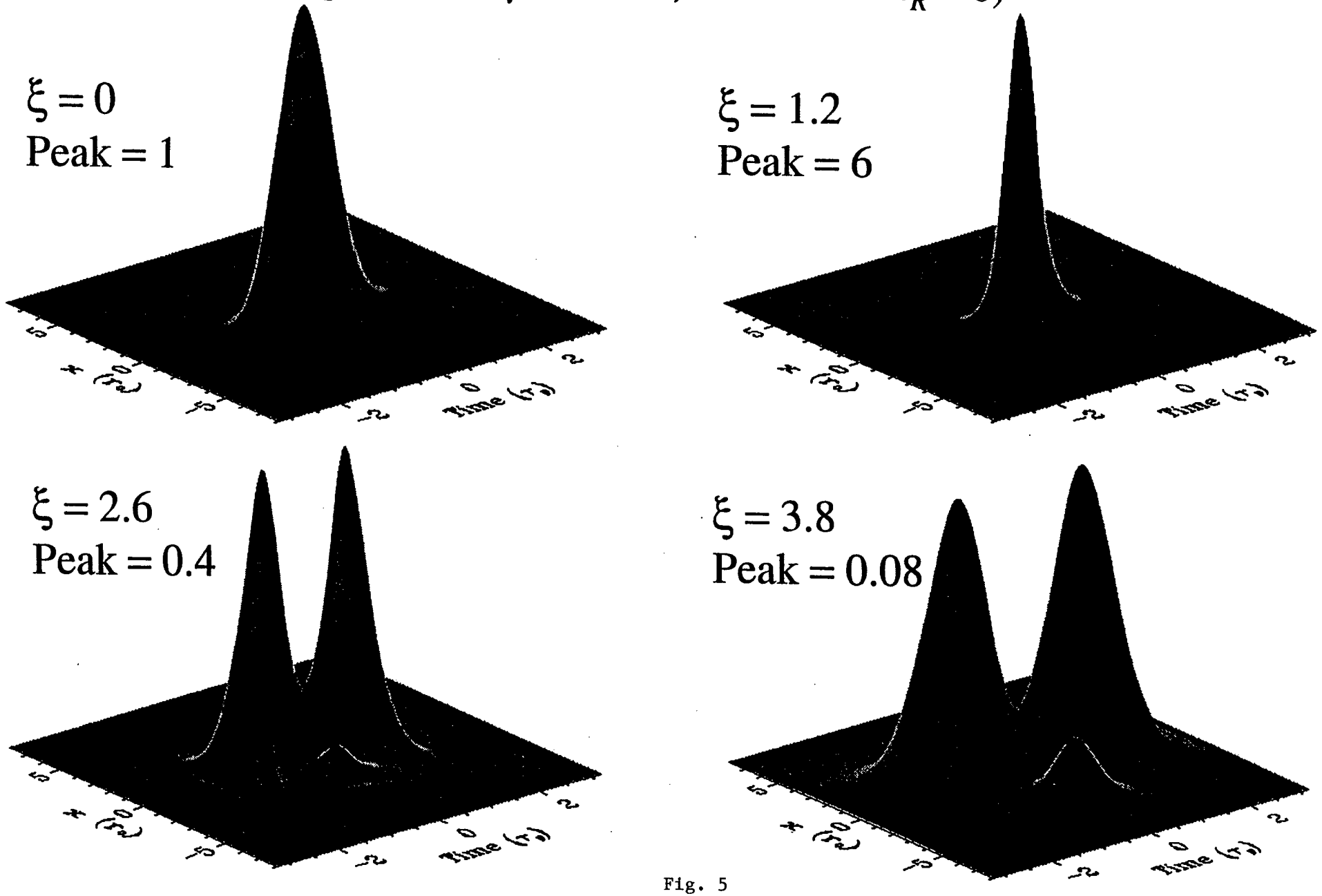

Fig. 5

Spectrum for 2nd Order Dispersion with Collapse

($p = 1.475$, $\gamma = 0.0755$, and $\delta = \sigma = \tau_R = 0$)

$\xi = 0$
Peak = 1

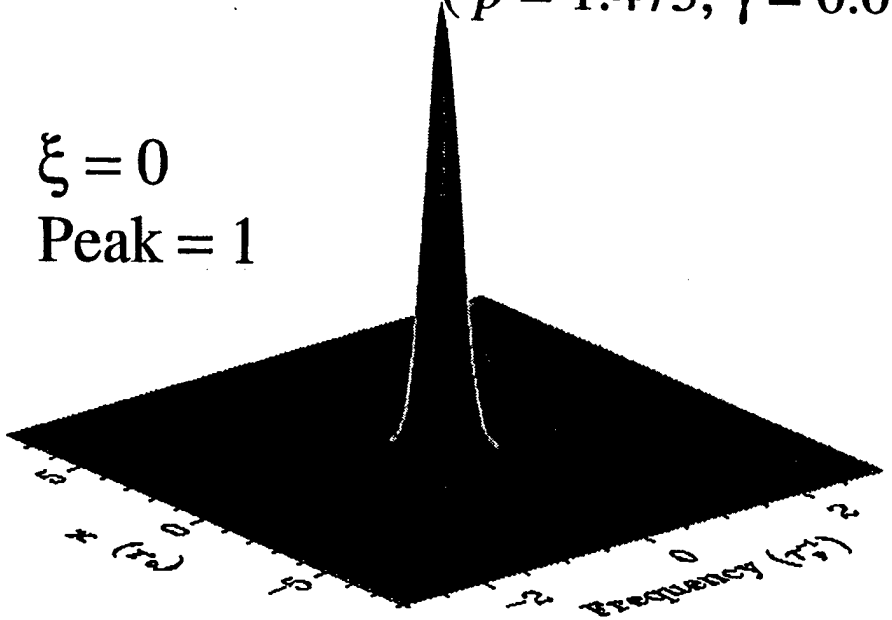

$\xi = 1.2$
Peak = 1.1

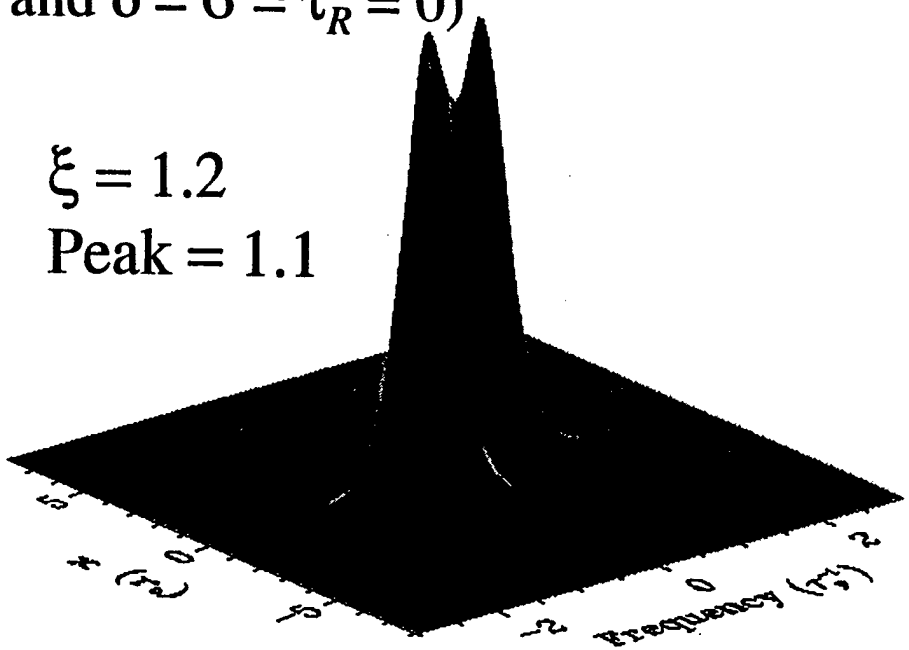

$\xi = 2.6$
Peak = 0.2

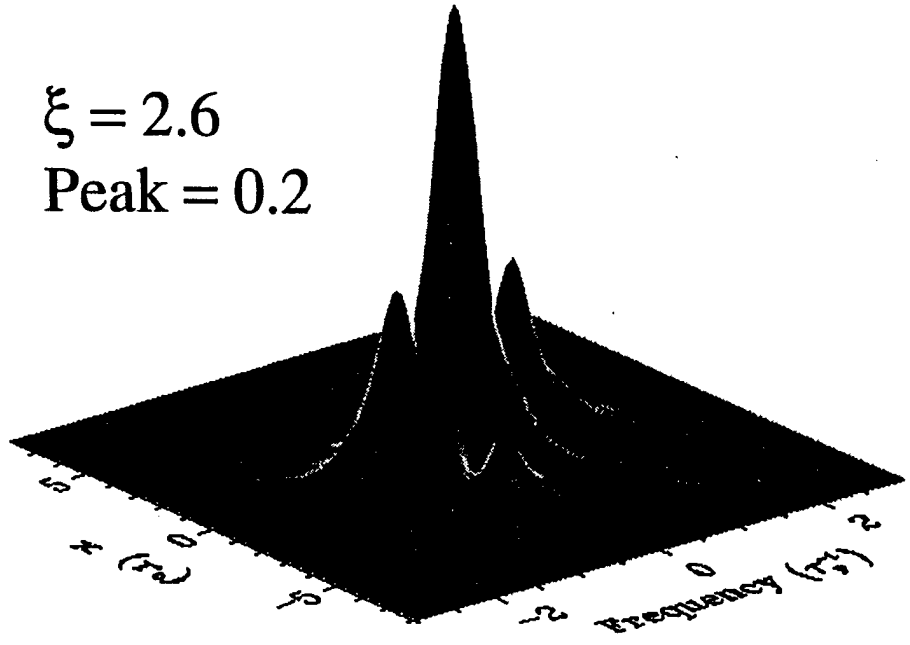

$\xi = 3.8$
Peak = 0.07

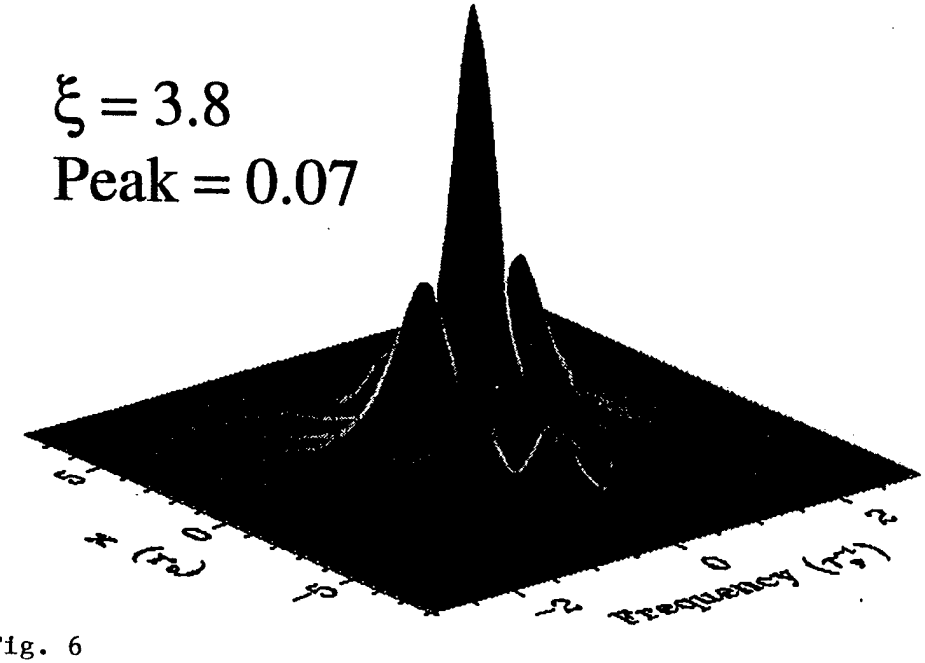

Fig. 6

Infrared Lasers & Millimeter Waves
Workshop
The Links Between Microwaves
& Laser Optics

21 Jan 1997 - 22 Jan 1997

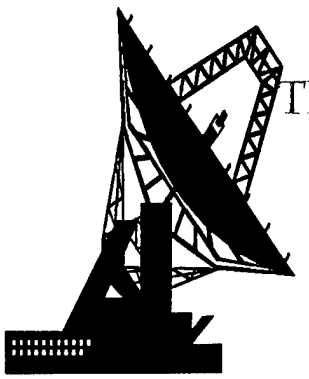

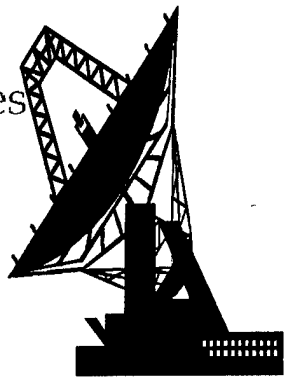

SECTION VI:

DOSIMETRY

The Wireless Technology Age: Near-field, Hotspot and Dosimetry Problems

by

Arthur W. Guy, Ph.D.
Wireless Technology Research, L.L.C.
18122 60th PL NE
Seattle, WA 98155

Introduction

The rapid development of new wireless communication and data transmission systems has spurred the application of new dosimetric techniques where exposure fields and energy absorption rates in exposed biological body tissues are now being quantified more rapidly and accurately than ever before. The new technology has been particularly valuable in allowing researchers to improve their experimental methodology and safety regulators to develop a better rationale for exposure standards. The proximity of portable wireless transmitting devices to the body of the user has presented some complicated problems in evaluating the exposure of biological tissues to near fields, the quantification of highly localized specific absorption rate energy in the tissues and the design of *in vivo* and *in vitro* exposure systems for evaluating the biological effects of such exposures.

Figure 1 illustrates the quantities and units used for guides and standards pertaining to the exposure of humans to electromagnetic fields. The guides are specified in terms of the electric field strength, E, expressed in units of volts per meter (V/m); the magnetic field strength, H, expressed in units of amperes per meter (A/m) and power density, P, expressed units of milliwatts per square centimeter (mW/cm^2). The latter may be obtained for a radiation field through a measurement of either E or H and relating the quantity to power density, P, by the equations shown at the bottom of the Figure. These equations have also been applied to near zone or non-radiation fields with the understanding that the calculated result is an "apparent" or "equivalent" power density rather than a true power density.

The specific absorption rate (SAR) of energy in exposed tissue expressed in units of watts per kilogram (W/kg), rather than power density, is the most important dosimetric quantity for evaluating exposure to wireless devices. SAR can be used as a meaningful quantity for relating any biological effect to electromagnetic fields. The SAR is a measure of the rate of absorbed energy which may or may not all be dissipated as heat. If other mechanisms of interaction are at work in the exposed tissues, some fraction of the SAR, even if infinitesimal, must be attributed to this interaction. Thus, the use of the quantity SAR does not imply that the only interaction mechanism is heat.

If one is to use the biological results from animal experiments for assessing the biological consequences of human exposure in order to establish safe levels of exposure, simply relating the incident energy measured with a survey meter, is not enough. When applied to human safety, the quantities that are related to thresholds of biological effects in exposed laboratory animals or in

vitro animal cells must be scaled either up or down to account for the differences in human shape and size as indicated in Figure 2. The characteristics of energy absorption are considerably different in animals and man exposed to the same incident energy, $I_{m,r}$. The scattered energy, $S_{m,r}$, transmitted energy, $T_{m,r}$, and reflected energy between tissue boundaries, $R_{m,r}$, vary markedly as a function of the wave length, exposed body size and shape, the exposed body orientation and the environment. In addition, any laboratory instrumentation in contact with the tissues of the animal will also perturb and often may considerably enhance the absorbed energy or SAR in the tissues of the exposed subject. Thus, one has to be extremely careful and be cognizant of the pitfalls of using instruments within the exposure field because the wiring between the animal and the instrumentation will also absorb electromagnetic energy. Extraneous currents are likely to be induced into the wires which can produce artifacts and lead to erroneous conclusions about the effect of the rf fields on the exposed subject. Instruments used in the presence of rf fields require very careful design. In order to relate the biological effects observed in the exposed laboratory animal to potential effects in exposed man, one has to quantify the fields in the tissues. Since the SAR has been the easiest quantity to measure and is an index of the internal electric field strength, its use has been widely accepted. The SAR quantity has been defined by the National Council on Radiation Protection and Measurements (NCRP) as an important quantity for use in nonionizing radiation dosimetry (NCRP, 1980). One should understand the difference, however, between spatially dependent term, SAR, which is defined for a point in the tissue and the term, average SAR, which is a whole body average of the SAR. For hand-held cellular telephones, the former is more important since the energy absorption is highly localized, resulting in much higher SAR at the surface tissues of the hand and head than the whole body-average SAR. Thus for cellular telephone exposure, we are concerned mainly with methods for quantifying the localized SAR distribution in the head.

SAR distribution in head of cellular telephone user

The most popular and frequently used method for quantifying the magnitude and distribution of the SAR in the head of a cellular telephone user is through the use of a powerful computer technique called the finite difference time domain (FDTD) method . The FDTD technique utilizes as input, the construction details including the RF radiating structure and excitation parameters of the telephone as well as the characteristics of the exposed body and its dielectric properties. This information is then fed into a computer and Maxwell's equations are solved using the FDTD method. The result is a detailed 3-dimensional pattern of the electric and magnetic fields and the SAR in tissue which may easily be visualized by standard graphical software. Given an electromagnetic source and an environment containing different geometries of materials or biological tissues, the method solves Maxwell's equations in the time domain. The method separates the model, for this case the human head and shoulders, into more than a million small cells or elements which may be cubical or rectangular shaped solid elements with sides of different dimensions. Each element or voxel is characterized in terms of tissue type, dielectric properties and density. A source such as a cellular telephone is modeled by separating it into voxels of proper conductivity and dielectric properties in the same manner as used for the human subject and is placed near the head of the model subject. The SAR in each voxel is then calculated on a

computer by stepping through short time intervals until the solution to Maxwell's equations converges to a steady state value. There are a number of papers covering the application of the FDTD technique to wireless technology in a recent special issue of the IEEE Transactions on Microwave Theory and Techniques (IEEE, 1996). Gandhi (1995) was one of the first to perfect such a model for the case of evaluating the exposure of a cellular telephone user to 840-MHZ to 900-MHZ rf fields. His model is based on Magnetic Resonance Imaging (MRI) scans of a human volunteer, obtained every 3 mm from the top of the head to the feet, providing a resolution of about 2 mm per pixel for each body cross sectional slice.. Fig 3 shows the overall view of one of Gandhi's FDTD scans where It can be seen that most of the energy is absorbed in the ear, where the top of the cellular telephone is placed. Some energy also is absorbed in the brain, but much less than in the ear. The highest tissue SARs found in the analysis of eight different cellular telephones approached about 1.5 W/kg specifically, in the ear, but in the brain itself, the SAR levels were down to 0.4 W/kg. This value is consistent with the analysis by Balzano (1995) based on actual measurements. Gandhi also did some measurements that confirmed his calculations. On the other hand, Niels Kuster (1993), using the same model as Balzano, measured SAR values well over 1.5 W/kg in the ear and brain tissues when looking at the highest exposure scenario. However, to obtain these higher values, Kuster placed the cell telephone antenna at distances much closer to the model head (atypical for most cell phone users) than used by Gandhi and Balzano. He also tested a phone with a shorter one quarter wavelength long antenna (not used in the United States) which results in higher SAR near the base of the antenna This issue is one that has to be resolved through agreement on antenna types and locations of the antenna relative to the head, typical of cellular telephone use.

Simulation of human exposure to cellular phones by means of laboratory animals

Exposure considerations for evaluating possible health effects of human exposure to cellular phones are quite different than those for other types of radio sources in the environment. Typical exposures to radio and television antennas, microwave dishes, mobile radios, small boat radars and marine radios involve whole-body illumination at a distance from the source. In such cases, RF energy is absorbed at all locations in the body, with peak values varying on the order of 20 times the whole-body average. Exposure standards for the general population are based on a large body of research data involving whole-body exposure of laboratory animals. IEEE/ANSI (1991) standards for the general population in uncontrolled environments limit whole-body SAR to 0.08 W/kg, and peak SAR to: a) 1.6 W/kg as averaged over a gram of tissue for the head and trunk of the body; and b) 4.0 W/kg as averaged over any 10 grams of tissue for the limbs. Note that the peak SAR values specified are derived from data looking at significant whole-body exposure of animals. Currently available measurements and calculations indicate that cellular phone use results in a whole-body SAR of less than 0.00088 to 0.004 W/kg in humans, with a much higher 1-gram average in the head of 0.25 to 4.0 W/kg—a ratio of head to whole-body absorption as high as 1000:1. Thus, research results from the whole-body exposures described above are of limited relevance to the assessment of cellular telephones, and new research should be based on exposure paradigms that truly duplicate human exposures. Whole-body average SAR, or, if possible, whole-head average SAR and peak SAR in the head should be related as closely as possible to human exposure to cellular phones or wireless instruments.

A typical SAR pattern resulting from human exposure to cellular telephones is shown in Figure 4 based on the mathematically-simulated, realistic model of the human head exposed to a mathematically- simulated cellular telephone discussed above. The figure illustrates the SAR in a horizontal slice (3 mm thick) of the head through the ear region, where the SAR was maximum. The peak brain surface SAR shown in Figure 1 is 0.4 mW/g, and the calculated peak SAR in the ear tissue shown is approximately 1.5 W/kg as averaged over a 2 mm x 2 mm x 3 mm voxel (less than a gram of tissue).

SAR levels and patterns vary with the type of telephone tested (Gandhi, 1995). For various phone models, maximum SAR was found to vary between 0.96 and 4.03 W/kg, with the maximum SAR averaged over a gram of ear tissue ranging from 0.16 to 0.69 W/kg. Peak SARs in brain tissue varied between 0.31 and 1.99 W/kg as averaged over a voxel and 0.10 to 0.41 W/kg as averaged over a gram. The corresponding whole-body average SAR for the exposure depicted in Figure 3 was 0.00081 - 0.00235 W/kg. Kuster *et al.* (1993) have measured peak SARs as high as 3.6 W/kg averaged over a gram of tissue in an exposed phantom head model. Generally the ratio of peak to whole-body average SAR will increase with increasing frequency as a result of the decreasing depth of penetration of the incident energy from rf sources.

In examining Figure 3 and comparing it with results obtained from conventional, whole-body *in vivo* exposure systems, it becomes increasingly clear that a highly localized, head-only exposure system is required for any *in vivo* exposure systems used to simulate human exposure to cellular telephones. For example, the literature indicates that, for whole-body exposures, whole-body SAR will be 70 to 100% of the peak values in the head. Thus, if we expose the entire body of a rat to levels that produce SARs in the brain that are roughly equal to those experienced by a person, the rat would be subjected to a whole-body average SAR as high as 4 W/kg. This represents a total, whole-body absorption of 1.2 watts—roughly twice the power available from a cellular telephone operating at maximum power. Many well-documented experiments have shown that whole-body exposure at this level will cause deleterious effects in exposed animals from thermal loading. Thus, a whole-body exposure will not produce a valid duplication of the low-level exposures from cellular telephones.

Basic design of animal head only exposure system

A number of approaches for generating exposures in small animals that are roughly analogous to human exposures are available. One option is a miniaturized or scaled-down cellular telephone antenna placed near the head of the animal, with the frequency proportionately scaled up to provide the same current distribution on the antenna. It has been shown (Balzano *et al.*, 1995) that it is the magnetic field related to the axial electric field or the current along the antenna which is primarily responsible for the SAR in the exposed tissues of the head. The radial electric field, proportional to the charge distribution along the antenna, contributes very little to the tissue SAR. Since the length of a typical cellular telephone antenna is close to one-half wavelength, the current is generally high at its midpoint. For a scaled-down antenna at the same frequency, however, this current would be greatly reduced, while the charge would be significantly increased. This situation results in a much lower magnetic field and a higher ratio between the radial and the axial

electric fields.

Another option is a small magnetic loop placed near the head of the animal. For the loop system, a high current and associated magnetic field could be maintained regardless of how much the loop is reduced in size. It is intuitively clear that the surface area of the localized exposure can be controlled by changing the size of the loop, and the SAR gradient penetrating into the head can be controlled by changing the distance of the loop from the head.

In addition to the work done by other investigators, for illustrative purposes, the author employed a crude rat model with an ellipsoidal volume of brain, surrounded by a thin shell of bone to simulate the skull of the animal. The SAR distribution was calculated by means of the admittance computer numerical model (Armitage *et al.*, 1983) which is valid when the size of the source and target are small compared to a wavelength. Though the conditions are marginal for this case, it was felt that the results would be qualitative enough to illustrate the point that loop source could produce the desired localized SAR distribution. To simplify the model, the simulated bone shell was placed to surround the entire ellipsoid. Since the exposure is highly localized at the head, the rest of the simulated body has very little effect on the calculated SAR pattern. The small current loop produced an SAR distribution that varied as expected with the size and spacing of the loop.

Figure 4 illustrates the highly localized SAR pattern calculated for a very small loop placed close to the head. This pattern is too localized to simulate the SAR distribution from human exposure to cellular phones. By increasing the size and spacing of the loop, however, the calculated results graphed in Figure 5 does begin to mimic more closely the size and shape of the SAR pattern from human exposure to cellular telephones.

Exposure of biological cell *in vitro* preparations to simulate human exposure to cellular telephones

In exposures of *in vitro* preparations to rf fields, it is desirable to maintain as uniform SAR as possible while keeping the temperature and environment conditions under precise control to prevent artifactual electrical and thermal "hotspots" from developing. In the past, a common exposure system frequently consisted of an rf radiation source, usually a microwave horn, to expose cells cultured in ordinary culture dishes or flasks suspended in free space or an anechoic chamber in front of the radiator.. Because the flasks were exposed in free space to a radiating field, the SAR was fairly nonuniform, and was highly dependent on the size and shape of containers, sharp discontinuities between the cell medium and air, and the polarization of the incident radiation. If not carefully controlled, this type of exposure can result in RF "hot-spots" in the medium. The SAR in the exposed cells and medium is highly dependent on the container shape, size and orientation.

Standard containers in air or liquid exposed in a TEM cell

Cell culture dishes or flasks may be exposed to RF radiation in a transverse electromagnetic

(TEM) cell. TEM cells provide exposure conditions most similar to the free-space environment and have thus been widely used in the past for these types of exposures. The TEM cell is able to simulate free space exposures in a relatively small space with considerably less power requirements. Also its design facilitates efficient forced air cooling. Figure 6. Illustrates an example of a TEM cell design. It consists of a rectangular cylinder containing a metal septum midway between the lower and upper walls of the cylinder. A coaxial connector is connected at one end so that the inner conductor tapers gradually from the round coaxial center conductor to a broad flat plate that forms the septum and the outer conductor is tapered from the cylindrical shape of the outer conductor or the coaxial connector to the rectangular shape or the cylinder walls. The opposite end of the rectangular cylinder and septum tapers down to a similar coaxial connector where a perfectly absorbing load can be attached to prevent any reflections from disturbing the field in the TEM cell. Since the TEM cell simulates free space radiation conditions in the region midway between the center septum and upper and lower walls, all of the polarization effects for free space radiation also apply to this method of exposure. However, if the exposed object is placed close to the septum or the upper and lower walls, the close proximity of its image to the near-by conducting surface will result in a different SAR pattern than that for free space. For a given frequency, the internal dimensions of the TEM cell cannot exceed certain limits without the introduction of higher-order modes of transmission. These modes can change the internal fields so they no longer resemble free space radiation fields. The height and width of the TEM cell should be less than one-half the wavelength of the highest frequency to be used. With careful design, however, a relatively pure TEM wave may be maintained in a larger TEM cell if no discontinuities are introduced that excite the higher-order modes. Since minimizing the energy coupling to an exposed body also minimizes the discontinuity caused by the body's presence, it may be possible to expose flask configurations with the low energy coupling polarizations. The author conducted an FDTD analysis of the SAR patterns in the culture medium for different flask orientations. Figure 7 illustrates the SAR pattern in the bottom layer of a 2x2x0.25cm rectangular culture medium exposed in the TEM cell shown in Figure 6 to a polarization where the x-axis is parallel to the broad face and perpendicular the long axis of the TEM cell, the y-axis is parallel to the narrow face and perpendicular to the long axis of the TEM cell, and the z axis is parallel to the direction of propagation along the long axis of the TEM cell. Thus the culture medium is located midway between the septum and the upper wall and oriented with its broad face perpendicular to the direction of propagation of the rf energy along the long axis of the TEM cell. For numerical analysis of the SAR pattern using the FDTD method, the culture medium was divided up into 13,000 cubes (voxels), with dimensions of 0.4 mm. A histogram and table of statistics for the SAR calculated for the 2601 voxels representing the bottom layer of the culture medium is shown in Figure 8. The coupling is fairly efficient for this orientation with a mean of 21.8 W/kg and a peak of 95.8 W/kg at the corners of the culture medium for 10 watts input to the TEM cell. The SAR distribution is very nonuniform for this case. When the culture medium was exposed midway between the septum and the upper wall while oriented with its broad face parallel to the broad face of the septum, the distribution shown in Figure 9 and histogram and table of statistics shown in Figure 10 were obtained. Here the SAR is much less, with a mean of only 0.252 and a peak of 1.96 W/kg. For this case the SAR distribution is quite uniform except near the outer edges of the culture medium . Figures 11 and 12 show the results of the SAR analysis for the case where the culture medium used in the previous exposure is lowered to set down on top of

the septum. The resulting SAR is again quite low but the pattern is quite nonuniform because of the effect of the image of the culture medium in the metallic septum of the TEM cell.

In order to ensure that appropriate SAR levels are utilized for *in vitro* exposures, it is important to know the highest levels of SAR to which humans are exposed when using a portable cellular telephone. Although a large amount of data is becoming available from theoretical calculations and experimental measurements of SAR in models of the human head, there is a great deal of disagreement in reported values. Peak values of SAR are usually expressed in terms of averages over a gram of tissue in the shape of a cube, averages over a voxel (3-dimensional cube) in a computer model, or an average over the volume occupied by a field sensor. None of these truly provide the SAR as averaged over a single *cell*, which is the ideal value for setting *in vitro* exposure levels.

Of the data available, peak values of SAR associated with the smallest voxels (2 mm x 2 mm x 3 mm) used for theoretical FDTD studies of the exposed head—once validated by experimental measurements—will probably provide the most accurate estimate of exposure at the cellular level. Reported values range from 1.06 to 1.99 W/kg in brain tissue and as high as 4.8 W/kg in other tissues. Although these numbers are an average over a volume much larger than a cell, there is probably not much variation of SAR throughout a single voxel (12 mm^3 volume) at the frequencies of current- and future-generation wireless communications systems. Based on the highest reported voxel SAR, therefore, a typical cell might be exposed to SAR as high as 2 W/kg in the brain and as high as 5 W/kg in other tissues.

A number of arguments and rationales have been raised for exposing *in vitro* samples above the value of 5 W/kg. Some favor increasing the exposure to the point where an effect is seen, and then decreasing the exposure level until the effect disappears. Others favor exposing at the 5 W/kg level and at levels ten times above and ten times below that value, in order to encompass all possible responses. It has been suggested by some investigators that a study will only provide useful information if some kind of quantifiable response is evoked; however, the only known quantifiable effects seen at these frequencies are related to high levels of exposure which produce heating. These types of thermal effects are not likely from exposure to cellular phones.

It is apparent from these results that exposures with relative uniform SAR distributions are possible within the TEM cell but considerable input powers will be necessary to bring SAR levels up to the maximum desired levels of 5 W/kg and above and cells must be restricted from the corners and restrained to the broad bottoms of the culture flasks to prevent them from being in nonuniform SAR and hot spots.

References:

Armitage, D.W., H.H. LeVeen, R. Pethig, (1983) "Radiofrequency-Induced Hyperthermia: Computer Simulation of Specific Absorption Rate Distributions Using Realistic Anatomical Models", Phys. Med. Biol., vol. 28, no. 1, pp. 31-42.

Durney CH, Massoudi H, Iskander M. F., (1986) Radiofrequency Radiation Dosimetry Handbook, 4th Ed. Report USAFSAM-TR-85-73. October 1986. Brooks AFB, TX:USAF SAM.

Kuster N, Schmid T, Meier K. "Untersuchungen der Absorption im extremem Nahfeld vo Sendern", Proceedings VDE Meeting, Bad Nauheim, Germany, November 9-10, 1993.

Gandhi, O.P., (1995), State of the Science Regarding RF Dosimetry, Measurements, and Certification, State of the Science Colloquium, University "La Sapienza" of Rome, Rome, Italy, 13-15 November 1995

Balzano Q, Garay O, Manning T., (1995), "Electromagnetic energy exposure of simulated users of portable cellular telephones." IEEE Transactions on Vehicular Technology 1995:44(3), 390-403.

Institute of Electrical and Electronics Engineers, "IEEE Standard for Safety Levels with Respect to Human Exposure to Radio Frequency Electromagnetic Fields, 3 kHz to 300 GHz", IEEE Standards Coordinating Committee SCC28 on Non-Ionizing Radiation Hazards, Approved September 26, 1991, IEEE Standards Board.

Rosen, Arye and Vander Vorst, Guest Editors, "Part II of two parts, Special Issue on Medical Application and Biological Effects of RF/Microwaves", IEEE Transactions on Microwave Theory and Techniques 1996:44(10).

List of figures:

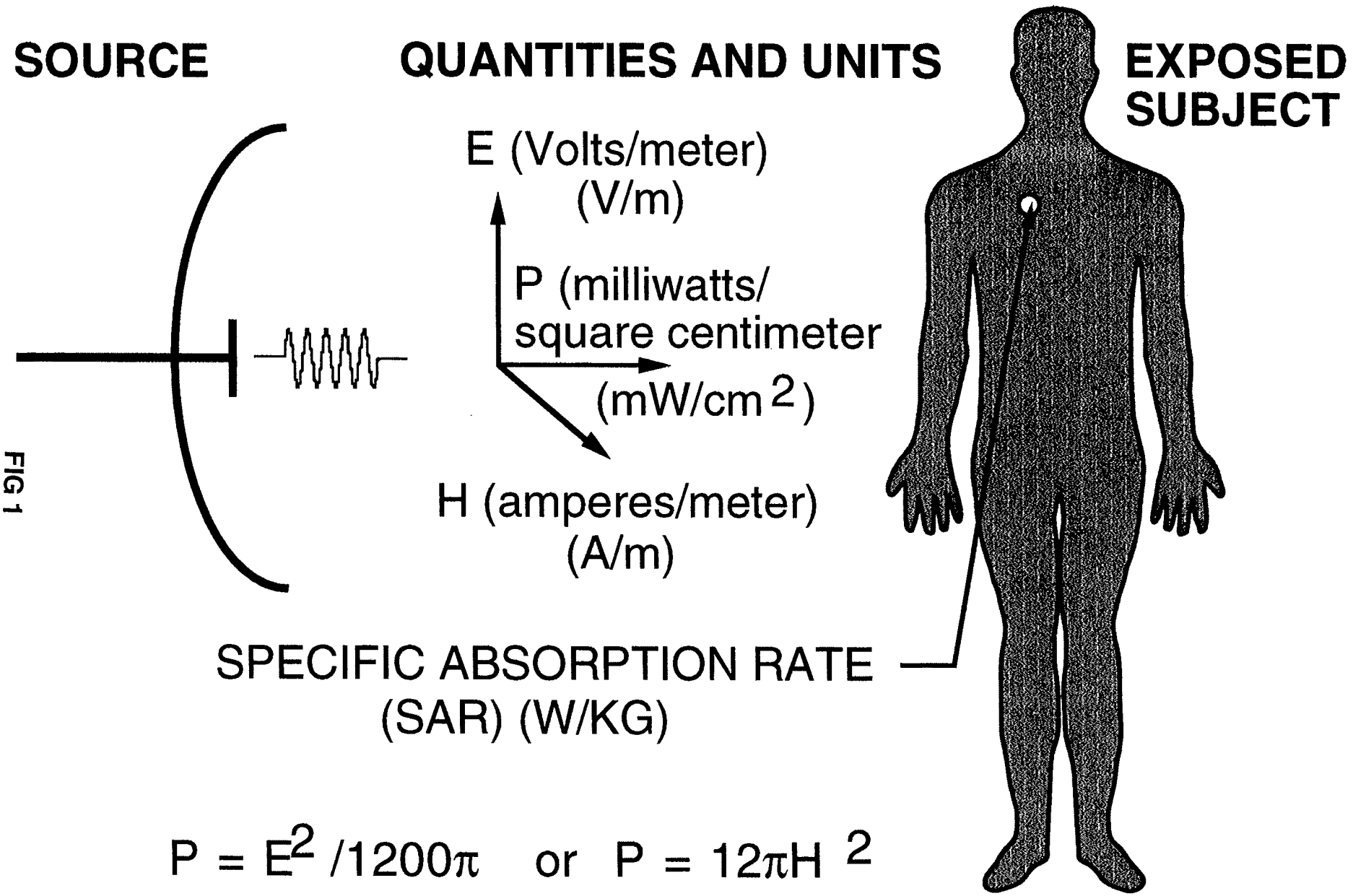
SOURCE
QUANTITIES AND UNITS
EXPOSED SUBJECT
E (Volts/meter) (V/m)
P (milliwatts/ square centimeter (mW/cm 2)
H (amperes/meter) (A/m)
SPECIFIC ABSORPTION RATE (SAR) (W/KG)
P = E2 /1200π or P = 12πH 2

FIG 1

NEED FOR SCALING
SOURCE IN ENVIRONMENT
SURVEY METER
I_m
S_m
T_m
R_m
SURVEY METER
BIOLOGICAL INSTRUMENT
FILTER
FIELD STRENGTH METER
TEMPERATURE SENSOR
T_r
R_r
I_r
S_r
LAB SOURCE

FIG 2

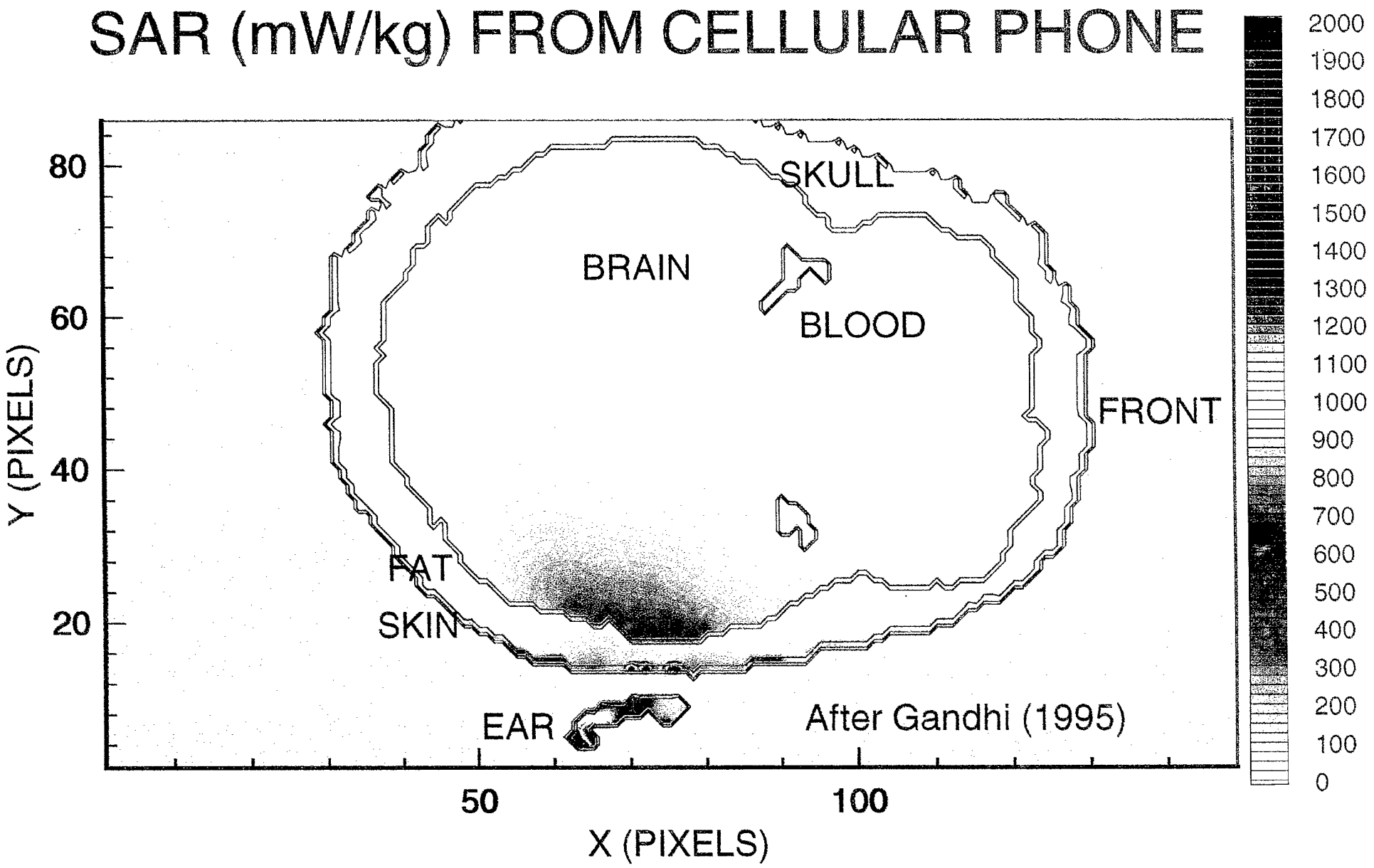
SAR (mW/kg) FROM CELLULAR PHONE
SKULL
BRAIN
BLOOD
FRONT
FAT
SKIN
EAR
After Gandhi (1995)
Y (PIXELS)
X (PIXELS)
80
60
40
20
50
100
2000
1900
1800
1700
1600
1500
1400
1300
1200
1100
1000
900
800
700
600
500
400
300
200
100
0

Approximate SAR in Double Shell Ellipsoidal Rat Exposed to 835 MHz Magnetic Loop Admittance Model, Loop I=300 ma

FIG 4

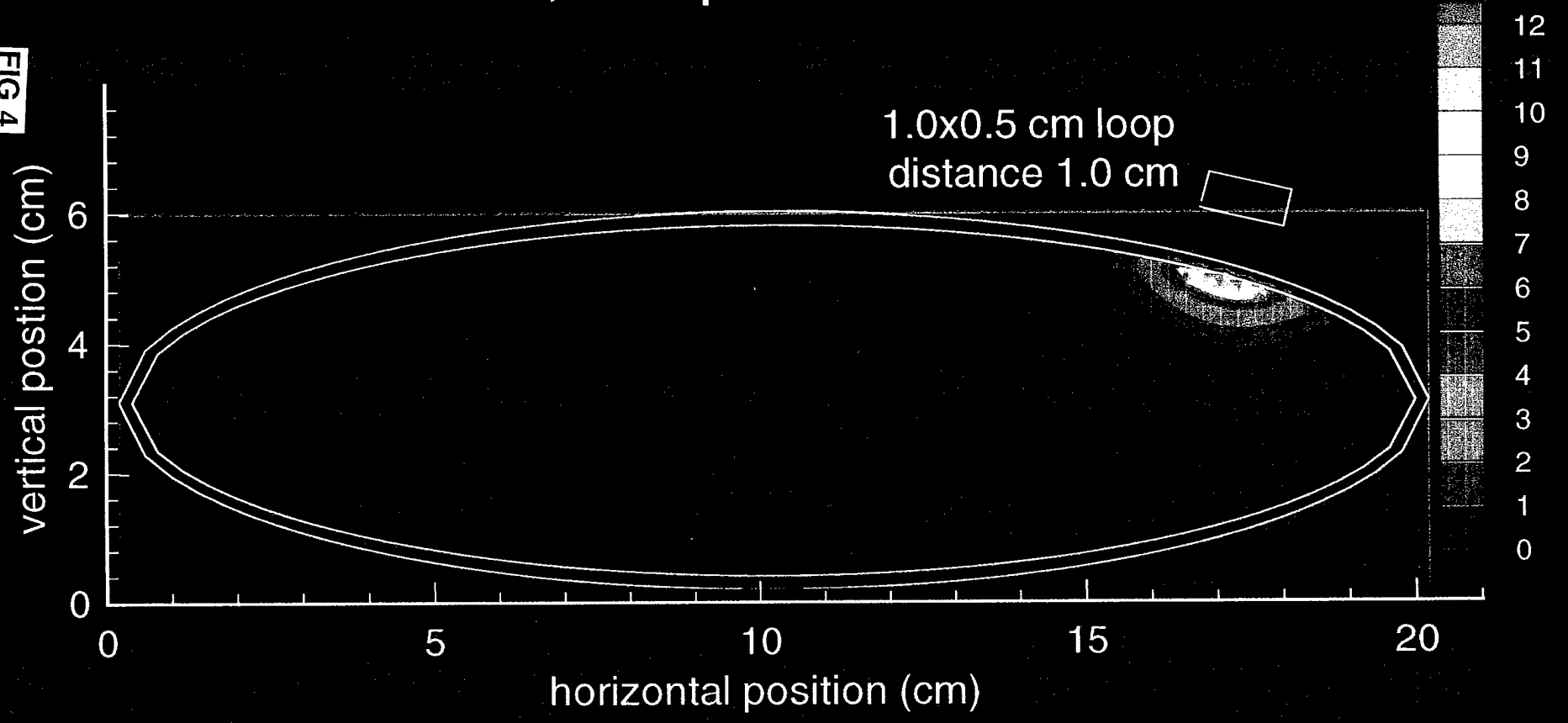

FIG 5

Approximate SAR in Double Shell Ellipsoidal Rat Exposed to 835 MHz Magnetic Loop Admittance Model, Loop I = 1 a

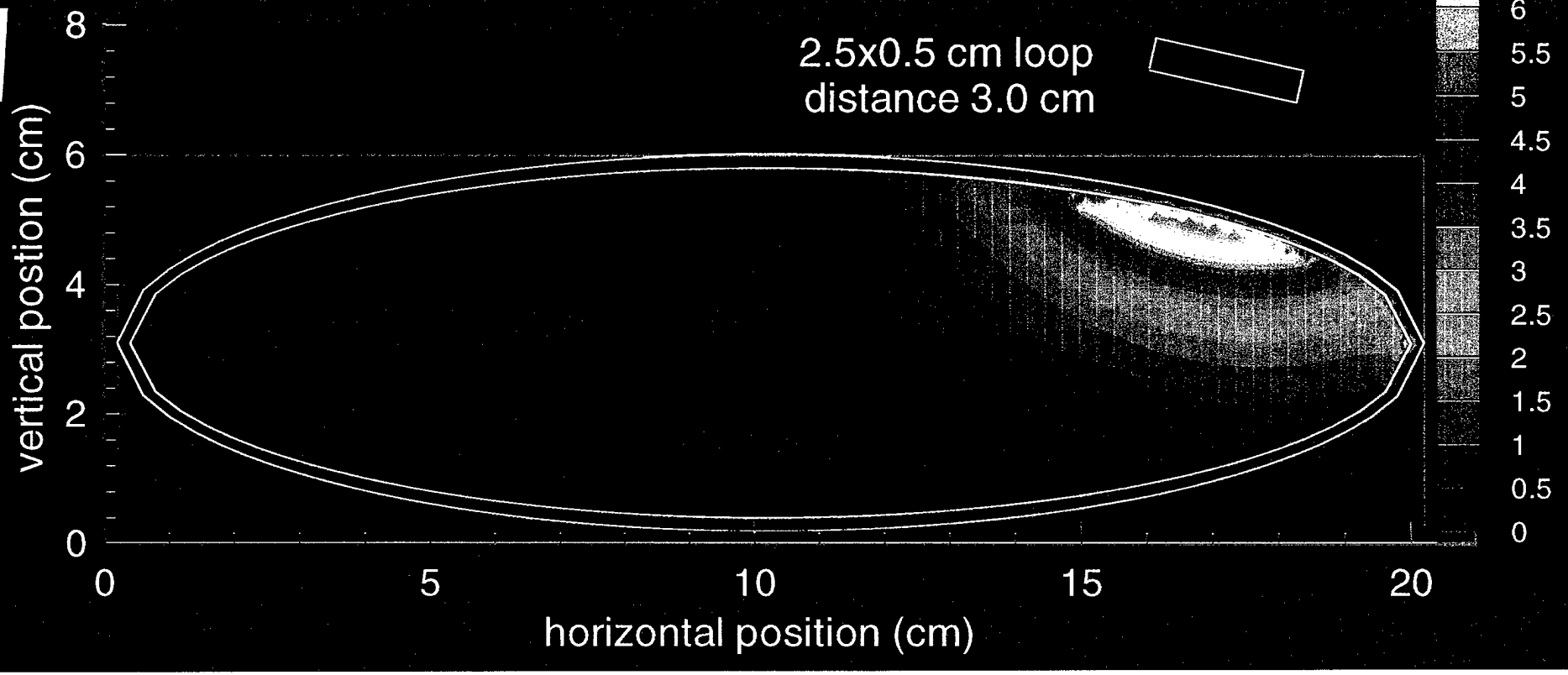

FIG 6

CROSS SECTIONAL VIEWS OF TEM CELL

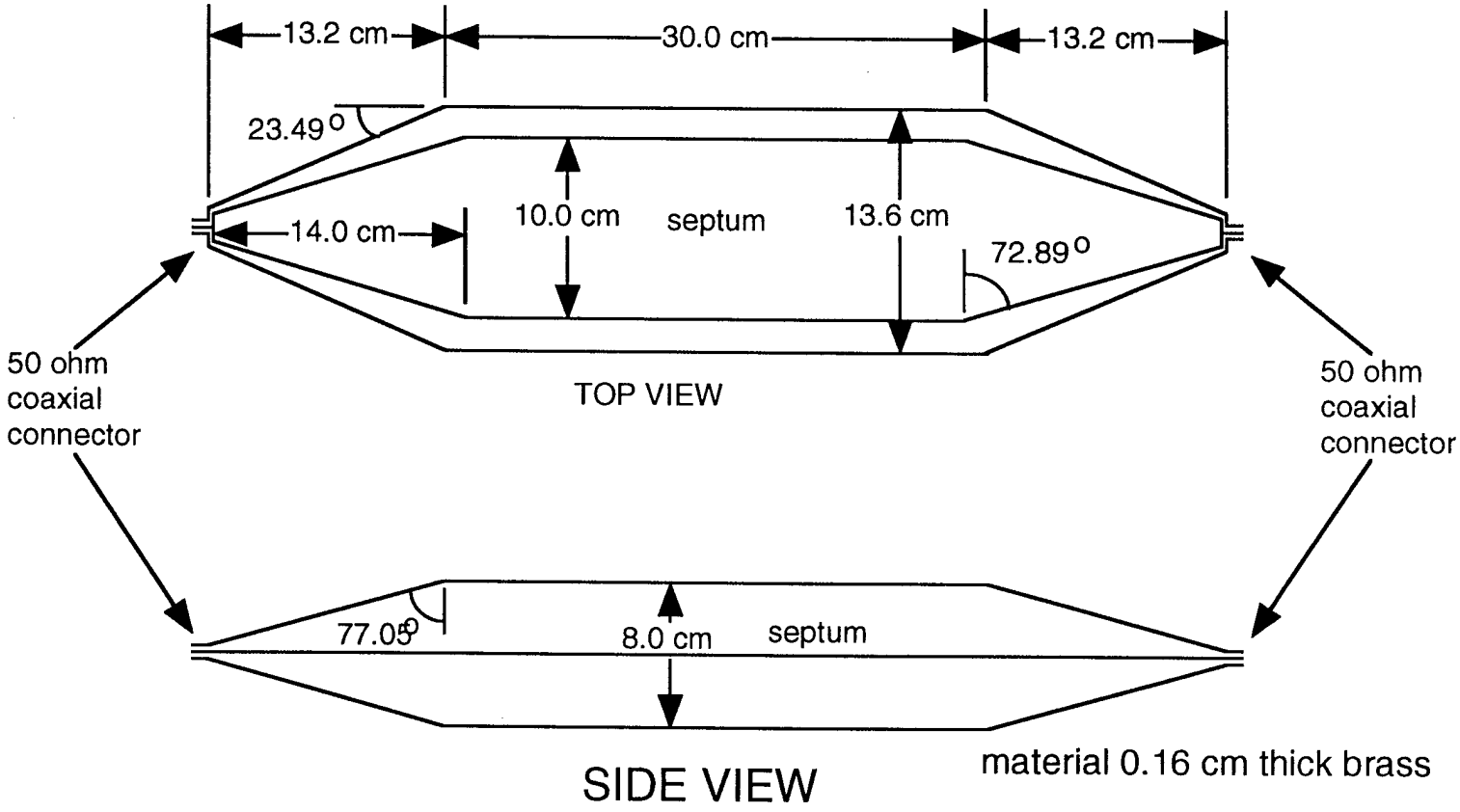

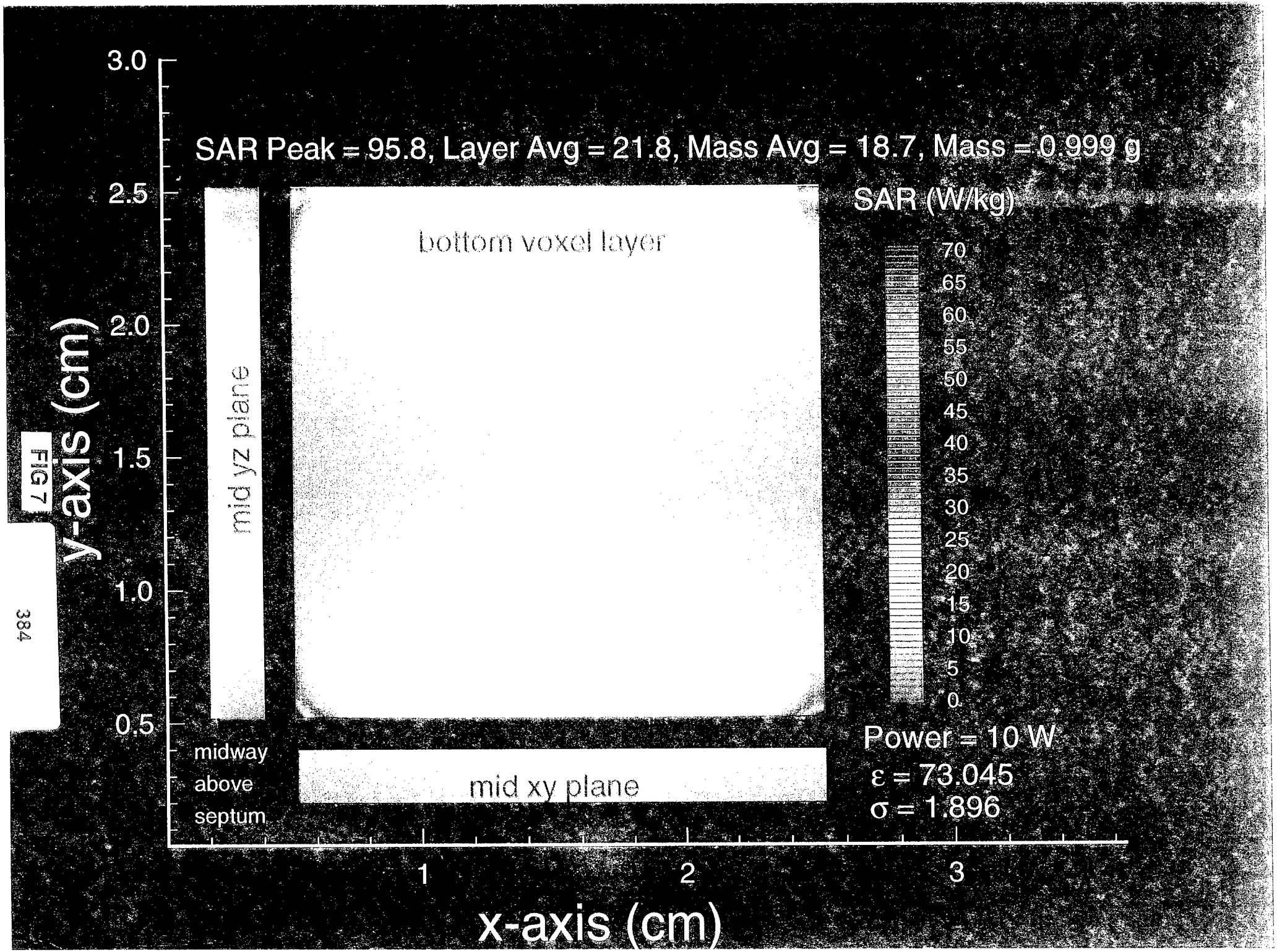
SAR Peak = 95.8, Layer Avg = 21.8, Mass Avg = 18.7, Mass = 0.999 g
SAR (W/kg)
70
65
60
55
50
45
40
35
30
25
20
15
10
5
0
bottom voxel layer
mid yz plane
mid xy plane
midway
above
septum
Power = 10 W
ε = 73.045
σ = 1.896
3.0
2.5
2.0
1.5
1.0
0.5
y-axis (cm)
1
2
3
x-axis (cm)

FIG 7

384

HISTOGRAM OF SAR IN EXPOSED CULTURE FLASK TEMC 20 (2cm square flask placed with broad face perpendicular to propagating wave)

(bottom layer)

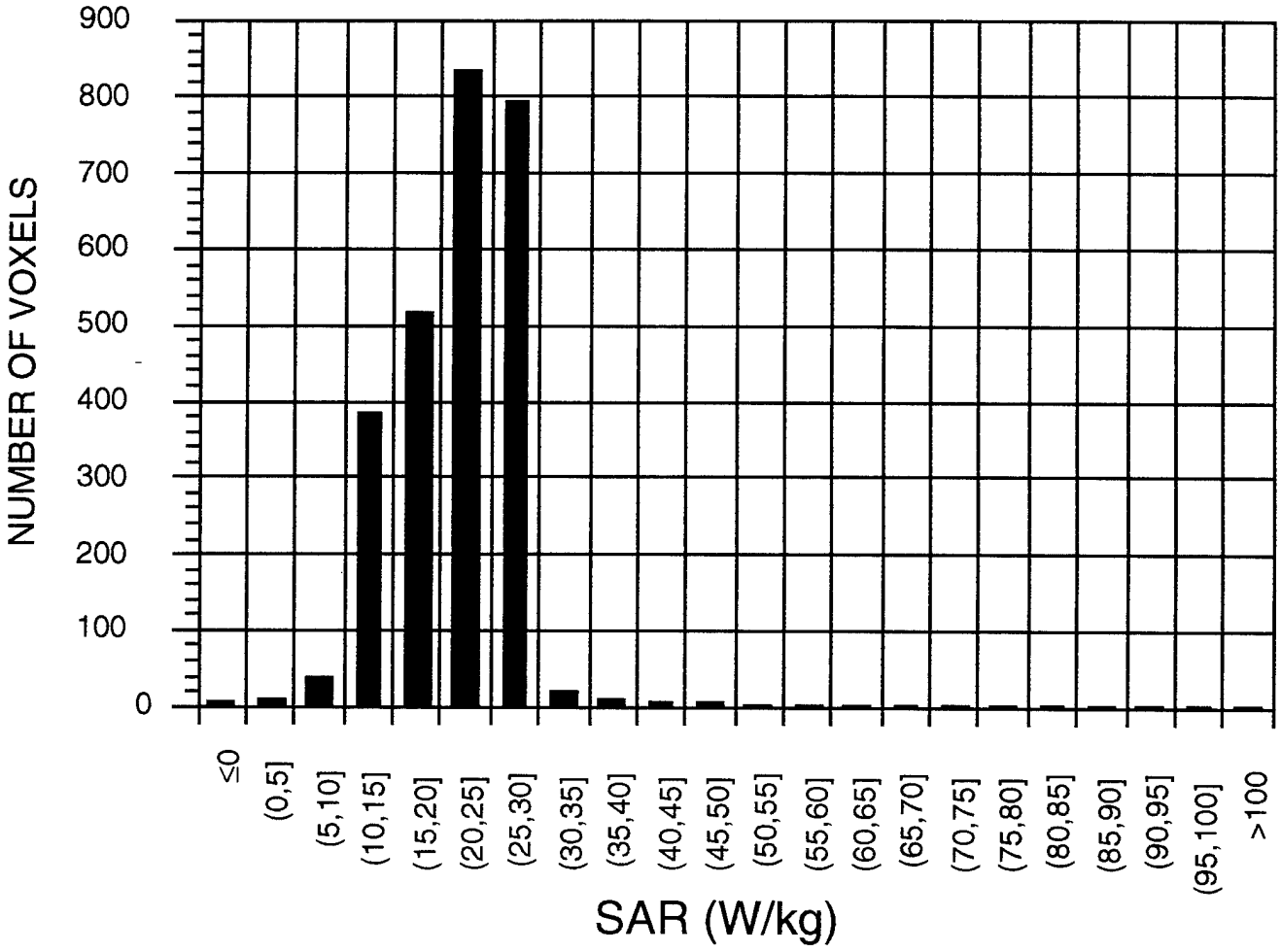

STATISTICS

Mean:	Std. Dev.:	Std. Error:	Variance:	Coef. Var.:	Count:
21.795	6.178	.121	38.165	28.345	2601

Minimum:	Maximum:	Range:	Sum:	Sum Squared:	# Missing:
6.886	95.822	88.936	56687.684	1334711.8	0

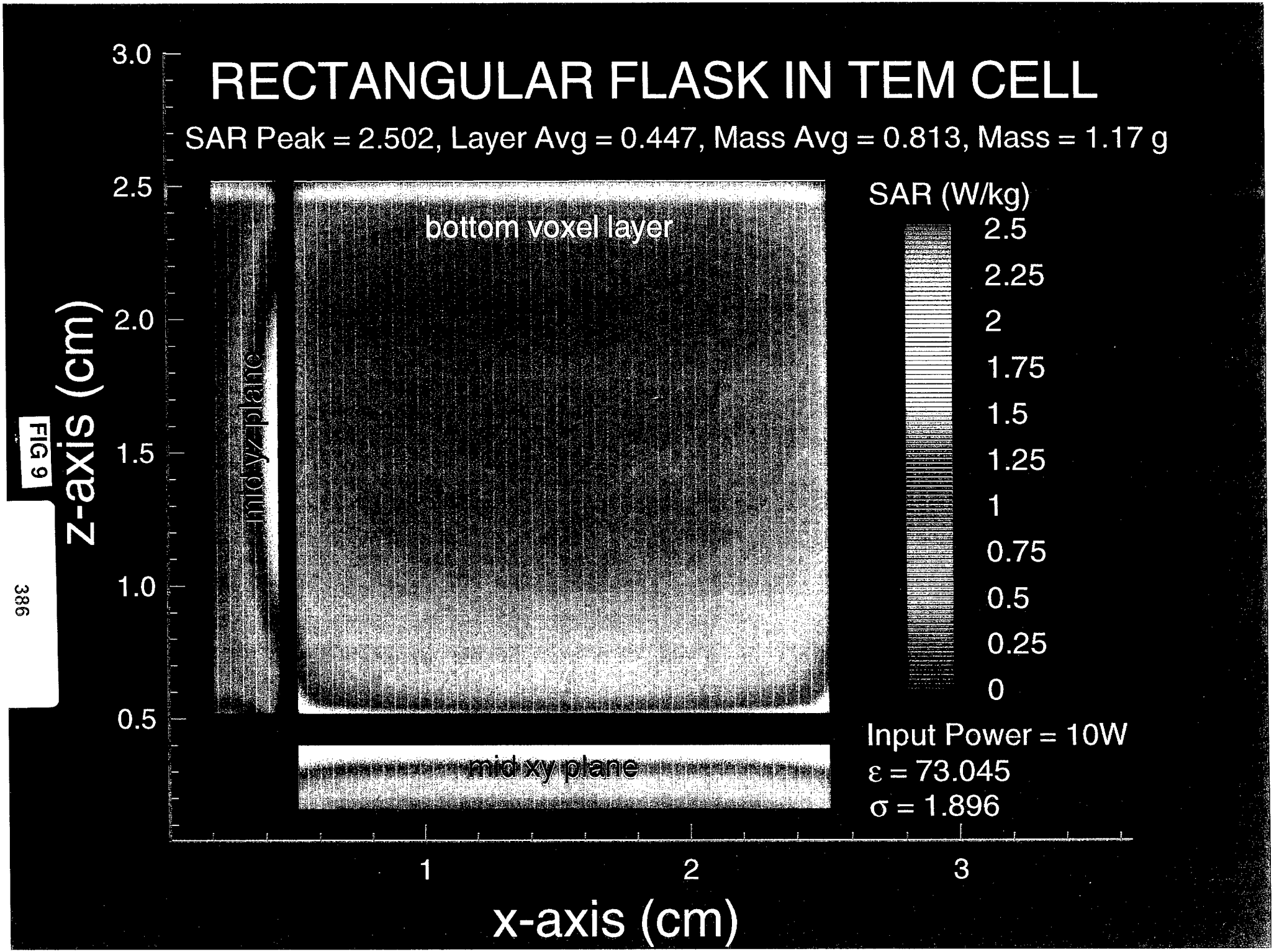
RECTANGULAR FLASK IN TEM CELL
SAR Peak = 2.502, Layer Avg = 0.447, Mass Avg = 0.813, Mass = 1.17 g
bottom voxel layer
mid yz plane
mid xy plane
SAR (W/kg)
2.5
2.25
2
1.75
1.5
1.25
1
0.75
0.5
0.25
0
Input Power = 10W
ε = 73.045
σ = 1.896
z-axis (cm)
3.0
2.5
2.0
1.5
1.0
0.5
1
2
3
x-axis (cm)

FIG 9

386

HISTOGRAM OF SAR IN EXPOSED CULTURE FLASK TEMC1 (2cm square flask sitting on septum)

(bottom layer)

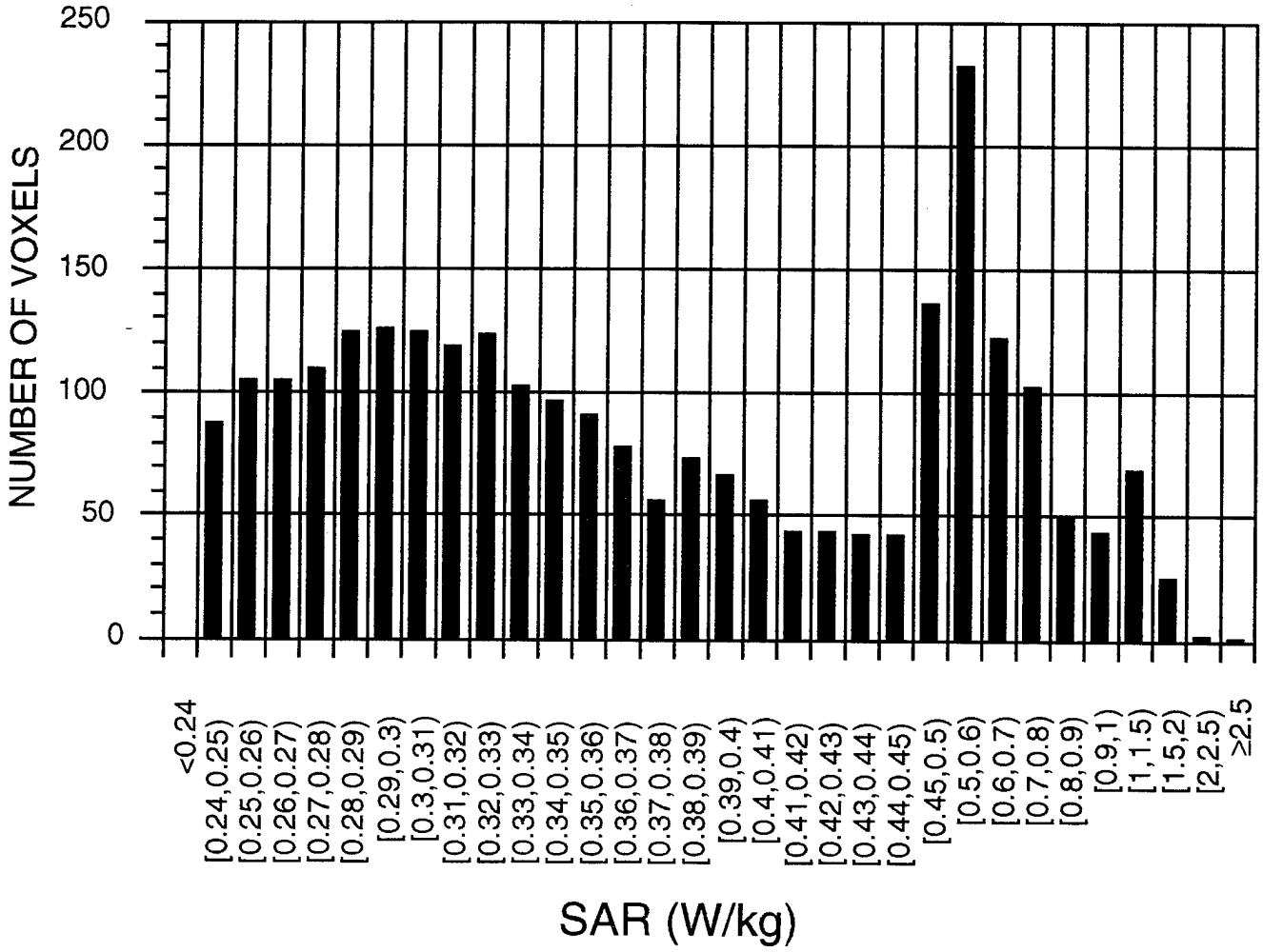

STATISTICS

Mean:	Std. Dev.:	Std. Error:	Variance:	Coef. Var.:	Count:
.447	.249	.005	.062	55.85	2601

Minimum:	Maximum:	Range:	Sum:	Sum Squared:	# Missing:
.242	2.502	2.261	1161.355	680.236	0

FIG 10

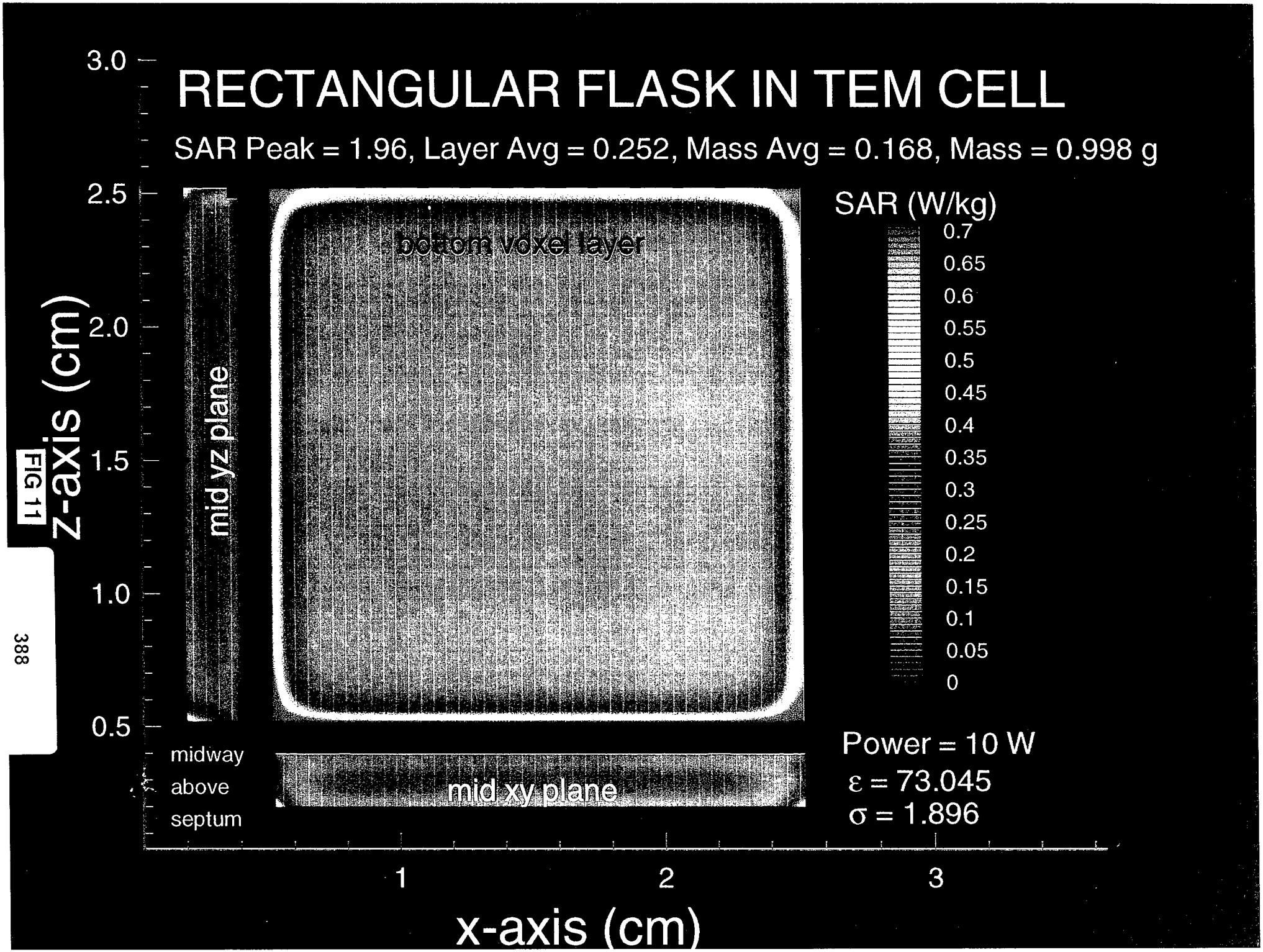
RECTANGULAR FLASK IN TEM CELL
SAR Peak = 1.96, Layer Avg = 0.252, Mass Avg = 0.168, Mass = 0.998 g
SAR (W/kg)
0.7
0.65
0.6
0.55
0.5
0.45
0.4
0.35
0.3
0.25
0.2
0.15
0.1
0.05
0
bottom voxel layer
mid yz plane
mid xy plane
midway
above
septum
Power = 10 W
ε = 73.045
σ = 1.896
Z-axis (cm)
3.0
2.5
2.0
1.5
1.0
0.5
1
2
3
x-axis (cm)

FIG 11

388

HISTOGRAM OF SAR IN EXPOSED CULTURE FLASK TEMC3 (2cm square flask suspended midway between septum and upper plate)

(bottom layer)

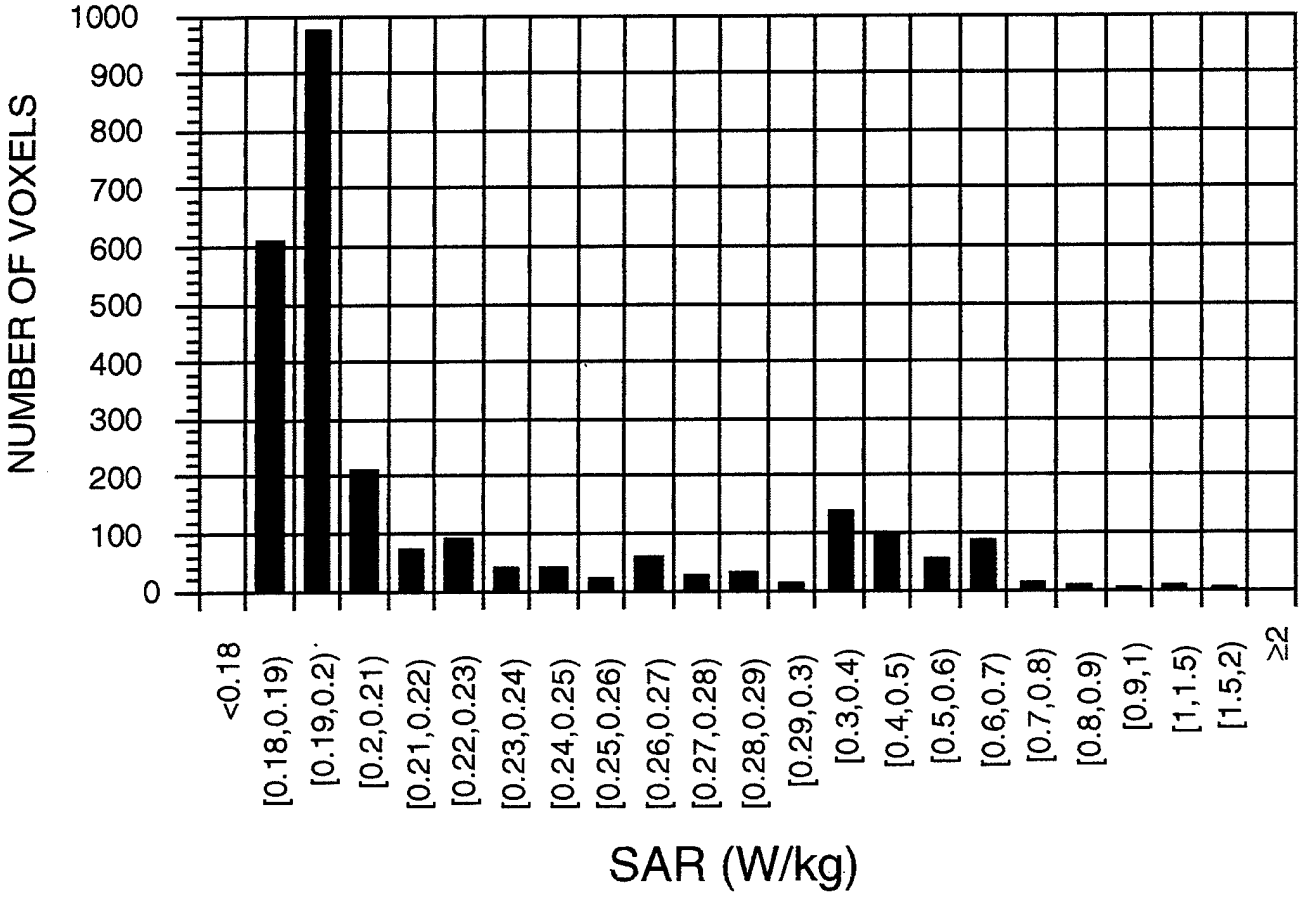

STATISTICS

Mean:	Std. Dev.:	Std. Error:	Variance:	Coef. Var.:	Count:
.252	.142	.003	.02	56.464	2601

Minimum:	Maximum:	Range:	Sum:	Sum Squared:	# Missing:
.186	1.955	1.77	655.714	217.988	0

FIG 12

DEPENDENCE OF RETINAL MODEL RESULTS ON BEAM SHAPE AND ABSORPTION COEFFICIENTS. D. E. Freund, The Johns Hopkins University Applied Physics Laboratory, Laurel, MD 20723

The determination of permissible levels of ocular exposure to laser light sources requires an understanding of the interaction of laser light with biological tissue. To address this issue, calculations are performed that compare retinal temperature increases resulting from exposure to uniform rectangular and circularly symmetric Gaussian beam sources; the effects of absorption coefficients is also investigated. Since most optical absorption occurs in the retinal pigment epithelium (RPE), it is modeled as a thin homogeneous absorbing sheet that is embedded in the fundus which, in turn, is modeled as a homogeneous medium having the thermal and optical properties of water. The RPE is also assumed to have the thermal properties of water, while its optical properties are taken from a range of values reported for humans and pigmented rabbits. The change in temperature within the fundus is obtained as a function of time by integrating the beam source with the fundamental Green's function solution to the heat diffusion equation. For moderate exposure times, temperature histories on the beam axis at a point just inside the retina are computed. The results indicate that temperature histories for rectangular and Gaussian beam sources have similar profiles. It is found numerically that the ratio of the temperature increases from the two different beam profiles is insensitive to the value of the absorption coefficient. It is also found analytically that the ratio of the temperature time derivatives is independent of absorption coefficient. Finally, in general, high (low) aspect ratio rectangular beams cause smaller (greater) temperature increases than a corresponding equal power Gaussian beam.

Supported by the U.S. Army and by U. S. Navy Contract N00039-95-C-0002.

Dependence of Retinal Model Temperature Calculations on Beam Shape and Absorption Coefficients

D. E. Freund, R. L. McCally, R. A. Farrell
The Johns Hopkins University
Applied Physics Laboratory
Johns Hopkins Road
Laurel, MD 20723

D. H. Sliney
U.S. Army Center
for Health Promotion
and Preventive Medicine
Aberdeen Proving Ground, MD 21010

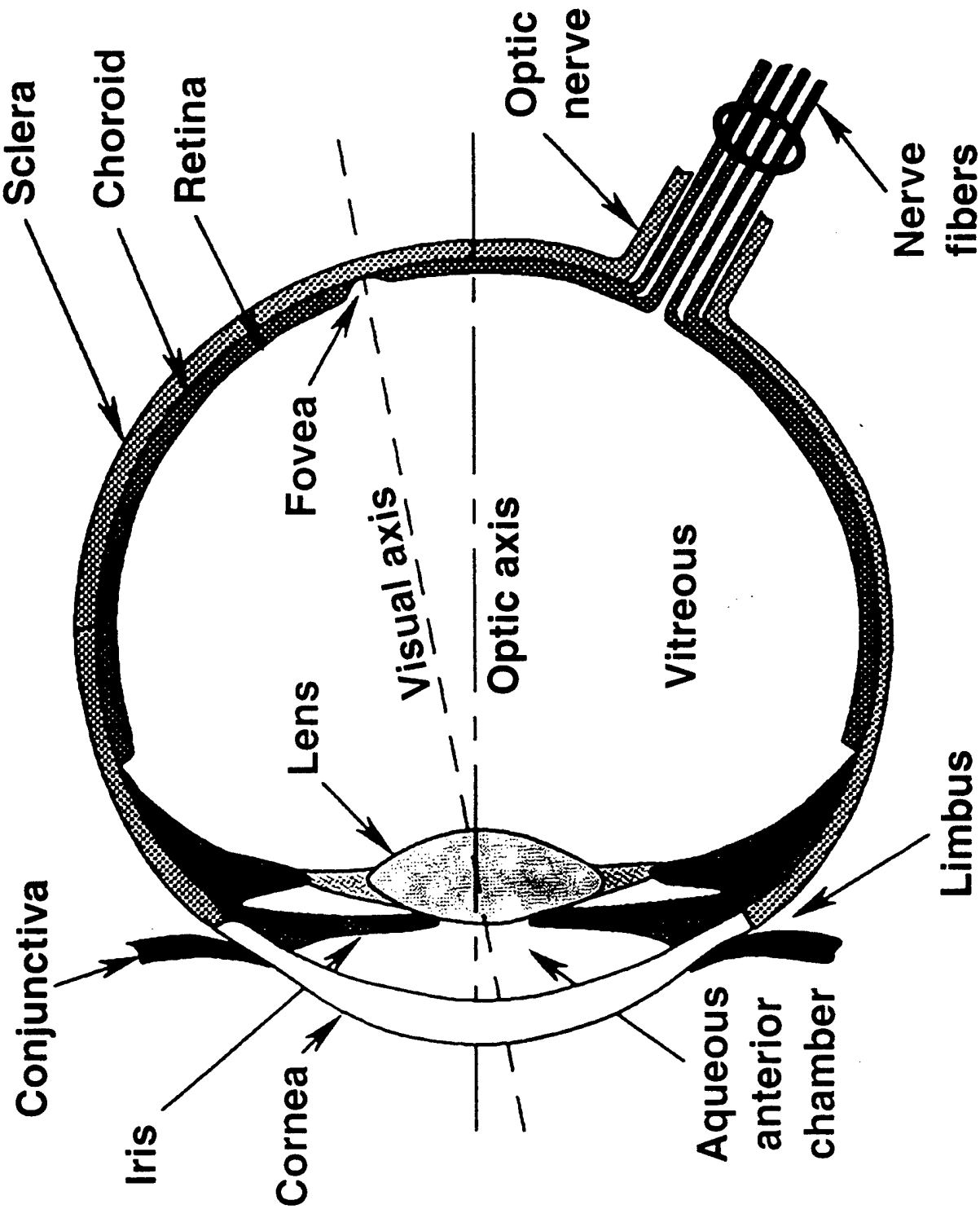
Sclera
Choroid
Retina
Optic nerve
Nerve fibers
Fovea
Visual axis
Optic axis
Vitreous
Lens
Limbus
Conjunctiva
Iris
Cornea
Aqueous anterior chamber

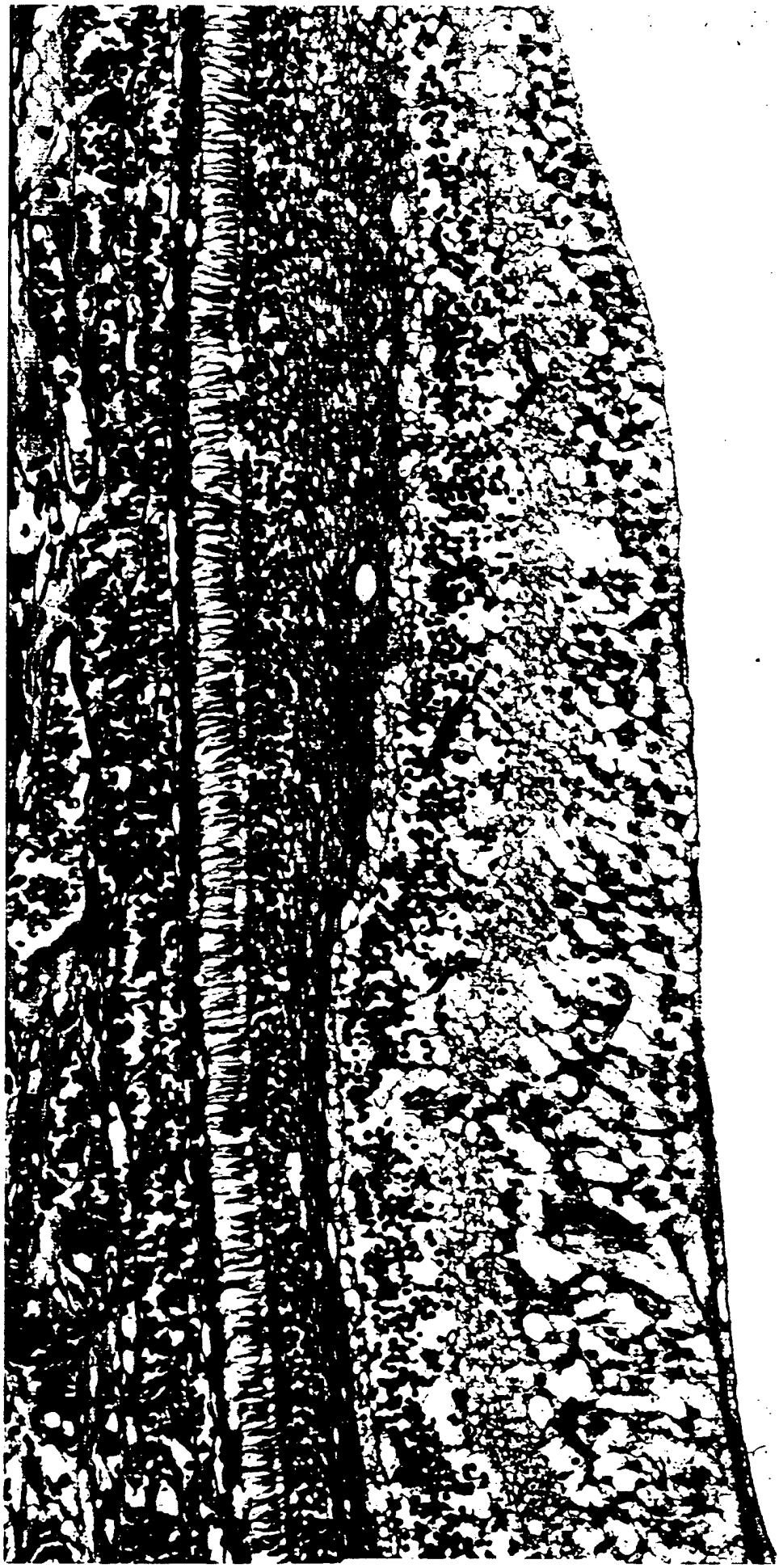

Retinal Thermal Model

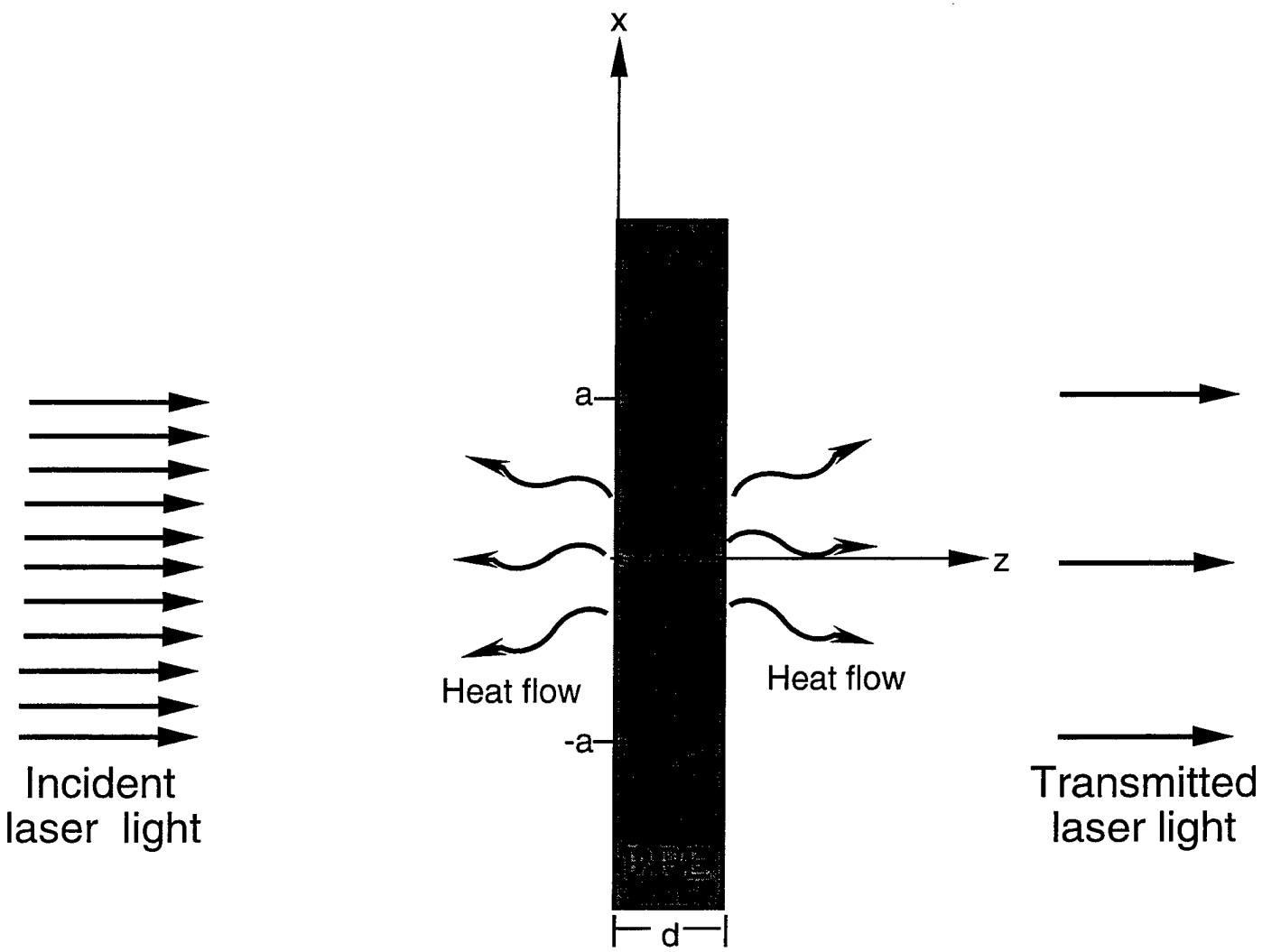

Beam Irradiance Profile

Uniform rectangular beam

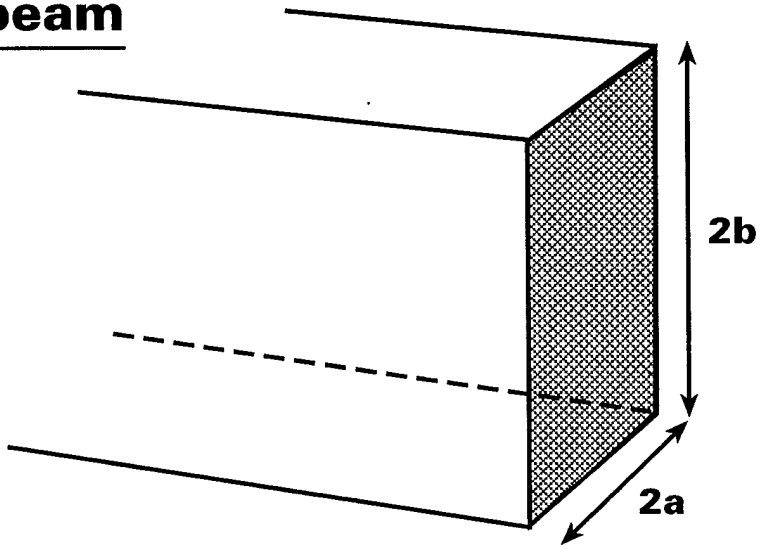

Circularly symmetric Gaussian beam

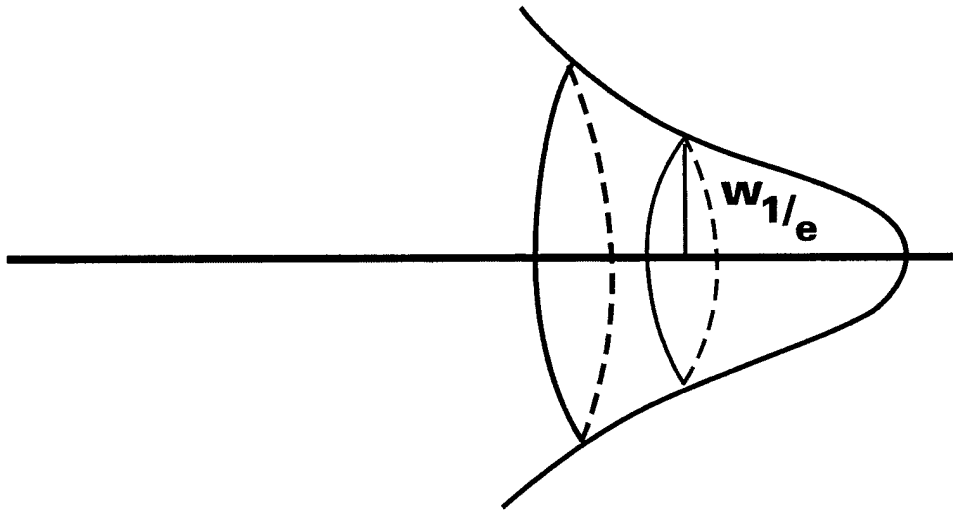

97-6844

Theoretical Expression for Temperature

Heat diffusion equation:

$$\frac{1}{\kappa}\frac{\partial T}{\partial t} - \nabla^2 T = \frac{\varepsilon}{\kappa \rho c}$$

Boundary and initial conditions:

$$\lim_{r \to \infty} T(\mathbf{r},t) = 0; \qquad T(\mathbf{r},0) = 0$$

Infinite domain Green Function:

$$G(\mathbf{r},\mathbf{r}';t,t') = \frac{\theta(t-t')\, e^{-|\mathbf{r}-\mathbf{r}'|^2/4\kappa(t-t')}}{8\rho c[\pi\kappa(t-t')]^{3/2}}$$

Solution:

$$T(\mathbf{r},t) = \int_0^{\tau} dt' \int_{-\infty}^{\infty} d\mathbf{r}'\; G(\mathbf{r},\mathbf{r}';t,t')\; \varepsilon(\mathbf{r}',t')$$

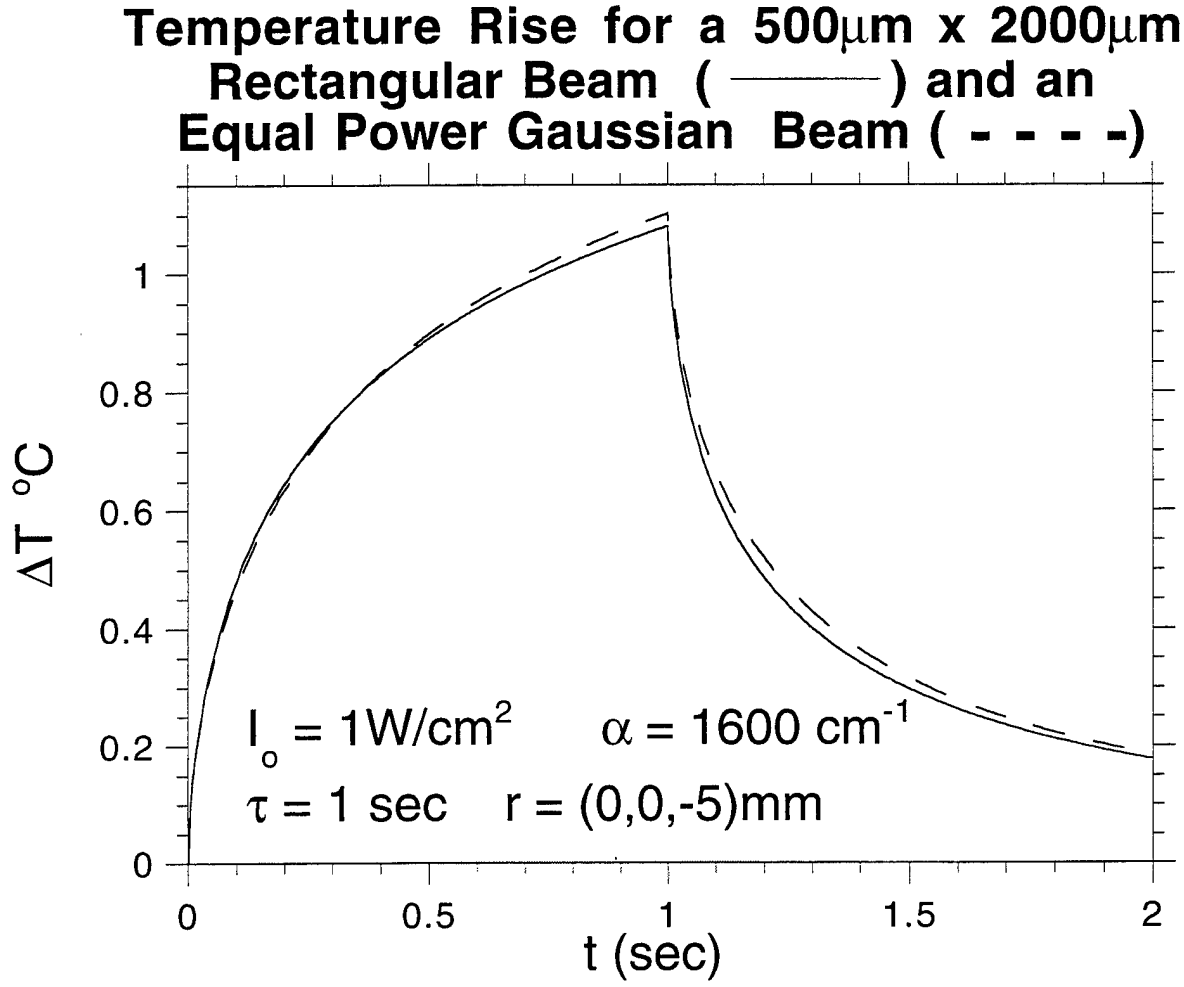
Temperature Rise for a 500μm x 2000μm
Rectangular Beam (———) and an
Equal Power Gaussian Beam (- - - -)
ΔT °C
t (sec)
0
0.2
0.4
0.6
0.8
1
0
0.5
1
1.5
2
I_o = 1W/cm^2
α = 1600 cm^{-1}
τ = 1 sec
r = (0,0,-5)mm

Maximum Temperature Rise for Equal Power Square (——) and Gaussian (- - - -) Beams

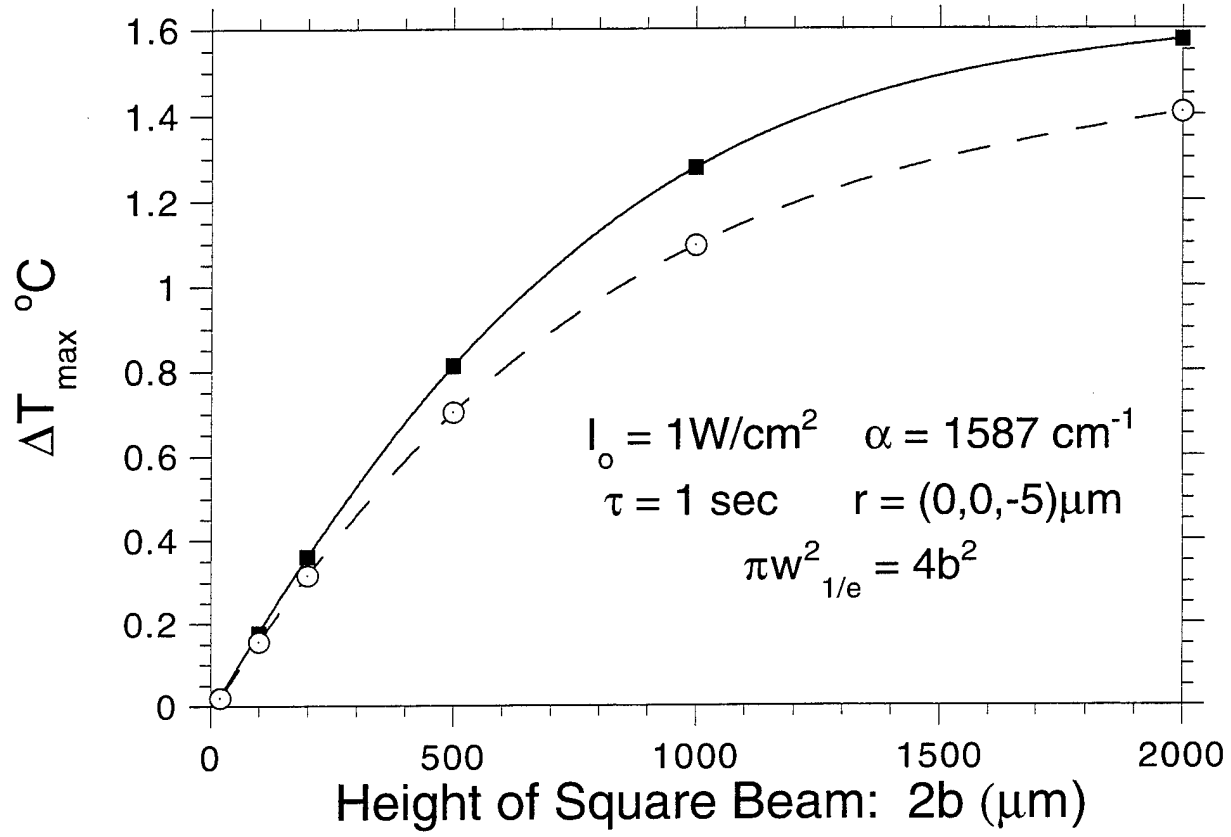

Maximum Temperature Rise for Equal Power Rectangular (———) and Gaussian (- - - -) Beams

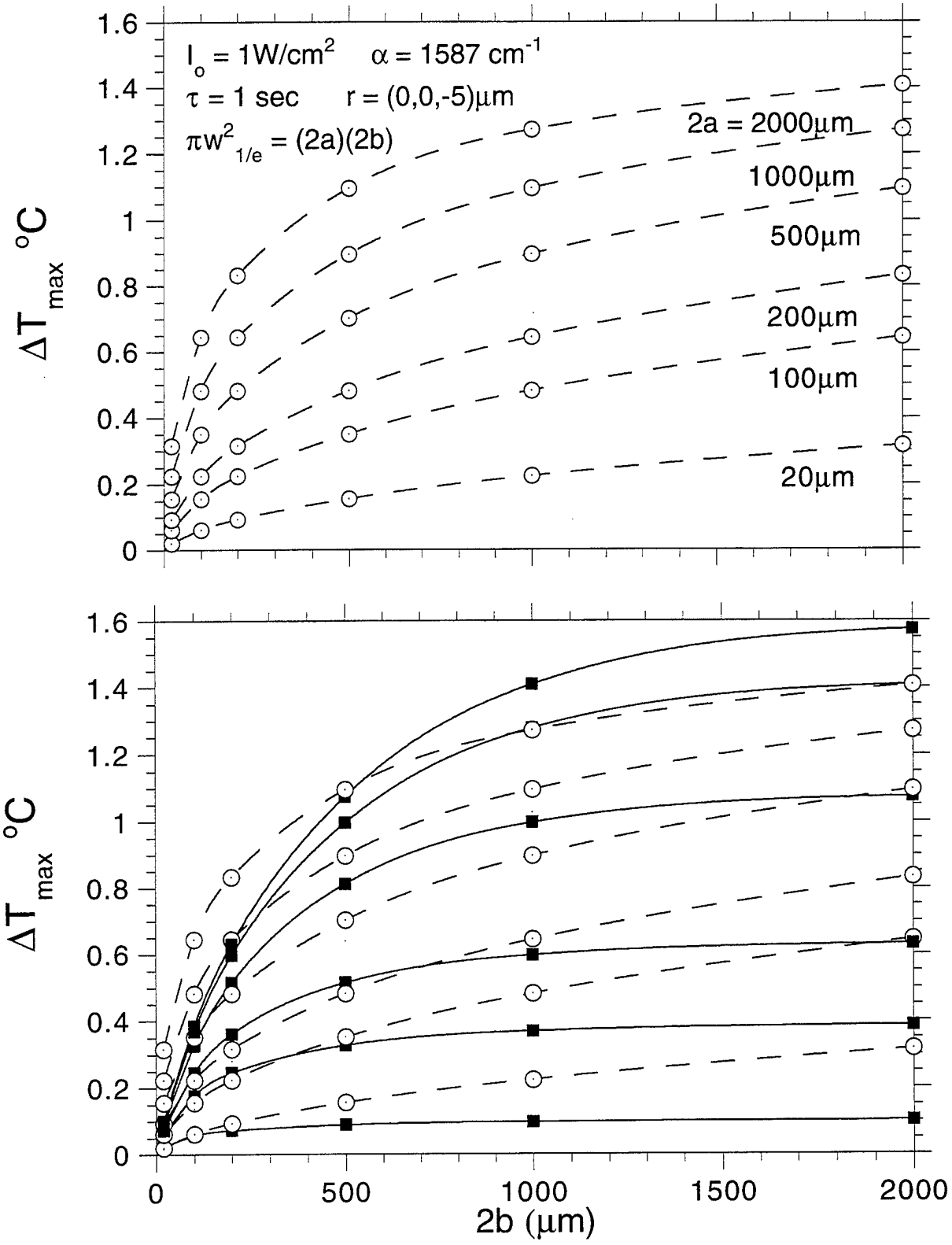

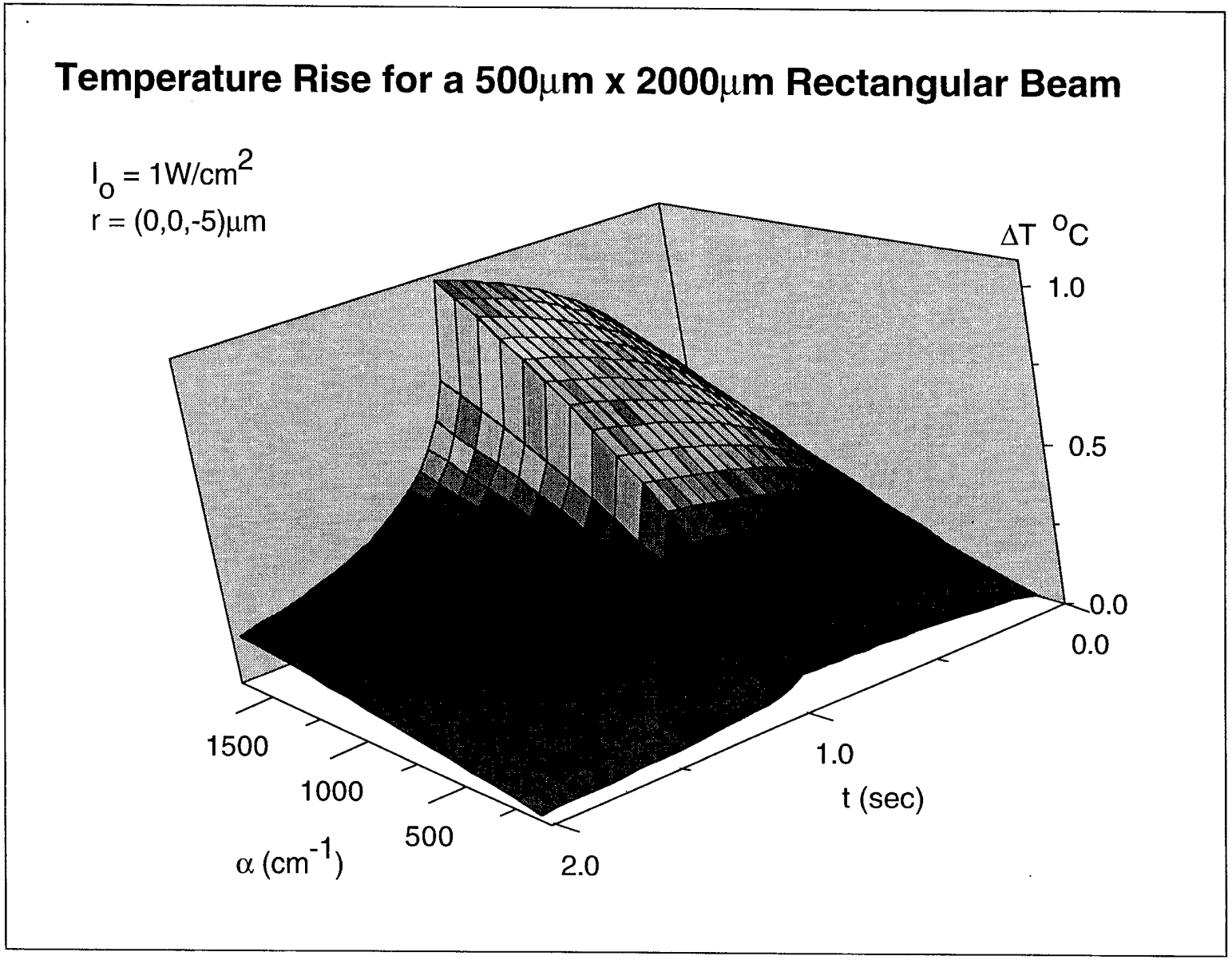
Temperature Rise for a 500μm x 2000μm Rectangular Beam
I_o = 1W/cm^2
r = (0,0,-5)μm
ΔT °C
1.0
0.5
0.0
0.0
1.0
t (sec)
2.0
1500
1000
500
α (cm^{-1})

Ratio of Temperature Rise for a 500μm x 2000μm Rectangular Beam to Temperature Rise for an Equal Power Gaussian Beam

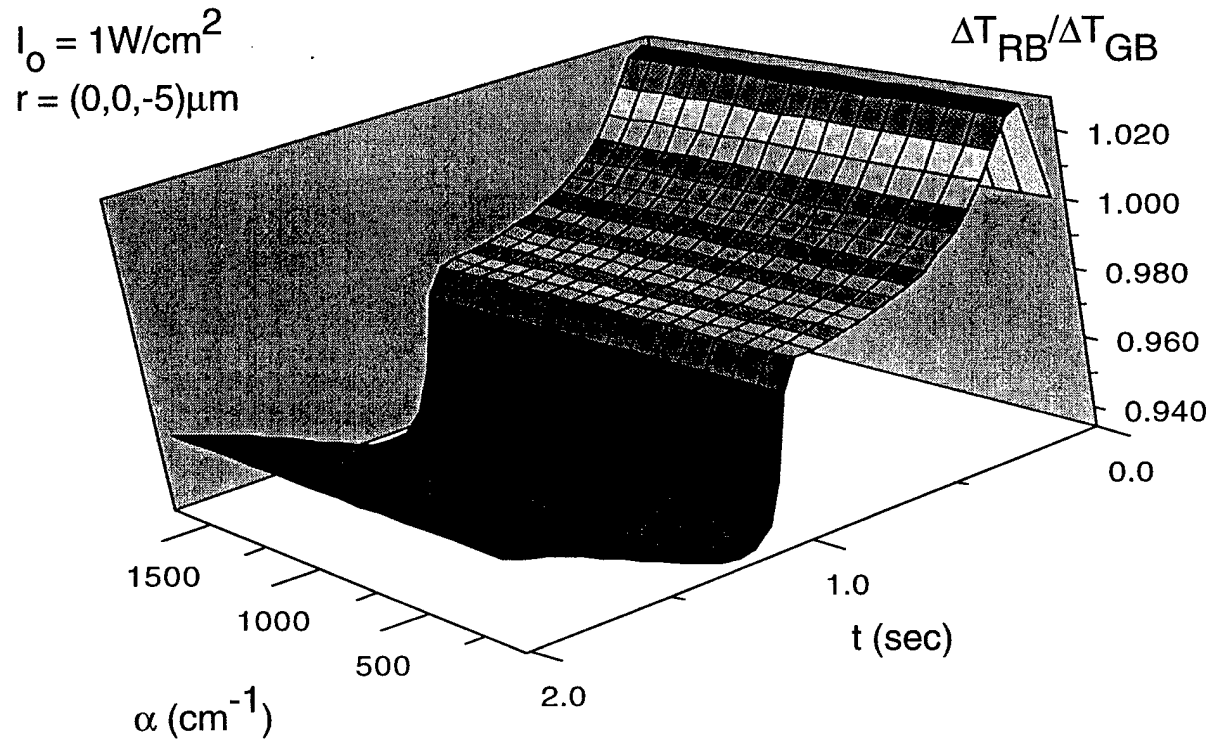

Heat Diffusion Equation for a Homogeneous and Isotropic Medium

$$\varepsilon(\mathbf{r},t) = \rho c\frac{\partial T}{\partial t} - \kappa\rho c\left[\frac{\partial^2 T}{\partial x^2}+\frac{\partial^2 T}{\partial y^2}+\frac{\partial^2 T}{\partial z^2}\right]$$

$$\left\{\begin{array}{l}\text{Rate at which}\\ \text{heat energy is supplied}\\ \text{to a unit volume at } \mathbf{r}\end{array}\right\} = \left\{\begin{array}{l}\text{Portion of heat energy}\\ \text{per unit time that}\\ \text{raises the temperature}\\ \text{of the unit volume}\end{array}\right\} - \left\{\begin{array}{l}\text{Portion of heat energy}\\ \text{per unit time that}\\ \text{leaves the unit volume}\\ \text{via conduction}\end{array}\right\}$$

Ratios of Time Derivatives of Temperature for Rectangular and Gaussian Beams

$$\mathcal{R}(x,y,t;a,b,w_{1/e},\kappa) = \left\{erf\left[\frac{a+x}{2\sqrt{\kappa t}}\right] - erf\left[\frac{x-a}{2\sqrt{\kappa t}}\right]\right\}\left\{erf\left[\frac{b+y}{2\sqrt{\kappa t}}\right] - erf\left[\frac{y-b}{2\sqrt{\kappa t}}\right]\right\} \Bigg/ \frac{4\exp\left[-r_{cy}^2 \Big/ \left(w_{1/e}^2 + 4\kappa t\right)\right]}{1 + 4\kappa t / w_{1/e}^2}$$

General Properties of $\mathcal{R}$:

- Independent of z
- Independent of RPE thickness and absorption coefficient
- Independent of mass density and specific heat of medium

Properties of $\mathcal{R}$ along the beam axes ($x = y = 0$):

- $\lim_{t \to \infty} \mathcal{R} = 4ab / \pi w_{1/e}^2$
- $\lim_{t \to 0} \mathcal{R} = 1$
- $\mathcal{R}(\gamma,\eta) = erf(\eta)erf(\gamma\eta)\left[1 + (\gamma\eta)^2\right] / (\gamma\eta)^2; \quad$ for $w_{1/e} = b,$
- $\mathcal{R}(\gamma,\eta) = erf(\eta)erf(\gamma\eta)\left[(\gamma\eta)\eta + \frac{\pi}{4}\right] / (\gamma\eta)\eta; \quad$ for $\pi w_{1/e}^2 = 4ab,$

where $\gamma \equiv b/a\ (b \geq a)$ and $\eta \equiv a/2\sqrt{\kappa t}$.

Ratio of Time Derivatives for Equal Power Rectangular and Gaussian Beams

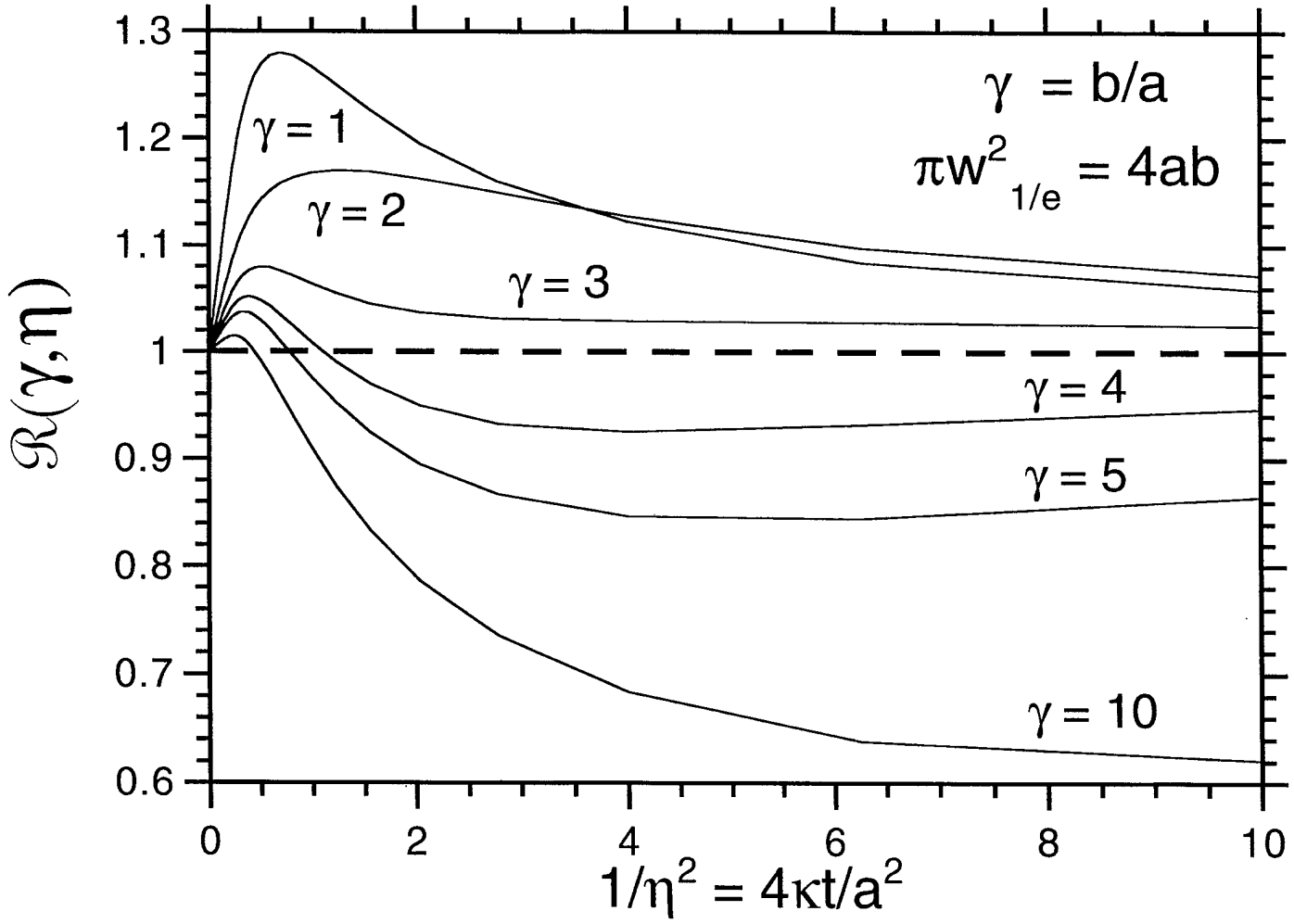

Maximum Temperature Rise for Equal Power Rectangular (———) and Gaussian (- - - -) Beams

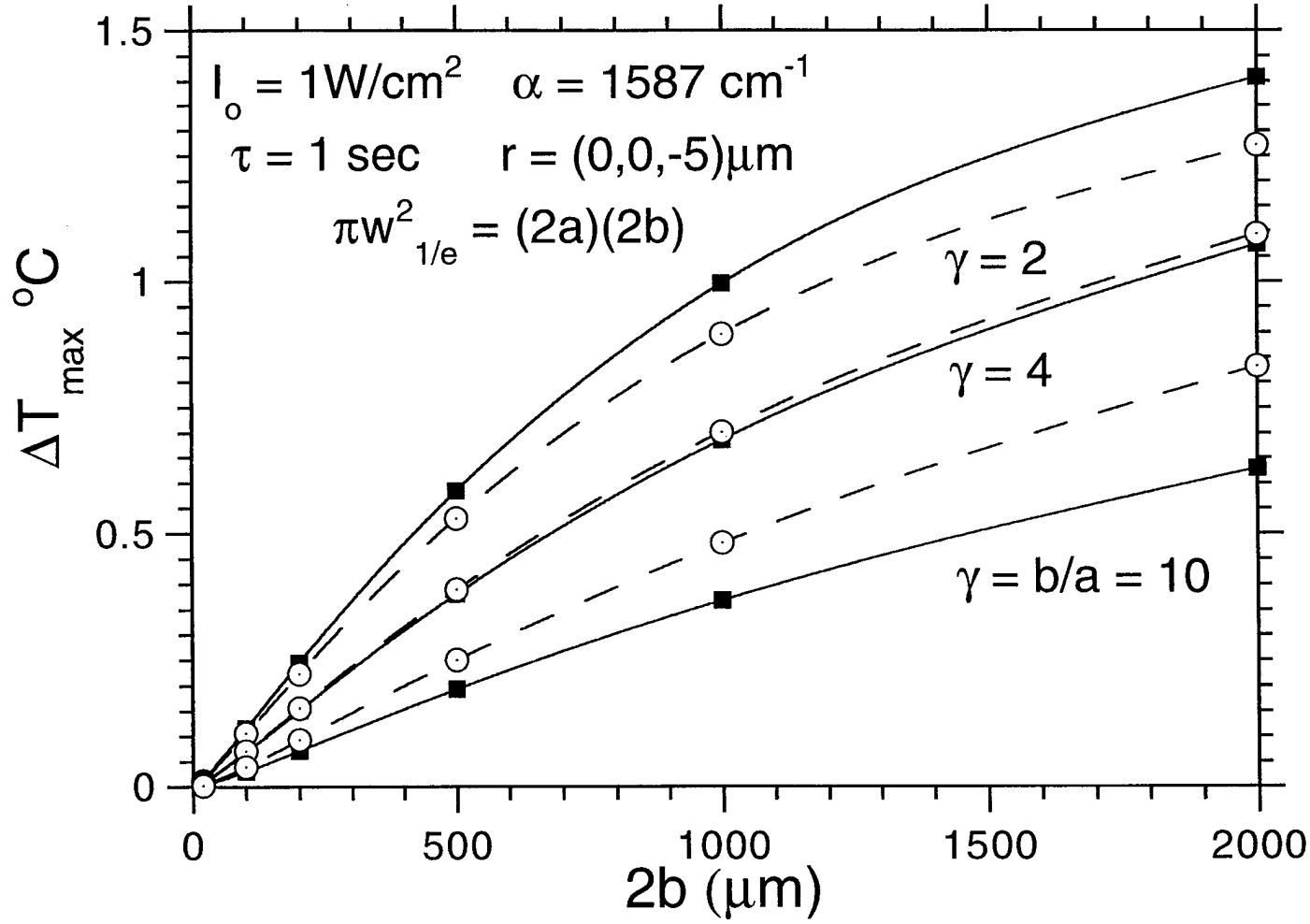

Conclusion

- The ratio $\Delta T_{RB}/\Delta T_{GB}$ is insensitive to the absorption coefficient.

- There is always an exposure duration short enough such that, along the axis, $\Delta T_{RB} > \Delta T_{GB}$.

- In general, high (low) aspect ratio rectangular beams cause a smaller (greater) ΔT than the corresponding equal power Gaussian beam.

Infrared Lasers & Millimeter Waves
Workshop
The Links Between Microwaves
& Laser Optics

21 Jan 1997 - 22 Jan 1997

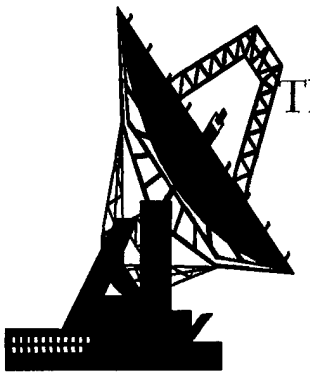

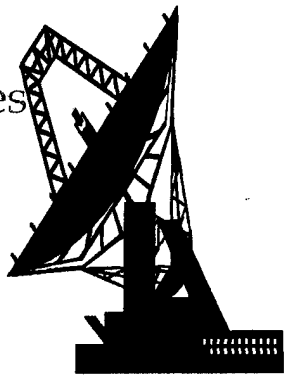

SECTION VII:

EXPOSURE STANDARDS: DEPENDENCE ON PENETRATION DEPTH, IRRADIATION AREA AND PEAK LIMITS.

The IEEE SCC-28 Standards-Setting Process

J. M. Osepchuk
Full Spectrum Consulting
Concord, MA

R. C. Petersen
Lucent Technologies Inc.
Murray Hill, NJ

From Research to Regulations

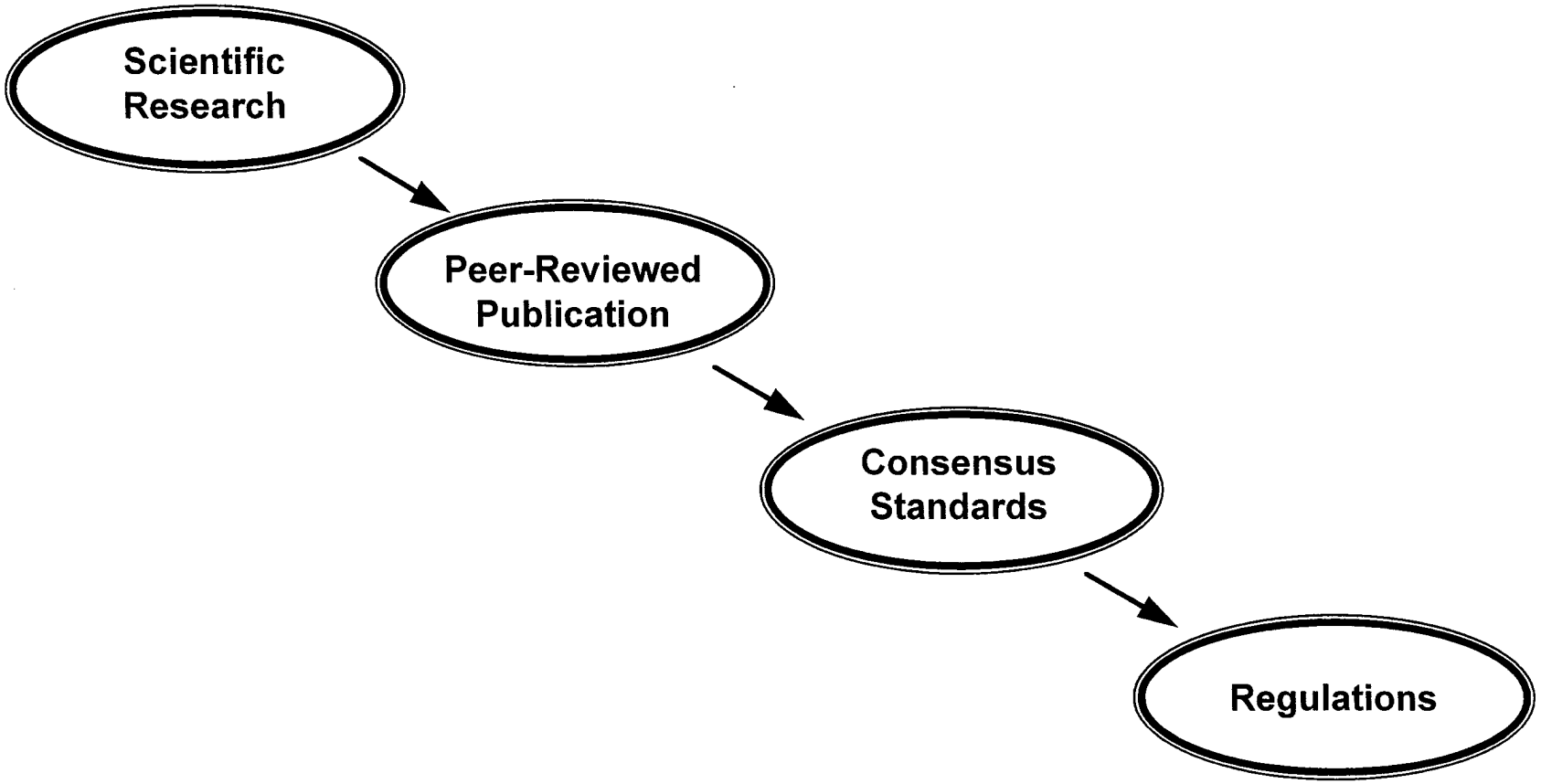

Standardization Activities in the USA

Two organizations that develop safety criteria for RF/microwave exposure are:

- **IEEE Standards Coordinating Committee 28**
- **The National Council on Radiation Protection and Measurements**

Institute of Electrical and Electronics Engineers (IEEE)

The IEEE, the largest professional society in the world, is composed of a number of professional societies, e.g., MTT, EMC, EMB, AP, VT. Many of these societies sponsor standards committees. Standards Coordinating Committees, sponsored by the IEEE Standards Board, develop standards on subjects that are of interest to two or more societies.

History of RF/Microwave Exposure Standards in the US (ANSI/IEEE)

1953 100 W/m^2 recommended to the US Navy

- **Based on simple thermal model**

1959 USASI C95 Committee chartered

- **Sponsored by USN and IEEE**

1966 ANSI C95.1-1966 approved

- **100 W/m^2 - thermal model**
- **10 MHz to 100 GHz**

History of RF/Microwave Exposure Standards in the US (ANSI/IEEE)

1974 ANSI C95.1-1974 approved

- **100 W/m^2 - thermal model**
- **Limits for E^2 and H^2**

1982 ANSI C95.1-1982 approved

- **Incorporates dosimetry**
- **Frequency dependent - single tier**
- **Based on threshold SAR for behavioral disruption**

History of RF/Microwave Exposure Standards in the US (ANSI/IEEE)

1988 ASC(ANSI) C95 Committee becomes IEEE SCC- 28

1991 IEEE C95.1-1991 approved

- SAR - based
- Two tier
- Induced current limits
- Relaxation for partial-body exposure
- Spatial averaging

History of RF/Microwave Exposure Standards in the US (ANSI/IEEE)

1992 IEEE C95.1-1991 is approved by the American National Standards Institute for use as an American National Standard (ANSI/IEEE C95.1-1992)

1996 Literature evaluation in progress for next revision. Some issues being examined are: averaging time, spatial peak SAR, necessity for two tiers

Institute of Electrical and Electronics Engineers

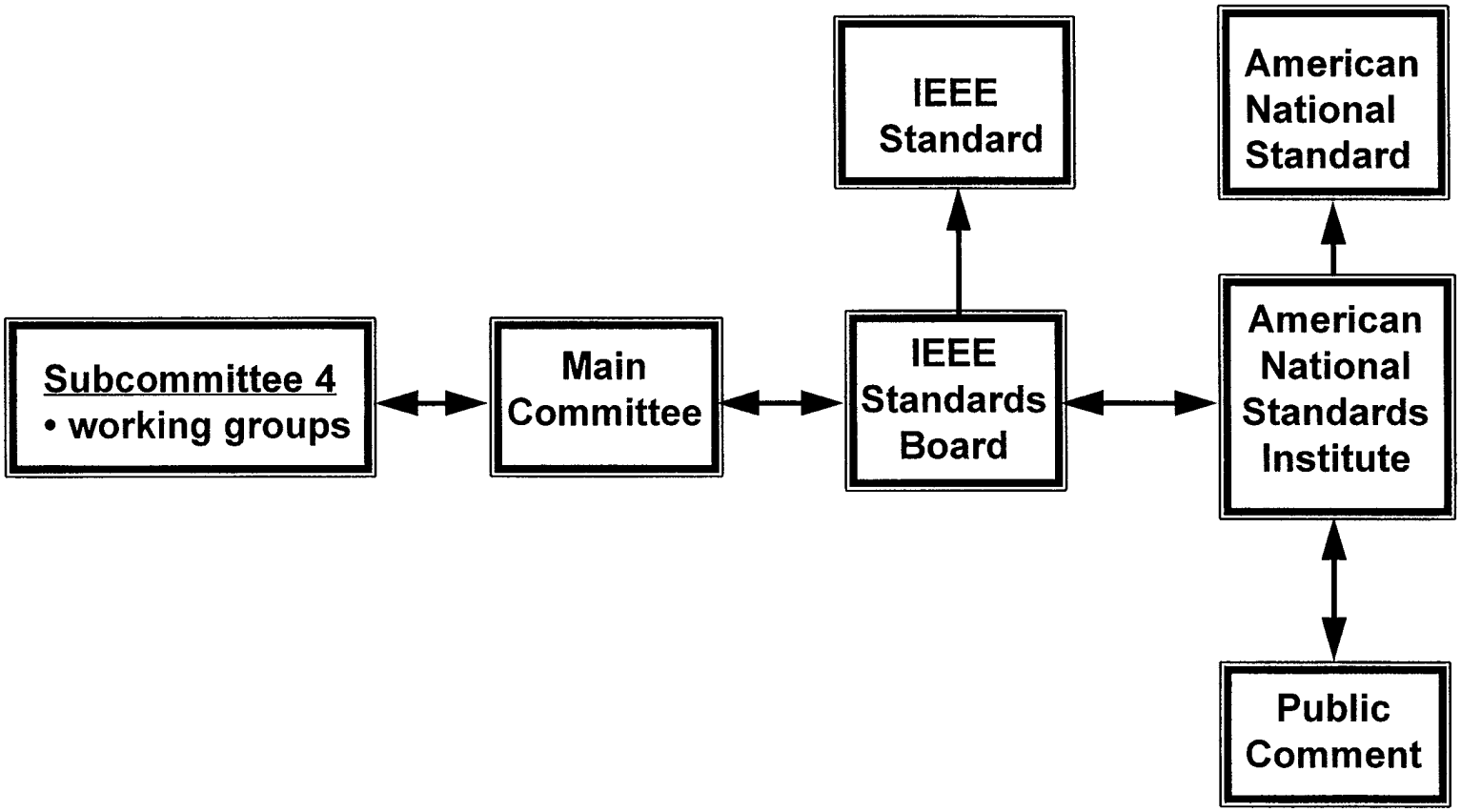

IEEE SCC-28 Standard-Setting Process

Approval of a Draft Standard by the IEEE Standards Board Requires:

Return of 75% of ballots

No more than 30% abstentions

At least 75% approval (not counting abstentions) after

- **All negative ballots have been addressed**
- **All unresolved negative ballots have been circulated to the balloting group (to allow change of vote)**

IEEE Standard for Safety Levels with Respect to Human Exposure to Radio Frequency Electromagnetic Fields, 3 kHz to 300 GHz - C95.1-1991

Membership: Affiliations - SC-4

Research:	university	37	(30%)
	nonprofit	8	(6%)
	military	15	(12%)
	non-military government	30	(24%)
Industry		12	(10%)
Industry - Consulting		4	(3%)
Government - Administration		5	(4%)
General Public & Independent Consultants		14	(11%)

IEEE Standard for Safety Levels with Respect to Human Exposure to Radio Frequency Electromagnetic Fields, 3 kHz to 300 GHz - C95.1-1991

Membership: Principle Disciplines - SC-4

	Number	Percentage
Physical Sciences	41	33
Life Sciences	54	43
Medicine	12	10
Radiology, Pharmacology, Toxicology	4	3
Others (Law, Medical History, Safety, etc.)	14	11

IEEE Standard for Safety Levels with Respect to Human Exposure to Radio Frequency Electromagnetic Fields, 3 kHz to 300 GHz - C95.1-1991

Literature Selection Criteria:

Relevance

Positive effects

Dosimetric quantifiability

Independent replication

IEEE Standard for Safety Levels with Respect to Human Exposure to Radio Frequency Electromagnetic Fields, 3 kHz to 300 GHz - C95.1-1991

Biological ValidationWorking Groups

Behavior	Genetics
Biorhythms	Modulation
Cardiovasculature	Hematology-Immunology
Central Nervous System	Metabolism-Thermoregulation
Development & Teratology	Oncology
Endocrinology	Combined Effects
Visual Systems	Physiology

IEEE Standard for Safety Levels with Respect to Human Exposure to Radio Frequency Electromagnetic Fields, 3 kHz to 300 GHz - C95.1-1991

Rationale:

During the literature assessment procedure, classifications of findings were made *without* prejudgement of mechanisms of effects

The intent was to protect exposed human beings from harm by *any* mechanism

IEEE Standard for Safety Levels with Respect to Human Exposure to Radio Frequency Electromagnetic Fields, 3 kHz to 300 GHz - C95.1-1991

Conclusions:

The most sensitive measures of potentially harmful biological effects were based on the disruption of food-motivated behavior in several animal species under widely-varying field parameters

IEEE Standard for Safety Levels with Respect to Human Exposure to Radio Frequency Electromagnetic Fields, 3 kHz to 300 GHz, C95.1-1991

<u>It was the consensus of the committee that</u>:

"Research on the effects of chronic exposure and speculations on the biological significance of of nonthermal interactions have not yet resulted in any meaningful alteration of the standard"

IEEE Standard for Safety Levels with Respect to Human Exposure to Radio Frequency Electromagnetic Fields, 3 kHz to 300 GHz - C95.1-1991

The MPEs (from 100 kHz to 6 GHz) are based on limiting the SAR to:

	Controlled Environments	Uncontrolled Environments
Whole-Body-Averaged	< 0.4 W/kg	< 8.0 W/kg
Spatial Peak (per gram)*	< 0.08 W/kg	< 1.6 W/kg

*Per gram of tissue in the shape of a cube

IEEE Standards Coordinating Committee 28 (Current Activities)

Literature evaluation is in progress

- **1100 citations in database**
- **Evaluations by topic**

Some issues that will be addressed are:

- **Microwave/millimeter wave averaging time**
- **The need for two tiers**
- **Spatial peak SAR and averaging volume**

IEEE SCC-28 - Subcommittee 4
Literature Evaluation Process

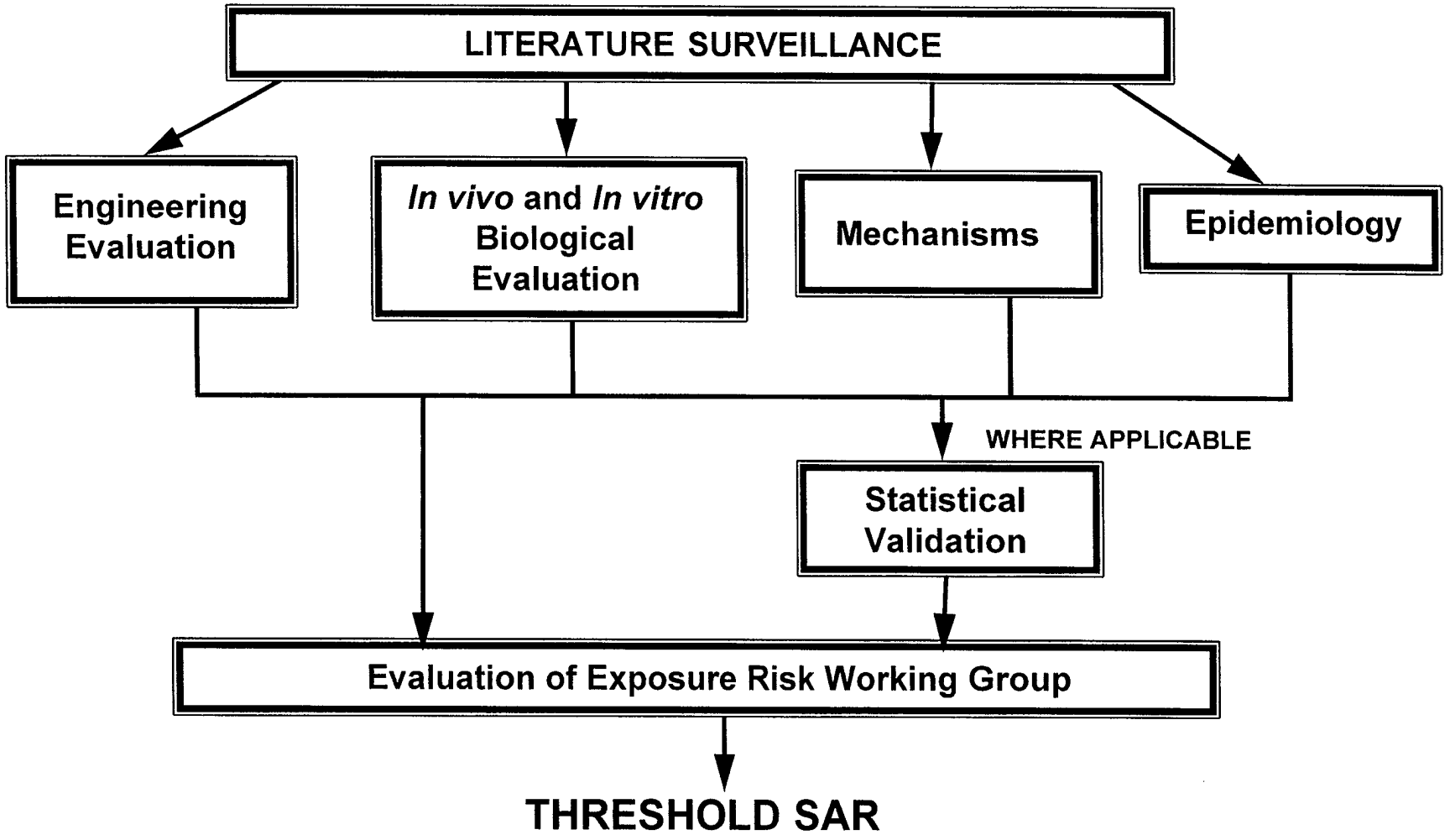

Basis for Laser Standard Development and Revision

M. L. Wolbarsht
Duke University
Durham, NC 27708

ABSTRACT

As increasingly more applications of lasers are formulated, the gaps in our quantitative data base of biological data are highlighted. In the past, just as now, research is tied to the need for safety data for specific applications. All too often in the past ambiguity or large disjunctions in the expression of the safety limits were ignored because "nobody uses a laser here anyway". Such a cavalier attitude is rarely possibly anymore as lasers are at all wavelengths and pulse durations, even as in the ultrashort pulse range where only guidelines have been offered to date due to lack of quantitative experimental information. As the gaps in our information are filled, another problem arises. The original formulation of the safety limits was intended more as a backup for the classification scheme, and there were only a few lasers to classify. As only a relatively few experts used the safety boundary equations either to classify new lasers or to deal with applications not easily covered by standard classification schemes, the mathematical formulations of the boundary conditions were not clearly stated and required cumbersome calculations and references to several tables before any correct answer could be determined. The next revision of the ACGIH and ANSI documents will embody some changes intended to simplify the calculations and make them more rational. Some examples are the use of dimensionally correct equations and decimal exponents.

stdrevms.baf/MSS.97

Where do standards cone from?

All standards are are derived from the same set of biological data, although they may differ to some extent from each other. The original ANSI Z-136.1 in 1976 was the first large scale examination of all the biological data available by a diverse team of experts to arrive at a consensus on the exposure boundaries for all wavelengths and exposure durations. Subsequent formulations have revised the exposure limits by taking account of new data or new conceptions (or in some cases misconceptions) of the old data. The standards also differ based on their revision schedules. For example, The ANSI Z-136.1 standard is revised on a 5-7 year cycle and the ACGIH on a yearly basis. On the other hand, the Federal Standard from the FDA CDRH has only been revised once since its original issue in 1976, although many individual variances have been granted. Thus, the best and most up to date guide to the exposure limits themselves is the latest ACGIH publication. It points the way to the ANSI revisions which follow, and to the variances from the FDA CDRH. The ANSI revision cycle has been recently been accelerated by the standards aimed at specialized user groups, such as optical fiber communications and health care. These ANSI standards are issued in between the revisions to Z-136.1 and may contain revised exposure conditions.

The exposure limits, and especially the classification schemes derived from them, as given in most international standards must be viewed with caution. The committee members from the various countries have rarely had any contact with the experimental programs that produced the exposure limit data. On the other hand, they frequently have political and commercial agendas behind their votes for or against certain exposure limit formulations.

To a large extent, the collection of data on laser injury thresholds has been designed to find only one value, the LD_{50}. This type of experimental design is a carry over from toxicology research in which lethal doses of compounds are sought. It is not as appropriate in the laser damage threshold field. Here, the data is more useful if the the slope of the regression line fitted to all other probabilities of damage is also known. This line also determines the LD_{50} value. However, experiments should be designed to locate the LD_{20} and LD_{80} values as they give much higher confidence levels for the slope and location of the regression line (Finney, 1947). The slope of the regression line also gives some insight into the type of tissue damage mechanism. When the slopes are different in different parts of the spectrum or for different exposure durations, then it is likely that the damage mechanisms are also different.

Formerly, the animal threshold data was checked against human data from volunteers and accidents. Such data is rarely available today. The types of ocular problems which formerly required enucleation, or removal, of the eye which allowed damaging level laser exposures before the operation are now treated in other ways. The number of laser accidents is certainly rising, unfortunately the data from those

occurring in the United States is rarely available for comparison due to litigation associated with the accidents.
There are many theories of laser injury and almost as many experiments to test them. The retina and other specific damage sites have complex anatomical features and usually involve more complex pathological reactions to the laser exposure. The injury reactions may be dependant also on laser wavelength and pulse duration, and even the extent of the exposed area. In spite of this background knowledge, the exposure limits are derived from empirical curve fitting to the experimental data. The theories are used for extrapolation and guidance in regions where there is no data. However, it must be emphasized that the vast majority of the MPE's, and etc. are related to curve fitting of available injury data. The exposure limits also reflect some concern about reasonable usage. Medical applications and other unusual exposure conditions may require more restrictive exposure limits due to the artificial ocular conditions or to prolonged or chronic viewing.

Revisions

The frequent revisions are made necessary by the need to modify the various discontinuities that are found to impact on new applications or new laser types. Sometimes there is a bit of luck and new data becomes available. A good example of that is the report on a program to find the injury thresholds near 1,500 nm presented at this meeting by the Army research group at Brooks Air Force Base (Zuclich et. al., 1997). Reinterpretation of older data sometimes is useful, as in the case of infrared cataracts (Wolbarsht, 1997)

Points that were filled in by extrapolation are reasons for revision when new data shows that the rationale for extrapolation was in error. Recent data from ultrafast pulse program of the Air Force group at Brooks Air Force Base (Rockwell et. al., 1997) suggests that the ANSI guidelines for pulses shorter than 1 ns may be set much too high. If the planned future experiments yield consistent results, these data would be the basis for revision of the exposure limits in this region.

One of the best recent examples of new data leading to a revision is connected with the limiting angular subtense of the source alpha$_{min}$, α_{min}. The correction factor C_E uses α_{min} as the limiting value for source size. The value of α_{min} is time dependent and may vary between 1.5 and 11 milliradians, mr. Sources are described in the latest revisions by the terms "small" and "large", which are separated by the value of α_{min}. Formerly, the small sources were termed "intrabeam viewing" or "point sources". The first is a laser range term and the latter is highly inappropriate for this category. 11 mr is about the angular subtense of the sun or moon and even a 1.5 mr source is far from producing the minimal retinal image expected of a point-like source. The older terms for a large source, extended source or diffuse reflection, are neither sufficiently general to cover projection systems or even exact enough to separate them from the present small source definition. The concept of source size is a difficult one to apply to lasers as the laser beam does not come from

a real source in geometrical optics terms. Rather, the laser beam is created in mid flight and the angular subtense of the source is based on the image size. For safety purposes, this image is the one on the retina.

The history of α_{min} is long and involved. It was invented late at night in a smoke-filled room in the SRI building in Rosslyn, VA across the street from an old CIA laboratory. Dick Honey, Dave Sliney, Art Vassiliadis and myself were part of a small group trying desperately to get the exposure limits in a format suitable for approval at the meeting of the ANSI Z-136 Executive Committee scheduled for the next day. It was a radically new concept. When first presented to the public, some accused those advocating the seemingly complex format of this correction factor of hidden motives, notably that it would insure consultation fees for them when they had to help others use it correctly. By now, most understand how to use the original time dependant correction factor. Possibly, that itself would have been grounds for a new formulation even if new data had not arisen. In any case, an experimental program led by Daniel Courant in France is suppling new data and even a new model (Courant et. al., 1997). This revision is in progress now and should be watched carefully in the future. The only safe prediction about it is that it will become more complex.

Revisions of the MPE's may be formal in nature. That is, equations in conjunction with graphs were substituted for tabular presentation of the exposure limit values. The format of the equations may be changed. Awkward mathematical terms may simplified. This may be facilitated by a general change to decimal exponents as shown:

$$t/\sqrt[4]{t} = t^{0.75}$$

$$n^{-1/4} = n^{-0.25}$$

A proposed change in the MPE's is to put all of the appropriate correction factors in each equation explicitly. An example of how this change would look is given in the MPE for the IRA in the 700-1,049 nm range:

$$1.8\ C_A\ (t/\sqrt[4]{t})\ \ mJ/cm^2 = 1.8\ C_A\ C_E\ t^{0.75}\ \ mJ/cm^2$$

Perhaps, the correction for multiple pulses based on $n^{-0.25}$ should also be given in each equation.

Future revisions

Biological data suitable to define the MPEs are difficult and expensive to gather. These considerations alone will make future data sparse. Nevertheless, there are many places where data is needed and gradually will become available.

One type of future revision that is needed is along quite another line, terminology. The laser exposure to the retina from a small source is evaluated in terms of the corneal irradiance in mW/cm^2 from a rate of delivery standpoint and corneal radiant exposure in mJ/cm^2 for the dose. The analogous terms for the large source are corneal radiance in $mW/sr/cm^2$ and integrated radiance in $mJ/sr/cm^2$, respectively. The terminology would be clearer and more logical if radiant exposure were replaced with irradiant (or irradiance) exposure and integrated radiance replaced by radiance exposure. Perhaps, an even better and simpler solutiion would be the single substitution of integrated irradiance for radiant exposure. This type of change of terminology is not likely to occur as the expects tend to make their judgements here on emotional rather than logical grounds. In any case, one big hope for the future is that all decisions on MPE's will be logical and another that the new data will arrive where it is needed the most.

References

American Conference of Governmental Industrial Hygienists (ACGIH) 1996 Threshold Limit Values (TLVs) for chemical substances and physical agents and Biological Exposure Indices (BEIs). Cincinnati, 1997.

American National Standard for the Safe Use of Lasers, ANSI Z136.1-1993, Laser Institute of America, 1993.

Courant, D., Naudy Vives, C., Dormont, D., Perot, J. and Garcia, J. Experimental determination of retinal damage thresholds induced by multiple picosecond laser pulses. ILSC'97, Laser Institute of America, Orlando, 1997.

FDA (Food and Drug Administration) 21 CFR Parts 1040.10 and 1040.11, Performance standard for laser products. Washington DC, 1976.

Finney, D., Probit Analysis. Cambridge U. Press, Cambridge, 1947.

Rockwell, B., Druessel, J., Hopkins, R., Payne, D., Kennedy, P., Toth, C., Roach, W., Phillips, S., Noojin, G., Stolarski, D. and Cain, C. Ultrashort laser pulse bioeffects and safety. ILSC'97, Laser Institute of America, Orlando, 1997.

Wolbarsht, M. L., Acute thermal cataracts from animal data. "Infrared lasers and millimeter waves" Workshop. Brooks Air Force Base, 1997.

Zuclich, J., Zwick, H., Schuschereba, S., Stuck, B., Boppart, S., Fujimoto, J. and Cheney, F. Ophthalmoscopic and pathological description of ocular damage induced by infrared laser radiation. ILSC'97, Laser Institute of America, Orlando, 1997.

SOME WEAKNESSES OF ANSI/IEEE C95.1-1992: NEEDS FOR ADDITIONAL DATA

Om P. Gandhi
Department of Electrical Engineering
University of Utah
Salt Lake City, Utah 84112

We will focus on the following three areas where the present safety guidelines are relatively weak and need additional data for proper justification.

1. As mentioned in the footnotes of Tables 1B and 2B of the ANSI/IEEE Standard [1], the present safety guidelines do not "adequately protect against startle reactions caused by transient discharges", i.e., for intermittent contacts with ungrounded or poorly grounded metallic objects in low-frequency electromagnetic fields. This lack of protection against transient discharges can result in accidents which may even be fatal in the event of a fall of a subject from a height.

   Therefore, there is a need for laboratory data on transient discharge currents as a function of frequency so as to protect against startle reactions and burns. These currents are likely to vary with the capacitance to ground of the metallic objects. We will propose laboratory experiments that may be done to develop the data to protect against such startle reactions.

2. Another weakness of the new ANSI/IEEE C95.1 safety guideline is the lack of scientific basis for increasing the power-density limit from 5 to 10 mW/cm^2 for frequencies in excess of 3.0 GHz for controlled environments and 15.0 GHz for uncontrolled environments. Data is extremely inadequate on the local and 1-g SARs that may result at the new higher power densities recommended in the 1992 ANSI/IEEE RF safety guidelines. Some calculations by Dimbylow and Gandhi [2] give SARs in excess of 8.0 W/kg for regions of the head including the eyes for frequencies of 2.0-3.0 GHz at the new safety limits. We will give some preliminary calculations of the SARs that point to the possibility that the new

proposed higher limits of power densities may result in 1-g SARs that are higher than the intended limits of 8.0 and 1.6 W/kg for controlled and uncontrolled exposures, respectively [1].

3. The proposed exclusion limits of low-power devices at higher microwave frequencies are not substantiated by the SAR data which are, by and large, not available at frequencies in excess of a few hundred MHz. According to the ANSI/IEEE C95.1-1992 safety guidelines [1], RF emitting devices for frequencies f in excess of 450 MHz need not be tested for SAR compliance if the radiated power is less than $7.0 \times 450/f_{\mathrm{MHz}}$ and $1.4 \times 450/f_{\mathrm{MHz}}$ for controlled and uncontrolled environments, respectively. We will present calculations of SAR distributions for radiating sources such as personal wireless devices which show that the 1-g SARs that one may obtain for the above suggested exclusionary power limits routinely exceed the 8.0 and 1.6 W/kg SAR limits suggested in the ANSI/IEEE safety guidelines.

References

1. ANSI/IEEE C95.1-1992, "IEEE Standard for Safety Levels With Respect to Human Exposure to Radio Frequency Electromagnetic Fields, 3 kHz to 300 GHz," published by the Institute of Electrical and Electronics Engineers, Inc., 345 East 47th Street, New York, New York, 10017.

2. P. J. Dimbylow and O. P. Gandhi, "Finite-Difference Time-Domain Calculations of SAR in a Realistic, Heterogeneous Model of the Head for Plane-Wave Exposure from 600 MHz to 3 GHz," *Physics in Medicine and Biology*, Vol. 36, pp. 1075-1089, 1991.

Infrared Lasers & Millimeter Waves
Workshop
The Links Between Microwaves
& Laser Optics

21 Jan 1997 - 22 Jan 1997

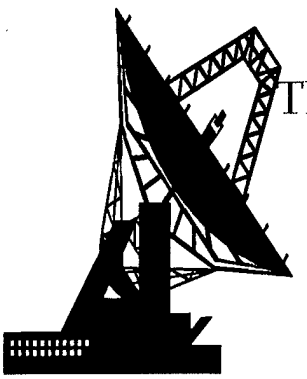

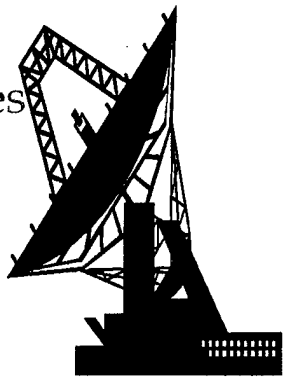

SECTION VIII:

PANEL DISCUSSION: GOALS FOR IMPROVED LASER & MICROWAVE STANDARDS

SYNOPSIS OF A PANEL DISCUSSION:
Goals for Improved Laser and Microwave Standards

Eleanor R. Adair, Rapporteur
Ronald C. Petersen, Moderator

Members of the Panel: Om P. Gandhi, John M. Osepchuk, Kenneth R. Foster, Marvin Ziskin, David Sliney, Bruce Stuck, Myron Wolbarsht, Russ McCally

Petersen: Does everyone agree that 10 s averaging time at 300 GHz is not adequate for the whole body?

Sliney: Thermal models are used for surface conduction, aperture average and volume. You have said that the SAR is not valid above 6 GHz. How about a step function? In talking about surface absorption, 10 s is too short for large and too large for small areas. We in the laser field do it in step functions.

Osepchuk: In the current Z136 laser standard you have 2 flux limits and 2 averaging times at 300 GHz.

Sliney: And you assume that equal energy absorbed is equally hazardous across frequencies. At the far IR we have a break.

Osepchuk: In the near future, will you be changing the duration for large areas?

Wolbarsht: We always stick to the data. We have a time function for area that blends into 10 seconds.

Sliney: As you know, laser sources in common use are pulsed and have small area. Extrapolation to the long term has been by thermal modeling. For us, exposure duration has not been an issue. In the past, the microwave standard reduced a power density of 100 mW/cm^2 to 10 mW/cm^2 at the highest frequencies to match us. But we also matched your standard at 10 mW/cm^2 there and now you have matched our averaging time of 10 sec.

Wolbarsht: There is a problem. The laser hazard is primarily to the eye. There is no such thing for microwaves. Optical gain must be considered.

Osepchuk: The laser standard exists at 300 GHz. But also, this is the upper limit of the RF/microwave standard and we must have a guideline to account for irradiation of larger surface areas.

Meltz: What will produce this? What is a common basis we can use for the two standards? Can we identify the sensitive organ?

McCally: At 300 GHz, the sensitive organ is either the skin or the cornea. But other things must be considered: pulsed, peak powers, continuous wave, etc.

Osepchuk: Let's ignore those additional problems now and concentrate on exposure duration. If we do correct thermal modeling, we should be able to work in the area factor. The laser community should lead the way on this.

Foster: Don't forget the L^2/D thing. The time constant is related to heat loss from the body (skin), i.e., the thermoregulatory time constant for the body. This problem becomes more important as you go to lower microwave frequencies where a large part of the body may be exposed.

Petersen: But the problem exists where the two standards meet.

Sliney: This dilemma over area is largely unusual for us. There are few data here. Insects use 300 GHz for communication (Callahan). In producing the laser standard, we have only solved problems where we had them. I expect it is good to tidy things up. We have a standard approach that should apply; but, the problem is capillary heat exchange, for example, choroidal blood flow.

Petersen: Will the Z136 committee investigate this question?

Sliney: IITRI developed a skin model some time ago. Freund and McCally have a model for small spots, as David described. Maybe these would constitute a first cut.

Foster: Sheldon Weinbaum's (New York) model is the gold standard.

McCally: The model used will depend on the situation being modeled. Long term exposure is one example, but you can ignore long-term responses for short exposures.

Petersen: We have a problem in how to draw the function for averaging time. As presently constructed, ours produces MPEs higher than they should be for the skin, at the lower GHz frequencies. My question is, should we reduce the averaging time to something like 10 s for all frequencies where the skin depth is the same? At the time we were discussing averaging times at the higher frequencies, an unnamed military scientist suggested for 10, 20, 30 GHz that an averaging time of close to 6 min would be appropriate. But I question this if the skin depths are approximately the same.

Sliney: You were always concerned with large exposure areas. But on another note, how about athermal effects? What I suggest is that you get someone to do similar experiments with millimeter waves and with IR lasers and see if you get the same results.

Stuck: Where does C95 have exposure limits above those specified in Z136?

Petersen: For short exposures above 30 GHz, where the averaging time is ~6 minutes, the exposure permitted will be higher.

Sliney: Does penetration depth vary monotonically with frequency?

Blick: Yes, log penetration depth varies monotonically with log frequency.

Sliney: You could use erythema or some other injury assessment, or histological data as endpoints for the proposed experiment. You could do it at Brooks where equipment at both frequencies is available.

Blick: I already have an approved protocol for a study of thermal pain in human subjects. This protocol will include 3 millimeter wave frequencies and 2 IR frequencies.

Glickman: Maybe there are other kinds of endpoints you could study.

Ziskin: Yes, especially if the penetration depth is essentially the same.

Petersen: Is there any reason to believe that there are differences in interaction mechanisms between millimeter wave and laser frequencies?

McCally: For lasers, we have well-characterized beams. This is not the case with millimeter wave sources.

Khiznyiak: With respect to short penetration depths, the epidermis has low water content so the maximal heating under millimeter wave exposure will be in the dermis. The same should be true for IR.

Foster: The epidermis is a thin layer. No appreciable heat will leave the skin. On the other hand, clothing may impede things.

Meltz: I am not sure that athermal is an overriding issue here. In the proposed experiment involving 2 frequencies, you should first look at the same bioeffect at a high intensity to determine similarities in response. But then you should look at progressively lower intensities to see if there may be differences that develop.

Petersen: It will take some time to design and conduct such an experiment. In the absence of data from this experiment, do we have enough information now to change the averaging time for frequencies below 300 GHz?

Foster: Models are a cheap way to go as a first pass. We could define hazards in terms of temperature rise.

---

2 minute gap in notes

Wolbarsht: In the microwave field, you must account for the fact that the exposures will always be longer. And we should always have dessert.

Petersen: Could I suggest that we agree to set up an ad hoc committee, comprised of members from the two standards-setting bodies, to work on the question of averaging time. We could, for example, select 3 people from the SCC28 committee system as members of this ad hoc group.

Sliney: The laser standard committee is under Wolbarsht's direction. They are the ones to provide members.

Wolbarsht: That is all right with me.

Sliney: At the same time, we should twist some arms to do some thermal modeling.

McCally: Fine. Freund and I can do thermal modeling, but we need some experiments to validate our products and to suggest parameter values.

Osepchuk: Unfortunately, there are currently no data. But if we had predictions from models and then found that a couple of points don't fit, this would be a good stimulus for further research.

Ziskin: I think it is important that we decide exactly what we are trying to protect against with our standards. Tissue damage? Corneal damage is probably the best end point.

Wolbarsht: But it has to be for a short exposure. The skin would be just as good as the cornea to measure tissue damage.

Kues: I have some relevant data in press at this time that I have collected on rabbit eyes exposed at 60 GHz. This research has been funded by Hewlett Packard. The animals were not anesthetised. They were restrained so that we could expose the cornea of one eye and use the other eye as a control. We measured corneal heating with an IR thermograph. In the first experiment, we exposed the cornea for 8 hours at a power density of 10 mW/cm^2 and SAW NOTHING. Then we did a second experiment, looking for cumulative damage. We exposed the same eye for 4 hours/day (at 10 mW/cm^2) for 5 days, and SAW NOTHING.

Glickman: Damage to the cornea is certainly a good endpoint.

Ziskin: Yes. Damage to the cornea means something.

Kues: We have plans to go to higher power densities in future studies.

Albanese: I believe that there are still some things missing and that a systematic review of each should be undertaken. Such matters as dermal reactions and problems with the immune system come to mind.

Petersen: Are there any other comments, or comments about the meeting in general?

Osepchuk: The plans to form a liaison group between the standards-setting bodies is a big, positive step.

Wolbarsht: The meeting is getting better.

Osepchuk: Good things have been said about the future. The meeting has been important and very productive.

Meeting closed.

Infrared Lasers & Millimeter Waves
Workshop
The Links Between Microwaves
& Laser Optics

21 Jan 1997 - 22 Jan 1997

LIST OF ATTENDEES

ATTENDEE LIST

21-Jan-97

LastName	FirstName	OrganizationName	EmailAddress	WorkPhone	FaxNumber
ABDELHAMIED	ADAM		ABDELHAMIED	(210) 536-5600	
ADAIR	ELEANOR	AL/OER	eadair@rfr.brooks.af.mil	(210) 536-4698	(210) 536-3977
ADAIR	ROBERT	DEPT. OF PHYSICS, YALE	adair@yalphz/physics.yale.edu	(203) 777-2955	(203) 432-6125
AKYEL	YAHYA		YAHYA AKYEL		
ALBANESE	RICHARD	AL/OES	ALBANESE	(210) 536-4839	(210) 536-2952
ALEXEEV	S.	CENTER FOR BIOMEDICAL PHYS	ziskiw@astro.ocis.temple.edu	(215) 707-7412	(215) 707-4324
BEASON	CHARLES	AL/OER	beason@rfr.brooks.af.mil	(210) 536-4041	
BLICK	DENNIS	SYSTEMS RESEARCH LABS	blick@rfr.brooks.af.mil	(210) 536-2547	(210) 536-2603
BRECHER	AVIVA	U.S. DOT, VOLPE NATL. TRANSP.	brecher@volpe1.dot.gov	(617) 496-3470	(617) 494-3688
BREWER	JOHN		brewer@hafa.net.gu	(671) 472-6473	(671) 477-2838
BROWN	CARROLL	SYSTEMS RESEARCH LABS	brown@rfr.brooks.af.mil	(210) 536-3197	(210) 534-2919
BURR	JOHN	BATTELLE PACIFIC NW LABS	jg_burr@pnl.gov	(509) 373-5172	(509) 376-6663
BURTON	RUSSELL	AL/CA	russell.burton@platinum.brooks.af.mil	(210) 536-3656	(210) 536-2371
CARTLEDGE	ROBERT		robert.cartledge@platinum.brooks.af.mil	(210) 536-3904	(210) 536-3903
CHALFIN	STEVEN	OPHTH DEPT - UTHSCSA	challffin@uthsca.edu	(210) 567-8411	(210) 567-8413
CHALFIN	STEVEN	UNIVERSITY EYE CONSULTANT	CHALFIN	(210) 567-5088	(210) 567-6584
CHERRY	ROBERT	HQDA (DACS-SF)	cherry@pentagon-hqdadds.acm.mil	(088) 225-7201	(088) 227-4055
COSTER	PERE		PERE COSTER		
D'ANDREA	JOHN		D'ANDREA		
DAYTON	TOM	SYSTEMS RESEARCH LABS	dayton@rfr.brooks.af.mil	(210) 536-4702	(210) 534-2919
DENNISTON	ROBERT	SYSTEMS RESEARCH LABS	denniston@rfr.brooks.af.mil	(210) 536-3197	(210) 534-2919
DENNY	JOHN	UT HEALTH SCI. CTR	DENNY	(210) 567-8439	(210) 567-8413
FOSTER	KEN		FOSTER		
FRANZEN	JOHN	AL/OES	franzen@integral.brooks.af.mil	(210) 536-5478	

LastName	FirstName	OrganizationName	EmailAddress	WorkPhone	FaxNumber
FREI	MEL	TRINITY	frei@rfr.brooks.af.mil	(210) 536-2036	
FREUND	DAVID	JHU/APL	freund@aplcomm.jhuapl.edu	(301) 953-6260	(301) 953-6904
FURSE	CINDY		FURSE		
GLICKMAN	RANDOLPH	UT HEALTH SCI. CTR	glilckman@uthscsa.ddu	(210) 567-8420	(210) 567-8413
GORSUCH	GREGORY	CMC (SD) HQMC	gorsuchg@mqg-smtp3.usmc.mil	(703) 614-1202	(703) 695-3231
GUY	ARTHUR		guy@u.washington.edu	(206) 485-6439	(206) 485-5963
HEYNICK	LOU		louhey@worldnet.att.net	(415) 494-6585	(415) 494-1151
HURT	WILLIAM	AL/OERS	hurt@rfr.brooks.af.mil	(210) 536-3167	(210) 536-3977
JAUCHEM	JAMES	AL/OERB	jauchem@rfr.brooks.af.mil	(210) 536-3572	(210) 536-3977
JUREK	DEBRA	SYSTEMS RESEARCH LABS	jurek@rfr.brooks.af.mil	(210) 536-3197	(210) 534-2919
KENNEDY	PAUL	AL/OEOP	paul.kennedy@platinum.brooks.af.mil	(210) 536-4791	(210) 536-3903
KHIZHNYAK	EUGENE	CTR.FOR BIOMED. PHY. TEMPLE	KHIZHNYAK	(215) 707-4012	(215) 707-4324
KIEL	JOHNATHAN	AAL/OERT	kiel@rfr.brooks.af.mil	(210) 536-3583	(210) 536-4716
KLAUENBERG	JON	AL/OER	klauenberg@rfr.brooks.af.mil	(210)-536-4837	
KUES	HENRY	JHU/APL	hak@aplcomm.jhuapl.edu	(301) 953-6259	(301) 953-6904
LAMBERT	LEROY		leroy.lambert@platinum.brooks.af.mil	(210) 536-6561	(210) 536-3903
LEONOWICH	JOHN	AL/OERS	leonowich@rfr.brooks.af.mil	(210) 536-3197	(210) 534-2919
LIOTTA	PHILIP	HQMC (SD),	liottap@wqg-smtp3.usmc.mil	(703) 614-1202	(703) 695-3231
LU	SHIN-TSU		lu@rfr.brooks.af.mil	(210) 536-5600	(210) 536-5382
LUND	JACK	USAMRD-BAFB	lund@laser.brooks.af.mil	(210) 536-4631	(210) 536-3450
MATHUR	SATNAM	MEKESSON BIOSERVICES, (USA	MATHUR	(210) 536-5601	(210) 536-5382
MAY	NOAL	FAA, AERONAUTICAL CTR.	nmay@mmacmail.jccbi.gov	(405) 954-3713	(405) 954-9112
MC CALLY	R.L.	JOHNS HOPKINS UNIV.	rmccally@jhuapl.edu	(410) 792-6201	(410) 792-6904
MEDINA	RICHARD	AL/OES	MEDINA	(210) 536-4839	(210) 536-2952
MELTZ	MARTIN	CERT/UNIV.OF TX. HLTH.SCI.CT	meltz@uthscsa.edu	(210) 567-5560	(210) 567-3446
MERRITT	JAMES	AL/OERB	merritt@rfr.brooks.af.mil	(210) 536-4703	(210) 536-3977
MITCHELL	JOHN		MITCHELL	(210) 696-2859	
MOSS	GENE		MOSS	(513) 841-4543	(513) 841-4488

LastName	FirstName	OrganizationName	EmailAddress	WorkPhone	FaxNumber
MURPHY	MICHAEL	AL/OER	murphy@rfr.brooks.af.mil	(210) 536-4833	(210) 536-3977
MYLACRAINE	KEVIN	SYSTEMS RESEARCH LABS	mylacraine@rfr.brooks.af.mil	(210) 536-3197	(210) 534-2919
OLSEN	RICHARD		olsen@rfr.brooks.af.mil	(210) 536-6535	(210) 536-6538
ORR	JOHN		jorr@swri.edu	(210) 522-2658	(210) 522-5517
OSEPCHUK	JOHN	FULL SPECTRUM CONSULTING	75754.3663@compuserve.com	(210) 587-5849	
PAKHOMOV	ANDREI	USHMRD	pakhomov@netxpress.com	(210) 536-5599	(210) 536-5382
PAKOMOVA	OLGA		OLGA PAKHOMOVA		
PETERSEN	RON	LUCENT TECHNOLOGIES,INC.	rcpetersen@lureut.com	(908) 582-6442	(908) 582-2846
POLSON	PETER	AUSA RESEARCH	ppolson@worldnet.att.net	(408) 257-3376	(408) 257-3376
POTASEK	M.J.	AL/OES	POTASEK	(210) 536-5709	(210) 536-2952
REDDIX	MICHAEL	NAVAL MEDICAL RESEARCH INS	reddix@rfr.brooks.af.mil	(210) 536-6552	(210) 536-6528
ROACH	PAT	AFOSR/NL	pat.roach@afosr.af.mil	(202) 767-8074	(202) 404-7475
ROBERTS	BRAD	U.S. ARMY CTR. FOR HEALTH PR	brad.roberts@CHPPM-CCMAIL.APGE	(410) 671-3353	(410) 671-5411
ROCKWELL	BENJAMIN		benjamin.rockwell@platinum.brooks.af.	(210) 536-4790	(210) 536-3903
RYAN	KATHY	DEPT. OF BIO., TRINITY UNIV.	ryan@rfr.brooks.af.mil	(210) 536-4825	(210) 736-7229
SAMN	SHERWOOD	AL/OES	samn@apache.brooks.af.mil	(210) 536-5708	(210) 536-2952
SEAMAN	RON	MCKESSON BIOSERVICES,	rseaman@rfr.brooks.af.mil	(210) 536-5595	(210) 536-5382
SHERRY	CLIFF	SYSTEMS RESEARCH LABS	sherry@rfr.brooks.af.mil	(210) 536-4767	(210) 534-2919
SMITH	MATT	BATTELLE PACIFIC NW LABS.	mh_smith@pnl.gov	(509) 373-2214	(509) 375-2019
SORENSEN	SHERRIE	AL/OER	sorensen@rfr.brooks.af.mil	(210) 536-2209	
STUCK	BRUCE		STUCK		
TRIBBLE	JERRI		trible@rfr.brooks.af.mil	(210) 536-1906	(210) 536-6528
VAN MATRE	BARRY		vanmatre@rfr.brooks.af.mil	(210) 536-6538	(210) 536-6538
VARANELLI	ARTHUR	RAYTHEON CO.	art16@ix.uetcom.com	(617) 860-1641	(617) 860-2210
WAGNER	KATRINA	AL/OER	wagner@delta.brooks.af.mil		
WALTERS	THOMAS	SYSTEMS RESEARCH LABS	walters@rfr.brooks.af.mil	(210) 536-3197	(210) 534-2919
WANG	YUN	ARMSTRONG LABORATORIES	WANG	(210) 536-5705	(210) 536-2952
WOLBARSHT	M.L.	DUKE UNIVERSITY	deryag@psych.duke.edu	(919) 660-5670	(919) 660-5672

LastName	FirstName	OrganizationName	EmailAddress	WorkPhone	FaxNumber
YACOVISSI	ROBERT	760 BUREAU OF MEDICINE & SU	nmc2rxy@bomed60.med.navy.mil	(202) 762-3448	(202) 762-0931
ZIRIAX	JOHN		ziriax@rfr.brooks.af.mil		
ZISKIN	MARVIN	TEMPLE UNIV. MED. SCH.	ziskin@astro.ocistemple.edu	(215) 707-4259	(215) 707-4324
ZUCLICH	JOSEPH	TASC	joe.zuclich@platinum.brooks.af.mil	(210) 536-4795	(210) 534-0420